LA-UR- 98-56

CONF-9708189--PROC.

Approved for public release; distribution is unlimited.

Title: INFRASOUND WORKSHOP FOR CTBT

Author(s): See attached agenda

Submitted to: INFRASOUND WORKSHOP FOR CTBT
August 25-28, 1997
Santa Fe, New Mexico

Los Alamos
NATIONAL LABORATORY

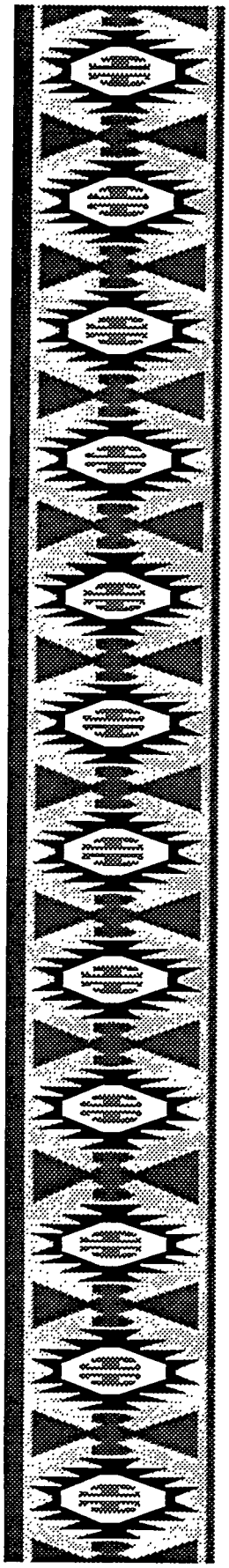

INFRASOUND WORKSHOP FOR CTBT MONITORING

August 25-28, 1997
Santa Fe, New Mexico

Sponsored By:
Los Alamos National Laboratory
U.S Department of Energy

DISCLAIMER

DISCLAIMER

Portions of this document may be illegible in electronic image products. Images are produced from the best available original document.

Contents

Infrasound Workshop for CTBT Monitoring
Santa Fe, New Mexico
25-28 August 1997

Foreword

by Rodney W. Whitaker, Los Alamos National Laboratory
Workshop Coordinator and Host

From 25 through 28 August 1997, the US Department of Energy and Los Alamos National Laboratory hosted, in Santa Fe, New Mexico, an International Infrasound Workshop for CTBT Monitoring . Over 60 partcipants from around the world attended the meeting and presented talks on sensors, signal processing and analysis, propagation, sources of noise and noise reduction, analysis of explosion data, and analysis of man-made and other natural sources. There were two and a half days of presentations and one-half day devoted to a tour of the DOE prototype infrasound array recently installed in Los Alamos. The informal atmosphere promoted much discussion among the attendees. During the last session, all participants contributed to a discussion of key technical issues and future work, which is summarized in this document.

In this document, you will find the Workshop Agenda, list of participants, and abstracts and view graphs from each presentation.

We gladly acknowledge the generous support of Ms. Leslie Casey, Program Manager of the DOE Comprehensive Test Ban Treaty Research and Development Program, for making the workshop possible. We also thank Jan Hull, Los Alamos Technical Associates, for meeting coordination support and Jill Warren and Fran Chavez, Los Alamos National Laboratory, for helping with the assembly of the proceedings.

Agenda

INFRASOUND WORKSHOP FOR CTBT MONITORING
Santa Fe, New Mexico
August 25-28, 1997

Monday, August 25

5:00 - 7:00 p.m. Registration and Welcome Reception -- *Poolside, Radisson Hotel*

Tuesday, August 26

7:30 - 8:30	Continental Breakfast -- *Poolside, Radisson Hotel*	
	TECHNICAL SESSIONS -- *Kachina Ballroom*	
8:30 - 8:45	Opening Remarks	Rodney W. Whitaker
8:45 - 9:00	Department of Energy Welcome	Leslie A. Casey
9:00 - 9:15	Los Alamos National Laboratory Welcome	David J. Simons Wendee M. Brunish
9:15 - 9:30	PTS/PREP COMM UPDATE A Progress Report on the Establishment of the IMS Infrasound Network	Douglas R. Christie
9:30 - 12:00	**SESSION ONE: ARRAY DESIGN AND SIGNAL PROCESSING**	
	9:30 - 9:50 Infrasound Array Design with Respect to Detection Slowness Estimation	Robert R. Blandford
	9:50 - 10:10 A Comparison of Several Automated Detectors for Infrasound Signal	Kevin D. Hutchenson
	10:10 - 10:30 Break	
	10:30 - 10:50 F-Statistics: A Tool for Infrasound Signal Detection	Haydar J. Al-Shukri
	10:50 - 11:10 Automatic Processing of Infrasonic Data at the Prototype IDC	Raymond J. Willemann Charles N. Katz
	11:10 - 11:30 Seismo-Acoustical Equipment Complex in Murmansk Region (Russia)	Oleg M. Raspopov
	11:30 - 12:00 Open Discussion	Thomas Armstrong, Moderator
12:00 - 1:00	Working Lunch -- *Dining Room, Radisson Hotel*	

1:00 - 5:00	**SESSION TWO: ARRAY PERFORMANCE AND NOISE REDUCTION**		
	1:00 - 1:20	Infrasound Detection: The French System	Elisabeth Blanc
	1:20 - 1:40	Capability Modeling of the Proposed International Monitoring System 60-Station Infrasonic Network	Dean A. Clauter
	1:40 - 2:00	Effects of Stratospheric Winds on Long Range Infrasonic Propagation	Joseph P. Mutschlecner
	2:00 - 2:20	High Altitude Wind Effects on Infrasound Network Performance	Lawrence C. Trost
	2:20 - 2:40	Permeable Hose Characteristics and Noise Reduction For Infrasound Monitoring	Terrance G. Barker
	2:40 - 3:10	Break	
	3:30 - 3:50	Noise Reducers for Infrasound Detection	Heinrich W. Haak
	3:50 - 4:10	Relationship Between the Normalized Cross-Correlation Function and the F-Statistic	Charles N. Katz
	4:10 - 5:00	Open Discussion	Douglas R. Christie, Moderator

6:30 - 9:00 Banquet -- *Board Room, Radisson Hotel*
Speaker: Ludwik J. Liszka
Swedish Institute of Space Physics

Wednesday, August 27

7:30 - 8:30 Continental Breakfast -- *Poolside, Radisson Hotel*

8:30 - 10:00	**SESSION THREE: EXPLOSION MONITORING**		
	8:30 - 8:50	About Estimations of the Explosion Sources Energy by Remote Acoustic Techniques	Sergey N. Kulichkov
	8:50 - 9:10	Long-Range Sound Propagation from Underground Surface, and Near Surface Bursts with Small Yields	Sergey N. Kulichkov
	9:10 - 9:30	Infrasound Monitoring System of Nuclear Explosion in the Atmosphere	Jin Lai Xie Zhao Hua Xie
	9:30 - 10:00	Open Discussion	Douglas O. Revelle, Moderator
10:00 - 10:40	**SESSION FOUR: DOE/LANL PROTOTYPE ARRAY**		
	10:00 - 10:20	Development of a Prototype Infrasound System	Rodney W. Whitaker
	10:20 - 10:40	Infrasound Sensor For CTBT Infrasound Array Application	Richard P. Kromer
	10:40 - 11:00	Break	

11:00 - 6:00	Lunch and Tour of US Department of Energy Prototype Infrasound Array at Los Alamos National Laboratory *Board bus at hotel front entrance*		

Thursday, August 28

7:30 - 8:30	Continental Breakfast -- *Poolside, Radisson Hotel*		
8:30 - 12:00	**SESSION FIVE: LONG RANGE PROPAGATION**		
	8:30 - 8:50	Numerical Modeling of Long Range Infrasonic Propagation	James H. Hunter
	8:50 - 9:10	Propagation Conditions and Localization of Infrasonic Sources	Ludwik J. Liszka
	9:10 - 9:30	Travel Times for Infrasonic Waves in the Atmosphere	Milton A. Garcés
	9:30 - 9:50	Break	
	9:50 - 10:10	Ukraine Infrasound Array proposal	Alexander Sytolenko
	10:10 - 12:00	Site, Site Survery, and Other Issues	Rodney W. Whitaker
12:00 - 1:00	Working Lunch -- *Dining Room, Radisson Hotel*		
1:00 - 2:20	**SESSION SIX: OTHER SOURCES OF INFRASOUND**		
	1:00 - 1:20	Infrasound from Mining Explosions, Space Shuttles and Meteors	Eugene Herrin
	1:20 - 1:40	The Infrasound Background for High Latitude CTBT Stations	Charles R. Wilson
	1:40 - 2:00	Bolides as Explosive Infrasonic Sources: CTBT Implications	Douglas O. Revelle
2:00 - 5:00	**SESSION SEVEN: DISCUSSION AND SUMMARY**		
	2:00 - 2:20	Final Discussion Related to Presentations	All
	2:20 - 2:40	Break	
	2:40 - 3:00	Discussion of Key Technical Issues for Future Work	Douglas R. Christie, Moderator
	3:00 - 5:00	Summary	Rodney W. Whitaker, Moderator

Infrasound Workshop Participants

Last Name	First Name	Organization	Mailing Address	State	ST	Zip	Country	Telephone	Fax	E-Mail
Afflerback	Gerald	ASC	Detachment 3, 1031 S. Hwy. A1A	Patrick AFB	FL	32925	USA	(407) 494-5512	(407) 494-9837	affle@aftac.gov
Al-Shukri	Haydar	ENSCO Inc.	445 Pineda Court	Melborne	FL	32940	USA	(407) 254-4122	(402) 254-3293	alshukri@fl.ensco.com
Albert	Don	U.S. Army, CRREL	72 Lyme Road	Hanover	NH	03755-1290	USA	(603) 646-4459	(603) 646-4397	dalbert@crrel.usace.army.mil
Armstrong	William	Los Alamos National Laboratory	EES-8, MS F659	Los Alamos	NM	87545	USA	(505) 667-9517	(505) 665-3681	wta@lanl.gov
Barker	Terrance	Maxwell Technologies	8888 Balboa Ave.	San Diego	CA	92123	USA	(619) 576-7756	(619) 576 7710	barker@maxwell.com
Blanc	Elizabeth	Commissariat A L'Energie Atomique	Laboratoire de Detection et de Geophysique BP 12,	91680 Bruyères le Chatel			France	33-1-6926-4996	33-1-6926-7023	blanc@ldg.bruyeres.cea.fr
Blandford	Robert	AFTAC	Suite 1450, 1300 N17th St.	Arlington	VA	22209	USA	(703) 247-1856	(703) 243-5379	rrb@cmr.gov
Breding	Dale	Sandia National Laboratories	MS 0979, Org. 5704	Albuquerque	NM	87185	USA	(505) 844-9084	(505) 844-5321	drbredi@sandia gov
Brown	David	Australian National University	Research School of Earth Sciences	Canberra	ACT	0200	Australia	61-6-249-4269	61-6-257-2737	djb@bullen.anu.edu.au
Brunish	Wendee	Los Alamos National Laboratory	EES-DO, MS F659	Los Alamos	NM	87545	USA	(505) 667-5724	(505) 665-3681	wb@lanl.gov
Bullard	Edwin	Chaparral Physics Consultants	7405 Capulin Road NE	Albuquerque	NM	87109	USA	(505) 822-8771		bullard@abq.com
Cable	Peter	BBN Systems and Technologies	Union Station	New London	CT	06320	USA	(860) 447-5913	(860) 447-1132	pcable@bbn.com
Casey	Leslie	U.S. Department of Energy	NN-20, 1000 Independence Av., SW	Washington	DC	20585-0420	USA	(202) 586-2151	(202) 586-0485	leslie.casey@hq.doe.gov
Cella	Luis	Autoridad Regulatoria Nuclear (ARN)	Av.del Libertador 8250	Buenos Aires 1429			Argentina	54-1-379-8377	54-1-379-8460	lcella@cae.cnren.gov.ar

Infrasound Workshop Participants

Last Name	First Name	Organization	Mailing Address	State	ST	Zip	Country	Telephone	Fax	E-Mail
Christie	Douglas	Provisional Technical Secretariat, CTBTO	Vienna Int'l. Center, P.O. Box 1200, A-1400	Vienna			Austria	43-1-21345-6138	43-1-21345-5877	dchristie@ctbto.un.or.at
Clauter	Dean	HQ AFTAC/TTR	1030 South Highway A1A	Patrick AFB	FL	32925-3002	USA	(407) 494-5263	(407) 494-2274	clauter@rayleigh.tt.aftac.gov
Dighe	Kalpak	Los Alamos National Laboratory	PO Box 1663, MS C300	Los Alamos	NM	87545	USA	(505) 665-1701		kdighe@lanl.gov
Garcés	Milton	University of Hawaii Manoa	PO Box 1599	Kailua-Kona	HI	96745-1599	USA	(808) 331-2745	(808) 329-1021	milton@hialoha.net
Gibson	Robert	BBN Corporation	1300 N. 17th St., Suite 1200	Arlington	VA	22209	USA	(703) 284-4787	(703) 284-4777	rgibson@bbn.com
Haak	Heinrich	Royal Netherlands Meteorological Institute	Seismology Division, P.O. Box 201	DeBilt		3730 AE	Netherlands	31-30-220-6341	31-30-220-1364	haak@knmi.nl
Hartmann	Gernot	BGR Hannover	Postfach 510153	30631 Hannover			Germany	49-511 643-3227	49-511 643-3663	Hart@sdac.hannover.bgr.de
Hedlin	Michael	University of California San Diego	9500 Gilman Drive	La Jolla	CA	92093-0225	USA	(619) 534-8773	(619) 534-2902	mhedlin@eos.ucsd.edu
Herrin	Eugene	Southern Methodist University	P.O Box 395, SMU Dept of Geology	Dallas	TX	75275	USA	(214) 768-2760	(214) 768-4291	herrin@passion.isem.smu.edu
Herrington	Preston	Sandia National Laboratories	P.O Box 5800, MS 0655	Albuquerque	NM	87185-0655	USA	(505) 844-9495	(505) 884-5321	pbherri@sandia.gov
Hodgson	Mark	Los Alamos National Laboratory	MS D460	Los Alamos	NM	87545	USA	(505) 665-5612	(505) 665-0854	mhodgson@lanl.gov
Hull	Jan	Los Alamos Technical Associates, Inc.	1200 Trinity Dr.	Los Alamos	NM	87544	USA	(505) 662-1740	(505) 662-1846	jhull@lanl.gov
Hunter, Jr.	James	University of Florida	414 NE 6th St.	Gainesville	FL	32601	USA	(352) 378-5284	(352) 392-5089	hunter@astro.ufl.edu
Hutchenson	Kevin	ENSCO Inc.	445 Pineda Court	Melbourne	FL	32940	USA	(407) 254-4122	(402) 254-3293	hutch@fl.ensco.com

Infrasound Workshop Participants

Last Name	First Name	Organization	Mailing Address	State	ST	Zip	Country	Telephone	Fax	E-Mail
Jih	Rong-Song	Defense Special Weapons Agency	HQ DSWA/PMP, 6801 Telegraph Road	Alexandria	VA	22310	USA	(703) 325-9203	(703) 325-2684	jih@cmr.gov
Katz	Charles	Science Applications International Corporation	10260 Campus Point Drive	San Diego	CA	92121	USA	(619) 546-6115	(619) 458-4993	katzc@cpva.saic.com
Kemerait	Robert	HQ/AFTAC	AFTAC/TT, 1930 Highway A1A	Patrick AFB	FL	32925	USA	(407) 494-7668	(407) 494-2274	kemerait@aftac.gov
Kromer	Richard	Sandia National Laboratories	MS 0655	Albuquerque	NM	87185	USA	(505) 844-1005	(505) 844-5321	rpkrome@sandia.gov
Kulichkov	Sergey	Institute of Atmospheric Physics	3 Pyzevsky	Moscow		109017	Russia	7 (095) 233-4876	7 (095) 233-1652	postmaster@iaph.msk.su
Liszka	Ludwik	Swedish Institute of Space Physics	Sorfors 634	UMEA		S-90588	Sweden	46-90-30297	46-90-30468	ludwik@irf.se
McCormack	David	Geological Survey of Canada	1 Observatory Crescent	Ottowa	ONT	KIA 0Y3	Canada	1 (613) 992-8766	1 (613) 992-8836	cormack@seismo.nrcan.gc.ca
McKisic	J. Michael	TRACOR Applied Sciences	1601 Research Boulevard	Rockville	MD	20850-3191	USA	(301) 838-6128	(301) 279-4655	mckisic@galileo.tracor.com
Morrow	Richard	U.S. Arms Control and Disarmament Agency	320 21St.	Washington	DC	20451	USA	(207) 736-7634		morrow@ivi.acda.gov
Munro	Philip	Geological Survey of Canada	1 Observatory Crescent	Ottowa	ONT	KIA 0Y3	Canada	1 (613) 995-4669	1 (613) 992-8836	munro@seismo.nrcan.gc.ca
Murphy	Timothy	ACIS	7105 Norwalk St.	Falls Church	VA	22043	USA	(703) 874-4006		
Mutschlecner	J. Paul	Los Alamos National Laboratory	121 Sierra Vista	Los Alamos	NM	87544	USA	(505) 672-3295		

Infrasound Workshop Participants

Last Name	First Name	Organization	Mailing Address	State	ST	Zip	Country	Telephone	Fax	E-Mail
Ostashev	Vladimir	New Mexico State University	Department of Physics, Box 30001 / Dept. 3D	Las Cruces	NM	88003-8001	USA	(505) 646-3707	(505) 646-1934	vostashe@nmsu.edu
Pilotte	Frank	AFTAC/TT	1030 South Highway A1A	Patrick AFB	FL	32925-3002	USA	(407) 494-2356	(407) 494-2274	ffp@rayleigh.aftac.gov
Raspopov	Oleg	Russian Academy of Sciences	Institute of Terrestrial Magnetism, Ionsphere and Radio Waves Propagation, Box 188	St. Petersburg		191023	Russia	(812) 310-5232	(812) 311-7758	oleg@omr.izmi.ras.spb.ru
Ray	Terrill	U.S Arms Control and Disarmament Agency	320 21st. Street NW	Washington	DC	20451	USA	(202) 736-4273	(202) 647-7663	rayte@acda.gov
Revelle	Douglas	Los Alamos National Laboratory	P.O. Box 1663, MS F659	Los Alamos	NM	87545	USA	(505) 667-1256	(505) 665-3681	dor@vega.lanl.gov
Roca	Jose	Autoridad Regulatoria Nuclear (ARN)	Av. del Libertador 8250	Buenos Aires 1429			Argentina	541 379-8567	541 379-8460	jroca@cac.cnren.gov.ar
Sandoval	Tom	Bechtel/Nevada	P.O Box 809	Los Alamos	NM	87544	USA	(505) 471-4354		
Simons	David	Los Alamos National Laboratory	PO Box 1663, MS D460	Los Alamos	NM	87545	USA	(505) 667-5930	(505) 665-0854	dsimons@lanl.gov
Sytolenko	Alexander	Cabinet of Ministers of Ukraine	Chief, National Space Agency of Ukraine, M. Hrushevsky St., 12/2	Kyjiv-002			Ukraine	(380) 44-293-0574	(380) 44-226-3605	

Infrasound Workshop Participants

Last Name	First Name	Organization	Mailing Address	State	ST	Zip	Country	Telephone	Fax	E-Mail
Timofeev	Vladimir	Cabinet of Ministers of Ukraine	Deputy Chief, Dept. on Issues of Technology, Ecology, Safety and Civil Protection M. Hrushevsky St.,12/2	Kyjiv-002			Ukraine	(380) 44-293-0574	(380) 44-226-3605	timofeev@ecprotec.freenet.kiev.ua
Trost	Lawrence	Sandia National Laboratories	Org. 5415, MS-0425, Sandia National Laboratories	Albuquerque	NM	87185	USA	(505) 844-8360	(505) 844-9293	lctrost@Sandia.gov
Valdez	Marsha	Los Alamos Technical Associates, Inc.	1200 Trinity Dr.	Los Alamos	NM	87544	USA	(505) 662-1807	(505) 662-1757	mvaldez@lata.com
Veloso	Alberto	Preparatory Commission for CTBTO	P.O Box 1250	Vienna A-1400			Austria	43-1-21345-6205	43-1-21345-5877	jveloso@unvienna.un.oz.at
Wheeler	Joseph	Boeing Company	PO Box 21233	Kennedy Space Center	FL	32813	USA	(407) 383-2831	(407) 269-6202	jwhee53394@aol.com
Whitaker	Rodney	Los Alamos National Laboratory	EES-8 MS F659	Los Alamos	NM	87545	USA	(505) 667-7672	(505) 665-3687	rww@lanl.gov
Willemann	Raymond	Center for Monitoring Research	1300 North 17th Street, Suite 1450	Arlington	VA	22209	USA	(703) 247-1830	(703) 243-8950	willmann@cmr.gov
Wilson	Charles	University of Alaska	Geophysical Institute, 1812 Musk Ox Trail	Fairbanks	AK	99709	USA	(907) 479-2419	(907) 474-7290	76654.2724@compuserve.com
Xie	Zhao Hua	Chinese Academy of Sciences	Computer Network Information Center, P.O Box 2719	Beijing 100080			China	(86+10) 6-253-3575	(86+10) 6-253-3527	xie@isa.ioa.ac.cn
Xie	Jin Lai	Chinese Academy of Sciences	Institute of Acoustics, P.O Box 2712	Beijing 100080			China	(86+10) 6-255-4482	(86+10) 6-255-3898	xie@isa.ioa.ac.cn

INFRASOUND WORKSHOP FOR CTBT MONITORING

25-28 August 1997

Santa Fe, New Mexico

Key Technical Issues and Recommendations for Further Work

Douglas Christie and Rod Whitaker

This brief document summarizes input provided by a broad spectrum of participants during the last session of the workshop.

Introduction

It is expected that the establishment of new infrasound stations in the global IMS network by the Provisional Technical Secretariat of the CTBTO in Vienna will commence in the middle of 1998. Thus, decisions on the final operational design for IMS infrasound stations will have to be made within the next 12 months. Though many of the basic design problems have been resolved, it is clear that further work needs to be carried out during the coming year to ensure that IMS infrasound stations will operate with maximum capability in accord with the specifications determined during the May 1997 PrepCom Meeting. Some of the papers presented at the Workshop suggest that it may be difficult to design a four-element infrasound array station that will reliably detect and locate infrasound signals at all frequencies in the specified range from 0.02 to 4.0 Hz in all noise environments. Hence, if the basic design of an infrasound array is restricted to four array elements, the final optimized design may be suited only to the detection and location of signals in a more limited pass-band. Several participants have also noted that the reliable discrimination of infrasound signals could be quite difficult if the detection system leads to signal distortion. Thus, it has been emphasized that the detection system should not, if possible, compromise signal fidelity.

Key Technical Issues

The material presented at the workshop has led to the identification of a number of specific technical areas that require further work.

(a) Design of a noise-reducing pipe array which will preserve signal fidelity and provide large improvement in signal-to-noise ratio at all frequencies between 0.02 to 4.0 Hz.

(b) Design of robust noise-reducing pipe arrays that will operate in a wide variety of hostile environments.

(c) Development of theoretical techniques which can be used to predict the response of pipe array and integrated pipe array/microbarometer systems to both wind-generated micropressure fluctuations and infrasonic signals.

(d) Development of infrasonic noise models for all environments.

(e) Determination of the frequency content, signal correlation properties, and morphology of infrasound signals from explosions with yields in the range from about 0.5 to 4.0 kT at distances of up to 4000 km for all upper atmospheric wind conditions.

(f) Optimal design of an infrasonic array that will provide good detection and location capability at all frequencies between 0.02 and 4.0 Hz.

(g) Development of other noise-reducing techniques, such as the use of properly designed barriers to suppress wind-generated micropressure fluctuations. One type was presented by Ludwik Liszka of Sweden.

(h) Development of optimal automatic signal detection techniques for infrasound signals, including techniques that can be used in the presence of continuous infrasonic background noise such as microbaroms.

(i) Development of techniques for accurate identification of all infrasonic signals from both man-made and naturally occurring sources.

(j) Consideration of in-the-field calibration that ideally would include some type of remotely controlled acoustic excitation.

Recommendations

1. Experimental and theoretical work should be carried out during the next year to determine standard robust designs for noise-reducing pipe arrays that can be used at infrasound stations located in wet, arid, or arctic environments. These pipe arrays should preserve signal fidelity and should provide a significant improvement in signal-to-noise ratio at all frequencies between 0.02 and 4.0 Hz. Results of the theoretical work should provide the response of both pipe arrays and integrated pipe array/ microbarometer systems to wind-generated noise and signals in the frequency band from 0.02 to 4.0 Hz.

2. Field and laboratory studies should be carried out on the design of wind-noise reducing structures that can reduce the influence of air turbulence at IMS infrasound stations located in high-wind areas.

3. Detailed studies, including correlation studies, should be carried out on the properties of the infrasonic background noise field in a wide variety of different environments.

These studies should make use of both existing data sets and new experimental observations.

4. To preserve signal fidelity and to improve discrimination capability, infrasound data should be sampled at 20 samples per second. Clarification of two CTBTO instrument specifications is also recommended: (a) the dynamic range should be interpreted as the system dynamic range and (b) the sensor response should be flat, to within 3 dB, and known over the pass-band of 0.02 Hz to 4.0 Hz.

5. Observational studies should be carried out of infrasound from large explosions at distances in the range of 100 to 4000 km. These studies should focus on detailed observations of the morphology, correlation properties, and frequency content of infrasound signals under all upper atmospheric wind conditions. Use of recently digitized data from observations of actual nuclear explosions, or other large explosions, could be beneficial to this effort. All signatory states should be encouraged to provide, as soon as possible, (e.g., updating at each PrepCom) advance notice to the Provisional Technical Secretariat of any large mining explosions or other large chemical explosions. This is a precursor to the Confidence Building Measures section of the treaty, and these explosions would be most useful as calibration events for the infrasound network during the PrepCom period.

6. An informal workshop on the use of infrasound for CTBT verification should be held in August or September 1998. This workshop should focus primarily on solutions to the problems described above that need to be resolved prior to the installation of IMS infrasound stations.

7. The design of a simple and cost-effective remotely controlled field calibration technique is needed that would include some acoustic source. Isolation of the sensor from the hoses and manifold would be desirable as well as good repeatability of the source. Innovative ideas are necessary in order to find a low-cost solution, if possible.

8. It is strongly recommended that any new ideas on site survey issues be forwarded to Douglas Christie in Vienna.

ESTABLISHMENT OF THE IMS INFRASOUND NETWORK

Dr. D. R. Christie

IMS - Infrasound
Provisional Technical Secretariat
Comprehensive Nuclear Test-Ban Treaty Organization
Vienna International Centre

ESTABLISHMENT OF THE IMS INFRASOUND NETWORK

- **CTBT**
- **PTS**
- **Summary: Working Group B Meeting**
- **1997/1998 PTS Work Program**
- **PTS Issues**
- **Technical Issues**

INFRASOUND

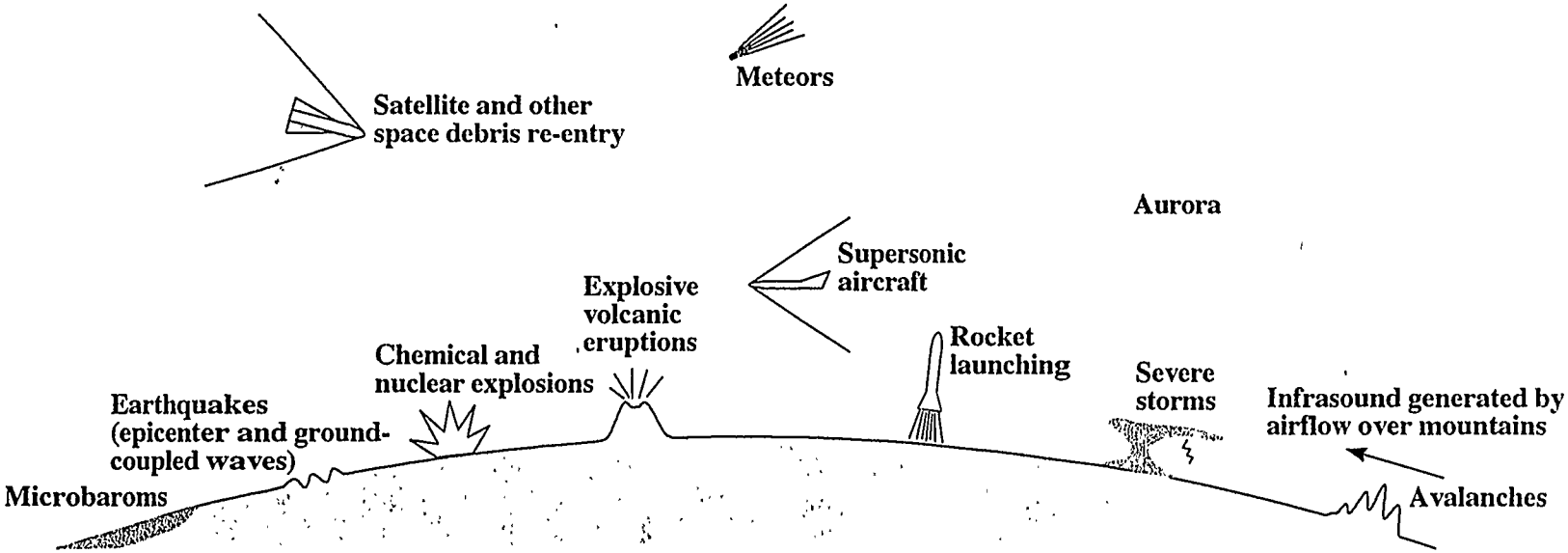
Meteors
Satellite and other
space debris re-entry
Aurora
Supersonic
aircraft
Explosive
volcanic
eruptions
Rocket
launching
Chemical and
nuclear explosions
Severe
storms
Infrasound generated by
airflow over mountains
Earthquakes
(epicenter and ground-
coupled waves)
Microbaroms
Avalanches

COMPREHENSIVE NUCLEAR TEST-BAN TREATY (CTBT)

- **Opened for signature on 10 September, 1996**

- **144 States have signed the Treaty**

- **6 States have ratified the Treaty**
  - **Fiji**
  - **Qatar**
  - **Uzbekistan**
  - **Micronesia**
  - **Japan**
  - **Mongolia**

- **44 designated States must ratify the Treaty before Entry Into Force**

- **Entry Into Force?**

The Provisional Technical Secretariat

MAJOR PROGRAMS

- **International Monitoring System (IMS)**
- **International Data Centre (IDC)**
- **Communications**
- **On-Site Inspection**
- **Evaluation** (evaluation of all procedures and products of the verification system)
- **Policy** (support for Preparatory Commission and Working Groups)
- **Administration, Coordination and Support**

IMS SECTION OF THE PTS

STAFF PROFILE

	1997	1998
• Management/ Training	1 D 3 P 2 G	1 D 4 P 2 G
• Seismic	4 P 3 G	6 P 4 G
• Infrasound	2 P 2 G	3 P 3 G
• Hydroacoustics	2 P 2 G	3 P 2 G
• Radionuclides	3 P 3 G	3 P 4 G
Total	27	35

INTERNATIONAL MONITORING SYSTEM

- **321 stations in 88 countries:**

Country	Total No. IMS Stations	Infrasound Stations
United States	38	8
Russian Federation	31	4
Australia	20	5
Canada	15	1
France	14	5
United Kingdom	11	4
China	11	2

Draft IMS Budget for 1998

Management, Co-ordination and Training	$1.8	million
Seismology	$ 16.2	million
Infrasound	$ 2.5	million
Hydroacoustics	$ 4.8	million
Radionuclides	$ 4.2	million
Total:	$29.5	million

Total Draft 1998 Budget for all Major Programs: approx. $68.8 million

1997 Infrasound Site Surveys

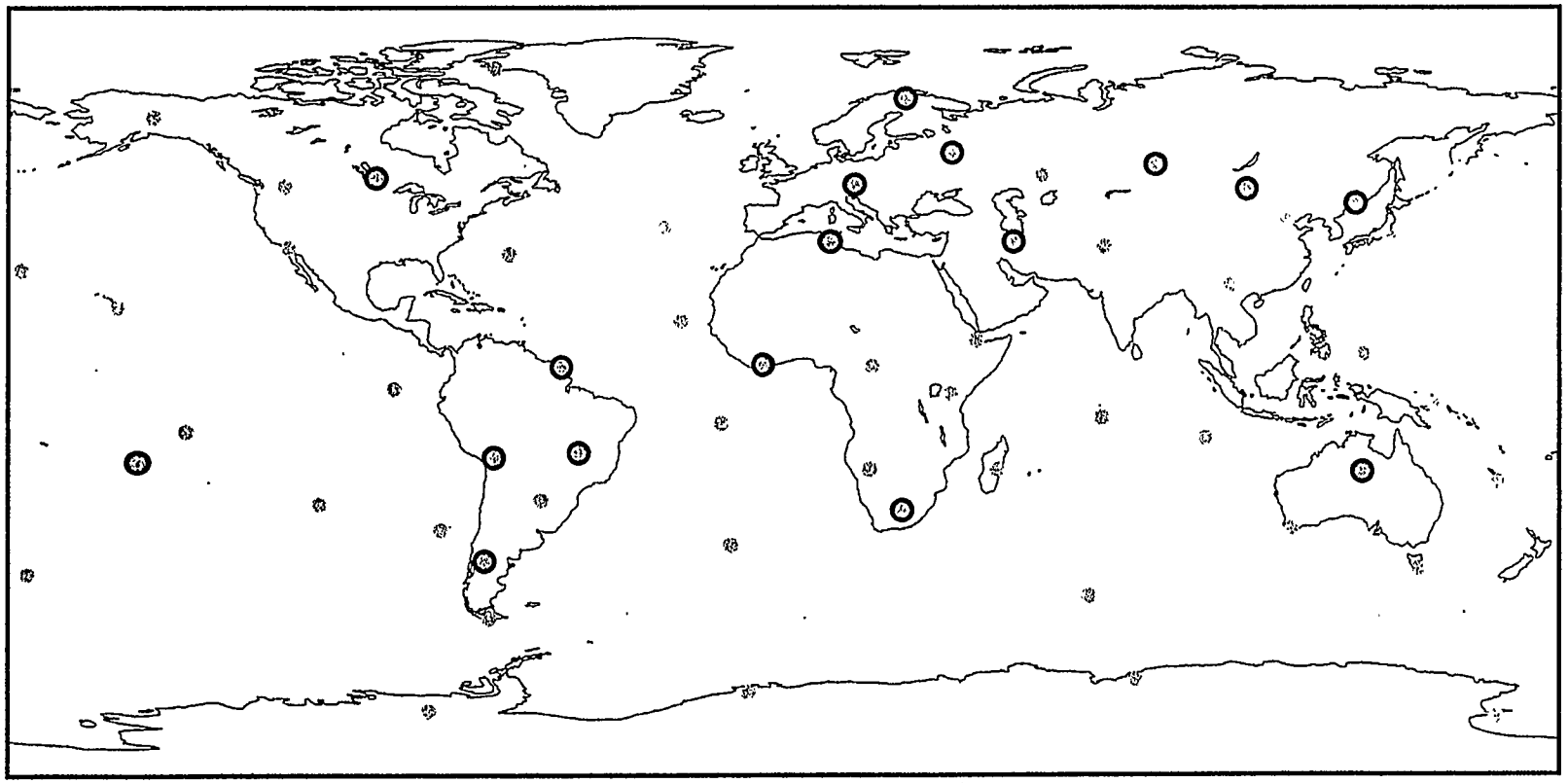

1998 Infrasound Work Program

Site Surveys

10 Site Surveys to be carried out. Surveys to be determined from a list of 23 specified stations.

Capital Investment

7 stations to be installed at sites surveyed in 1997.

Certification

5 stations to be fully certified and operational by the end of 1998.

ISSUES

A. PTS Procedural Issues

B. Technical Issues

- Supply of Equipment
- Site Survey Requirements:
  - Sloping ground?
  - Other topographical limitations.
- Spacing Between Array Elements (Array Configuration)
- Wind-Noise Reducing Pipe Array Design
  - Problems due to snow, freezing rain, precipitation, dust, sand etc.
  - Protection from animals, insects etc.
  - Configuration and size: need signal-to-noise enhancement at all frequencies between 0.02 and 4 Hz

INFRASONIC ARRAY DESIGN PARAMETERS

Design requirements:
a) Good detection capability at all frequencies
b) Good directional capability at all frequencies

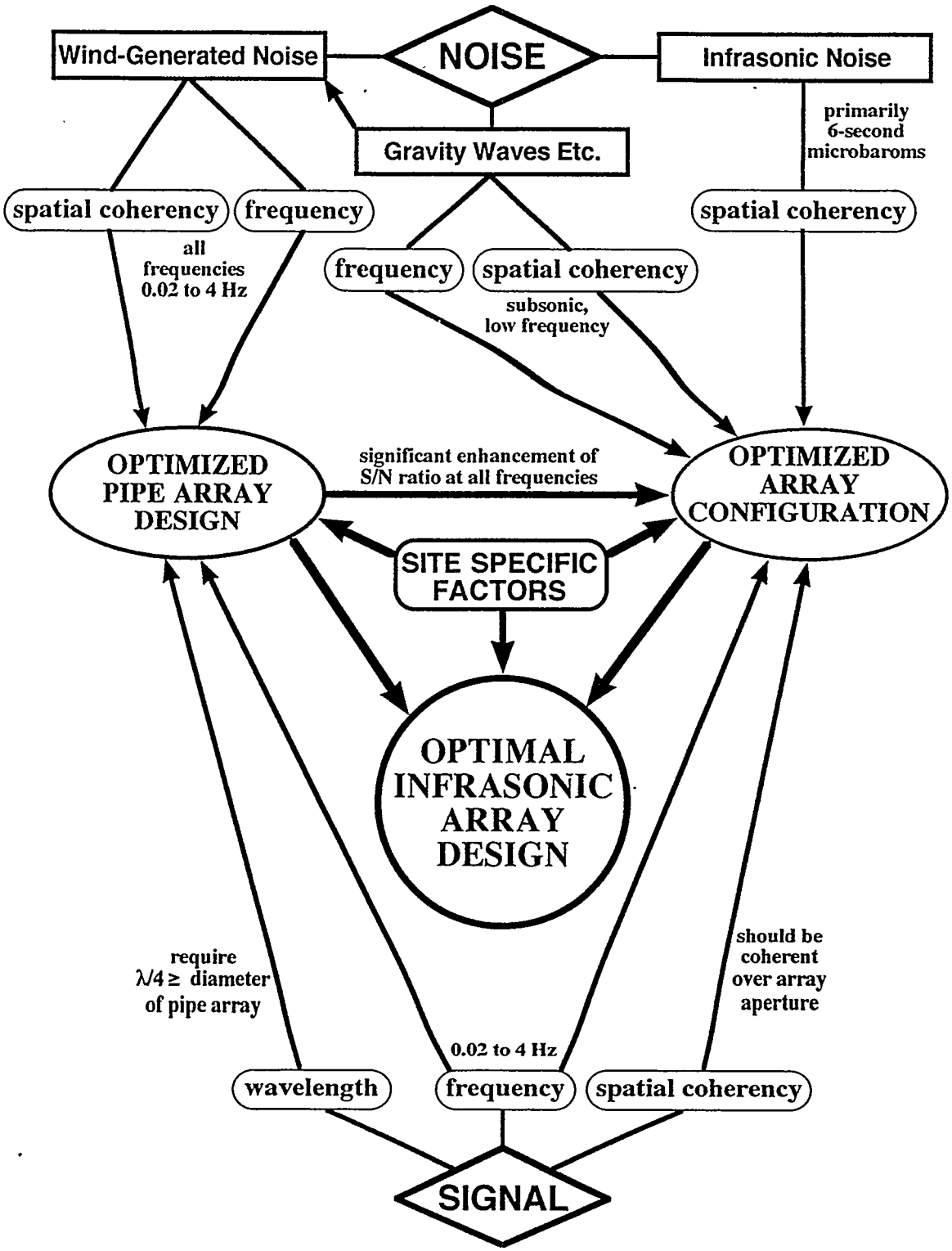

WIND-NOISE REDUCING PIPE ARRAYS

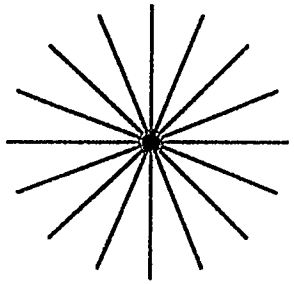

≤ 1.5 Hz

50 m

(a) Porous hose (15 mm I. D.) (Warramunga, Australia)
- good noise reduction at high frequencies

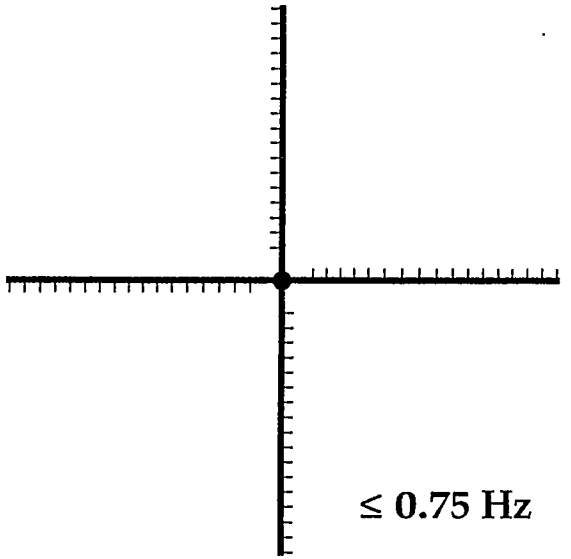

≤ 0.75 Hz

100 m

(b) Graduated steel pipe . Each arm has 33 capillary ports spaced at 1.52 m intervals. (Warramunga)

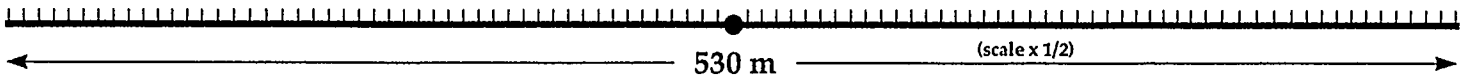

530 m (scale x 1/2)

(c) Single graduated steel pipe . Each arm has 174 capillary ports spaced at 1.52 m intervals. (United States Air Force 1952)
- good background noise reduction at long periods

≤ 0.14Hz

CARPET PIPE ARRAY

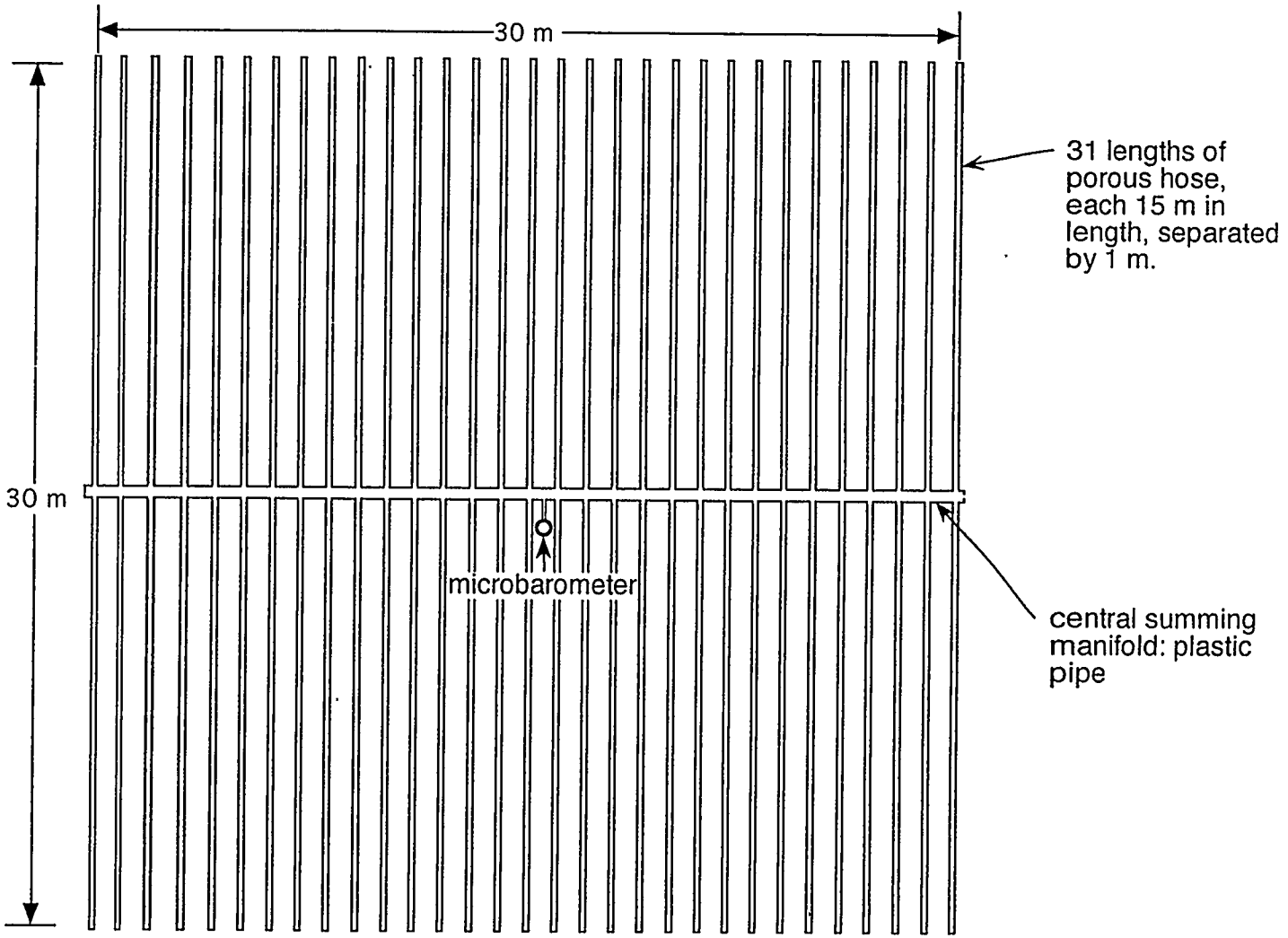

Protected Porous Hose

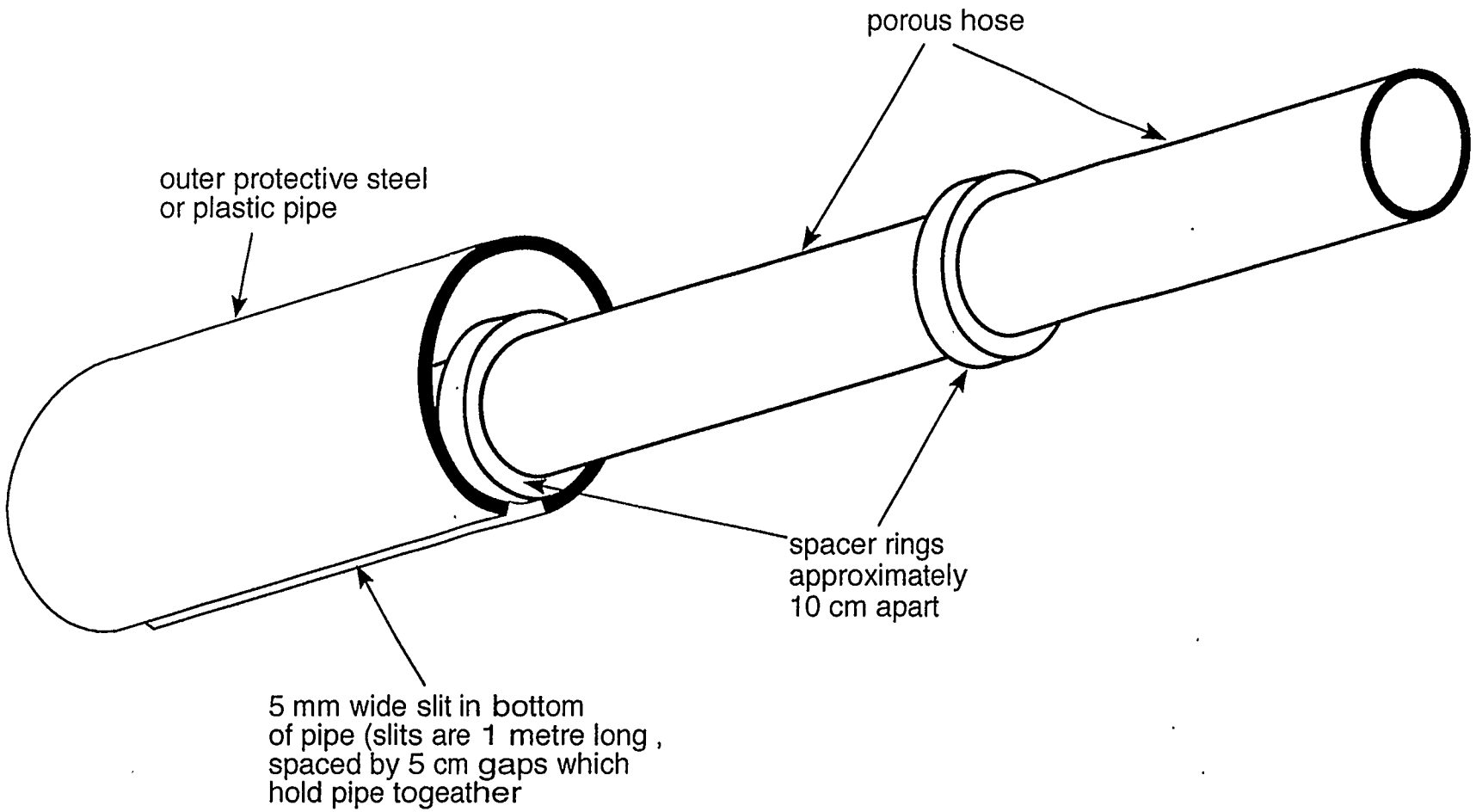

Pipe Arrays for IMS Infrasound Stations

- **PrepCom Approved Specification:**
  Detection capability at all frequencies between 0.02 and 4 Hz.

- **Design Requirement:**
  Wind-noise suppression at all frequencies between 0.02 and 4 Hz.

- **Design Problem:**

  (a) **Detection of 4 Hz signals:**
  - **Must use small diameter (~20 m) pipe array.**
  - **Good performance at 4 Hz, but poor performance at longer periods.**

  (b) **Noise reduction at longer periods:**
  - **Must use larger diameter (~100 m) pipe array.**
  - **Not suitable for detection of high frequency signals.**

Pipe Array Design: Possible Solutions

4-Element Array

1. **Determine design with enhanced signal-to-noise ratio at all frequencies (0.02 and 4 Hz).**

   - **Unresolved problem**

2. **Optimise pipe-array design for maximum signal-to-noise ratio at dominant frequency (0.2 Hz).**

   - **Poor detection capability at high frequencies.**

   - **Poor discrimination capability.**

3. **Install independent high frequency and low frequency pipe arrays with 2 microbarometers at each array element.**

   - **Inefficient use of resources.**

   - **Coherency and spatial aliasing problems unresolved.**

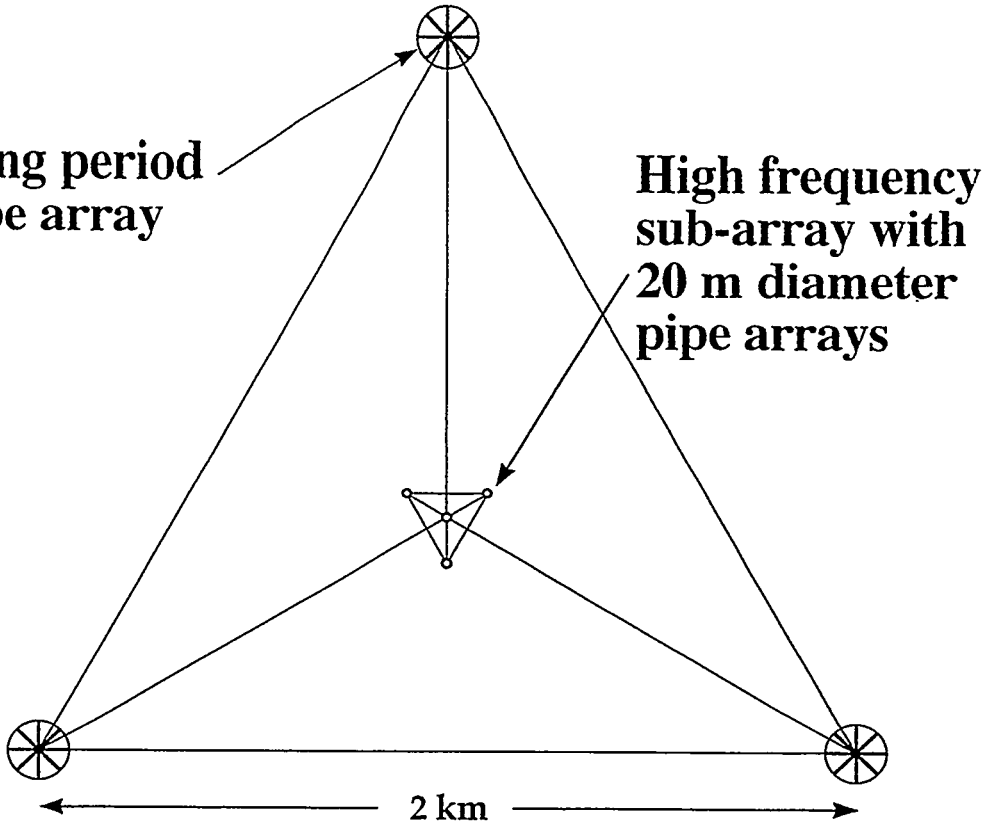

7-ELEMENT ARRAY

All technical problems resolved.

- Good noise suppression at all frequencies.
- Good detection capability at all frequencies.
- Resolves spatial aliasing and signal coherence problems.
- Detrimental influence of microbaroms is reduced.
- Good discrimination capability.

Cost	
4-element array:	$180000
4-element array with small-aperture tripartite sub-array:	$205000

SUMMARY

Problems which need to be resolved:

1. **Optimal array size.**

2. **Optimal configuration and practical number of array elements.**

3. **Optimal design for pipe filters.**

INFRASOUND ARRAY DESIGN WITH RESPECT TO DETECTION AND SLOWNESS-ESTIMATION

Robert Blandford

Air Force Technical Applications Center
1300 N 17th Suite 1450
Arlington, VA 22209

Detection by means of an F-statistic correlator detector, and slowness estimation by means of optimized beamforming are evaluated for CD 4-element arrays of 1 to 3 km aperture for signal correlation estimates from nuclear test infrasound waveform data spanning 1 to 80 seconds signal period, 1 to 40 km sensor spacing, and source distances of 700 to 10,000 km.

The frequency-wavenumber dispersion parameters determined by Mack and Flinn (1971) are found to model the data satisfactorily, and, also using observed S/N as a function of frequency for 2 kt explosions, it is found that the 1 km aperture array gives the best detection and location capability. Capability is much better in the 4-1 second pass band than in the 10-20 second passband due to better S/N and greater bandwidth. The larger apertures are unsatisfactory for the 4-1 second period band due to the loss of signal correlation at the larger sensor spacings.

Design of Infrasonic Arrays

CTBT Informal Infrasound Workshop
Santa Fe, New Mexico

Robert R. Blandford
AFTAC, Directorate of Nuclear Treaty Monitoring

August 26, 1997

Design of Infrasonic Arrays

- Trade-off between array aperture and signal correlation.
- Large Aperture Microbarograph Array (LAMA) and AEDS signal correlation data.
- Detection theory for partially correlated signals in noise.
- Slowness estimation theory for partially correlated signals in noise.

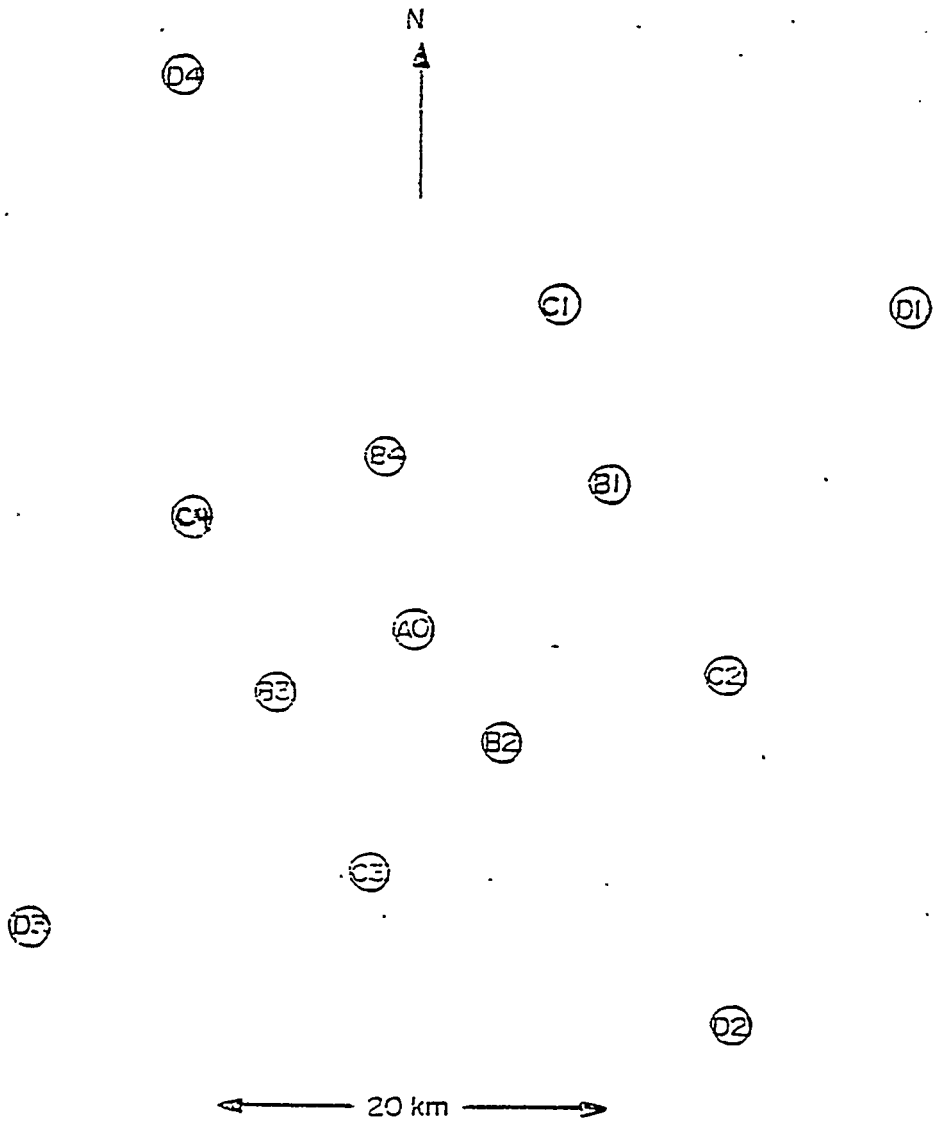

Plan of the Large Aperture Microbarograph Array (LAMA).

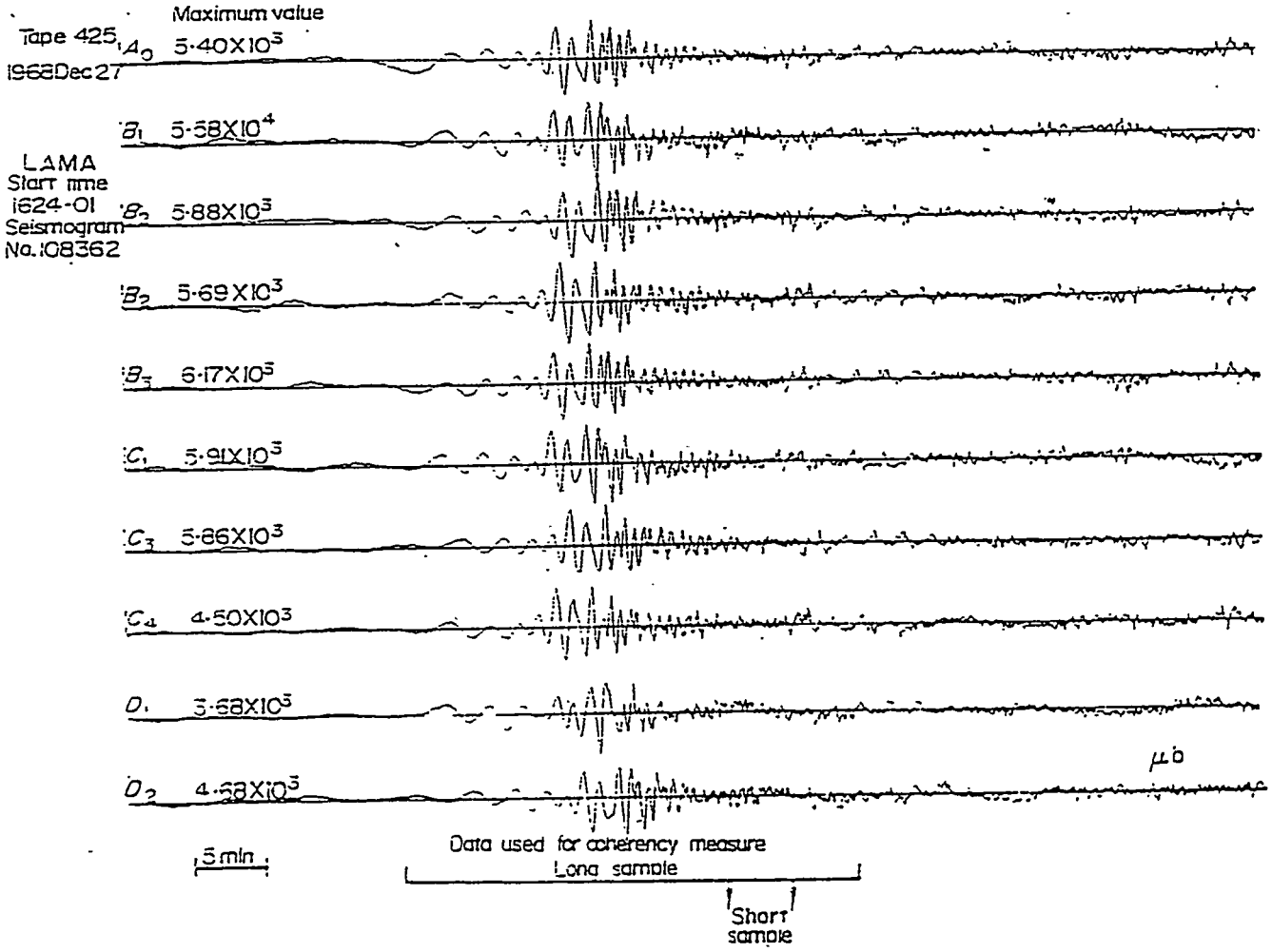

Individual LAMA channel recordings of the acoustic-gravity waves generated by a presumed nuclear explosion in China (Event 1).

Representation of Coherence
Mack and Flinn (1971)

$$\gamma^2 = \left| \frac{\sin(2\pi k_o x \sin\Delta\theta)}{2\pi k_o x \sin\Delta\theta} \right|^2 \cdot \left| \frac{\sin(2\pi\Delta k y)}{2\pi\Delta k y} \right|^2$$

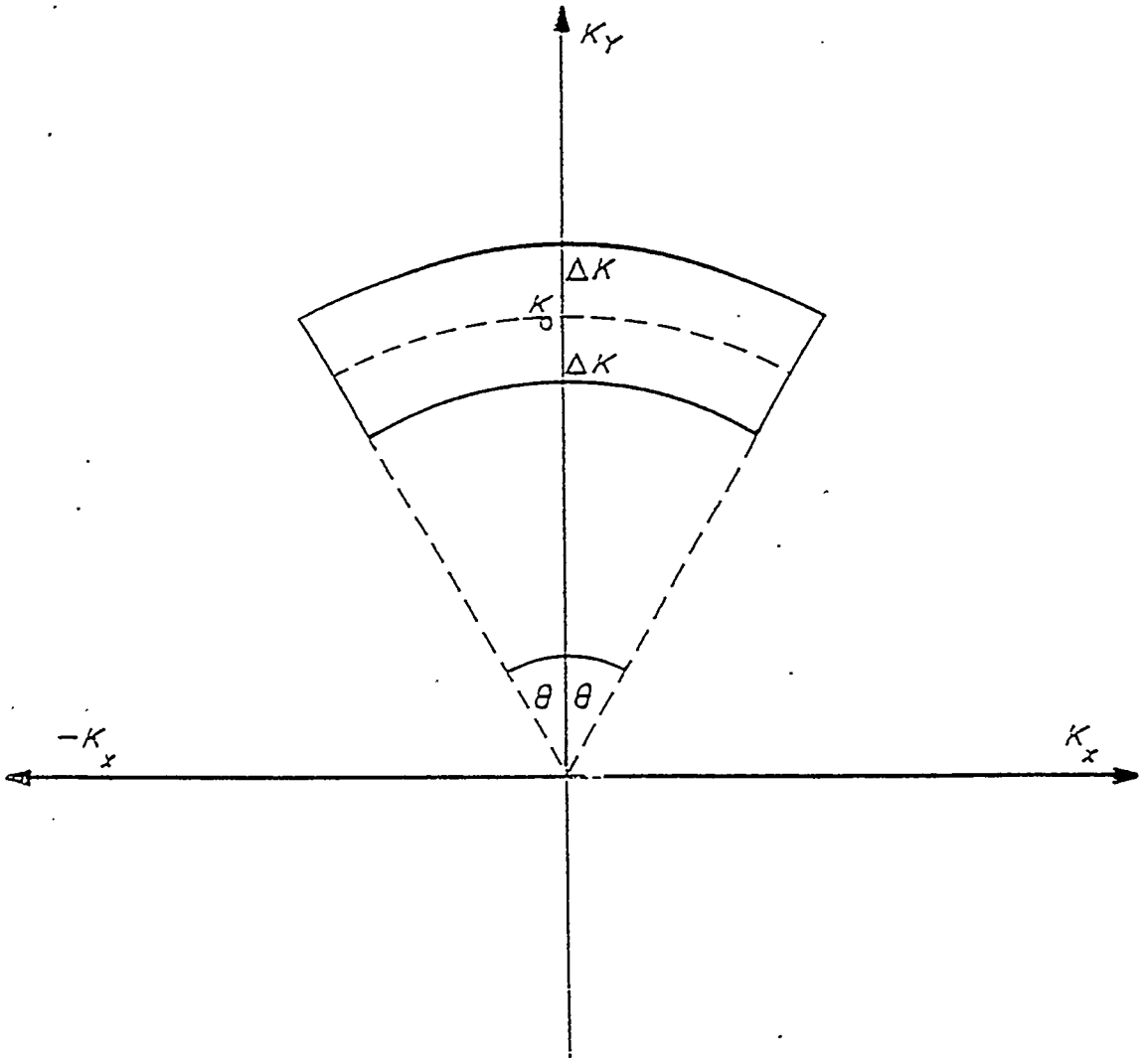

Wavenumber representation of waves at the same frequency but having a range of azimuth and velocity.

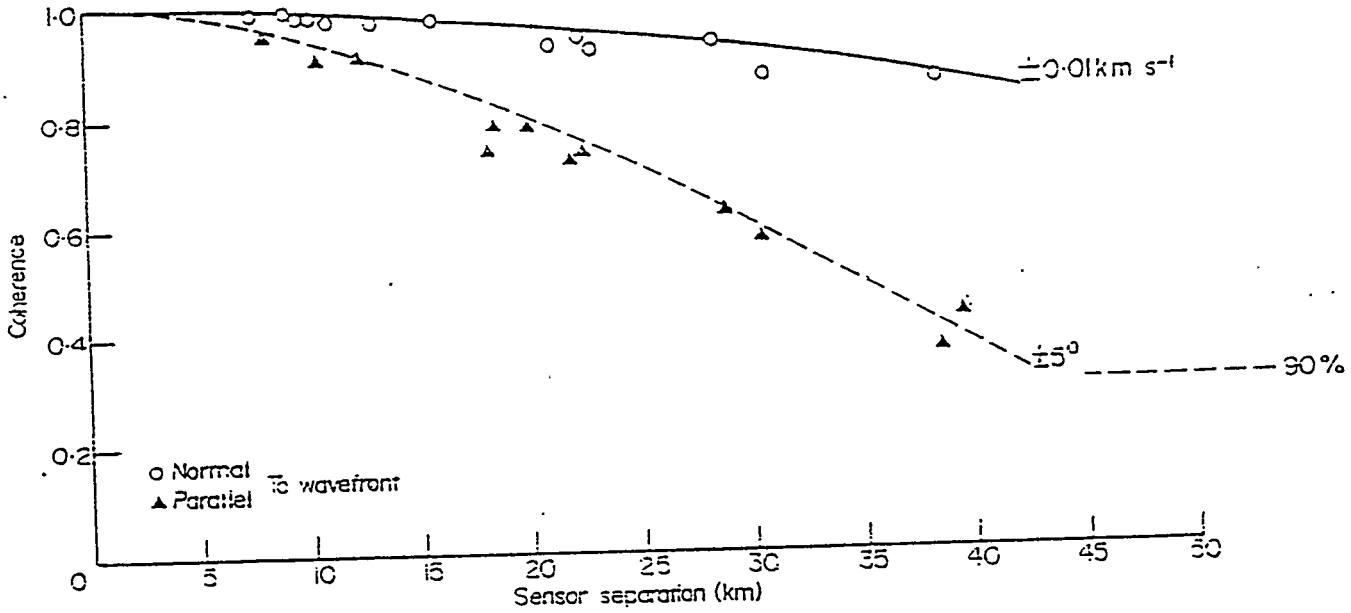

Coherence versus microbarograph separation for Event 1 at a period of 42·8 s.

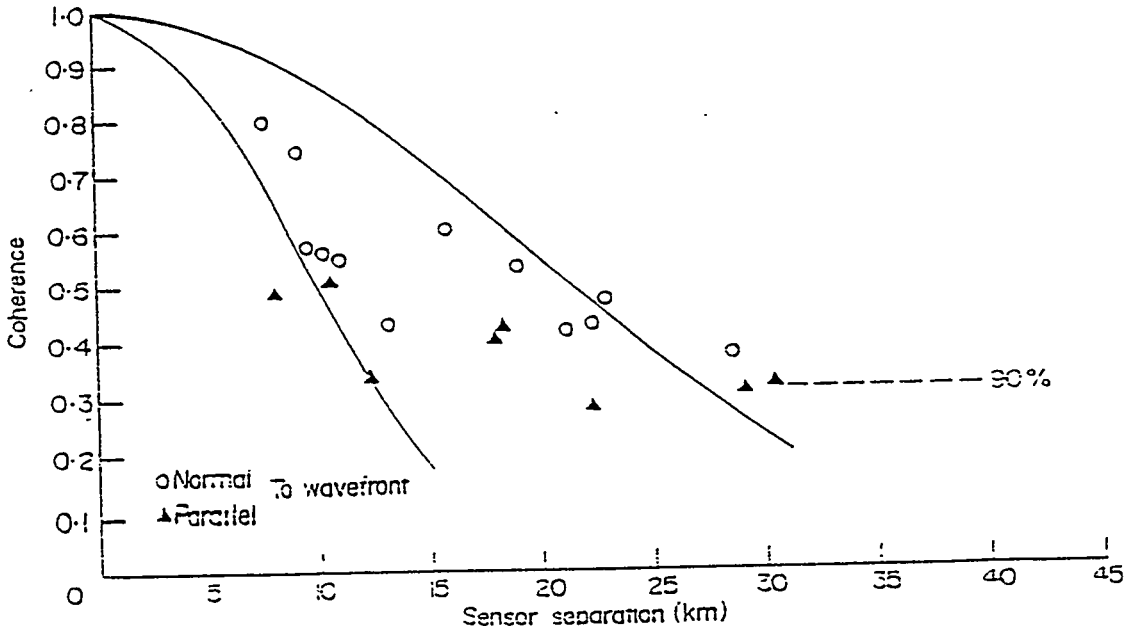

Coherence versus microbarograph separation of Event 1 at a period of 10·7 s.

Representation of Coherence
Mack and Flinn (1971)

$$\gamma^2 = \left| \frac{\sin(2\pi k_o x \sin\Delta\theta)}{2\pi k_o x \sin\Delta\theta} \right|^2 \cdot \left| \frac{\sin(2\pi\Delta k y)}{2\pi\Delta k y} \right|^2$$

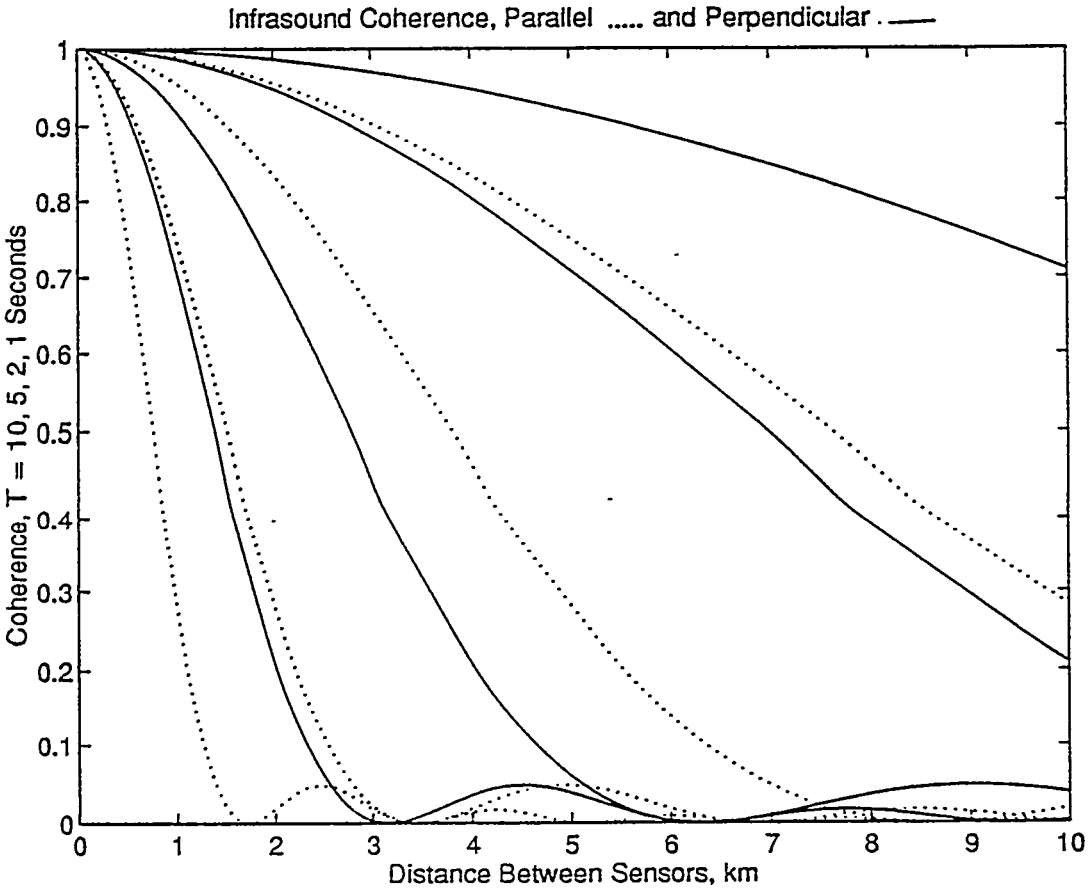

Coherence as a function of intersensor distance for T=10, 5, 2, 1 seconds according to equation (2) using Δc=0.015 km/sec and $\Delta\theta$=5 degrees as determined from Mack and Flinn (1971), parallel and perpendicular to the wavefront.

Signal Models for Azimuth Estimation in Arrays

- Fixed but unknown
- Stochastic-Identical (Perfect Correlation)
- Stochastic

$$y_j = s_j(t - T_j(\theta)) + n_j(t)$$

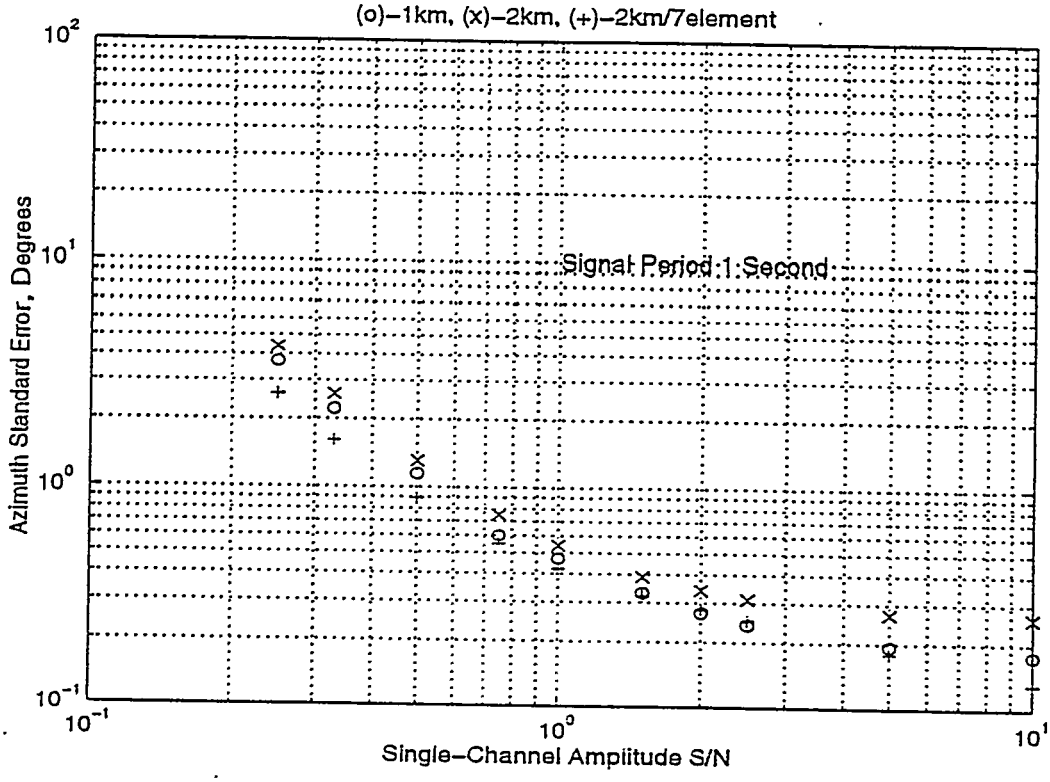

Azimuthal error as a function of signal-to-noise for a signal period of 1 seconds for the 4-element 1 and 2 km aperture arrays and for the 2 km, 7-element array. From equation (4).

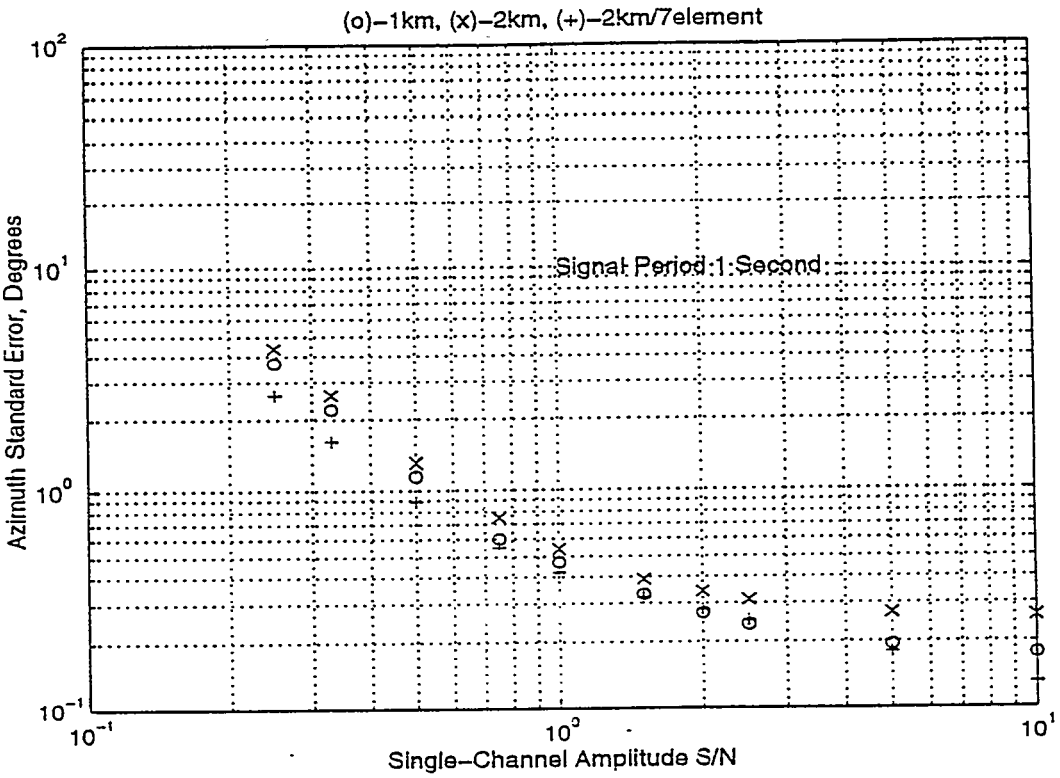

Azimuthal error as a function of signal-to-noise for a signal period of 1 seconds for the 4-element 1 and 2 km aperture arrays and for the 2 km, 7-element array. From equation (4).

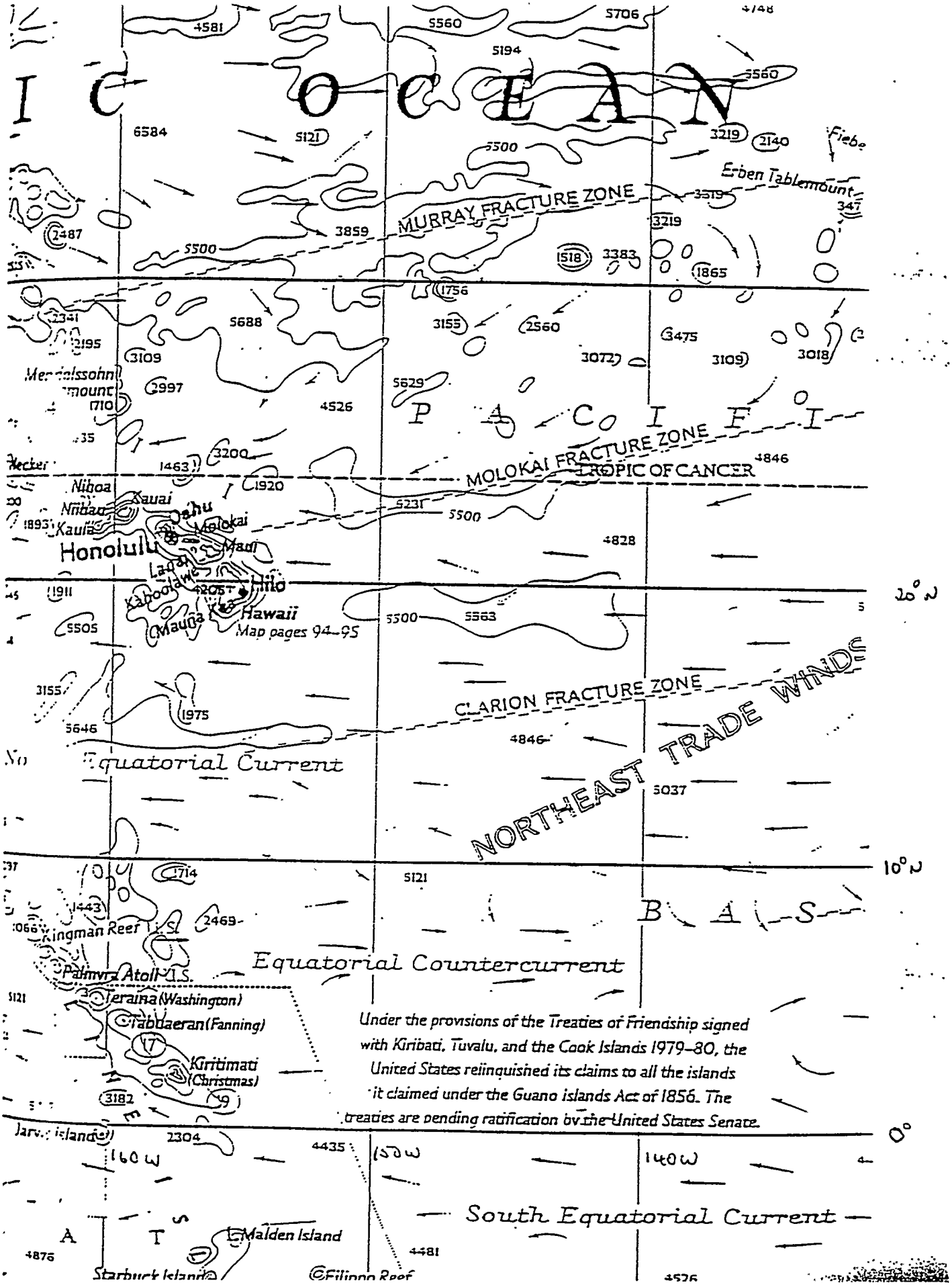
I C O C E A N
MURRAY FRACTURE ZONE
Erben Tablemount
MOLOKAI FRACTURE ZONE
TROPIC OF CANCER
P A C I F I
CLARION FRACTURE ZONE
NORTHEAST TRADE WINDS
Equatorial Current
Equatorial Countercurrent
South Equatorial Current
B A S
A T S
Honolulu
Hilo
Hawaii
Map pages 94–95
Oahu
Kauai
Maui
Molokai
Lanai
Niihau
Kingman Reef U.S.
Palmyra Atoll U.S.
Jarvis Island
Malden Island
Starbuck Island
Filippo Reef
Kiritimati (Christmas)
Tabuaeran (Fanning)
Teraina (Washington)
Under the provisions of the Treaties of Friendship signed with Kiribati, Tuvalu, and the Cook Islands 1979–80, the United States relinquished its claims to all the islands it claimed under the Guano Islands Act of 1856. The treaties are pending ratification by the United States Senate.
160 W
150 W
140 W
10° N
0°

PALMYRA

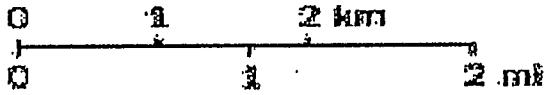

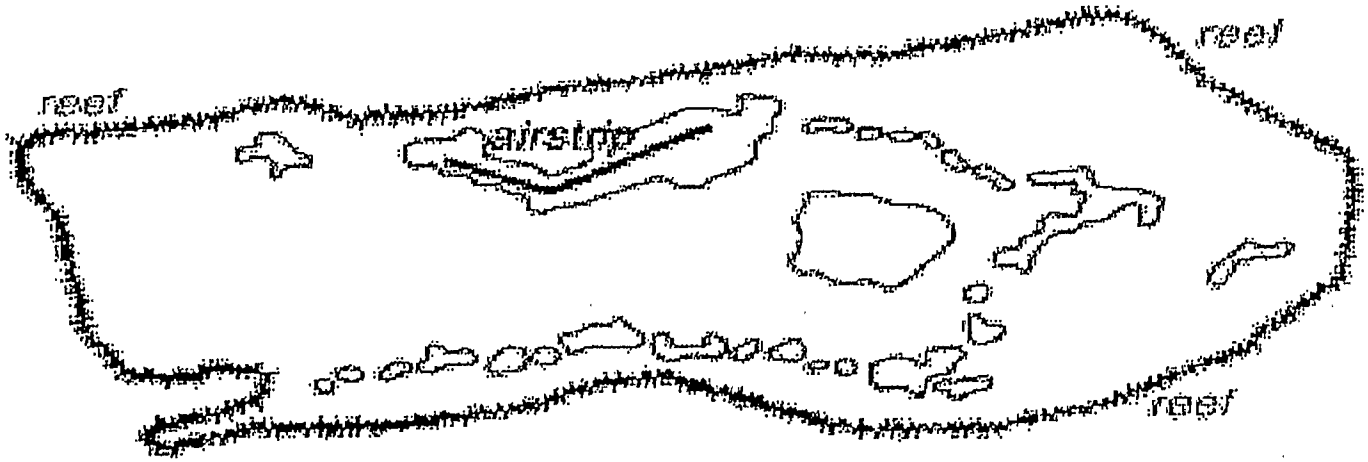

North Pacific Ocean

Petit, 2.2 kt, near Tanana, ~15:00, 19 June 1962 at Palmyra (Small Fry)

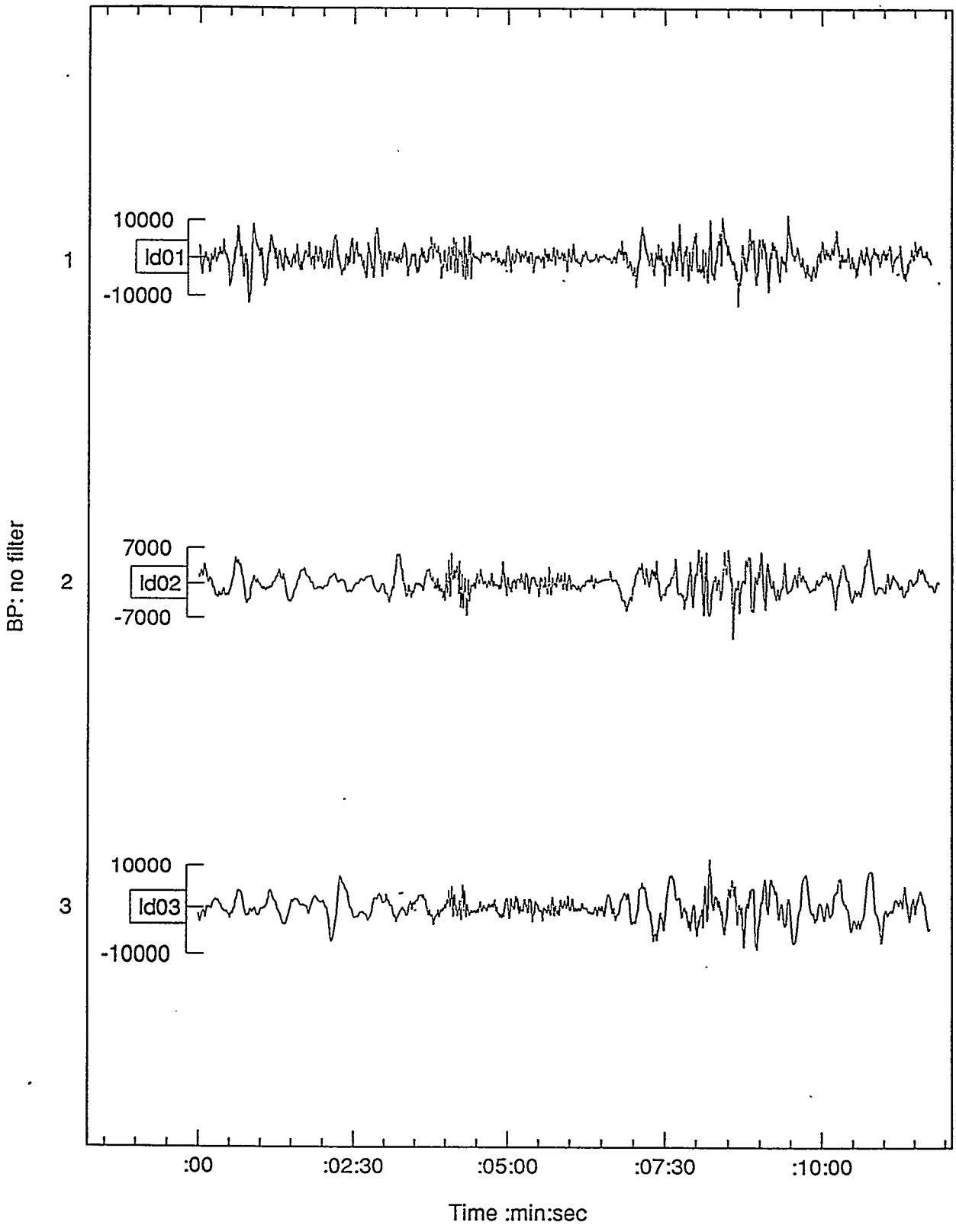

Tanana, 2.6 kt,1.65N, 157.28W, 16:08:52, 25 May 1962 at Palmyra (Small Fry)

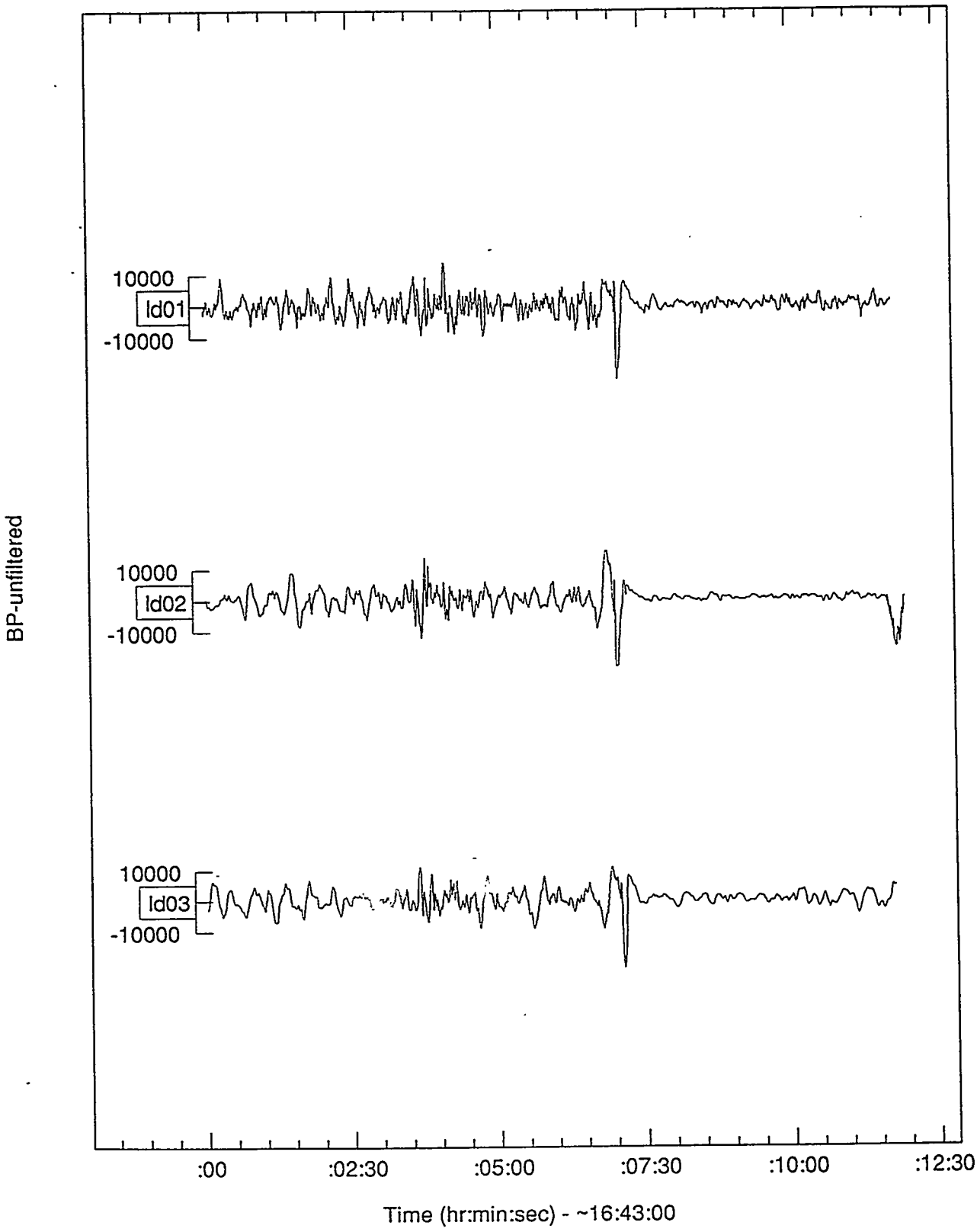

Tanana, 2.6 kt,1.65N, 157.28W, 16:08:52, 25 May 1962 at Palmyra (Small Fry)

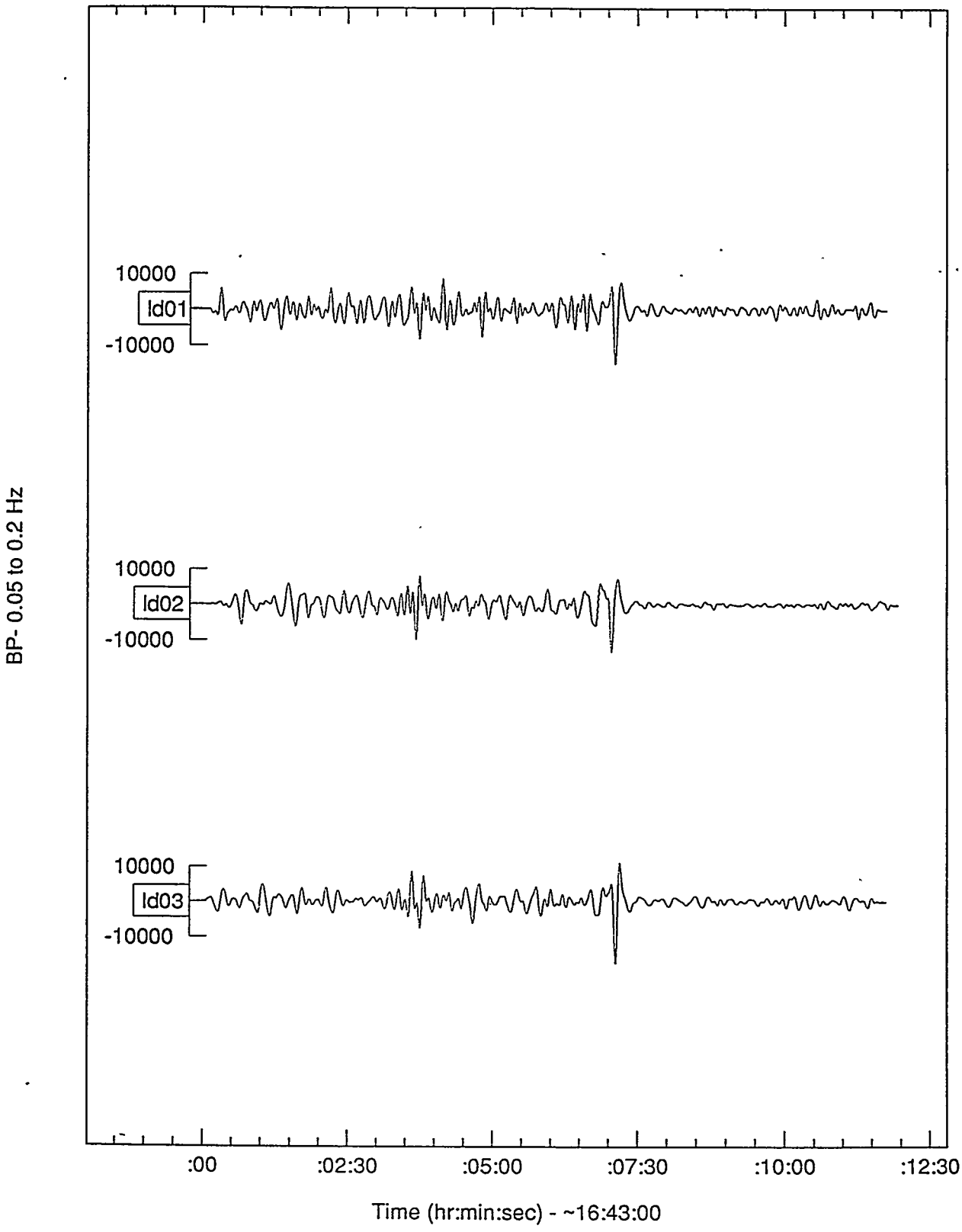

Tanana, 2.6 kt,1.65N, 157.28W, 16:08:52, 25 May 1962 at Palmyra (Small Fry)

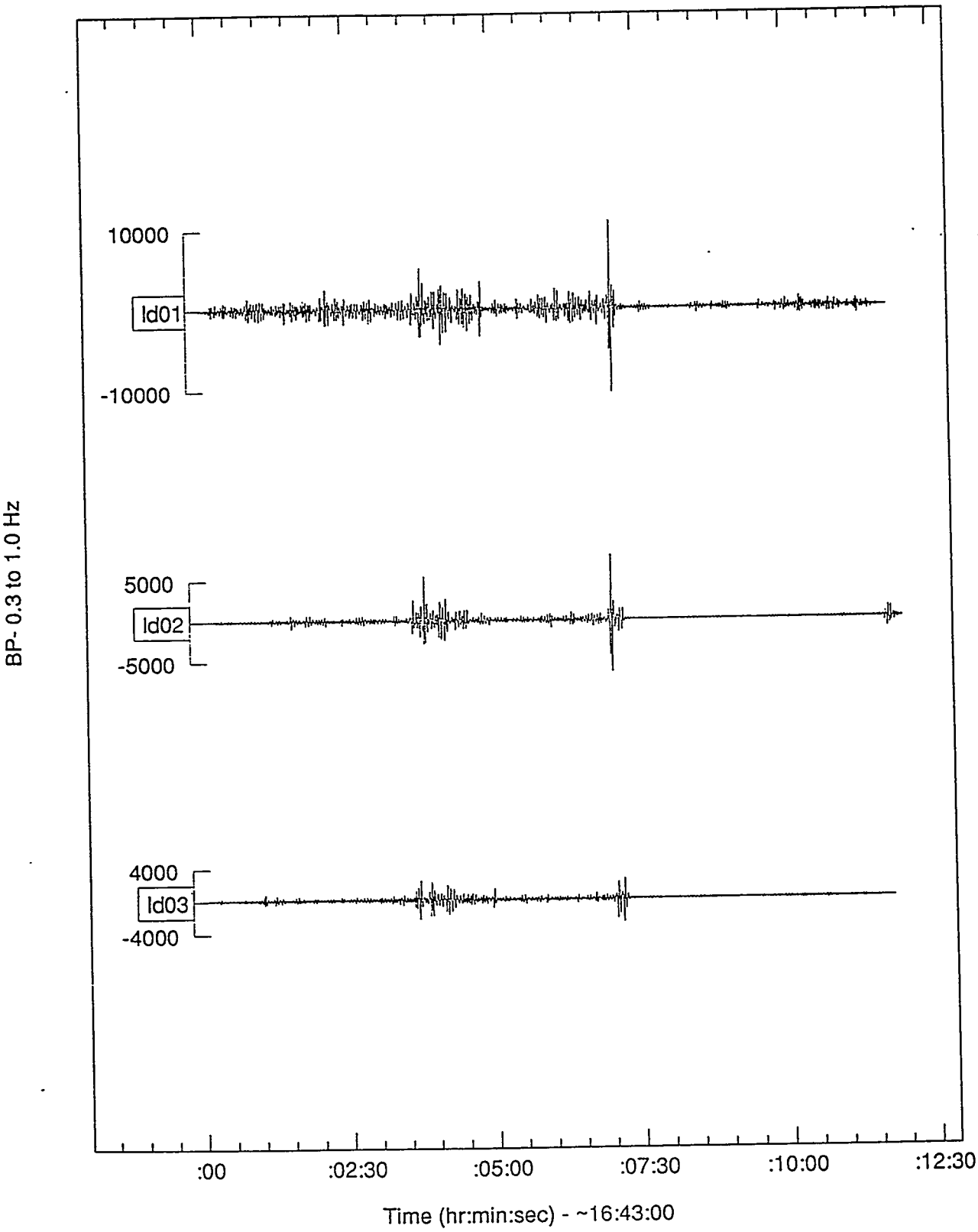

Cross-Correlation of Aligned Traces 1/2, 1/3, 2/3 Tanana at Palmyra (Small Fry)								
BP (Hz) T (sec)	Observed Signal Correlation				Corrected for Background Noise			
	Signal 1		Signal 2		Signal 1		Signal 2	
.025-0.1	-.02		.85		U		1.18	
20	.35	.29	.94	.85	4.3	U	1.36	1.30
0.05-0.2	.50		.72		1.3		1.2	
10	.34	.46	.88	.87	.54	.96	1.3	1.3
0.1-0.5	.72		.69		.90		1.04	
4	.62	.84	.59	.68	.80	.85	.81	.86
0.2-0.5	.64		.96		.81		1.4	
3	.70	.82	.63	.68	.83	.90	.98	.82
0.3-1.0	.58		.84		.67		.96	
2	.48	.69	.22	.60	.55	.72	.26	.64
0.5-2.0	.38		.71		.44		.77	
1	.28	.40	.02	.21	.35	.44	.03	.22

Tanana, 2.6 kt,1.65N, 157.28W, 16:08:52, 25 May 1962 at Palmyra (Small Fry)

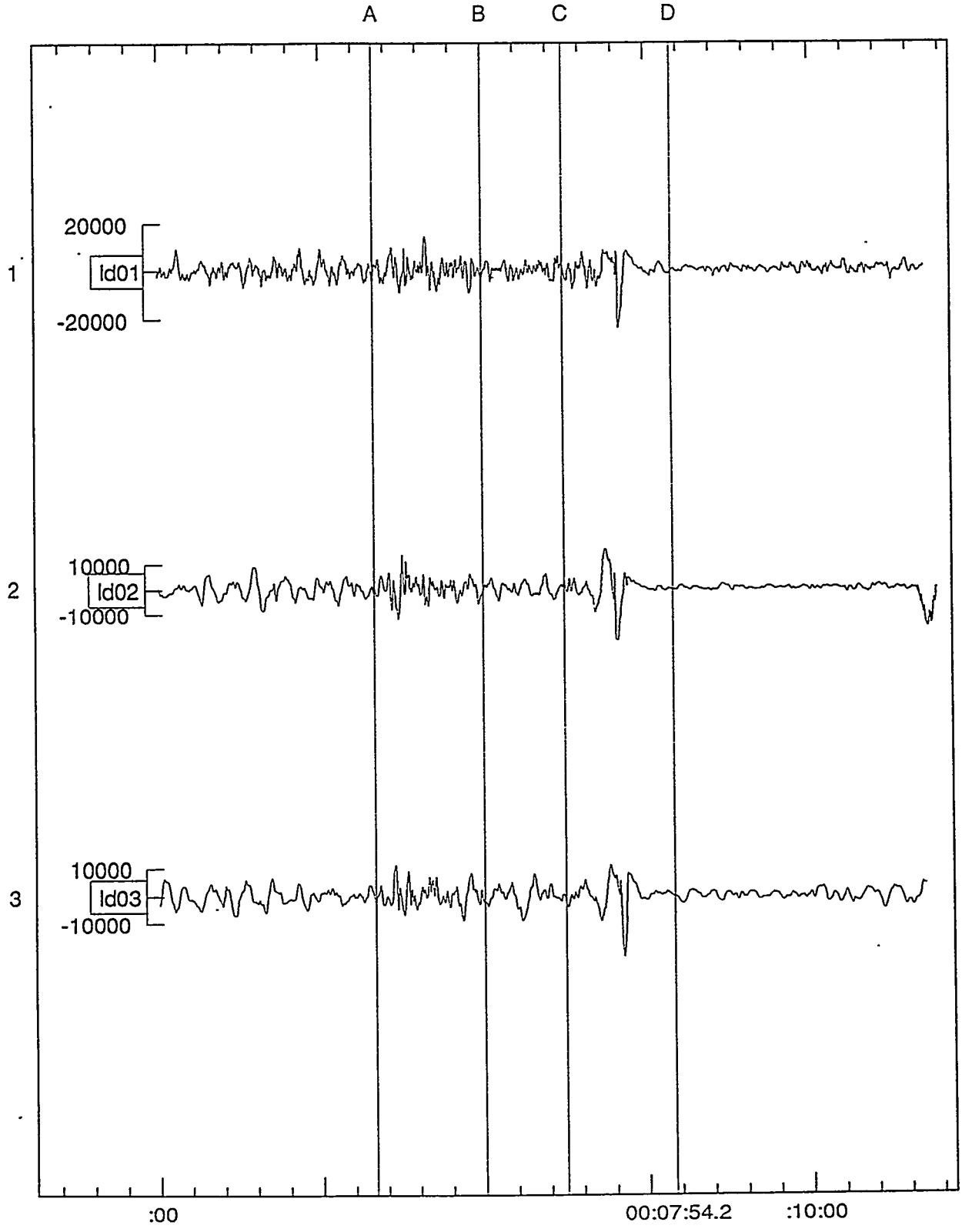

Signal Windows: 1, A-B; 2, C-D

Tanana, 2.6 kt,1.65N, 157.28W, 16:08:52, 25 May 1962 at Palmyra (Small Fry)

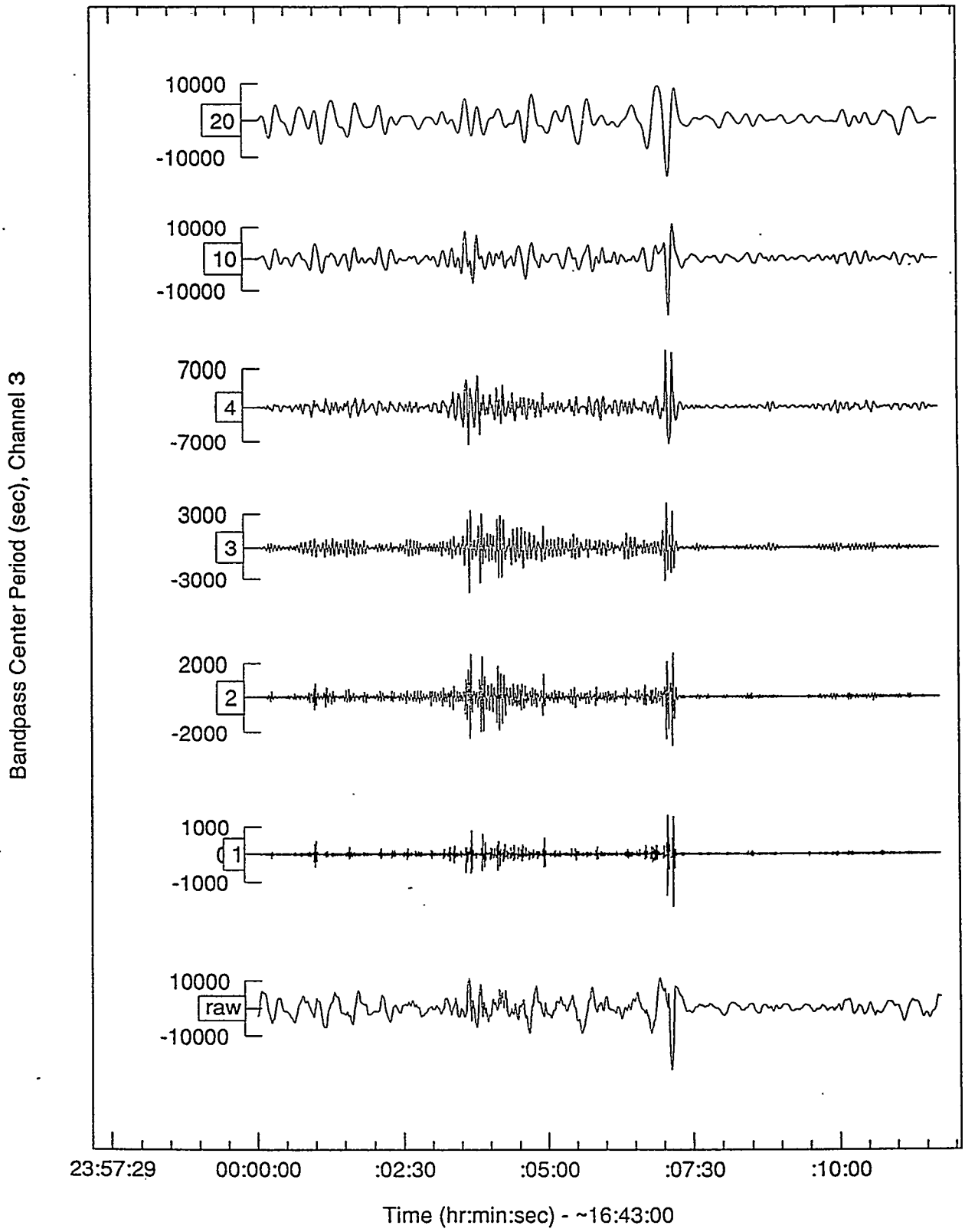

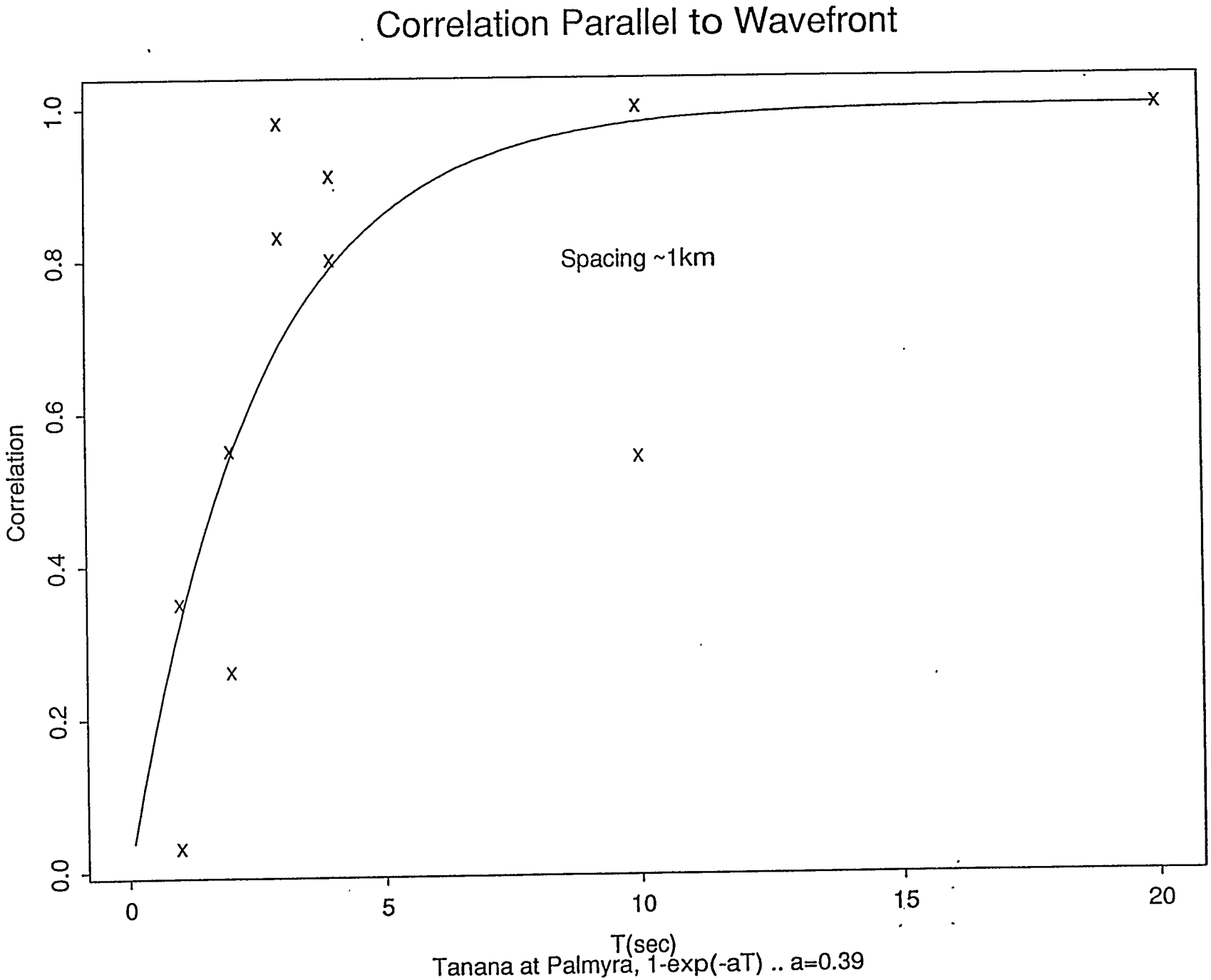
Correlation Parallel to Wavefront
Spacing ~1km
Correlation
0.0
0.2
0.4
0.6
0.8
1.0
0
5
10
15
20
T(sec)
Tanana at Palmyra, 1-exp(-aT) .. a=0.39

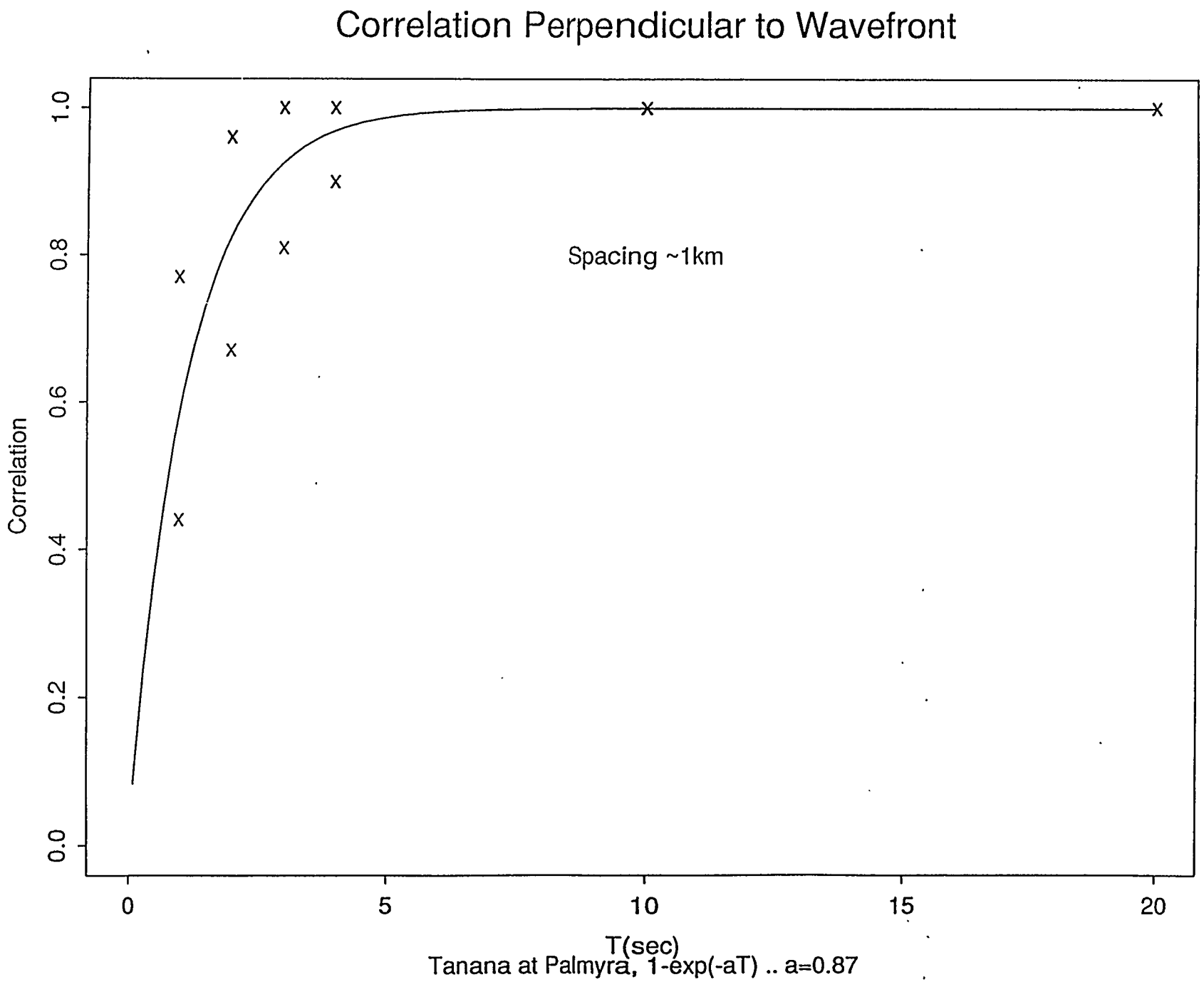
Correlation Perpendicular to Wavefront
Spacing ~1km
Correlation
0.0
0.2
0.4
0.6
0.8
1.0
0
5
10
15
20
T(sec)
Tanana at Palmyra, 1-exp(-aT) .. a=0.87

Comparison of Predicted and Observed Infrasound Correlation for Sensor Spacing of 1 km				
	Prediction, Mack and Flinn (1971) Δc=0.015 km/sec $\Delta\theta$=5°		Fitted Observations Tanana at Palmyra	
Signal Period (sec)	2	1	2	1
ρ parallel to wavefront	.75	.28	.54	.32
ρ perpendicular to wavefront	.92	.70	.82	.58

Twelve (12) observations from T= 1 to 20 seconds were fitted to the expression $1-exp(-aT)$. a was found to be 0.39 parallel to the wavefront, and 0.87 perpendicular. Considering the scatter in the small amount of data which is available for analysis, the observations seem not inconsistent with the predictions of Mack and Flinn although there is some indication of a lesser correlation, which would suggest the use of smaller arrays than those suggested using the data of Mack and Flinn.

Comparison of Observed and Theoretical Infrasound Signal Correlations							
Period (sec)		20	10	4	3	2	1
10 km spacing, Petit at Oahu (~2195 km)							
Perpendicular to wavefront 1-2	Observed (raw) (250-350 sec window)	>.91	>.56	>.29	>.35	>.13	>-.09
	Theoretical	.92	.71	.06	0	0	0
Parallel to wave-front 1-3	Observed (raw) (250-350 sec window)	>.68	>.41	>-.15	>-.28	>-.25	>-.09
	Theoretical	.75	.28	.05	0	0	0
1 km spacing, Tanana at Palmyra (708 km)							
Perpendicular to wavefront 1-3	Observed (Corrected Average Signals A-B & C-D	1	1	.95	.90	.82	.60
	Theoretical	.999	.997	.98	.96	.92	.71
Parallel to wavefront 2-3	Observed (Corrected) Average Signals A-B & C-D	1	.77	.80	.90	.40	.19
	Theoretical	.997	.99	.93	.88	.75	.28

Observed correlation at Oahu is biased lower than the true value because the available data does not include pre-signal noise which is needed to correct signal correlation estimates for the effects of noise. If the negative values of correlation at short periods at Oahu can be taken to indicate the standard errors of the Oahu correlation estimates, ~0.25,then the theoretical (Mack and Flinn, 1971), and observed data seem consistent, although there is a suggestion that, for estimates perpendicular to the wavefront, that the observed correlations are greater than the theoretical.

Assuming that the true correlation must decline with distance for the Palmyra data parallel to the wavefront, suggests a value of ~0.2 for the standard error of the estimates. Such a standard error would seem to allow the theoretical and observed data to be consistent at Palmyra, although there is a suggestion that the observed correlations are less that the theoretical. Analysis of Petit at Palmyra gives similar observed correlation values.

F Detectors

- Detect on ratio of array beamed power to mean-over-channels residual power. Ratio is an F statistic (Ratio of Chi-squares) Will detect only in presence of signal correlation.
- $pF(q, N_1, N_2, \lambda)$ is the cumulative integral of F from 0 to q with N_1 and N_2 degrees of freedom and non-centrality parameter λ.
- $N_1=2BT$, where B is the bandwidth in the range 0.075 to 1.5 Hz for bandpasses centered from 20 to 1 sec.; T is ~100 seconds. $N_2=(N-1)N_1$ where N is the number of channels in the array.
- $\lambda=2BT(S/N)_{beam}$ where $(S/N)_{beam}$ is the power signal-to-noise on the beam.
- For 1 false alarm per day (FAR), T=100 sec implies 1-pF=0.0016 for central F ($\lambda=0$). For the range of values of B this corresponds to a range for q of $q_T=3.2$ to 1.3.
- Probability of detection (PD) is $1-pF(q_T, N_1, N_2, \lambda)$

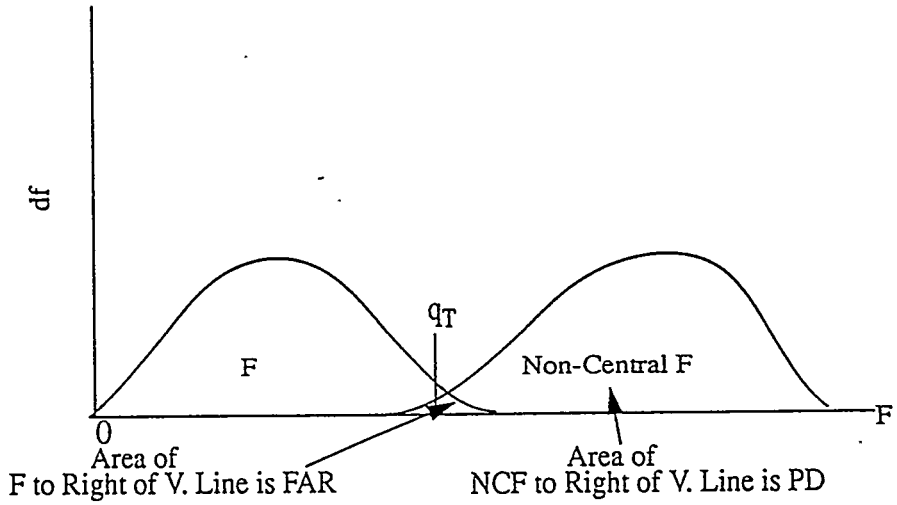

Azimuth Standard Error for Perfectly Correlated Signals

$$\sigma_a = \left(\frac{180}{\pi}\right)\cdot\left(\frac{1}{2\pi}\right)\cdot\left(\frac{1}{2BT}\right)^{\frac{1}{2}}\cdot\left(\frac{1}{N\cdot snr}\right)^{\frac{1}{2}}\left(1+\frac{1}{N\cdot snr}\right)^{\frac{1}{2}}\left(\frac{\lambda}{\sigma}\right)$$

Azimuth Standard Error for Less-than-perfect Correlation

$$\sigma_a = \left(\frac{180}{\pi}\right)\cdot\left(\frac{1}{2\pi}\right)\cdot\left(\frac{1}{2BT}\right)^{\frac{1}{2}}\cdot\left(\frac{1}{N\cdot snr}\right)^{\frac{1}{2}}(\lambda^2)(2N)^{\frac{1}{2}}(\tilde{\theta}'\cdot D_P^{-1}\cdot\tilde{\theta})^{\frac{1}{2}}$$

where $\tilde{\theta} = (k_y,-k_x)'$. and $D_P = P_s^{-1}\cdot D$

where P_s is the power spectrum, and

$$D = \sum_{j,k} c_{jk}\cdot F_{kj}^{s}\cdot(\vec{r}_j-\vec{r}_k)\cdot(\vec{r}_j-\vec{r}_k)'$$

where $\vec{r}$ are element coordinates,

and $F_{kj}^{s} = P_s^{-1}\cdot f_{kj}^{s}$

where f_{kj}^{s} is the signal covariance matrix.

In this application the off-diagonal elements of F_{kj}^{s} are equal to the correlation.

The signal-to-noise enters the calculation of D through the relation for the matrix for c_{jk}:

$$C = F_s\cdot\left(F_s+\frac{1}{snr}\cdot I\right)^{-1}$$

It does not appear possible to write the expression for D in pure matrix notation.

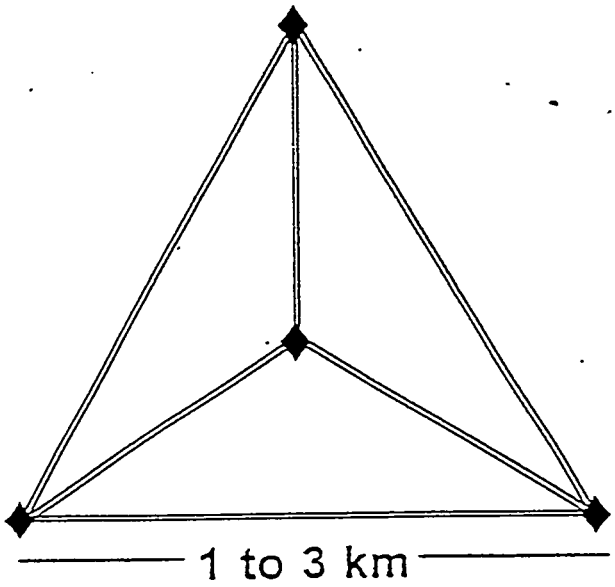

FIGURE 1 : 4 ELEMENT INFRASOUND ARRAY CONFIGURATION

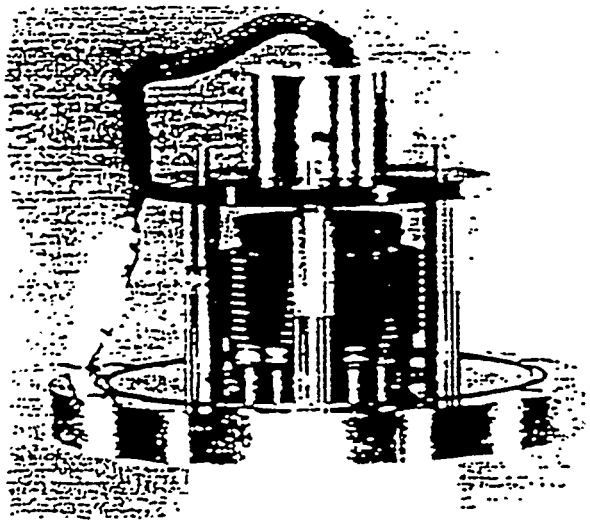

FIGURE 2 : WIDEBAND MICROBAROGRAPH

	Period (sec)					
d (km)	20	10	5	2l	1l	0.5
1	0.00	0.01	0.06	0.38	1.4	3.8
2	0.02	0.06	0.24	1.4	3.8	5.7
3	0.03	0.14	0.54	2.7	5.2	6.0
4	0.06	0.24	0.93	3.7	5.7	6.0
8	0.24	1.0	2.9	5.7	6.0	6.0

Beam signal Loss (dB), *imperfect correlation*, 4 element CD Array, d km on a side.

	Period (sec					
d (km)	20	10	5	2	1	0.5
1	41.3/41.4	14.6/14.7	4.5/4.5	1.26/1.39	0.46/0.66	0.20/0.65
2	20.6/20.7	7.3/7.4	2.2/2.4	0.63/0.90	0.23/0.75	0.10/2.87
3	13.7/13.9	4.9/5.0	1.39/1.71	0.42/0.86	0.15/1.49	0.07/33.6
4	10.3/10.5	3.6/3.9	1.12/1.42	0.32/1.02	0.12/3.31	0.05/3.95
8	5.2/5.5	1.8/2.3	0.56/1.25	0.15/4.54	0.06/4.56	0.02/117

Azimuth Error (deg), (*perfect signal correlation/(imperfect correlation*), 4 element CD Array, d km on a side Single element amplitude signal-to-noise of 0.75. Signal window of 60 sec.

Calculation of Signal Correlation in the Presence of Noise

$$\rho = \frac{C_{ij}}{A_s}$$

Where C_{ij} is the cross correlation between two channels and where A_s is the autocorrelation, assumed here to be the same on each channel. The cross-correlation corrected for noise, under the assumption that the noise is stationary, is given by:

$$\rho_c = \frac{C_{ij}}{A_s - A_n}$$

where A_n is the autocorrelation before the signal.

To estimate detection thresholds, and standard errors of azimuth estimates at those thresholds, it is necessary to calculate signal-to-noise and correlation as we multiply measured source powers by factors of interest. We need estimates not only of the total signal power but also of the correlated signal power (which is measured by the correlation) and the uncorrelated signal power. This uncorrelated power influences the appearance of the beam in the time domain; it is reduced by beamforming but nonetheless enhances the signal-to-noise on the beam if the beamed signal is compared to pre-signal noise. We see that the correlated signal power is:

$$A_{s,c} = \rho_c \cdot (A_s - A_n)$$

and the uncorrelated signal is:

$$A_{s,uc} = (1 - \rho_c) \cdot (A_s - A_n)$$

Now in the case of a reduced amplitude source we may multiply A_{sc} and $A_{s,uc}$ by a suitable factor, f, to obtain $A'_{s,c}$ and $A'_{s,uc}$, where c and uc refer to correlated and uncorrelated. Then

$$\rho' = \frac{A'_{s,c}}{A'_{s,c} + A'_{s,uc} + A_n}$$

would be the correlation for the same signal with reduced amplitude, in the original noise.

For application to determine probability of detection and errors of azimuth estimates using theoretical correlation estimates, we also need the signal-to-noise on an individual channel, $(S/N)_P$.

$$(S/N)_P = (A'_{s,c} + A'_{s,uc})/A_n$$

. Detection and Location Parameters for CD Infrasound (1,2,3) km Aperture Arrays Derived from Mack and Flinn(1971) correlations, and $(S/N)_p$ from Tanana as observed at Palmyra, reduced by a factor of 5.

Signal Parameters				Theoretical Mean Correlation, ρ,			Non-centrality Parameter $\lambda = 2BT*(S/N)_{beam}$		
T_c (sec)	B (Hz)	q_T	$(S/N)_P$	1	2	3	1	2	3
20	.075	3.23	.540	.998	.995	.99	6.5	6.5	6.5
10	.15	2.53	.620	.995	.98	.96	14.9	14.6	14.3
4	.4	1.70	.880	.97	.89	.77	55.2	48.8	42.0
3	.3	1.88	.920	.95	.81	.63	41.6	34.8	26.5
2	.7	1.41	1.36	.89	.63	.39	130	87.2	50.4
1	1.5	1.32	6.40	.63	.22	.065	652	168	46.0

T_c is the center period for the detection filter passband with bandwidth B and time duration T=100 sec. q_T is the F detection threshold for one false alarm per day. $(S/N)_P$ is the power signal to noise ratio on a single channel of the event Tanana as seen at Palmyra. The theoretical mean correlation for the arrays was computed using the parameters Δc=0.015 km/sec and $\Delta\theta = 5^0$. $(S/N)_{beam}$ is given for a 4-element array by $\dfrac{\rho \cdot f \cdot (S/N)_P}{\frac{1}{4} \cdot [(1-\rho) \cdot f \cdot (S/N)_P + 1]}$

where f is the factor giving the reduction of signal power; for this table, $f = 1/5$. This is equivalent to (1/5)th of the yield or 0.52 kt.

Detection and Location Estimates for CD Infrasound (1,2,3) km Aperture Arrays Derived from Mack and Flinn(1971), and the Event Tanana as observed at Palmyra. Estimates for the Event Tanana as observed at Palmyra with Amplitude reduced by a factor of $5^{1/2}$

T_c(sec)	Visual $(S/N)_{beam}$ Amplitude			Probability of Detection With F using Simple Beam PD			Azimuth Estimate with Optimum Weighted Beam Standard Error, σ_θ °		
	1	2	3	1	2	3	1	2	3
20	1.05	1.05	1.05	.02	.02	.02	110	55	37
10	1.06	1.06	1.06	.02	.02	.02	35	17.7	12.1
4	1.08	1.08	1.07	.48	.37	.26	6.6	3.6	2.7
3	1.08	1.08	1.06	.29	.18	.09	5.6	3.2	2.6
2	1.12	1.10	1.07	.99	.85	.39	1.9	1.3	1.3
1	1.38	1.24	1.17	1.0	.96	.07	.34	.42	1.02

T_c is the center period for the detection filter passband. Detection and azimuth estimates are for a time window of 100 sec. The "Visual" amplitude is given by dividing the estimate for the single-channel noise power in front of the signal into the sum of the noise plus correlated signal power plus 1/4 the uncorrelated signal power (for a 4-element array), and then taking the square root. The probability of detection is computed for an correlation F detector with a false alarm rate of one per day and for a signal with 1/5th the power (yield~0.52kt) of Tanana at Palmyra. The azimuth estimate assumes that detection has selected the proper window over which to estimate the azimuth. Thus, if detection probability is low, the significance of the azimuth estimate is questionable. It appears that one should construct 1 km aperture arrays and detect at 1 Hz. Note that azimuth error would be larger for larger arrays if azimuth were determined by the maximum of the simple beam instead of the optimum weighted beam.

Summary

- Infrasound signal coherence observed in the period range 1-20 sec at ~1 km separation for the 2.6 kt event Tanana recorded at Palmyra, a distance of 700 km, is consistent with parameters estimated by Mack and Flinn (1971) to represent the signal coherence of a Chinese event recorded at LAMA at a distance of ~90° in the period range 10-80 sec at 7 to 40 km separation. Petit (2.2kt) at Oahu (~2000 km) is also in agreement for 10 km separation for periods of 20, 10 and 4 seconds. Correlation is nearly zero, in agreement with MF, for T = 2 and 1 seconds.

- These parameters, together with the observed single-channel S/N of Tanana at Palmyra make it possible to determine the ~1kt nuclear event detection threshold and azimuth estimation standard error for infrasound CD arrays as a function of array aperture.

- Arrays with apertures of 1 km have the lowest detection threshold and smallest standard error of azimuth estimation as compared to arrays with apertures of 2 and 3 km. This capability occurs at periods of 1 and 2 seconds. The loss of capability for the larger arrays is due to the loss of correlation of the 1 and 2 second signals at the larger spatial intervals.

- There is very little capability at 10 and 20 second periods. For detection this is mostly due to the low bandwidth of the long-period signals, although S/N is also slightly lower. for these low-yield shots. For location it is due also to the small array aperture as compared to the wavelength.

- Detection statistics reported in the 1950's for 1-2 kt events at such distances routinely reported peak amplitude detections at periods near 5 seconds, independent of distance. A fitted formula (AFTAC Tech Memo 87, 19 October 1956) gave $\log Y = -2.00 + 2.84 \log T +/- 0.28$ with data spanning the range 0.2 to 500 kt. This is consistent with observations of Tanana at Palmyra, suggesting that the 1-2 second energy also propagates to greater distances but was not reported due to the instrument response which peaked at 13 seconds and was 4 dB down at 2 seconds. Further archival recovery and experimental research is sorely needed to obtain good data on 1-2 second period data at distances of 1000-4000 km for yields of 1-4 kt and at sensor spacings of 1-3 km.

A COMPARISON OF SEVERAL AUTOMATED DETECTORS FOR INFRASOUND SIGNALS

Kevin D. Hutchenson and Haydar J. Al-Shukri

ENSCO, Inc.
445 Pineda Ct.
Melbourne, FL 32940

Under the IMS, a network of infrasonic arrays is expected to be deployed in the next few years. This network should consist of approximately 50 to 60 arrays consisting of four elements to be distributed around the globe. These arrays will be deployed to monitor potential atmospheric and near-surface nuclear tests under the Comprehensive Test Ban Treaty (CTBT). Data from these arrays must be processed routinely.

Several existing and new procedures are currently in use or have been proposed for automated infrasound signal detection. Although not an exhaustive list, these detectors include: (1) Array Signal Detector by Lag Closure, using cross-correlation functions to determine the delays of a propagating signal and assuming that the sum of the delays along a closed path is zero, (2) F-detector, which in general represents the ratio of the beam power to the power of the difference between the individual channel and the beam, (3) Power detector using a standard STA/LTA ratio, and (4) an Autoregressive filter/detector process. Each of these have been examined for the automated detection capability using both synthetic and real data.

The F-statistic detector has been found to be the most successful of the automated detectors, when factors of capability, missed detections, false alarms, turning, etc, are considered.

A Comparison of Several Automated Detectors for Infrasound Signals

K.D. Hutchenson and Haydar J. Al-Shukri
ENSCO, Inc., Melbourne, Florida
August, 1997

ENSCO, Inc.

INTRODUCTION

- ✧ Problems exist distinguishing between noise and signal.
- ✧ Several existing and new procedures currently proposed for automated infrasound signal detection:
  1. Power detector:
     - Uses a standard STA/LTA ratio
  2. Lag Closure detector:
     - uses a cross-correlation function to determine the delays of a propagating signal
     - detect when the sum of the delays along a closed path is zero
  3. F-statistics detector:
     - represents the ratio of the beam power to the power of the difference between the individual channel and the beam
  4. Autoregressive filter/detector process.

Automated Processing

- Detection process must be completely without human intervention after some initialization step.
- Detection step must be computationally faster than real-time.
- Must be reliable.
  - Few false alarms
  - Few missed events

NOISE and Signal

- Noise can be either random or coherent.
  - Wind eddies
  - Microbaroms
- Signals are coherent.
- Signals can be masked by both coherent and incoherent noise.

Typical Infrasonic Data

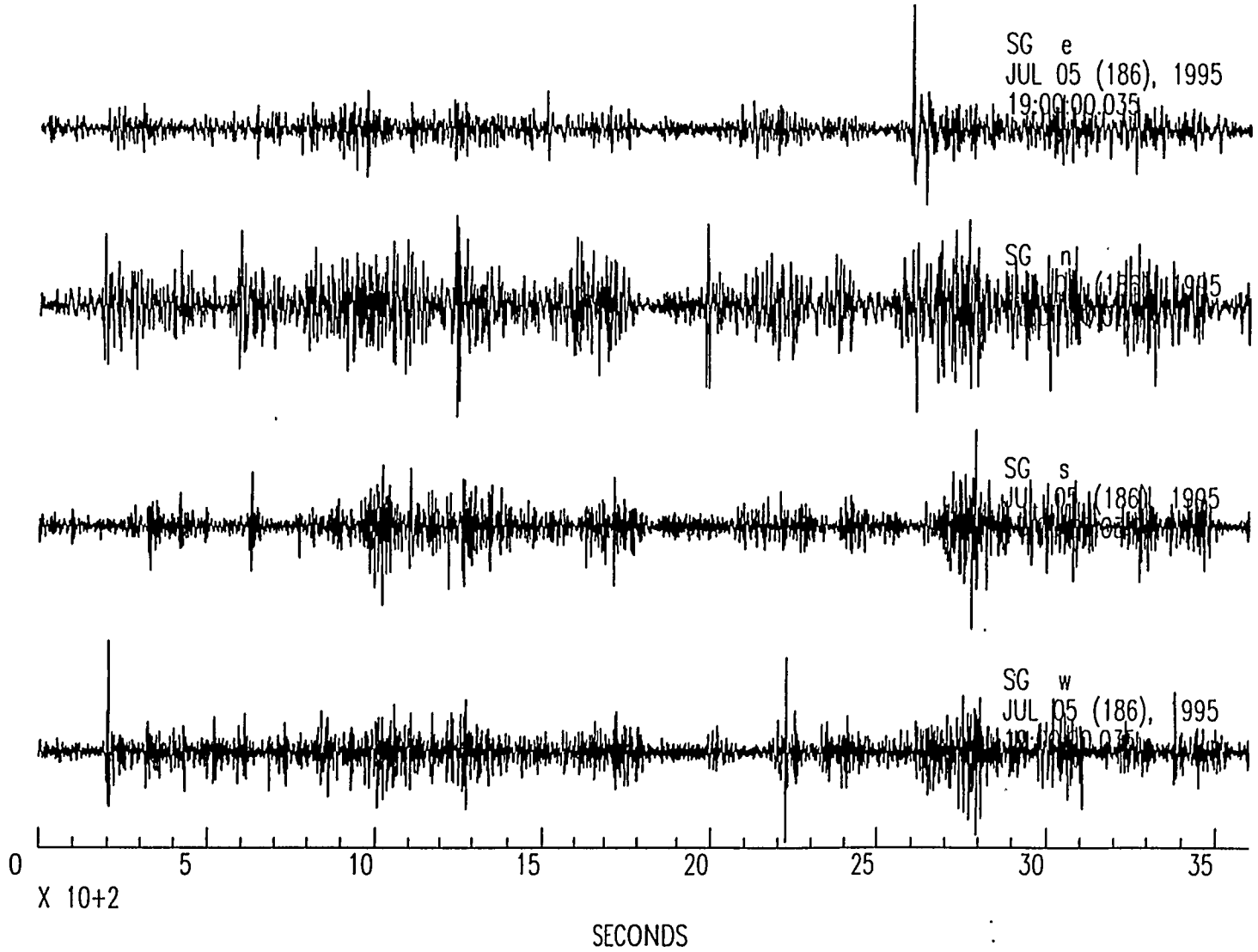

ENSCO, Inc.

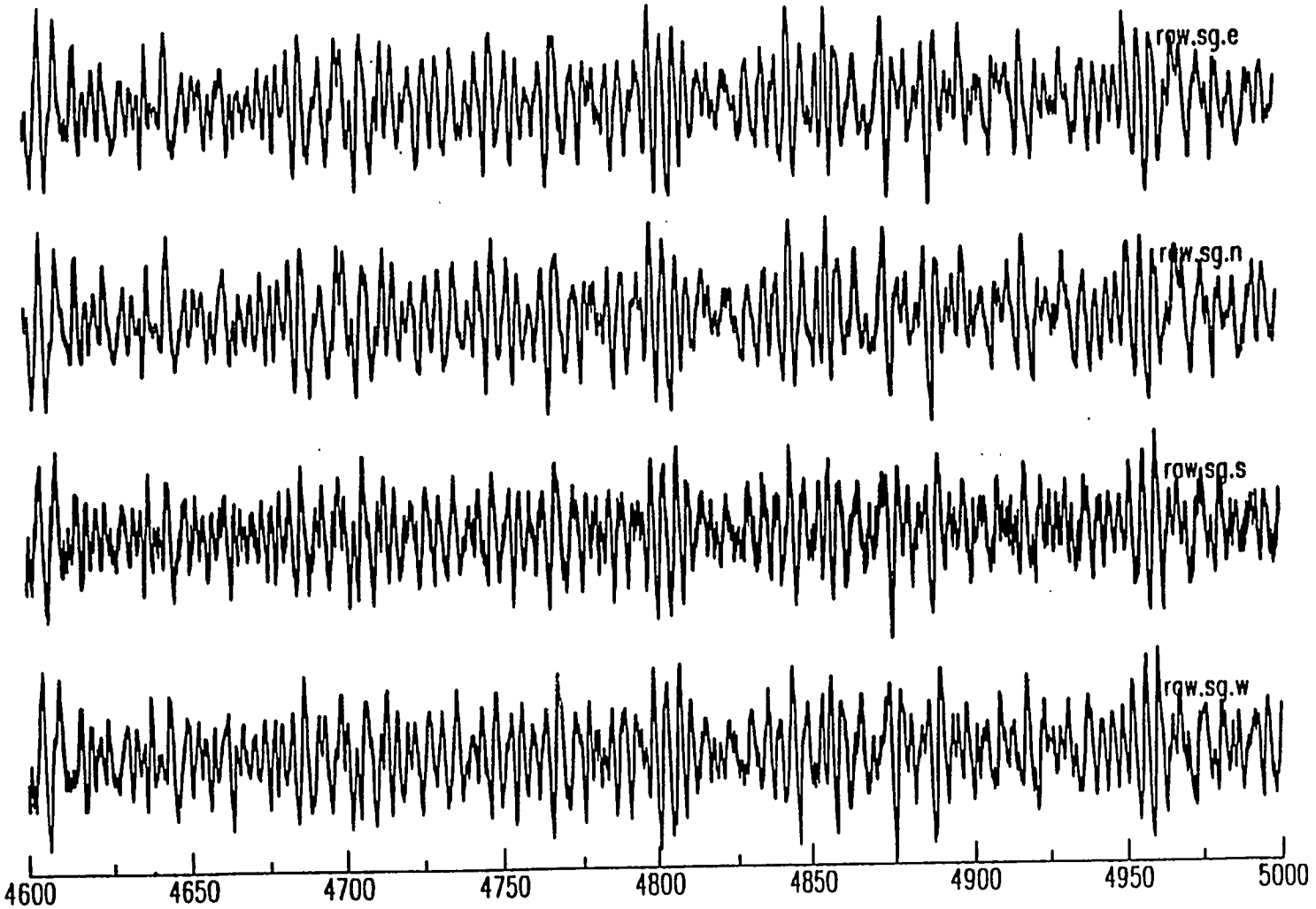

Coherent Microbaroms Signal at SG Array

ENSCO, Inc.

PRE-DETECTION PROCESSING:

- **Bandpass Filter.**
  - **Coherency is preserved.**

- **Autoregressive Filter.**
  - **Noise coherency is destroyed.**
  - **Signal coherency is degraded.**

Raw, Band-Pass, and AR Data

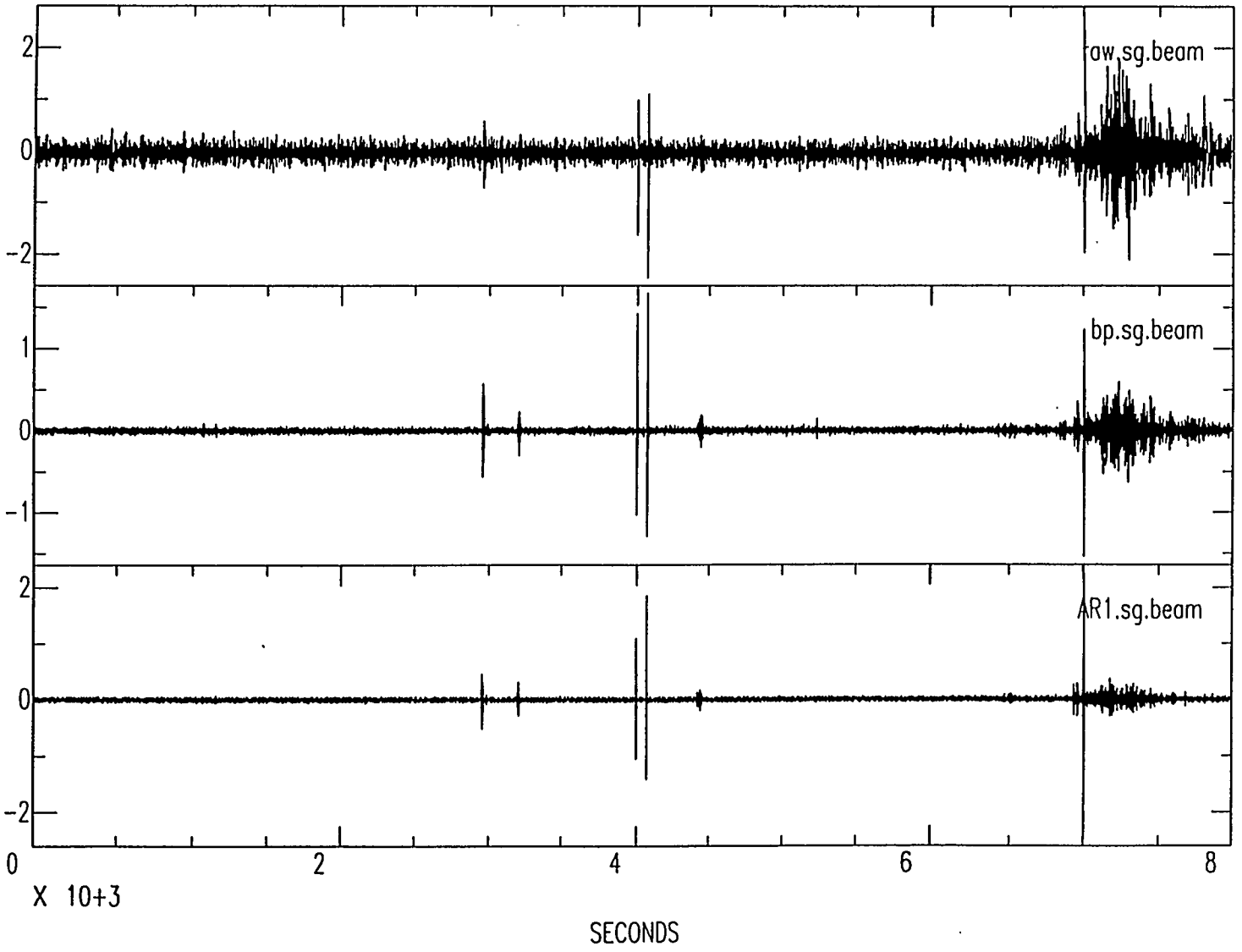

ENSCO, Inc.

Raw, Band-Pass, and AR Data

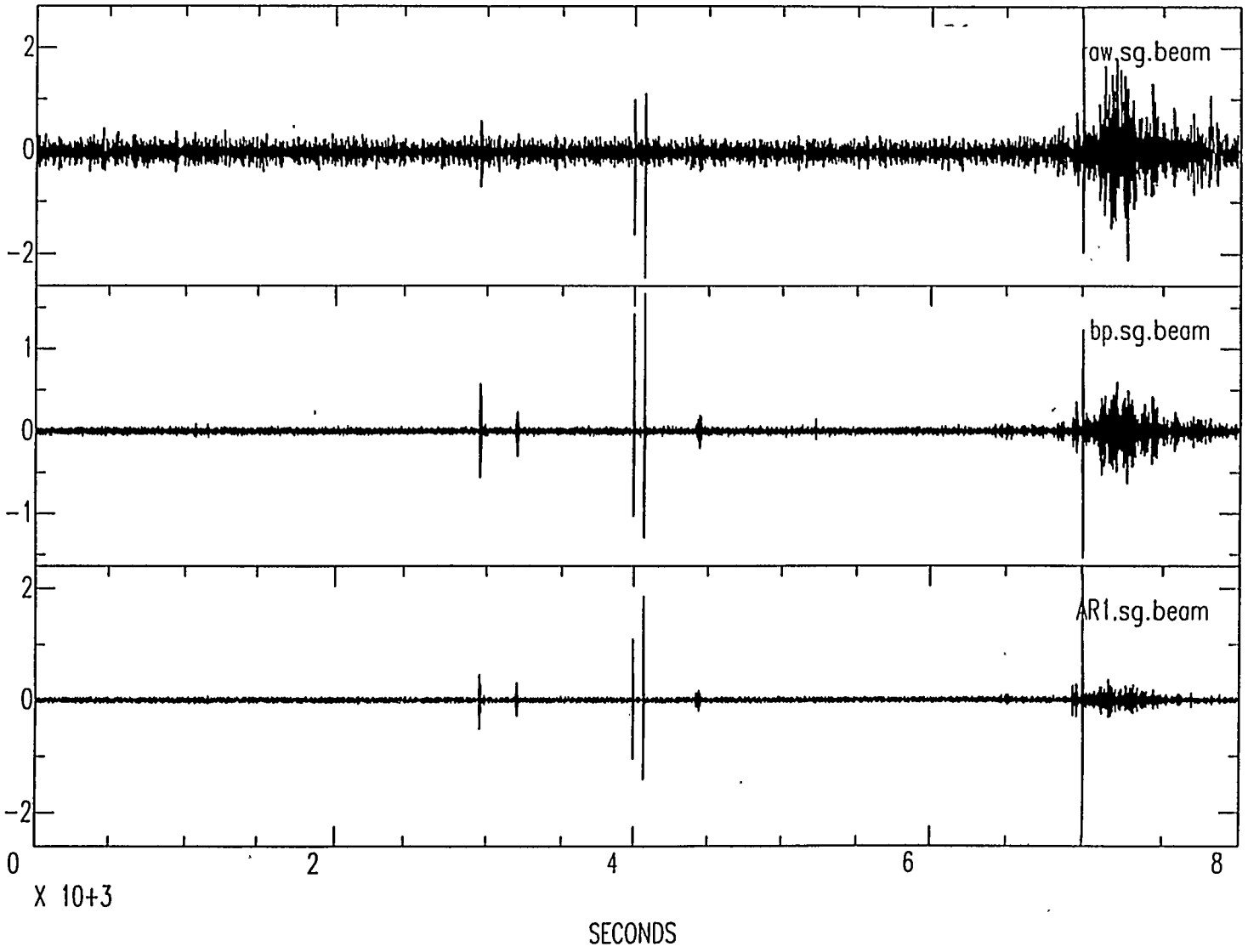

ENSCO, Inc.

ENSCO, Inc.

Power Detector

$$SNR = \frac{\sum_{i=1}^{N} stav_i}{\sum_{j=1}^{M} ltav_j}$$

SNR = signal-to-noise ratio

stav = short-term average

ltav = long-term average

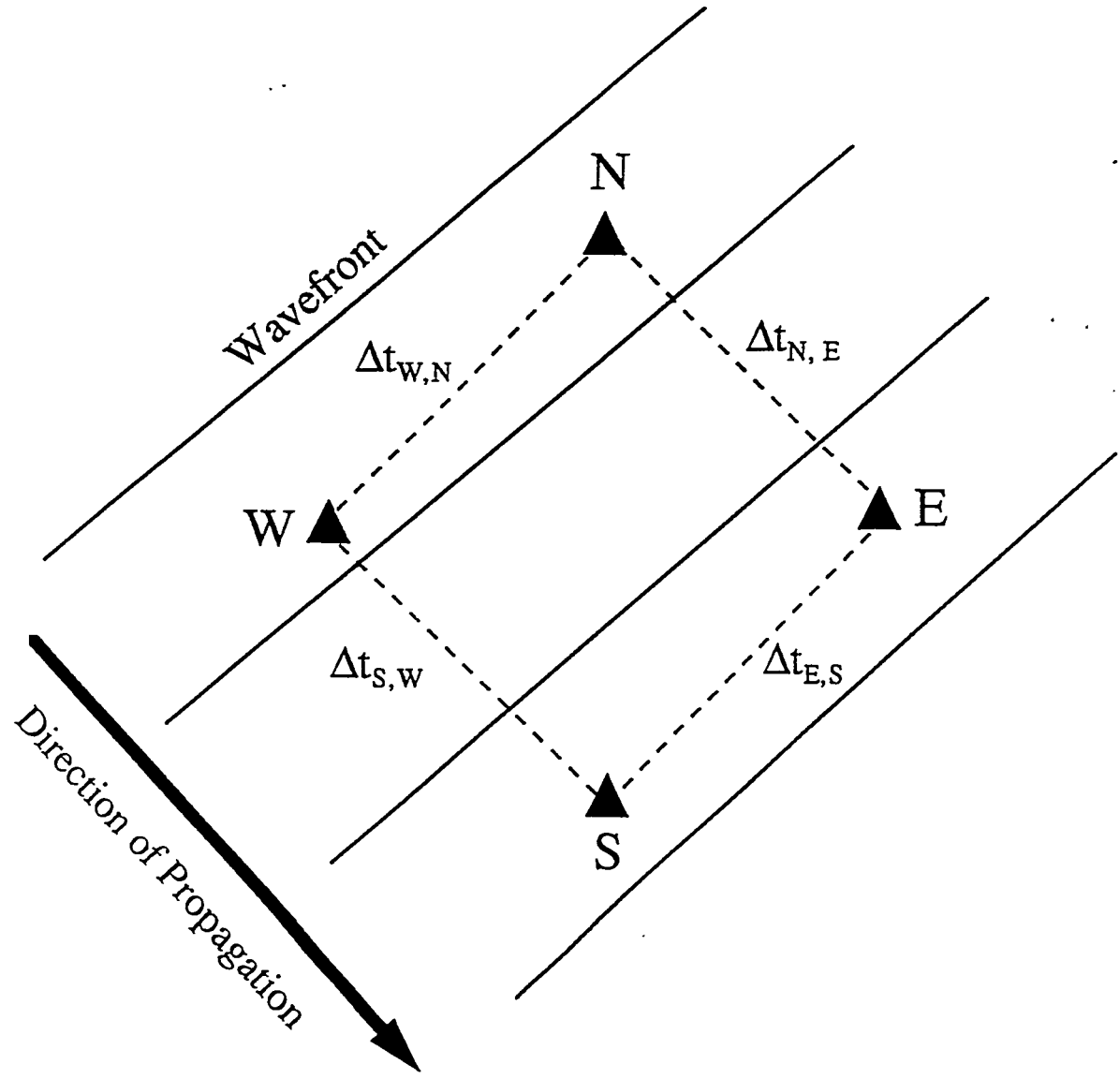

$$\Delta t_{N,E} + \Delta t_{E,S} + \Delta t_{S,W} + \Delta t_{W,N} = 0$$

ENSCO.

Lag-Closure

$$c(t) = \int_{-\infty}^{\infty} f(\tau - \Delta t_n) f(t + \tau) d\tau$$

✧ **At** $t = \Delta t_n$ **, c(t) maximize at c(**Δt_n**), or**

$$c(t)_{max} = c(\Delta t_n)$$

Lag-Closure

- The time delay between the arrivals at elements b and a can be represented by

$$\Delta t_{b,a} = t_b - t_a$$

- For any arbitrary closed path through the array, the sum of the delay times is

$$\Delta t_{a,b} + \Delta t_{b,c} + \Delta t_{c,a} = (t_a - t_b) + (t_b - t_c) + (t_c - t_a)$$

- Since the delay times are given by the lags at the cross-correlation maximum, the sum of those lags equals zero, or

$$\Delta t_{a,b} + \Delta t_{b,c} + \Delta t_{c,a} = \tau_{a,b} + \tau_{b,c} + \tau_{c,a} = 0.0$$

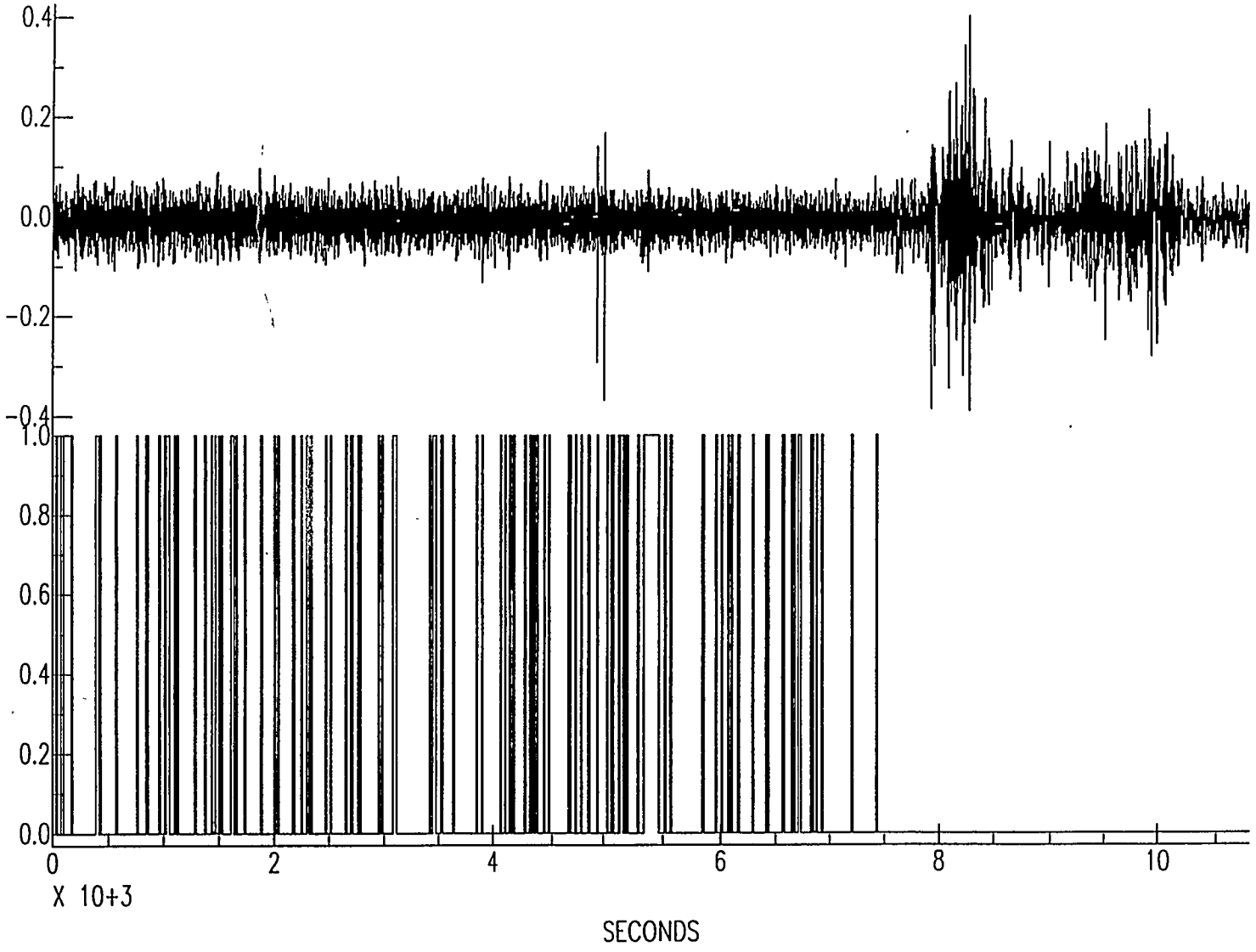

ENSCO, Inc.

Lag-Closure Detector: BP Data

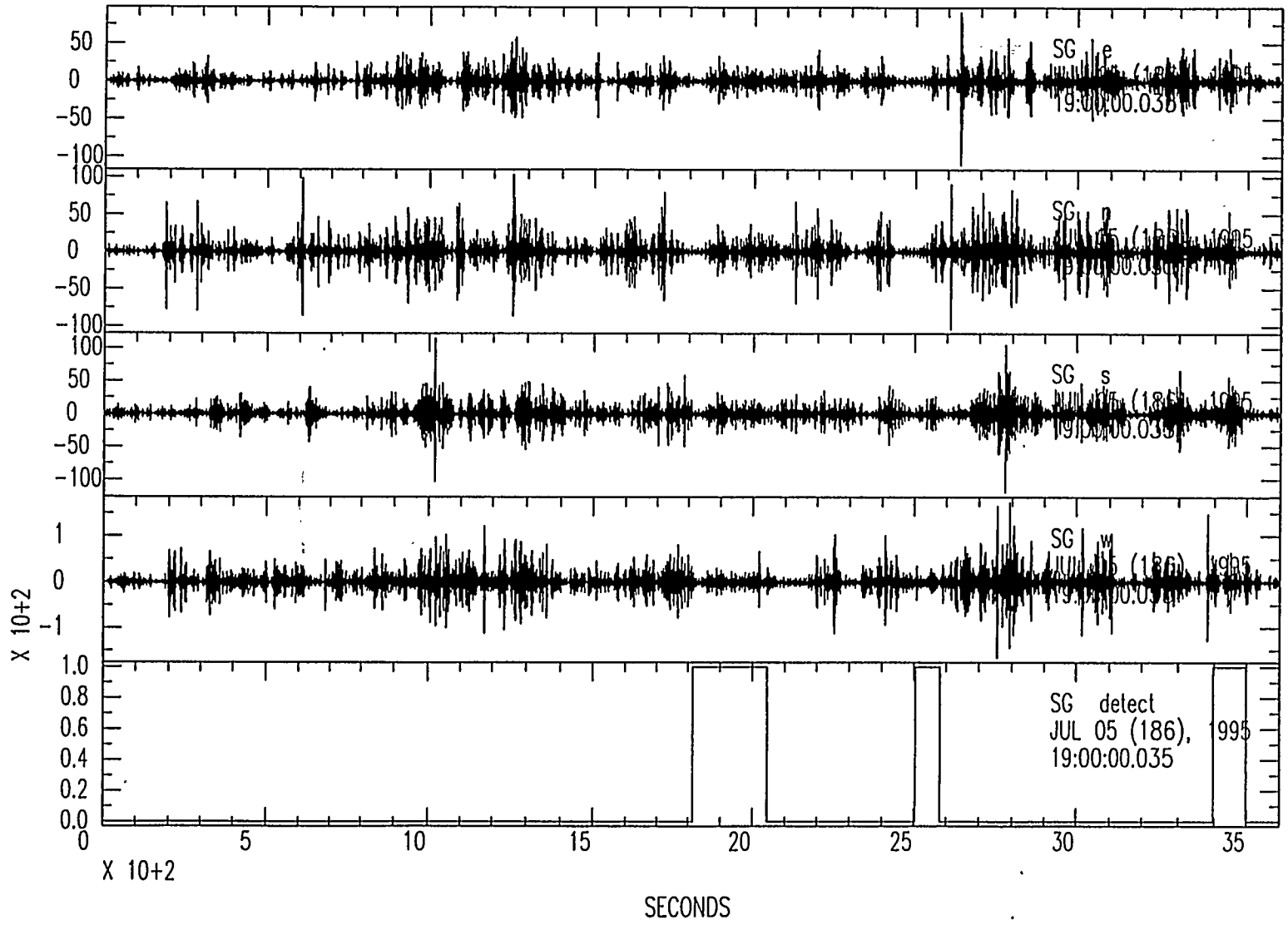

ENSCO, Inc.

Lag–Closure Detector: BP Data

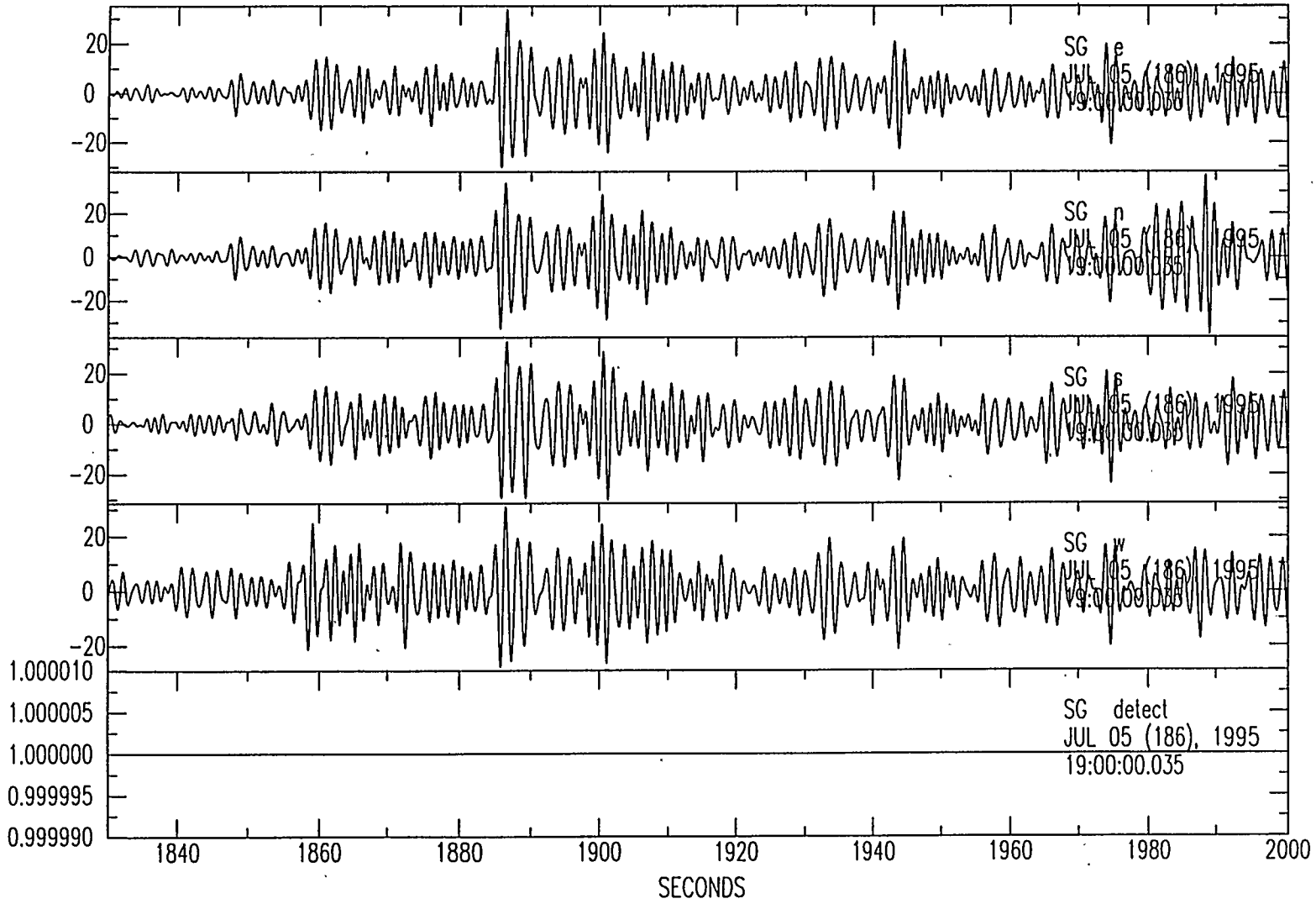

ENSCO. Inc.

Lag-Closure Detector: BP Data

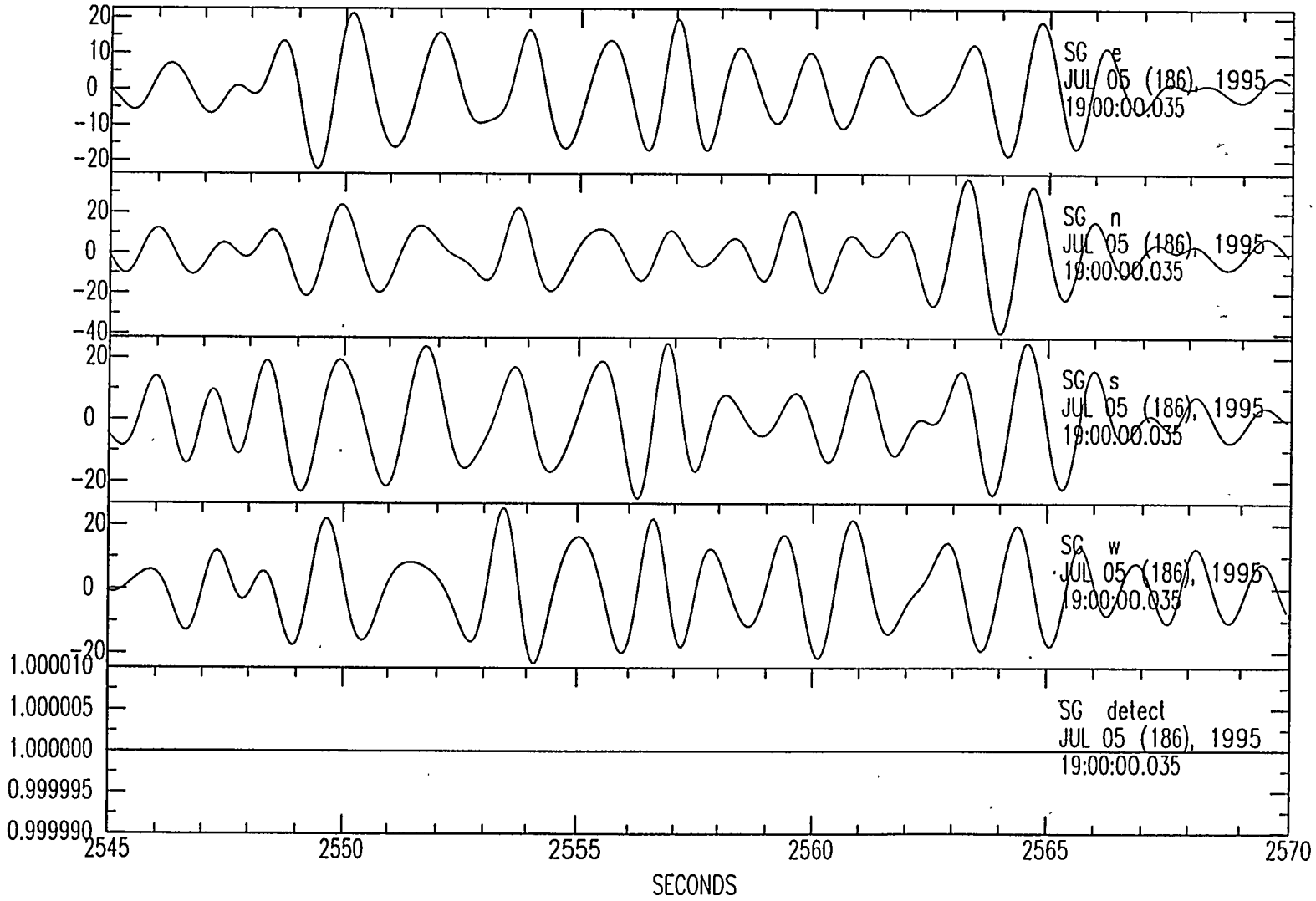

ENSCO, Inc.

Lag-Closure Detector: BP Data

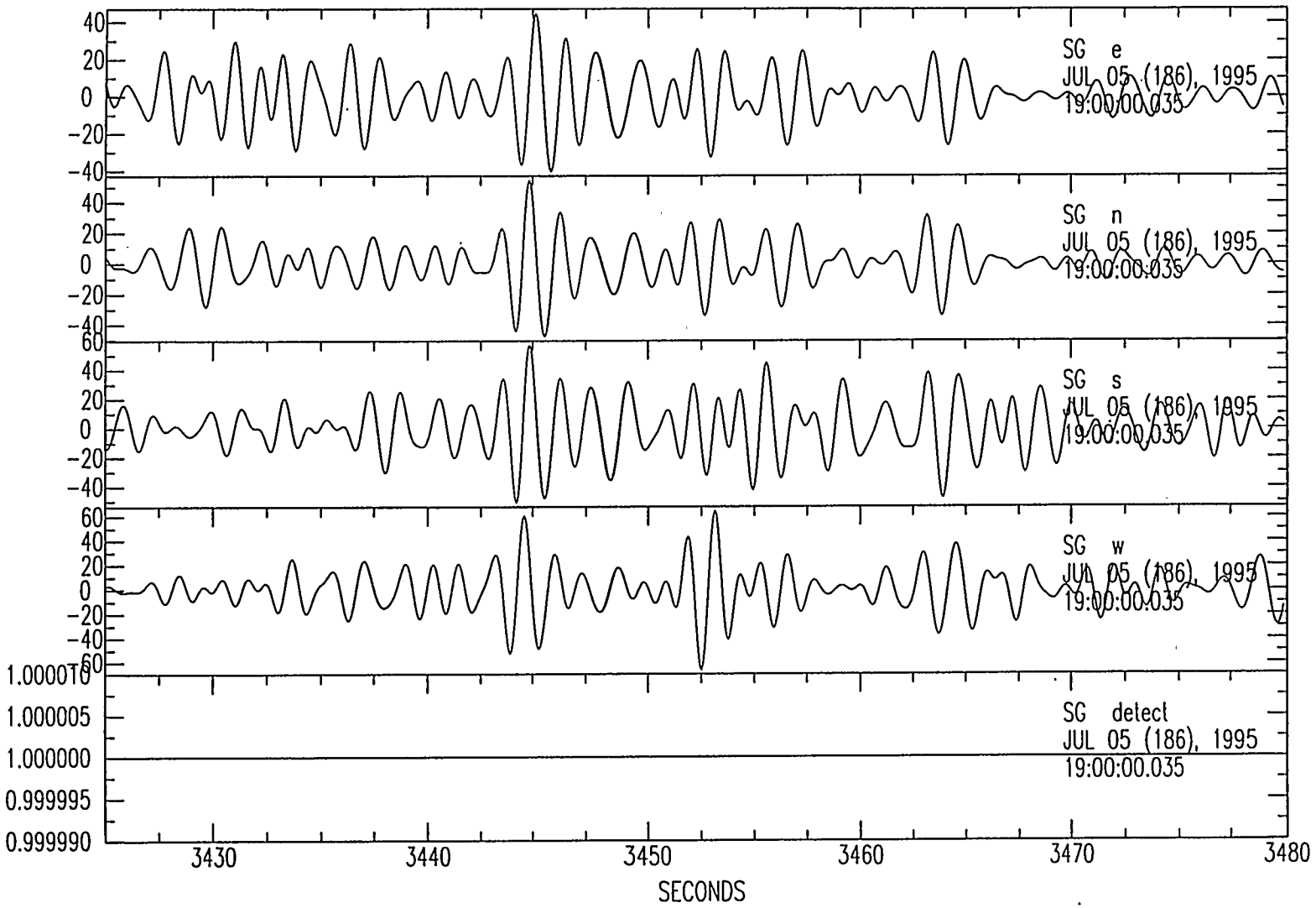

ENSCO. Inc.

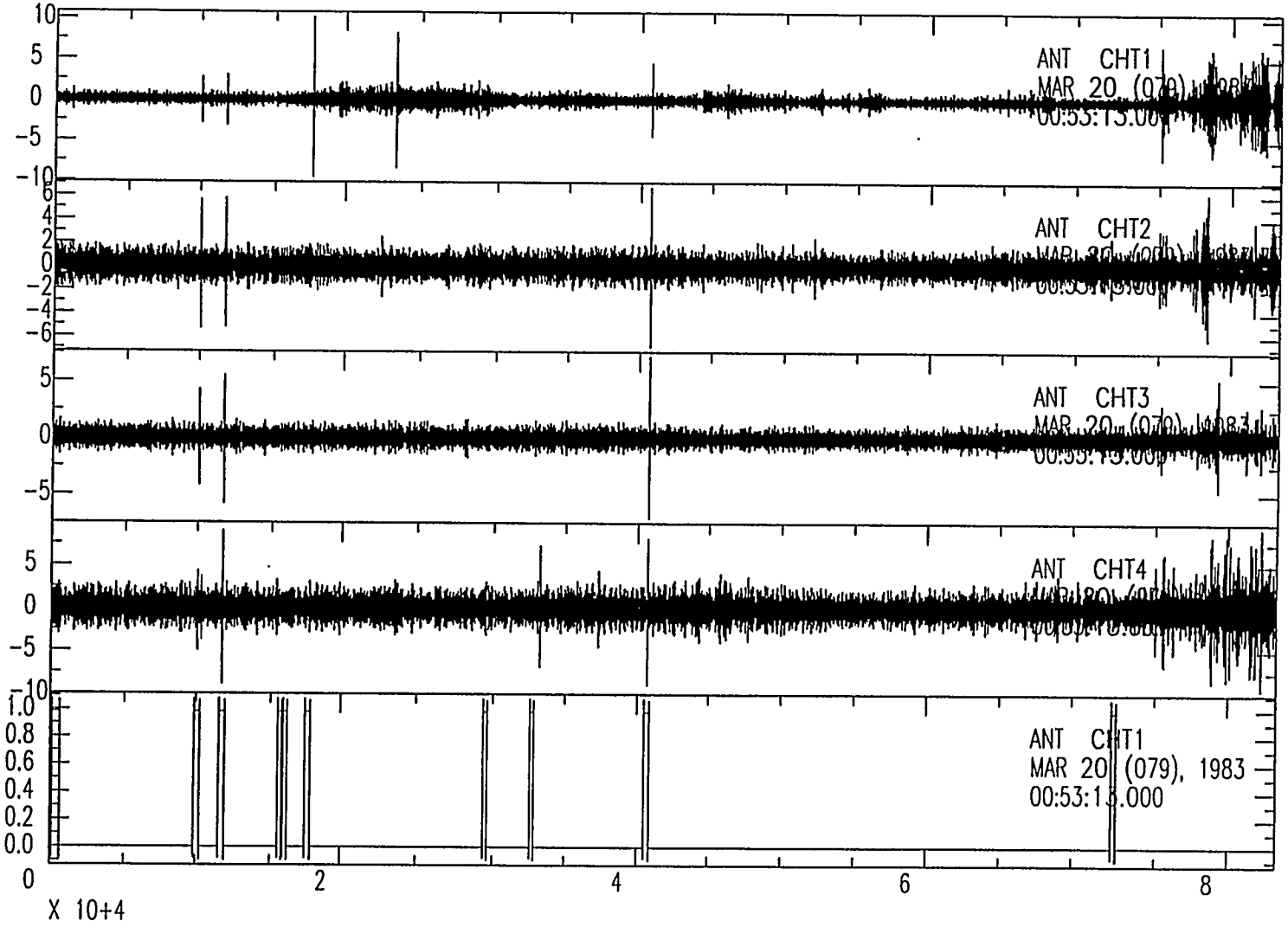
ANT CHT1
ANT CHT2
ANT CHT3
ANT CHT4
ANT CHT1
MAR 20 (079), 1983
00:53:15.000
X 10+4

ENSCO, Inc.

Lag-Closure Detector: BP Data

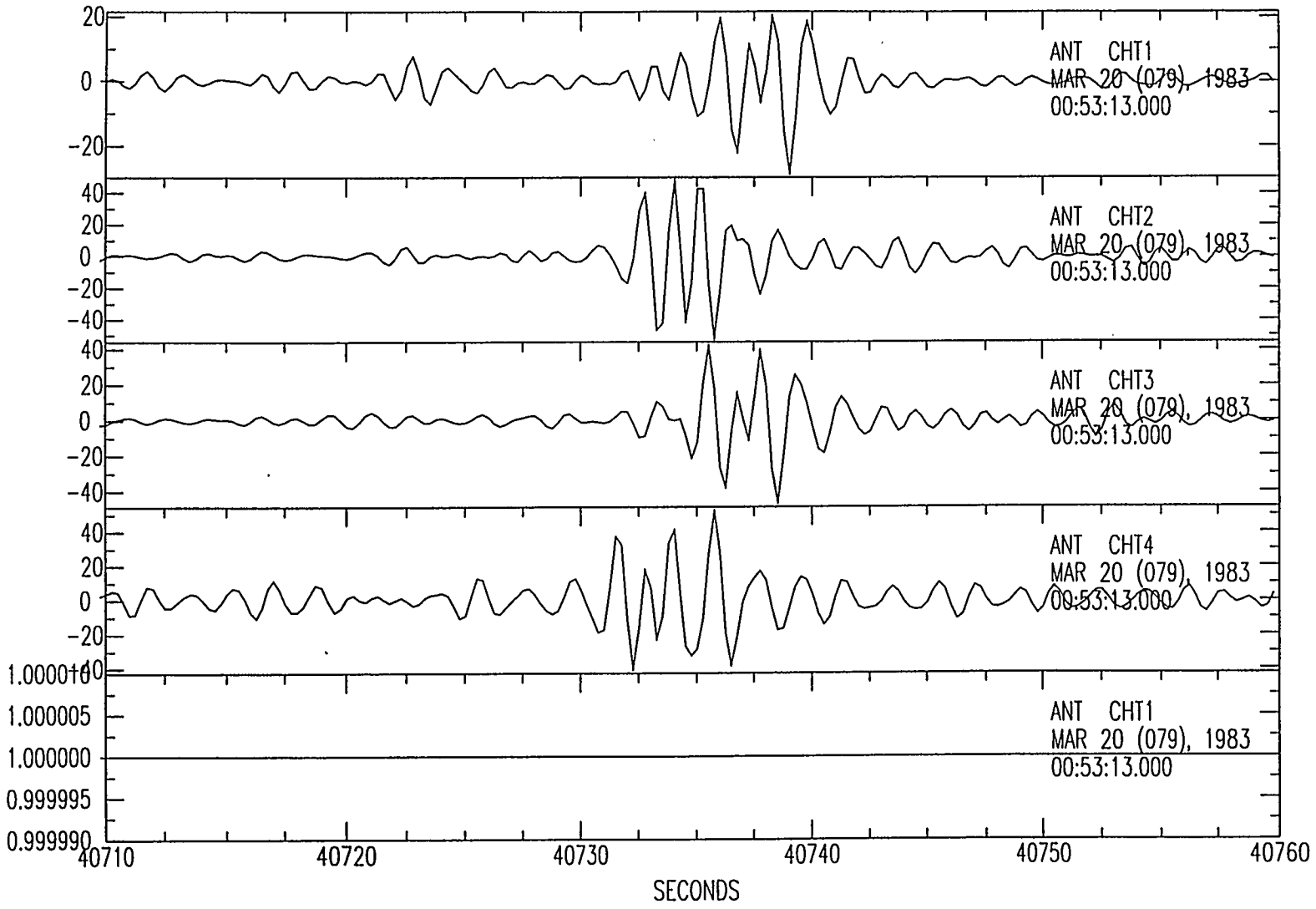

ENSCO, Inc.

F-Statistic

$$F = (N-1)\frac{\sum_{j=1}^{P} \hat{S}^2}{\frac{1}{N}\sum_{j=1}^{P} S_i^2 - \sum_{j=1}^{P} \hat{S}^2}$$

F = statistical value for the F-detector for the time window

N = number of points in the stations

P = number of stations in the array

S_i = raw time series channel

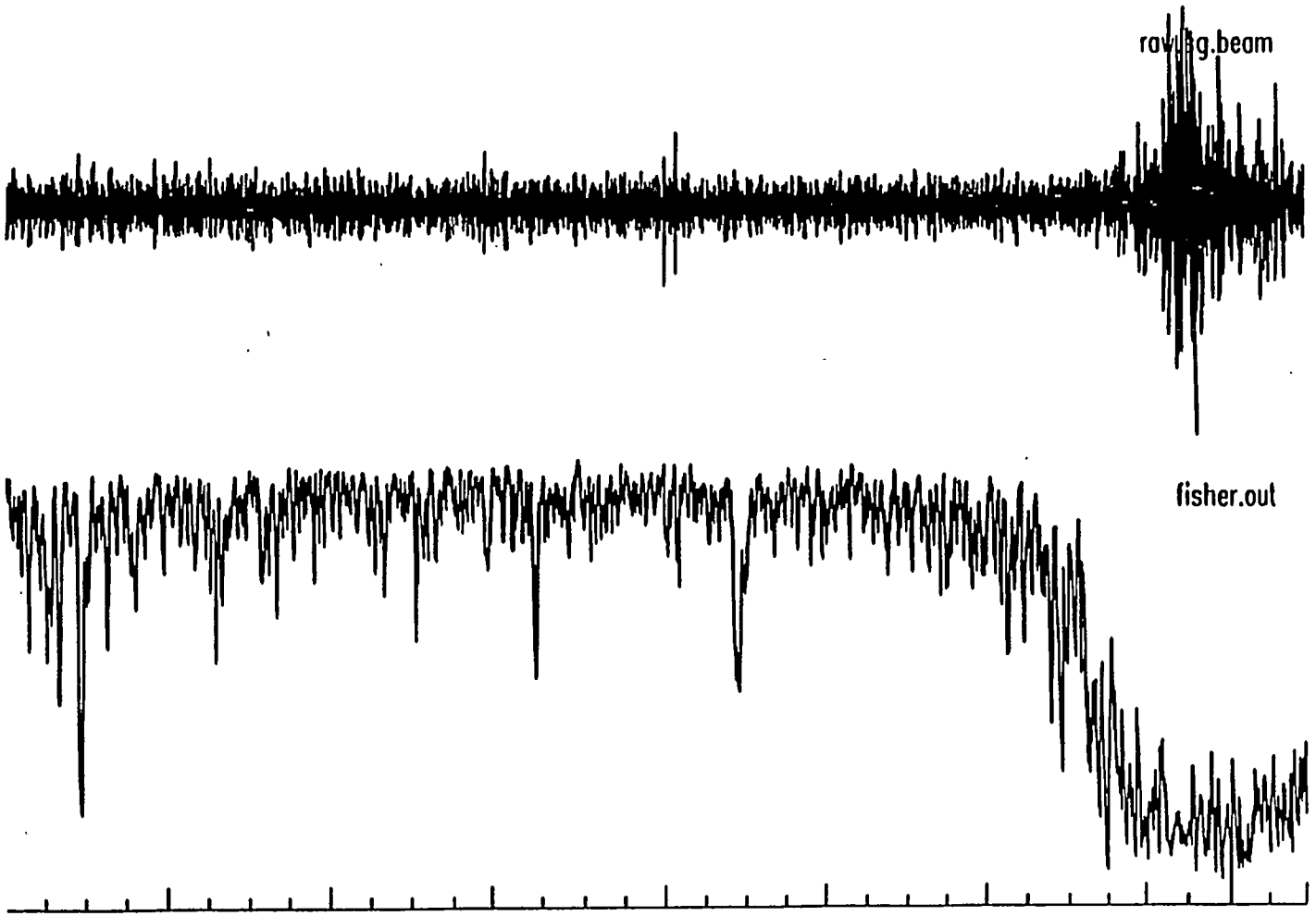

Beam of Raw Data and F-delector Values

ENSCO, Inc.

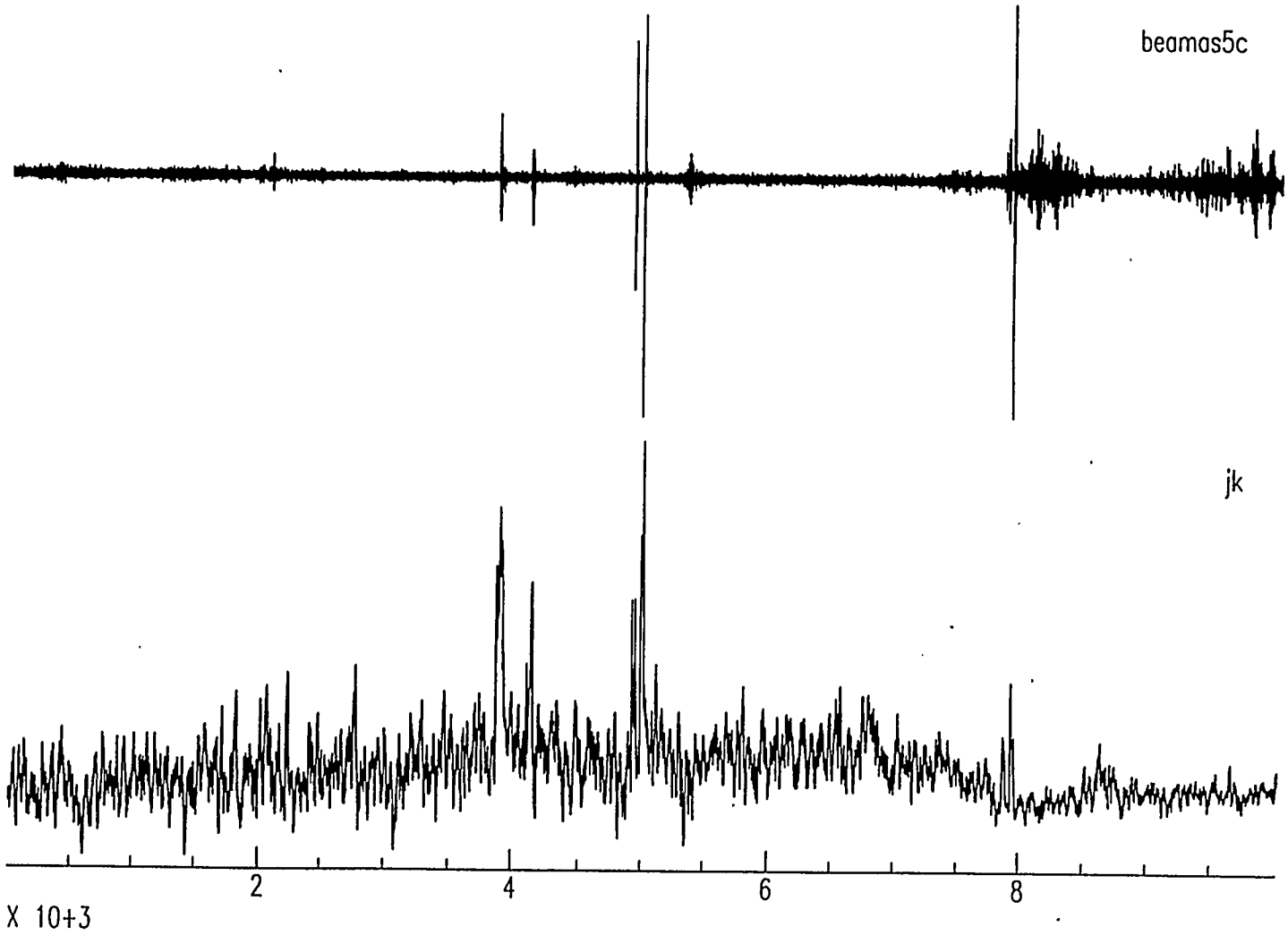

Beam of Filtered [AR] Data and F-detector Values

ENSCO, Inc.

CONCLUSIONS

- Each process represented can be easily automated:
  - Power detector
  - Lag Closure detector
  - F-Statistic detector
  - Bandpass filter
  - Autoregressive filter

- Power detector:
  - Limitations
  - Single channel (element or beam)
  - Threshold level not known in advance
  - Little improvement by filtering process

CONCLUSIONS

- **Lag Closure detector:**
  - Good detector
  - False alarm rate is relatively high
  - Need additional processing for onset time

- **F-Statistic detector:**
  - Good detector
  - Least number of false alarms/missed detections
  - Can detect secondary arrivals in the same signal
  - Accurate detection time

- **F-Statistic detector provides best results of evaluated list.**

F-STATISTICS: A TOOL FOR INFRASOUND SIGNAL DETECTION

Haydar J. Al-Shukri and Kevin D. Hutchenson

ENSCO, Inc.
445 Pineda Ct.
Melbourne, FL 32940

The infrasonic technique is one of the proposed methods for monitoring a Comprehensive Test Ban Treaty. For such a treaty to be effective, reliable technologies must be developed to detect and identify low-yield explosions. Under the proposed International Monitoring System, approximately 60 infrasonic arrays are expected to detect potential atmospheric explosions.

This paper presents a new and simple approach to analyze the F-statistic function, a multi-channel statistical procedure which uses the coherency of signals recorded by an array as a detection criteria. The new approach is to use the derivative of the F-statistic in the detection process. The derivative seems to offer a dramatic improvement to the detection capability even during periods of high energy microbaroms. The efficiency of this approach was evaluated according to the following characteristics: (1) the capability of being operated in an automatic mode, (2) the number of missed detection, (3) the number of false alarms, (4) the capability of processing data in a real time fashion, and (5) simplicity and flexibility of the tuning process.

A suite of synthetic and real data were used for the evaluation process. Data were collected which contain a variety of infrasonic signals and noise. Real data were collected from arrays at St. George, Utah; Los Alamos, New Mexico (both are small aperture arrays); Windless Bight, Antarctica; and Fairbanks, and Alaska. Results indicate that if a carefully selected pre-detection process (bandpass filter or autoregressive filter) is used, the derivative of the F-statistic may provide the best approach for detecting coherent signals from array data. A low coefficient (2 or 3) autoregressive filter was found to be an effective pre-detection process.

F-Statistics: A Tool for Infrasonic Signal Detection

Haydar J. Al-Shukri and K.D. Hutchenson
ENSCO, Inc., Melbourne, Florida
August, 1997

F-Detector for Infrasonic Signals

$$F = \frac{T(C-1)}{C(T-1)} \frac{\sum_{i=1}^{T}\left[\sum_{c=1}^{C} X_{ct}\right]^2}{\sum_{i=1}^{T}\sum_{c=1}^{C} X_{ct}^2 - \frac{1}{C}\sum_{i=1}^{T}\left[\sum_{c=1}^{C} X_{ct}\right]^2} \quad (1)$$

$$F = \frac{T(C-1)}{C(T-1)} \frac{\sum_{i=1}^{T}\left[\sum_{c=1}^{C} X_{ct}\right]^2 - \frac{1}{T}\left[\sum_{i=1}^{T}\sum_{c=1}^{C} X_{ct}\right]^2}{\sum_{i=1}^{T}\sum_{c=1}^{C} X_{ct}^2 - \frac{1}{C}\sum_{i=1}^{T}\left[\sum_{c=1}^{C} X_{ct}\right]^2} \quad (2)$$

F = statistical value for the F-detector for the time window

T = number of points in the window

C = number of stations in the array

X = time series.

ENSCO, Inc.

Major Problems in Infrasonic Data

- **Coherent Noise**
  - Long Duration
  - High Amplitude
- **Wind Noise**
  - Random
  - Short Duration (bursts)
  - High Amplitude

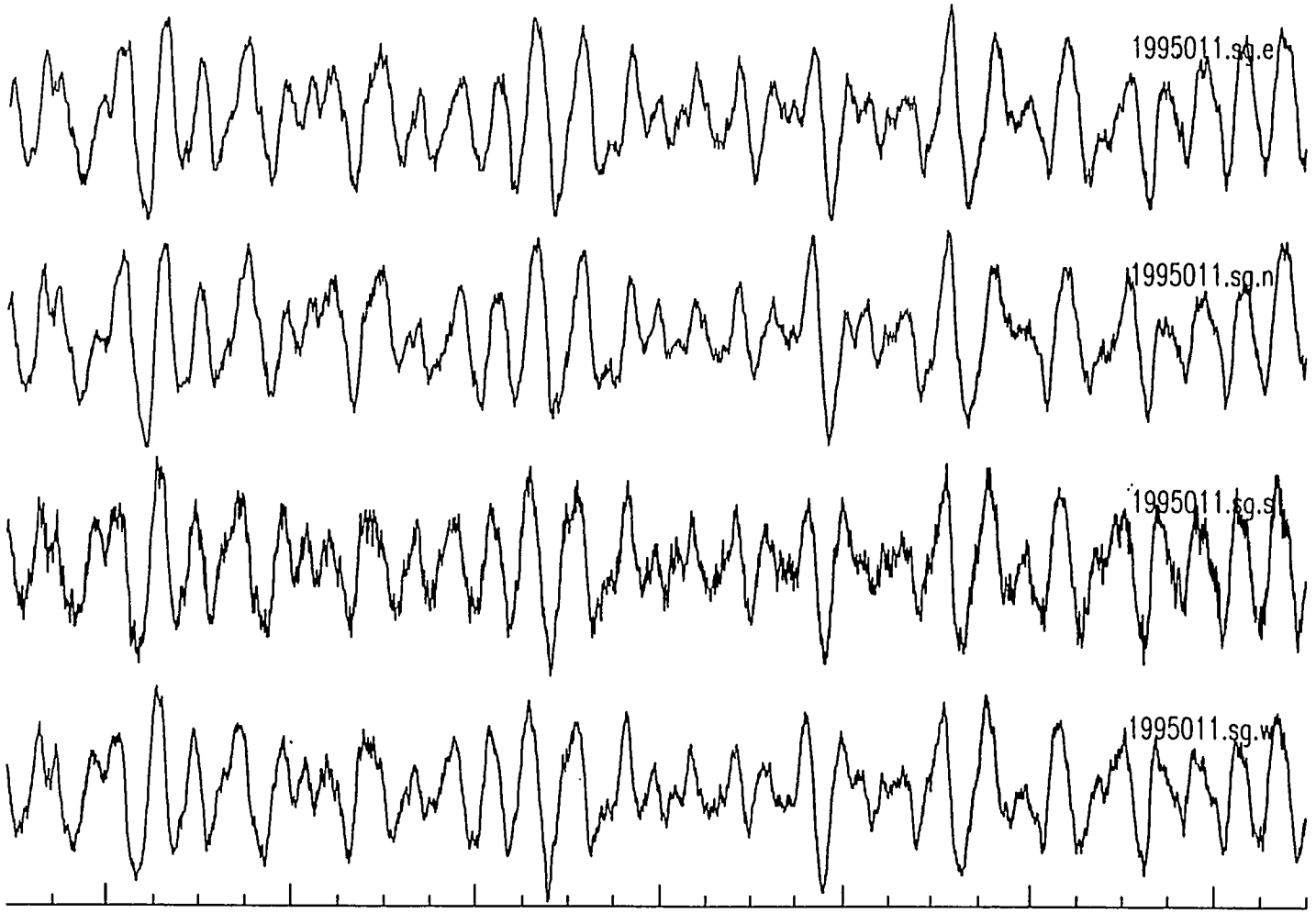

Coherent Microbaroms at St. George Arry

ENSCO, Inc.

ENSCO, Inc.

F-Statistics: Requirements

- ✧ Array Data (multichannel process)
- ✧ Infinite Velocity Shift (Best Beam)
- ✧ Pre-detection Signal Enhancement

ENSCO, Inc.

Why the F-Statistic Detector?

- ✧ Detects Coherency (only)
- ✧ Works on a Small Number of Channels
- ✧ Small Number of False Alarms
- ✧ Small Number of Missed Detections
- ✧ Computationally Fast
- ✧ Can Be Automated
- ✧ Potentially an Accurate Process for Onset-Time Determination

Typical Infrasonic Data

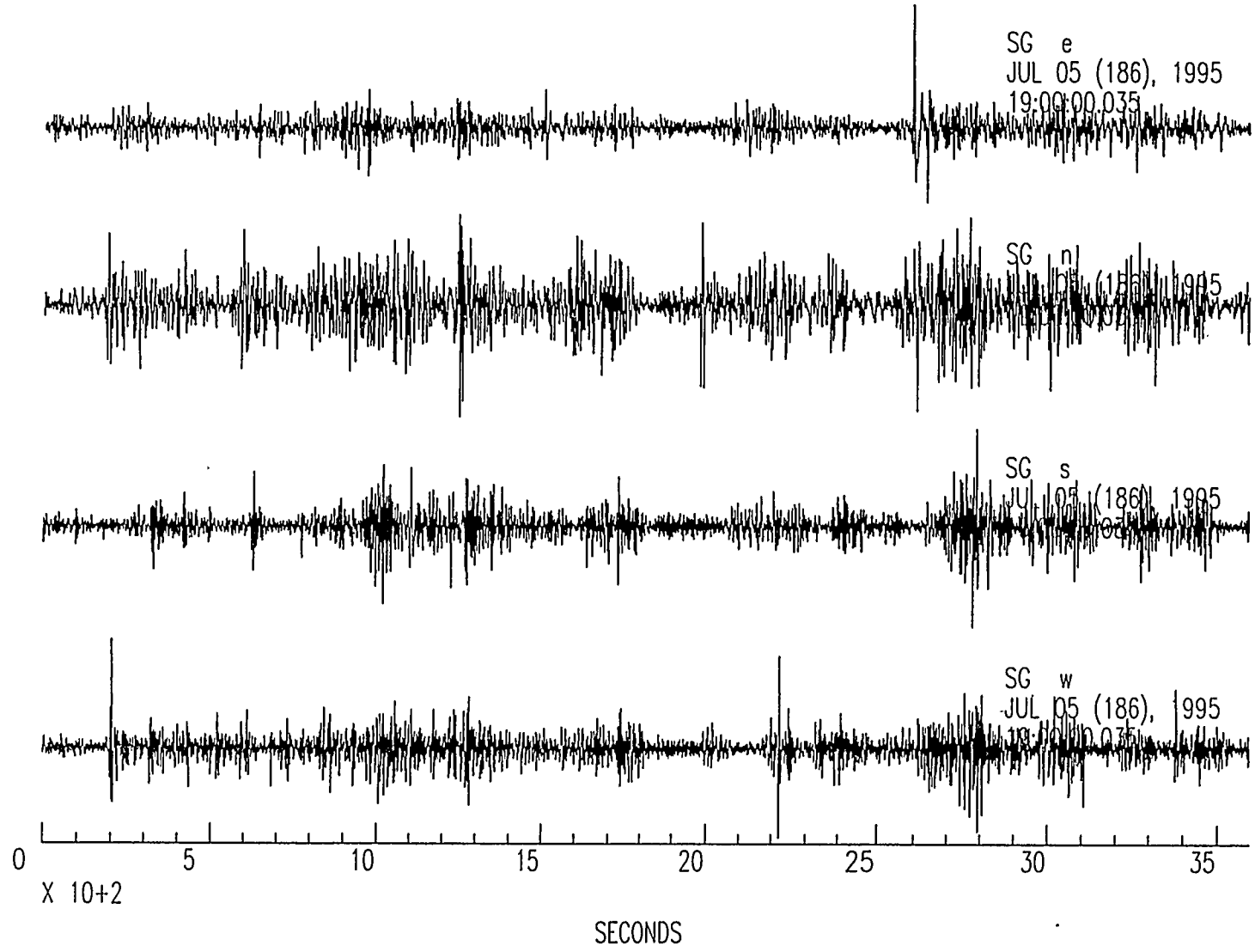

ENSCO, Inc.

Raw Data and Its Beam, SG Array

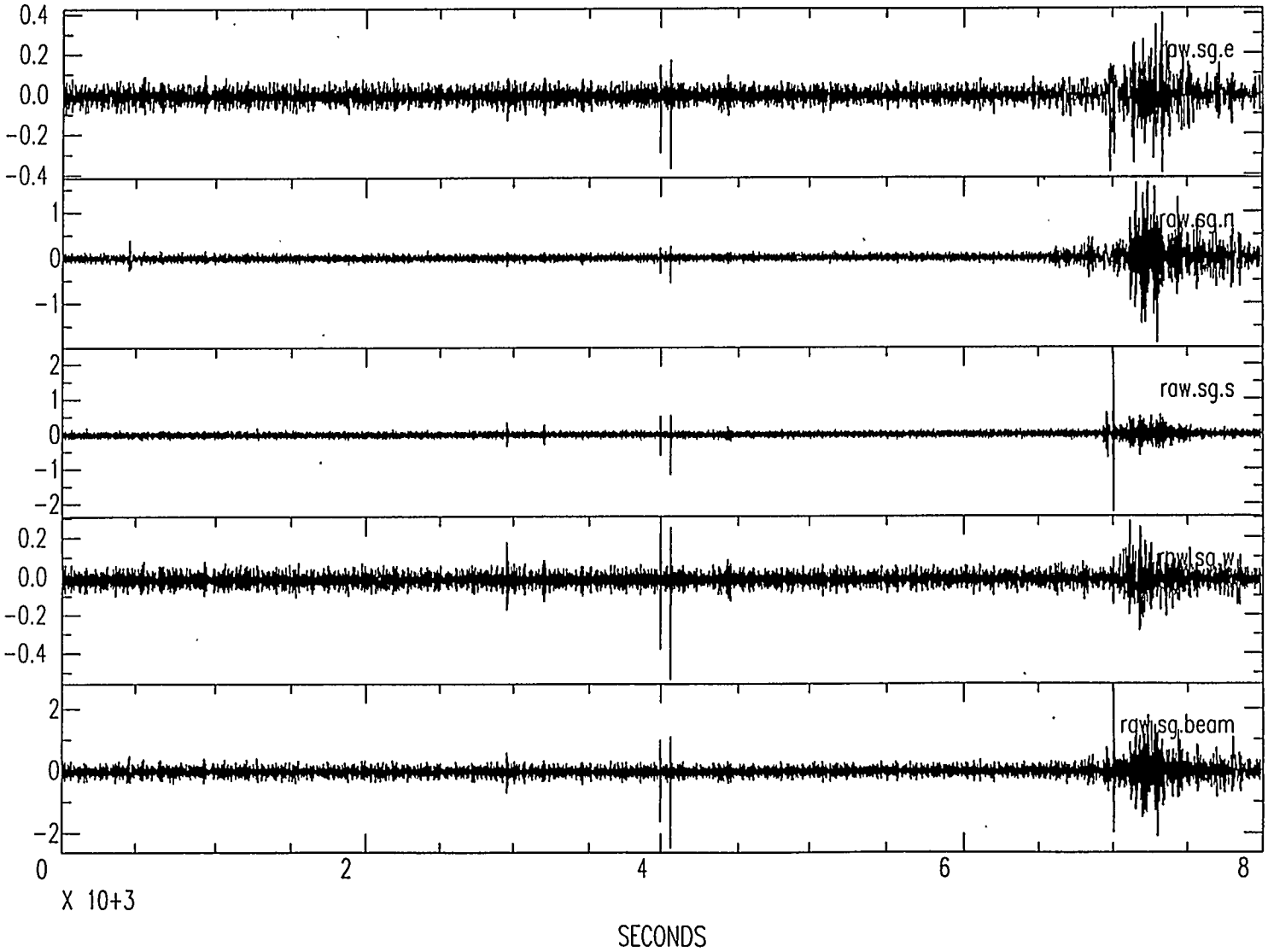

ENSCO, Inc.

F-detector: Raw Data

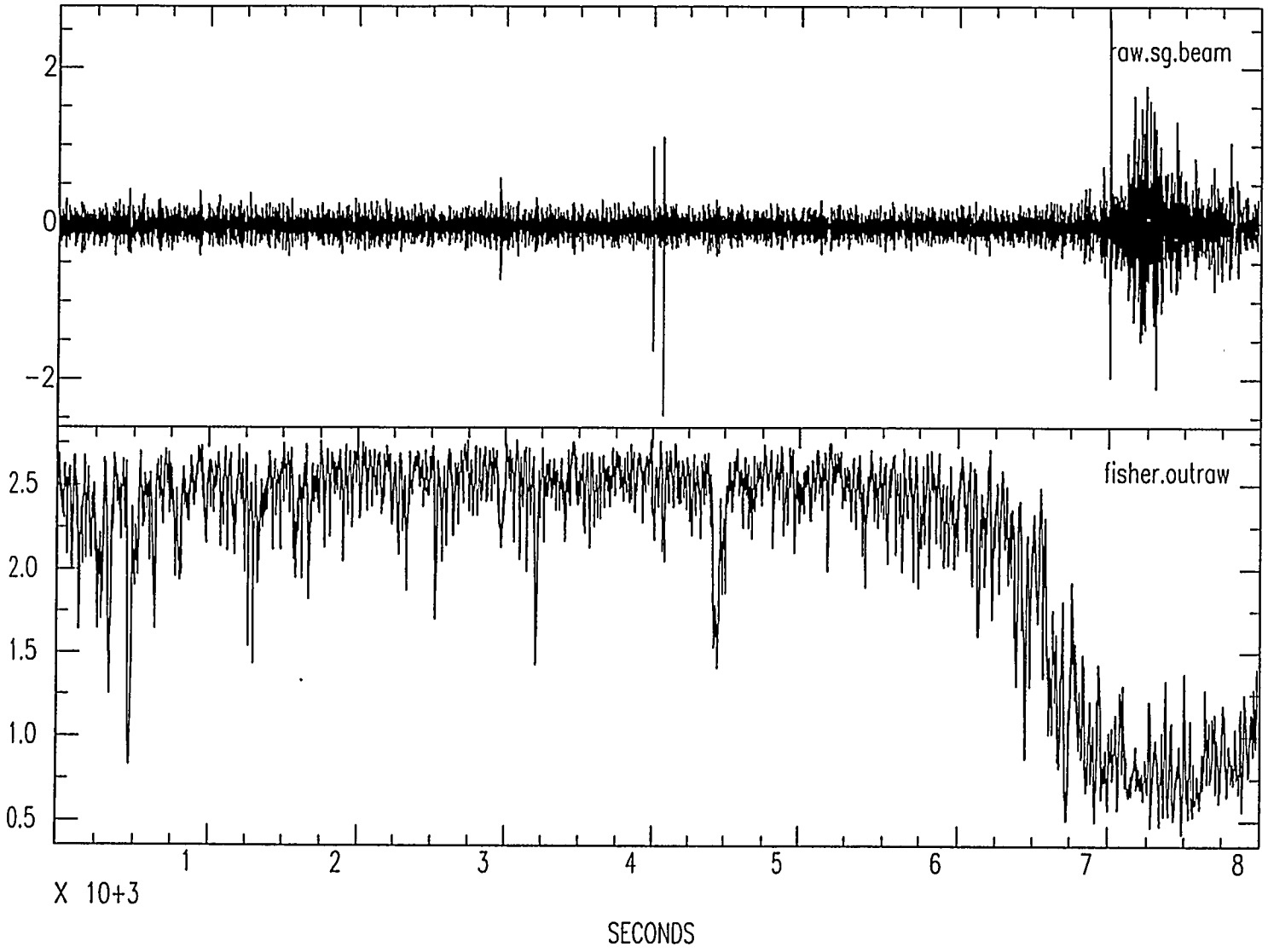

ENSCO, Inc.

AR Infrasonic Data Form SG Array

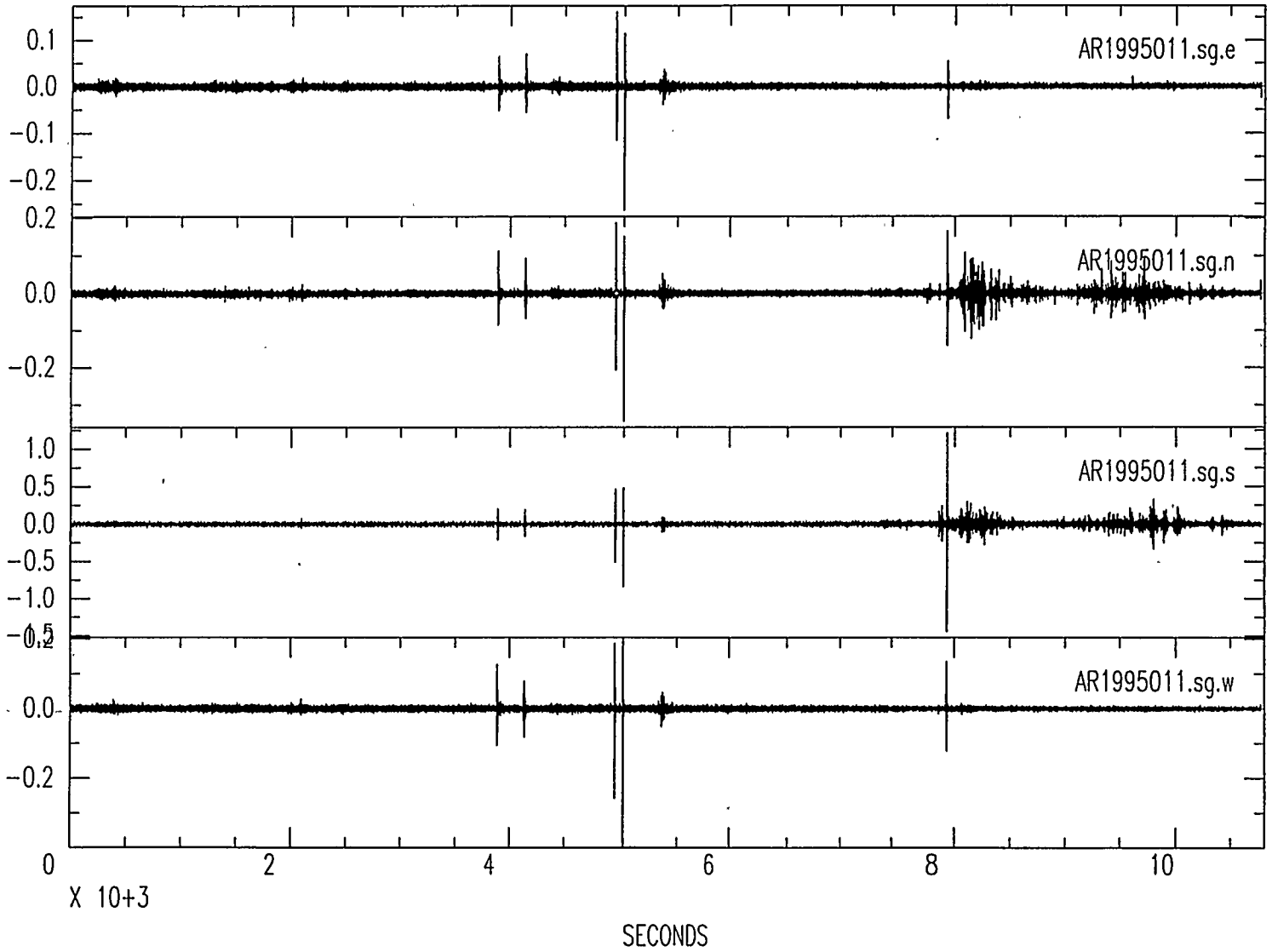

ENSCO. Inc.

Raw, Band-Pass, and AR Data

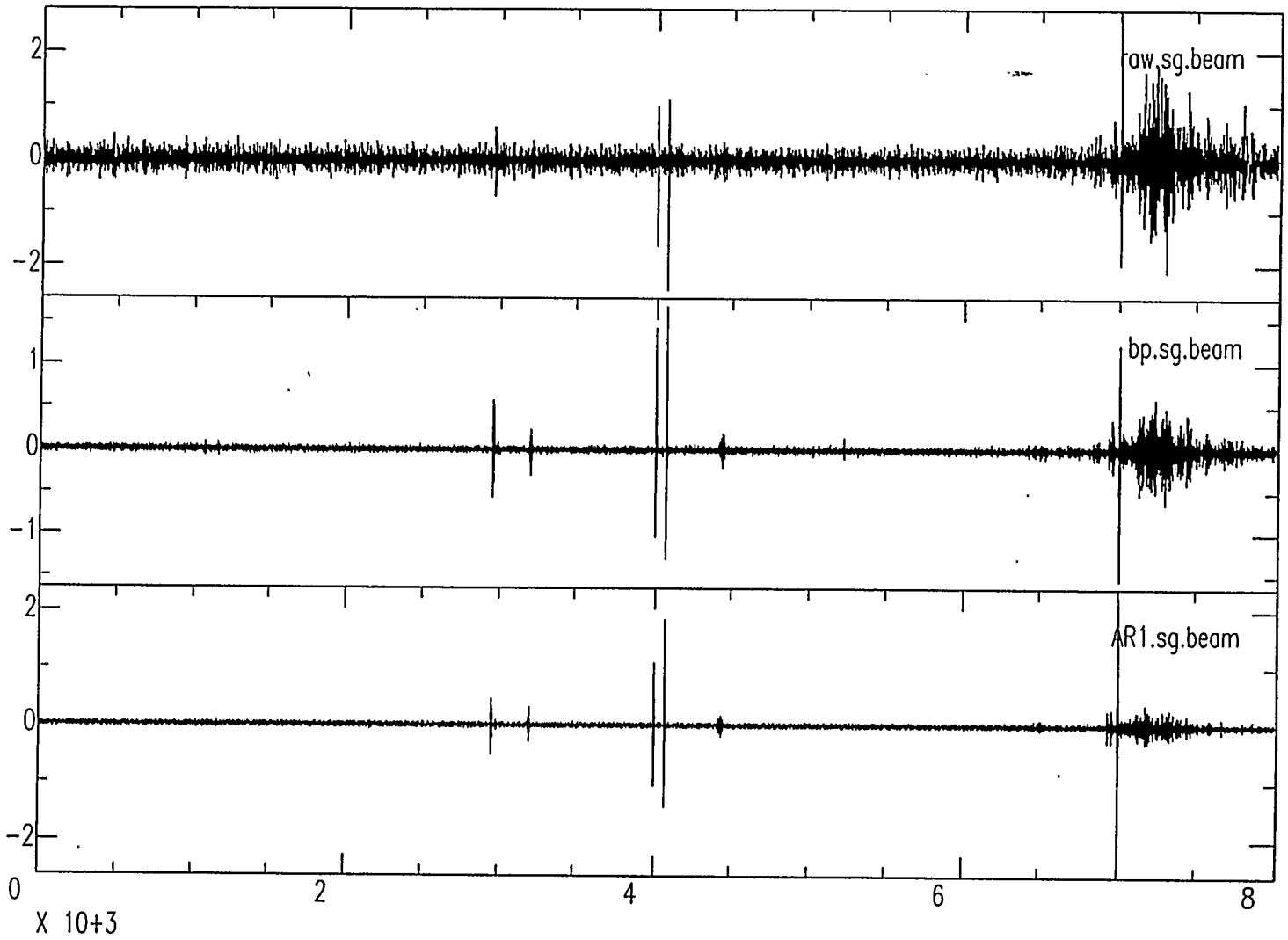

ENSCO, Inc.

Advantages and Disadvantages of:

- ✧ Autoregressive (AR) Filter
- ✧ Bandpass (BP) Filter

BP and AR

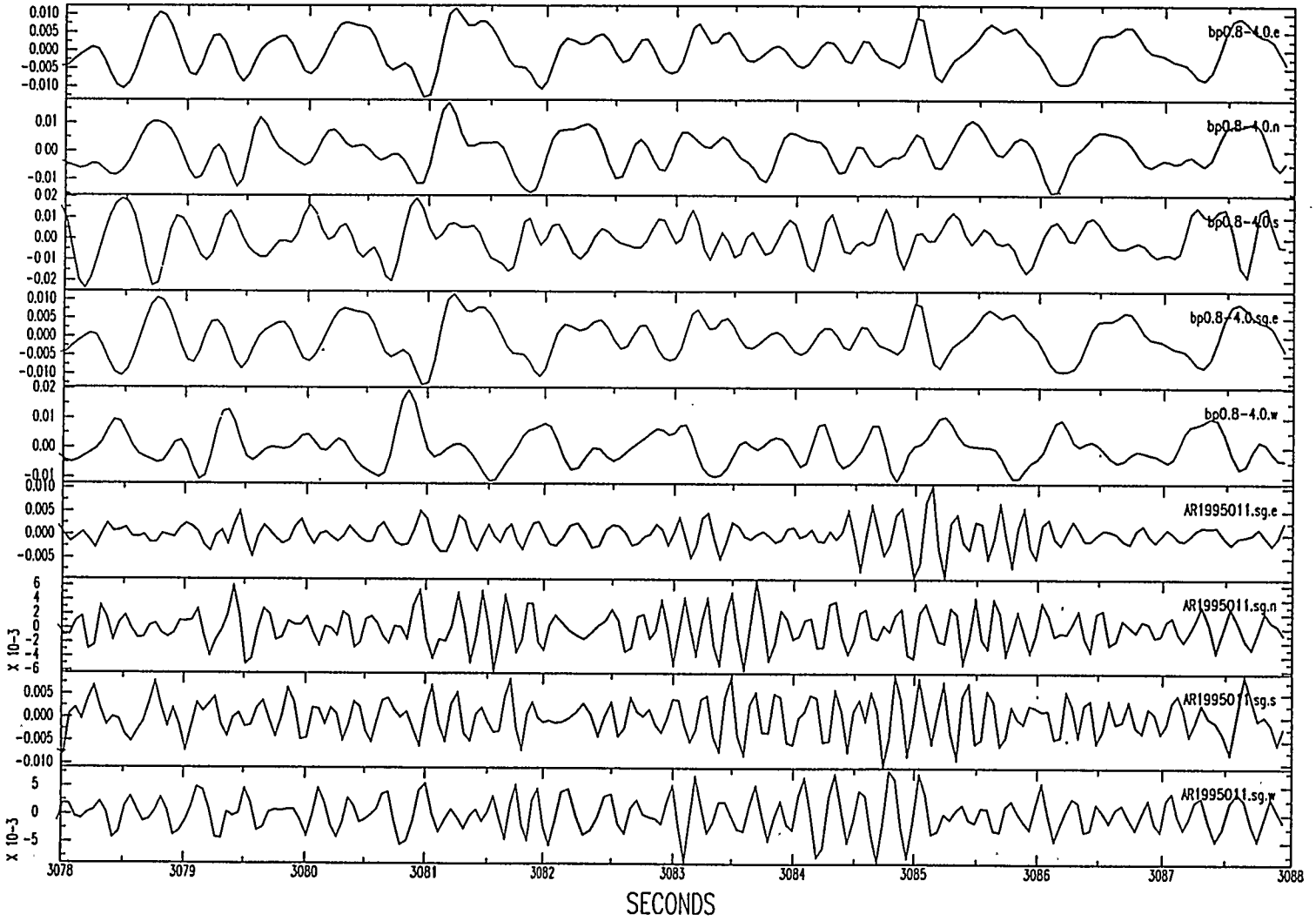

ENSCO, Inc.

BP and AR

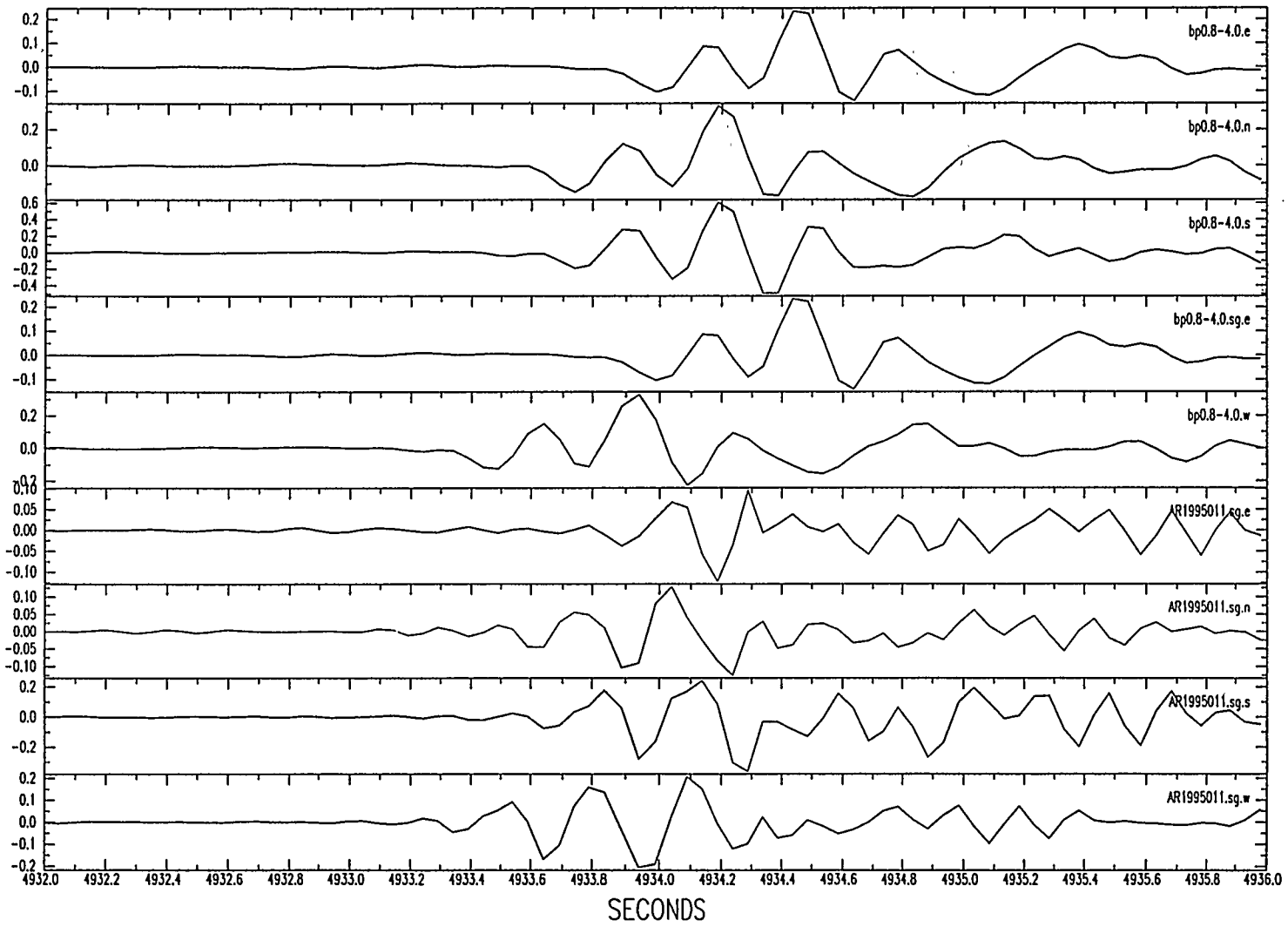

ENSCO, Inc.

F-statistics: AR Data and BP Data

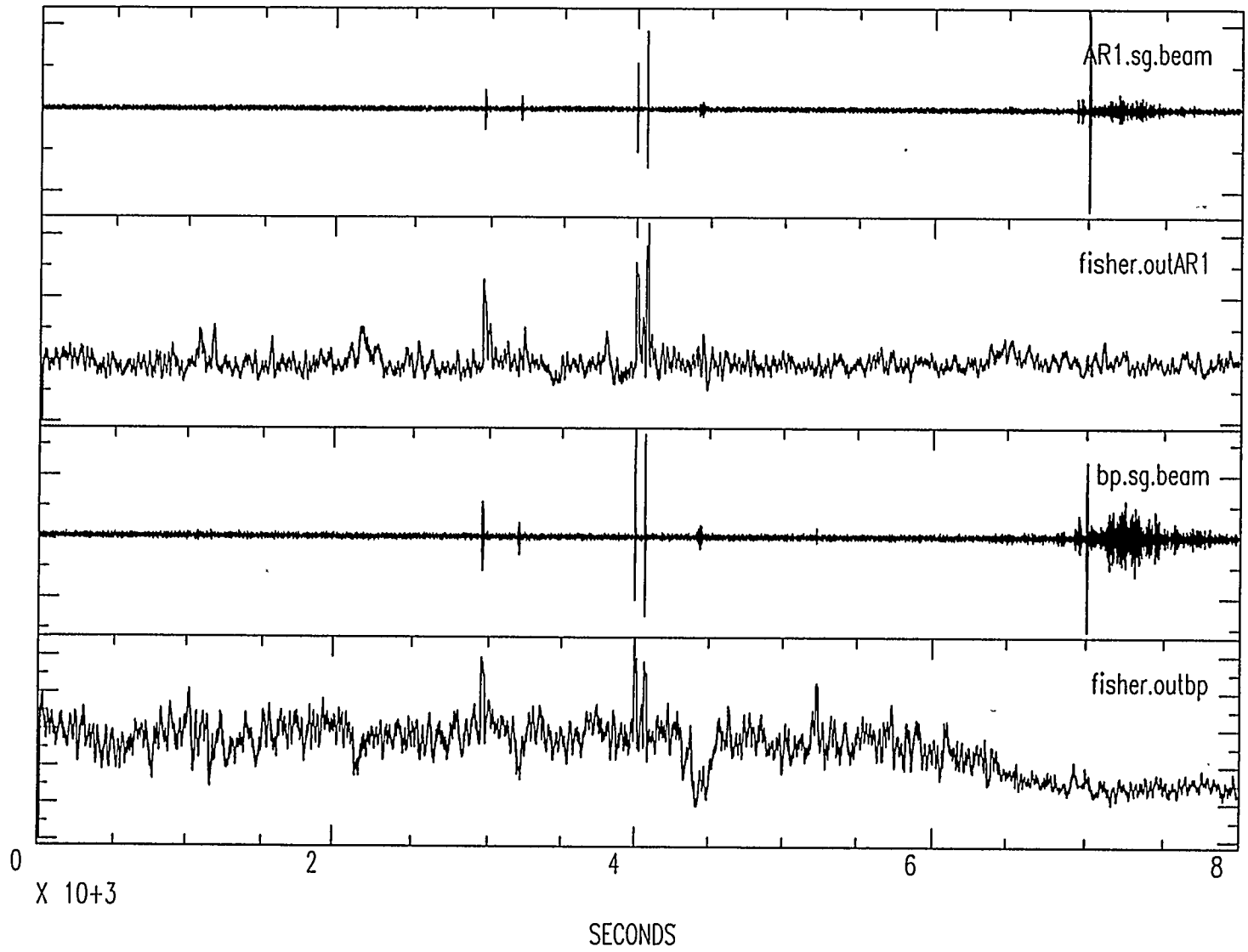

ENSCO, Inc.

Raw, Band-Pass, and AR Data

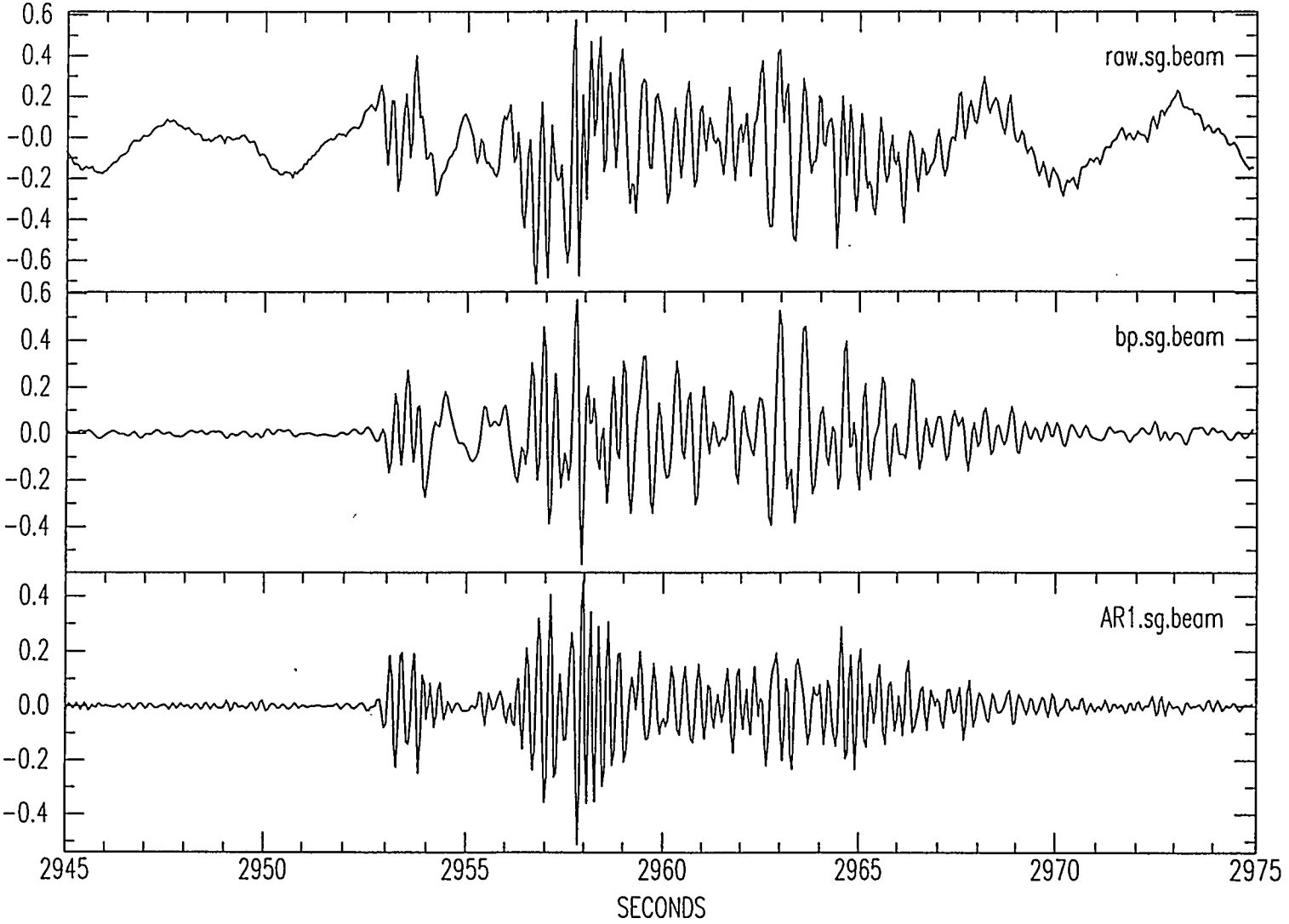

ENSCO, Inc.

Onset-Time Estimation

- ✧ Uses the Derivative of the F-Statistic Function
- ✧ Uses a Simple Power Detector

F-detector: Raw Data

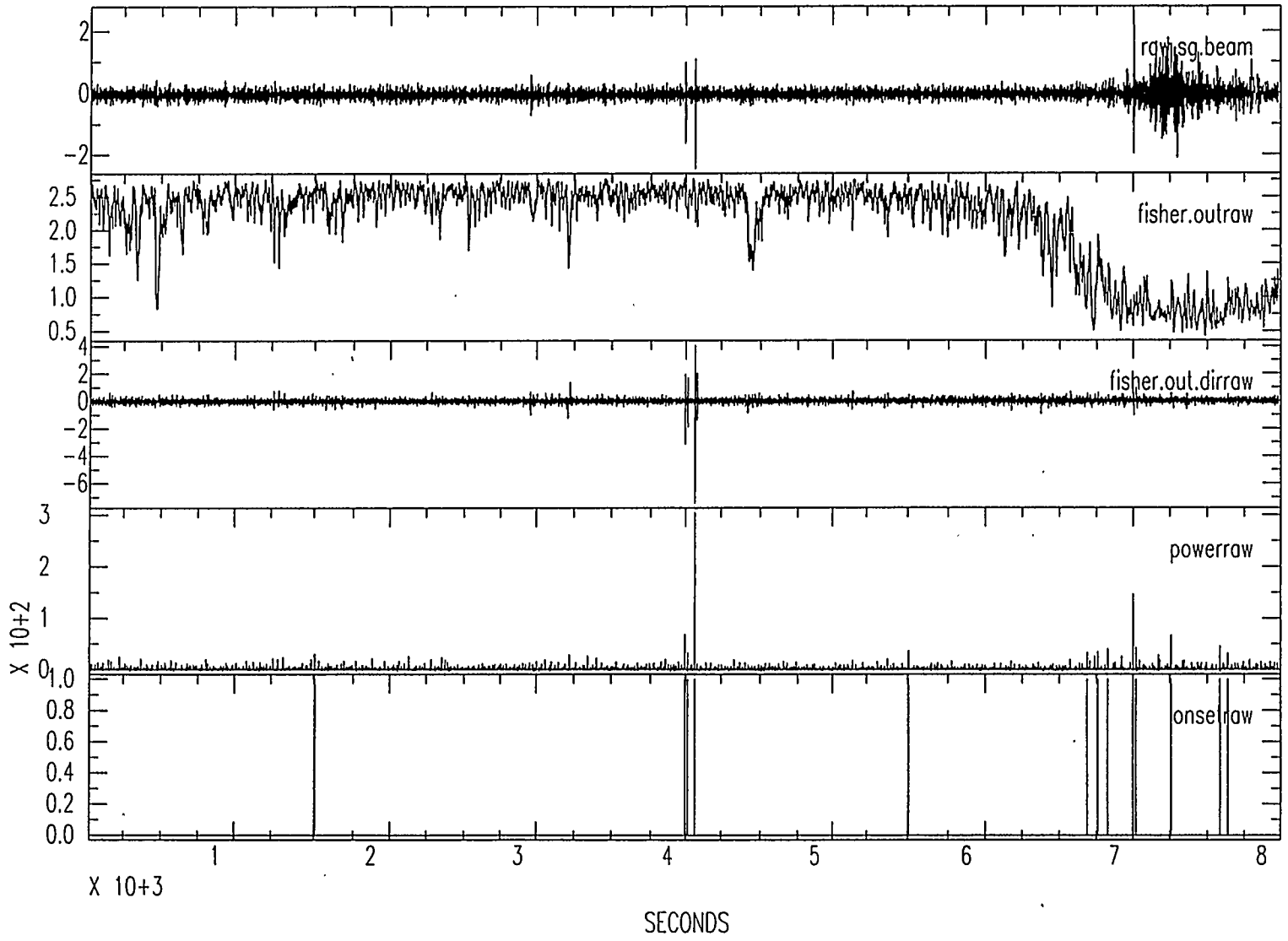

ENSCO. Inc.

F-detector: BP Data

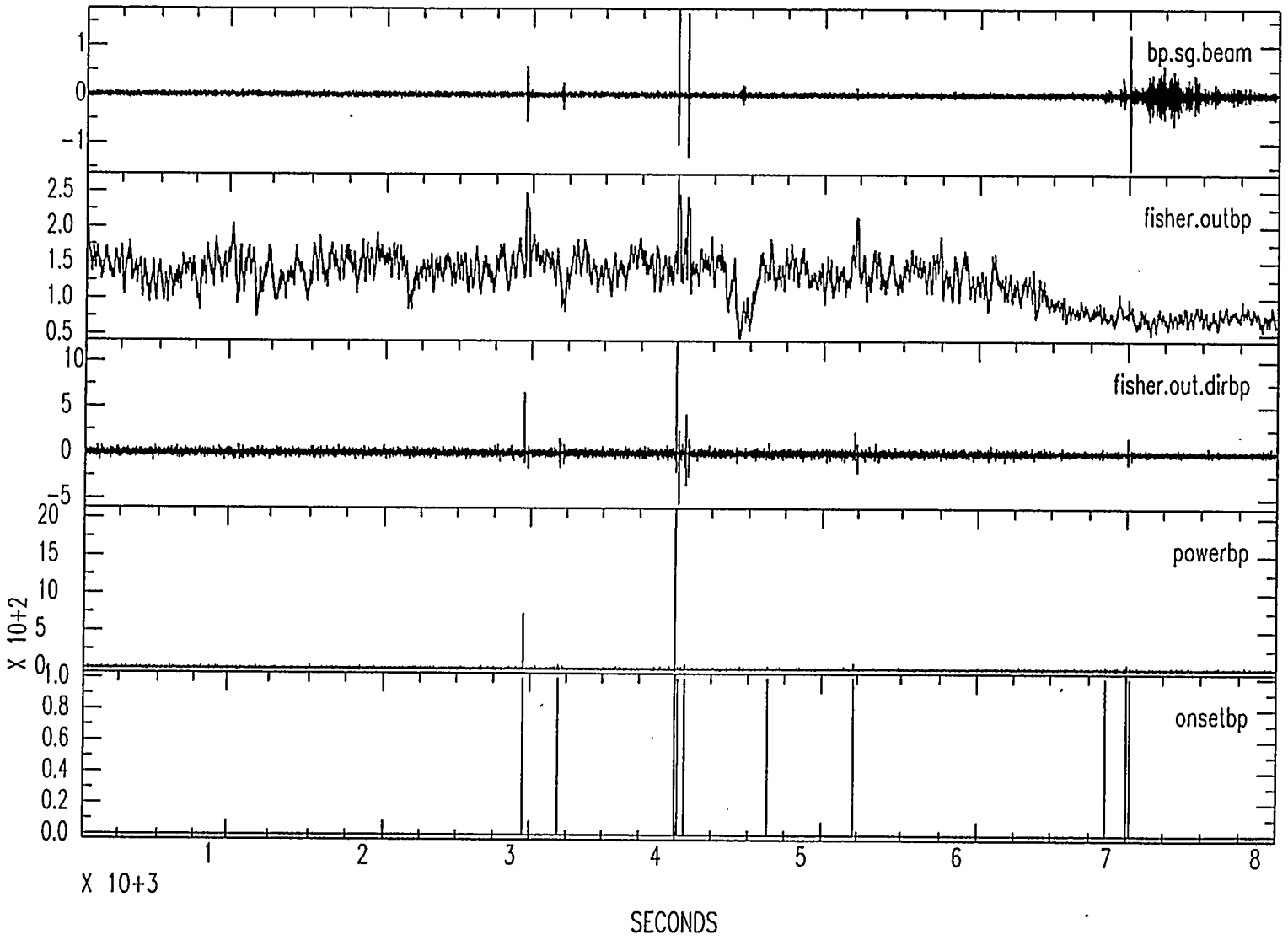

ENSCO, Inc.

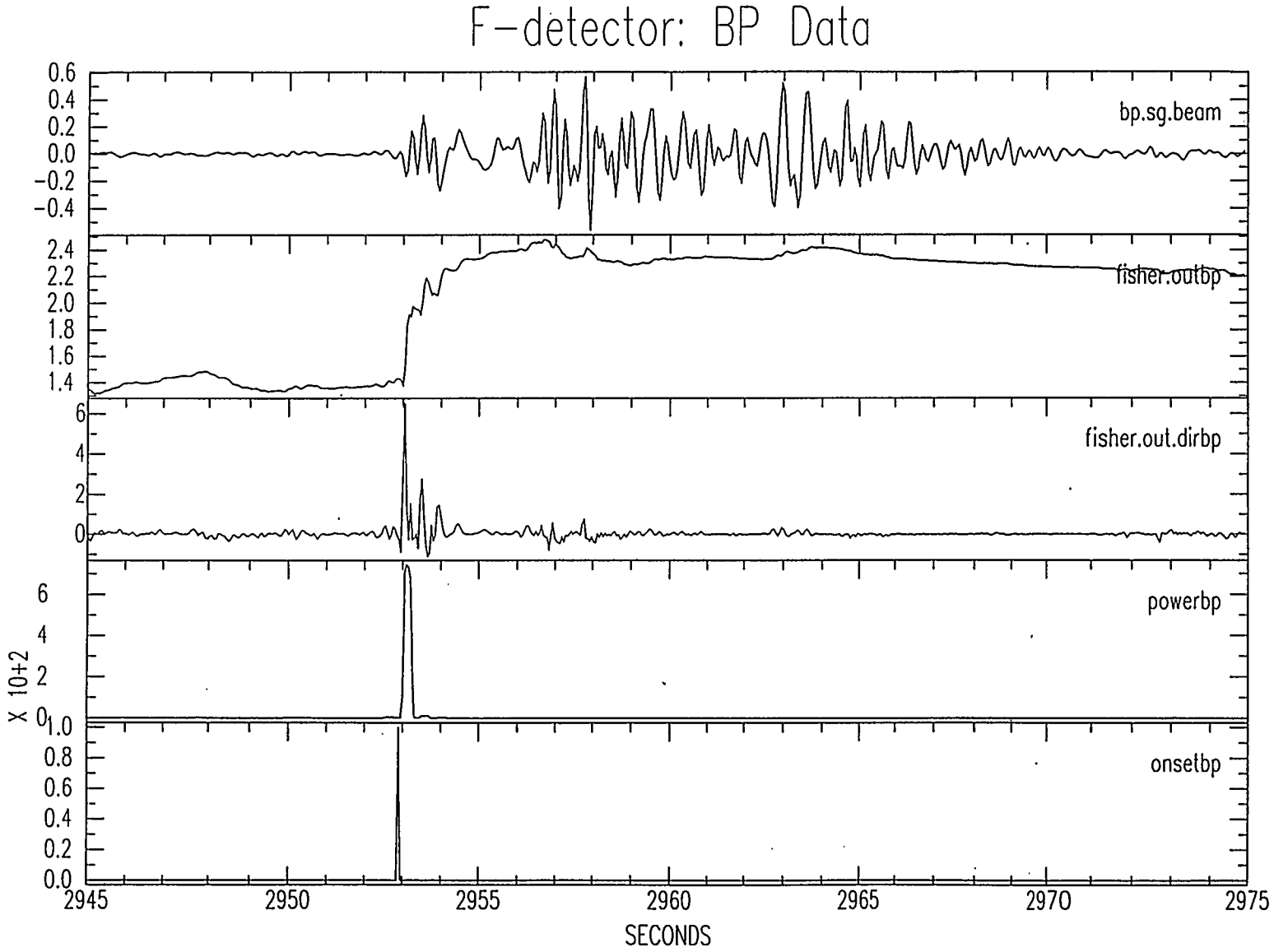
F-detector: BP Data
bp.sg.beam
fisher.outbp
fisher.out.dirbp
powerbp
onsetbp
X 10+2
SECONDS
2945
2950
2955
2960
2965
2970
2975

ENSCO, Inc.

F-detector: BP Data

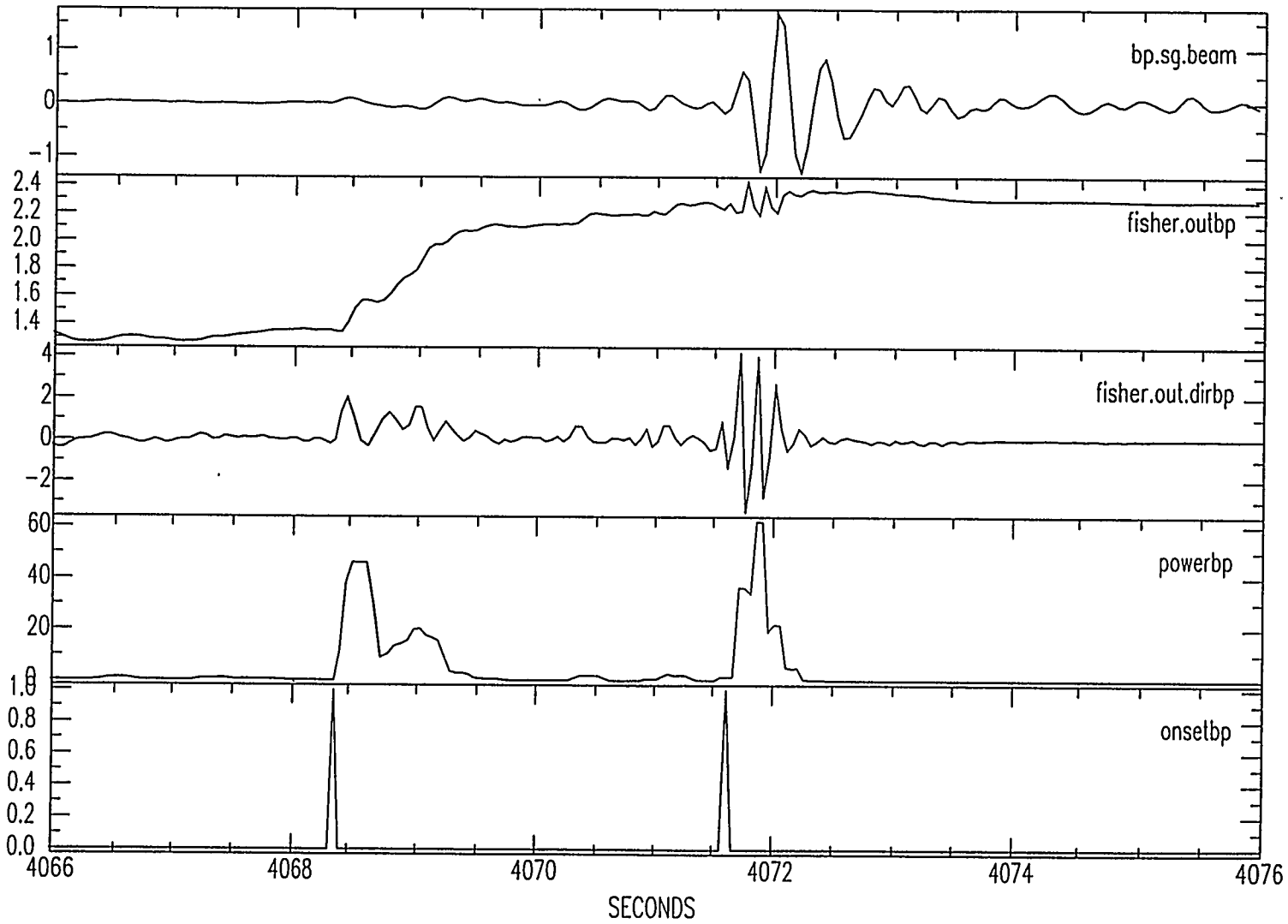

ENSCO, Inc.

F-detector: AR Data

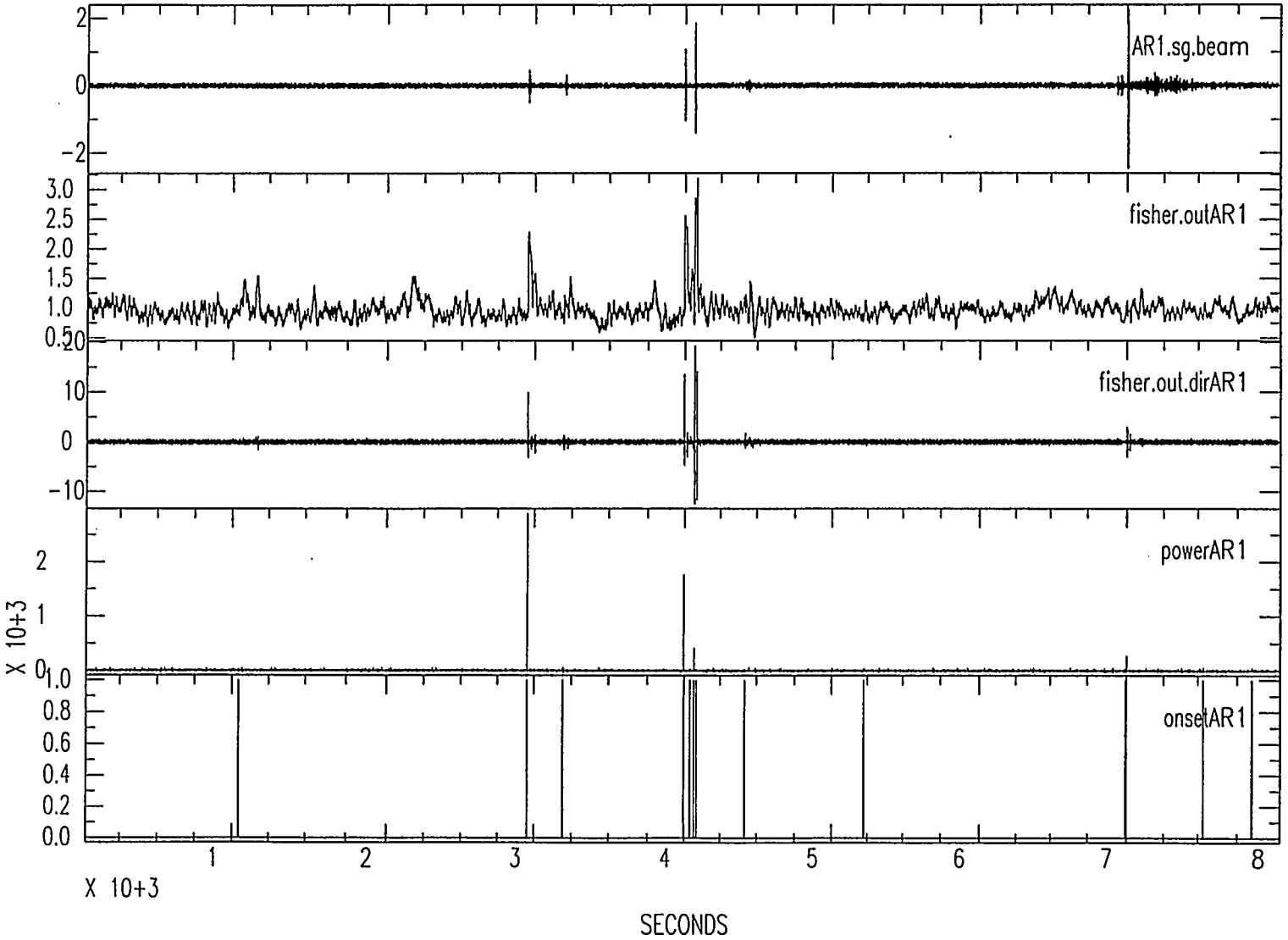

ENSCO, Inc.

F-detector: AR Data

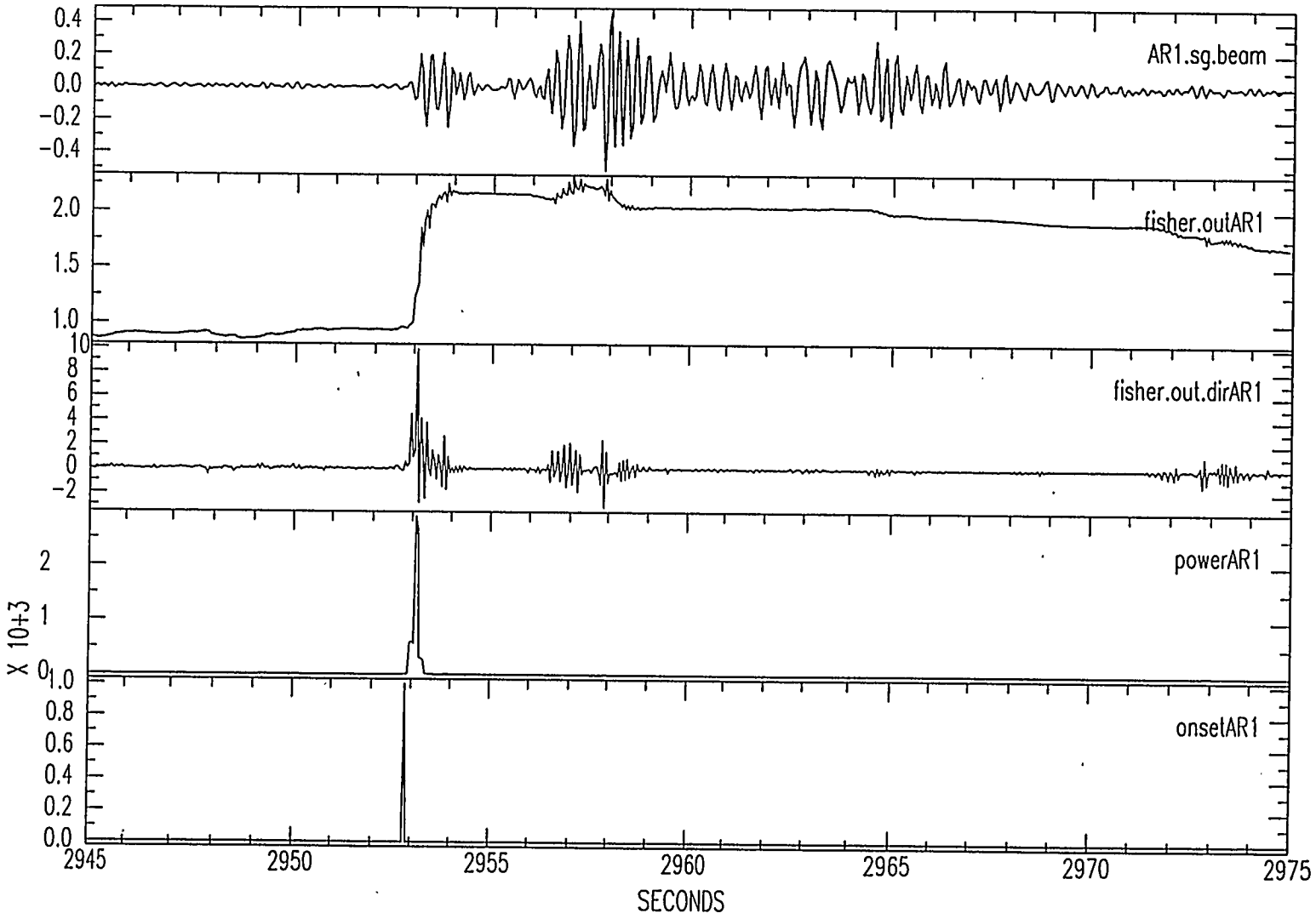

ENSCO, Inc.

F-detector: Onset-time Estimation

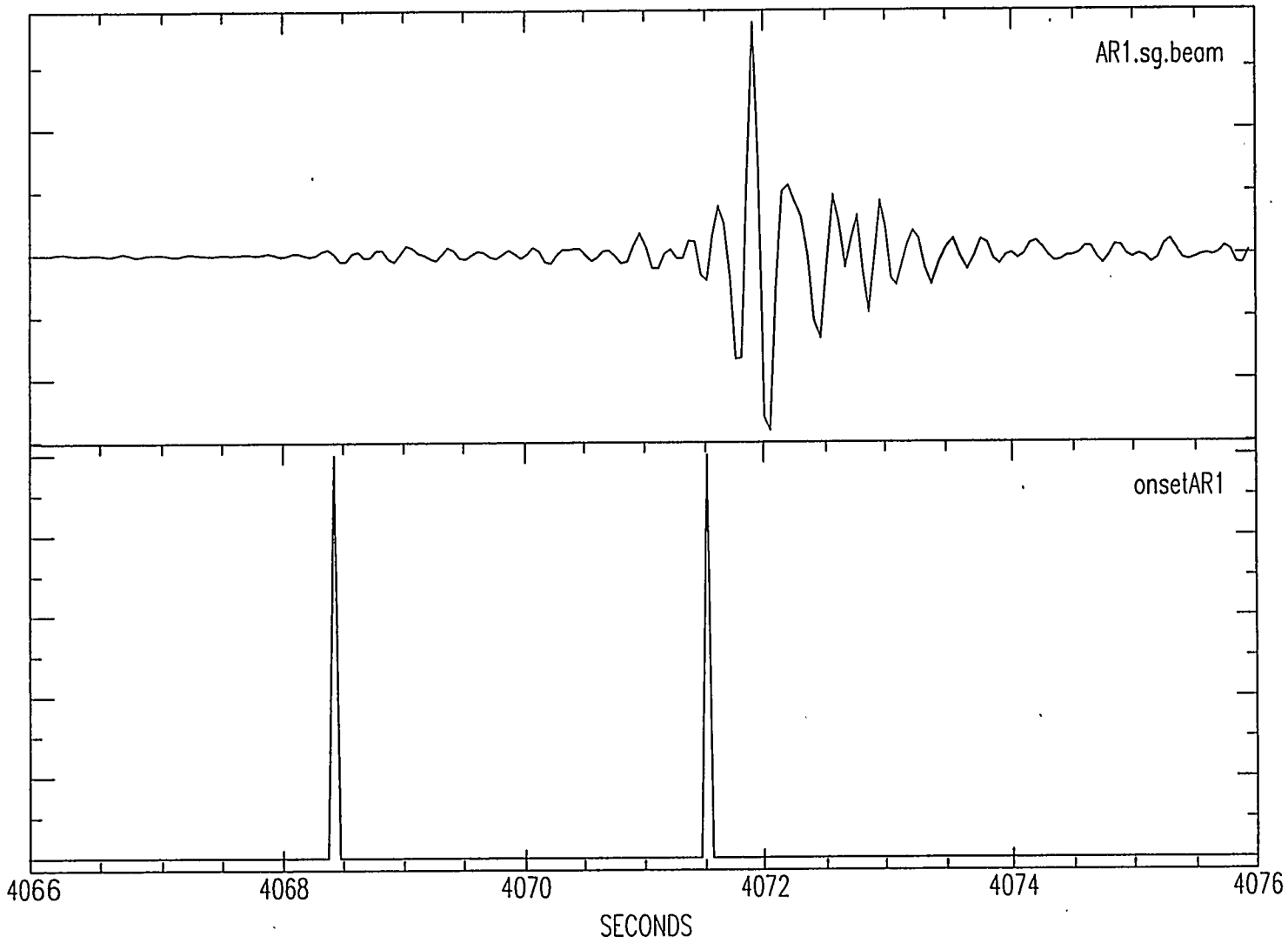

ENSCO, Inc.

ENSCO, Inc.

Examples

- Minuteman Missile Demolition
- Antarctica Data
- Nuclear Tests
  - Tanana
  - Chetco

SG Array Data [raw]: Minuteman Missile Demolition

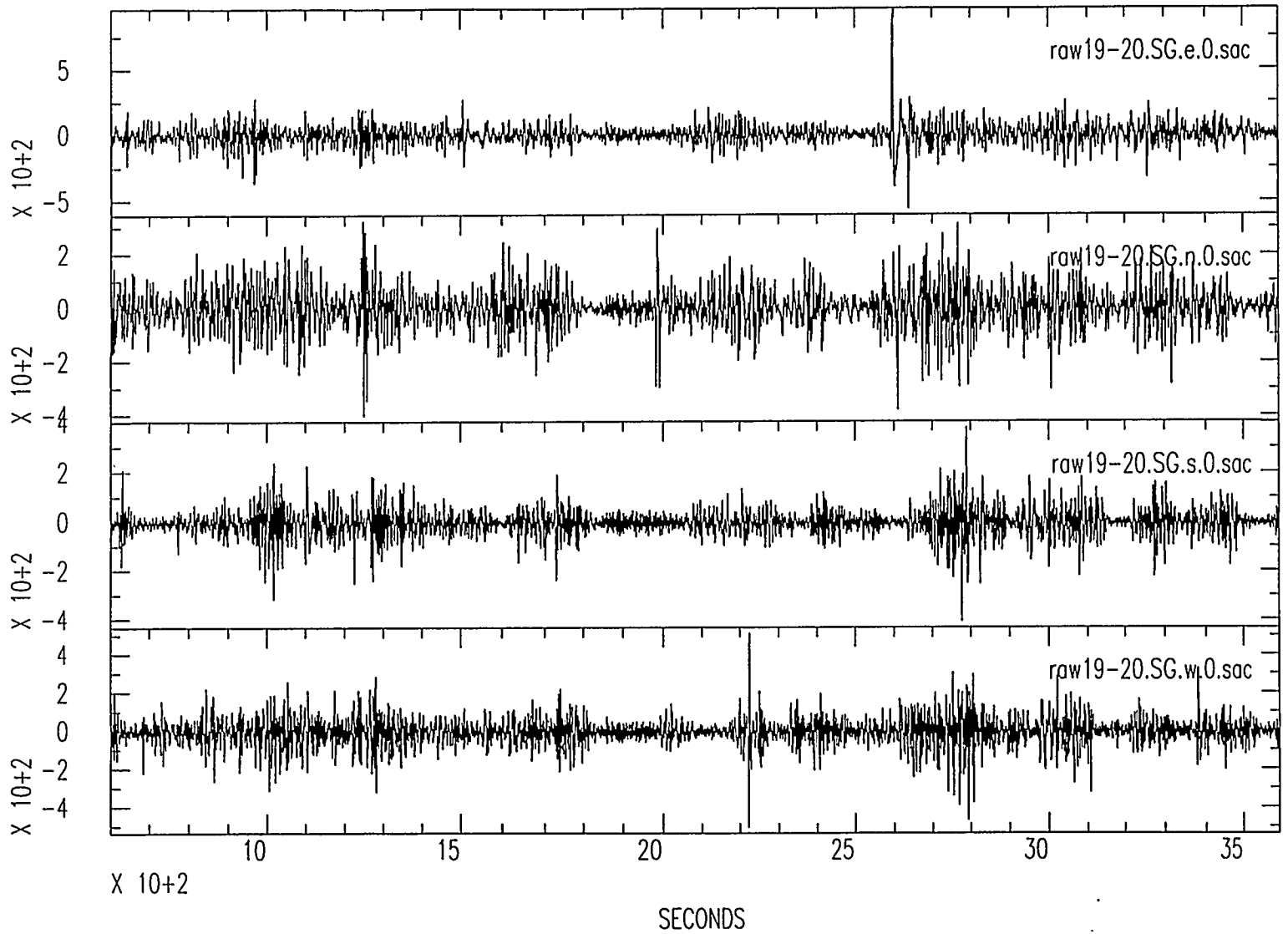

ENSCO, Inc.

SG Array Data [AR]: Minuteman Missile Demolition

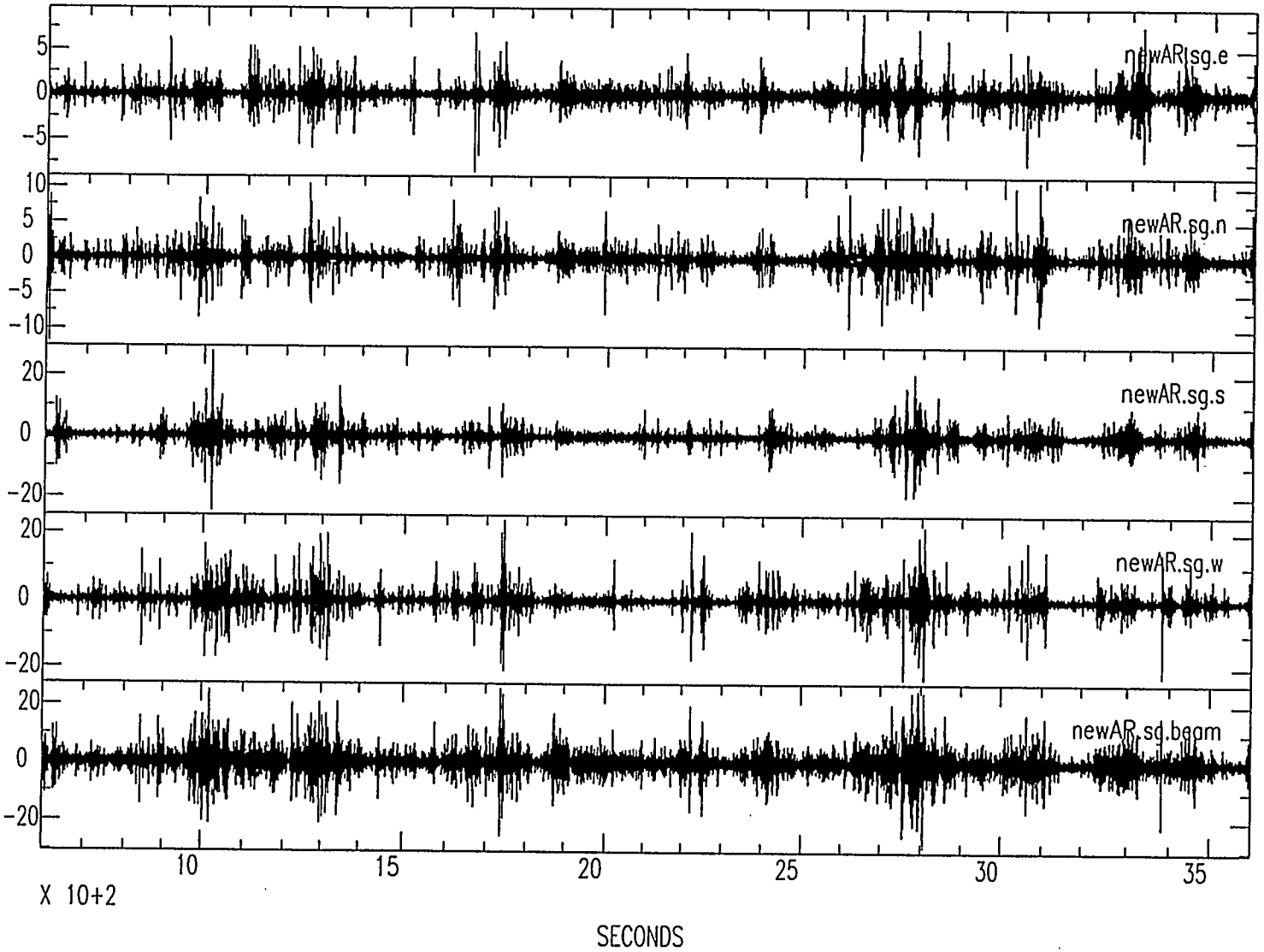

ENSCO, Inc.

F--detector: Minuteman Missile Demolition Signal [AR]

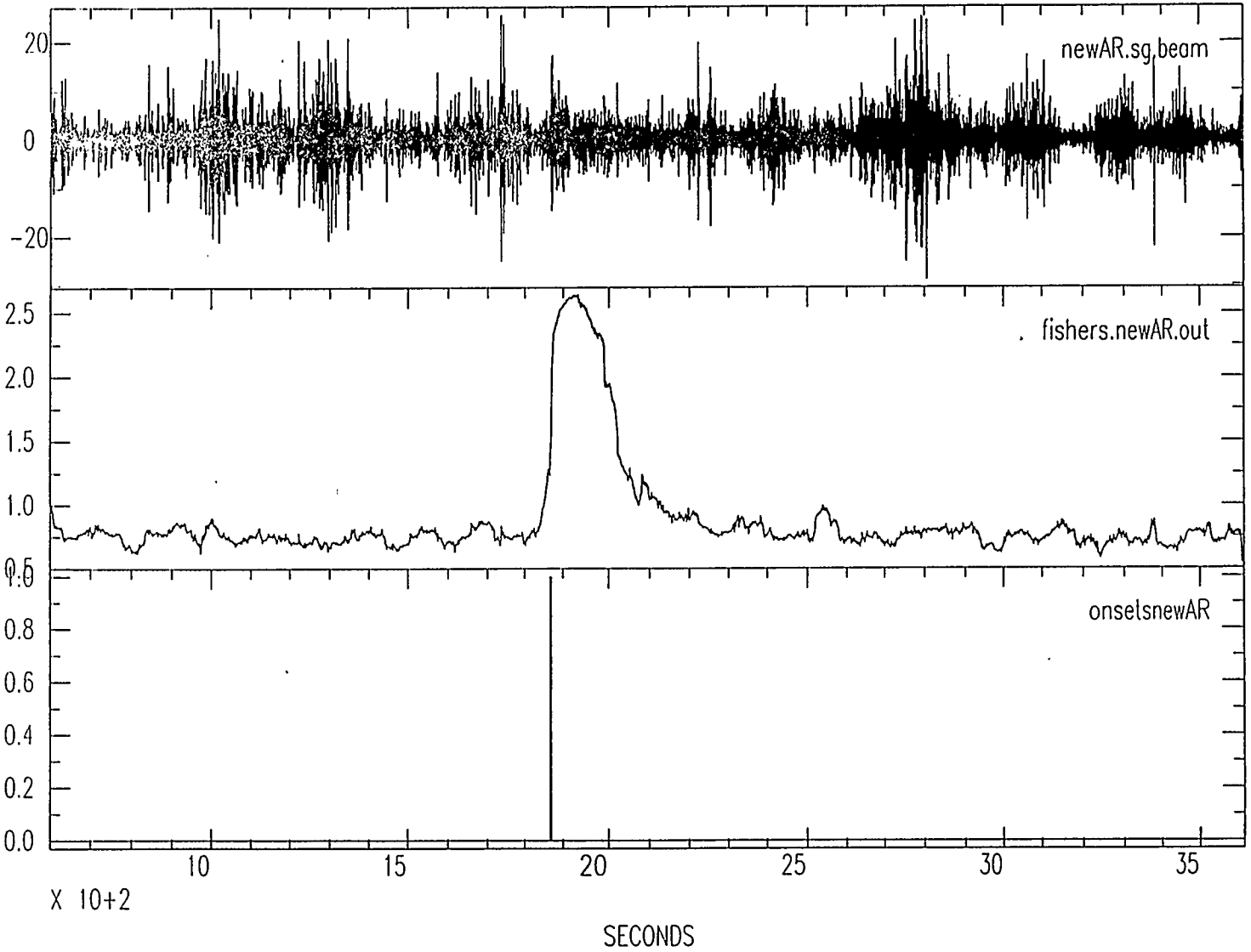

ENSCO, Inc.

F-detector: Minuteman Missile Demolition Signal [BP]

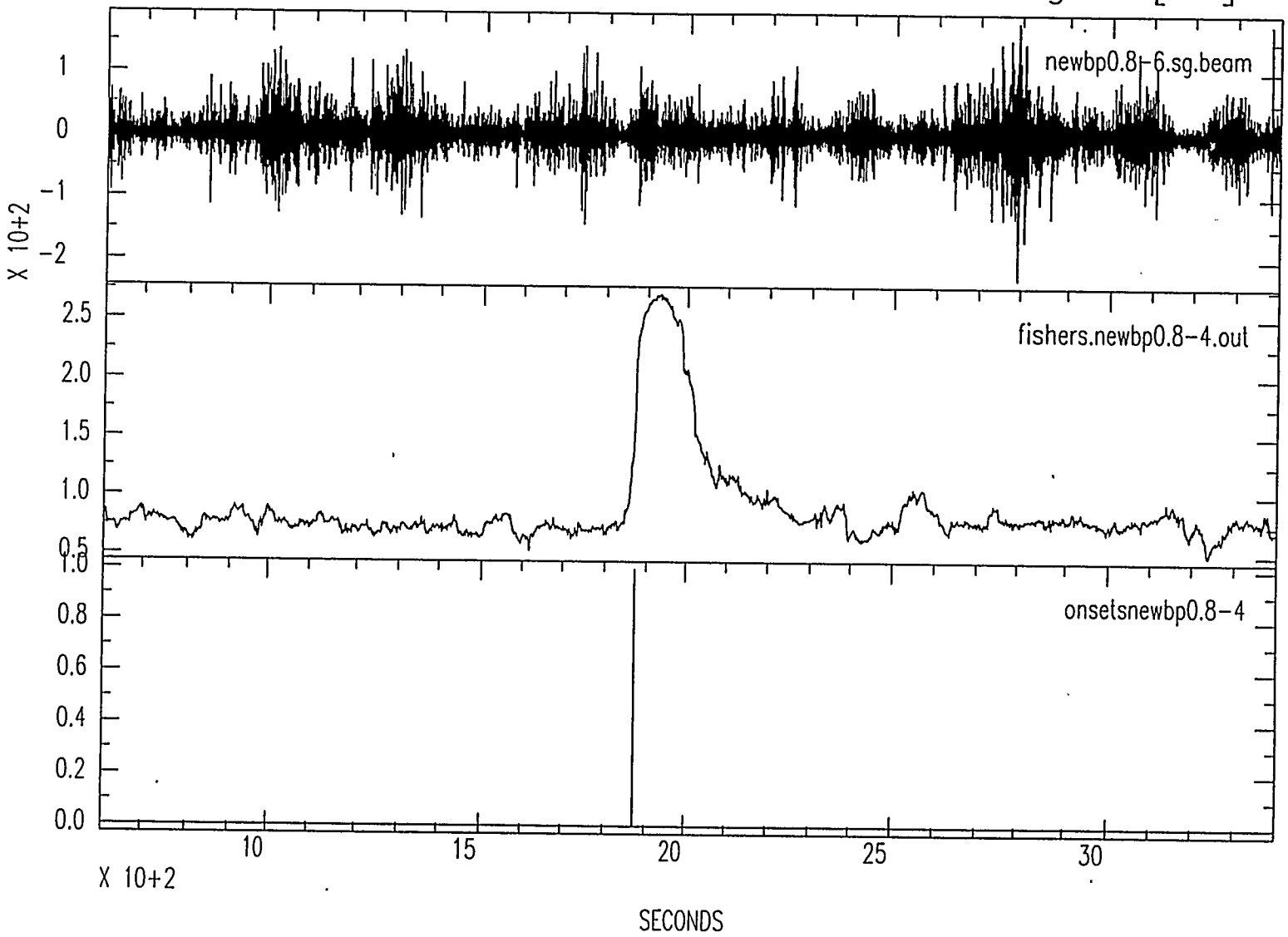

ENSCO, Inc.

F-detector: Minuteman Missile Demolition Signal [BP]

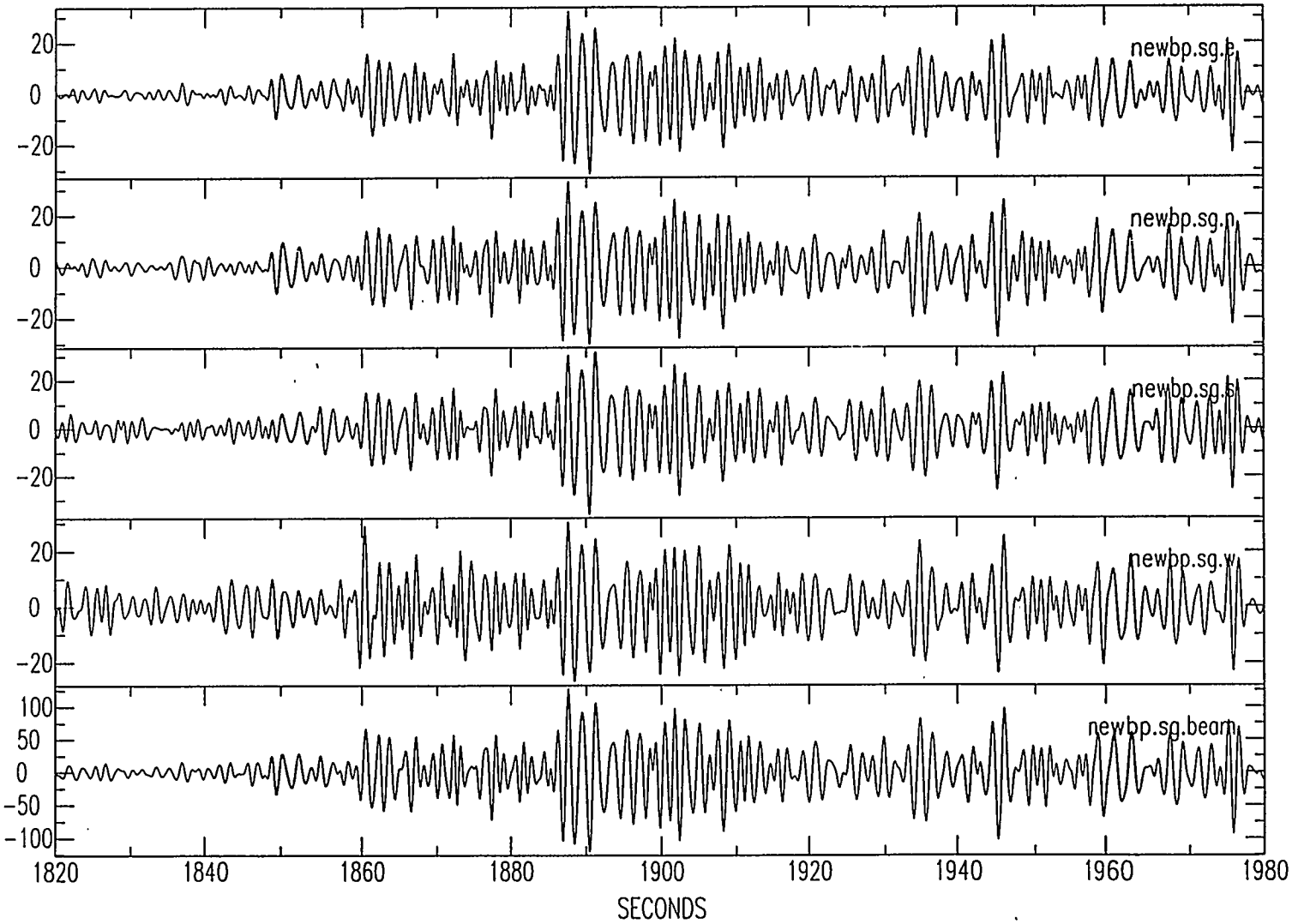

ENSCO, Inc.

Data from Antarctica

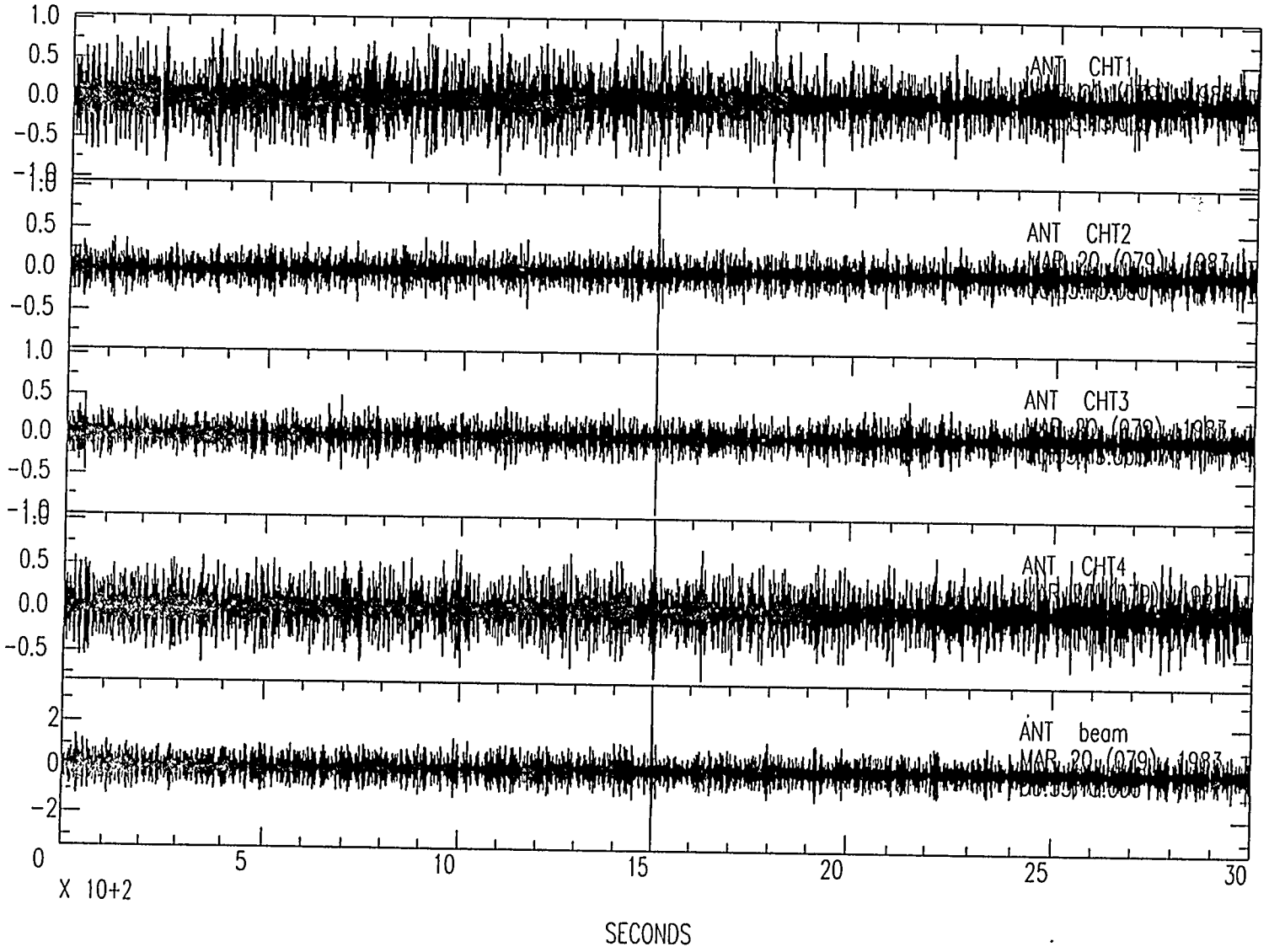

ENSCO, Inc.

F-detector: Data from Antarctica

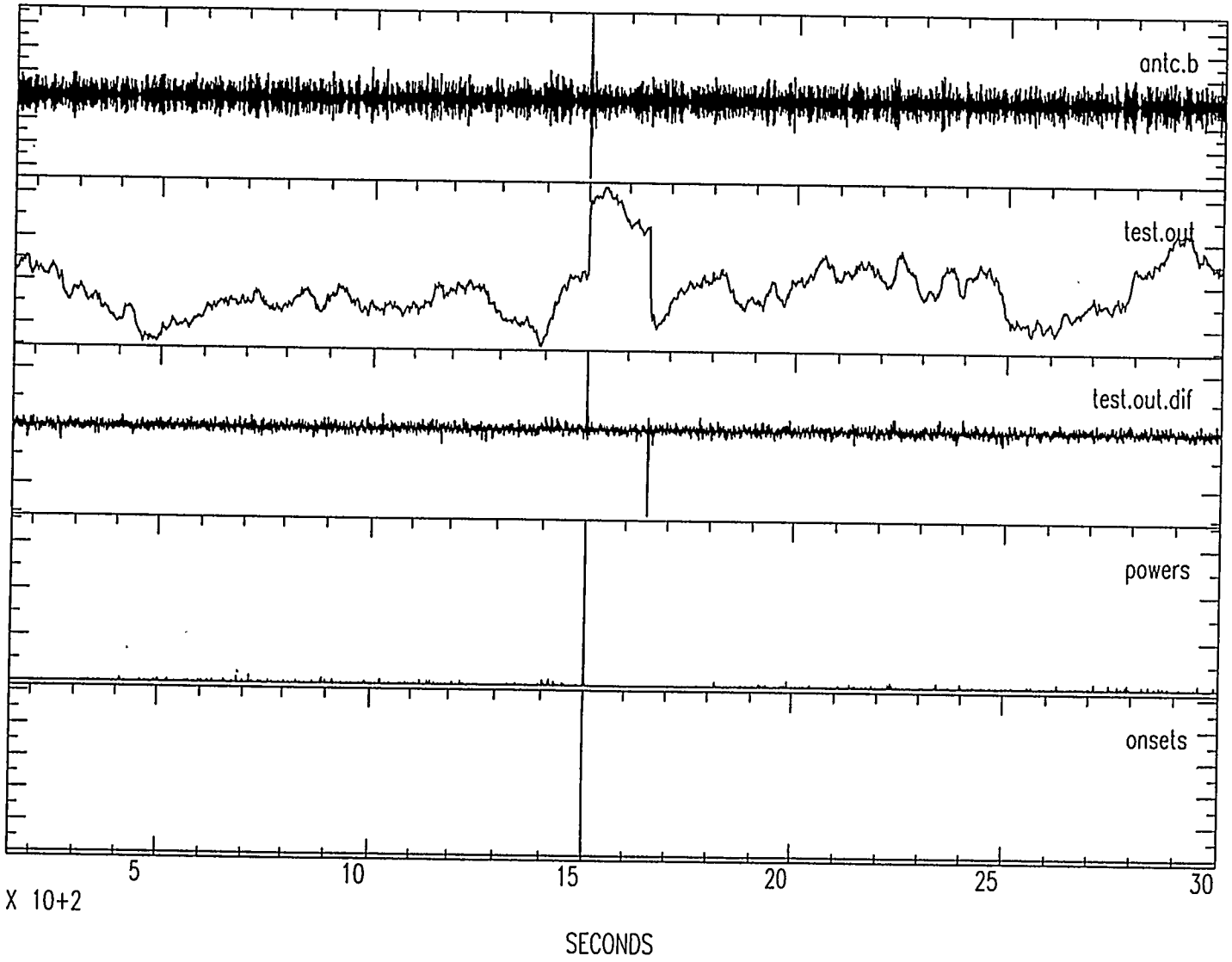

ENSCO, Inc.

Tanana Nuclear Test Recorded by SF Array

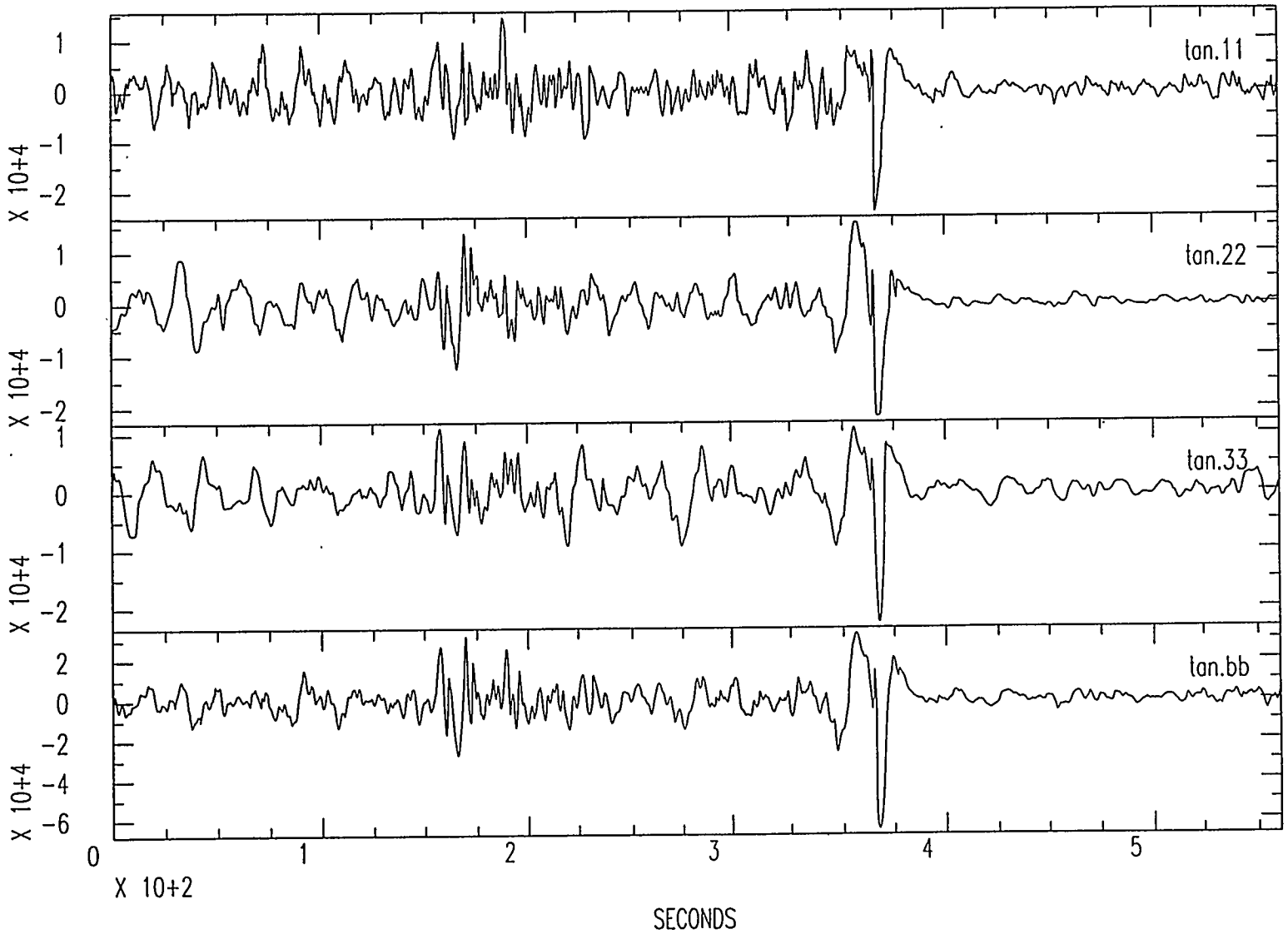

ENSCO. Inc.

Tanana Nuclear Test Recorded by SF Array

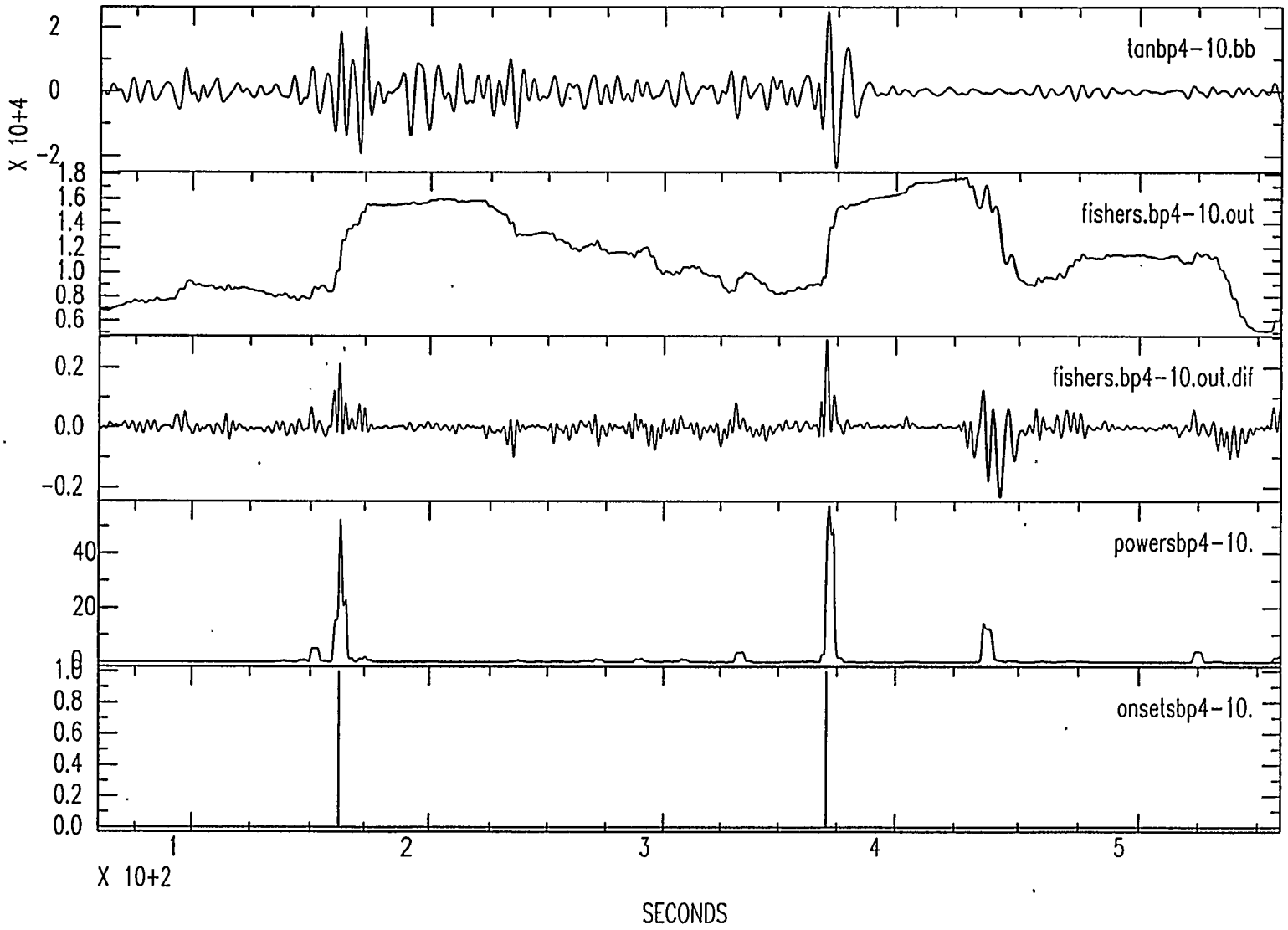

ENSCO, Inc.

Tanana Nuclear Test Recorded by SF Array

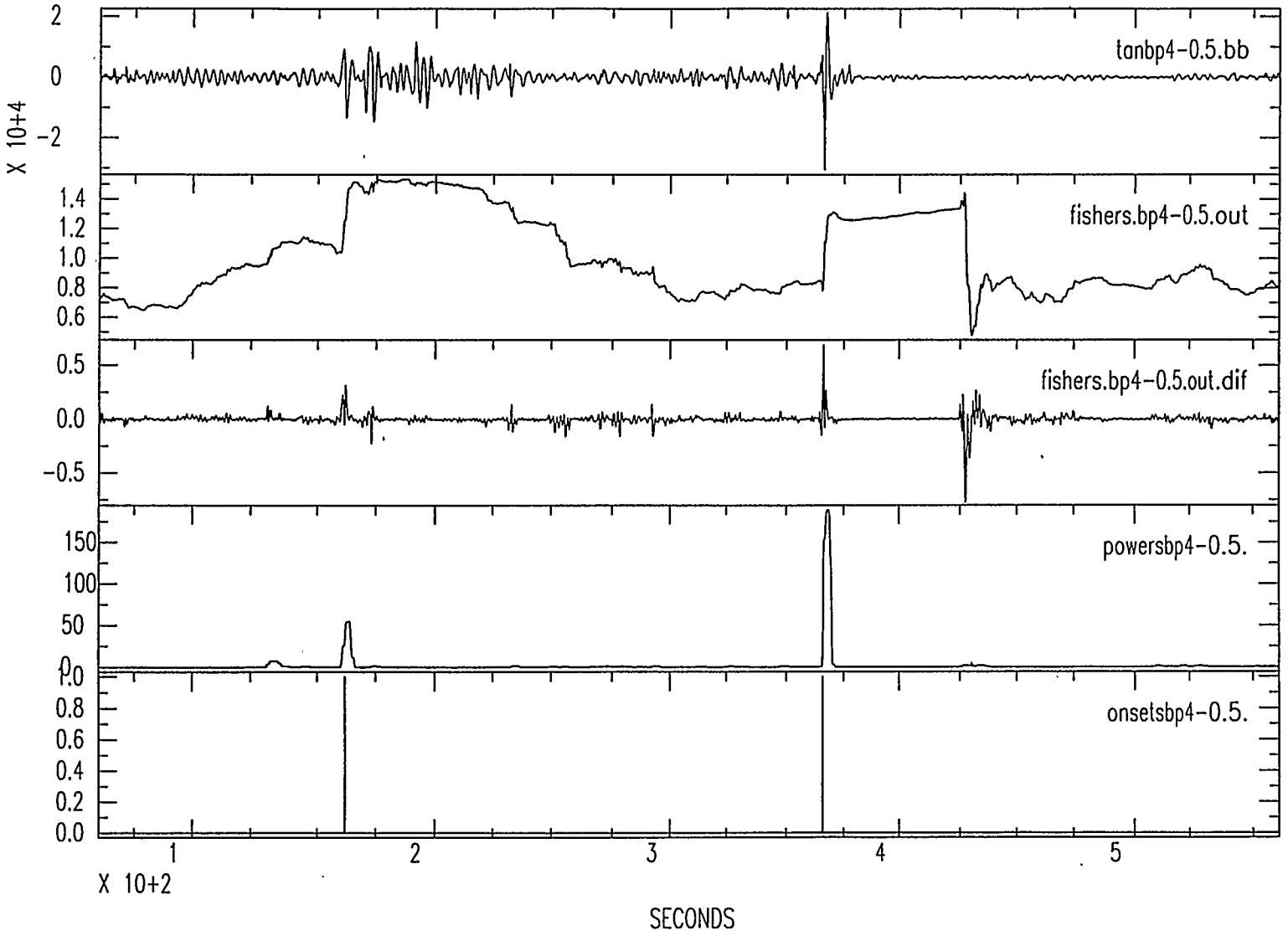

ENSCO, Inc.

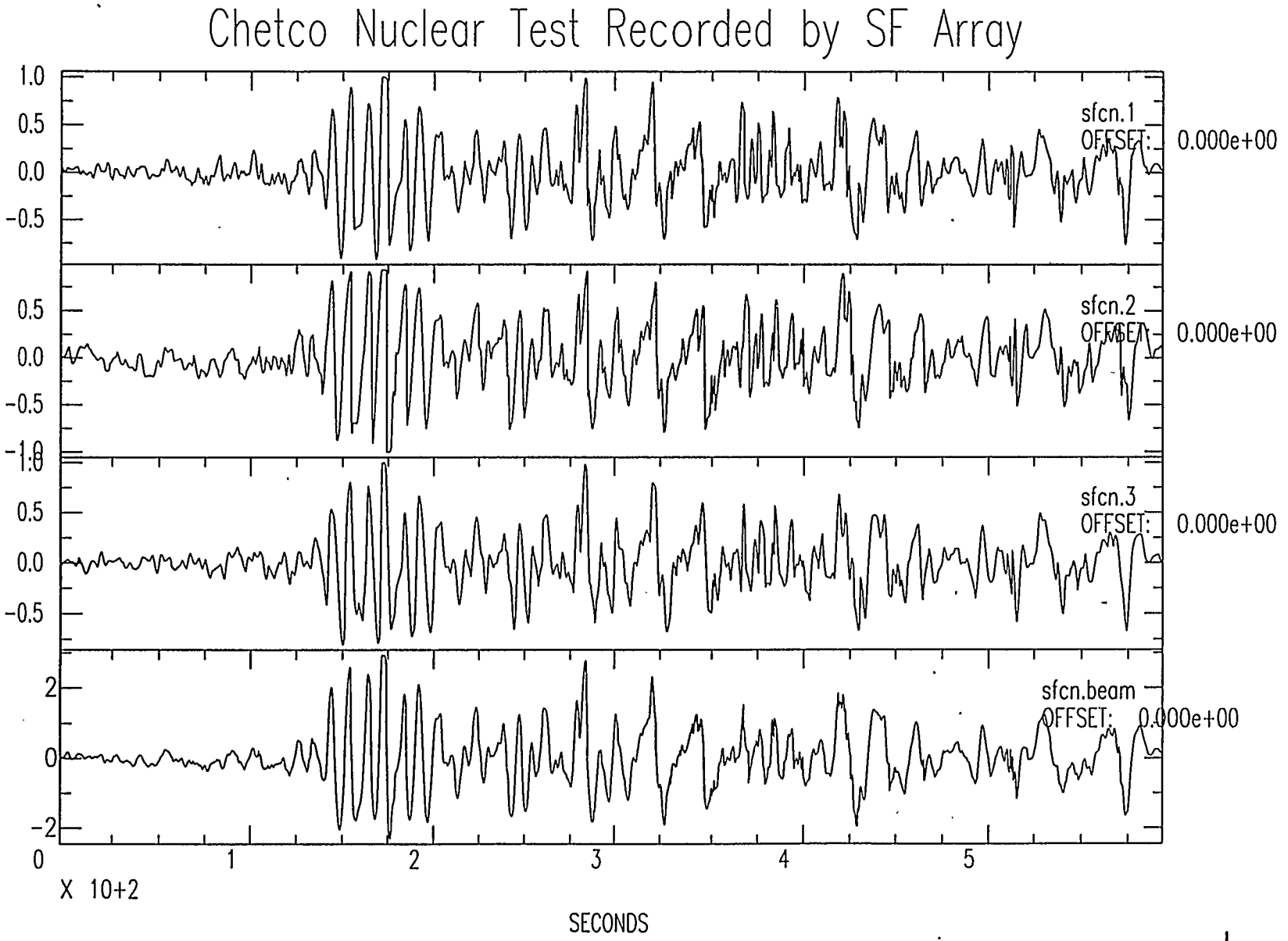
Chetco Nuclear Test Recorded by SF Array
1.0
0.5
0.0
-0.5
sfcn.1
OFFSET: 0.000e+00
0.5
0.0
-0.5
-1.0
sfcn.2
OFFSET: 0.000e+00
1.0
0.5
0.0
-0.5
sfcn.3
OFFSET: 0.000e+00
2
0
-2
sfcn.beam
OFFSET: 0.000e+00
0
1
2
3
4
5
X 10+2
SECONDS

ENSCO, Inc.

Chetco Nuclear Test Recorded by SF Array

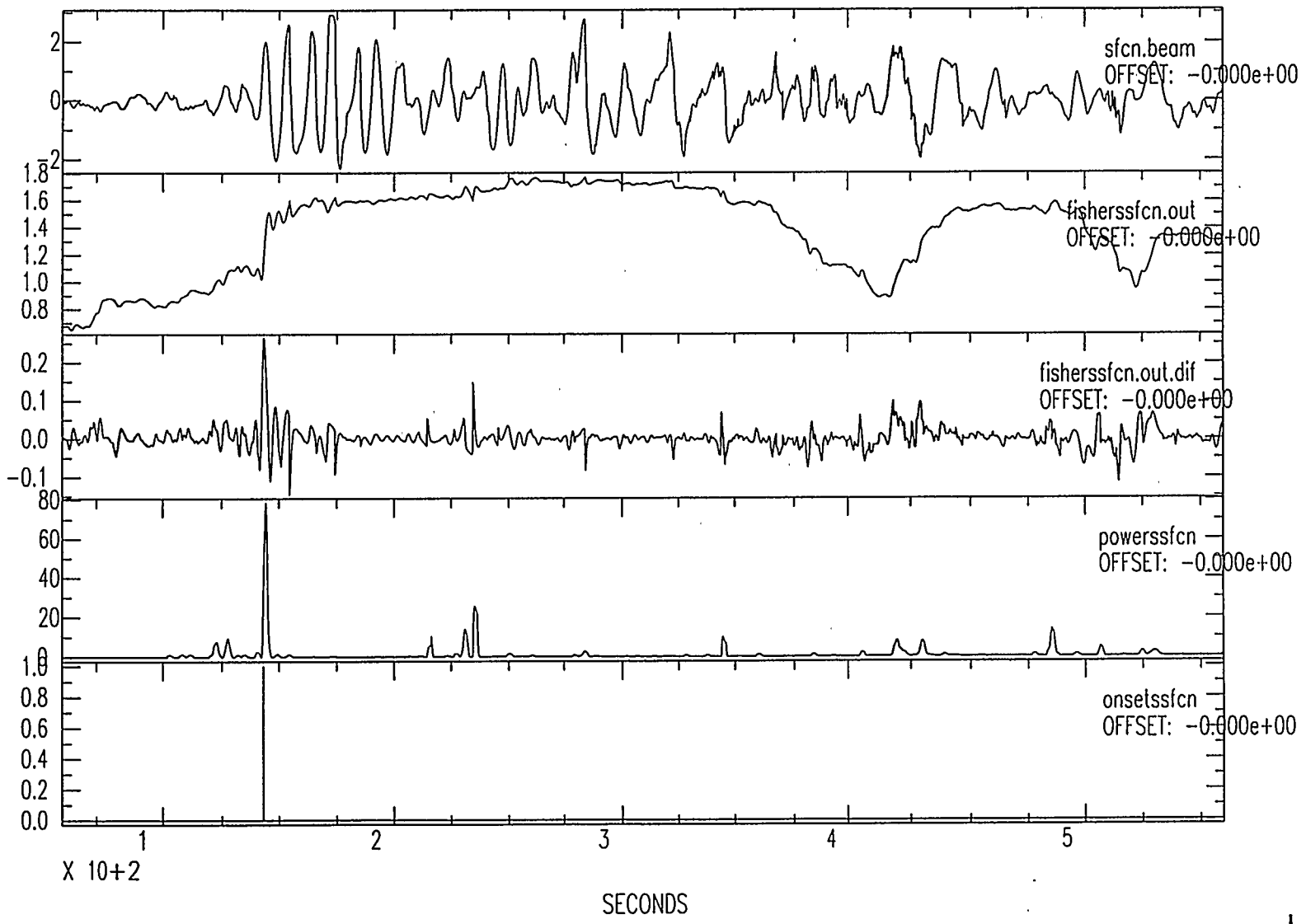

ENSCO, Inc.

ENSCO, Inc.

Conclusion

- The F-Statistic detector is a reliable process for detecting infrasonic events.
- The detector has the following characteristics:
  - Works on a small number of channels
  - Small number of false alarms
  - Small number of missed detections
  - Computationally fast
  - Can be automated
- Pre-detection signal enhancement is essential, especially during periods of microbaroms.
- The F-Statistic detector is an accurate onset-time estimator.

AUTOMATIC PROCESSING OF INFRASONIC DATA AT THE PROTOTYPE IDC

Raymond J. Willemann, Charles N. Katz, and J. Wang

Science Applications International Corporation
Center for Monitoring Research
1300 North 17th Street, suite 1450
Arlington, VA 22209

Infrasonic data received at the IDC will be automatically processed to produce a bulletin of "events", that is locations and times of transient sources of signals received at several stations. The resulting automatic event lists are released as intermediate products. The automatic event lists are also the starting point for subsequent interactive analysis of the data, which produces the final product of the IDC. Given the data volume expected at the CTBTO IDC and the limited number of analysts, reasonably accurate automatic event lists are crucial.

Automatic processing of infrasonic data at the Prototype IDC begins with "detection", that is identification of discrete times in which a signal from a potentially interesting origin has arrived at the array. We have developed a procedure for detection that finds times at which coherence across the array is large and either the power or the coherence increases quickly, indicating onset of a transient signal. The coherence measure is the F-statistic and the power is measured on a beam directed at the slowness vector of high coherence. The procedure is designed to reliably detect transient signals while minimizing the number of detections on continuous signals such as microbaroms.

The next step in automatic processing is "feature extraction", that is measurement of signal properties. We have implemented measurement of

- the slowness vector and its uncertainty, based on the Cramer-Rao lower bound.
- spectral properties, including dominant period and corner frequency
- onset time, duration and other features in multiple frequency bands.

Preliminary classification of detections is based on these features. The primary purpose of classification of infrasonic detections is to identify noise detections, which are ignored in subsequent automatic processing. After preliminary classification, non-noise detections from different stations are associated with origins, and origin locations and times are estimated.

The Prototype IDC currently receives data from five infrasonic arrays, which are processed in near real time. Detection rates are generally low, indicating successful rejection of continuous signals. Nevertheless, the approach detects natural transient signals of interest. Arrivals are currently classified based on estimated slowness alone. A database of detection feature values is being accumulated, however, which may later allow additional detections to be correctly classified as noise before the association process.

Automatic Processing of Infrasonic Data at the Prototype IDC

R. J. Willemann, C. N. Katz, and J. Wang
(willmann@cmr.gov, jinwang@cmr.gov,katzc@cpva.saic.com)
Science Applications International Corporation
Center for Monitoring Research
300 North 17th Street, suite 1450
Arlington, VA 22209
USA

Infrasonic data received at the IDC will be automatically processed to produce a bulletin of "events", that is locations and times of transient sources of signals received at several stations. The resulting automatic event lists are released as intermediate products. The automatic event lists are also the starting point for subsequent interactive analysis of the data, which produces the final product of the IDC. Given the data volume expected at the CTBTO IDC and the limited number of analysts, reasonably accurate automatic event lists are crucial.

Automatic processing of infrasonic data at the Prototype IDC begins with "detection", that is identification of discrete times in which a signal from a potentially interesting origin has arrived at the array. We have developed a procedure for detection that finds times at which coherence across the array is large and either the power or the coherence increases quickly, indicating onset of a transient signal. The coherence measure is the F-statistic and the power is measured on a beam directed at the slowness vector of high coherence. The procedure is designed to reliably detect transient signals while minimizing the number of detections on continuous signals such as microbaroms.

The next step in automatic processing is "feature extraction", that is measurement of signal properties. We have implemented measurement of

- the slowness vector and its uncertainty, from the Cramer-Rao lower bound.
- spectral properties, including dominant period and corner frequency.
- onset time, duration and other features in multiple frequency bands.

Preliminary classification of detections is based on these features. The primary purpose of classification of infrasonic detections is to identify noise detections, which are ignored in subsequent automatic processing. After preliminary classification, non-noise detections from different stations are associated with origins, and origin locations and times are estimated.

The Prototype IDC currently receives data from five infrasonic arrays, which are processed in near real time. Detection rates are generally low, indicating successful rejection of continuous signals. Nevertheless, the approach detects natural transient signals of interest. Arrivals are currently classified based on estimated slowness alone. A database of detection feature values is being accumulated, however, which may later allow additional detections to be correctly classified as noise before the association process.

Automatic Processing of Infrasonic Data at the Prototype IDC

R. J. Willemann, C. N. Katz, and J. Wang
Science Applications International Corporation
Center for Monitoring Research
300 North 17th Street, suite 1450
Arlington, VA 22209
USA

Los Alamos Array

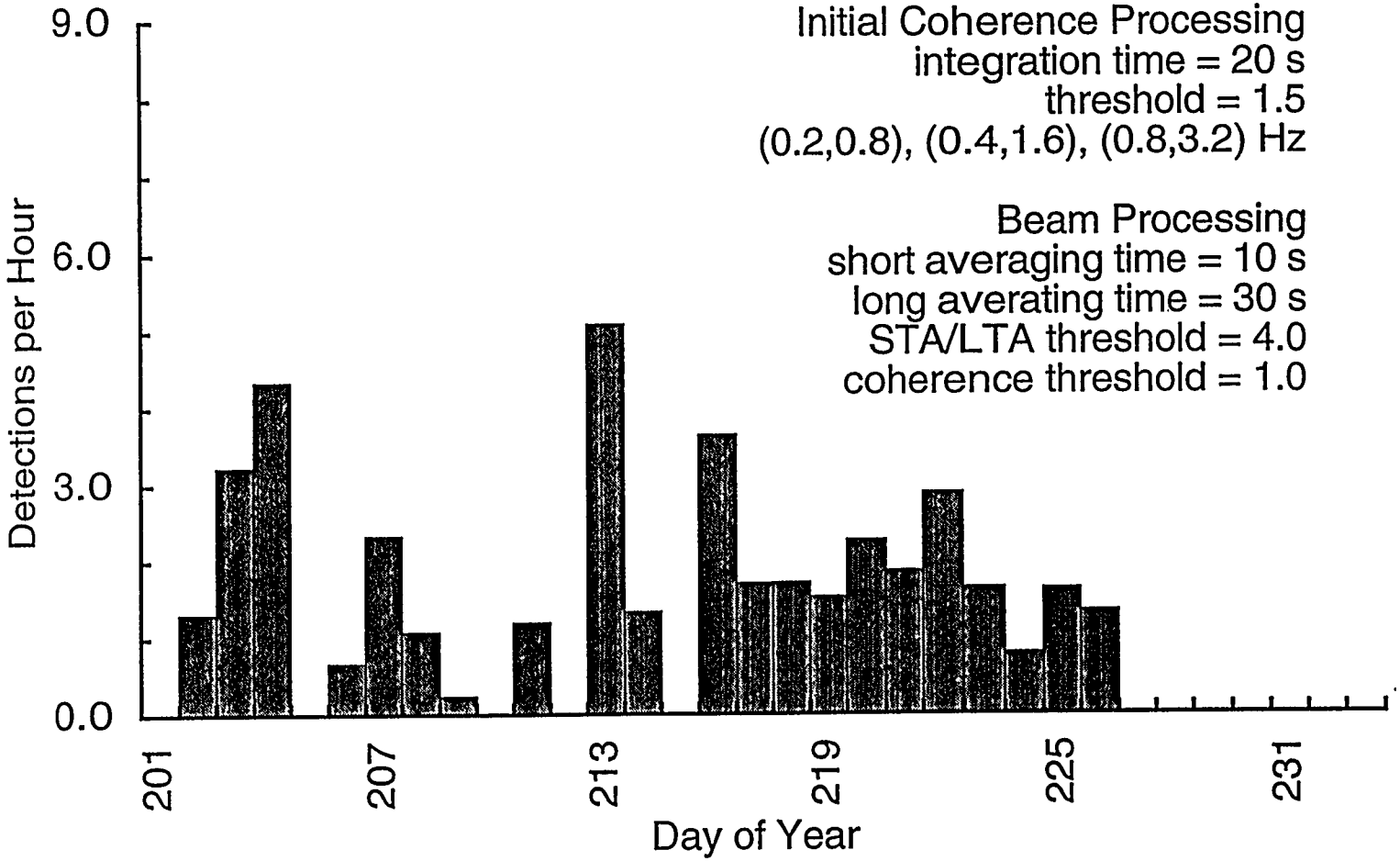

Detection Algorithm

A four-stage process is applied to moderate length (30 minute) data intervals:

- Slowness-plane directed search for coherence (peaks in normalized cross-correlaton or F-statistic) over short integration times (20 – 120 seconds)
- Beam-forming at the center of coherence clusters.
- STA/LTA search for rapid power increases at particular times.
- Confirmation that coherence exceeded a threshold at the same time as the STA/LTA trigger.

St. George Array

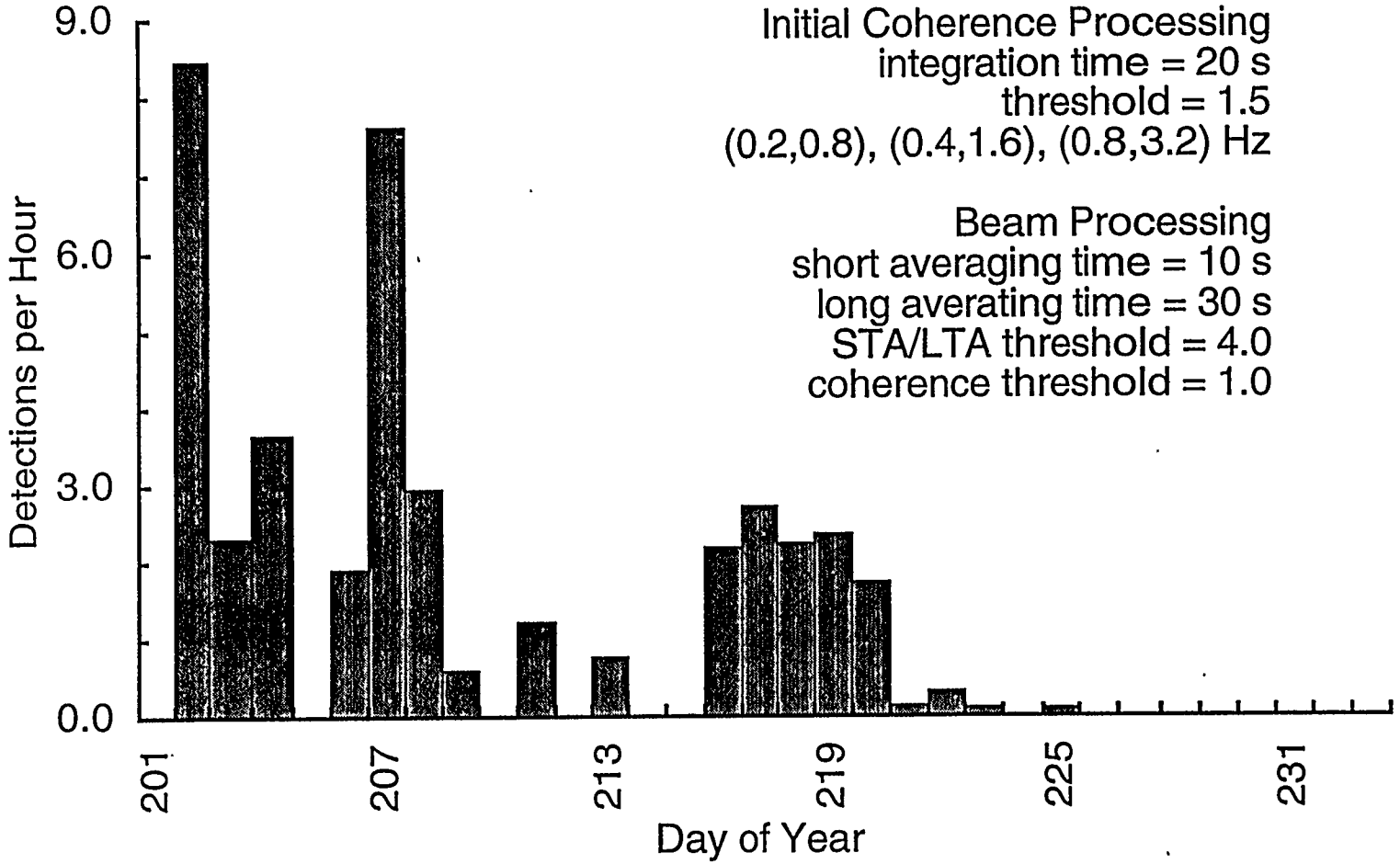

Pinedale Array

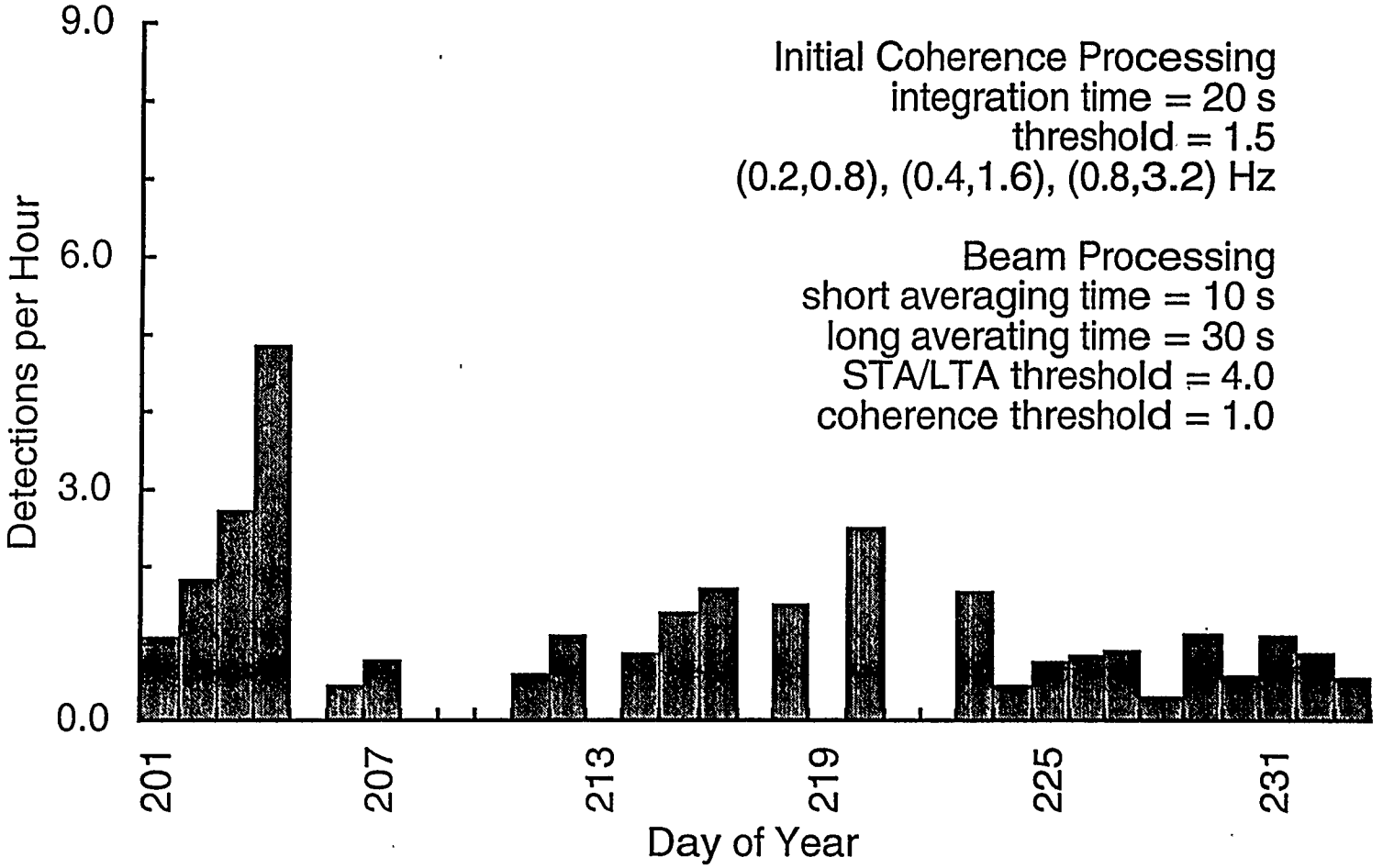

Texess Array

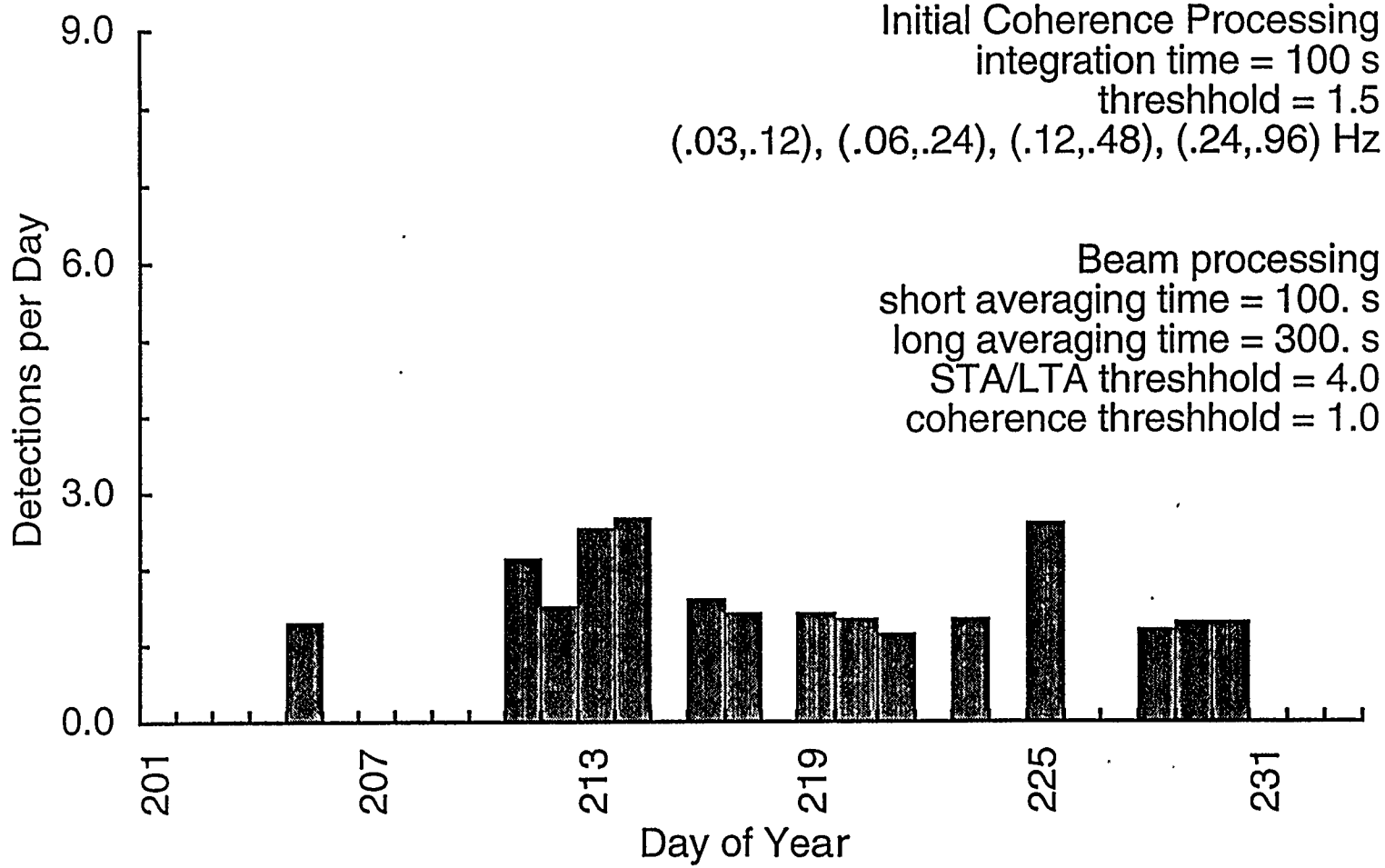

	Detections per hour or 24 hours				Detection Count				Hours of data successfully processed			
DOY	LSAR	PDIAR	SGAR	TXIAR	LSAR	PDIAR	SGAR	TXIAR	LSAR	PDIAR	SGAR	TXIAR
201	0.00	1.09	0.00			6			2.0	5.5	6.5	
202	1.32	1.83	8.47	0.00	31	44	199		23.5	24.0	23.5	2.0
203	3.23	2.73	2.31	0.00	21	60	15		6.5	22.0	6.5	10.0
204	4.34	4.85	3.66	0.00	89	114	75		20.5	23.5	20.5	5.5
205	0.00	0.00	0.00	1.30				1	1.0	23.0	1.0	18.5
206	0.67	0.45	1.91	0.00	14	5	41		21.0	11.0	21.5	7.5
207	2.33	0.79	7.60	0.00	14	11	38		6.0	14.0	5.0	14.5
208	1.08		2.96	0.00	14		34		13.0		11.5	14.5
209	0.23	0.00	0.60	0.00	5		13		21.5	6.5	21.5	23.5
210	0.00	0.00	0.00	0.00					20.5	24.0	21.5	24.0
211	1.20	0.60	1.22	2.13	24	13	25	2	20.0	21.5	20.5	22.5
212		1.11		1.50		5		1		4.5		16.0
213	5.08		0.77	2.53	33		5	2	6.5		6.5	19.0
214	1.33	0.88	0.00	2.67	4	18		2	3.0	20.5	3.0	18.0
215		1.40		0.00		21				15.0		21.0
216	3.64	1.70	2.18	1.60	20	23	12	1	5.5	13.5	5.5	15.0
217	1.70	0.00	2.72	1.41	40		64	1	23.5	3.5	23.5	17.0
218	1.71	1.50	2.23	0.00	35	9	48		20.5	6.0	21.5	19.0
219	1.52	0.00	2.36	1.41	35		53	1	23.0	3.0	22.5	17.0
220	2.26	2.50	1.74	1.33	43	20	33	1	19.0	8.0	19.0	18.0
221	1.86	0.00	0.14	1.14	40		3	1	21.5	1.0	21.5	21.0
222	2.88		0.33	0.00	62		7		21.5		21.5	18.5
223	1.64	1.67	0.11	1.33	18	20	2	1	11.0	12.0	18.0	18.0
224	0.79	0.45	0.00	0.00	15	9			19.0	20.0	22.0	17.0
225	1.62	0.77	0.11	2.59	30	18	2	2	18.5	23.5	19.0	18.5
226	1.33	0.85	0.00	0.00	12	20			9.0	23.5	9.0	18.5
227		0.91		0.00		21				23.0		17.5
228		0.30		1.20		7		1		23.0		20.0
229		1.13		1.30		27		1		24.0		18.5
230		0.58		1.30		14		1		24.0		18.5
231		1.11		0.00		26				23.5		18.5
232		0.88		0.00		21				24.0		17.5
233		0.56		0.00		10				18.0		11.5
max	5.08	4.85	8.47	2.67	89	114	199	2	23.5	24.0	23.5	24.0
avg	1.74	1.02	1.73	0.77	29	23	37	1	14.9	16.3	15.5	16.8

Features Extracted

Each of 12 features are extracted in an arbitrary number of bands.
Cepstral features are extracted in a broad frequency band.

Times	onset, termination, peak amplitude, energy mean
Levels	rms noise, peak signal, total energy
Energy Moments	mean, spread, skewness, kurtosis
Complexity	total time above threshold and number of threshold crossings
Cepstral	variance, peak and delay time at peak of both trend and residual from noise spectral equalization

Output from Signal Processing

Arrival Record	time, azimuth, slowness and S/N of signal.
Feature Records	onset, duration, energy moments, *etc.* in each of the specified feature extraction bands.
Detector Traces	azimuth, slowness, and S/N in each integration interval.
Detection Beams	filtered shift & sum beams at the azimuth and slowness of the arrival, from several minutes before onset to several minutes after termination.

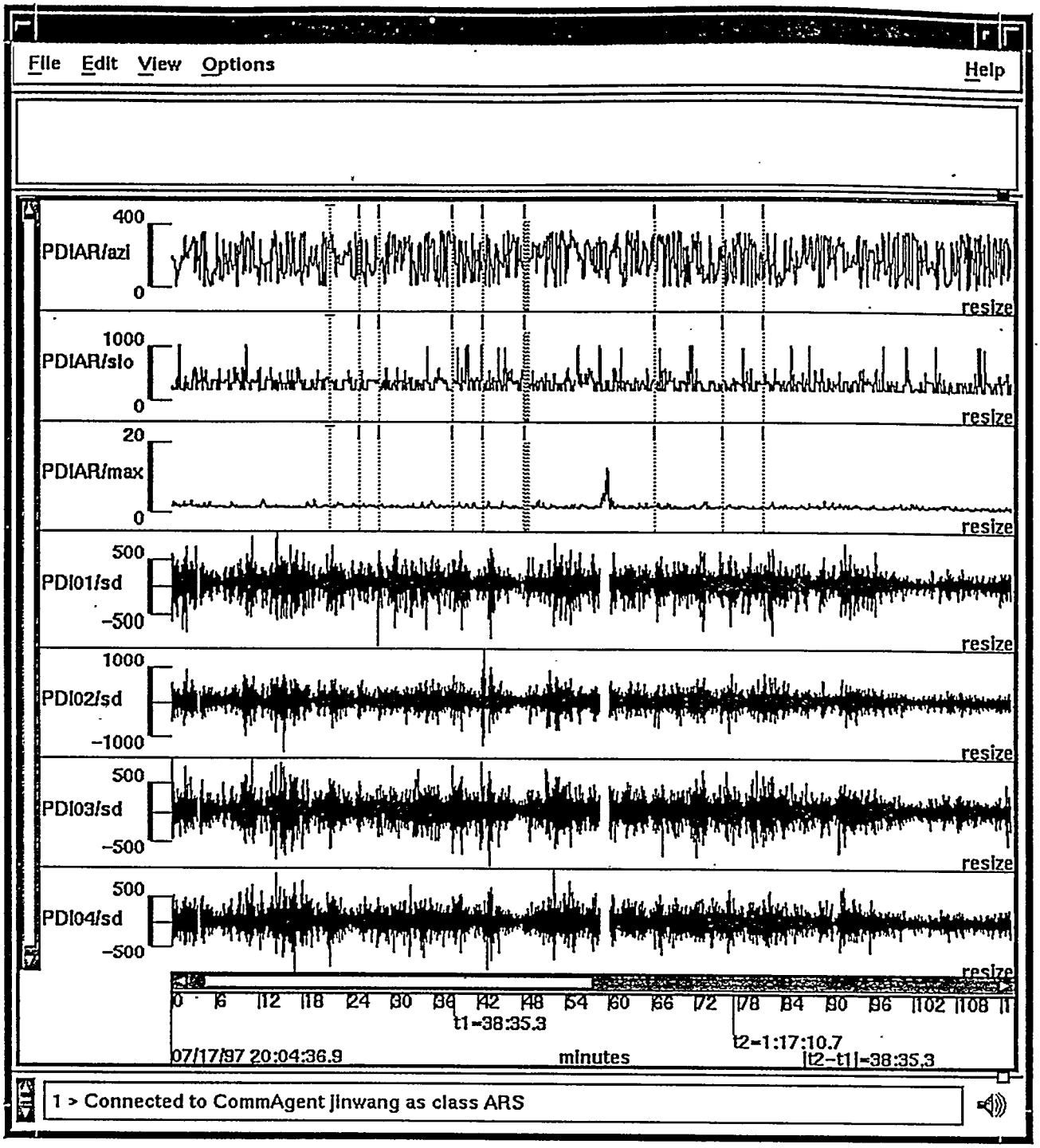
File Edit View Options
Help
400
PDIAR/azi
0
resize
1000
PDIAR/slo
0
resize
20
PDIAR/max
0
resize
500
PDI01/sd
-500
resize
1000
PDI02/sd
-1000
resize
500
PDI03/sd
-500
resize
500
PDI04/sd
-500
resize
0 6 12 18 24 30 36 42 48 54 60 66 72 78 84 90 96 102 108
t1=38:35.3
t2=1:17:10.7
07/17/97 20:04:36.9
minutes
|t2-t1|=38:35.3
1 > Connected to CommAgent jinwang as class ARS

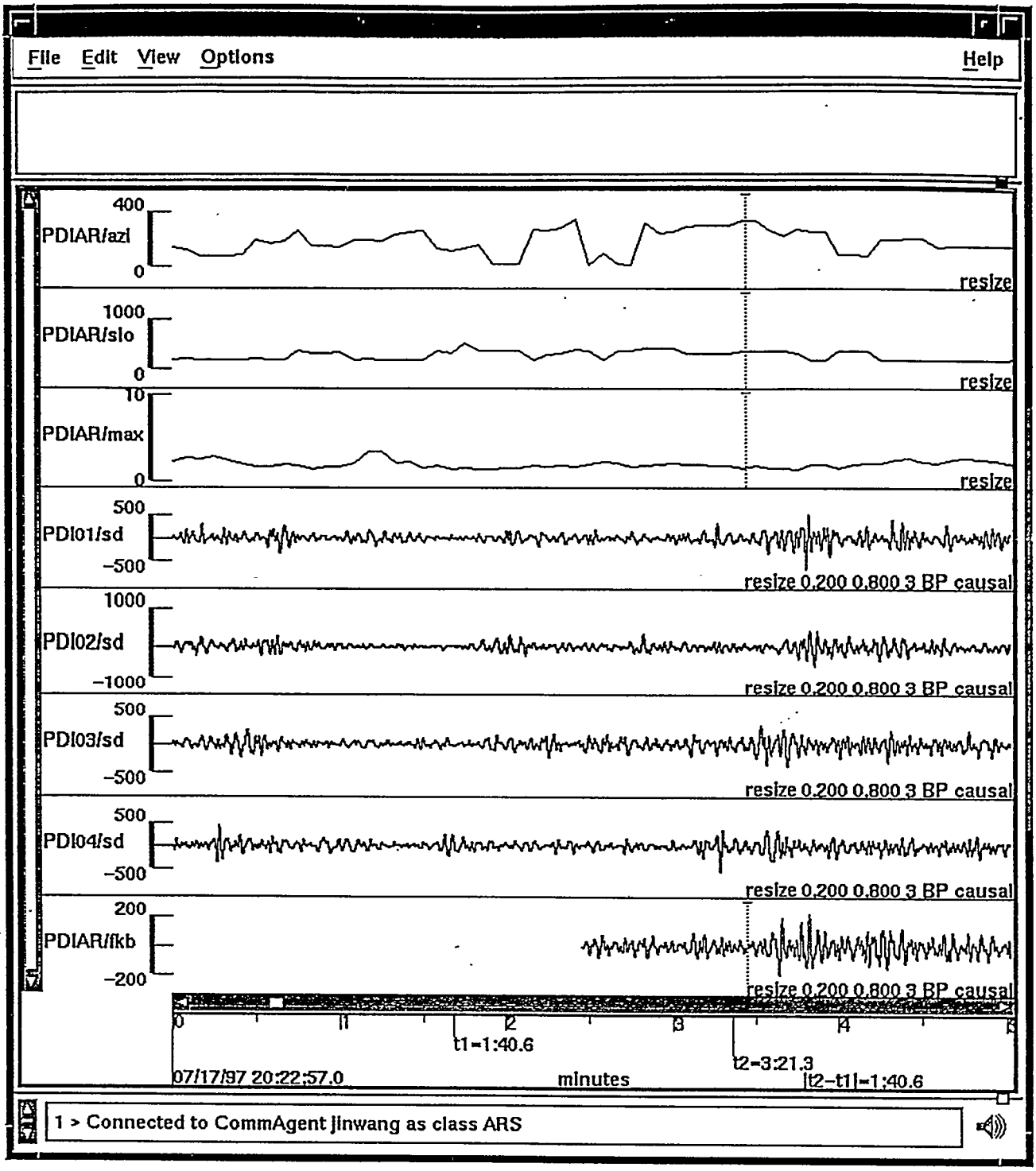
File Edit View Options Help
400
PDIAR/azi
0
resize
1000
PDIAR/slo
0
resize
10
PDIAR/max
0
resize
500
PDI01/sd
-500
resize 0.200 0.800 3 BP causal
1000
PDI02/sd
-1000
resize 0.200 0.800 3 BP causal
500
PDI03/sd
-500
resize 0.200 0.800 3 BP causal
500
PDI04/sd
-500
resize 0.200 0.800 3 BP causal
200
PDIAR/fkb
-200
resize 0.200 0.800 3 BP causal
0
1
2
3
4
t1=1:40.6
t2=3:21.3
07/17/97 20:22:57.0
minutes
|t2-t1|=1:40.6
1 > Connected to CommAgent jinwang as class ARS

Measurement of Azimuth and Slowness

- Compute X-correlation at each point on a refinement grid.
- Perform two one-dimensional cuble interpolations around the best point.
- Size of the refinement grid will overlap adjacent points on the detection grid.
- Number of grid points required (10 - 40 in each direction?) is to be determined.

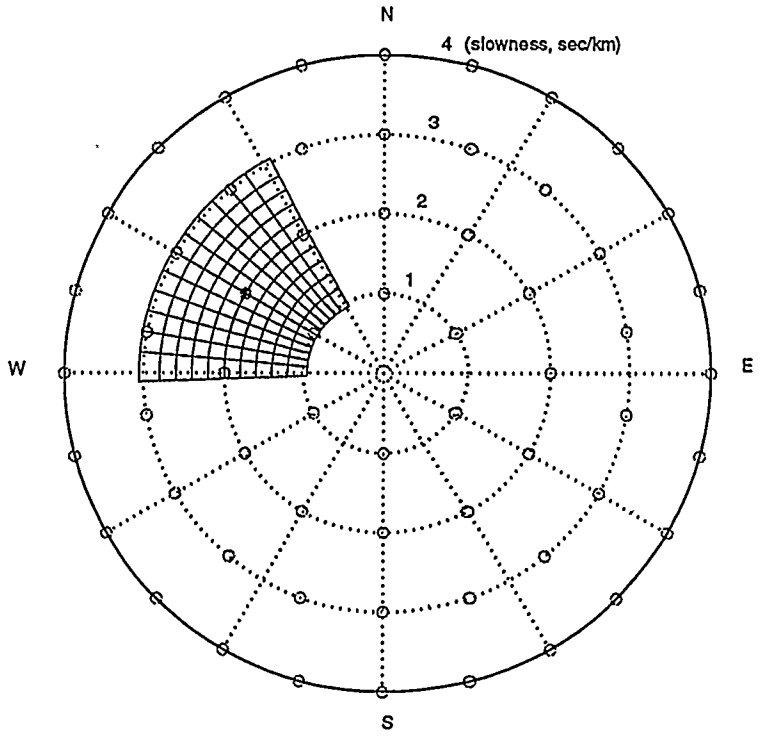

Evaluation of Azimuth and Slowness Measurement

Tests using synthetic data with known azimuth and slowness

- Using real array geometry at small DOE arrays.
- Signals are perfectly correlated.
- Noise is independent on each channel.
- Four sets of wavefrom are tested:

	F_c	Slow(s/km)	Azi. (deg.)
▽	1.0	2.1	30
◁	1.0	2.7	30
∇	0.5	3.0	60
Δ	0.5	4.0	60

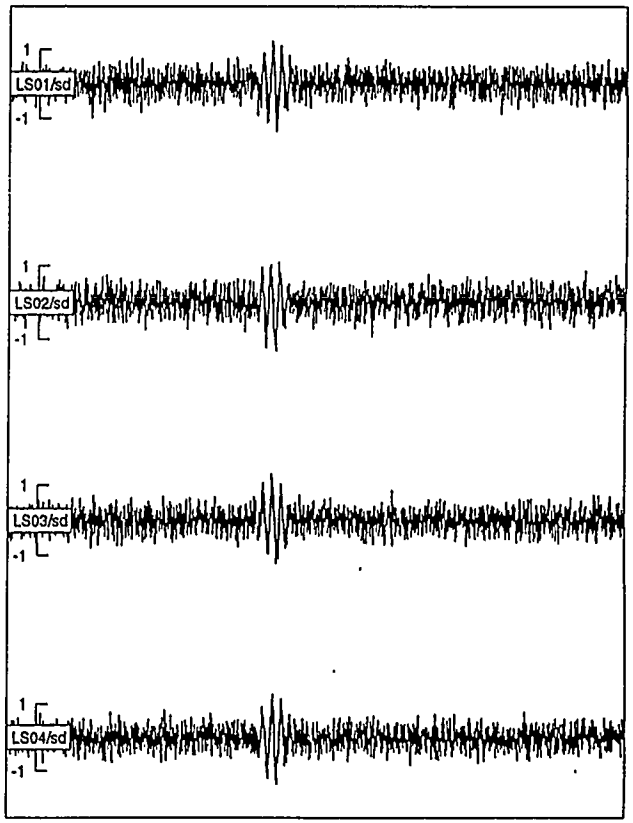

Synthetic waveform (0.5/4.0/60)

Evaluation of Azimuth and Slowness Measurement

- Values from manual FK analysis are generally in agreement with values used to generate synthetics.

- Values from automatic X-correlation processing are highly dependent on refinement parameters.

- Six sets of refinement parameter are tested:

#	Width of vel. (m/s)	Number of bins
0	25	16
1	100	40
2	100	80
3	50	40
4	50	80
5	50	160

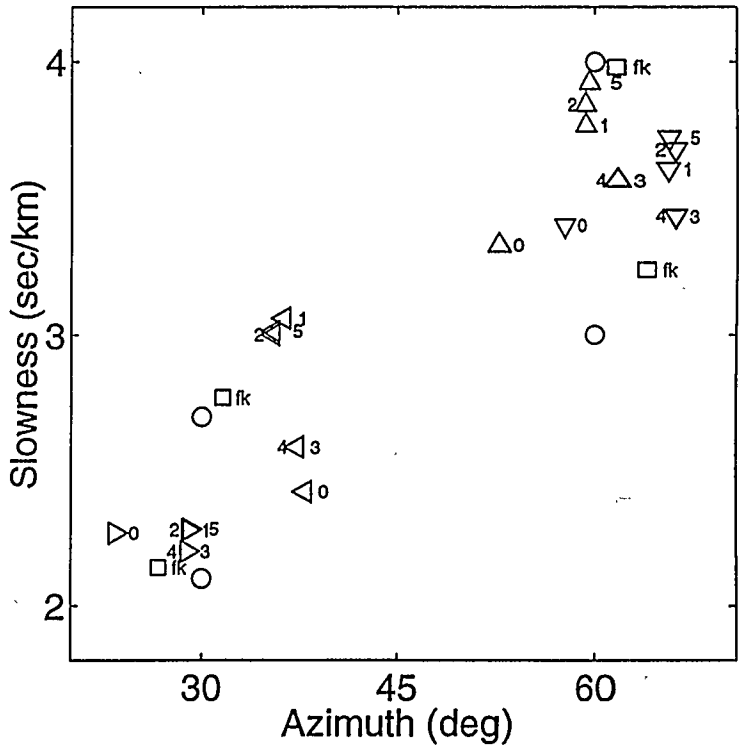

Uncertainty of Azimuth and Slowness

Computed from Cramer-Rao lower bound

- ❑ implicit assumption of uncorrelated noise
- ❑ assumes perfectly correlated signals
- ❑ includes effect of array geometry
- ❑ includes effect of signal to noise ratio
- ❑ includes effect of signal frequenncy content

$$\sigma_{azi} = \frac{180}{\pi}\frac{\lambda}{2\pi}\frac{1}{\sqrt{2BT}}\frac{1}{\sqrt{M}}\frac{1}{\sqrt{SNR}}\left[\frac{d\Phi}{d\phi}^T K_r \frac{d\Phi}{d\phi}\right]^{-1/2}$$

$$\sigma_{slow} = \frac{\lambda}{2\pi}\frac{s}{\sqrt{2BT}}\frac{1}{\sqrt{M}}\frac{1}{\sqrt{SNR}}[\Phi^T K_r \Phi]^{-1/2}$$

Evaluation of Azimuth and Slowness Uncertainty

- Manual FK analysis gives an alternate estimate of the azimuth and slowness of real signals.

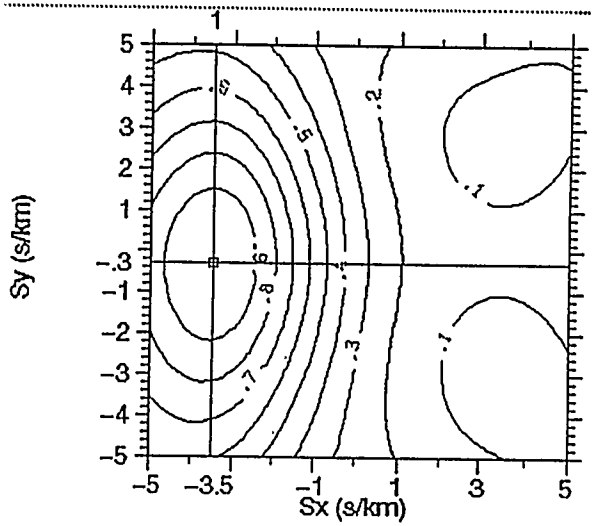

Evaluation of Azimuth and Slowness Uncertainty

Azimuth and slowness of real signals from manual FK analysis genally agree, but not automatic cross-correlationprocessing and within Cramer-Rao Lower Bound.

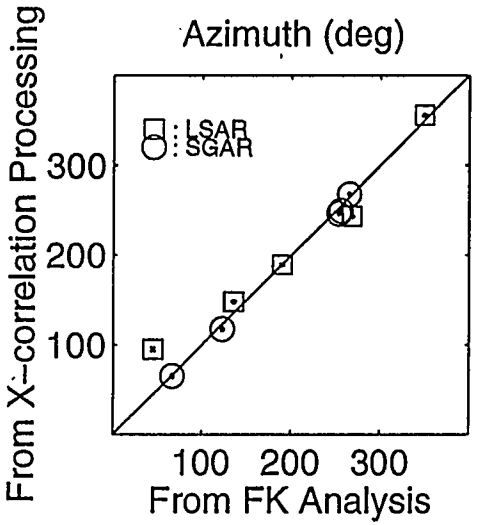

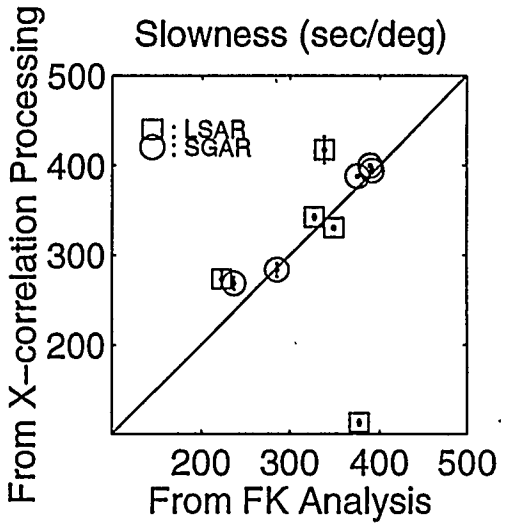

SEISMO-ACOUSTICAL EQUIPMENT COMPLEX IN MURMANSK REGION

E. O. Kremenetskaya, I. A. Kuzmin

Kola Regional Seiemological
Center KSC RAS, Apatity

Oleg M. Raspopov

S. Petersburg Filial IZMIRAN
P.B.188
St. Petersburg, 191023, Russia

Sergey N. Kulichkov

Institute of Atmospheric Physics
Russian Academy of Sciences
3 Pyzevsky, Moscow 109017, RUSSIA

The acoustic and seismology equipment complex (ASEC) was installed on Kola Peninsula at 18 km from Apatity. Equipment complex based on Apatity Regional Small Aperture Seismology Array included 9 seismometers and connected with Norwey seismology array NORSAR via satellite. Apatity seismological array NORSAR via satellite. Apatity seismological array was added by microbarographs network included 3 microbarographs. The main aim of ASEC is the simultaneous registration of atmospheric and Earth crust oscillations generated by the some sources. The programs for ASEC include registration of explosions in open and underground mains and registration of following seismic after-shocks, as well registration of microbaroms and microseisms, generated simultaneously in Atlantic ocean region during ciclonic and storm activity. Microbarom and microsesm data will be use for investigations of a short period (T=1-12h) changes of temperature and wind velosities into stratosphere (H=30-50 km) and termosphere (H90-120km). Microseisms will be use for a determination of the position of the oscillation sources and the changes of the parameters of the microbaroms will characterize the thermodynamic regime of the stratosphere and the thermosphere. The ASEC creation was supported by Russian Foundation for Basic Research.

Seismo-Acoustical Equipment Complex in Murmansk Region (RUSSIA)*

E.O.Kremenetskaya, I.A.Kuzmin,
Kola Regional Seismological Center KSC RAS, Apatity,
Murmansk Region, 184200, Russia
O.M.Raspopov
S.-Petersburg Filial IZMIRAN, P.B.188, St.-Petersburg,
191023, Russia, E-mail: oleg@omr.izmi.ras.spb.ru
S.N.Kulichkov
Institute of Physics of the Atmosphere RAS, Pyzhevskiy
per. 3, Moscow, 109017, Russia

Abstract

The acoustic and seismological equipment complex (ASEC) was installed on Kola Peninsula at 18 km from Apatity. The equipment complex is based on Apatity Regional Small Aperture Seismological Array that includes 9 seismometers and is connected with Norway seismological array NORSAR via satellite. Apatity seismological array was complemented by microbarographs network that consists of three microbarographs. The main purpose of ASEC is the simultaneous registration of atmospheric and Earth crust oscillations generated by the some sources. The programs for ASEC include registration of explosions in open and underground mines and registration of the following seismic after-shocks as well as registration of microbaroms and microseisms generated simultaneously in Atlantic ocean region during cyclonic and storm activity. The microbarom and microseism data is used for investigations of short period ($T = 1 \div 12$ h) changes of temperature and wind velocities in stratosphere ($H = 30 \div 50$ km) and thermosphere ($H = 90 \div 120$ km). Microseisms can be used for determination of the position of the oscillation sources, and the changes of the parameters of the microbaroms characterize the thermodynamic regime of the stratosphere and the thermosphere.
The hard- and sofrware development for Apatity seismic array and complemented by hard- and software for acoustic waves registration allows to record and process the signals in real time and to transfer this information to the international data base.
The ASEC creation was supported by Russian Foundation for Basic Research.

*Presented on INFRASOUND WORKSHOP FOR CTBT MONITORING, Santa Fe, New Mexico, August 25 - 28, 1995

Introduction

Kola Regional Seismological Center of Kola Scientific Center (KRSC) of the Russian Academy of Sciences (RAS), Institute of Atmospheric Physics of RAS, St.Petersburg Filial of IZMIRAN (SPbF IZMIRAN), and Polar Geophysical Institute of KSC of RAS initiated complex observations of atmospheric infrasound oscillations, seismic oscillations, and geomagnetic disturbances in 1988. This joint project has the goals: 1. To study the thermodynamic regime of the stratosphere and thermosphere basing on microbarom and microseism investigations; 2. To study the atmospheric infrasonic oscillations associated with the ionospheric disturbances.

Originally the recording of infrasound oscillations was carried out at Loparskaya obs. (68.6^0 N, 33.3^0 E) (Figure 1) where ionospheric and geomagnetic observations were simultaneously carried out. In 1990 the three-position set of microbarographs was installed. It permitted to carry out the estimation of azimuths of arriving waves. Microseism registration was carried out nearby, at Apatity obs. that is 150 km to the south from Loparskaya obs. (Figure 1). This made it possible to carry out the simultaneous observation of microbaroms and microseisms generated by cyclonic activity above ocean. In this case the microseism parameters provide the information about temporal variations of the source power, while the microbarom parameters give information on source location and variations in the stratospheric and thermospheric parameters.

The microbarographs were modernized and replaced at Apatity in 1994 where earlier the Kola Regional Small Aperture seismological Array was installed (67.61^0 N, 32.99^0 S). This array included 9 seismometers and was connected with Norwegian seismological array via satellite (Figure 2). The seismological array in Apatity was complemented by

microbarograph network consisted of three microbarographs. The main goal of the installation of the joint Acoustic and Seismic Equipment Complex (ASEC) is the investigation of the problems mentioned above and the investigation of acoustic signals generated by near-surface explosions [1,2,3]. The location of ASEC gives a good possibility for the study the explosions problem because a few open mines are located at Kola peninsula. In this paper we describe the acoustic equipment and some results obtained by the recently installed acoustic array.

Microbarograph system and its testing.

During the summer of 1994 tree liquid microbarographs were installed at the Apatity seismic array site of Kola Regional Seismological Center of the Russian Academy of Sciences (KRSC). The Apatity seismic array site is located 13 km to the east from Apatity town (Figure 1). Figure 3 displays the array geometry along with the newly installed devices.

The liquid microbarographs allow to register an infrasound signals in a most interesting frequency range 1 - 0.01 Hz and are simple to operate that was reason why this type of sensor has been selected [4]. A typical liquid microbarograph design is shown in Figure 4. One of the output holes (4) is kept open into atmosphere, other is coupled with a volume (not shown) separated from the atmosphere. The relative liquid level in the capacitors (2) changes under a difference between the atmospheric pressure and the pressure in the volume. Deviation of liquid level from the balance is transformed into electric signal by capacity-voltage converter.

Microbarographs are installed on the concrete basements coupled with the bedrock.

The outputs are connected to the ADC in central hub by symmetric communication lines in order to suppress the interference. Three spare channels of the existing data acquisition system, sampling rate 40 Hz, were used to transfer a data to KRSC in Apatity. Effective frequency band of infrasound data is registered to 1 - 0.1 Hz because of these channels were originally designed to register seismic data therefore their frequency band and sampling rate are not quite conforming with infrasound signals. However, their bandwidth is large enough to record most interesting phenomena except the internal gravitation waves.

The operation of set of the microbarographs and of seismic array is similar, therefore microbarographs relative phase responses should be either identical or carefully measured. To obtain the relative phase shifts the following measurements have been made. All microbarographs were placed close each other near the central hub and were linked with the data acquisition system. The input holes of microbarographs normally opened into atmosphere were coupled by rubber tubes with a single puncture. Such a connection leads that the pressure in measuring chambers of microbarographs will be identical, thus the phase shifts between microbarographs output yield a relative phase responses. The data were recorded during several hours. For further processing time histories free of spikes about of an hour length have been chosen. To estimate a relative phase shifts and a coherency of acoustical signals the method described in [5] has been applied.

Figure 4a shows the output signals coherency, Figure 4b represents the phase shifts. High coherency of the analyzed signals confirms that the estimates are confident. These results will be used further by more comprehensive software when estimating arrival

angles infrasound atmospheric oscillations.

The next step was to asses the threshold sensitivity. Figure 5 shows a response of the recording system obtained by imposing a step function 2.5 dyne/cm^2 amplitude to the input of a microbarograph. In spite of this estimation is quite rough, a conclusion that the threshold pressure sensitivity is not less than 1 dyne/cm^2 can be made.

Software installed at the SUN workstation in KRSC extracts infrasound data from the data stream, filters it by the anti-aliasing Butterwort low pass filter that has corner frequency 1.5 Hz slope 80 dB/decade, resamples it to 4 Hz sampling rate and stores the outcome on the hard disk afterward.

The atmospheric oscillation recordings are often affected by the wind initiated the air turbulence near the ground hence the data selection is necessary before the processing. The effective indicator of the true infrasound signal is a coherency between the microbarographs output. Thus the first step for selecting the efficient signal was the calculation of a coherency spectra between microbarographs.

Some results as an example of the acoustic signal registration

Registration on explosions.

The explosions in open mines in Olenegorsk and Kirovsk (Figure 1) were used as the test signals for standartization and checking the identity of microbarographs operation. The distance from ASEC to Kirovsk mine is 33 km and to Olenegorsk mine is 60 km. Figure 7 shows the example of registration of the explosion in Kirovsk mine on June 22, 1994. Upper three curves represent acoustic signals, and the next nine curves are the records of the seismic signals at ASEC. The lower three curves are from seismographs

located at Kirovsk near the mine. They give the information about the explosion time. One can clearly see the phase shift of the acoustic signal arrival that permits to determine the azimuth of the signal arrival equal to 80 degrees that coincides with the direction to Kirovsk mine with the accuracy of 1^0.

The parameters of the acoustic signal from the explosion in Olenegorsk open mine on February 10, 1995 are shown in Figure 8. In the Figure one can see the acoustic signals from three microbarographs as well as the coherency, the variations of the signal amplitude (root mean square (RMS)) and the azimuth of the signal propagation. The wave arrival azimuth prove to be 4 degrees that corresponds to Olenegorsk direction with accuracy 2^0.

The example of registration of long-distance propagation of acoustic waves generated by the explosion is shown in Figure 9. In this Figure one can see the signals from the large explosion at Plesetsk rocket range that were registered at Loparskaya on February 27, 1991, 12.09 UT. The distance from Plesetsk to Loparskaya is about 600 km. Azimuth of Plesetsk direction from Loparskaya is 160 degrees. Figure 10 shows the coherency of microbarograph signals and the calculated azimuth of the wave propagation before (12.06 UT) and during the registration of explosion signals (12.10 UT). For the explosion wave packet the calculated azimuth varied from 140 to 180 degrees if the microbarographs coherency is more than 0.75. Thus the accuracy of the azimuth detections occurs to be +/-20 degrees. The variations in the determined azimuth value could be associated with the atmospheric nonhomogeneities produced by warm atmospheric front located to South-East from Loparskaya during the explosion time.

Registration of microbaroms

The convenient objects for the development of a methods of long-term observation of acoustic signals and the useful signal selection are microbaroms. They are generated during the atmospheric cyclonic activity above ocean, they have quasi-sinusoidal signal shape in the periods range from 3 to 8 seconds, and their generation continues for hours. The microbarom source is usually located on the back side the a cyclone.

For the microbarom registration the useful signal selection was carried out by means of the coherency analysis of the signals from all microbarographs. The succession of microbaroms was registered during three days from February, 9 till February,11, 1995. Besides the explosion in Olenegorsk mine was registered as well at 10.20 UT on February, 10, 1995. One can see from Figure 11 that the development of three cyclones above Atlantic ocean occurs. One of the cyclones is close to Kola peninsula and moves towards North-East. The 15 minutes plots of the signal coherency of microbarographs on February, 10, 1995 is shown in Figure 12. One can see that during the whole day the good coherency of acoustic waves with periods from 3 to 8 seconds is observed. In Figure 13 the distribution of the power spectra of microbaroms is shown for the same day. The increase of the oscillation period from 5 to 8 seconds was observed during the day. The plots of microbarom amplitude variations (RMS) on February, 9, 1995 for oscillations with periods of T=3,4,6,and 8 seconds are presented in Figure 14. Zero of the abscissa axis corresponds to 00 UT on February 9, 1995. One can see that from the second half of February 10, 19995 the increase of the signal power takes place that is associated with approach of the back side of the cyclon that was moving near Kola peninsula. The plots of azimuth variations of acoustic waves arrivals are presented in Figure 15. The azimuth

varies from 50 to 75 degrees during three days that is associated with the source shift southward. One can clearly see the peak near 10 UT on February 10, 1995 in the plot. This peak corresponds to the explosion time in Olenegorsk mine at 10.20 UT that was discussed in the previous section of this paper.

The analysis of seismic signals on February 9-11, 1995 indicates that the microseism generation occurs during these days. The plots of microseism and microbarom amplitude variations on February 10, 1995 are shown Figure 16 for the wave periods of 3,4,6, and 8 seconds. The amplitude of the microseisms is practically stable. It means that the change of the microbarom amplitude is not the result of the change of the source power, but it is the result of the acoustic wave propagation in the atmosphere and the change of the source location relatively the point of waves detection.

Conclusions

1. Joint Acoustic and Seismic Equipment Complex (ASEC) was created in Apatity (Kola peninsula) in 1994-1995 basing on the Apatity seismic array connected by satellite with NORSAR seismic network.
2. The test registration of explosions in several mines and microbaroms showed the identity of microbarographs operation and confirmed the possibility of a correct determination of the direction of the oscillation source.
3. The hard- and software developed for Apatity seismic array and complemented by the software for acoustic waves registration allows to record and process the signals in real time and to transfer this information to the international data base. Thus Apatity could be a convenient location for the station connected with CTBT/IMS infrasound network.

4. The developed method of microbarograph signal coherency provides the possibility to select the useful signal, however the acoustic noise problem requires the further development.

The ASEC creation was supported by Russian Fundation for Basic Research.

References.

1. Kuzmin, I.A., Fedorenko, Yu.V., Grachev, A.I., Kulichkov, S.N., and Raspopov, O.M., Joint seismic and acoustic equipment complex for infrasound measurements in polar region, Apatity, Kola Scientific Center RAS, 1995, 26 p., (in Russian)

2. Kuzmin, I.A., Fedorenko, Yu.V., Grachev, A.I., Kulichkov, S.N., and Raspopov, O.M. Initial results of newly installed acoustic array, NORSAR Scientific Report, No 2-94/95, Semiannual Technical Summary, Oct.1, 1994 - March 31, 1995, Kjeller, 1995

3. Kulichkov, S.N. Long-range sound propagation in the atmosphere, Izvestiya RAS, Physics of the atmosphere and ocean, v.28, No4, 1992, 339-360, (in Russian)

4. Bovsheverov, V.M., Grachev, A.I.,Lomadze, S.O., and Matveev, A.K., Liquid type of microbarograph, Izvestiya RAS, Physics of the atmosphere and ocean, v.15, No11, 1979, 1215-1218, (in Russian)

5. Bendat, J.S., and Piersol, A.G., Random data. Analysis and measurement procedures., John Wiley & Sons, 1988

Figure captions.

Figure 1. The map of Kola peninsula.

Figure 2 The seismological network related to NORSAR-system.

Figure 3. Scheme of the seismograph (A and B) and microbarograph (MB) locations at Apatity testing area.

Figure 4. Principal scheme of the microbarograph: 1 - liquid; 2 - capacitor plates; 3 - body; 4 - output holes; 5 - electronics.

Figure 5. Result of the measurement of relative phase-frequency response of the microbarographs. A - coherency, B - phase difference.

Figure 6. The response of the acoustic measuring system on injection of 0.1 cm^2 of air into microbarograph (in relative units).

Figure 7. Record of acoustic and seismic signal of explosion at Kirovsk open mine on July 22, 1994, located at 33 km distance from Apatity.

Figure 8. The parameters of acoustic signal of explosion at Olenegorsk open mine on February 10, 1995, 15 20 UT. A - signal recorded, B - azimuth, C - coherency, D - amplitude (RMS).

Figure 9. The record of acoustic signals of the explosion at Plesetsk rocket range on February 7, 1991, 12 09 UT.

Figure 10. Coherency and azimuth of acoustic signals of Plesetsk explosion registered by microbarographs before (12 06 UT) and during explosion wave packet (12 10 UT).

Figure 11. The maps of meteorological situation on February 9 - 10, 1995 during microbarom registration at Apatity

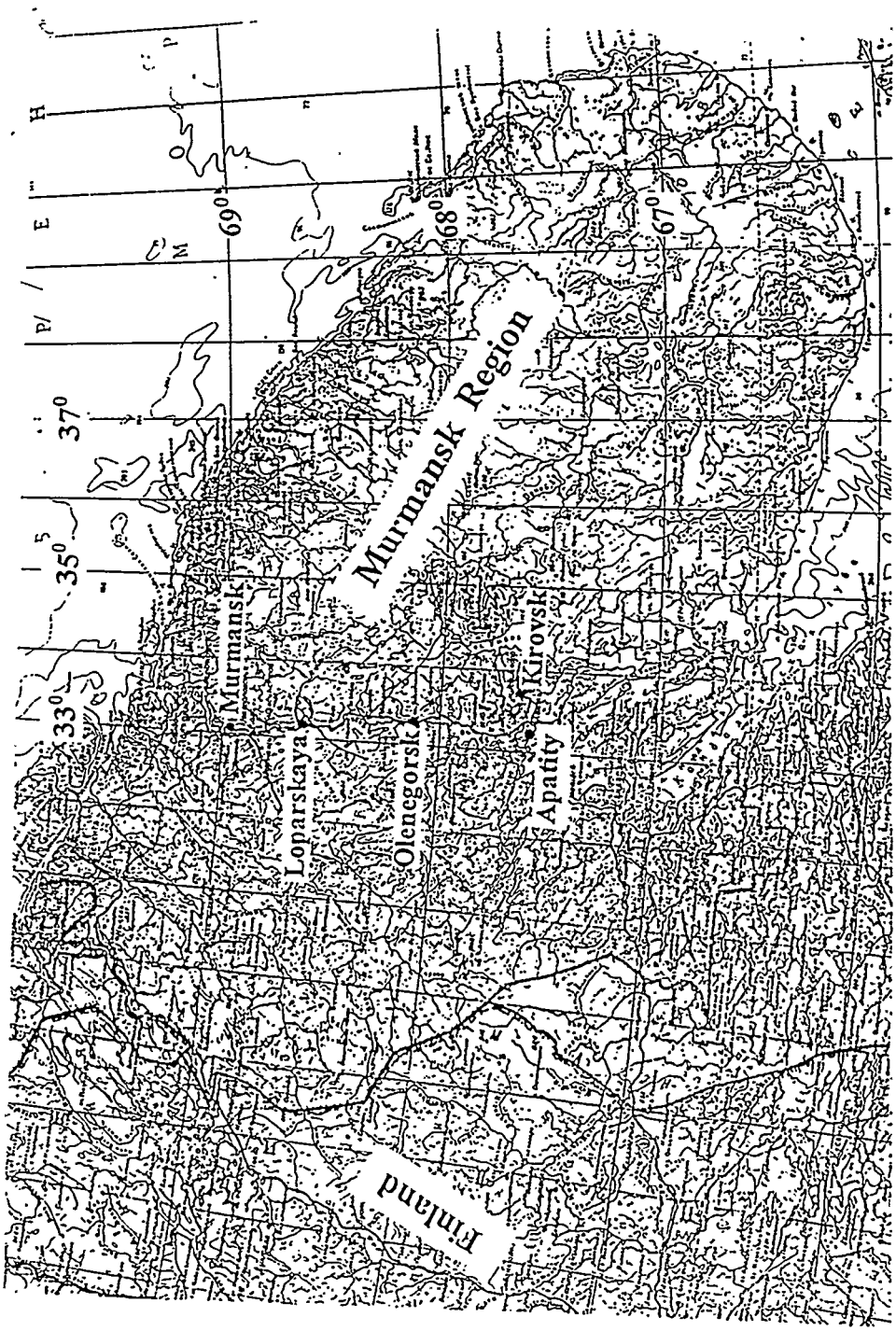
Murmansk Region
Murmansk
Loparskaya
Olenegorsk
Kirovsk
Apatity
Finland
33°
35°
37°
69°
68°
67°

Figure 1.

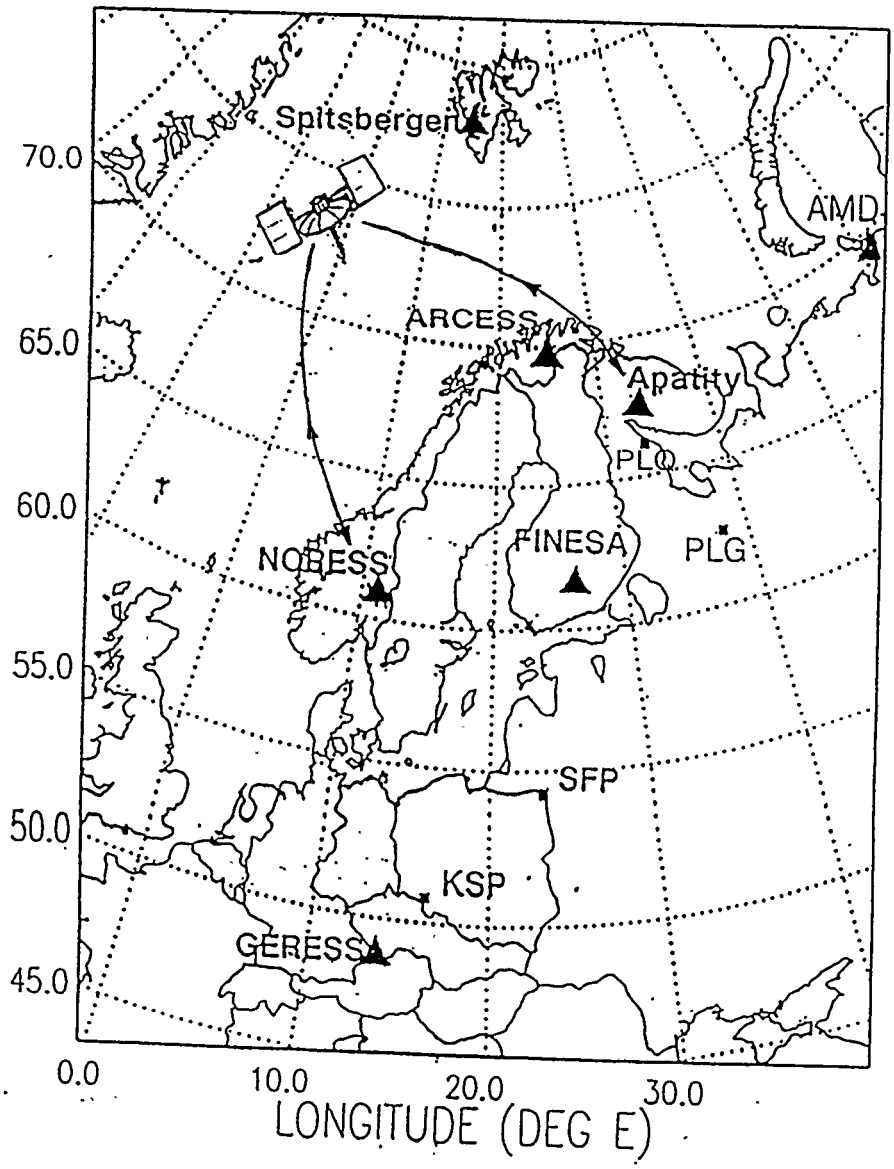
Spitsbergen
AMD
ARCESS
Apatity
PLO
NORESS
FINESA
PLG
SFP
KSP
GERESS
70.0
65.0
60.0
55.0
50.0
45.0
0.0
10.0
20.0
30.0
LONGITUDE (DEG E)

Figure 2.

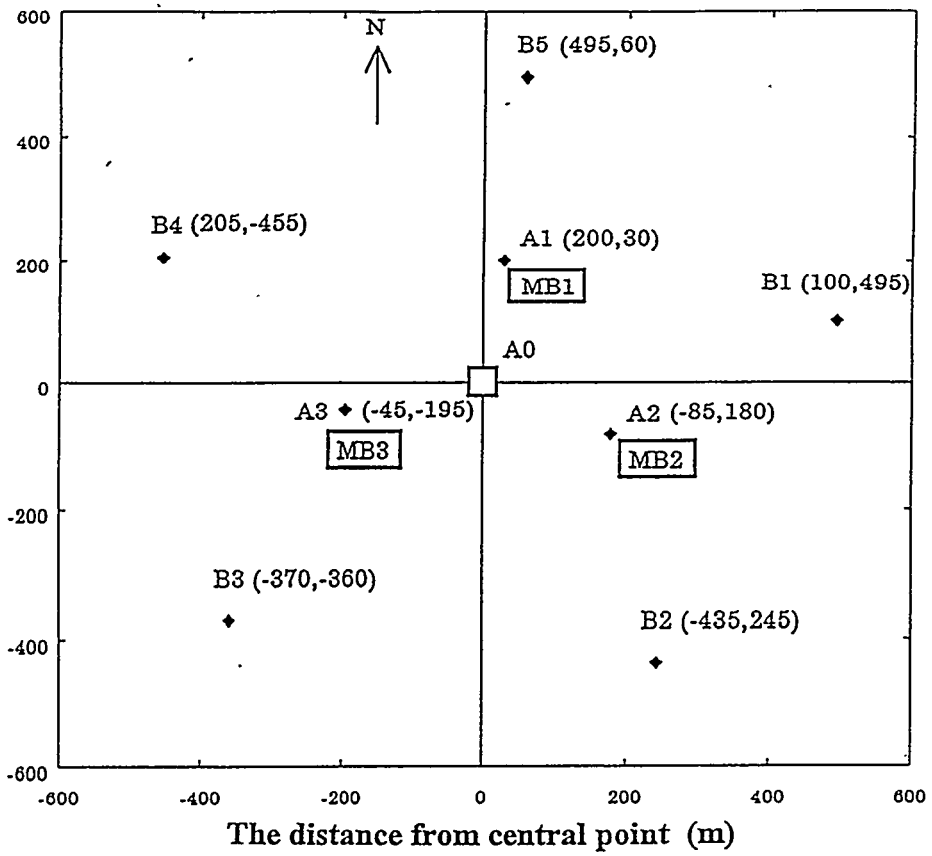
N
B5 (495,60)
B4 (205,-455)
A1 (200,30)
MB1
B1 (100,495)
A0
A3 (-45,-195)
MB3
A2 (-85,180)
MB2
B3 (-370,-360)
B2 (-435,245)
600
400
200
0
-200
-400
-600
-600
-400
-200
0
200
400
600
The distance from central point (m)

Figure 3.

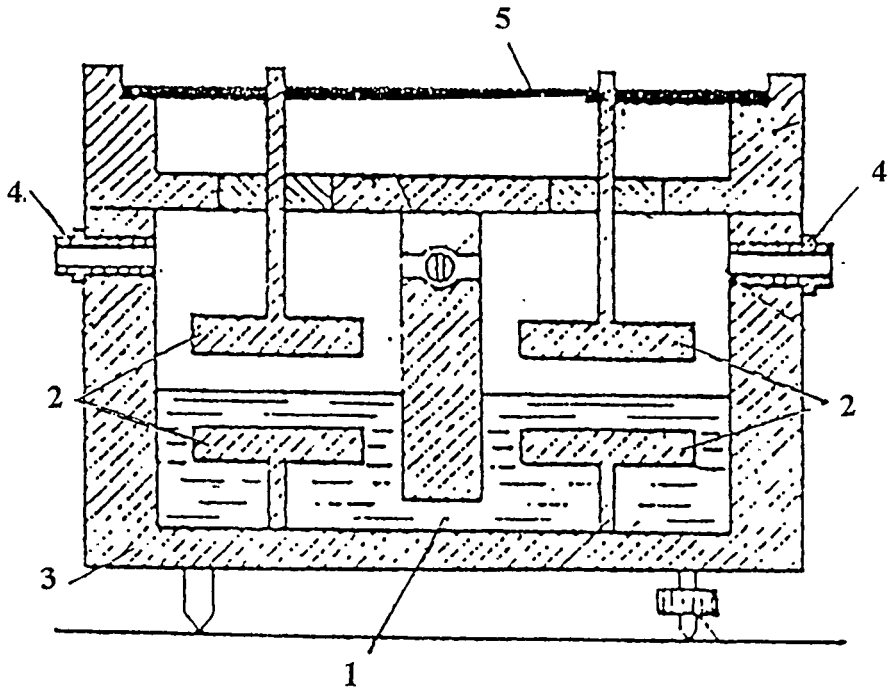

Figure 4.

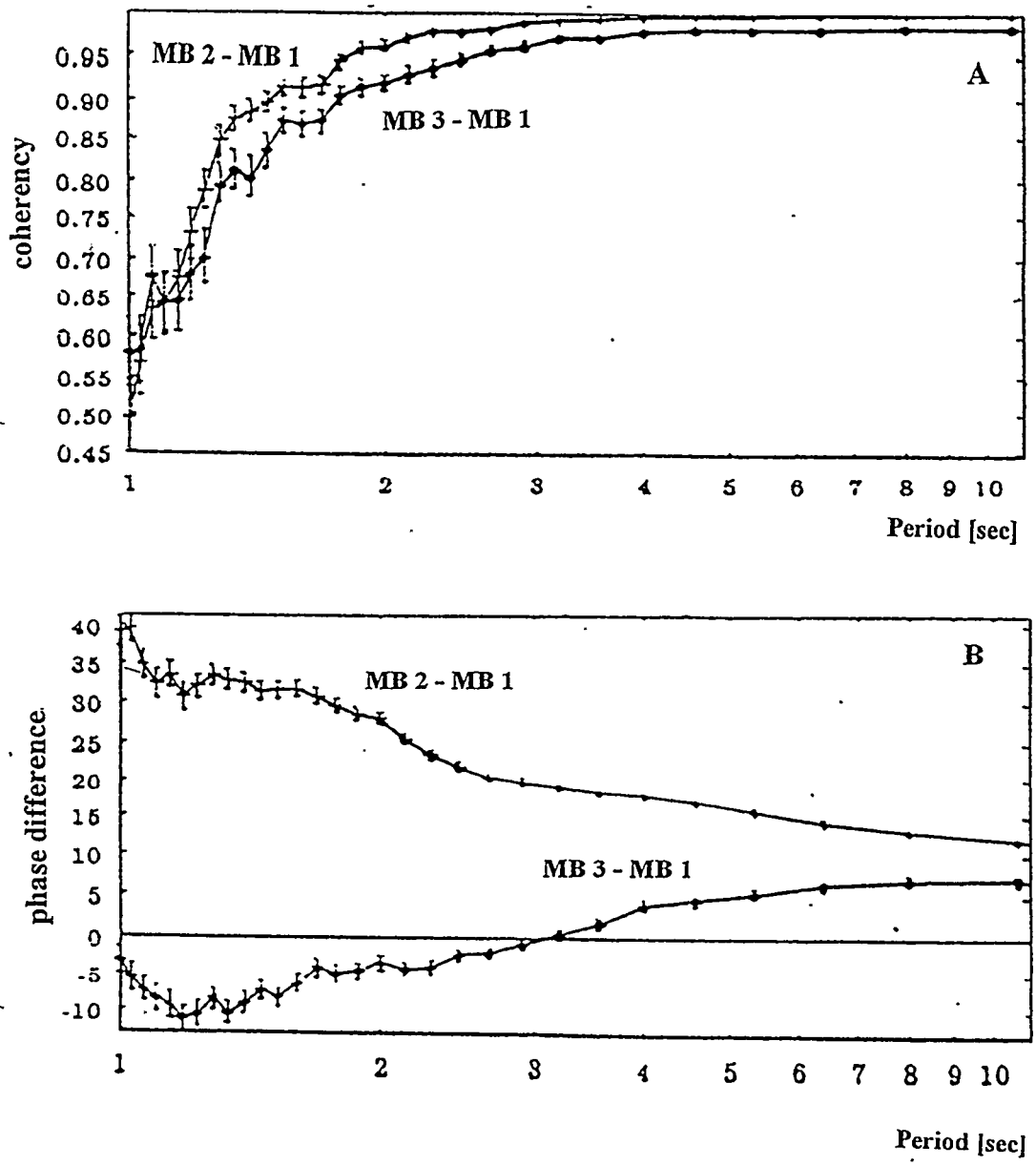
A
MB 2 - MB 1
MB 3 - MB 1
coherency
0.95
0.90
0.85
0.80
0.75
0.70
0.65
0.60
0.55
0.50
0.45
1
2
3
4
5
6
7
8
9
10
Period [sec]
B
MB 2 - MB 1
MB 3 - MB 1
phase difference
40
35
30
25
20
15
10
5
0
-5
-10
1
2
3
4
5
6
7
8
9
10
Period [sec]

Figure 5.

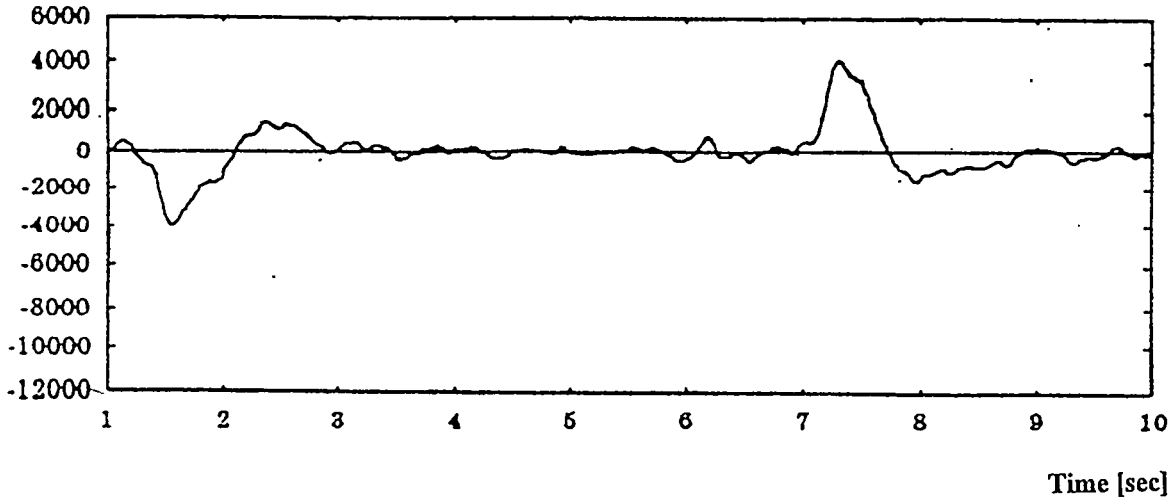
6000
4000
2000
0
-2000
-4000
-6000
-8000
-10000
-12000
1
2
3
4
5
6
7
8
9
10
Time [sec]

Figure 6.

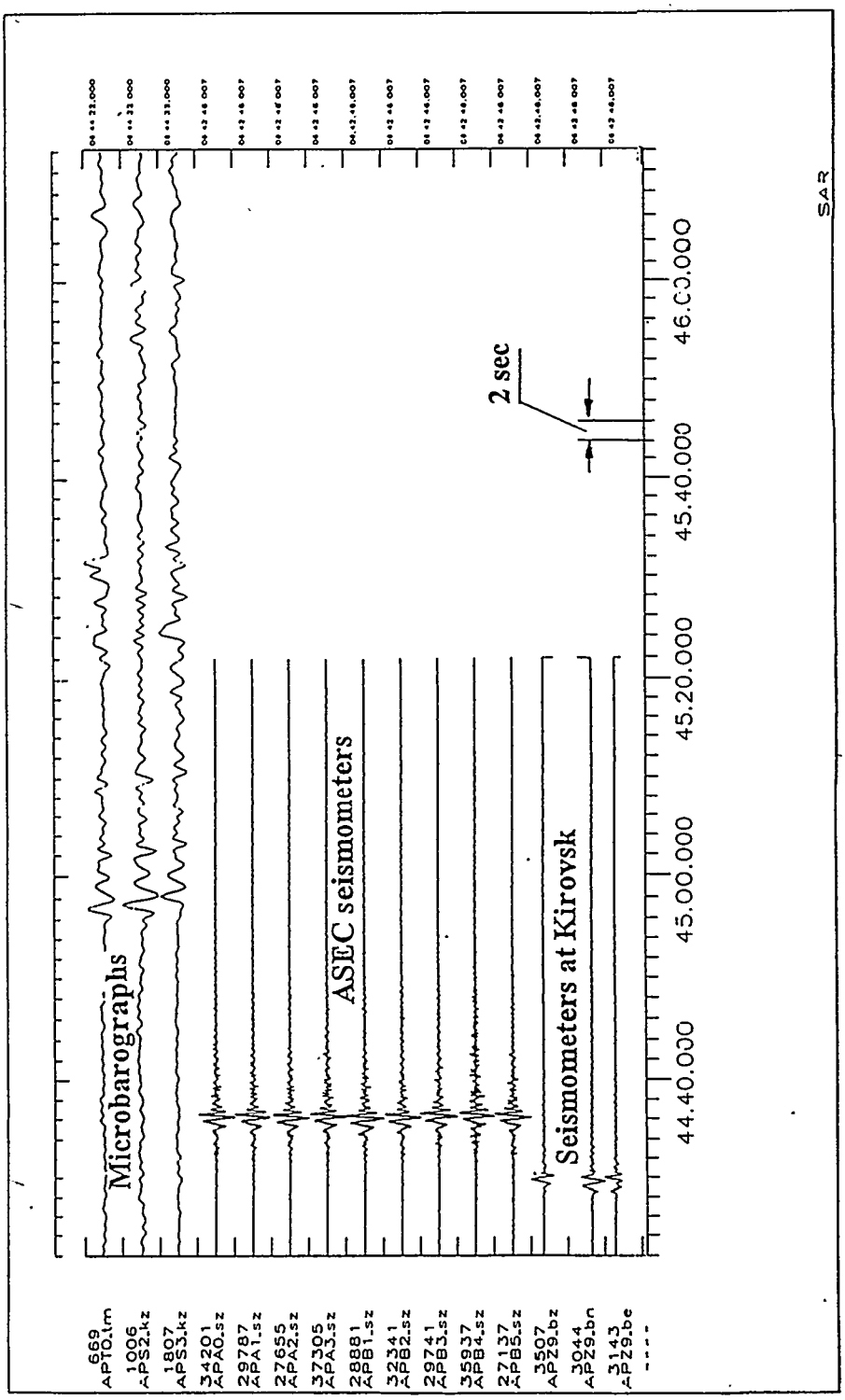
Microbarographs
ASEC seismometers
Seismometers at Kirovsk
2 sec
44.40.000
45.00.000
45.20.000
45.40.000
46.00.000
SAR

Figure 7.

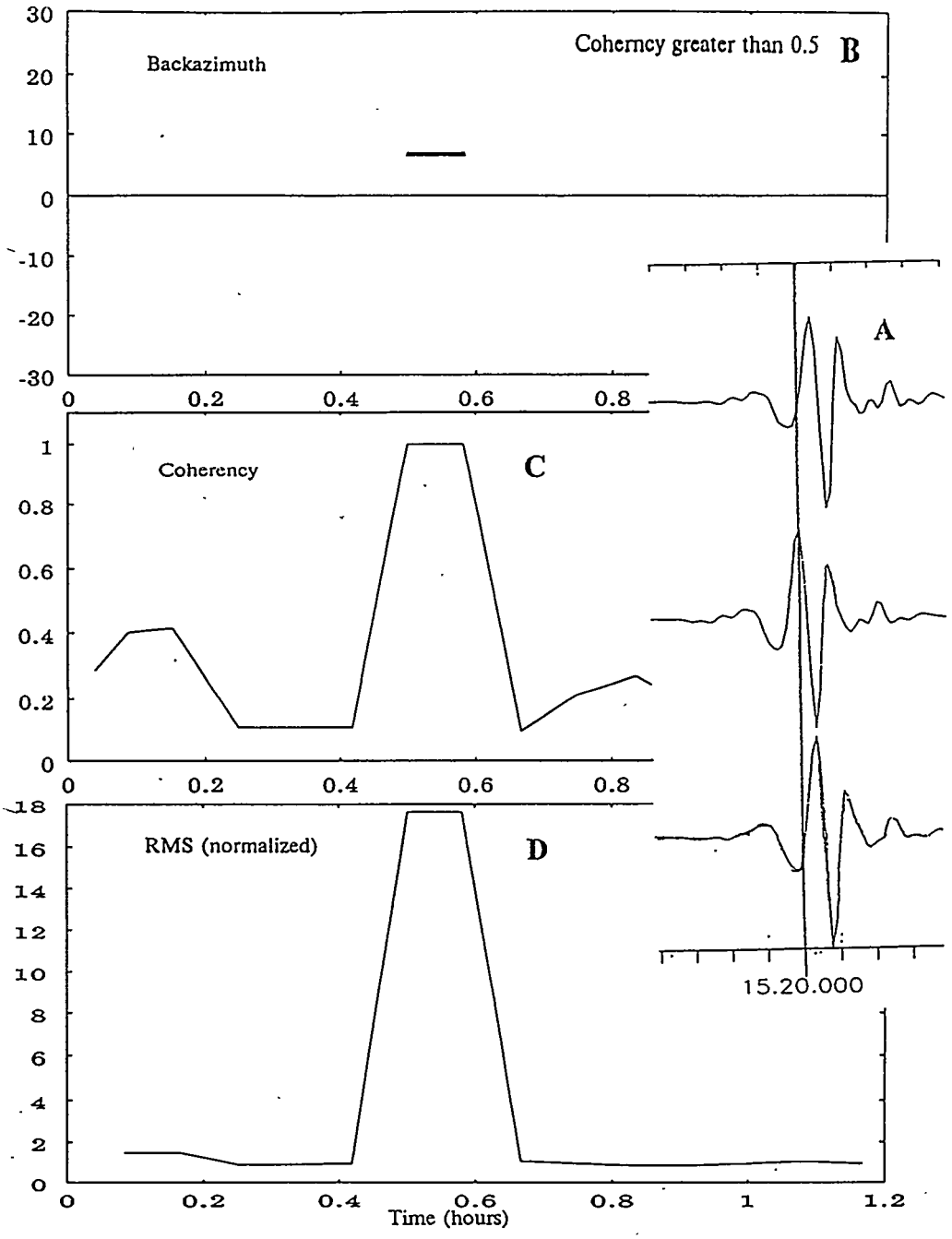
Backazimuth
Coherncy greater than 0.5
B
A
C
Coherency
D
RMS (normalized)
15.20.000
Time (hours)

Figure 8.

Loparskaya February 27, 1991

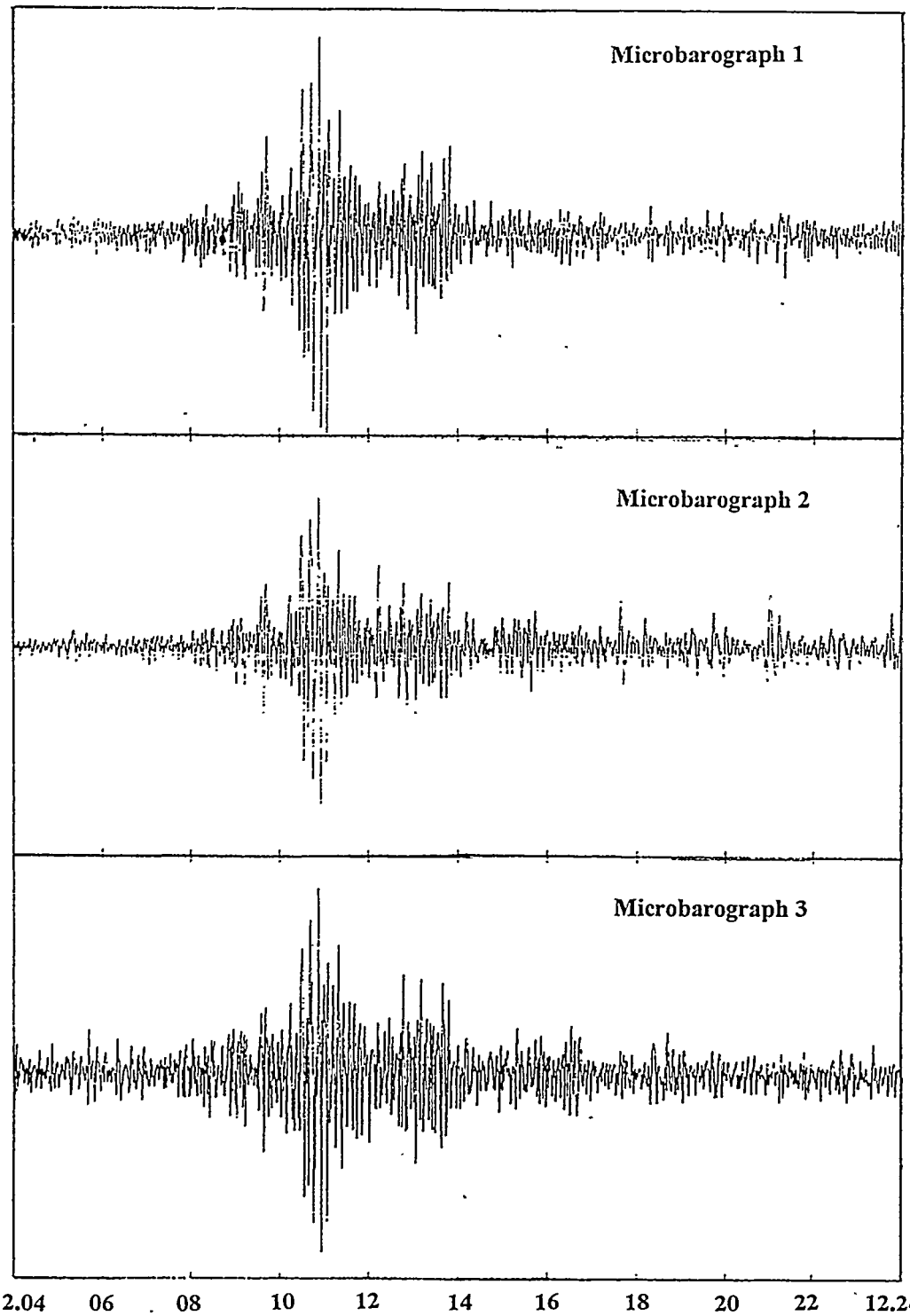

Figure 9.

Loparskaya February 27, 1991 12 06 UT

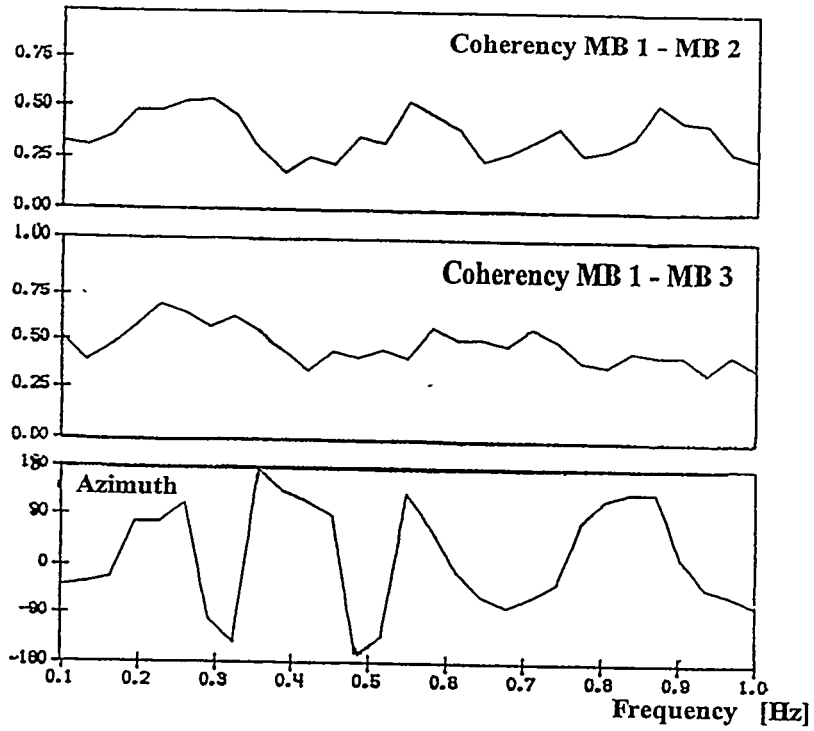

12 10 UT

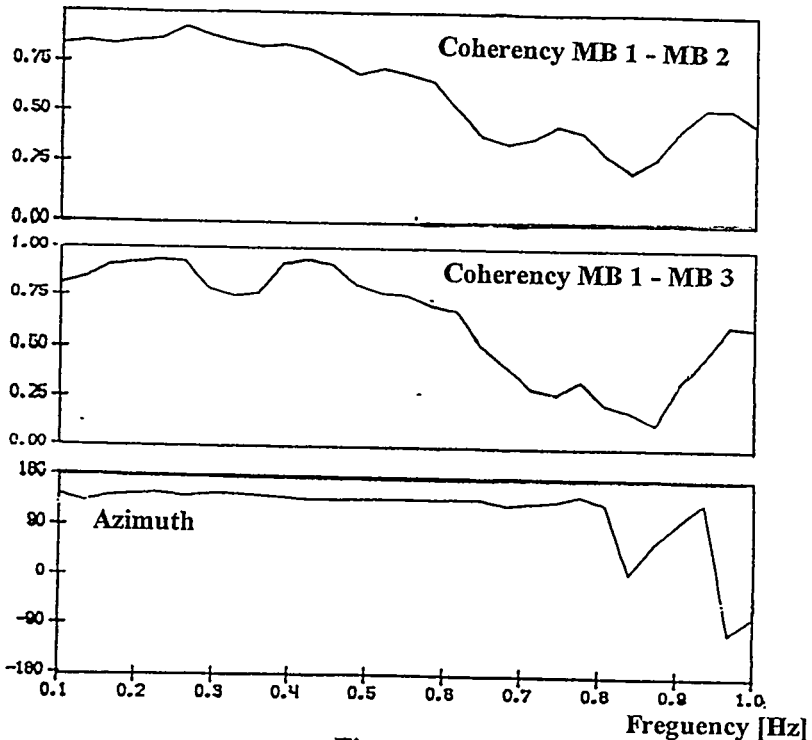

Figure 10.

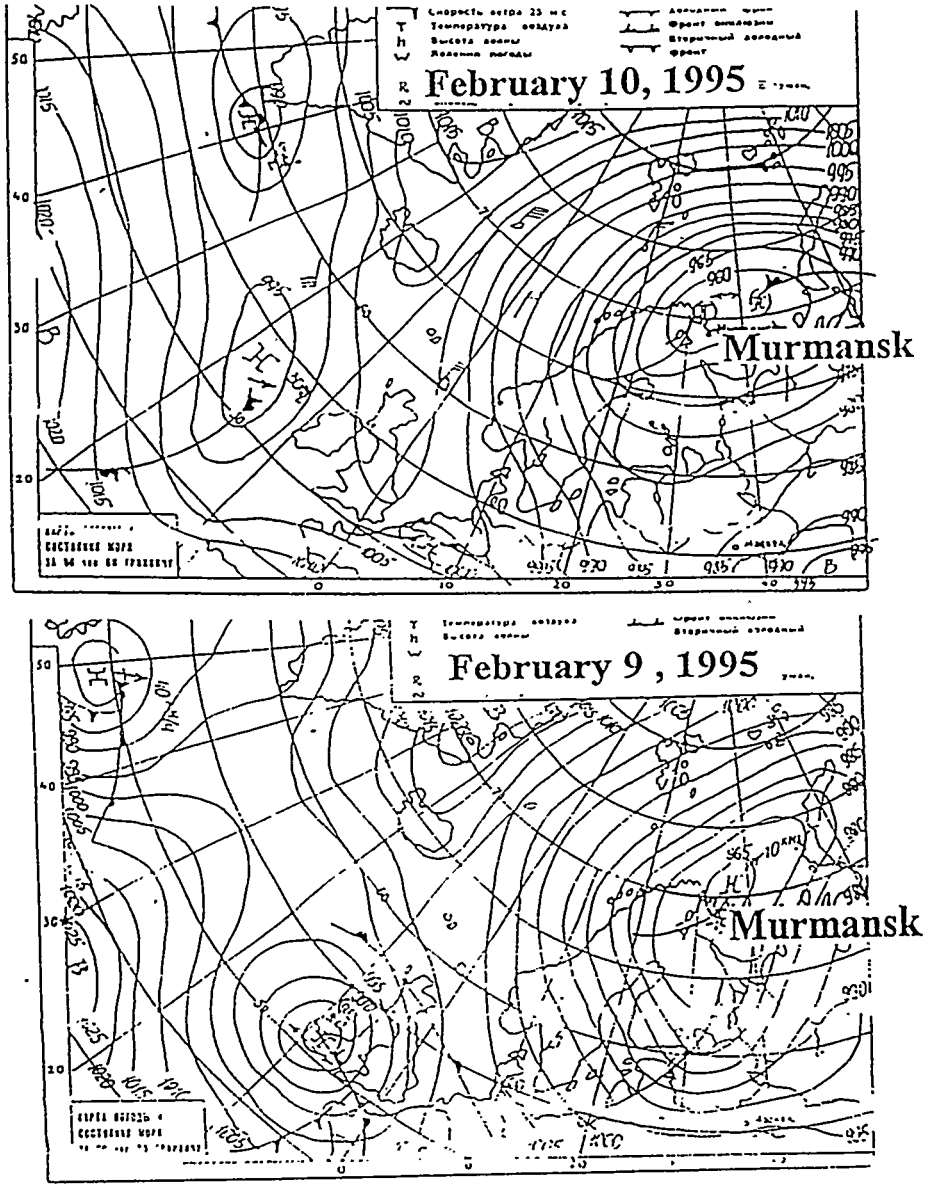

Figure 11.

10 February 1994

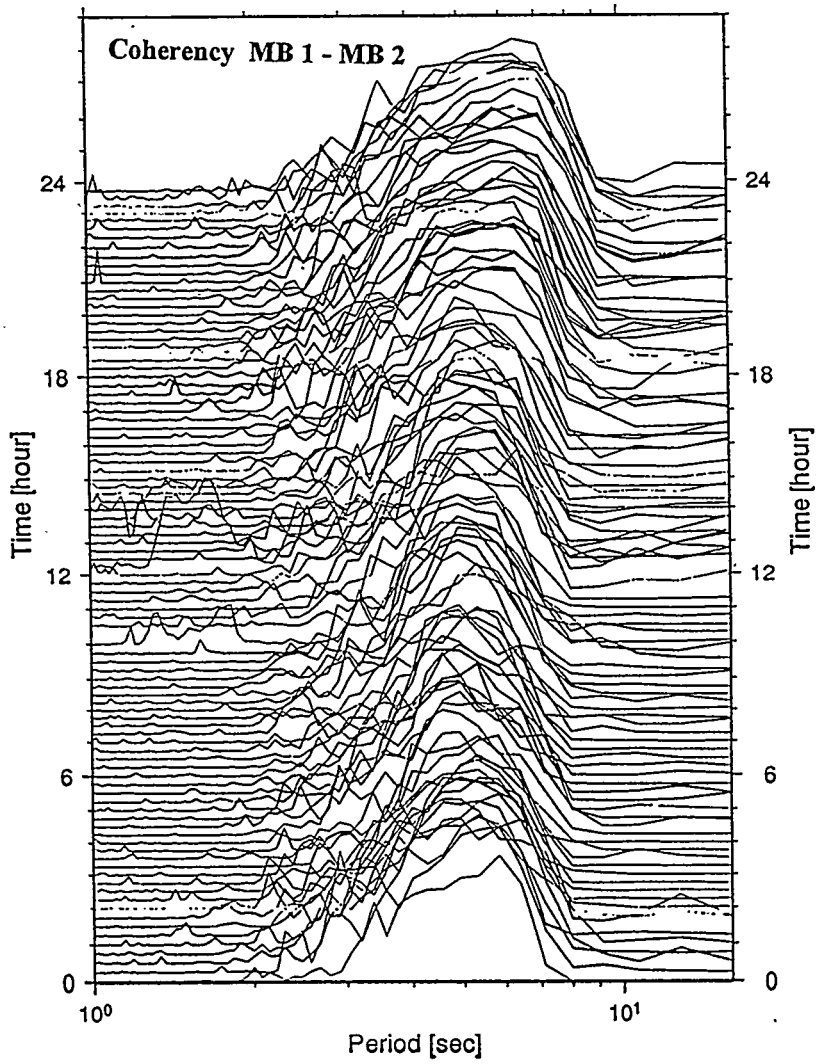

Figure 12.

10 February 1995

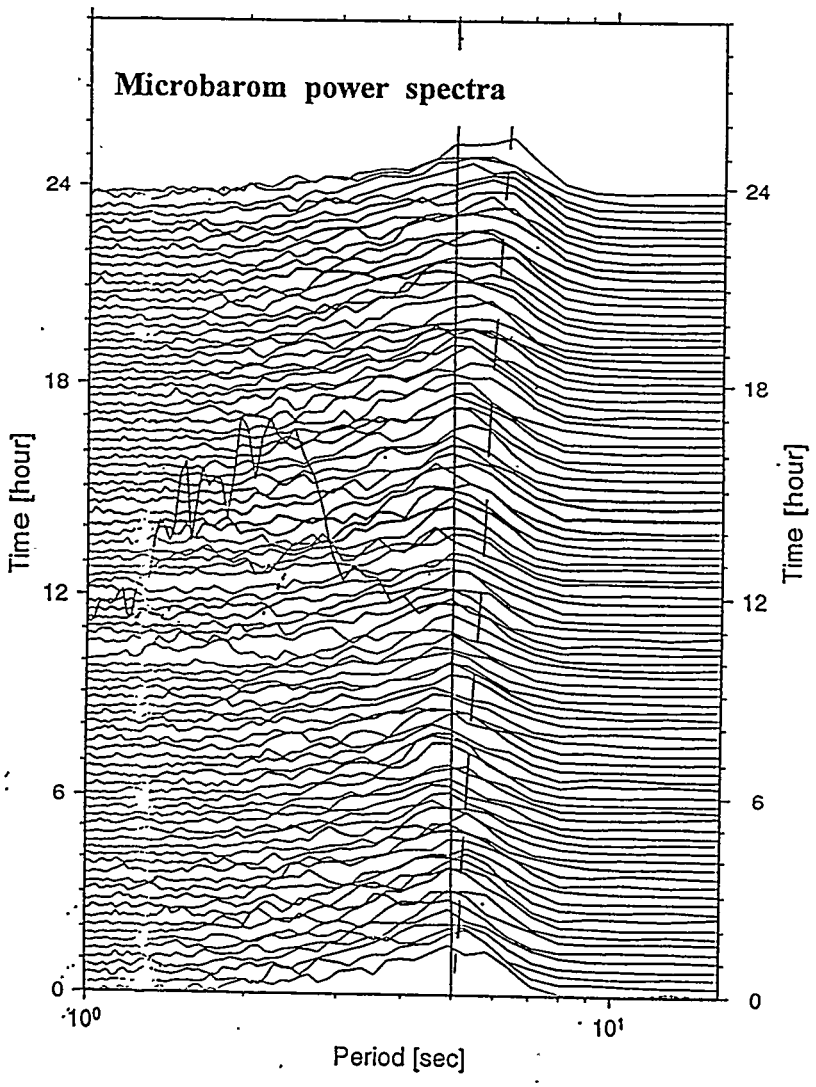

Figure 13.

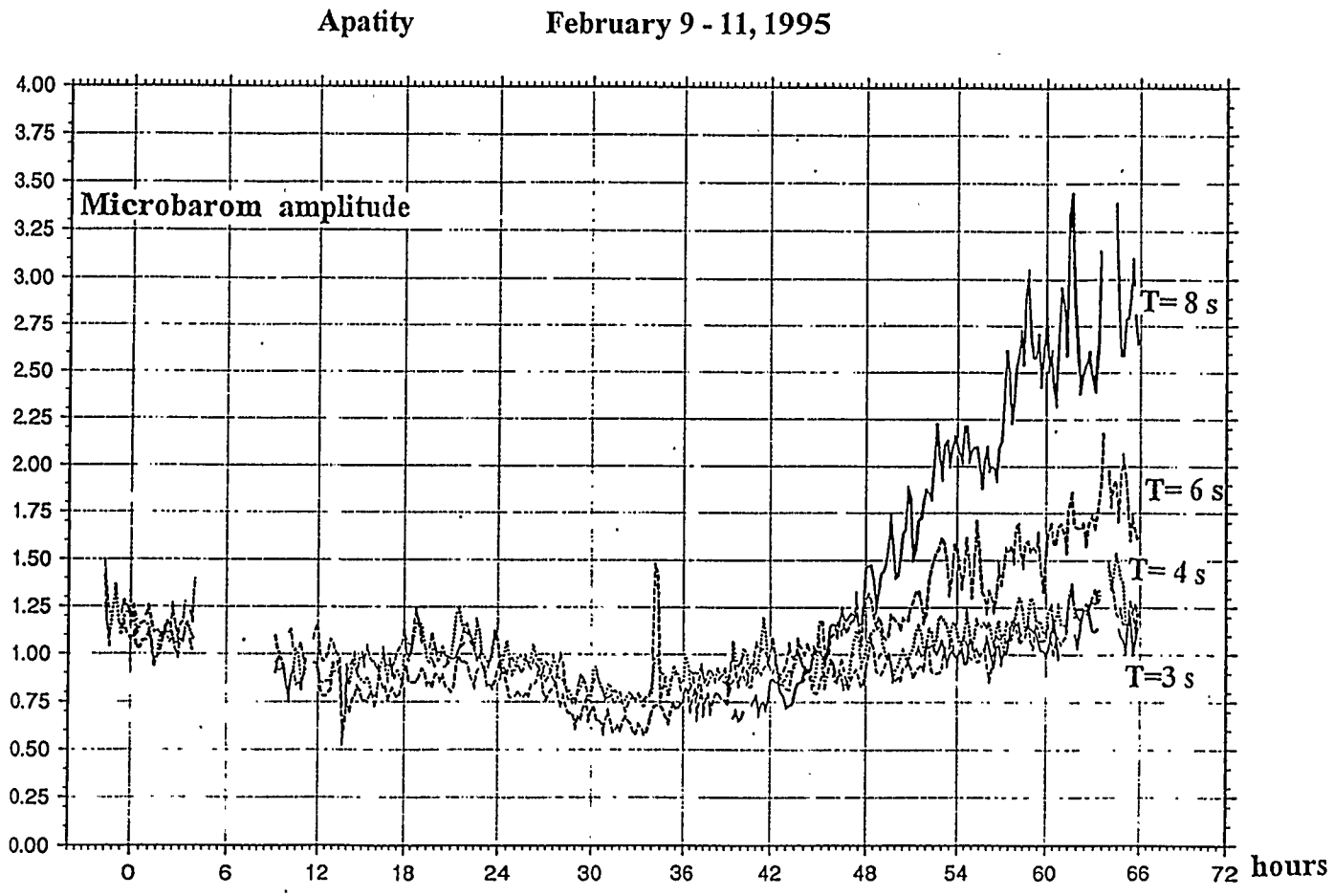
Apatity February 9 - 11, 1995
Microbarom amplitude
T= 8 s
T= 6 s
T= 4 s
T=3 s
4.00
3.75
3.50
3.25
3.00
2.75
2.50
2.25
2.00
1.75
1.50
1.25
1.00
0.75
0.50
0.25
0.00
0
6
12
18
24
30
36
42
48
54
60
66
72
hours

Figure 14.

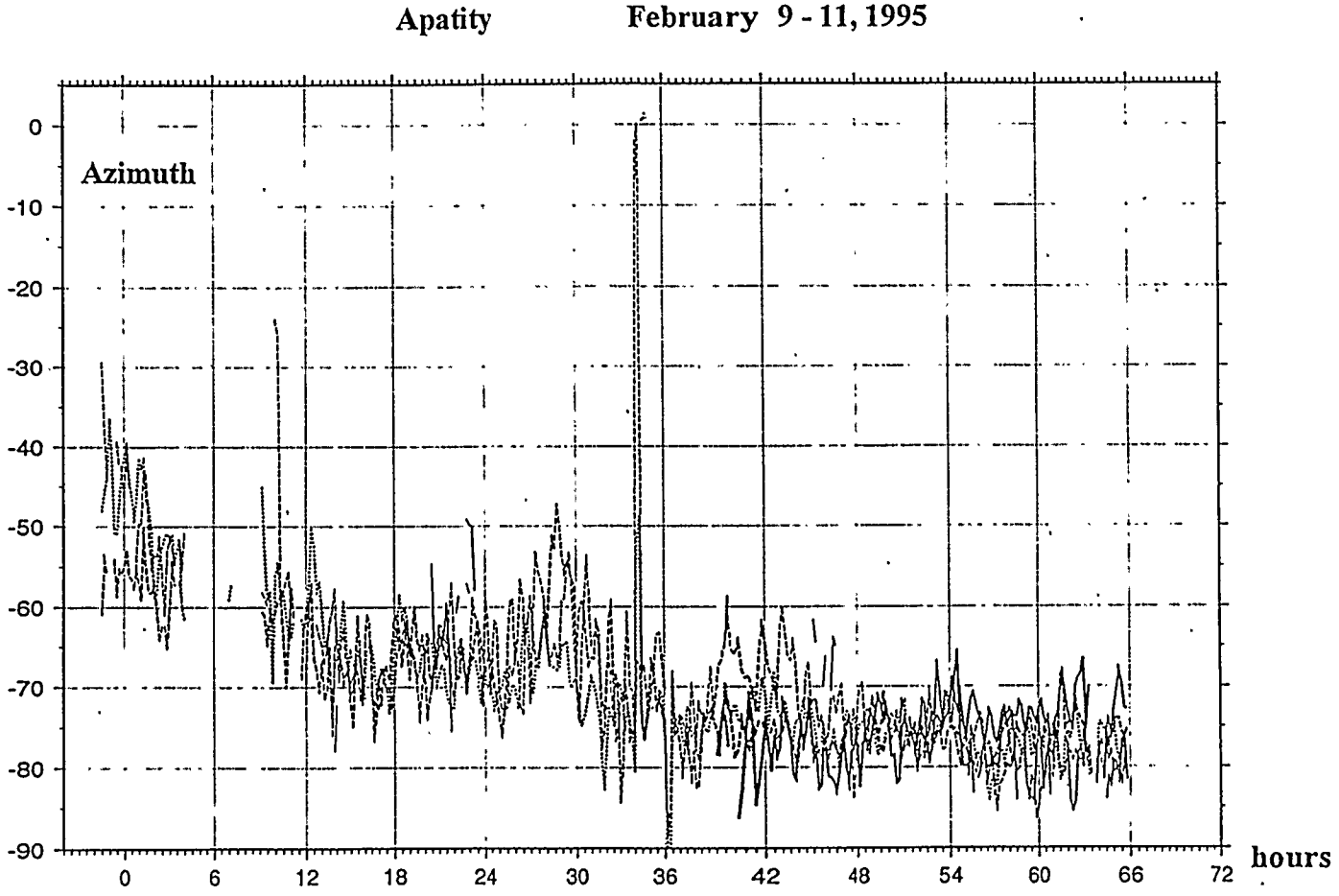
Apatity
February 9 - 11, 1995
Azimuth
0
-10
-20
-30
-40
-50
-60
-70
-80
-90
0
6
12
18
24
30
36
42
48
54
60
66
72
hours

Figure 15.

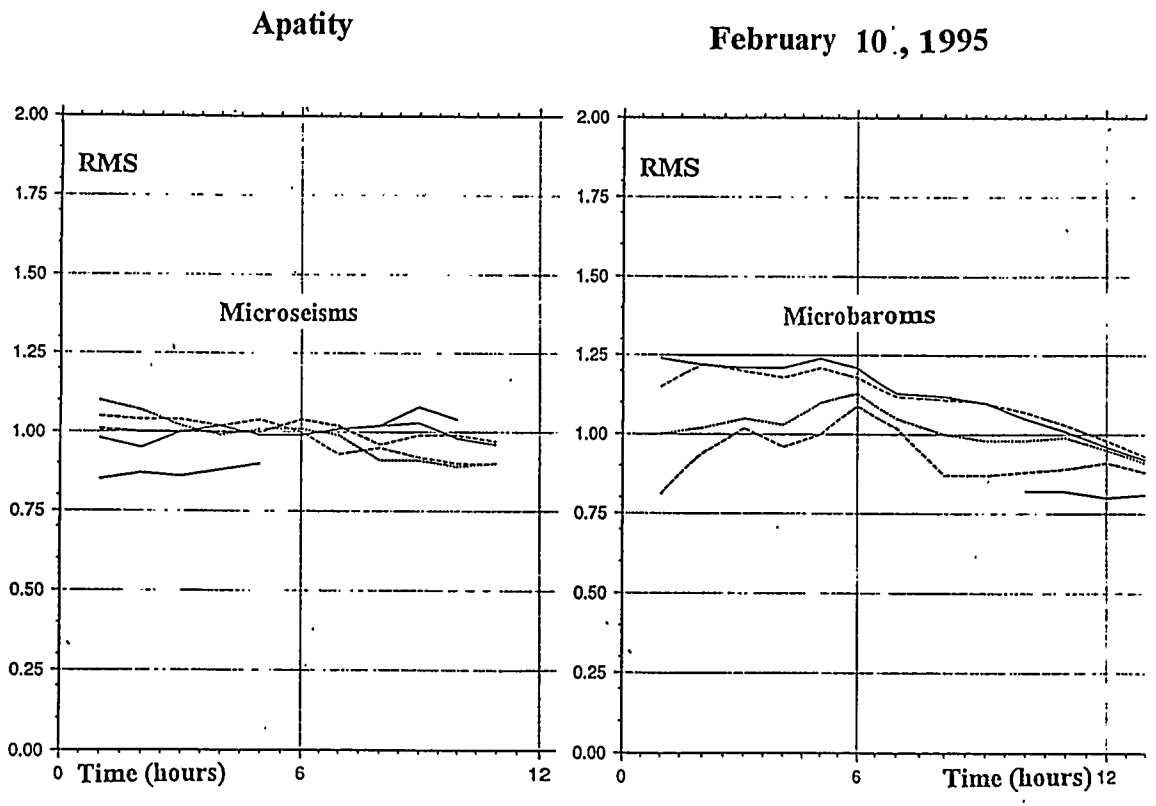
Apatity
February 10, 1995
RMS
Microseisms
RMS
Microbaroms
2.00
1.75
1.50
1.25
1.00
0.75
0.50
0.25
0.00
0
6
12
Time (hours)
Time (hours)

Figure 16.

INFRASOUND DETECTION - THE FRENCH SYSTEM

Elisabeth Blanc

CEA/DASE/LDG
BP 12, 91680
Bruyères le Chatel, France

An experimental station developed by CEA/DASE has been set up at Flers (Normandy), France. This station is a four element array, whose characteristics correspond to the request of the experts of the Conference of Disarmament for the CTBT infrasound monitoring network. The purpose of this presentation is to summarize the most important results obtained at Flers during 1.5 year of permanent measurements.

Most of the infrasounds measured at the Flers station are microbaroms produced by the ocean swell, atmospheric waves associated to severe weather and high frequency infrasounds generated by the Concorde supersonic aircraft. The signature of theses disturbances is characteristic. Well identified infrasound as microbaroms or Concorde infrasounds can be used for testing the system and defining the best adapted automatic processing methods. Last results obtained with PMCC method are presented.

A second station in Bretagne has been added for determining the location precision and for testing the event association methods. Several different configuration of porous hoses for noise reduction have been tested and circular hoses seems to be a well adapted configuration. Noise measurements in different vegetation conditions were intensively performed in France. Measurements in French Guyana allowed to evaluate noise and vegetation effects in quite different conditions. Infrasounds produced by the Ariane rocket on April 16, 1997 have been used for the estimation of the detectability in different environment conditions.

INFRASOUND DETECTION THE FRENCH SYSTEM

E. Blanc, Y. Cansi, G. Claque, D. Fouquet, A. Le Pichon
J.L. Plantet, Y. Moreno, G. Ruzié

Commissariat a l'Energie Atomique,
Département Analyse Surveillance Environnement
BP 12, 91680 Bruyères le Chatel
France

Infrasound detection

- **The French system**
  - sensors
  - infrasound arrays
  - data processing
- **Infrasounds from a nuclear explosion**
  - Examples of researched signals
  - Propagation laws
- **Detection capability of the CTBT infrasound network**
- **Infrasound noise and noise reduction**
  - Noise characteristics, different kind of hoses configurations vegetation effect
- **Infrasounds from natural sources**
  - Severe weather, Volcanic eruptions, Ariane 5

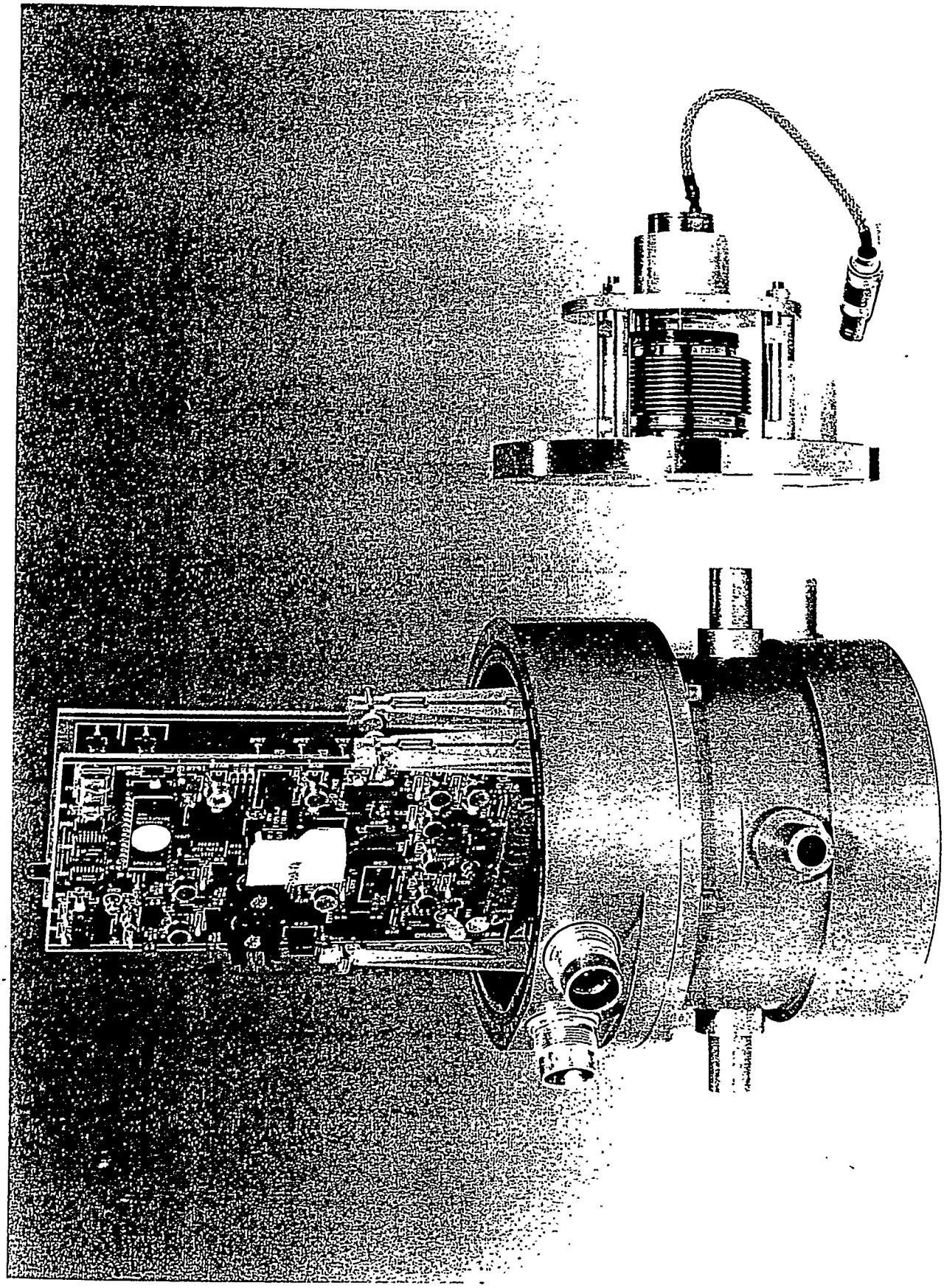

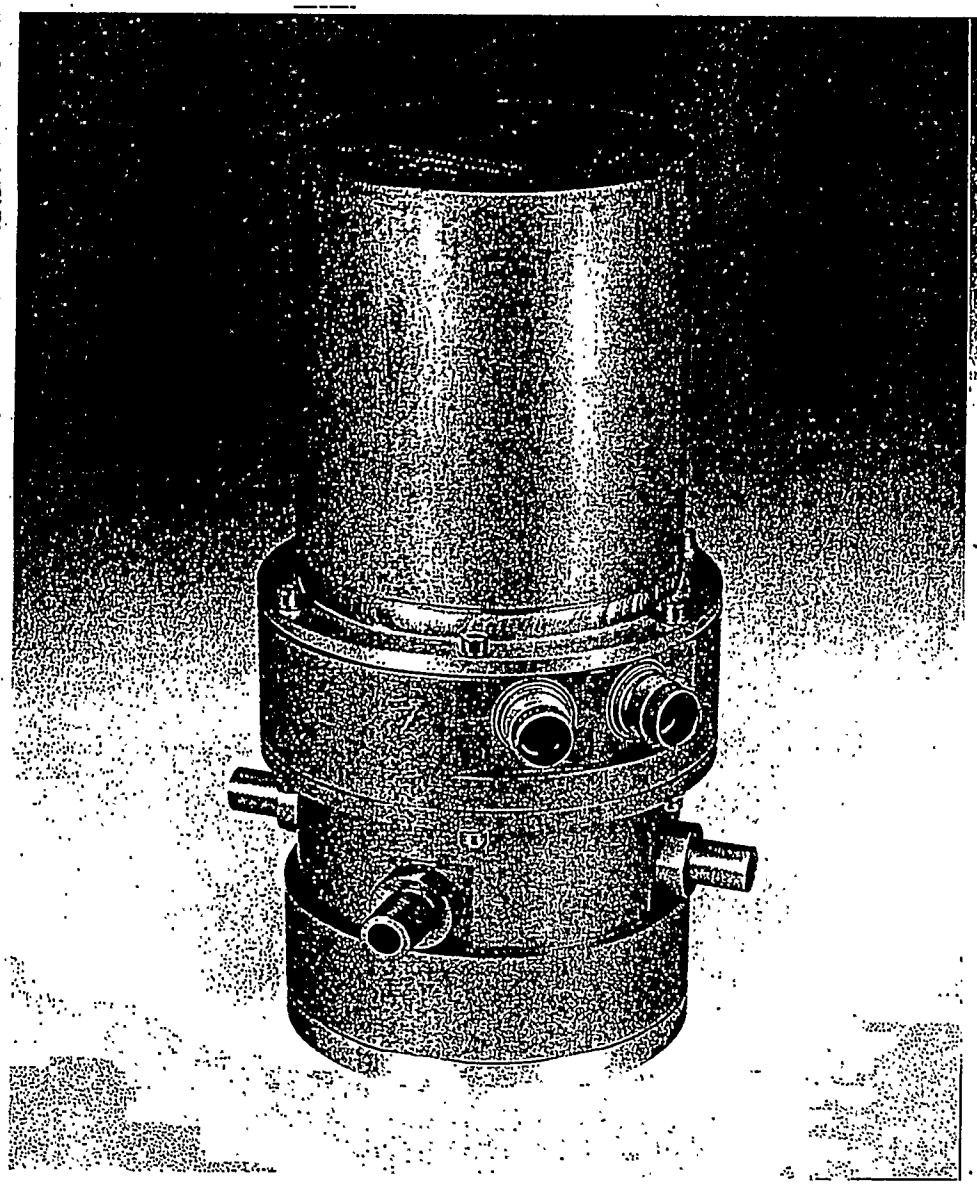

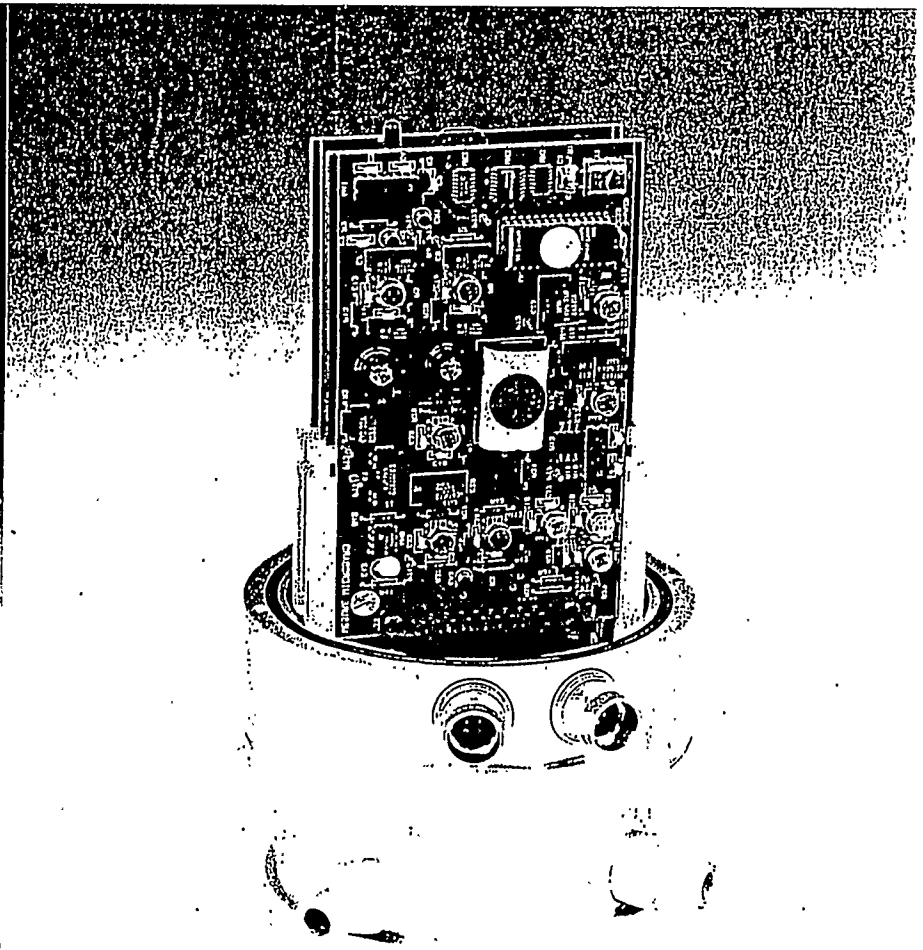

The MB2000 microbarometer frequency response

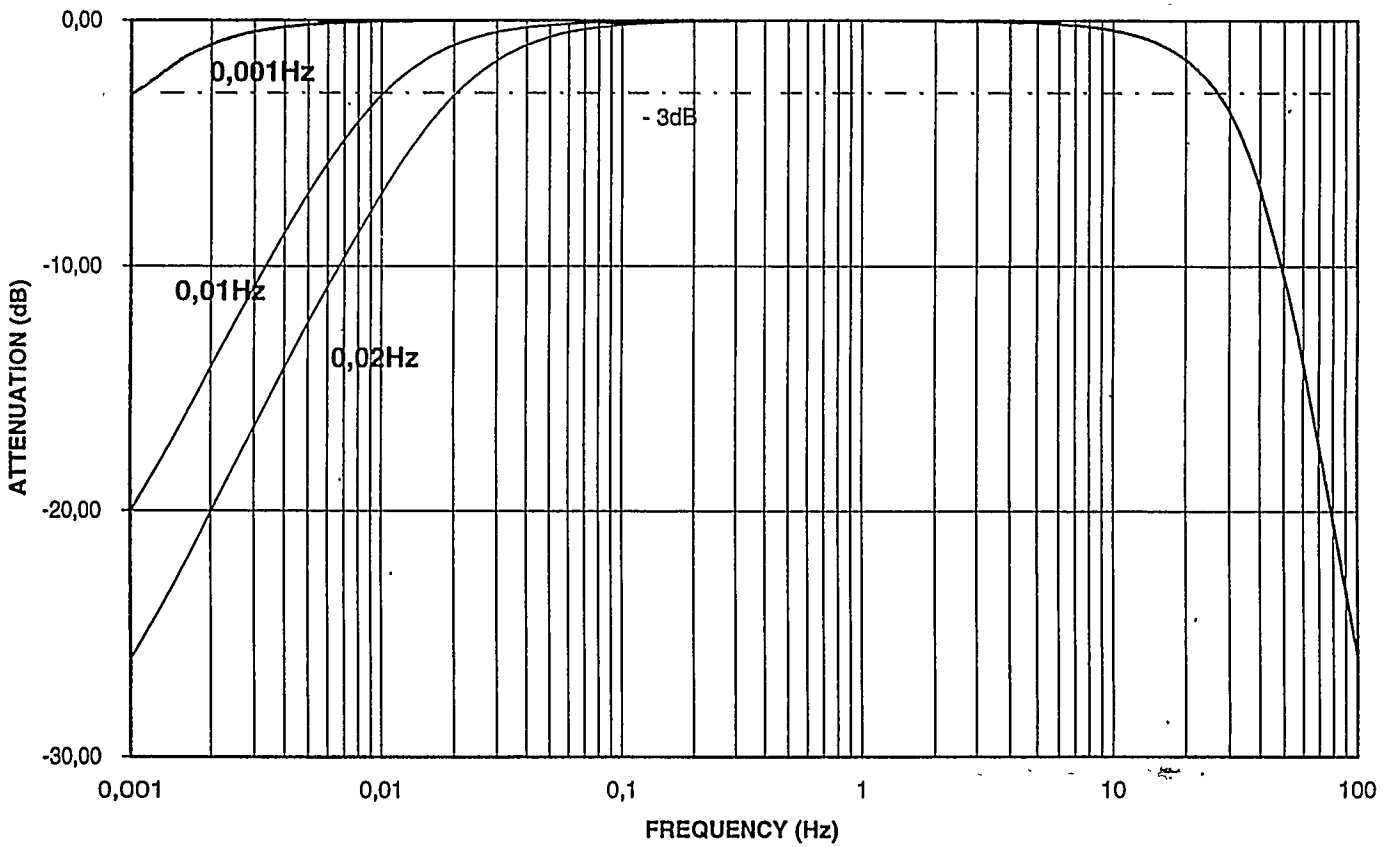

Electronic and background noises on a MB 2000 microbarometer

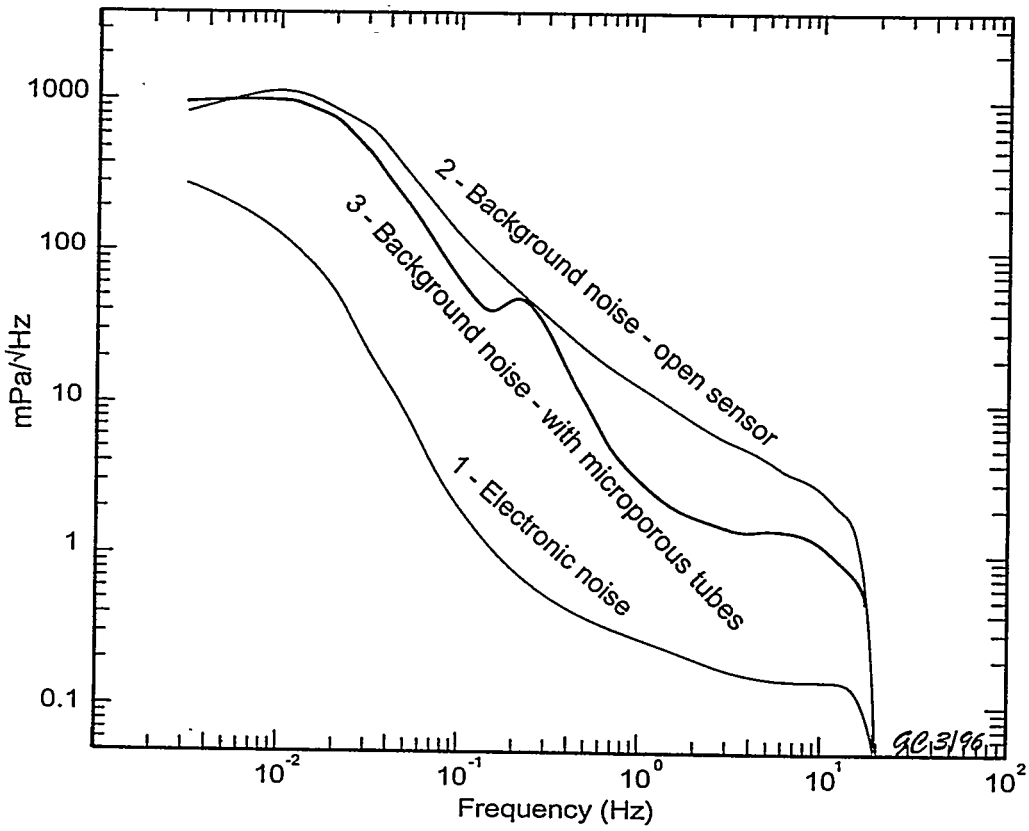

Comparison between the CEA infrasound station and the Expert Group proposals

(Report of the Infrasound Experts Group, December 15, 1995)

Expert group (95)

	Sensor minimum characteristics proposed by GSE	CEA sensor 20 bits ADC filtered outpout	CEA sensor 24 bits ADC no filtered .
Sensor			
Sensitivity		100 mV/Pa (1)	1 mV/Pa
Pass band	0.02-5 Hz	0.01-27 Hz (2)	0-27 Hz
Antialiasing filter	10 Hz	8 Hz	10 Hz
Sampling frequency	20 Hz - 10Hz	20 Hz - 10Hz	25 Hz
Amplitude range of sensor		200 hPa pp	200 hPa pp
Electronic noise		4 mPa pp	4 mPa pp
Dynamic range		134 dB	134 dB
digitizing unit			
Digitizing range		20 Vcc	20 Vcc
Digitizing outpout		20 bits	24 bits
LSB (filtered data)		0,19 mPa	1,19 mPa
Electronic noise (peak to peak)		21 LSB	3 LSB
Sensitivity of atmospheric pressure outpout (used for calibration)		1 mV/hPa	1 mV/hPa
Amplitude range outpout	100 Pa pp	200 Pa pp	20000 Pa pp
Electronic noise	10 mPa pp	4 mPa pp	4 mPa pp
Dynamic range	80 dB	94 dB	134 dB.

(1) also suitable for 16 bit ADC

(2) 0.001-27 Hz option

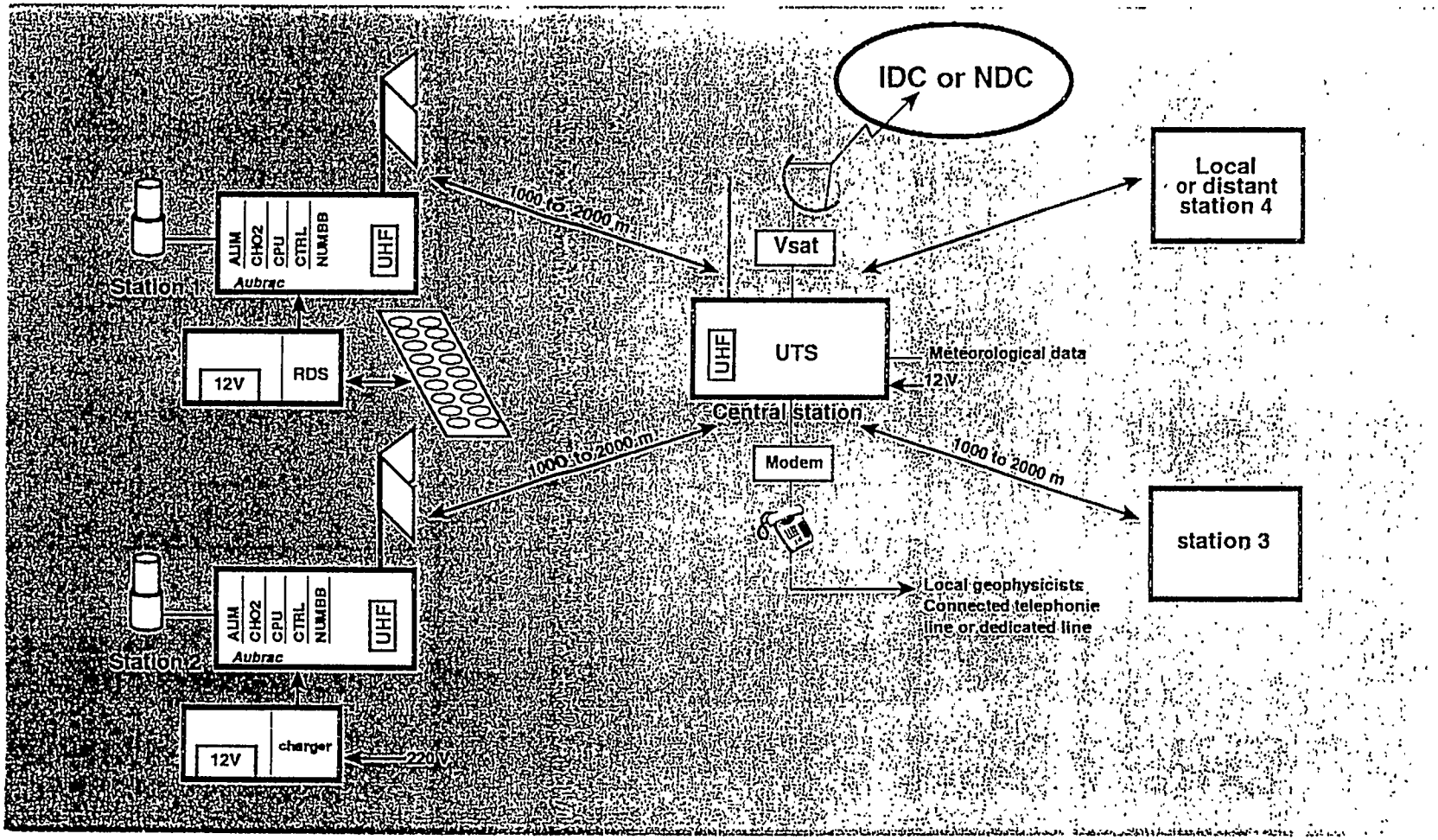

Figure 2 *Infrasound array. The central station is directly connected to the IDC over a VSAT satellite link. Local data processing is also possible by telephone line.*

PMCC method

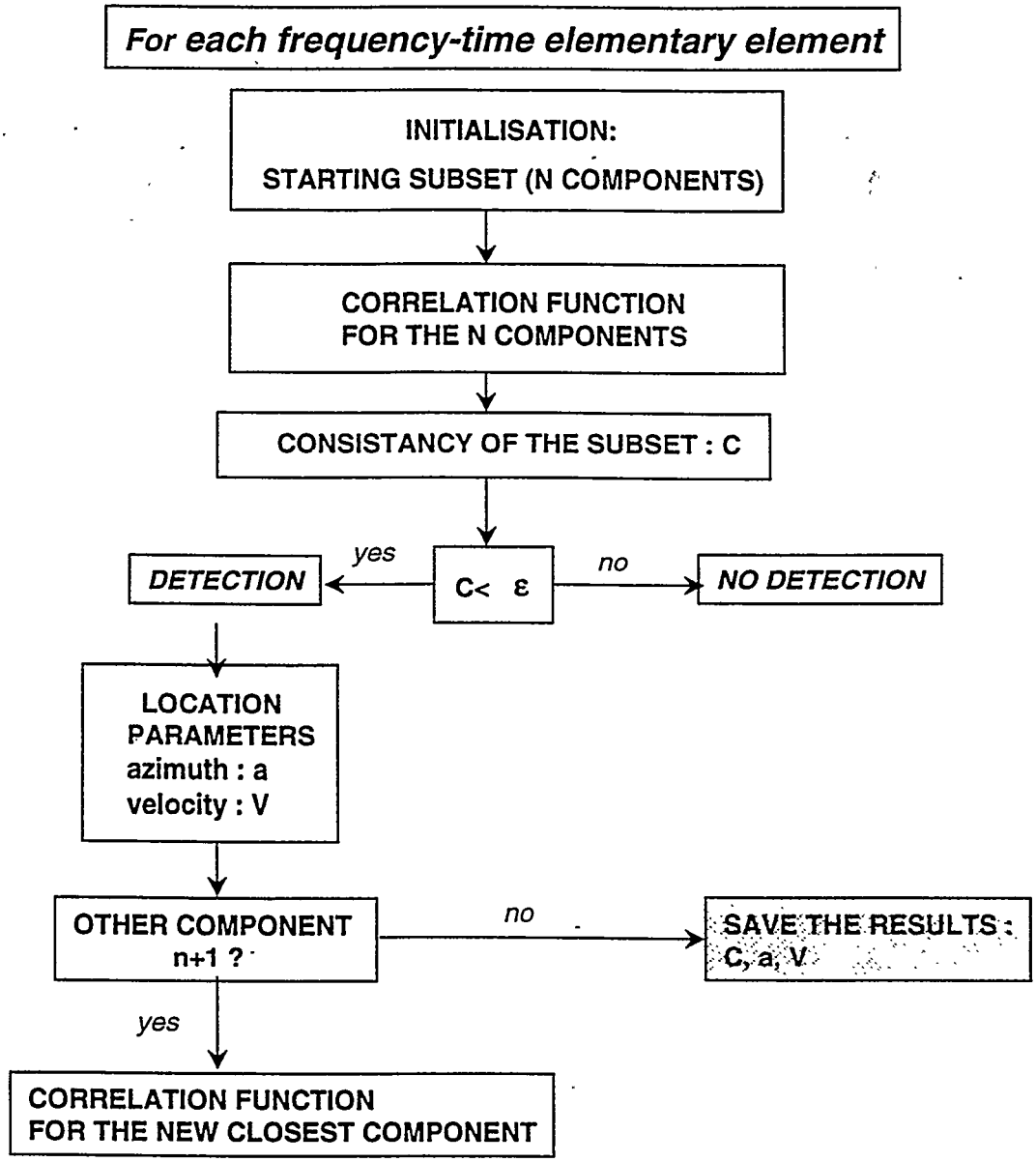

DASE/LDG - E. BLANC - 25/08/97

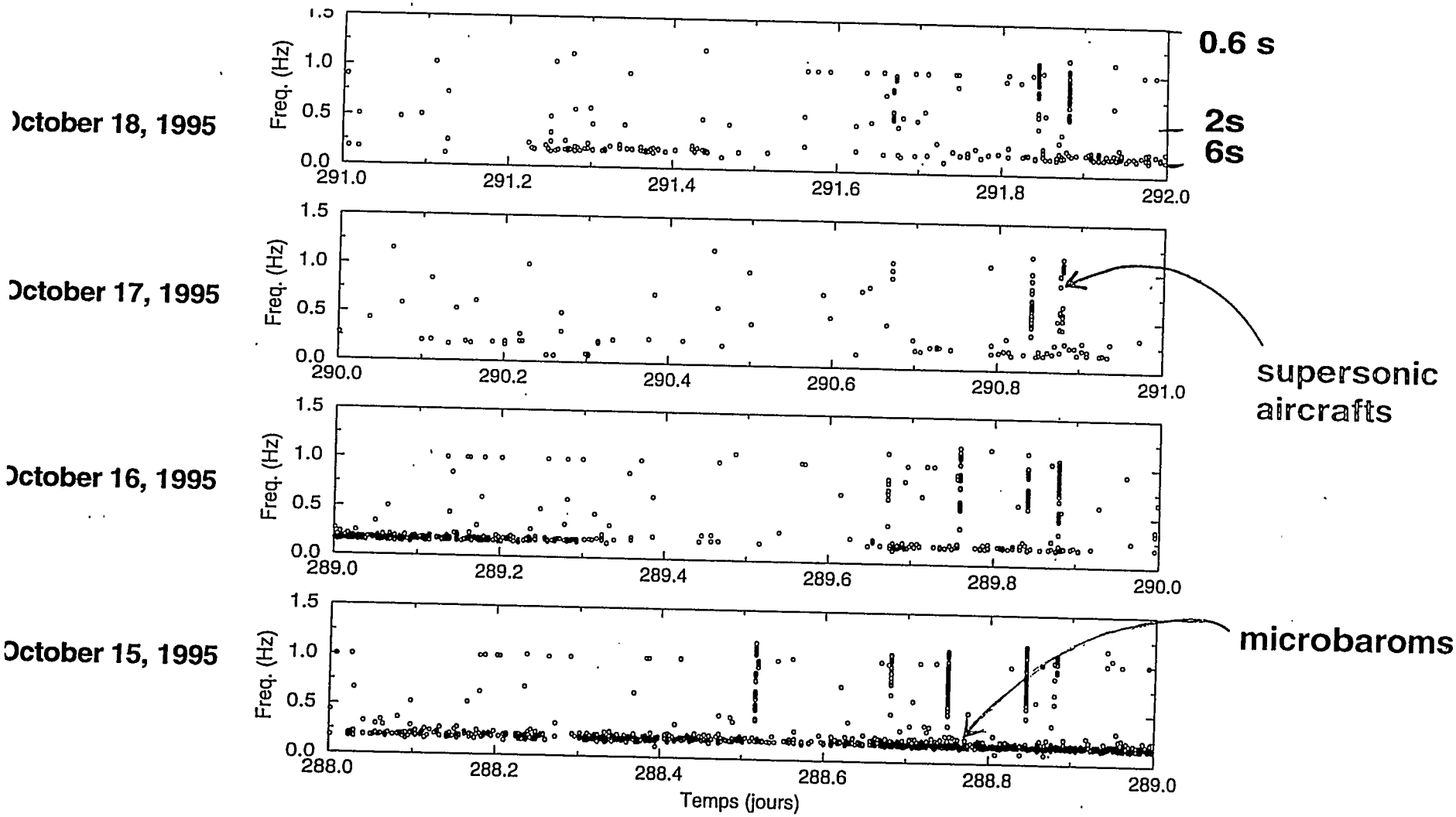

FLN infrasound network (4 components)
4 days of measurements

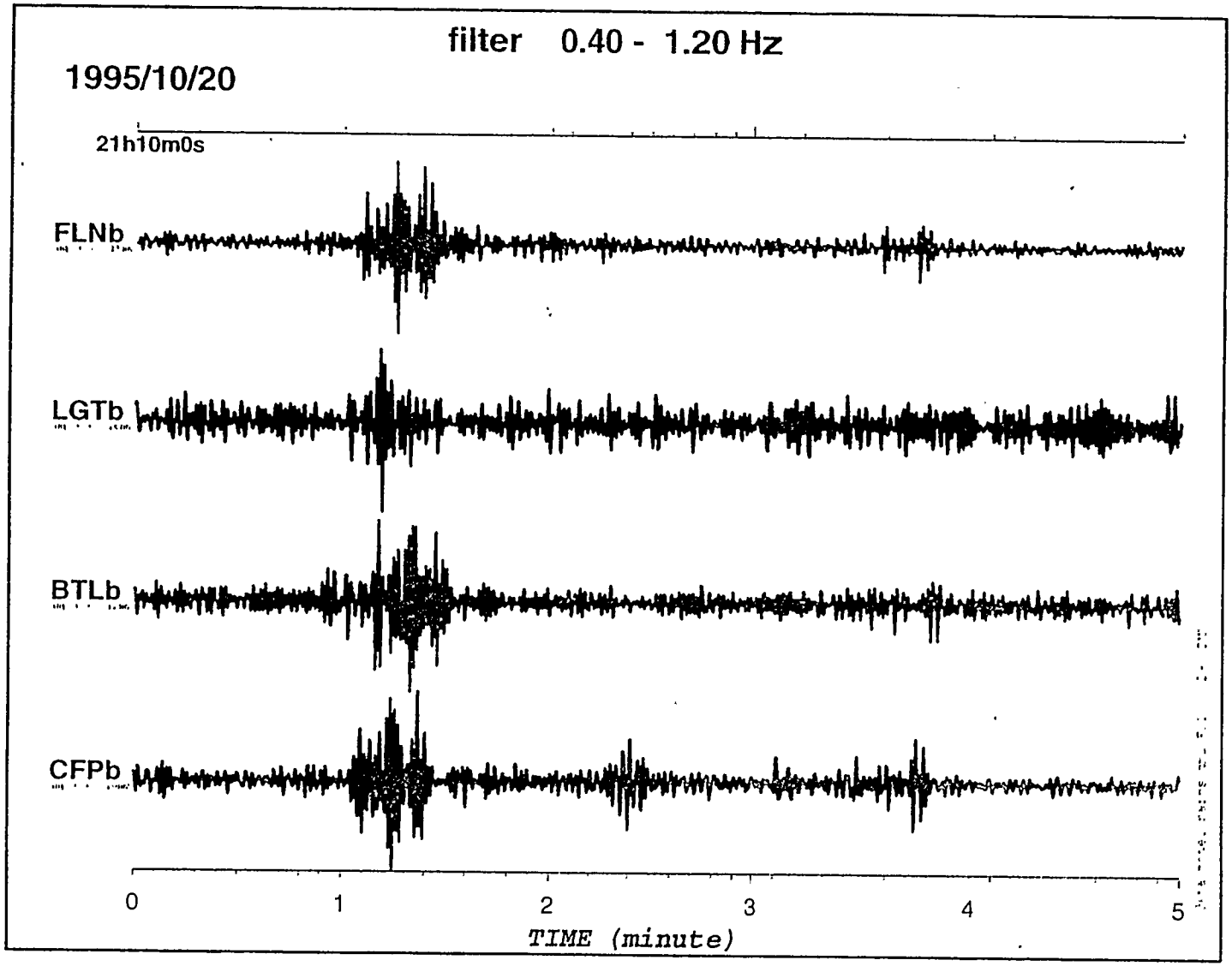
filter 0.40 - 1.20 Hz
1995/10/20
21h10m0s
FLNb
LGTb
BTLb
CFPb
0
1
2
3
4
5
TIME (minute)

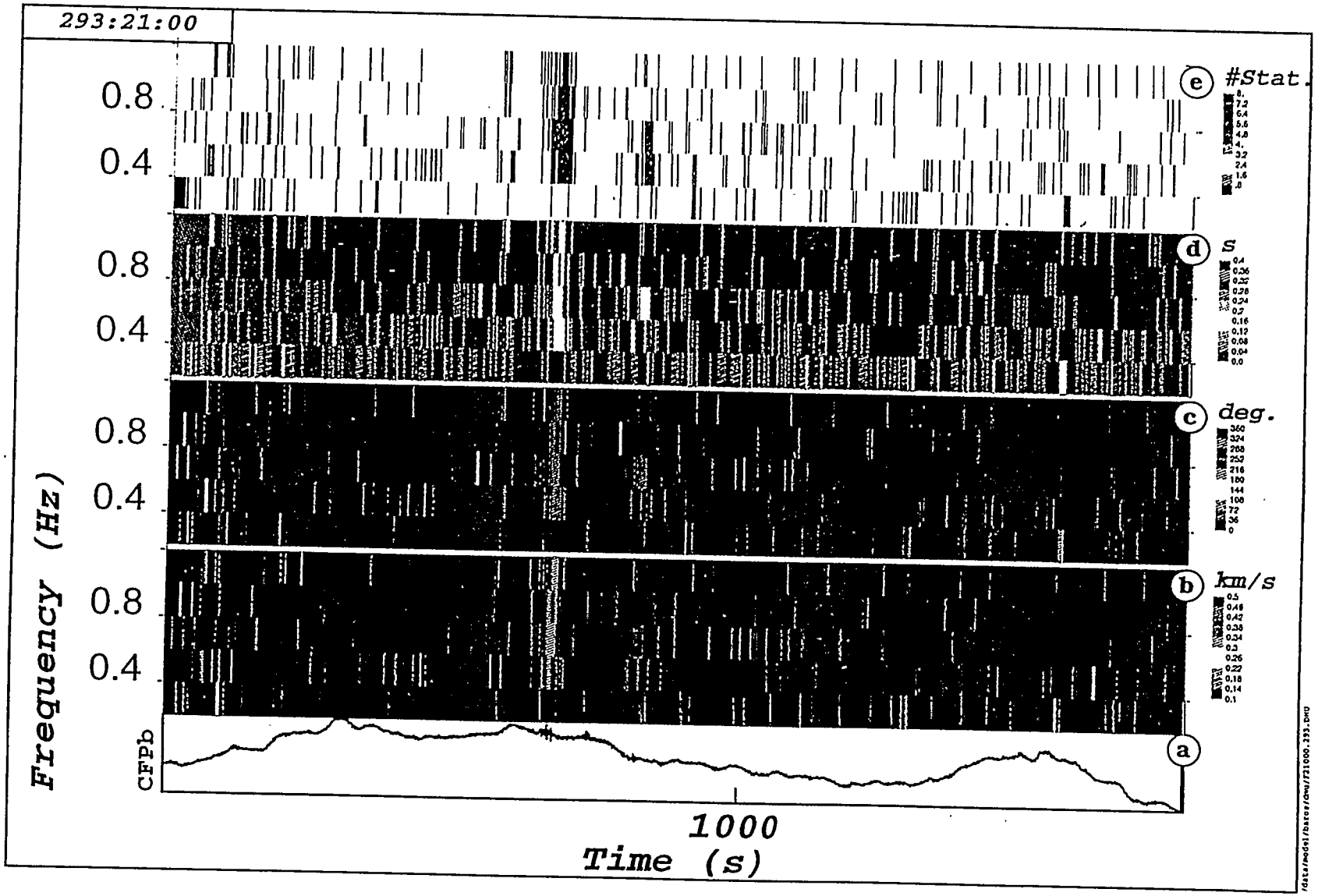
293:21:00
0.8
0.4
0.8
0.4
0.8
0.4
0.8
0.4
Frequency (Hz)
e
#Stat.
d
S
c
deg.
b
km/s
a
cFpb
1000
Time (s)

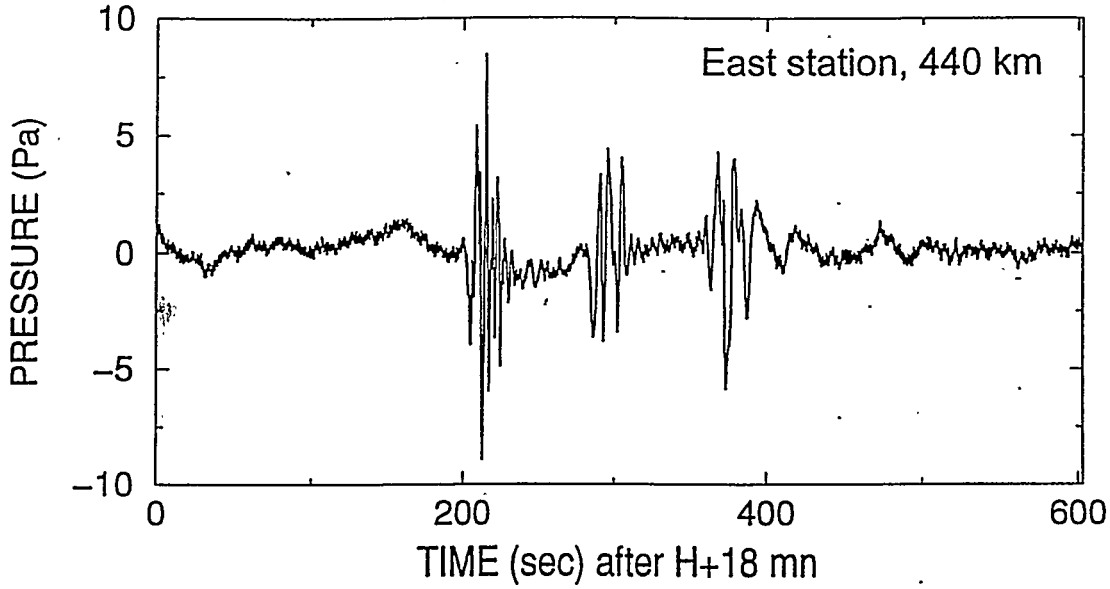

Figure 2: signals measured by the LDG during nuclear tests of a few kilotons at 440 km East of the explosion point. The different arrivals are produced by reflections of the waves in the upper layers of the atmosphere.

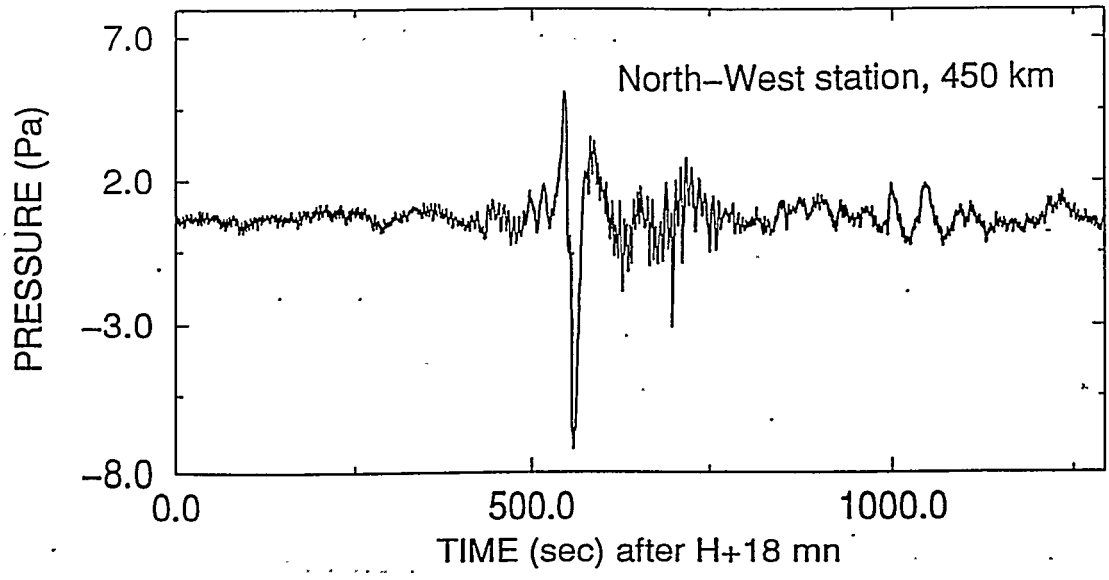

Figure 3: same as Figure 2 for measurements at 450 km in the North-West direction

PROPAGATION OF THE INFRASOUNDS IN THE ATMOSPHERE

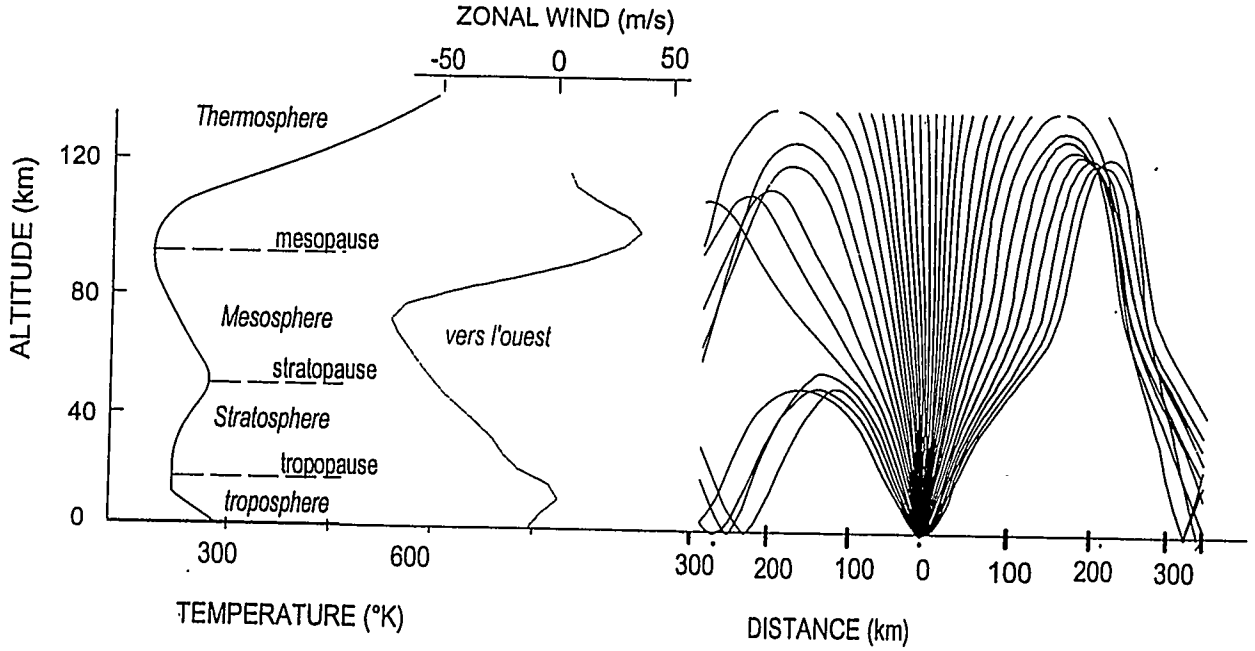

Figure 1 : Acoustic ray tracing (right) and temperature (left) and wind (center) profiles corresponding to conditions possible in the Northern hemisphere in summer.
The waves are reflected in the stratosphere and thermosphere's temperature increase levels. They are submitted to the stratospheric winds which drag the acoustic energy in the wind direction.

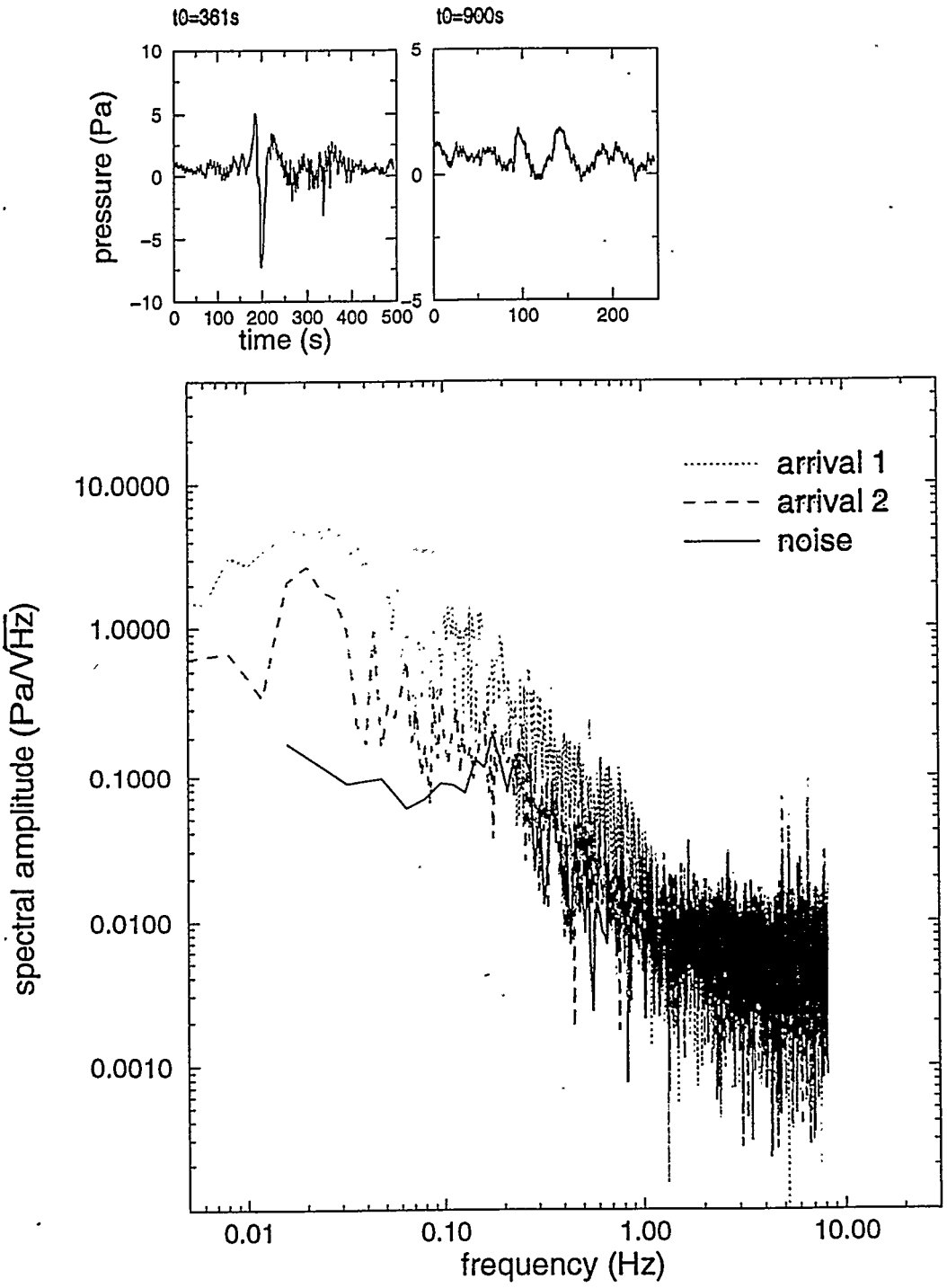

Figure 5: Same as Figure 4 for the signals of Figure 3

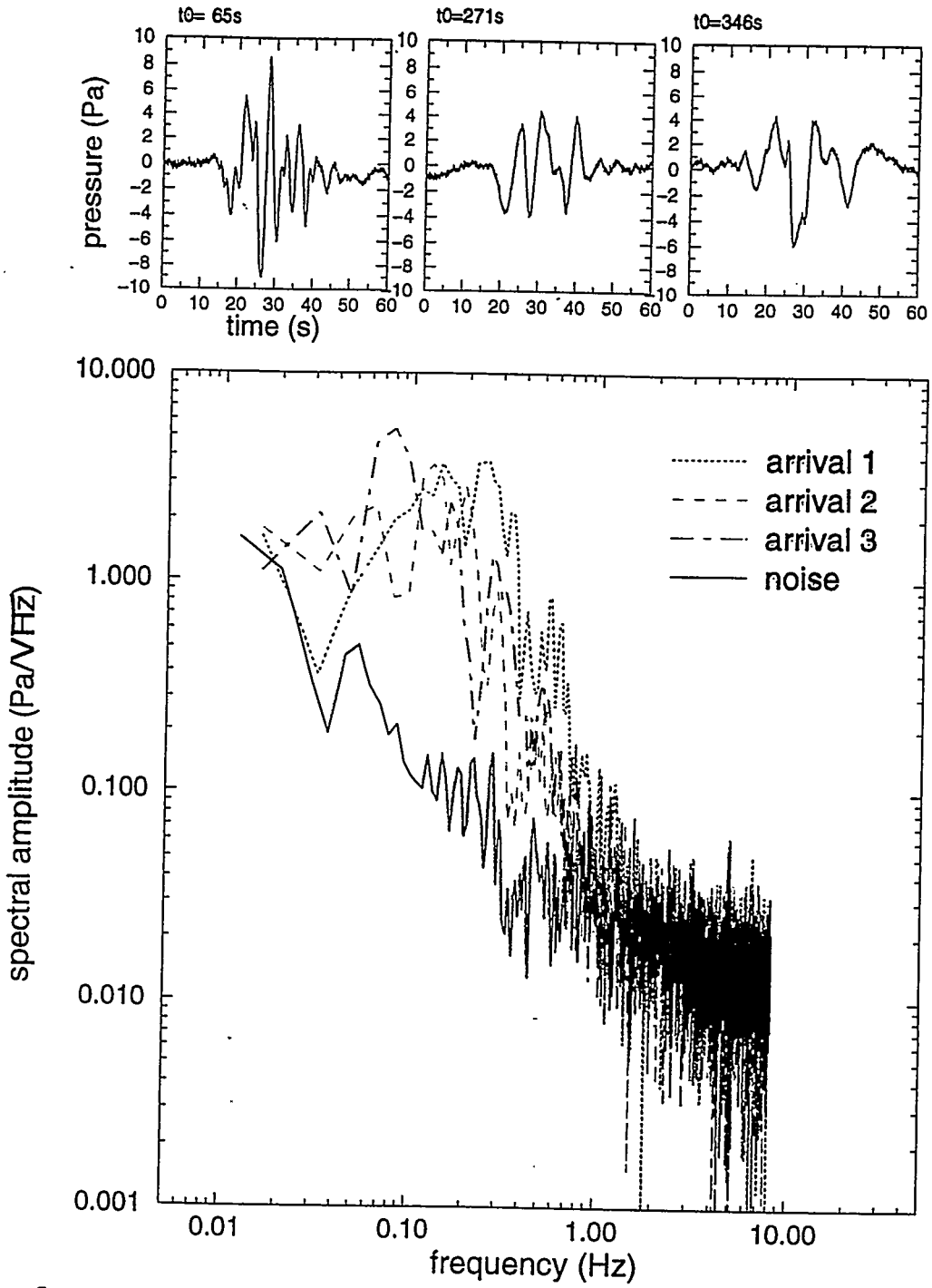

figure 4: Comparison of the spectra of the different arrivals of Figure 2 with a noise spectrum measured little before the test. The upper part of the figure shows the details of the signals corresponding to the different arrivals.

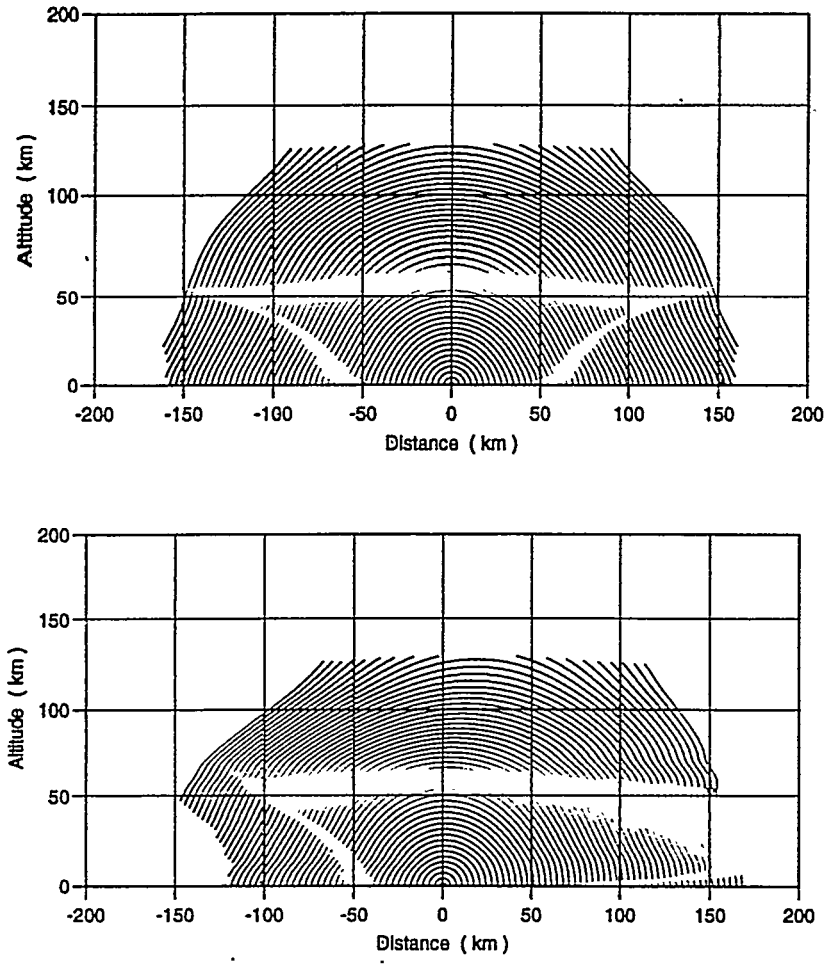

Figure 8 : The wave fronts have bee determined for a 5 kt explosion without wind (top) and in the presence of winds (bottom)

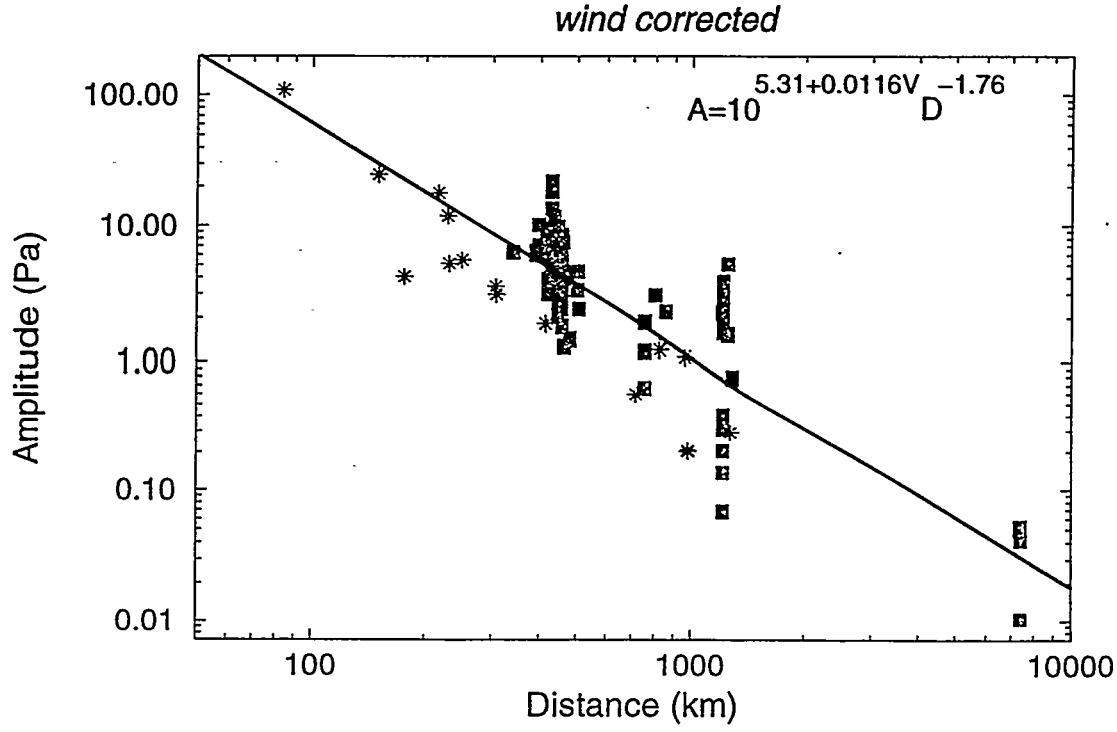
wind corrected
5.31+0.0116V −1.76
A=10 D
100.00
10.00
1.00
0.10
0.01
Amplitude (Pa)
100
1000
10000
Distance (km)

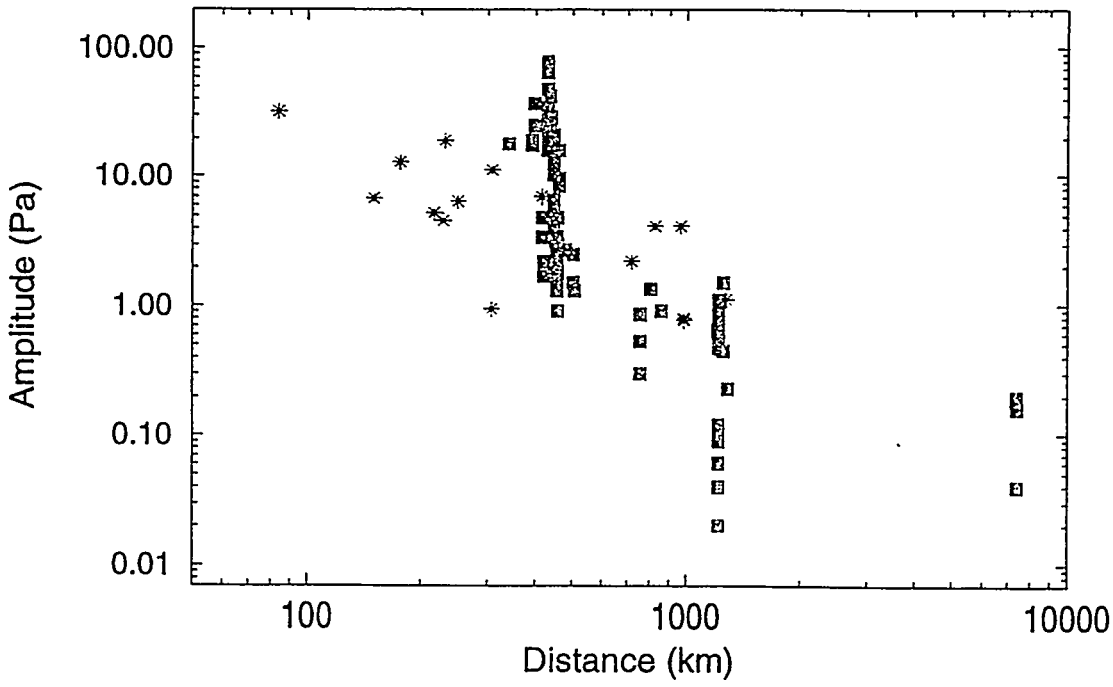
100.00
10.00
1.00
0.10
0.01
Amplitude (Pa)
100
1000
10000
Distance (km)

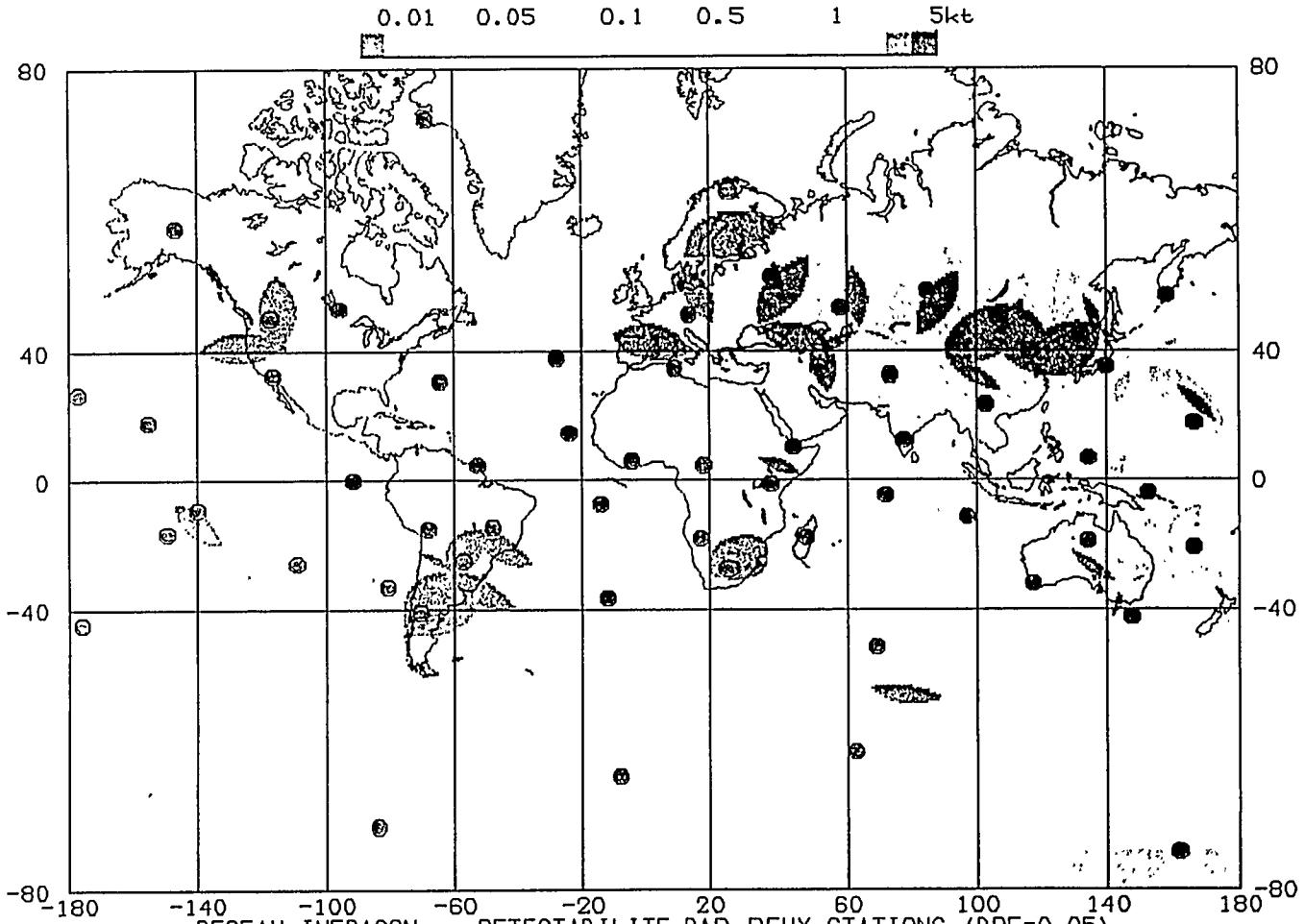

RESEAU INFRASON - DETECTABILITE PAR DEUX STATIONS (BDF=0.05)

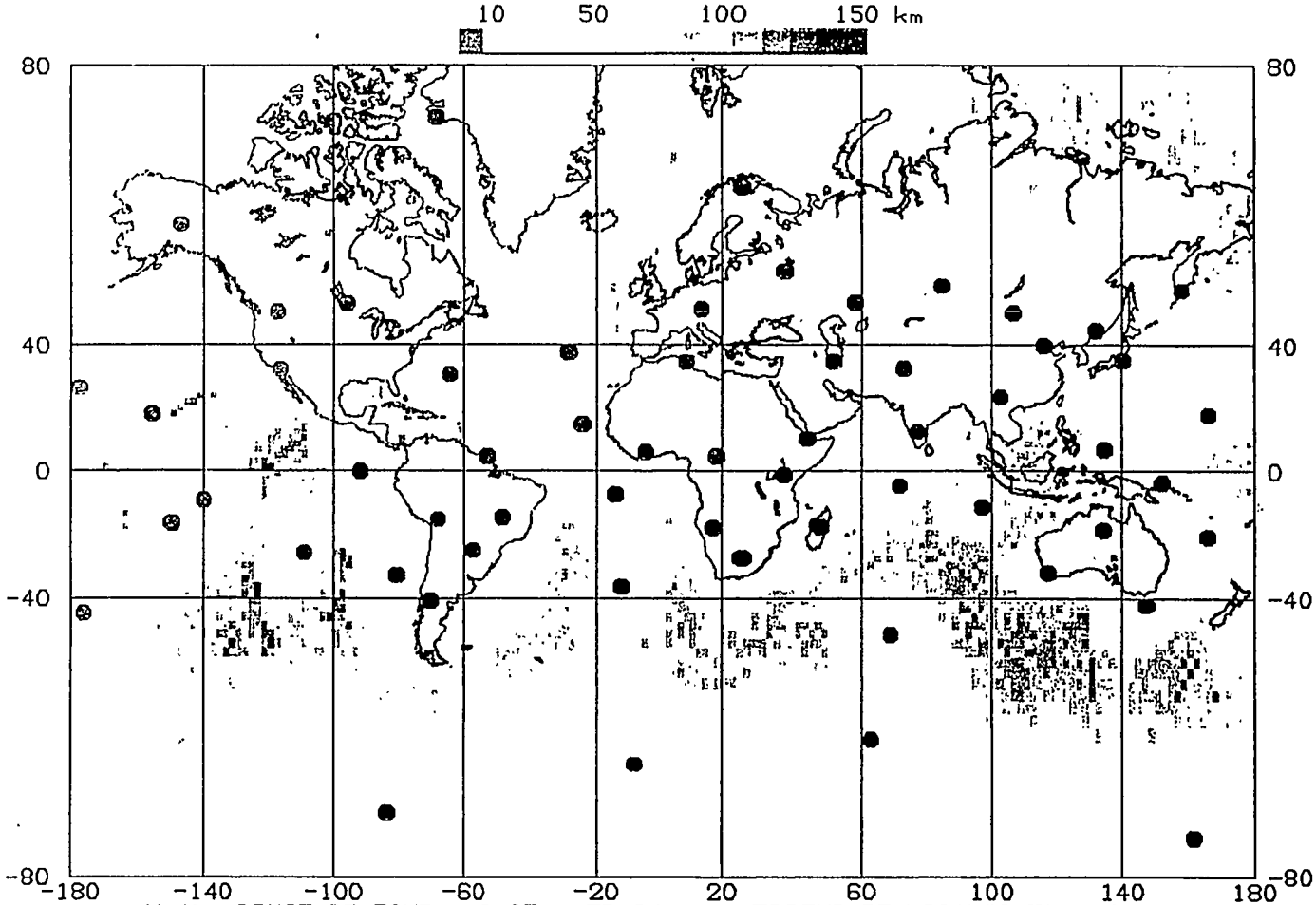
10 50 100 150 km
80
40
0
-40
-80
-180 -140 -100 -60 -20 20 60 100 140 180
W=1kt BRUIT DE FOND = 0.05 - ER=2degres ERREUR DE LOCALISATION EN KM

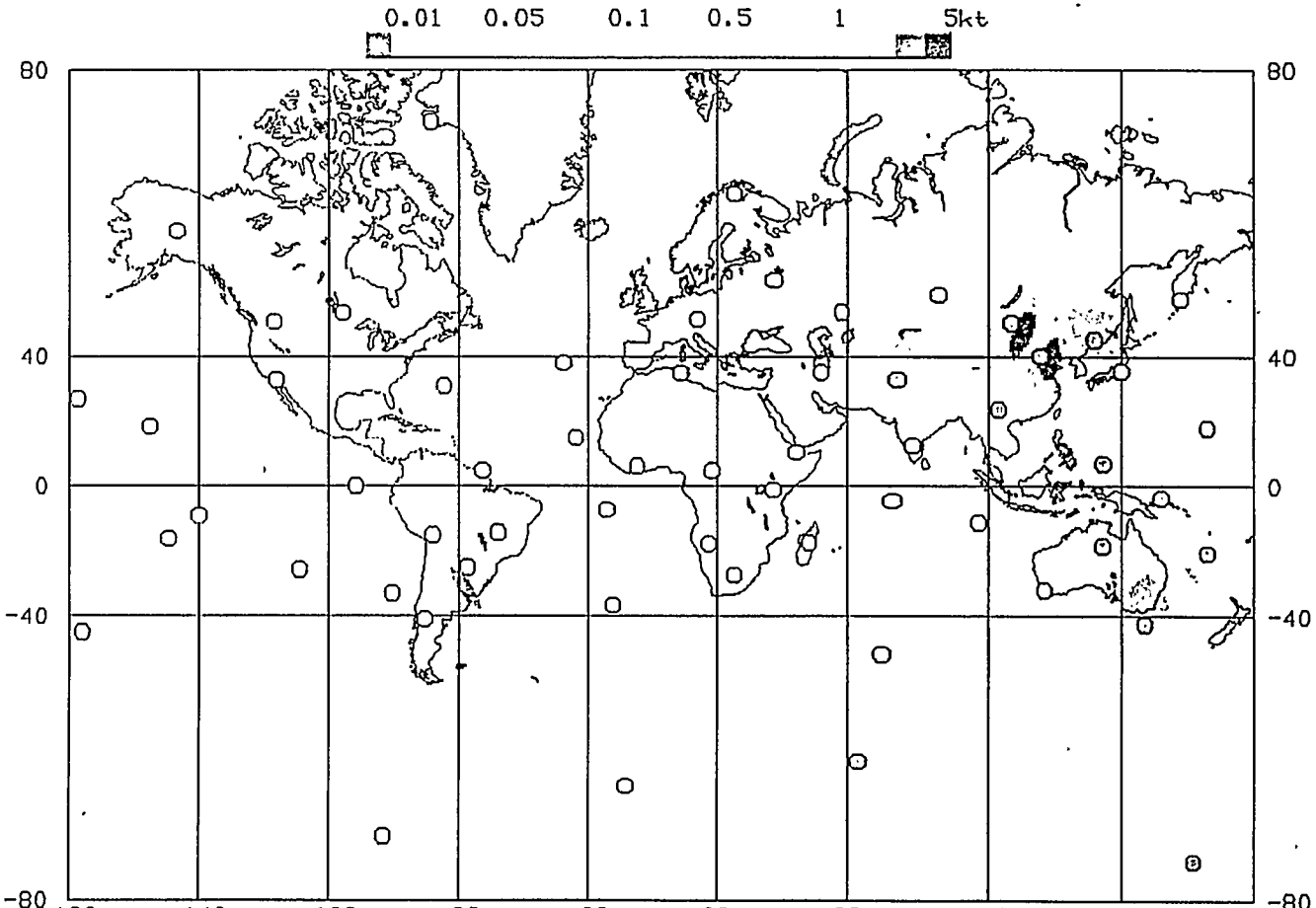

RESEAU INFRASON - DETECTABILITE PAR TROIS STATIONS (BDF=0.05)

Atmospheric noise

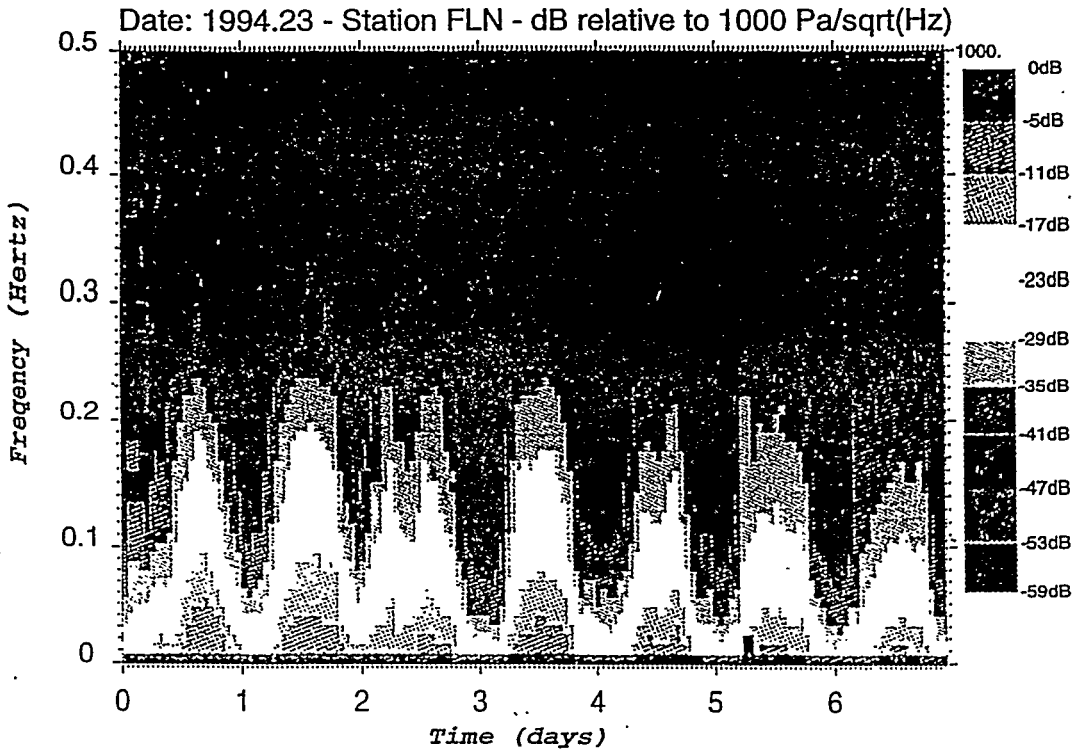

Figure 10 : Measurements were performed at the Flers station between 23 and 29 January 95. Noise significantly increases during the day, under the effect of wind-related local turbulence.

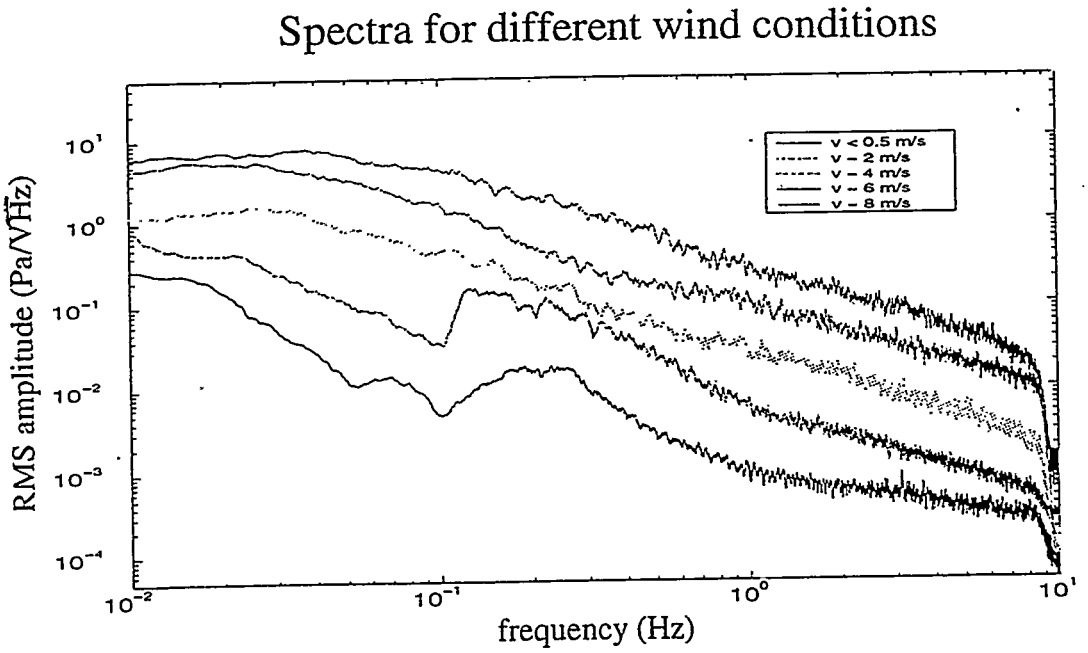
Spectra for different wind conditions
RMS amplitude (Pa/√Hz)
frequency (Hz)
v < 0.5 m/s
v ~ 2 m/s
v ~ 4 m/s
v ~ 6 m/s
v ~ 8 m/s

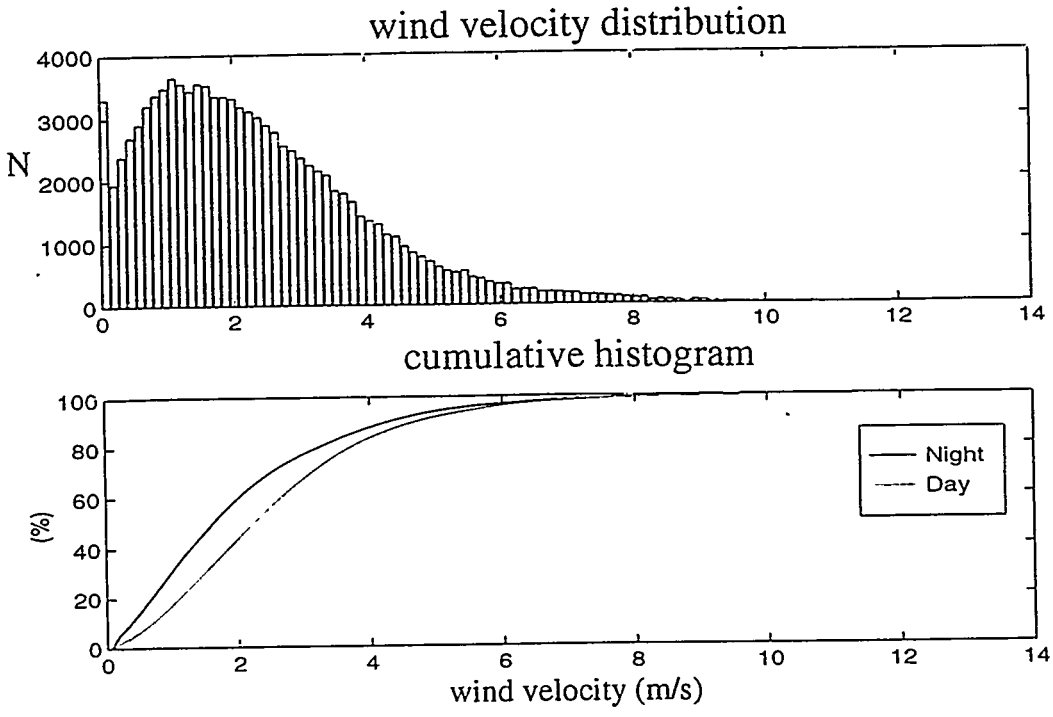
wind velocity distribution
N
cumulative histogram
(%)
Night
Day
wind velocity (m/s)

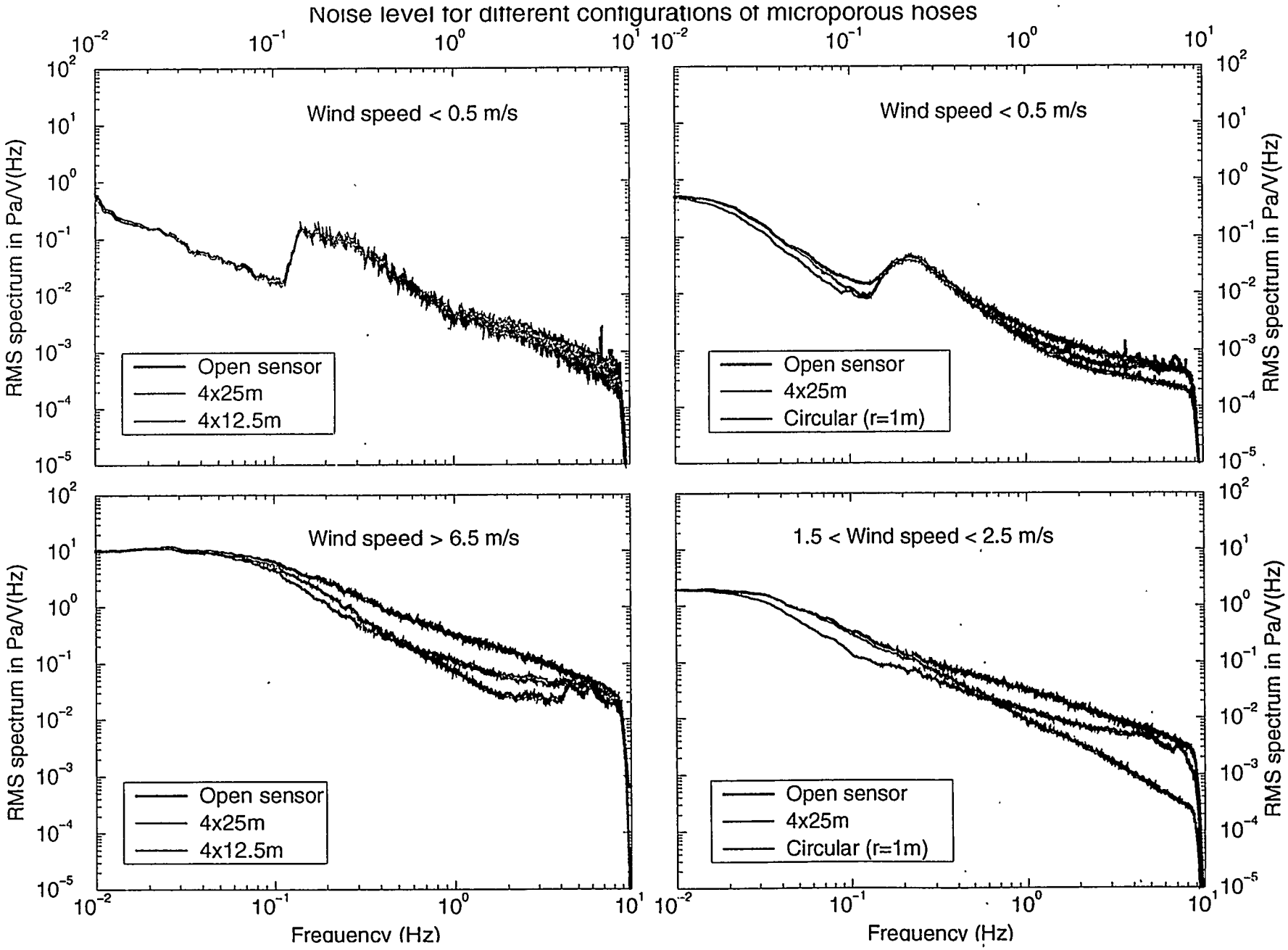
Noise level for different configurations of microporous hoses
Wind speed < 0.5 m/s
Open sensor
4x25m
4x12.5m
Wind speed < 0.5 m/s
Open sensor
4x25m
Circular (r=1m)
Wind speed > 6.5 m/s
Open sensor
4x25m
4x12.5m
1.5 < Wind speed < 2.5 m/s
Open sensor
4x25m
Circular (r=1m)
RMS spectrum in Pa/V(Hz)
Frequency (Hz)

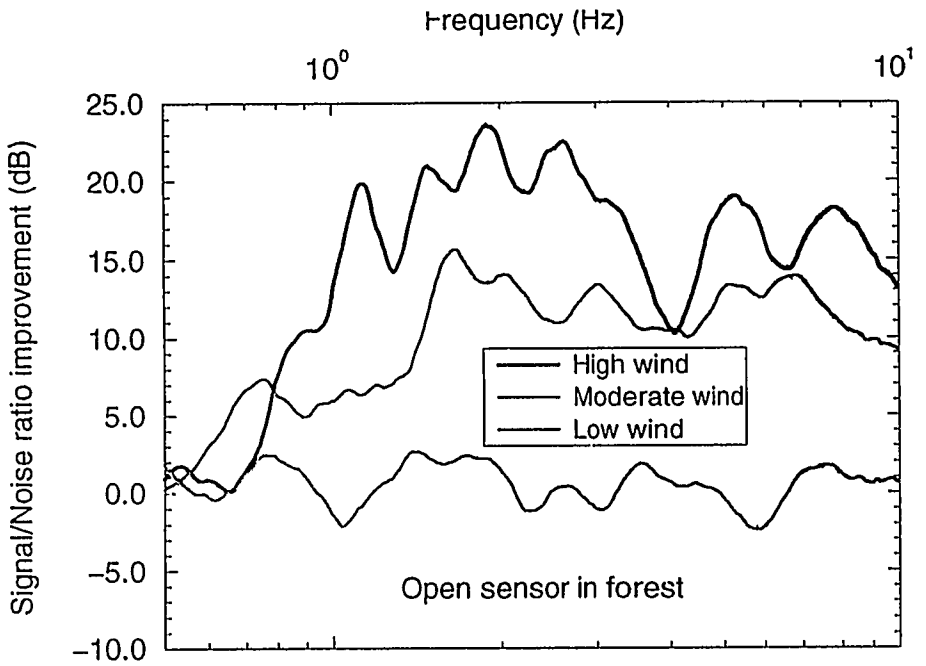

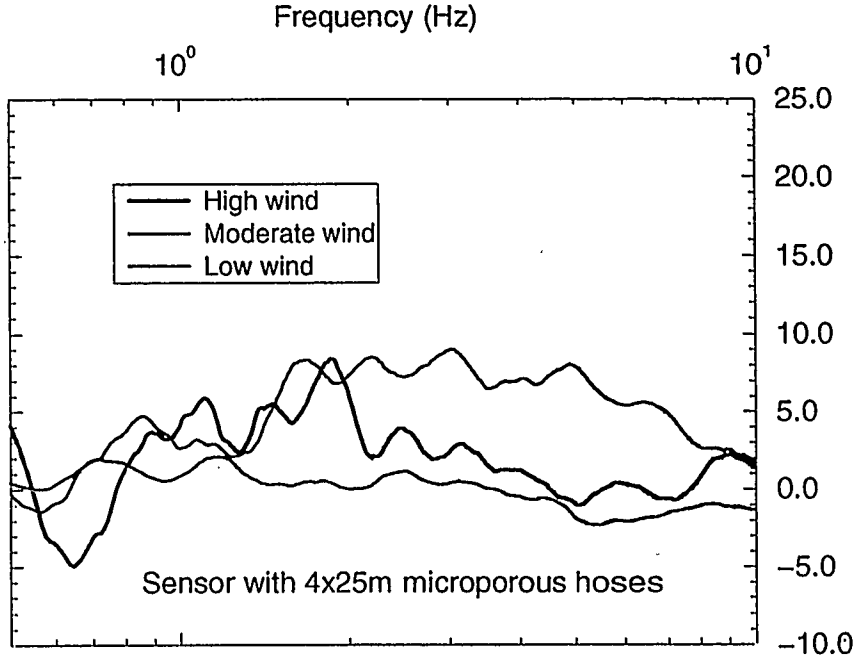

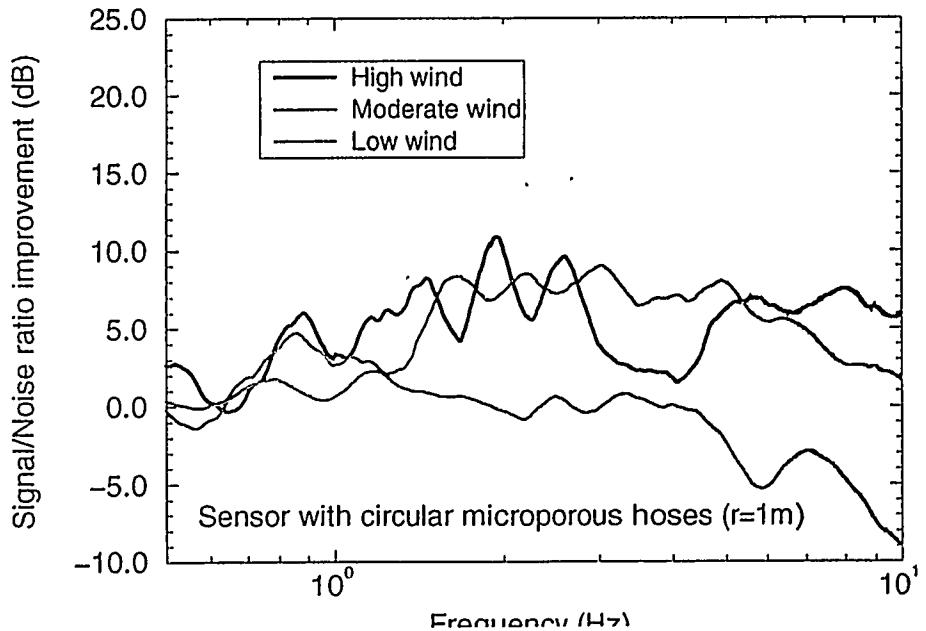

Effects of hoses and forest on the Concorde detection

Noise spectra (wind velocity ~ 0.5 m/s)

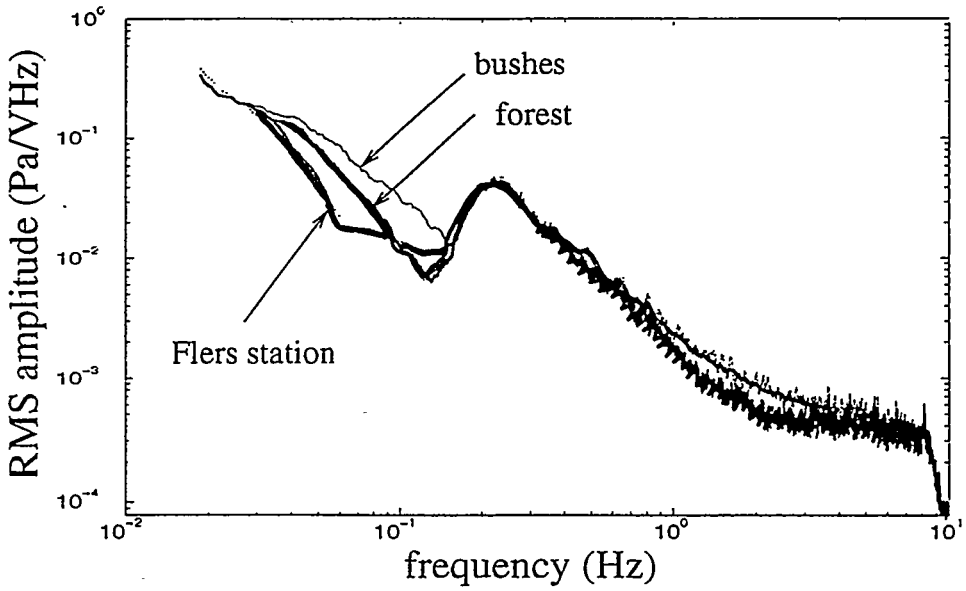

Noise spectra (wind velocity ~ 3.5 m/s)

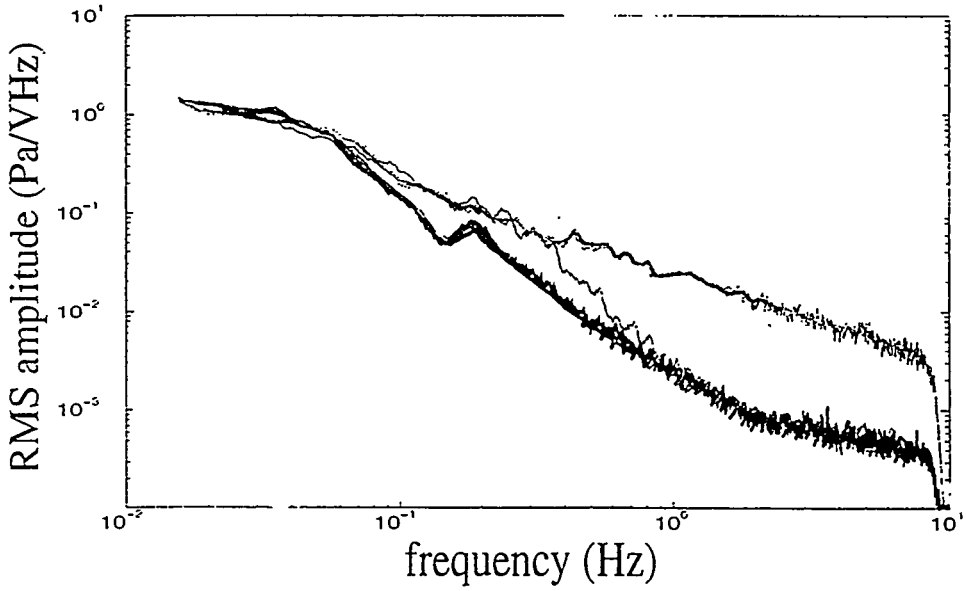

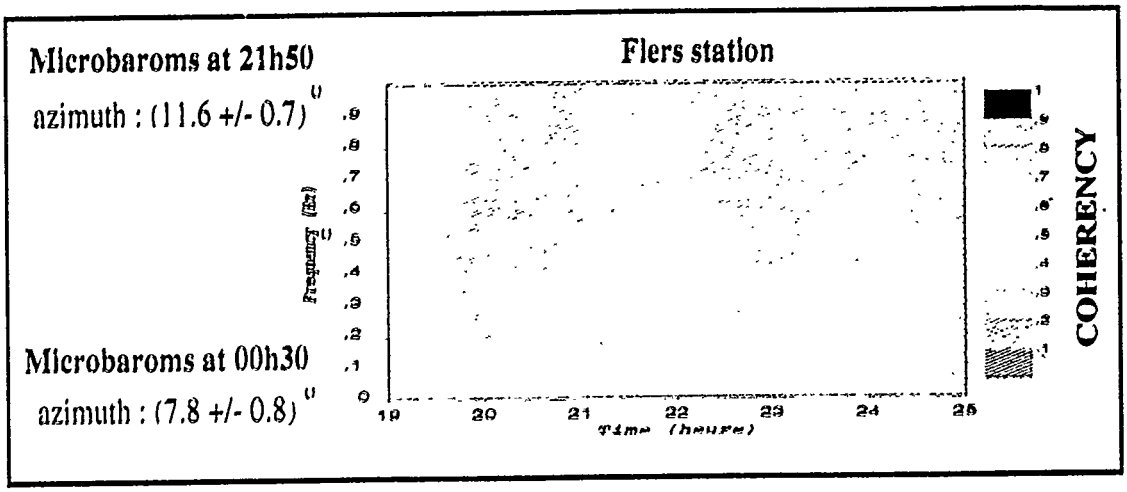
Microbaroms at 21h50
azimuth : (11.6 +/- 0.7)°
Microbaroms at 00h30
azimuth : (7.8 +/- 0.8)°
Flers station
Frequency (Hz)
Time (hours)
COHERENCY

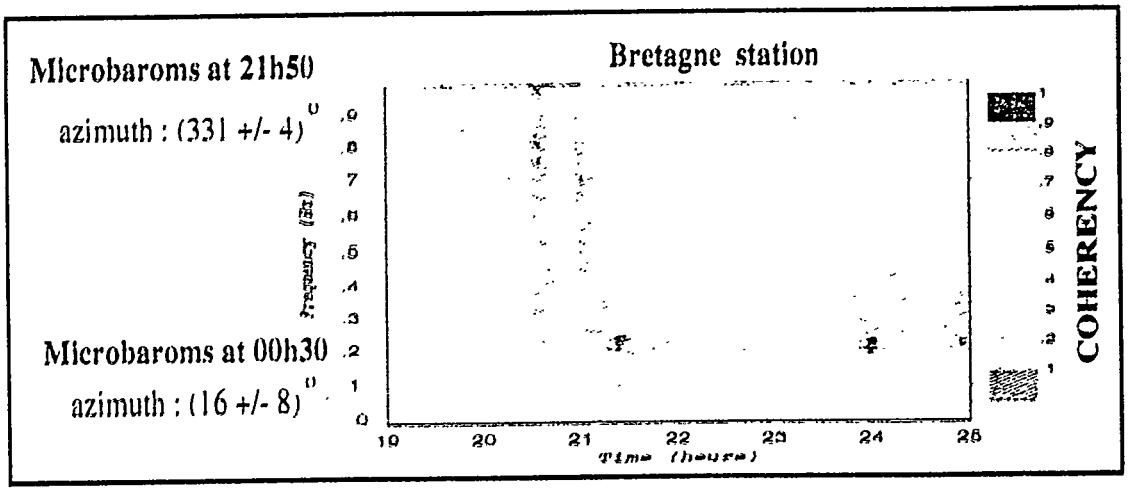
Microbaroms at 21h50
azimuth : (331 +/- 4)°
Microbaroms at 00h30
azimuth : (16 +/- 8)°
Bretagne station
Frequency (Hz)
Time (hours)
COHERENCY

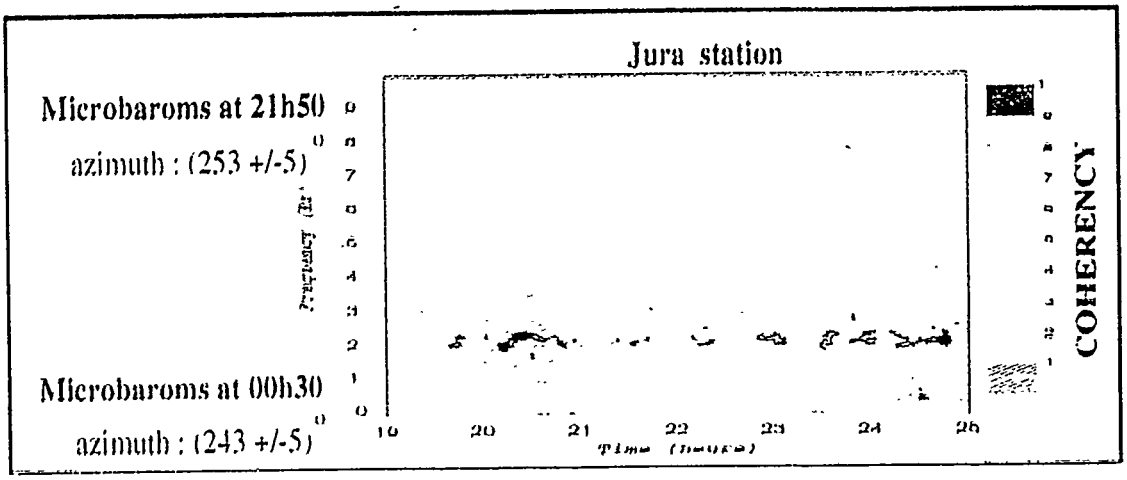
Microbaroms at 21h50
azimuth : (253 +/-5)°
Microbaroms at 00h30
azimuth : (243 +/-5)°
Jura station
Frequency (Hz)
Time (hours)
COHERENCY

azimuth variation of the microbarom source

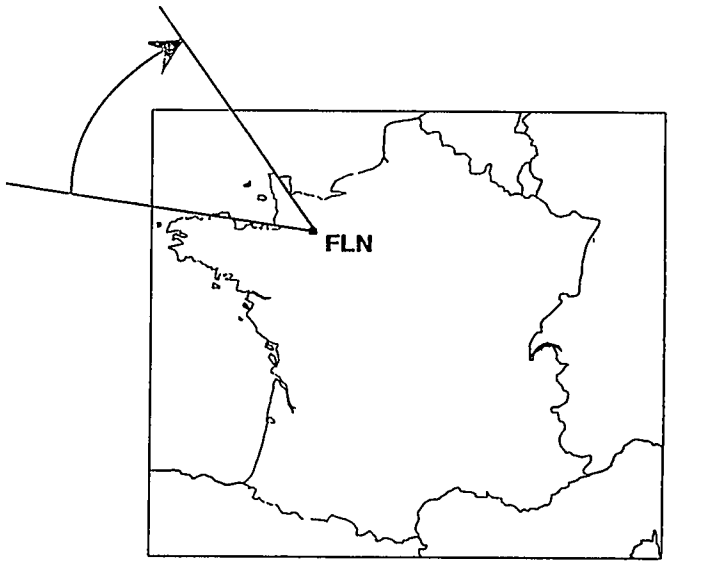

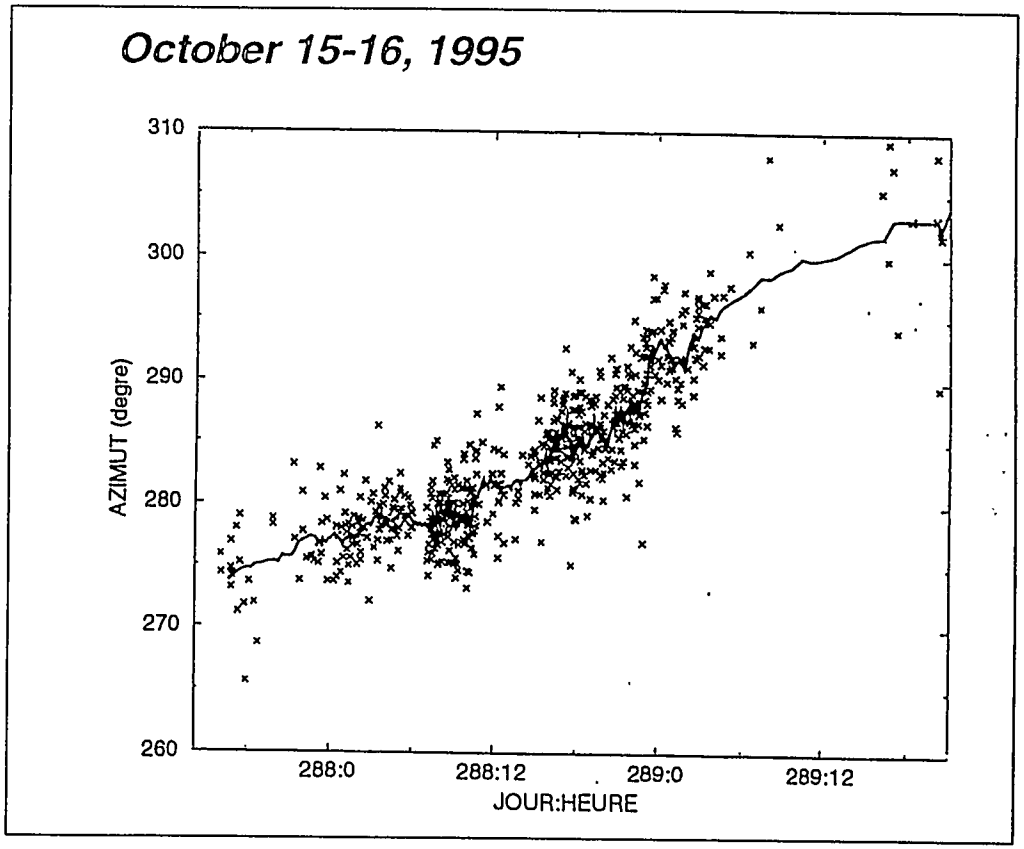

OBSERVATION OF THE OCEAN SWELL MOTION FROM MICROBAROM SIGNALS

Example of atmospheric waves at Flers

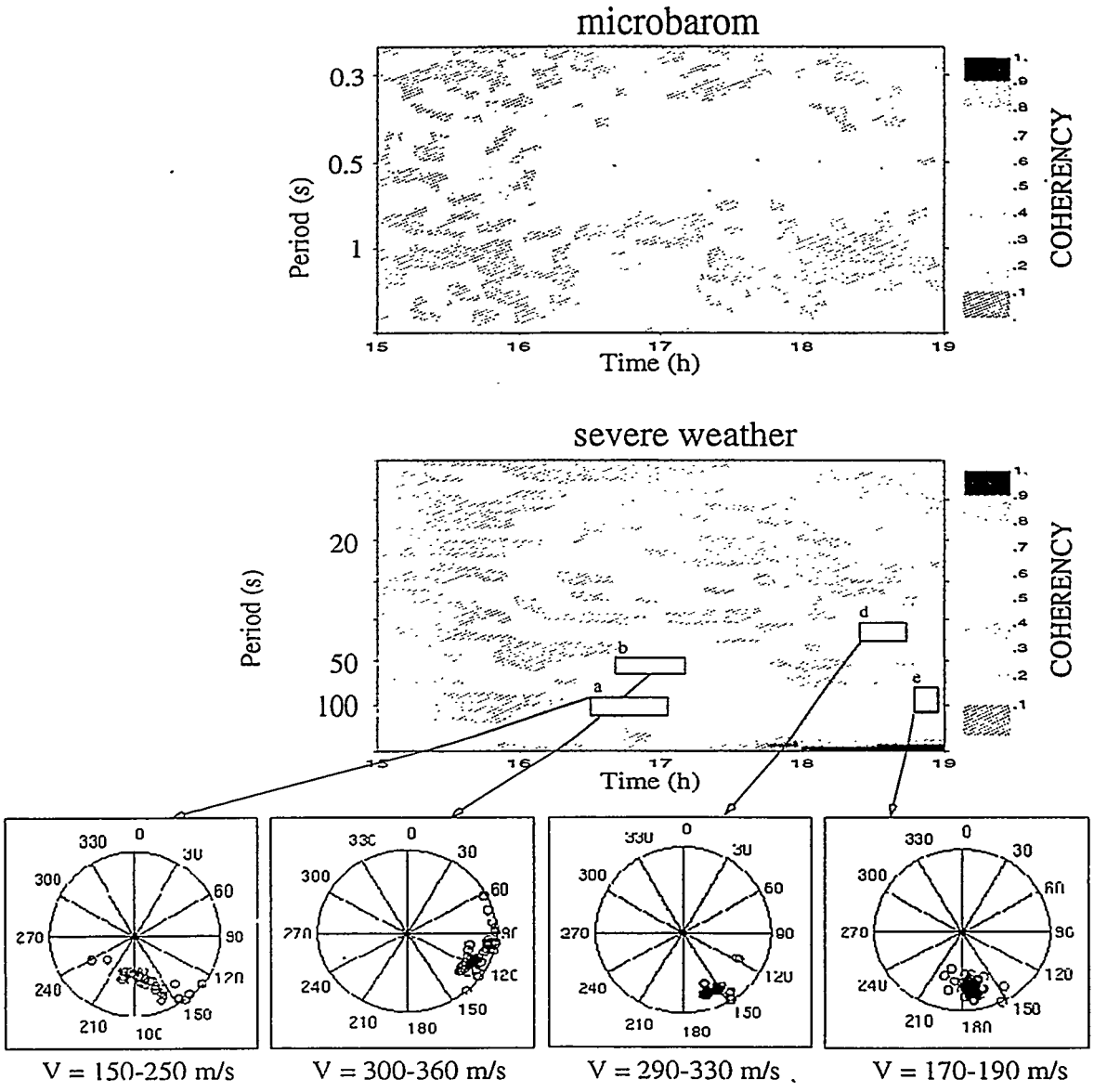

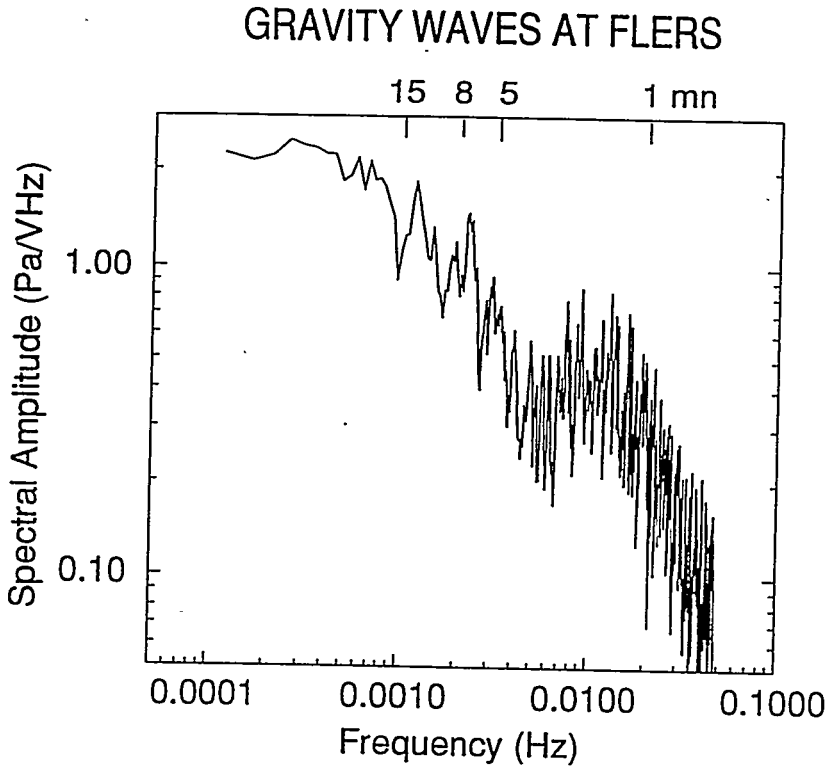

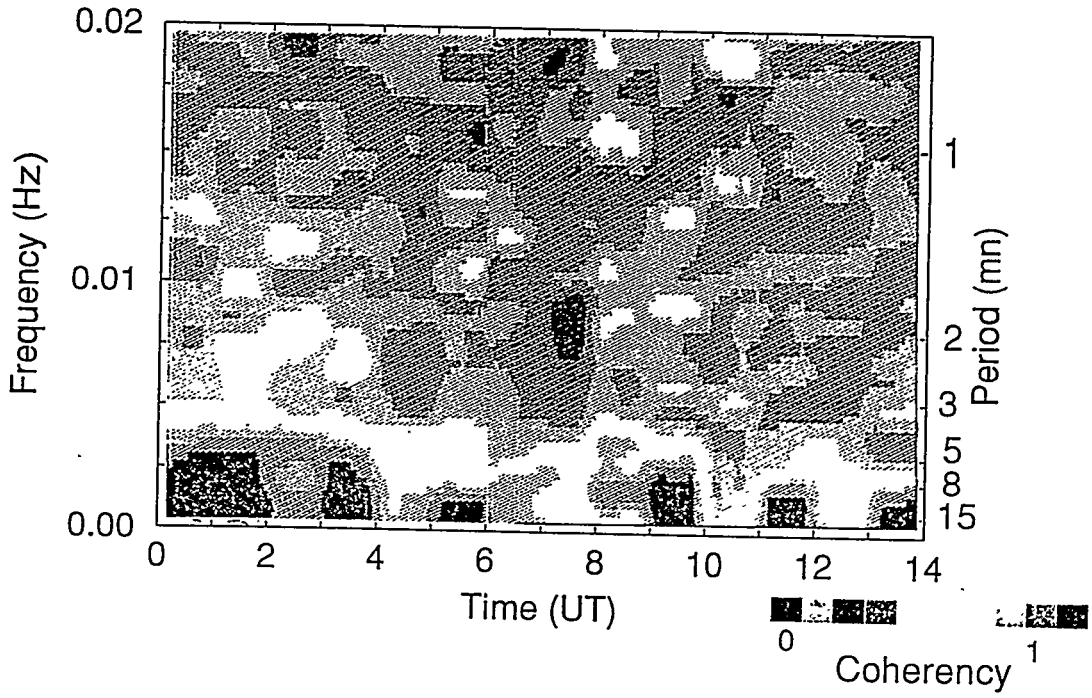

The gravity waves period is higher than the Brunt Vaissala period (about 5 mn).
Gravity waves are attenuated in the measurements because they are outside the sensor bandwidth. Their amplitude is however strong and they are observed and used for testing the system.

Ariane V launching (Kourou, 04/16/1997, 23H08 TU)

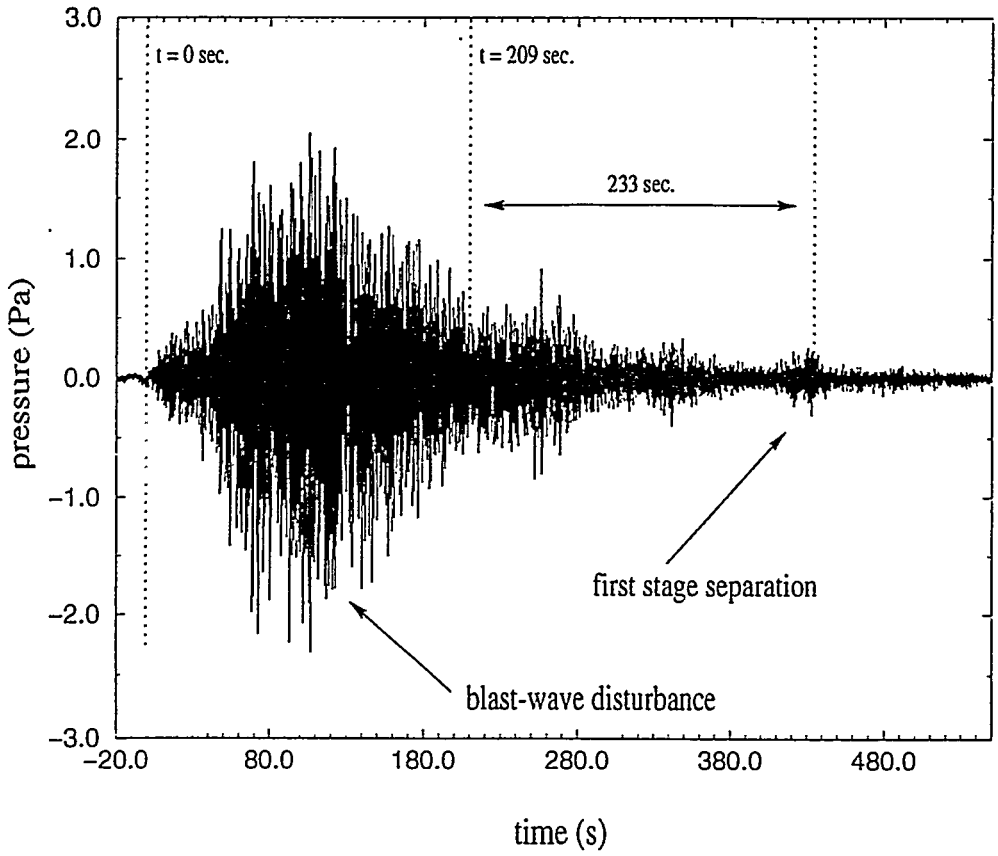

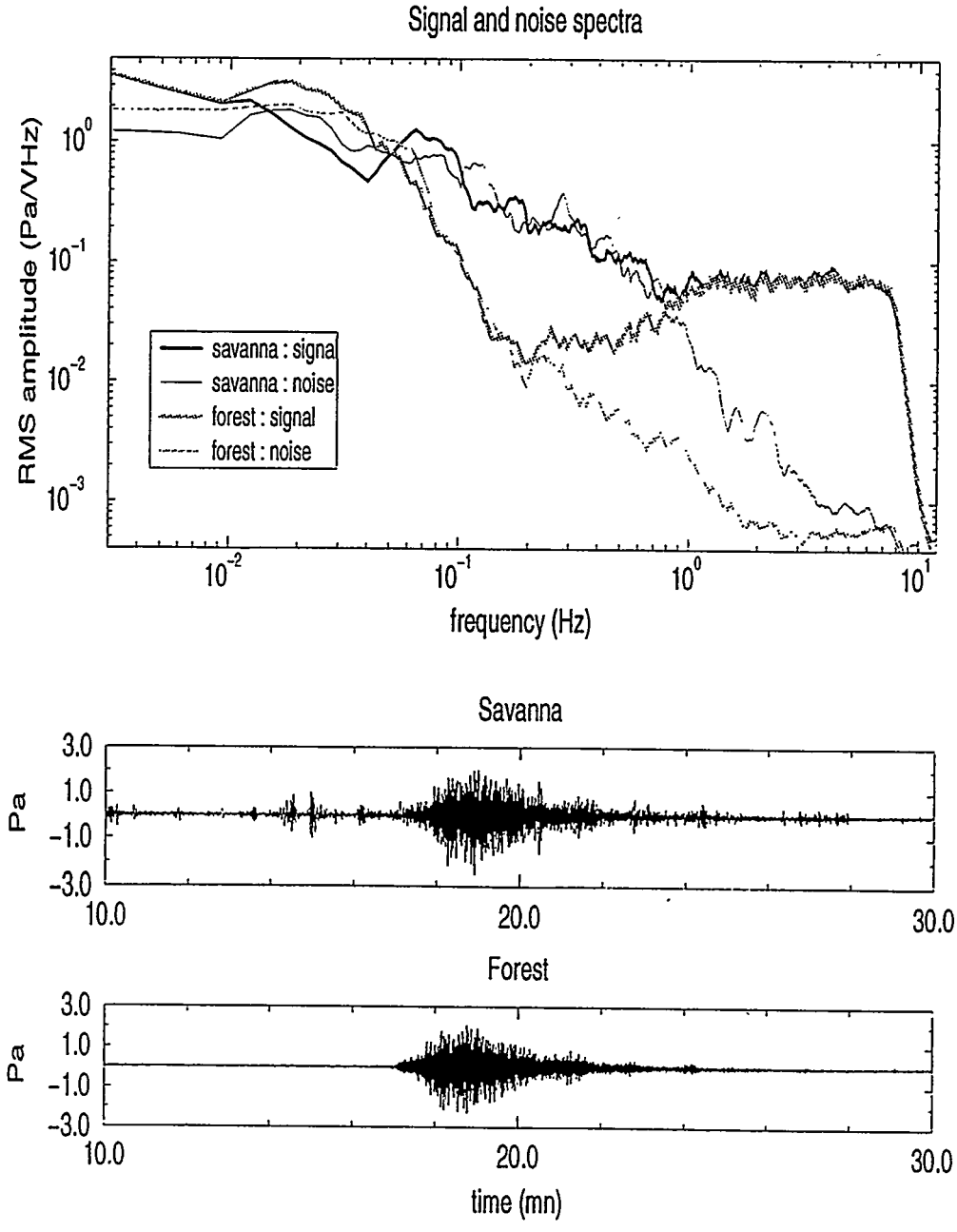
Signal and noise spectra
RMS amplitude (Pa/√Hz)
10^{0}
10^{-1}
10^{-2}
10^{-3}
savanna : signal
savanna : noise
forest : signal
forest : noise
10^{-2}
10^{-1}
10^{0}
10^{1}
frequency (Hz)
Savanna
Pa
3.0
1.0
-1.0
-3.0
10.0
20.0
30.0
Forest
Pa
3.0
1.0
-1.0
-3.0
10.0
20.0
30.0
time (mn)

CAPABILITY MODELING OF THE PROPOSED INTERNATIONAL MONITORING SYSTEM 60-STATION INFRASONIC NETWORK

Dean A. Clauter and Robert R. Blandford

Air Force Technical Applications Center
1300 N 17th Suite 1450
Arlington, VA 22209

We have modeled the detection and location capability of the International Monitoring System (IMS) proposed 60-station infrasonic network using a statistical model which assumes a log normal distribution of signal and noise. Model inputs were determined empirically from infrasonic data of US nuclear tests. Amplitude as a function of source distance was determined after normalizing the amplitude by the square root of the yield. An empirical relationship was derived for the background noise as a function of wind speed. Modeling results indicate that the proposed 60-station international network with 4-element arrays will achieve detection capabilities for two stations at the 90% confidence level between 0.1 kilotons (kt) over land areas and 0.7 kt over ocean areas. Location uncertainties are based on empirically determined azimuth and arrival time errors. The location radius of uncertainty circle at the 90% confidence level ranges from 50 kilometers over land to 150 kilometers over the southern ocean areas.

Capability Modeling of the Proposed International Monitoring System 60-Station Infrasonic Network

by Dr. Dean Clauter and Dr. Robert Blandford
Air Force Technical Applications Center (AFTAC)

sponsored by AFTAC

ABSTRACT

We have modeled the detection and location capability of the International Monitoring System (IMS) proposed 60-station infrasonic network using a statistical model which assumes a log normal distribution of signal and noise. Model inputs were determined empirically from infrasonic data of US nuclear tests. Amplitude as a function of source distance was determined after normalizing the amplitude by the square root of the yield. An empirical relationship was derived for the background noise as a function of wind speed. Modeling results indicate that the proposed 60-station international network with 4-element arrays will achieve detection capabilities for two stations at the 90% confidence level between 0.1 kt over land areas and 0.7 kt over ocean areas. Location uncertainties are based on empirically determined azimuth and arrival time errors. The location radius of uncertainty circle at the 90% confidence level ranges from 50 km over land to 150 km over the southern ocean areas.

Keywords: Infrasonic, Infrasound, detection and location modeling

Objective

AFTAC had an infrasonic nuclear monitoring mission until 1974. Currently, the mission is being reestablished by the international community. For support to the United States delegation at the Comprehensive Test Ban Treaty (CTBT) talks in Geneva, we modeled the detection thresholds and the location uncertainty of the proposed 60-station international infrasonic network consisting of 4-element arrays. We used actual data from nuclear tests of known yields, origin times, and locations recorded at historical infrasonic stations and included these as empirical inputs to the modeling program. We have three objectives for this presentation. Our first objective is to describe our method and show our modeled detection and location capability for the 60-station infrasonic network. Our second objective is to demonstrate that both azimuth and arrival times can be used to reduce the area of the location uncertainty ellipse. Our third objective is to convey to the research community the additional work that we anticipate is needed to improve location methods in order to meet international expectations.

Research Accomplished

The model for signal detection thresholds model was first developed for the determination of seismic detection and location capabilities (Sereno, 1990). The model assumes a log normal distribution of signals and noise amplitudes. The probability of detection is given by the expression:

$$P_{ijk} = R_i \times \Phi\left[\frac{\log S_{ijk} - \log N_{ijk} - \log SNR_{ijk}}{\left(\sigma_{Sijk}^{\ 2} + \sigma_{Nijk}^{\ 2}\right)^{1/2}}\right]$$

where

P_{ijk} is the probability of detection at the ith station for the jth epicenter and the kth event.

R_i is the reliability of the station i, assumed to be 95%.

S_{ijk} is the signal amplitude. This number is a function of distance and was empirically determined and will be shown in the first figure.

N_{ijk} is the station noise amplitude, for which we developed an empirical relationship between station noise and wind speed. We assumed that for 4-element arrays, we can also reduce the wind noise for a single sensor by a factor of 2.

SNR_{ijk} refers to the signal-to-noise ratio expected for a detection. This number is 1.5, based on empirical experience.

σ_{Sijk} refers to the log standard deviation of the signal. This number was empirically determined to be 0.3 log units. We used this number for all station-event pairs.

σ_{Nijk} to the log standard deviation of the noise background. This number was empirically determined to be about 0.4 log units for a number of our stations. We used this number for all stations.

Φ is the probability density function.

In Figure 1, we show our empirically determined amplitude distance relationship. The horizontal axis is in kilometers, and the vertical axis is in microbars. The black crosses are nuclear events from Nevada Test Site (NTS) shots, and the Dominick series of tests in the Pacific. The X's are ammonia nitrate and fuel oil (ANFO) explosions, which had their size corrected for the equivalent nuclear energy. The amplitudes observed were scaled to 1 kt by square root scaling of the yield. Shots at the surface were multiplied by a factor of 2 in yield to account for the surface reflection. In addition, amplitude corrections were made for the wind direction for the ANFO shots, but not the others. A least squares scaling was done on the events which give the relationship between pressure and range given at the bottom of the slide. From the scatter, a log signal deviation of 0.28 was determined of the individual points from the best fitting straight line. This is thought to be due in large part to the variation in the upper level winds.

We determined the mean wind speed in meters per second on an annual and monthly basis from meteorological stations adjacent to our old infrasonic stations. There was a period of 36 months for which we have data of background noise measurements made four times per day at each sensor. The arrays had Daniels pipes to suppress noise. We took those noise levels and plotted them versus mean annual wind speed in meters per second, taken at the standard meteorological height of 10 meters. The empirical relationship obtained is plotted in Figure 2. The circles represent yearly averages. In order to obtain the extremes, we looked at particularly calm or windy months and plotted the noise values versus the monthly means. One observation from this graph is that the noise rarely goes below about 0.3 microbars. This level must represent the zero-wind background noise levels which are presumably usually due to propagating infrasound signals from distant storms. Note also that the noise varies quadratically with speed. High wind speeds along with few land areas contribute to the problem in the southern ocean areas of finding suitably spaced sites. In these areas the arrays may have to be expanded to 16 elements to achieve the required detection and location thresholds. In the modeling, meteorological stations near proposed sites or other data were used to estimate the typical wind speed at a site and the derived empirical relationship between wind speed and noise was used to model the noise. Other effects besides wind speed contribute to wind noise. These included the vegetation and topography of the sites. These differences contribute to the scatter of the data points along the best fitting empirical relationship.

Based on the model and empirical data described above, we show our detection capability for the proposed international 60-station network in Figure 3. The detection capability is modeled for detection by two stations at the 90% confidence level. The detection contours are in Kilotons (KT). Over land areas the network will have a detection threshold considerably below 1 KT, and only approaching 1 KT in the remote ocean areas. The objective of the international community is to be at or below 1 KT worldwide.

In addition to modeling the detection thresholds, the location uncertainty was modeled. Inputs required for determining the location uncertainty in addition to the probability of detection are the standard deviation in the velocity and azimuth. Figure 4 shows the azimuth uncertainty for Dominic and NTS events as a function of distance. From these data, a standard deviation of 1.8 degrees was used in the modeling for events less than 27 degrees distant from the event. For events between 27 and 35 degrees, linear interpolation was used to a value of 7 at 35 degrees; between 35 and 91 degrees, 12.2 was used; and 27.5 was used for stations at greater distances from the event. These values could be reduced if the conditions of the upper level winds are known.

Figure 5 is a graph of the mean wind speed as a function of distance from the Novaya Zemlya test site to our infrasonic stations at the distances indicated. The average standard deviation from this test site is 5.17 meters per second which represents a velocity error of 1.7%. This is probably the best one can do for a calibrated test site where station bias has been removed without independent meteorological information.

In Figure 6 shown is the radius of uncertainty circle for the 60-station network where arrival time is not considered in the solution. The errors over land range from 50 - 150 kilometers, whereas over water they exceed 1000 kilometers.

In Figure 7 we have assumed a 5% uncertainty in the arrival time and factored it into the uncertainty estimate for the uncertainty circle. Note that we have reduced our error considerably for location.

If we assume a 2% uncertainty in velocity, we get an uncertainty radius of around 100 kilometers over most ocean areas and, in the worst case, 225 kilometers as shown in Figure 8.

We have taken the worst case in the southern ocean areas and shown in Figure 9 that when the velocity uncertainty falls beneath 10%, there is a significant drop in the radius of uncertainty circle. The international community's goal is 100 kilometers or less for location uncertainty everywhere. Some array sites may be supplemented by more than 4-element arrays to help meet this goal.

Conclusions and Recommendations

1. The detection threshold for the 60-station, 4-element array international infrasonic network at the 90% level for two stations to detect a signal is below 1 KT.

2. Location uncertainty can be reduced considerably using both arrival times and azimuth of incoming signals.

3. Location uncertainties with a 5% velocity uncertainty vary from approximately 50 - 100 kilometers over land areas and from 200 - 300 kilometers over ocean areas for 1 KT events. With satellite observations, both azimuth and velocity errors may be significantly reduced, giving a more precise event location.

4. Future research will be necessary to meet the goals for location accuracy of events required by the international community. Since there are several infrasonic phases that all travel at different velocities, one must identify the detected phase arrival times before they can be used to constrain location. This is not a simple procedure since not all phases are identified with a particular event. The event may have to be located first with azimuth information, and this information used to identify the phase in a second iteration. In addition, corrections for azimuth and velocity bias may be possible by knowing the velocity of the upper level winds with the Upper Atmospheric Research Satellite and other satellites. These winds have large standard deviations so that a dynamic model will have to be developed.

References

Sereno, Thomas J. Jr., **Simulation of the Detection and Location Capability of Regional Seismic Networks in the Soviet Union**, SAIC technical report 91/1061, March 1, 1991.

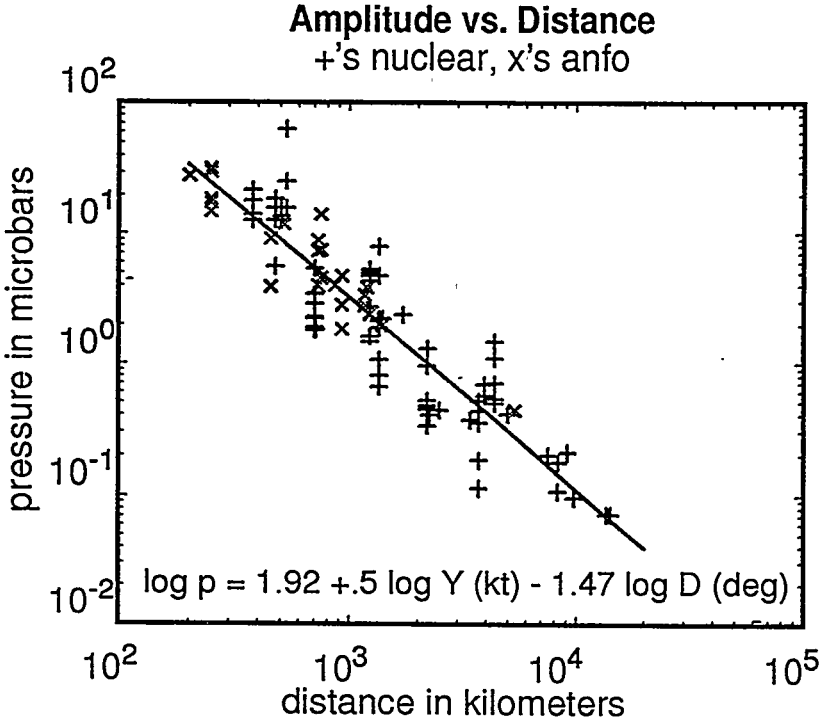

Figure 1. Amplitude versus distance relationship for infrasonic waves based on nuclear tests and ANFO data.

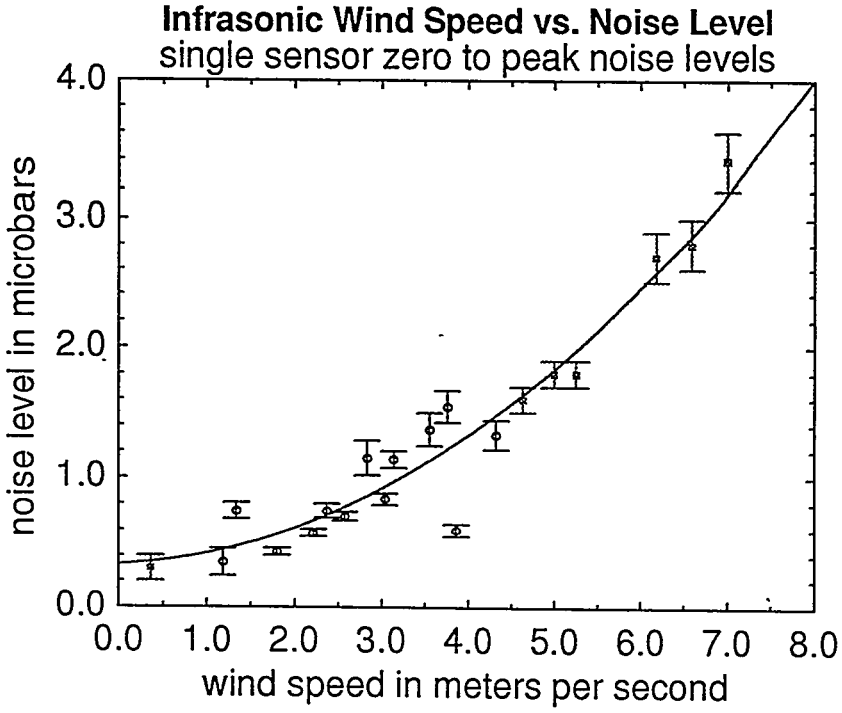

Figure 2. Model for wind speed versus noise level based on infrasonic and meteorological data; circles yearly, squares monthly averages.

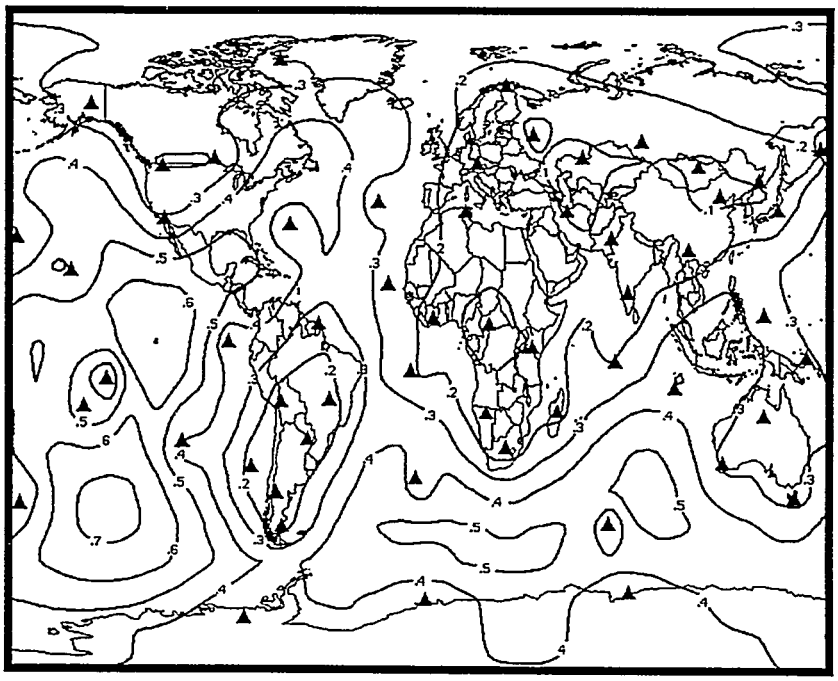

Figure 3. Detection capability at the 90% confidence level for two stations for the 60-station infrasonic network with 0.1 KT contours.

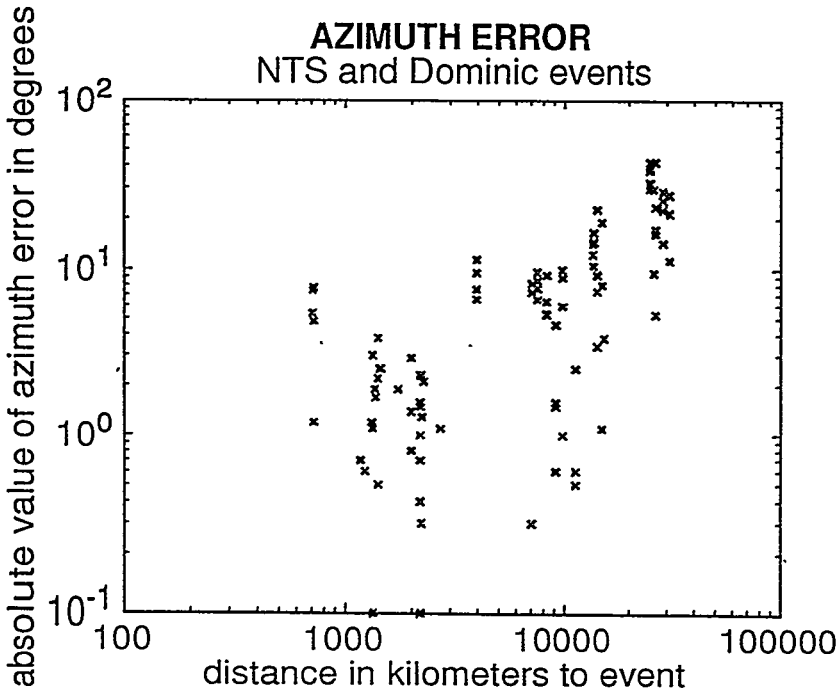

Figure 4. Azimuth error as a function of distance from the events

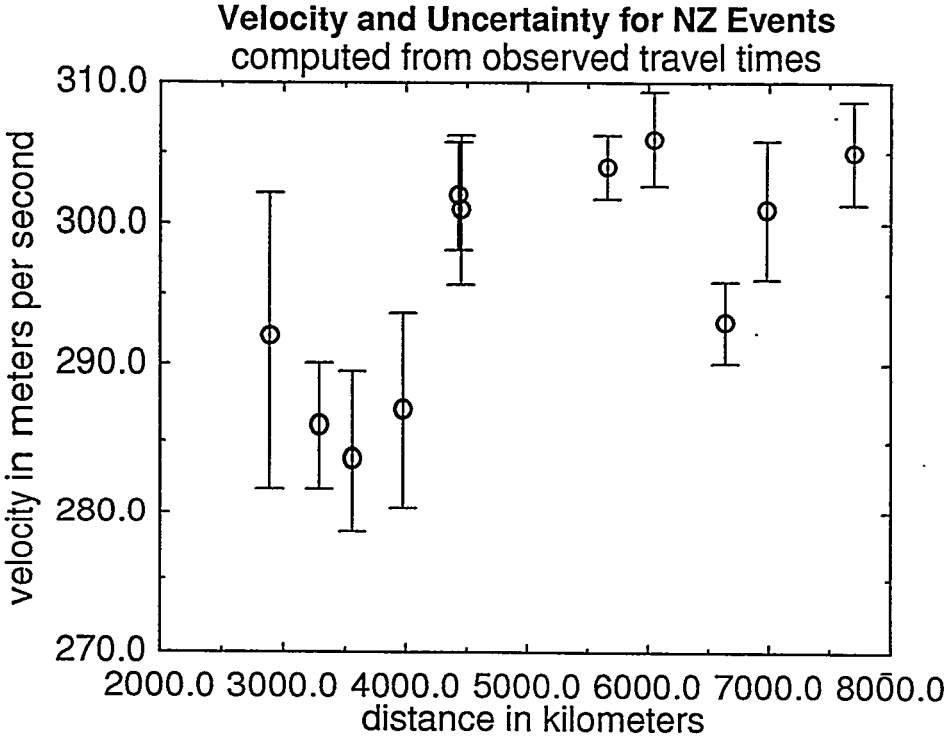

Figure 5. Velocity and velocity uncertainty for events from the Novaya Zemlya test site recorded by the Dawn Star (AFTAC) infrasonic network.

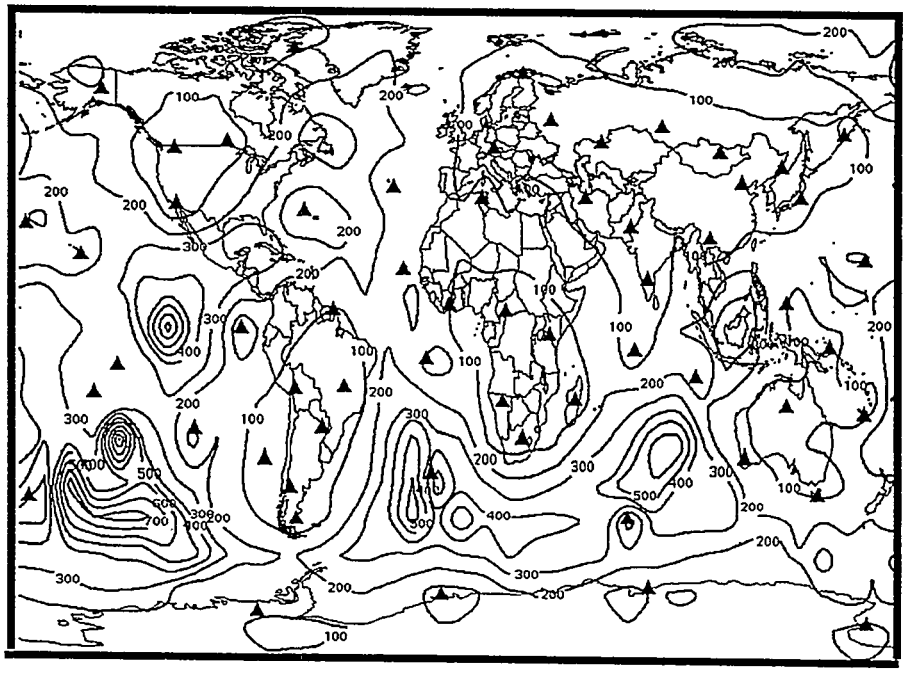

Figure 6. Contours of radius of uncertainty circle (kilometers) for 100% velocity uncertainty, 1 Kiloton sources.

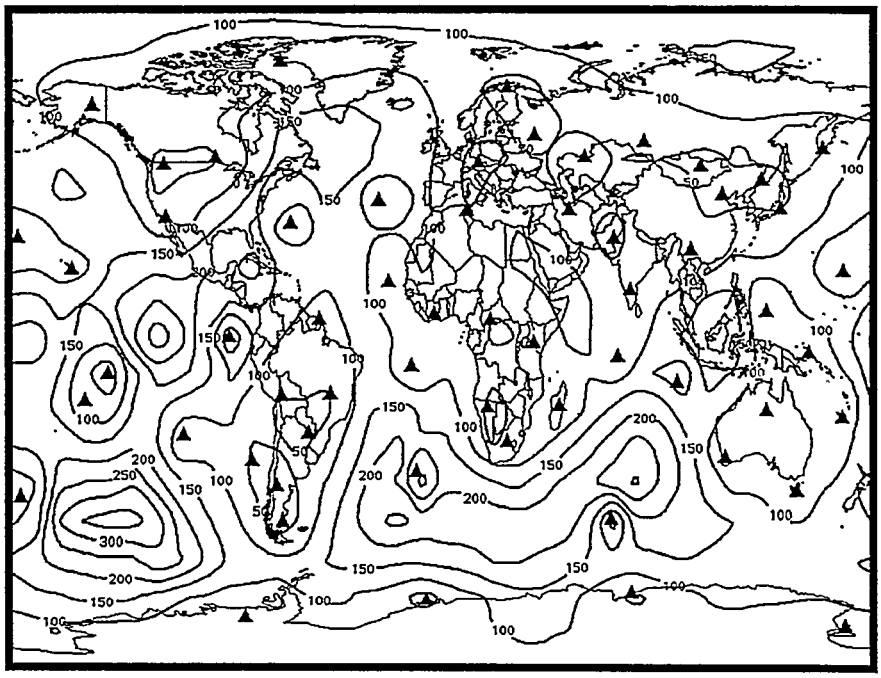

Figure 7. Contours of radius of uncertainty circle (kilometers) for 5% velocity uncertainty, 1 Kiloton sources.

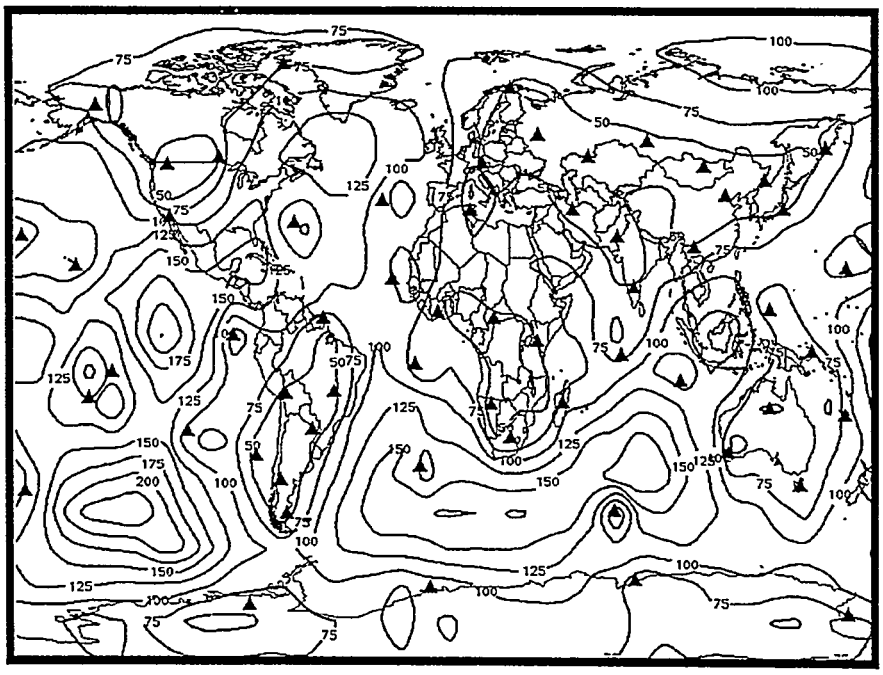

Figure 8. Contours of radius of uncertainty circle (kilometers) for 2% velocity uncertainty, 1 Kiloton sources.

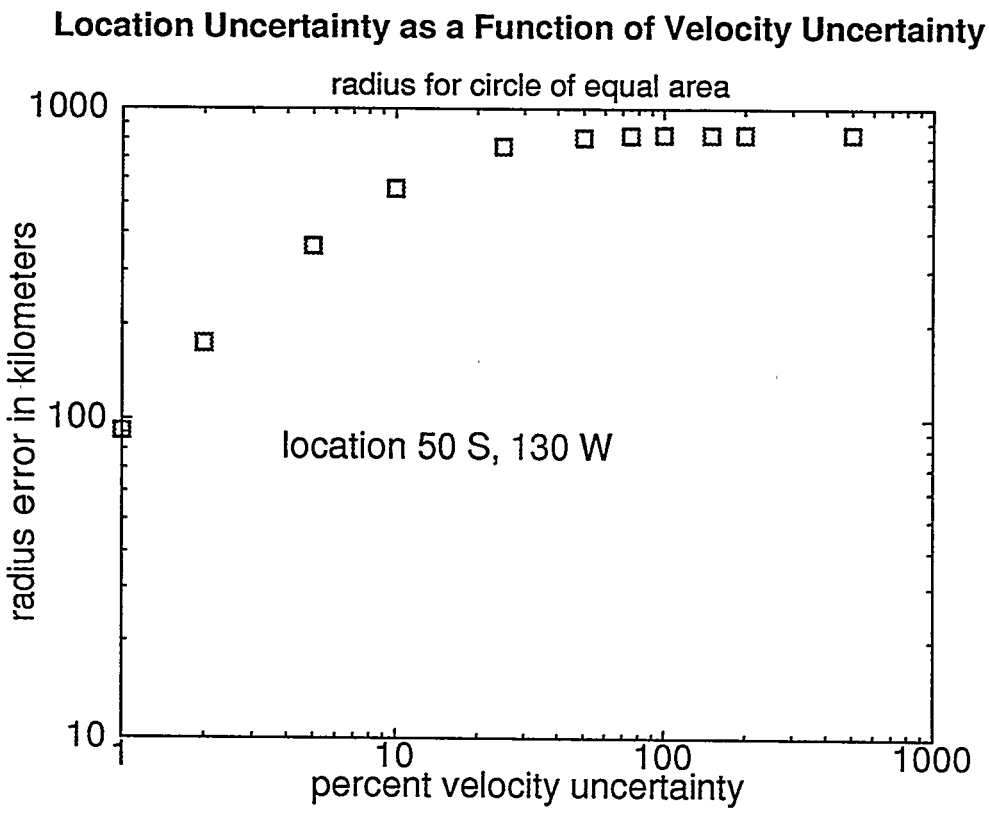

Figure 9. Location uncertainty improves considerably if the velocity uncertainty is known to 10% or better.

EFFECTS OF STRATOSPHERIC WINDS ON LONG RANGE INFRASONIC SIGNALS

Joseph Paul Mutschlecner, Rodney W. Whitaker, and Lawrence Auer

Los Alamos National Laboratory
Los Alamos, NM 87545

Stratospheric winds play a central role in determining the propagation of infrasonic signals at long ranges (hundreds to thousands of kilometers). These winds and the temperature profile determine the refraction of the ozonospheric signals and the effectiveness of the return of signals from the layers near fifty kilometers in height to the earth. The following figure illustrates the effect of stratospheric winds on signals. These infrasonic observations of atmospheric nuclear tests by the Sandia National Laboratory were made at St. George, Utah, over a period of years. The observed amplitudes are scaled to one kiloton and displayed versus day of the year. At this location, directly east of the test site, the amplitudes are strong in the winter and greatly reduced in the summer.

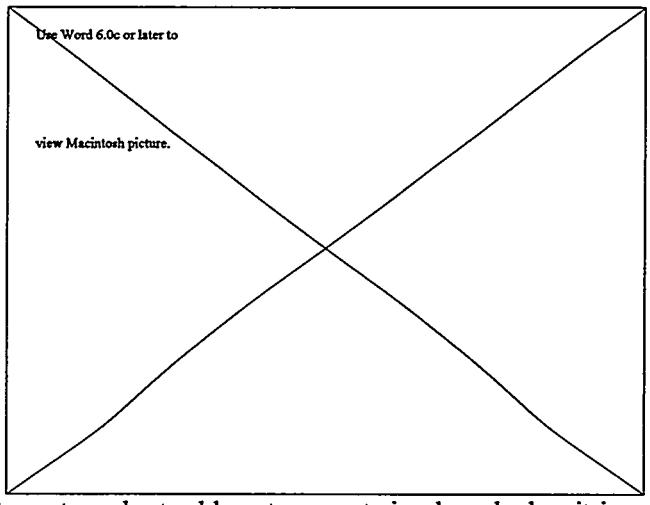

It is of obvious importance to understand how to correct signals and when it is necessary to do so. We have analyzed an archival data set of infrasonic signals from atmospheric nuclear tests at the Nevada Test Site. The observations, by the Sandia National Laboratory, were made primarily at a set of stations surrounding the test site at or near the first bounce return distance over a period of several years and included a large range in explosive yield. Our analysis indicates that an appropriate correction is given by

$$Ac = Ao * 10^{(-k*Vd)}$$

where Ac is the corrected amplitude, Ao is the observed amplitude, Vd is the stratospheric wind velocity vector near fifty kilometers altitude directed towards the receiver from the source, and k is an empirical onstant. The value of k is approximately 0.02 s m-1 near the first bounce distance but appears to vary with range. We illustrate the general effect of the of the correction by application to on several data sets and discuss the applicability of the method at multibounce distances from a source. The work was supported by the Department of Energy Office of Non- Proliferation and National Security.

EFFECTS OF STRATOSPHERIC WINDS ON LONG-RANGE INFRASONIC SIGNALS

J. Paul Mutschlecner, Rodney W. Whitaker, and Lawrence H. Auer

Los Alamos National Laboratory

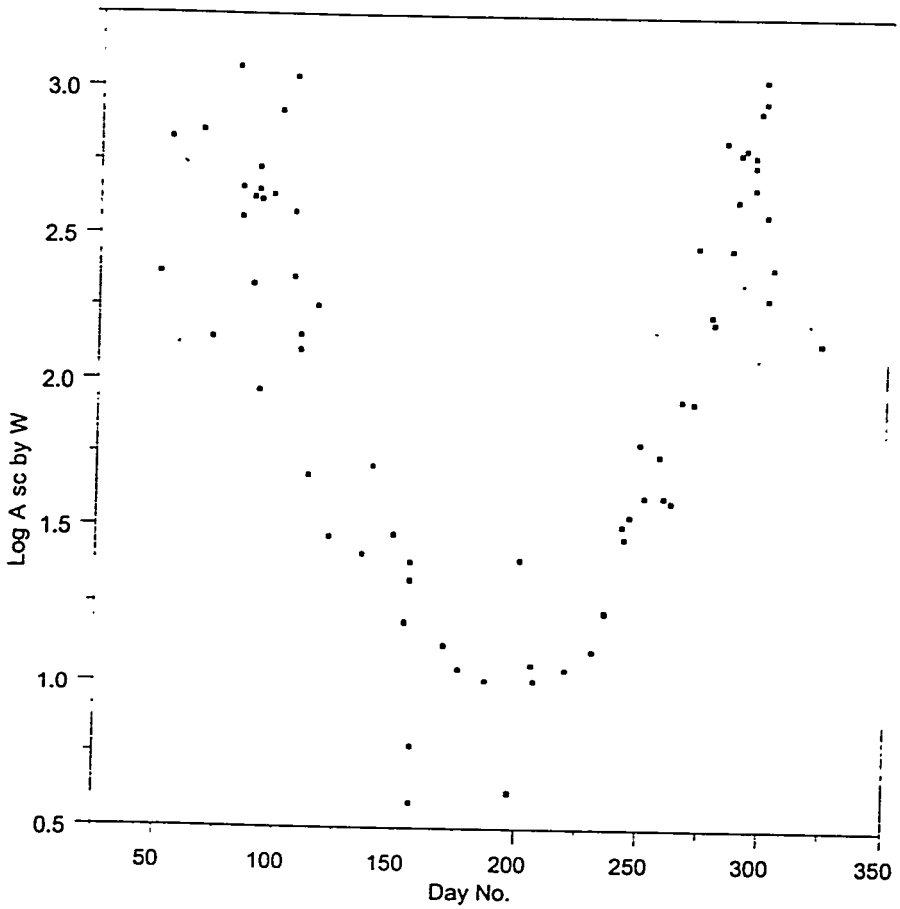

NTS DATA, ST. GEORGE, AZIMUTH 90 DEG.

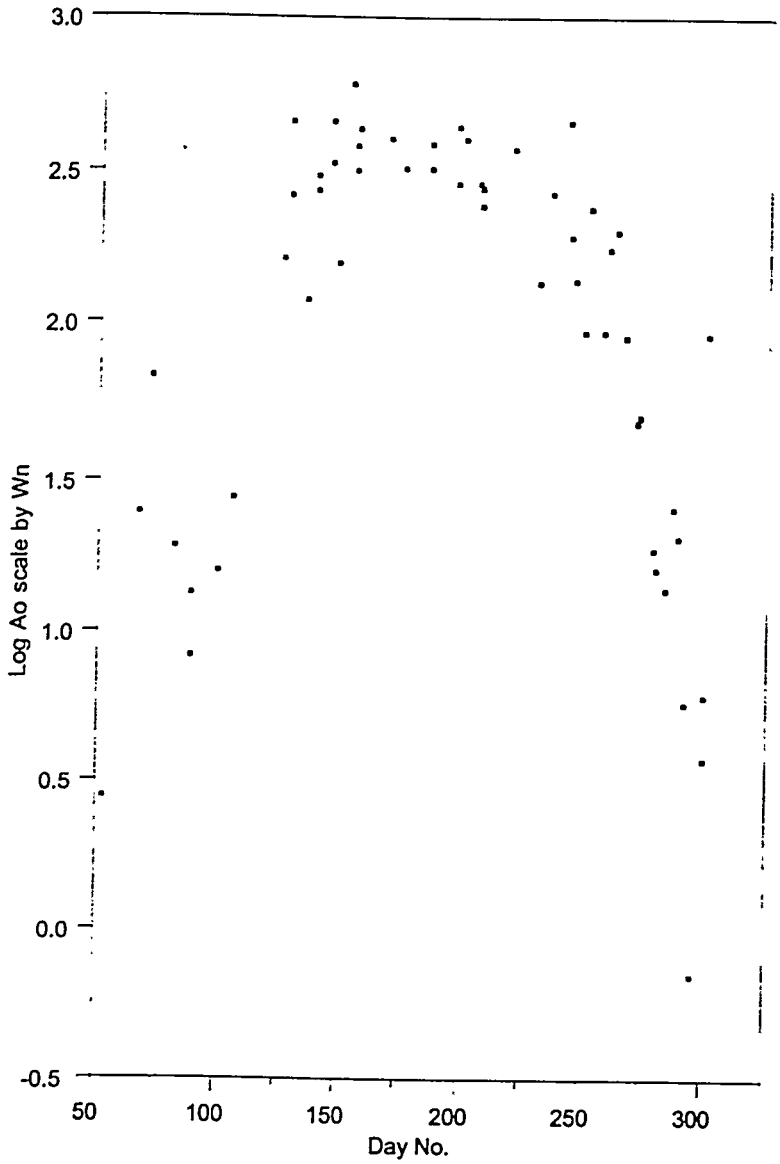

NTS DATA, BISHOP, AZIMUTH 278 DEG.

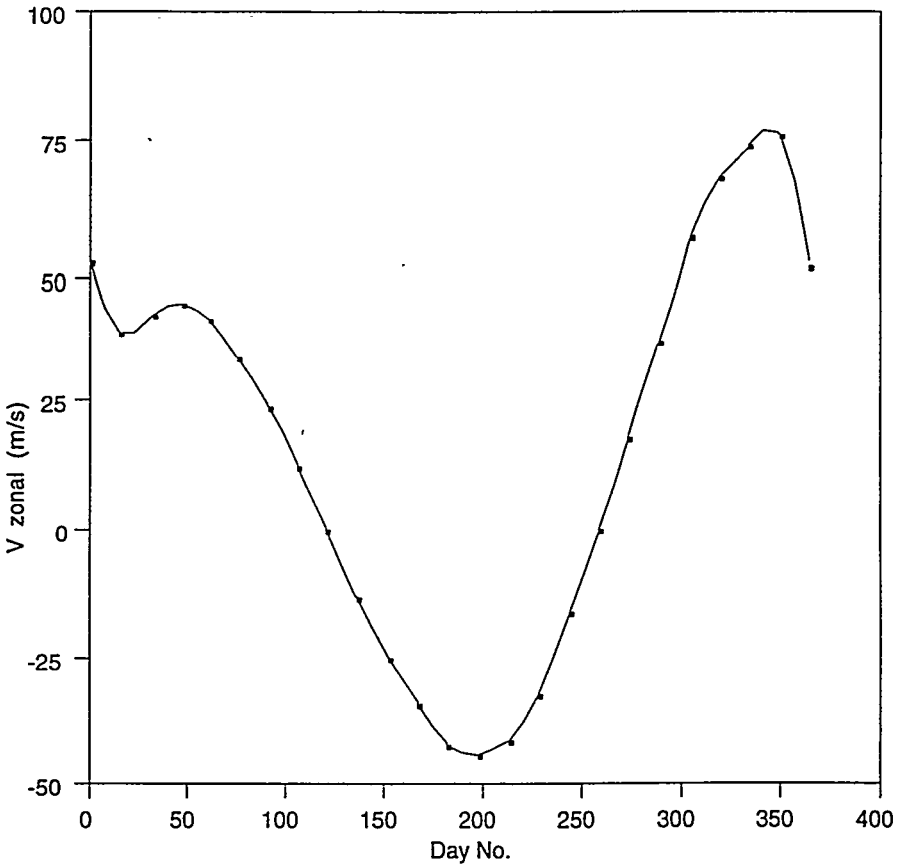

ZONAL WIND (SCI) at 50 KM and 35 N LATITUDE

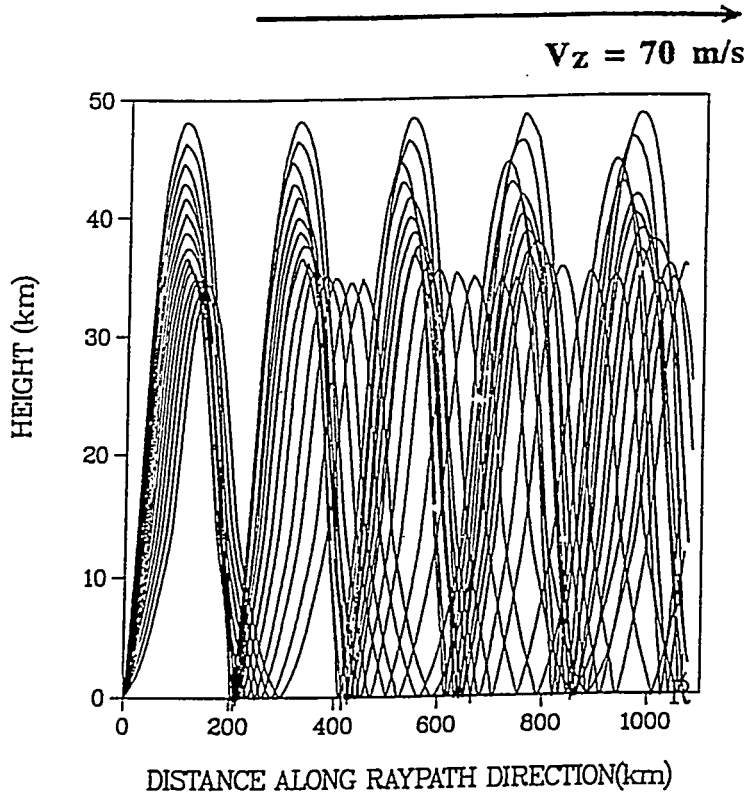

NOVEMBER WINDS

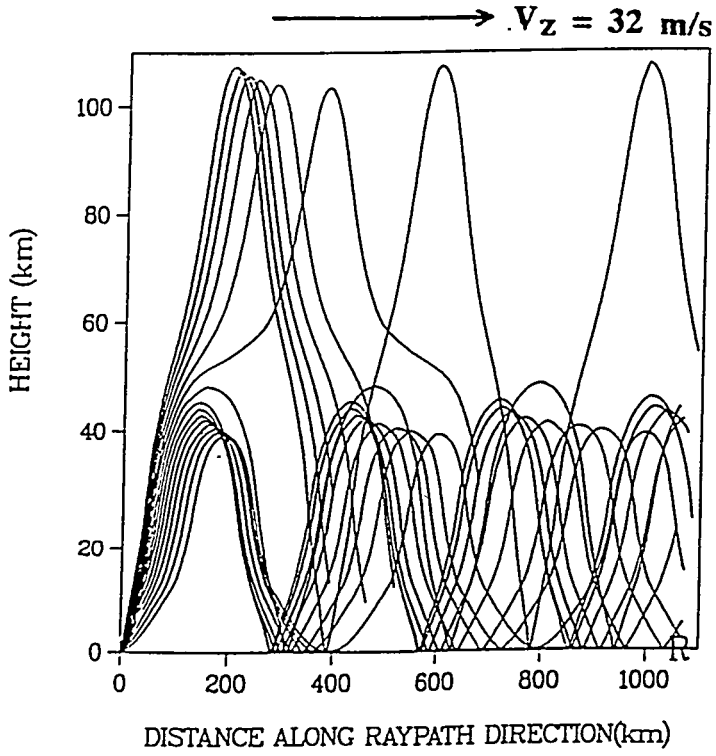

MARCH WINDS

SNL Observations of NTS Atmospheric Nuclear Events

- Period: 1951-1958
- Number of Events: 79
- Yield Range: 0.5 ton to 74.3 kilotons
- Amplitude Range: μbar to few mbars
- Stations: 8 (typically 5-6 per event)
- Single Broad-Band Microbarographs

Other Features:

Tropospheric and Ionospheric Signals
Average Velocities
1.2 ton HE Calibration Shots
Selected Wave Forms (in progress)

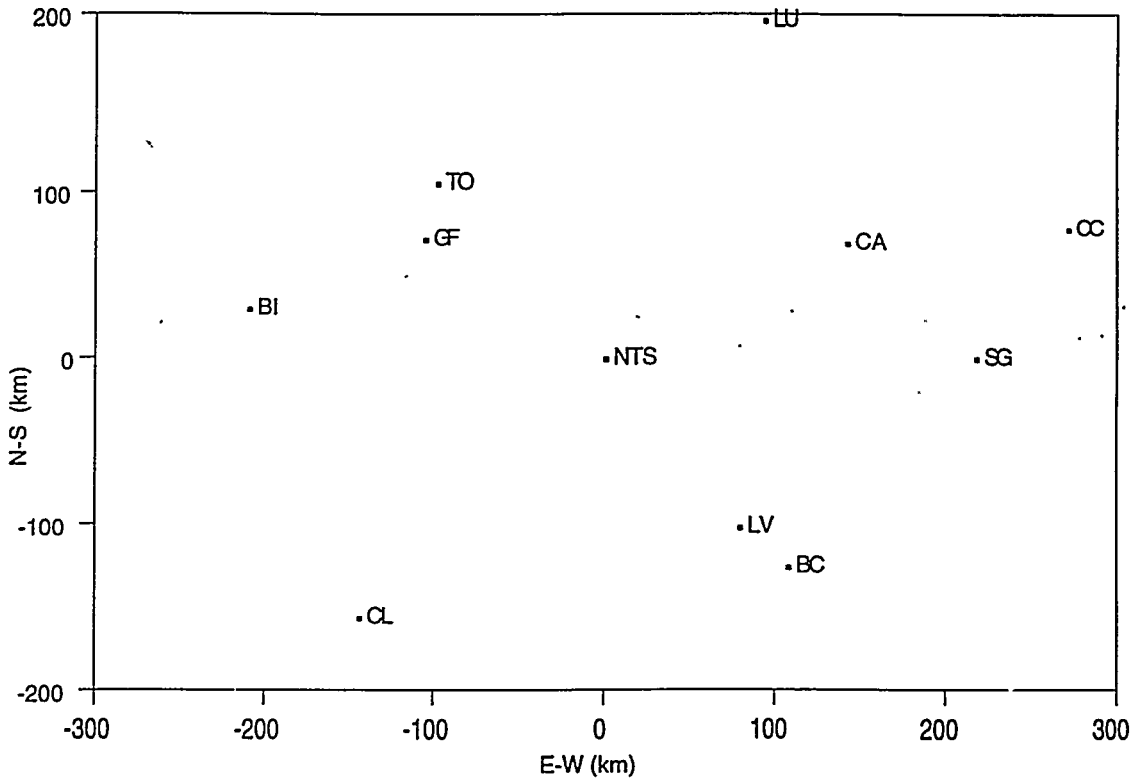

SANDIA LAB STATIONS

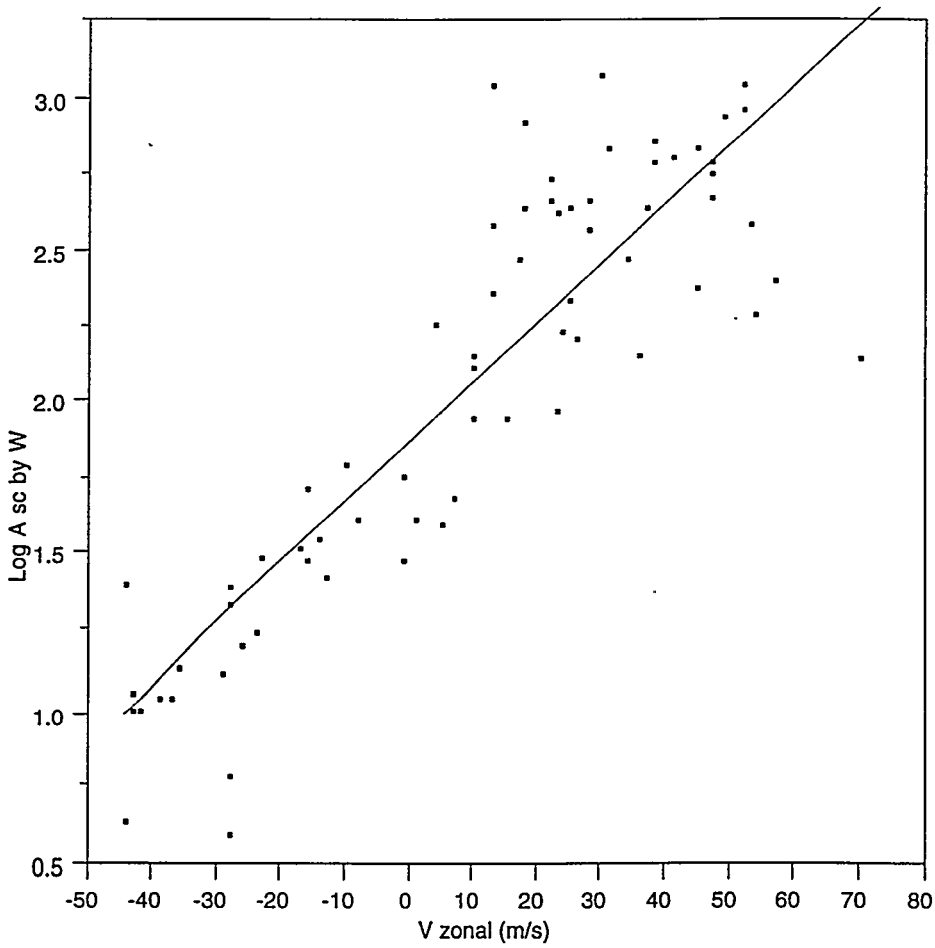

NTS DATA SCALED WITH WIND, ST. GEORGE

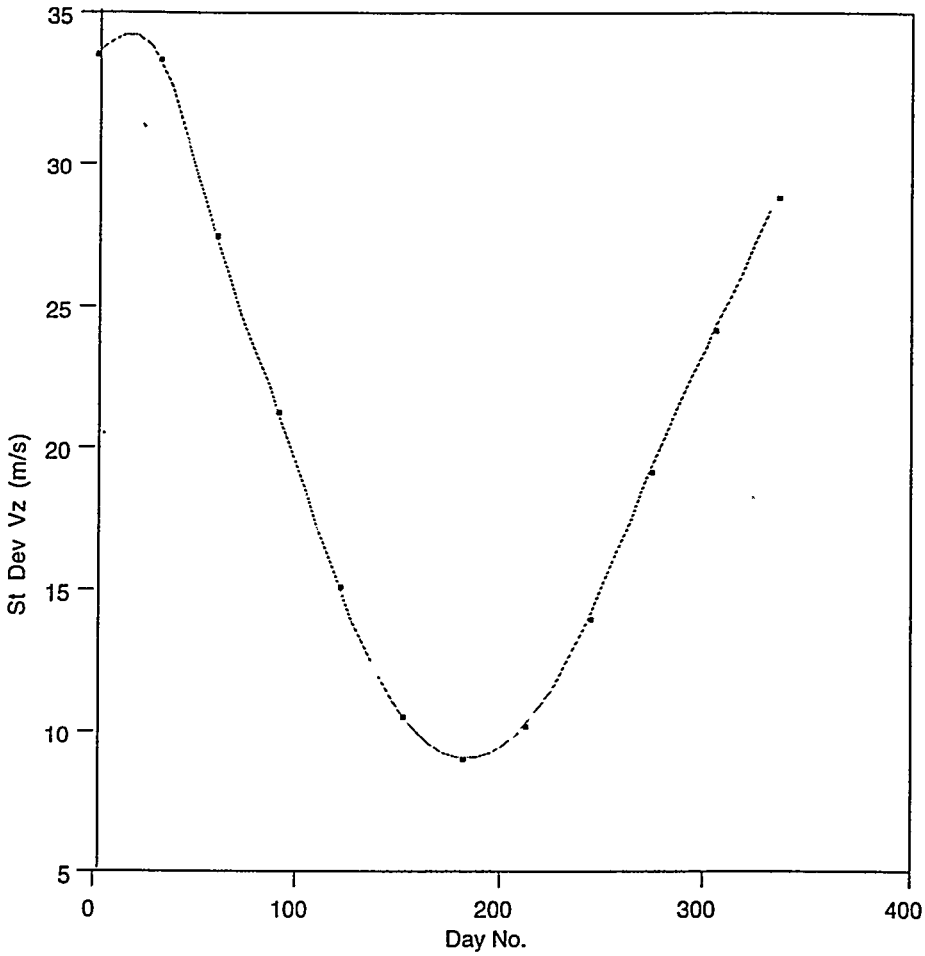

STANDARD DEVIATION OF THE ZONAL SCI WIND

DATA FITTING EQUATIONS

RANGE SCALING:

$$A_{obs} = C \cdot \left(\frac{R}{W^m} \right)^s \cdot 10^{k \cdot V_d}$$

MULTIVARIATE FIT:

$$Log\ A_{obs} = C + s \cdot Log\ R + n \cdot Log\ W + k \cdot V_d$$

where

$$n = -m \cdot s$$

FOR ONE STATION (CONSTANT RANGE):

$$Log\ A_{obs} = C + n \cdot Log\ W + k \cdot V_d$$

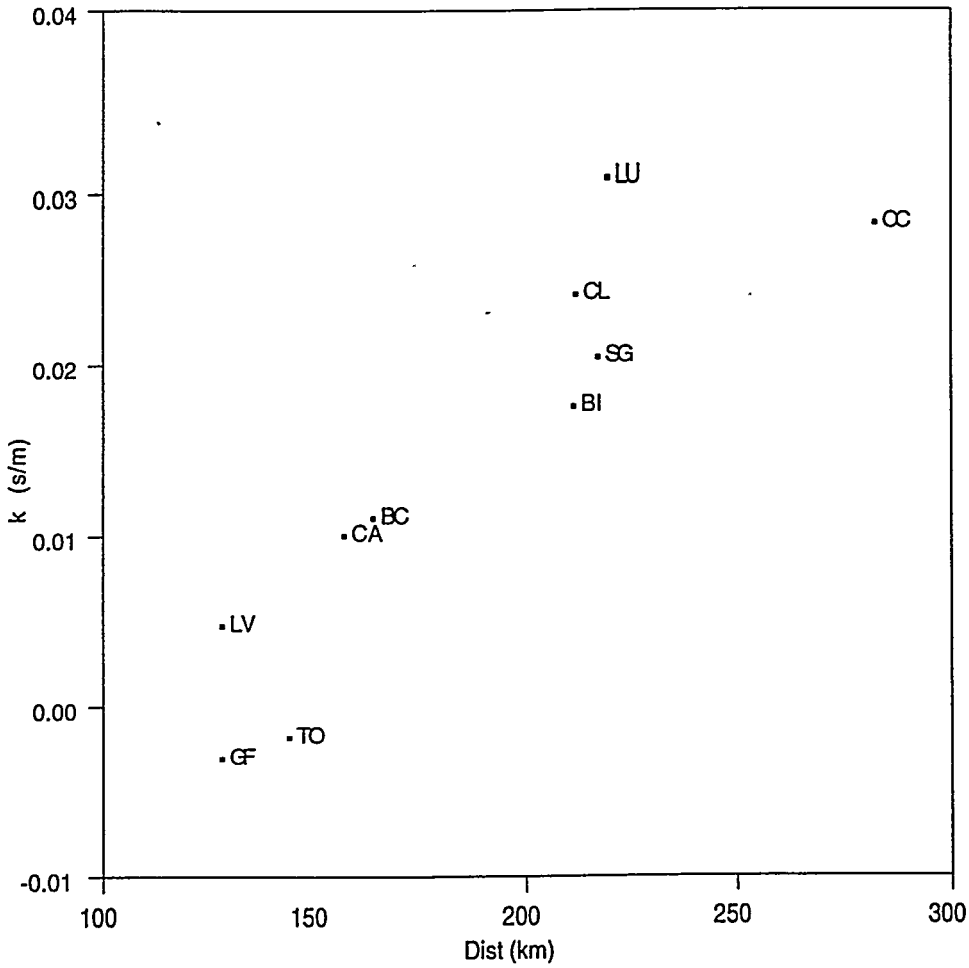

k DETERMINATION BY STATION, NTS DATA

Results from the Analysis of the NTS Data

- $Log\ A_{obs} = C + n \cdot Log\ W + k \cdot V_d$
- and $A_{corr} = A_{obs} \cdot 10^{-kV_d}$
- $k = f\ (R)$
- $k \approx 0.019\ s / m$ at first bounce distances
- $n \approx 0.45$

Does the Correction Method Apply to Longer Ranges ?

Trial Applications to Several Other Data Sets:

- LANL White Sands HE Data
- LANL Earthquake Data
- Longer Range NTS Data (TS-UK)

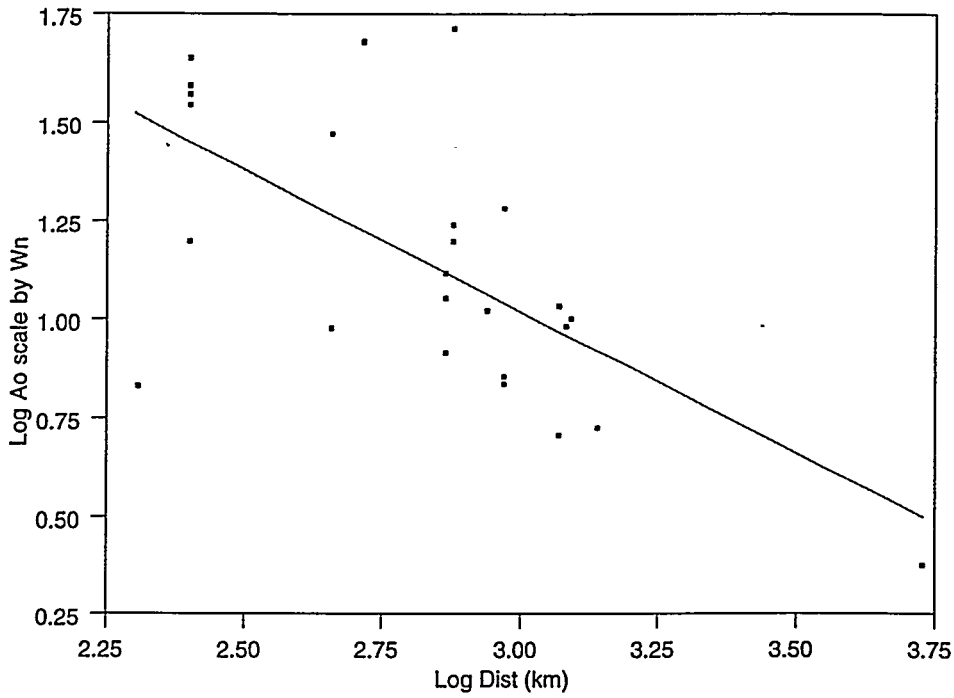

LANL HE DATA, FIT WITHOUT WINDS

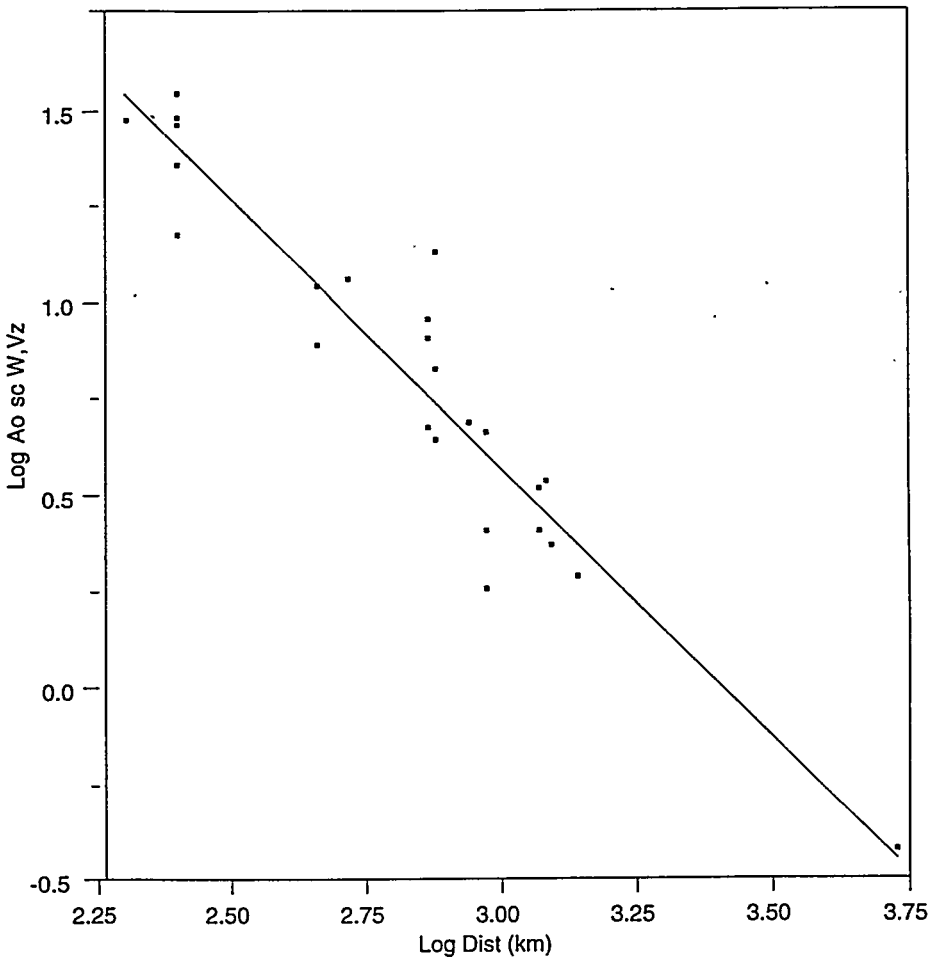

LANL HE DATA, FIT WITH WINDS

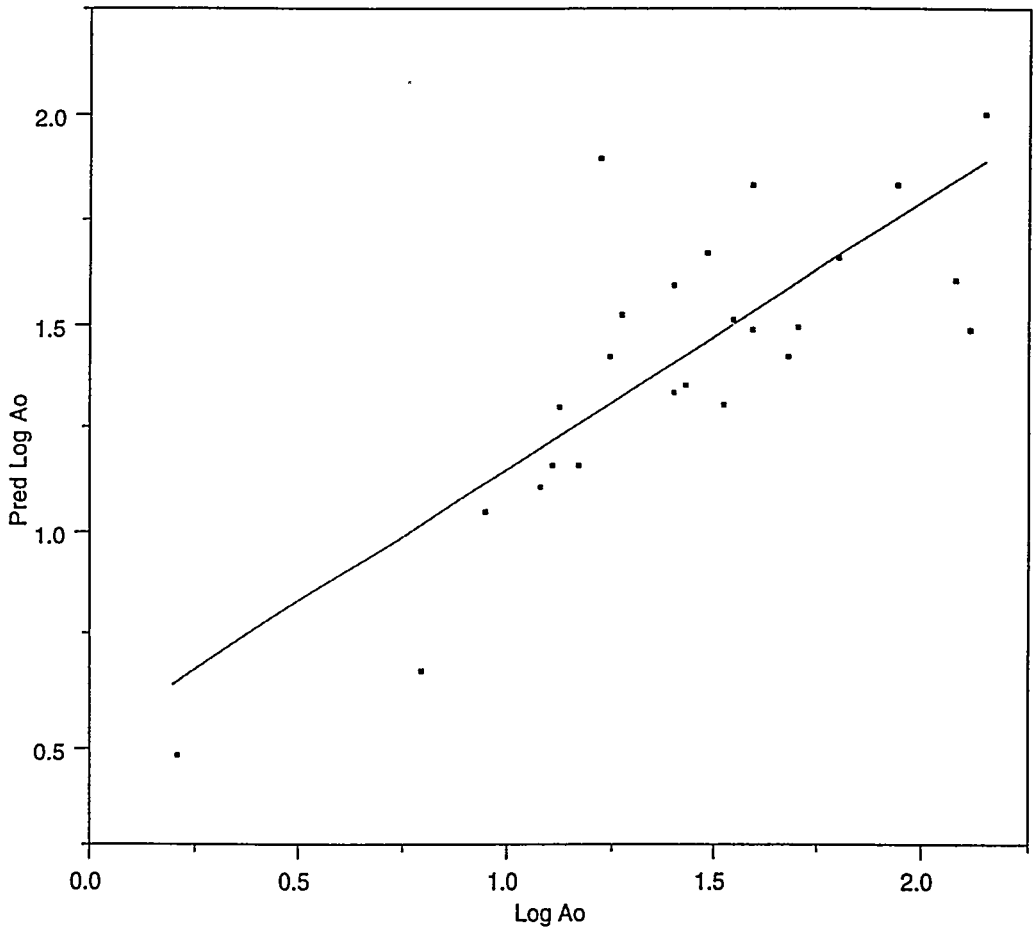

LANL HE DATA, FIT WITHOUT WINDS

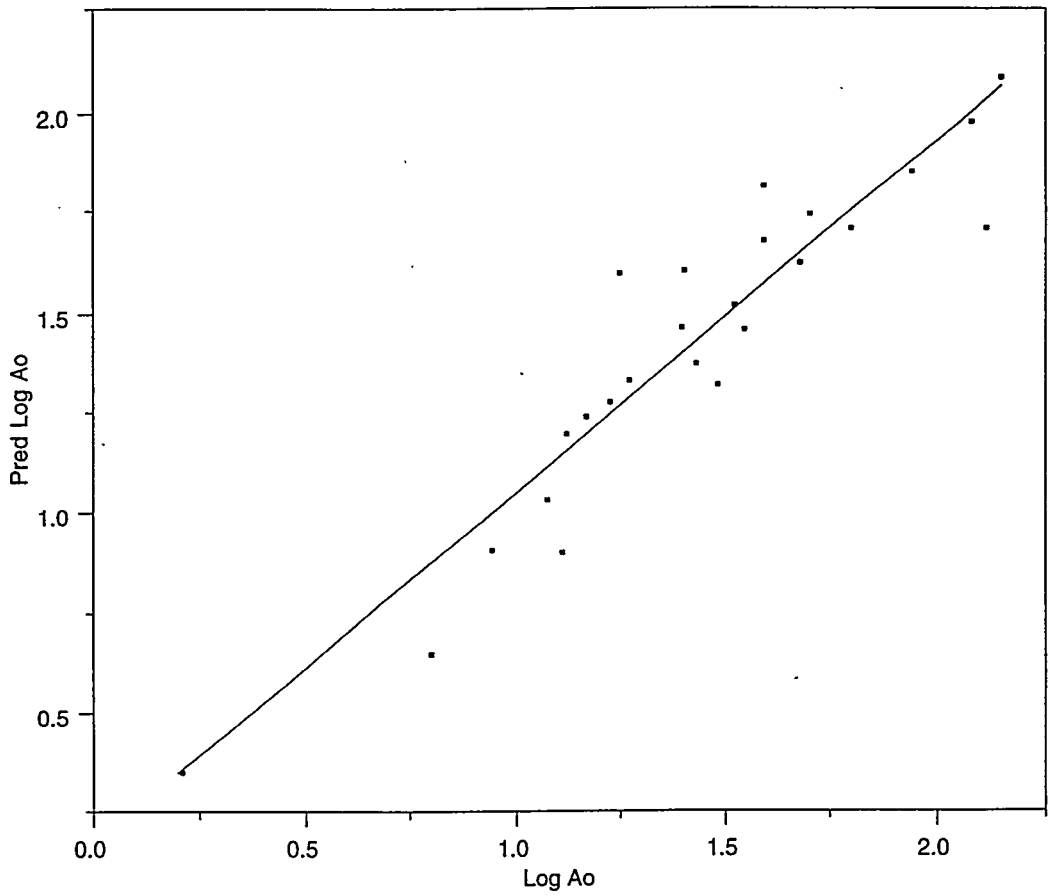

LANL HE DATA, FIT WITH WINDS

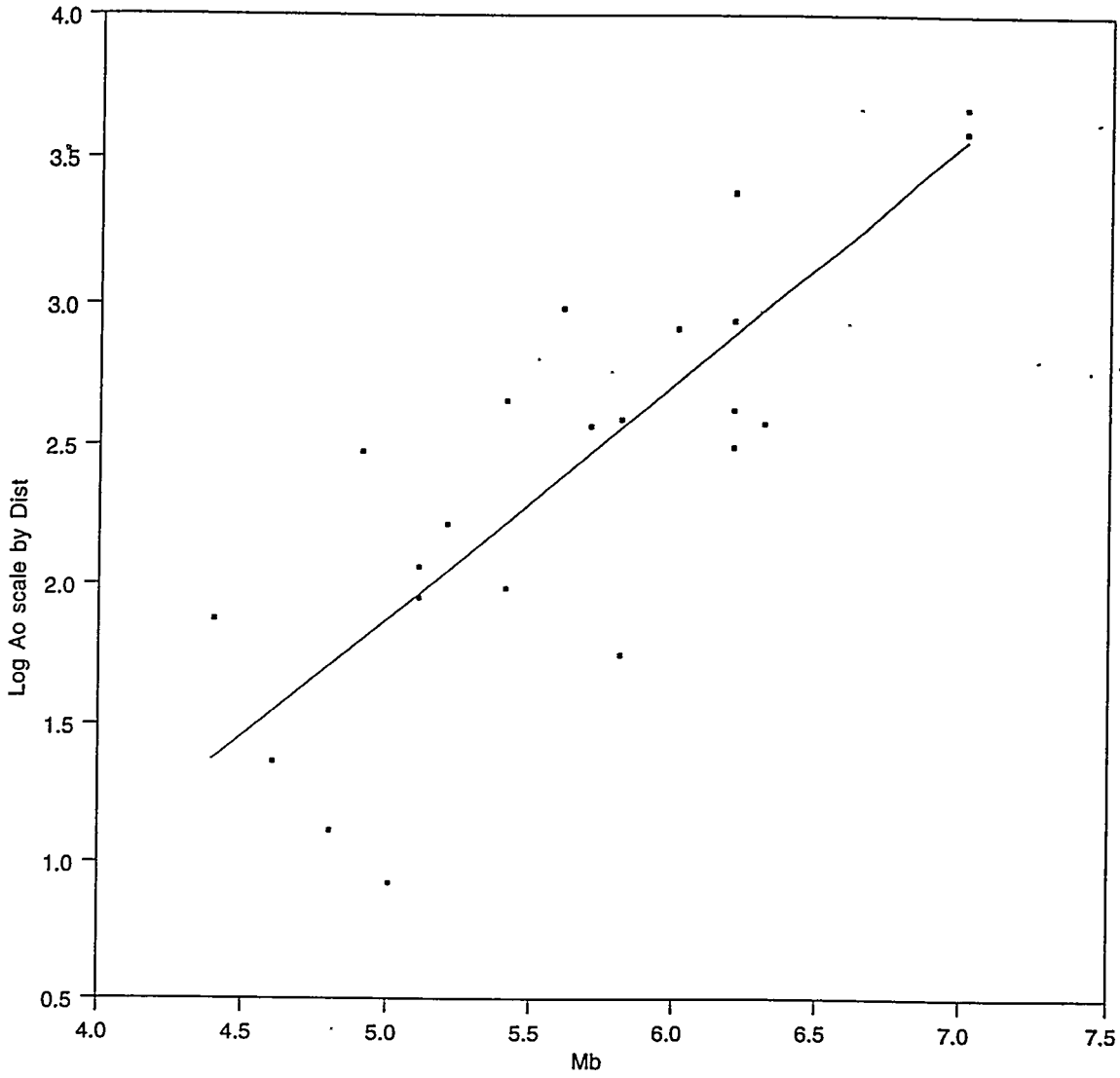

LANL EQ DATA, FIT WITHOUT WIND

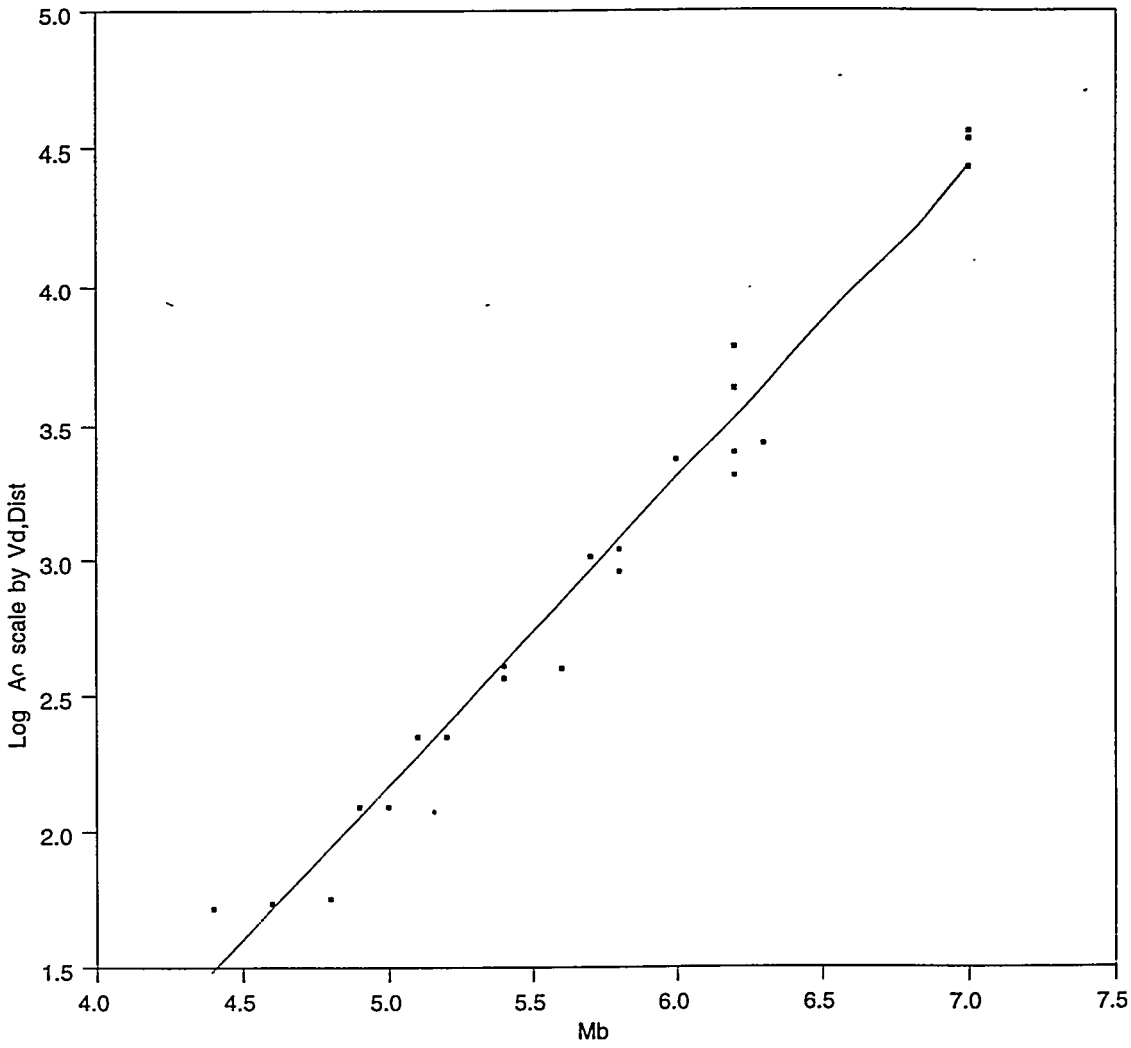

LANL EQ DATA, FIT WITH WIND

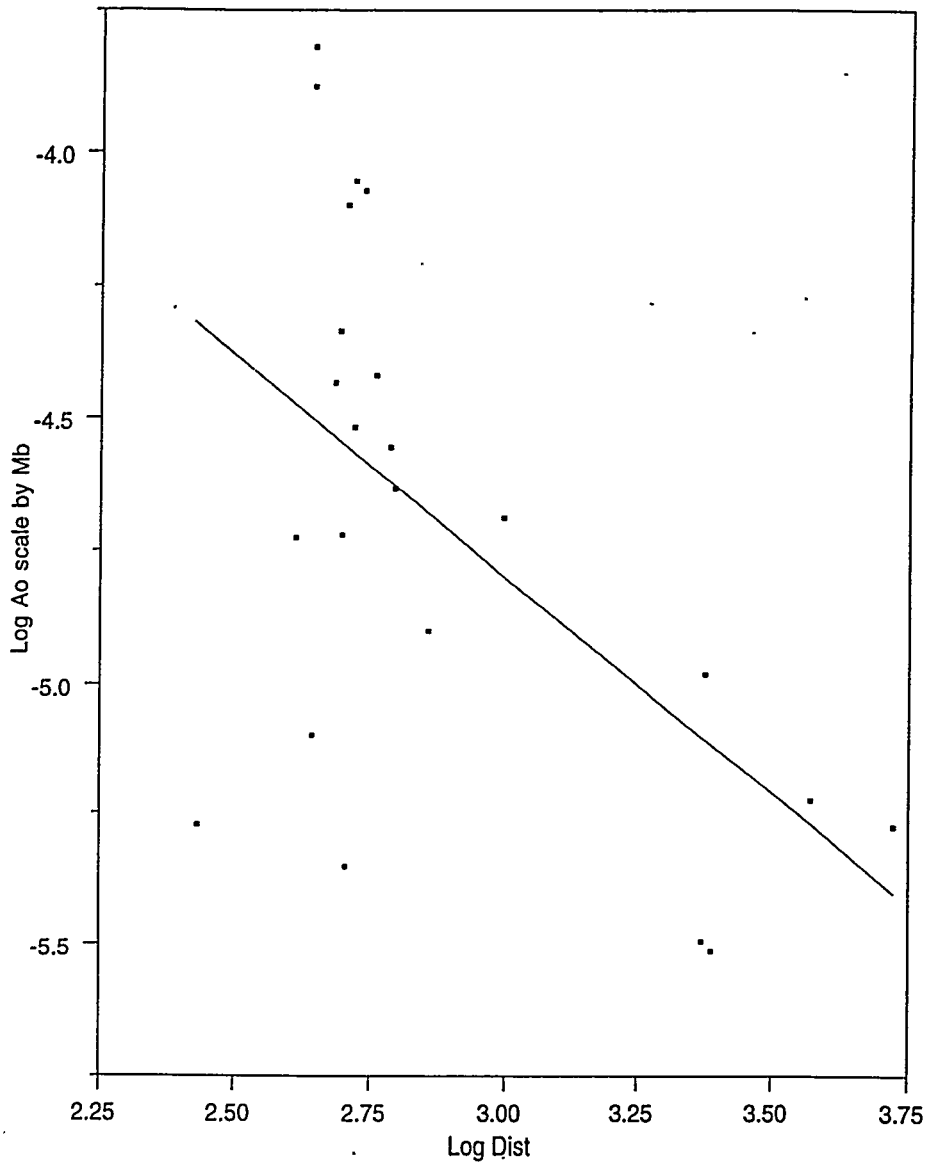

LANL EQ DATA, FIT WITHOUT WIND

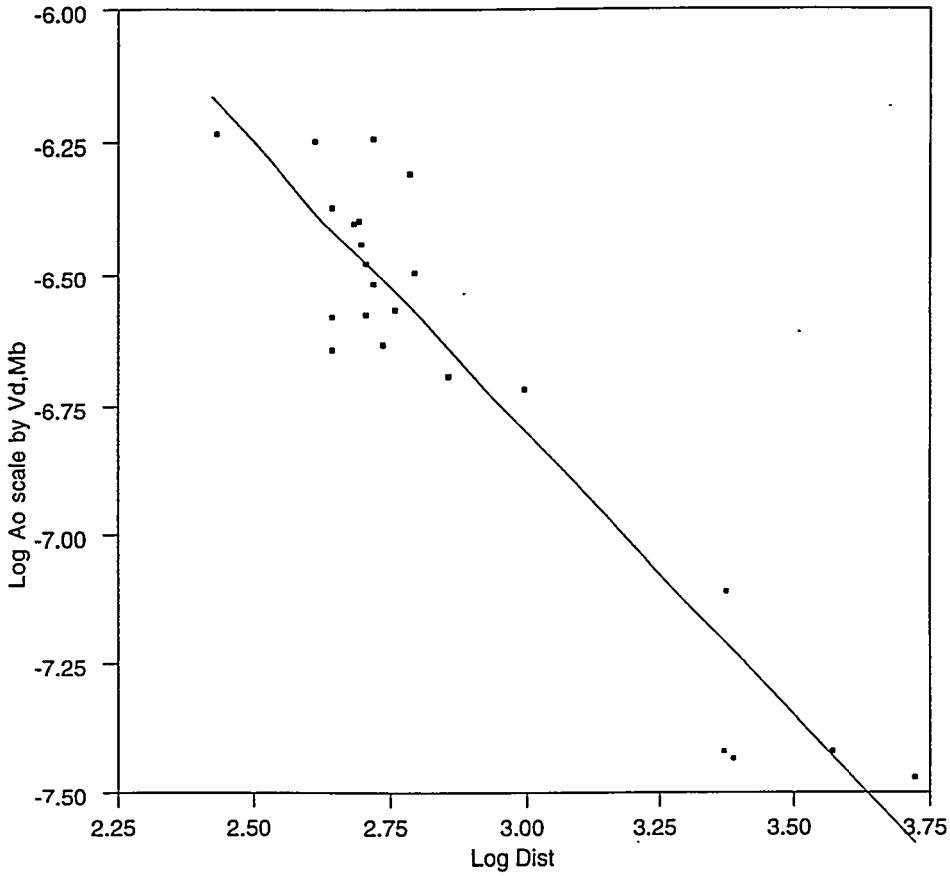

LANL EQ DATA, FIT WITH WIND

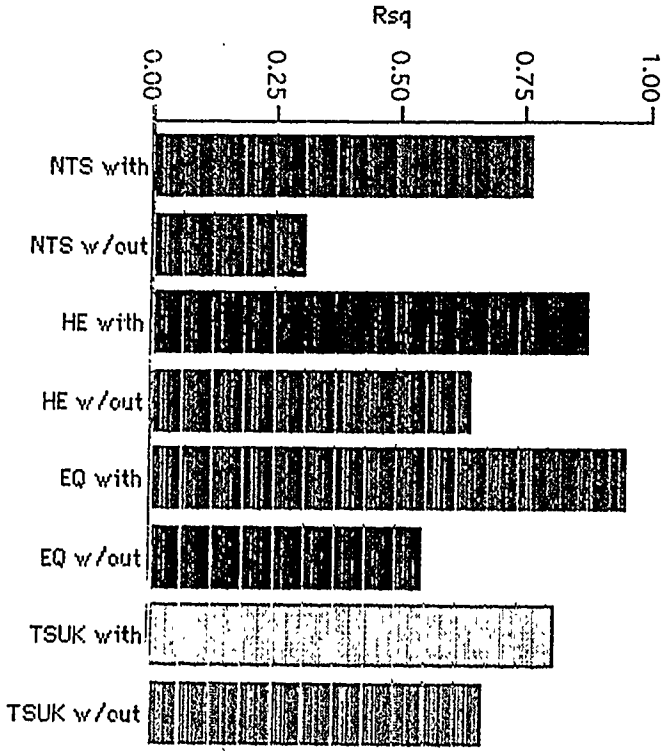
Rsq
0.00
0.25
0.50
0.75
1.00
NTS with
NTS w/out
HE with
HE w/out
EQ with
EQ w/out
TSUK with
TSUK w/out

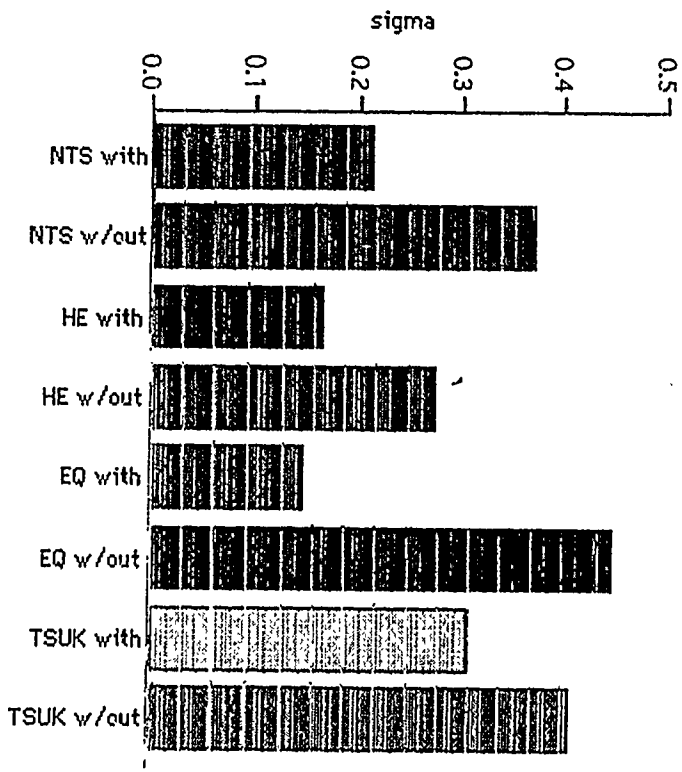
sigma
0.0
0.1
0.2
0.3
0.4
0.5
NTS with
NTS w/out
HE with
HE w/out
EQ with
EQ w/out
TSUK with
TSUK w/out

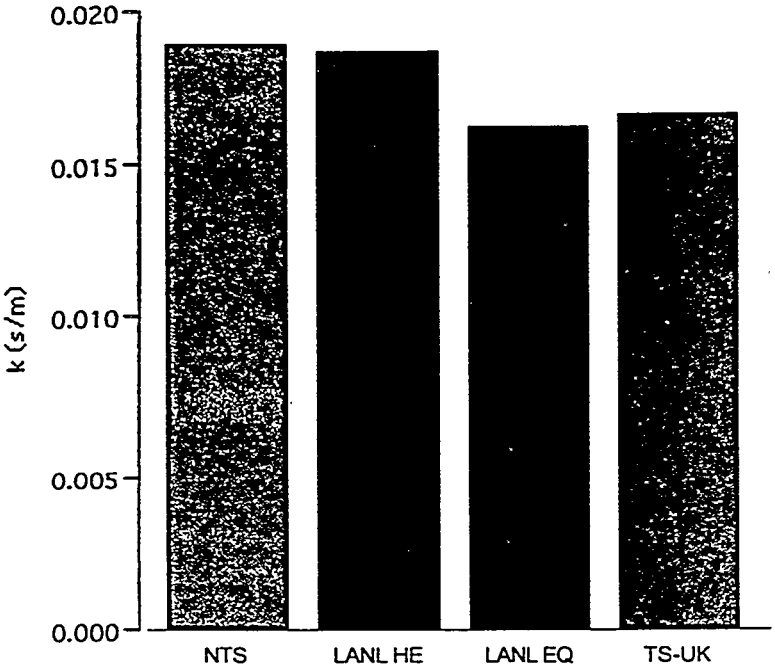

k DETERMINATIONS

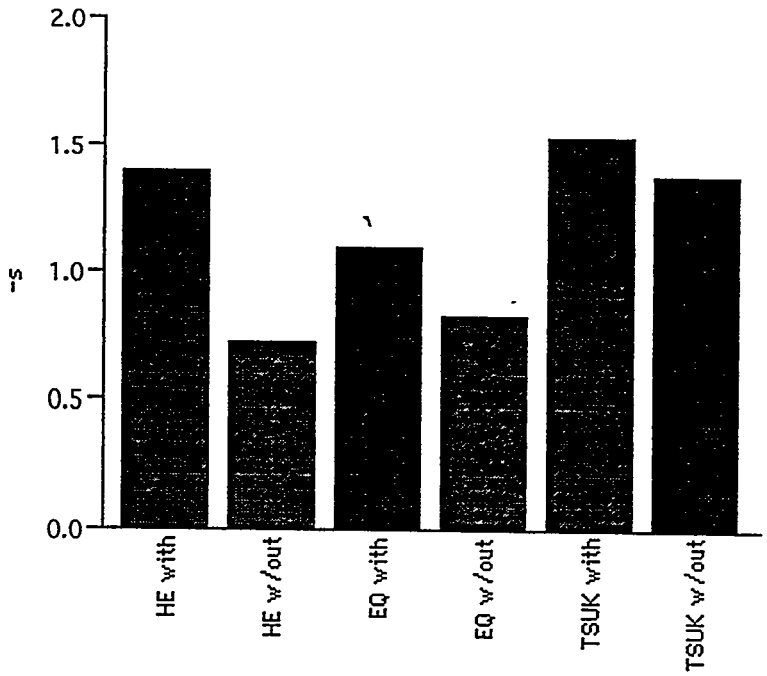
2.0
1.5
1.0
0.5
0.0
-s
HE with
HE w/out
EQ with
EQ w/out
TSUK with
TSUK w/out
s DETERMINATIONS

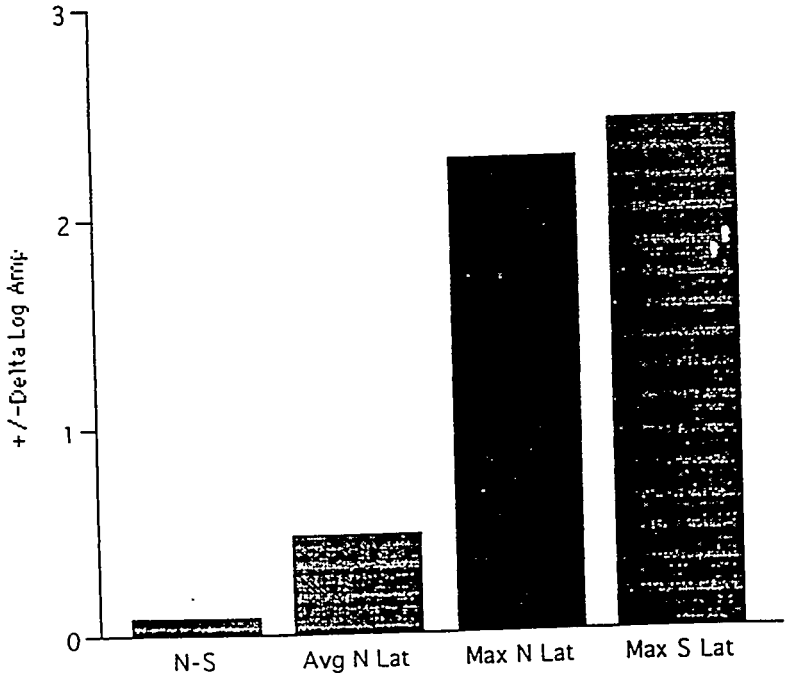

PREDICTED EFFECTS OF WIND ON AMPLITUDE

Conclusions and Recommendations

- Analysis of the NTS Data Provides a Method for the Correction of Amplitude for Stratospheric Wind Effects (several 100 km in range)

- Application to Longer Range Data Sets Indicates that the Method is Applicable to Long Ranges (several 1000 km in range)

- Future Efforts:
  1. Theoretical understanding of the correction (use of Pierce-type modal model)
  2. Analysis of a selected set of the NTSwaveforms
  3. Propose an observational effort to confirm and expand the method using HE explosions

POSSIBLE INFRASOUND

PROPAGATION EXPERIMENT

- 10 to 12 HE Explosions About 1 Month Apart
- Yield Approx. 5 Tons
- Microphones at "Bounce" Distances Out to About 1000 km. to the East and to the West
- At Least One Array of Microphones to East and West
- Dedicated Rocketsondes and/or Satellite Data to Provide Upper Atmospheric Wind Velocities
- Confirm Ability to Model Results

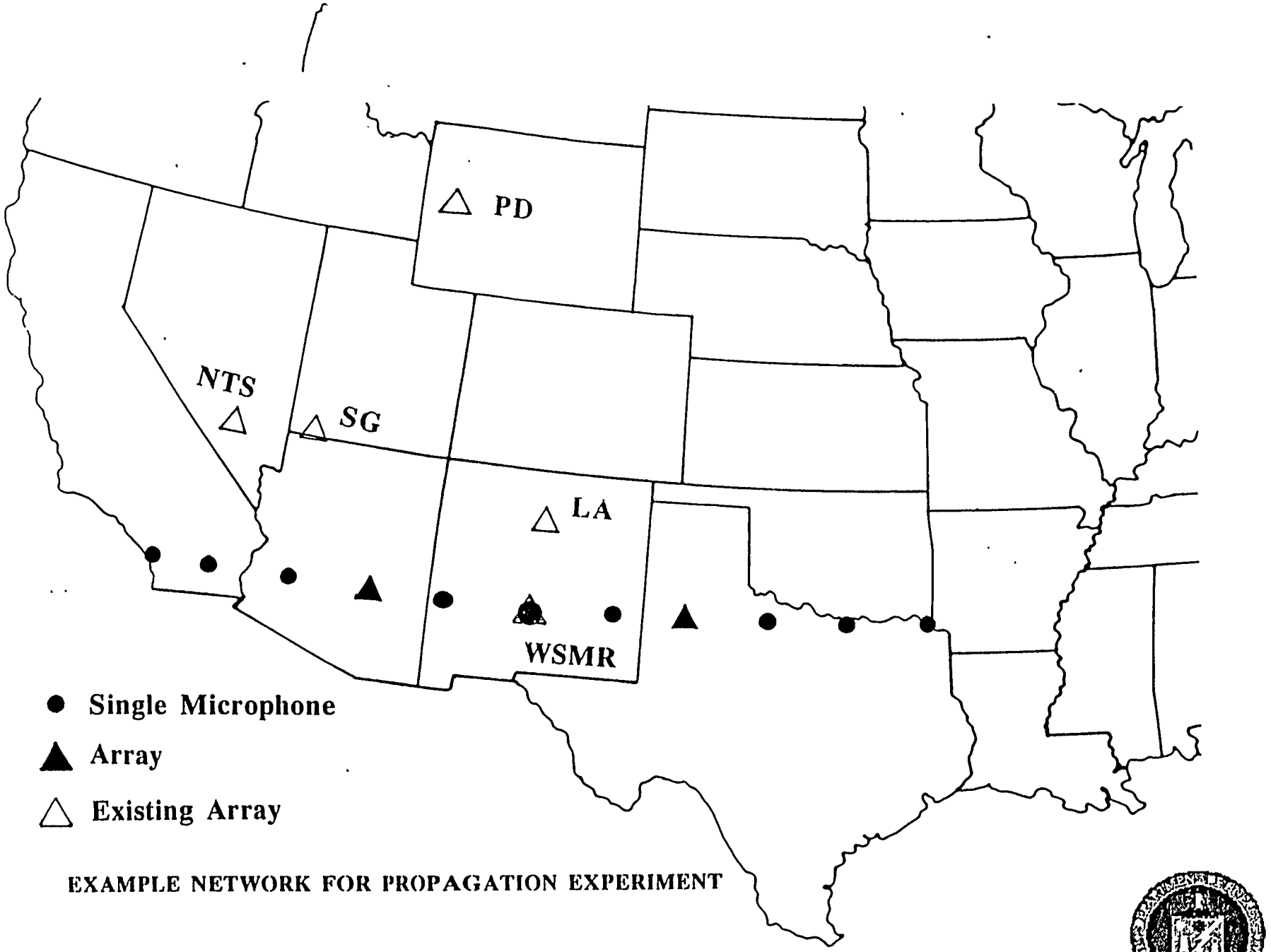

EXAMPLE NETWORK FOR PROPAGATION EXPERIMENT

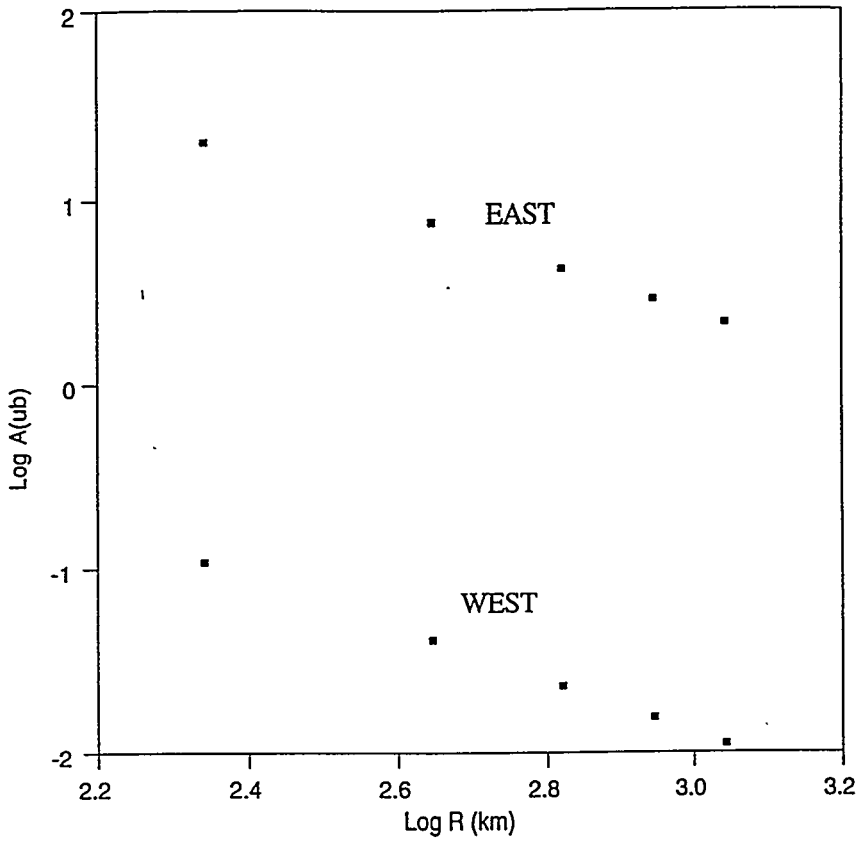

PREDICTED AMPLITUDES

5 TONS ANFO

V = 60 m/s

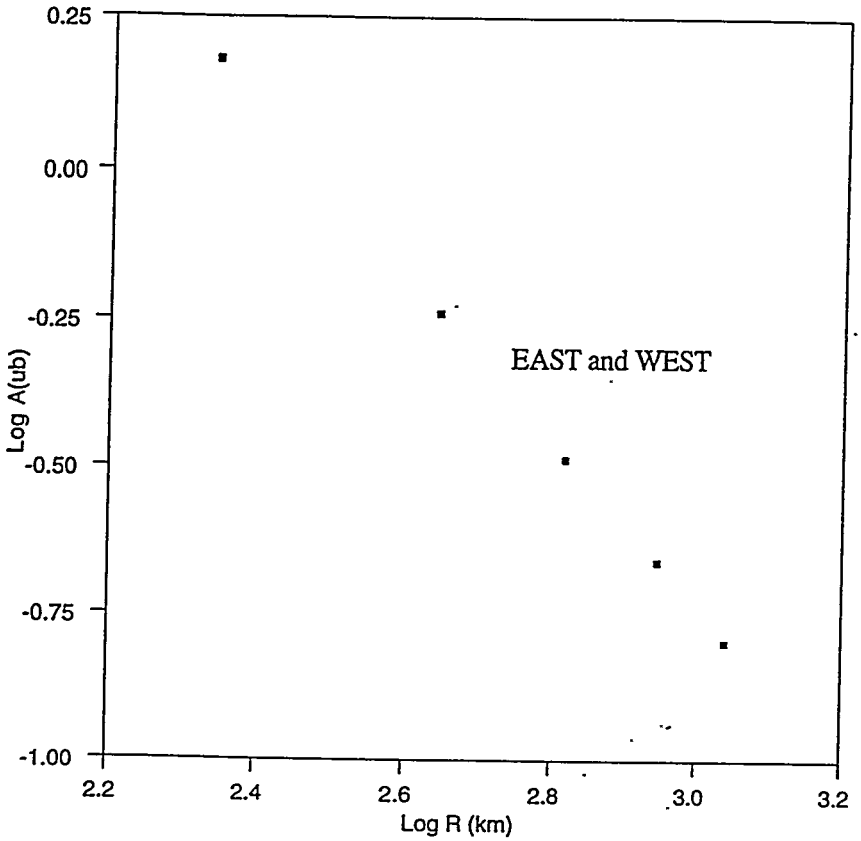

PREDICTED AMPLITUDES

5 TONS ANFO

V = 0 m/s

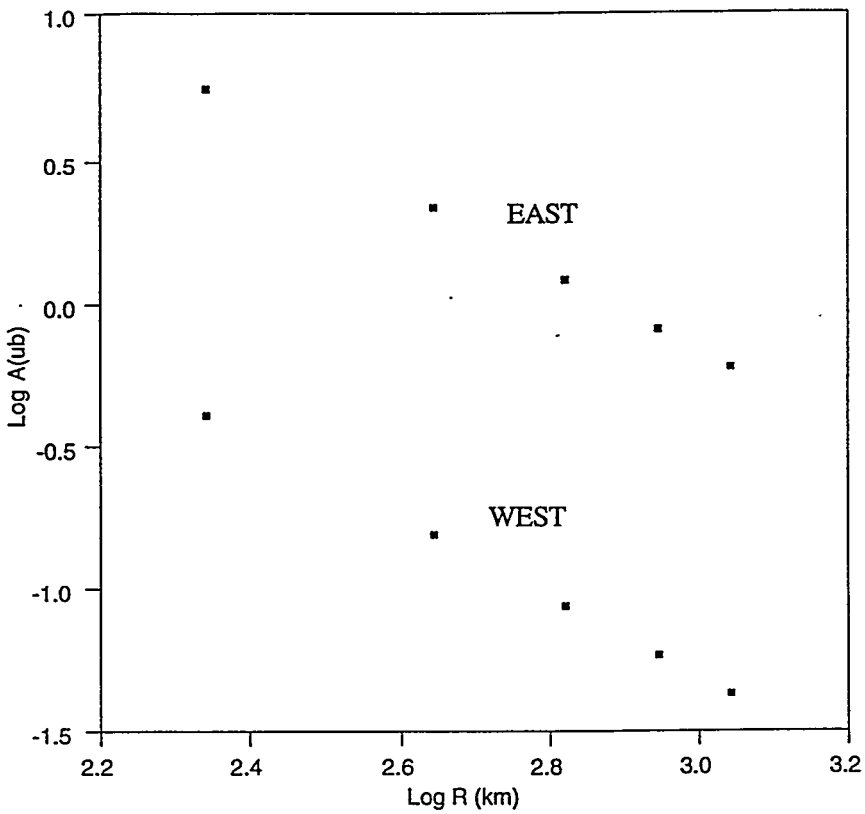

PREDICTED AMPLITUDES

5 TONS ANFO

V = 30 m/s

ANTICIPATED RESULTS OF INFRASOUND PROPAGATION EXPERIMENT

- Effects of Wind upon Signal Amplitude to Large Ranges
- Effects on Winds upon Average Signal Velocity
- Changes in Spectral Characteristics of Signals
- Understanding of E-W Asymmetry
- Azimuth Deviations Caused by Winds
- Some Tropospheric Signals

HIGH ALTITUDE WIND EFFECTS ON INFRASOUND NETWORK PERFORMANCE

Lawrence Trost

Sandia National Laboratory

Currently there is disagreement on the effects of 50 km winds on infrasound propagation. Many researchers feel it is highly important, while other do not view it as a major influence. In order to gain a first order impression of the effects that the 50 km winds might have on IMS network performance, a series of simulations were made using the IVSEM computer code. In these simulations, the detection performance of the WP330R infrasound network against small (subkiloton) events was analyzed for a number of months with different average wind conditions, with and without a LANL derived wind correction factor. It was found that on the average, the simulation predicted better performance for the network with the wind correction than without. It was also found that the geographic coverage of the network varied greatly throughout the year. Regions of decreased detection performance, found mostly in the Southern Hemisphere, remained stable if the wind correction was not used. When wind effects were factored in, the position of those regions shifted radically with the season, and the size varied greatly. In view of these differences, research is warranted to better understand the physics of infrasound propagation under the influence of high altitude winds.

High Altitude Wind Effects on Infrasound Network Performance

Lawrence C. Trost

Sandia National Laboratories

August 26, 1997

Sandia is a multiprogram laboratory operated by Sandia Corporation, a Lockheed Martin Company, for the United States Department of Energy under Contract DE-AC04-94AL85000.

Sandia
National
Laboratories

High Altitude Winds

- Some (but not all) researchers believe that 50 km winds have major effects on propagation
- Network performance would be affected by these winds
- 50 km winds vary by time of year
- Network performance will therefore vary according to the time of year

Methodology

- The IVSEM model was used
- One run was made with the wind correction removed
- Three runs were made simulating three times of the year: March, September, and December

Integrated Verification System Effectiveness Model

- IVSEM is designed to provide quick estimations of network effectiveness
- IVSEM contains 4 models: Seismic, Hydroacoustic, Infrasound, and Radionuclide
- Only the infrasound model was used for this effort

Simulation Assumptions

- 1 kt and notional lower yield event
- WP-330R network with 4 element stations
- Signal to noise threshold of 2
- Station noise based on yearly average wind speeds
- 3 runs with wind correction, 1 without
- Three times of year: March, September, and December

Sandia National Laboratories

Detection Probability
1 kt, 1 km, WP330R
No Wind Correction

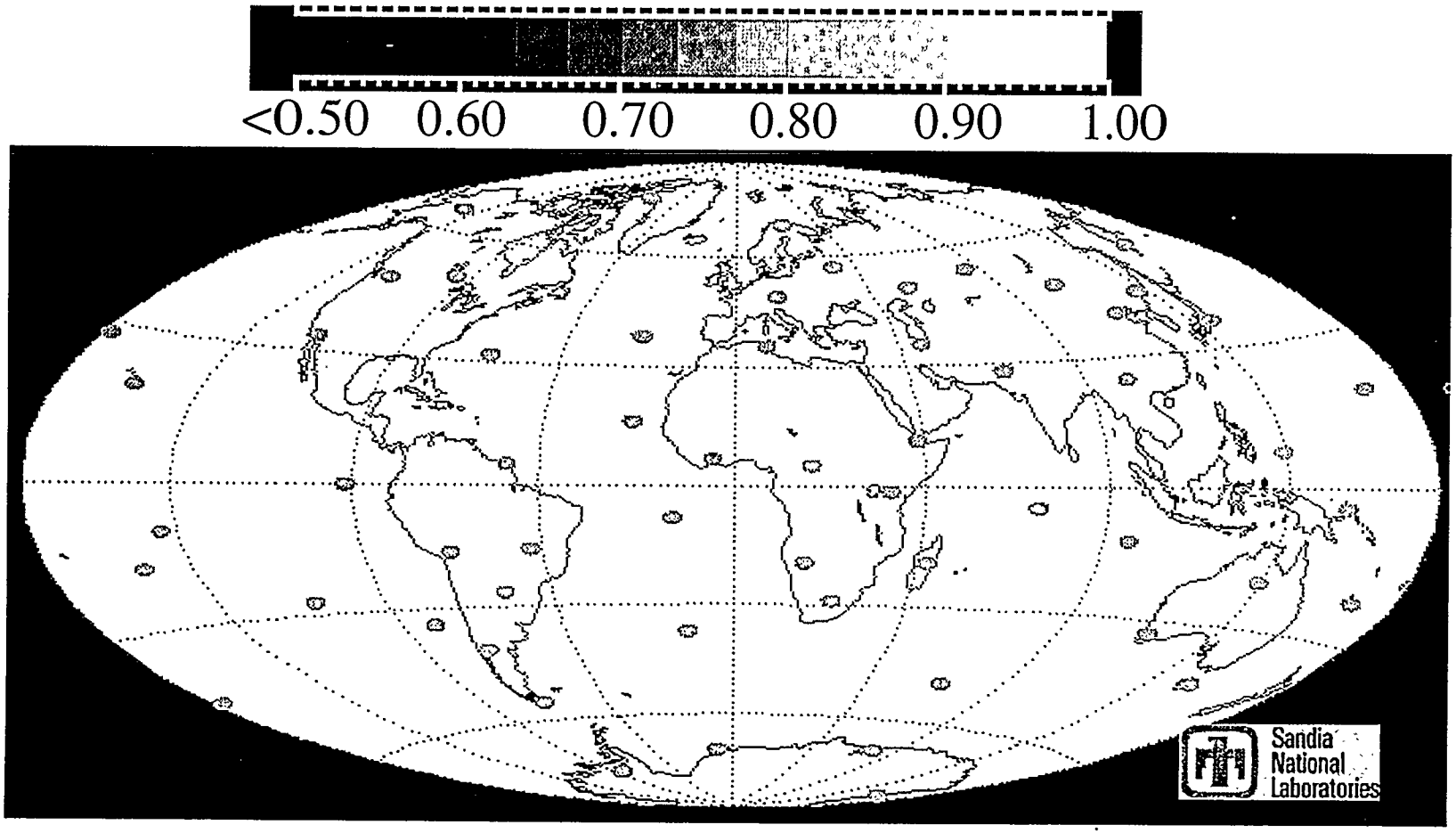

Detection Probability
1 kt, 1 km, WP330R
March Wind Correction

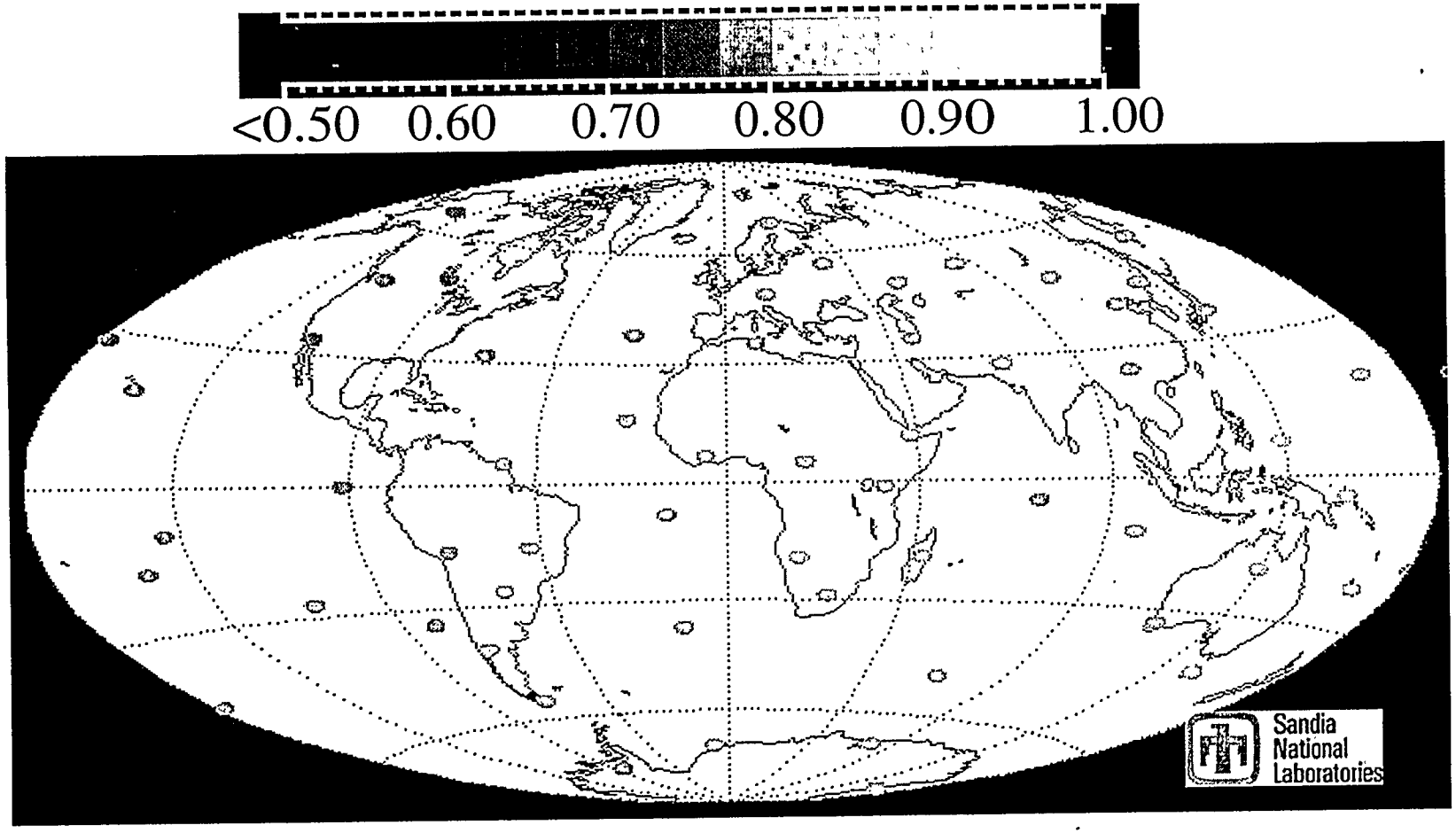

Detection Probability
Lower Yield, 1 km, WP330R
No Wind Correction

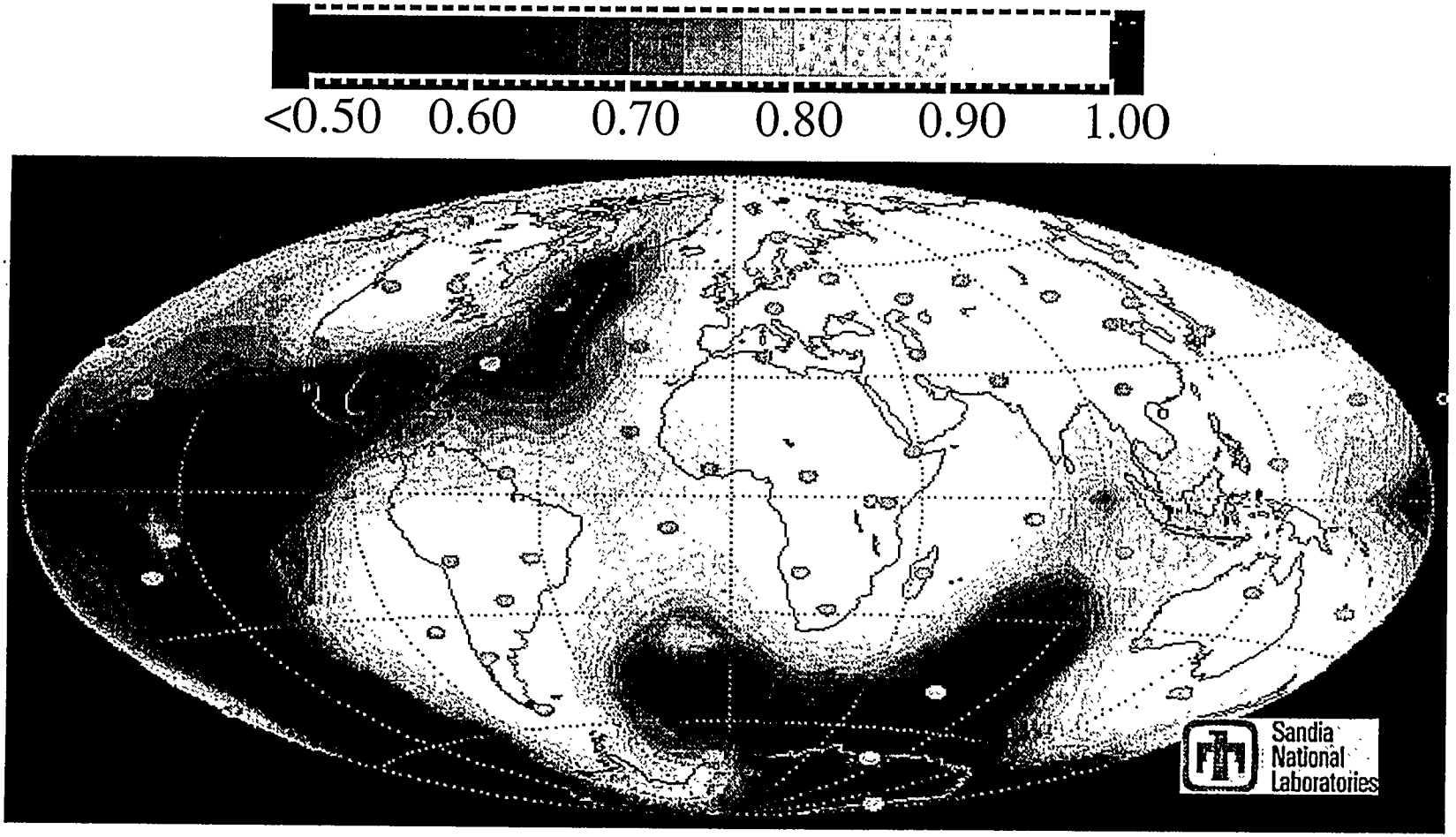

Detection Probability
Lower Yield, 1 km, WP330R
March Wind Correction

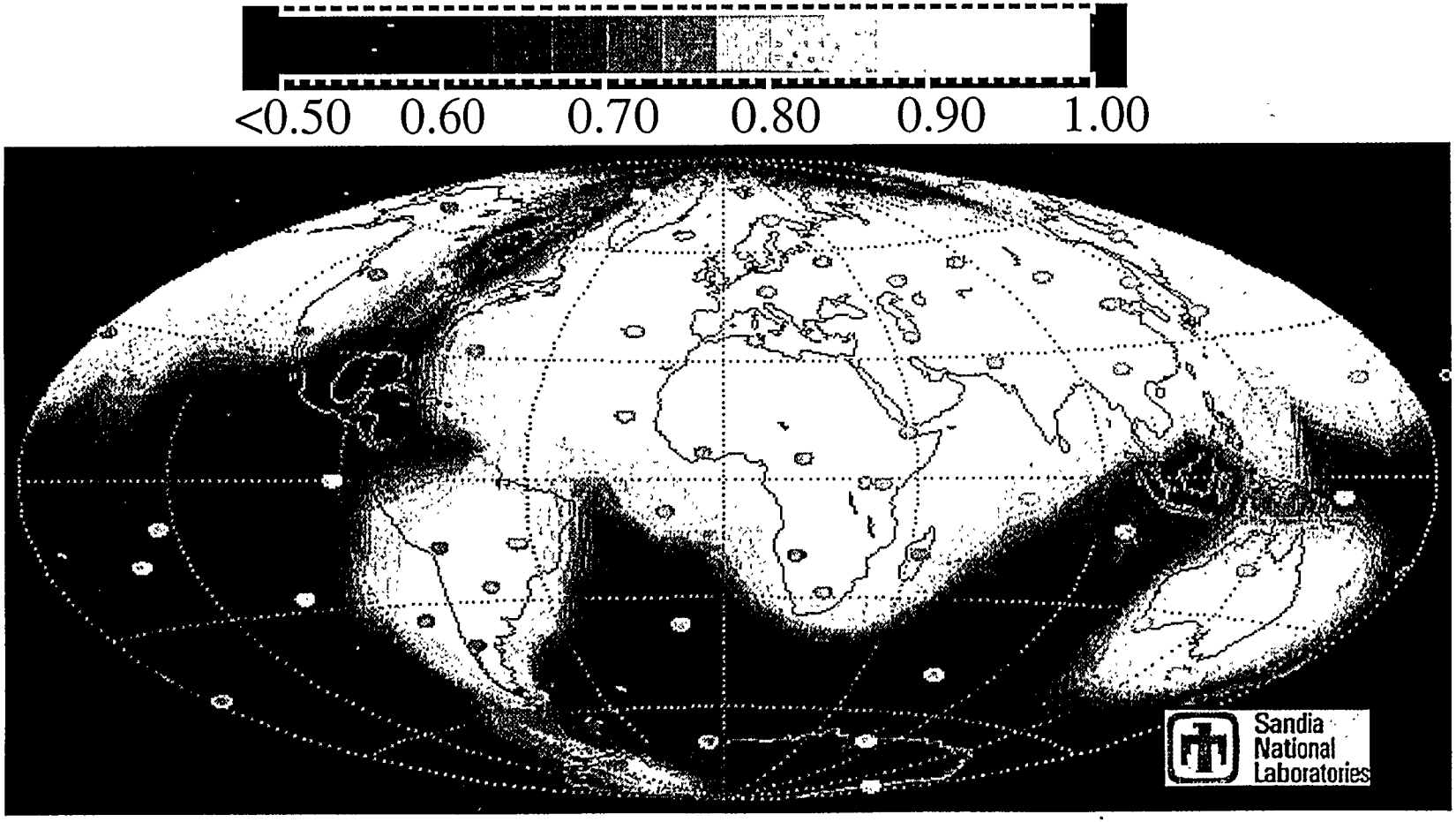

Detection Probability
Lower Yield, 1 km, WP330R
September Wind Correction

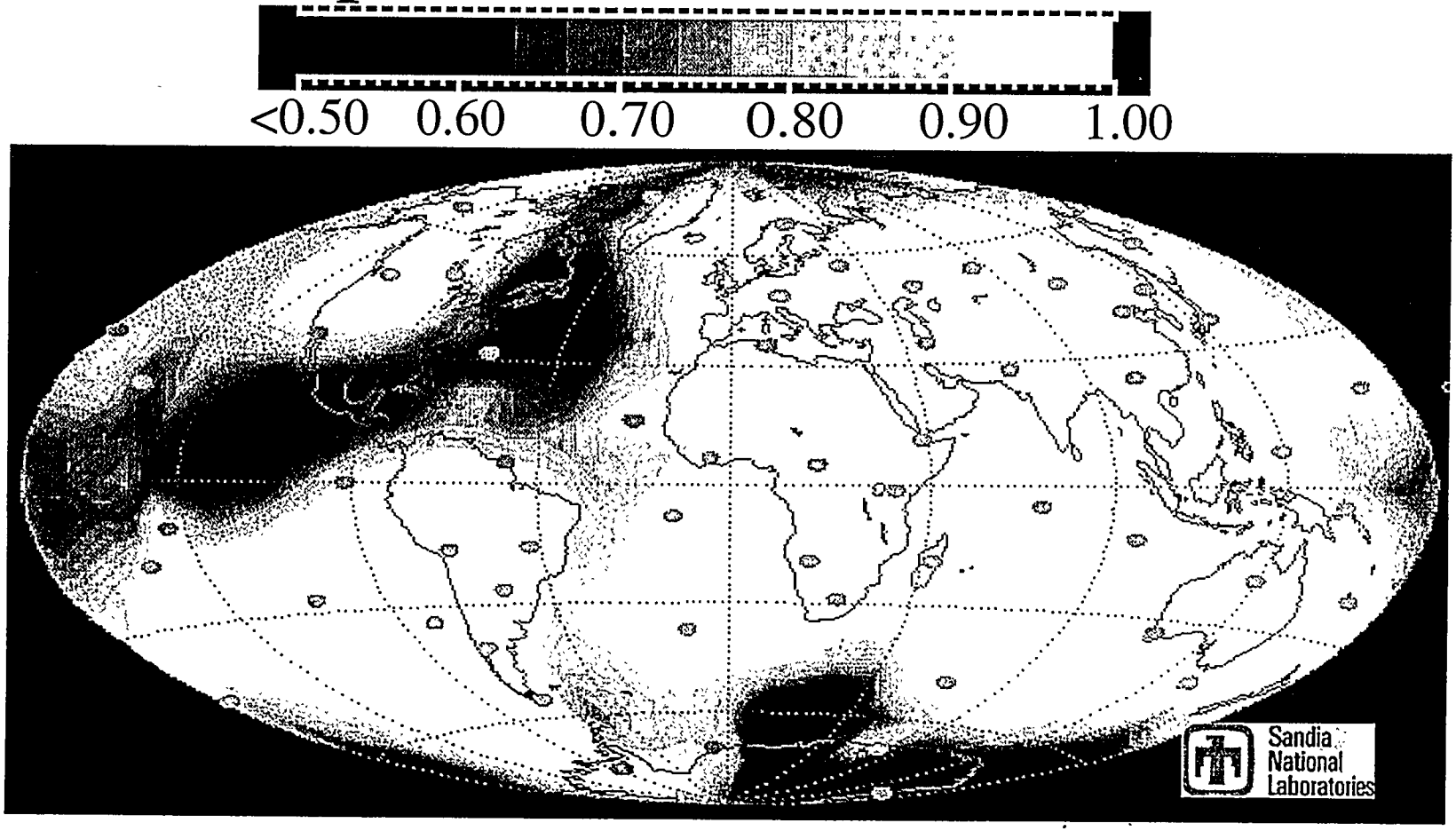

Detection Probability
Lower Yield, 1 km, WP330R
December Wind Correction

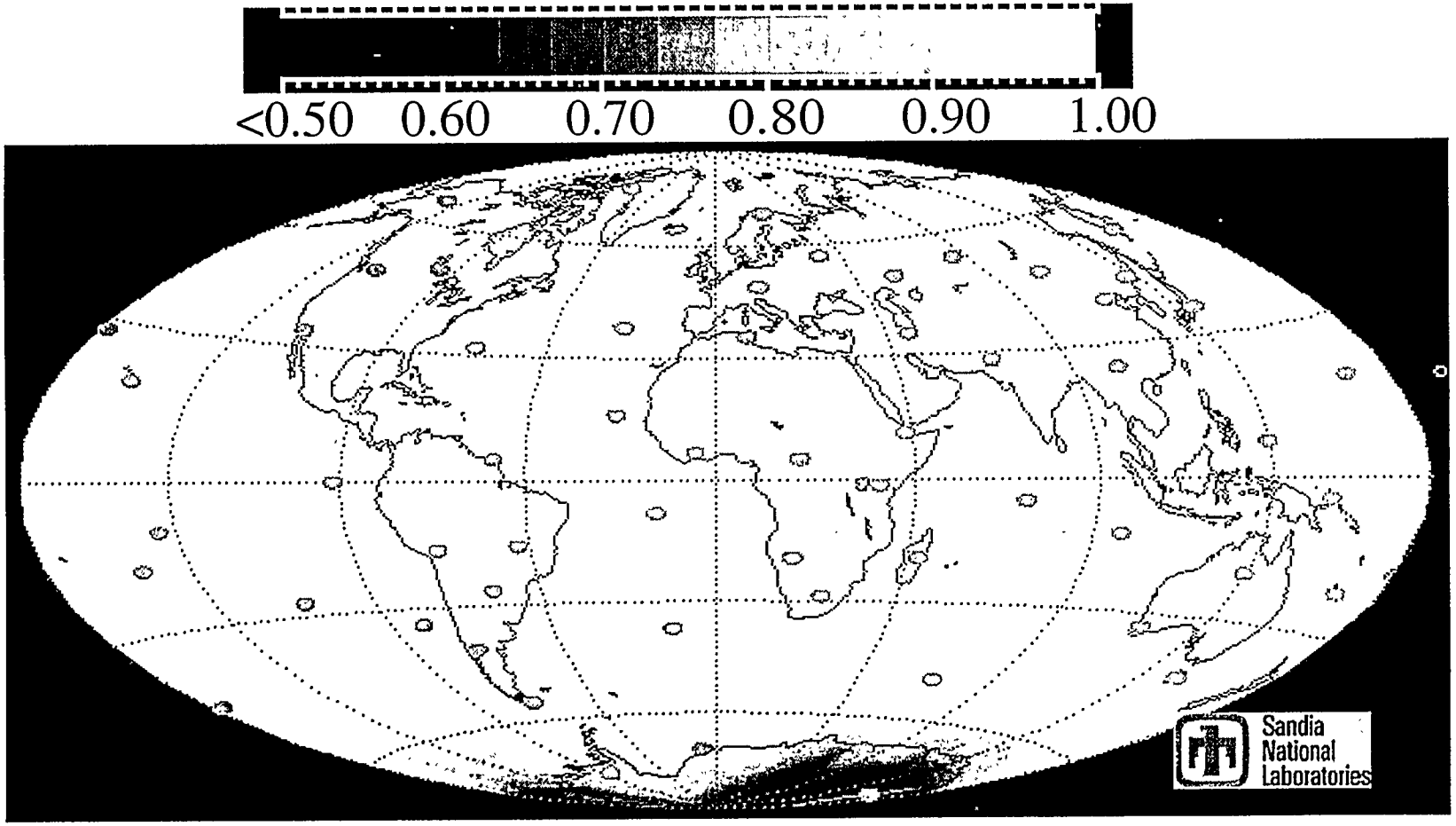

Conclusions

- 50 km winds could have a major effect on network performance against small yield events
- The regions of poor detection performance would vary with the time of year
- Research is needed to confirm the effects of these winds

Sandia National Laboratories

PERMEABLE HOSE CHARACTERISTICS AND NOISE REDUCTION FOR INFRASOUND MONITORING

Keith L. McLaughlin, Terrance G. Barker, and Darin E. Wilkins,

Maxwell Technologies
8888 Balboa Blvd.
San Diego, CA 92123

The proposed CTBT infrasound monitoring network consists of between 50 and 60 4 - station arrays. Many of the infrasound stations will be co-located or adjacent to seismic systems and work in concert. Each infrasound station is intended to consist of a broadband microbaragraph equipped with several hundred meters of noise reduction hose. The permeable hose design replaces Daniels microphone pipes for the purposes of spatially averaging wind eddy generated pressure fluctuations. Useful detection thresholds for infrasound stations will be directly related to the effectiveness of the noise reduction hose arrays. We present an analysis of the differential equations that describe the acoustics of infrasound recording with a permeable hose as opposed to the discrete set of coupled equations that have traditionally been used to describe a Daniels pipe. We have implemented solutions to the differential equations using the finite - difference code Maxhose, which is an implicit Crank-Nickelson time-stepping second order code. The code includes the effects of atmospheric loading, calibration/test volumes, and finite volume manifolds and transducers attached to the hose. It may be generalized to multiple hoses connected to finite volume manifolds. Traditionally, the momentum term is neglected in computing hose response. We have included this term and found its effect to be significant under some circumstances. The code accepts arbitrary atmospheric pressure as a function of position and time to simulate wind noise and propagating signals. We show results for atmospheric loading in which the noise power spectra decay as inverse frequency and inverse wavenumber. Future plans include Monte Carlo simulations of noise reduction properties of multiple hose configurations. It is shown that a hose may be characterized by a characteristic time constant, and a characteristic length, l. The time constant is related to permeability of the hose and the characteristic length is related to both flow resistance and permeability of the hose. Signal to noise improvement is directly proportional to the characteristic length of the hose. The low pass filer corner frequency of the system is determined by the characteristic time. Wavelengths of the pressure field shorter than characteristic length are averaged over the length of the hose. The finite difference code, Maxhose, is used to model both operational hose designs as well as calibration configurations. A simple experimental calibration is described to measure the characteristic times and lengths of permeable hoses. Calibration results are shown for commercially available soaker hose. Typical measured characteristic times are between 10 to 20 milliseconds, while characteristic lengths are between 100 and 300 meters. Of particular note are the effects of hose degradation during a typical San Diego winter as demonstrated by a reduction in characteristic length of the hose by a factor of 2. An operational system would have experienced a comparable degradation of signal - to - noise over time. Simple calibration systems can be designed to track such hose characteristics, and modeled using simple finite-difference codes to predict system performance.

Permeable Hose Characteristics and Noise Reduction For Infrasound Monitoring

Infrasound Workshop, Santa Fe NM, 25-28 August 1997

Keith McLaughlin, Terry Barker, Darin Wilkins

Maxwell Technologies
8888 Balboa Ave. San Diego, CA 92123
619-576-7763 FAX 619-576-7763
scatter@maxwell.com, barker@maxwell.com,
wilkins@maxwell.com
http://www.maxwell.com/products/geop

Maxwell TECHNOLOGIES
Federal Division

Outline

- **Introduction**
- **Flow properties and spectra of permeable hoses**
- **Expected SNR improvements**
- **Simple diagnostic methods for test hose systems**
- **Effects of hose degradation on SNR improvement**
- **Description of numerical code, *Maxhose*, for modeling hoses**
- **Using numerical modeling with wind noise models to understand performance of hose configurations**

Log10(W) Threshold for 2 Infrasound Stations - Proposed IMS

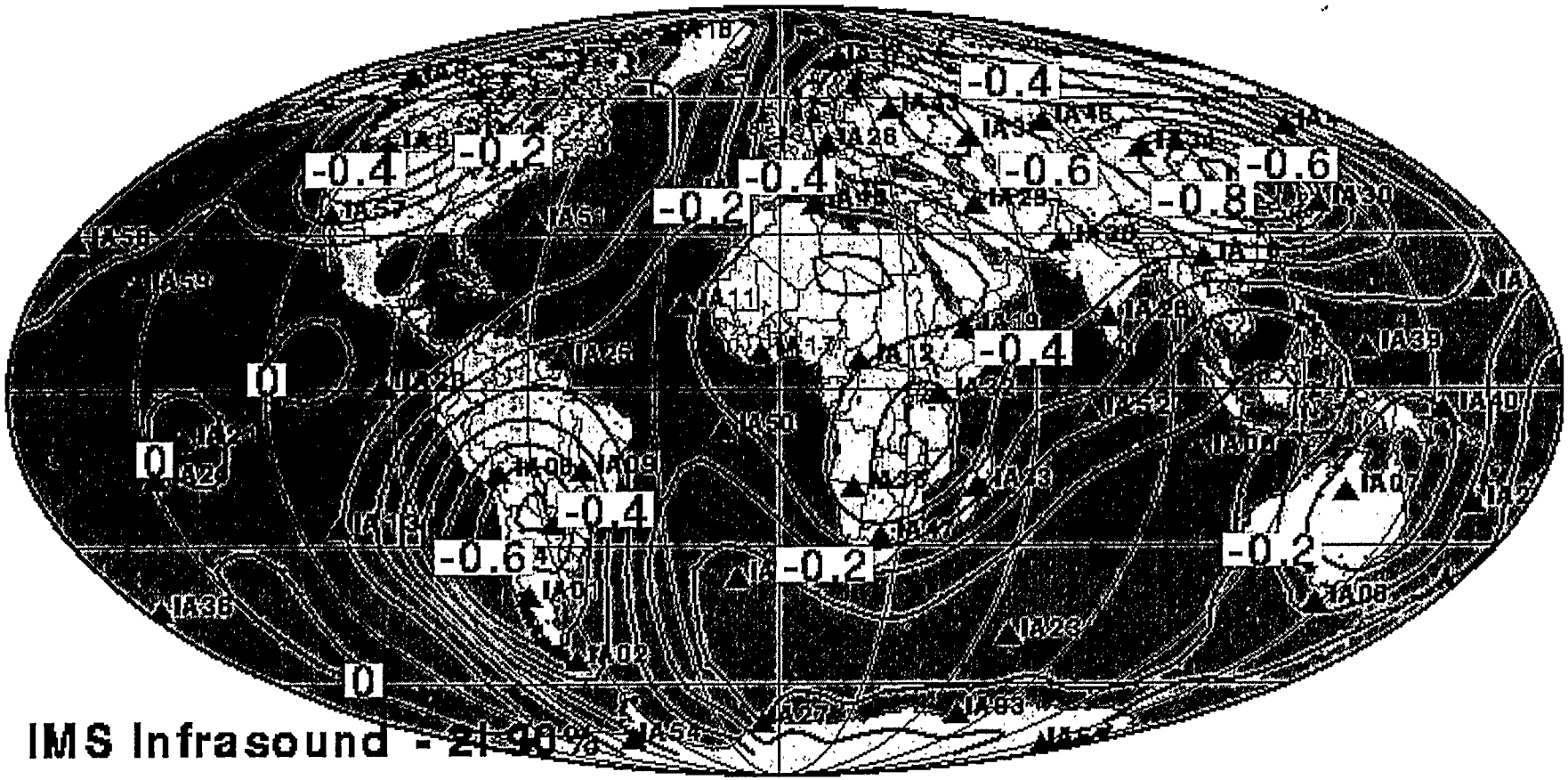

Log10(W) Threshold for 3 Infrasound Stations - Proposed IMS

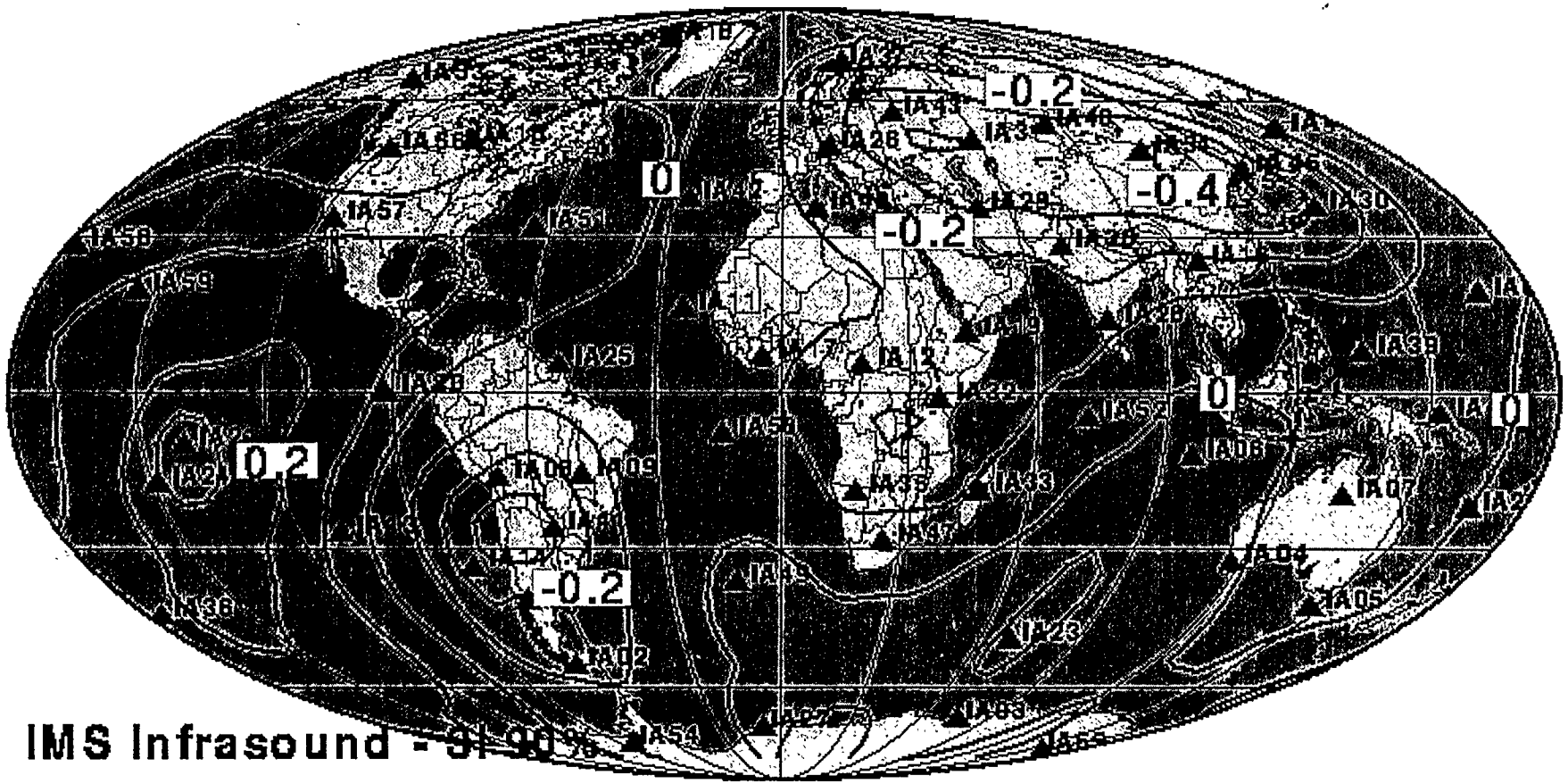

IMS Infrasound - 3 of 90 %

Atmospheric Turbulence and Permeable Hose

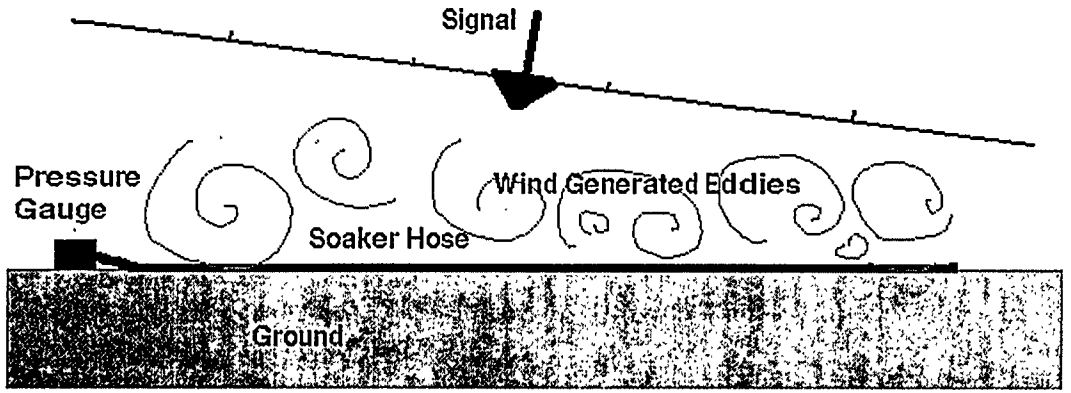

Wind generates turbulent eddies which are seen as pressure fluctuations.

The eddies move slowly across the ground and hence are spatially incoherent.

The permeable hose spatially "averages" the incoherent noise and reduces the wind generated noise.

Signals are coherent across the hose

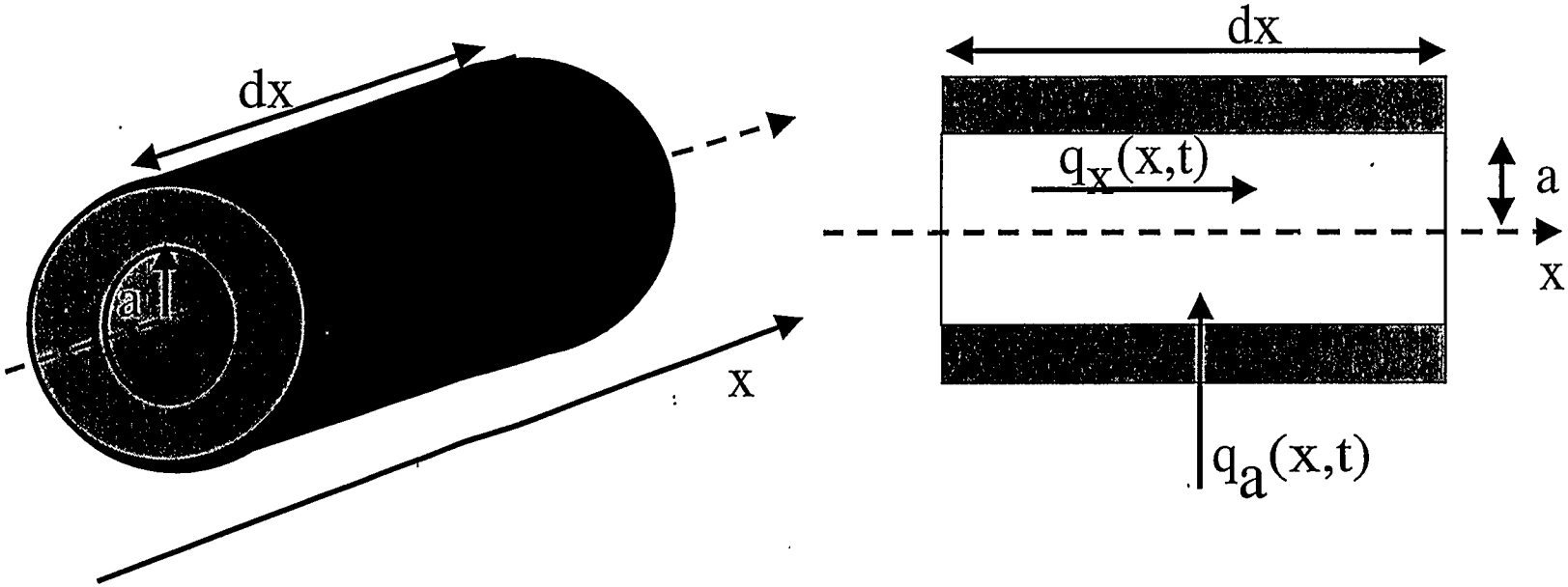

Hose element of length dx and radius a.
Mass flow along hose, $q_x(x,t)$.
Mass flow into hose, $q_a(x,t)$.

$$\dot{m}(x,t) = \rho(x,t)dV = q(x,t) = q_a(x,t) - (q_x(x+dx,t) - q_x(x,t))$$

A Hose Element

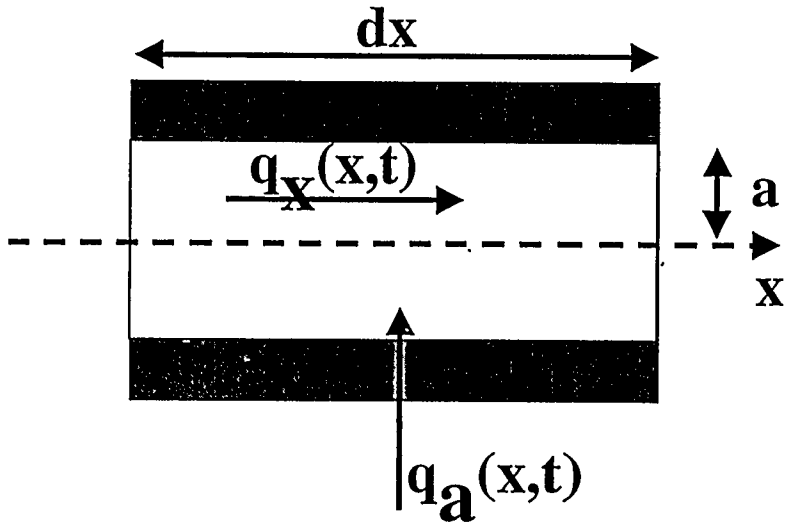

Conservation Of Mass

$$\dot{m}(x,t) = \rho(x,t)dV = q(x,t) = q_a(x,t) - (q_x(x+dx,t) - q_x(x,t))$$

Diffusive Flow Into/Out Of The Hose

$$q_a(x,t) = 2\pi a e(p_a(x,t) - p(x,t))dx$$

Steady State Viscous Flow Along the Hose

$$q_x = (1/\nu)\partial p(x,t)/\partial x$$

Partial Differential Equation

$$2\pi a e(p_a(x,t) - p(x,t)) - (1/\nu)\frac{\partial^2 p(x,t)}{\partial^2 x} - \dot{p}(x,t)\pi a^2/(RT) = 0$$

Transform to the frequency - wavenumber domain

$$p(x,t) = \iint \hat{p}(\omega,\kappa)\exp(-i\omega t)\exp(-i\kappa x)d\omega d\kappa .$$

$$\hat{p}(\omega,\kappa) = \frac{1}{(1+i\omega/\omega_0+(\frac{\kappa}{\kappa_0})^2)}\hat{p}_a(\omega,\kappa)$$

$$\tilde{p}(\omega,x) = \int \frac{1}{(1+i\omega/\omega_0+(\frac{\kappa}{\kappa_0})^2)}\hat{p}_a(\omega,\kappa)\exp(-i\kappa x)d\kappa$$

Permeable hose acts as a low-pass spatial and temporal filter

Low-pass corner frequency, ω_0

Low-pass wavenumber, κ_0

A plane-wave signal is low-pass filtered with time constant, τ_0

Now we observe that a far-field signal has the form

$$\hat{p}_a(\omega,\kappa) = \delta(\kappa)\tilde{p}_s(\omega)$$

so the signal pressure in the hose is simply

$$\tilde{p}_{signal}(\omega) = \frac{1}{(1+i\omega/\omega_0)}\tilde{p}_s(\omega).$$

The typical soaker hose has a characteristic time constant,

$\tau_0 = 2\pi/\omega_0 = a/(2RTe) < 0.2$ seconds

Noise Reduction and SNR Improvement

$$\hat{p}(\omega,\kappa) = \frac{1}{(1+i\omega/\omega_0+(\frac{\kappa}{\kappa_0})^2)}\hat{p}_a(\omega,\kappa)$$

The large wavenumbers are attenuated proportional to

$$(1+i\omega/\omega_0+(\frac{\kappa}{\kappa_0})^2)^{-1}$$

characteristic wavenumber for the hose:

$$\kappa_0^2 = (2\pi/\lambda_0)^2 = 2\pi aev = 4\pi Av/(RT)/\tau_0 \sim (2\pi/(200meters))^2$$

There fore Signal to Noise Ratio improvement depends upon the characteristic length of the hose:

$$SNR \sim |(1+i\omega/\omega_0+(\frac{\kappa}{\kappa_0})^2)/(1+i\omega/\omega_0)|$$

$$\sim |(1+if\tau_0+(\lambda_0/\lambda)^2)/(1+if\tau_0)|$$

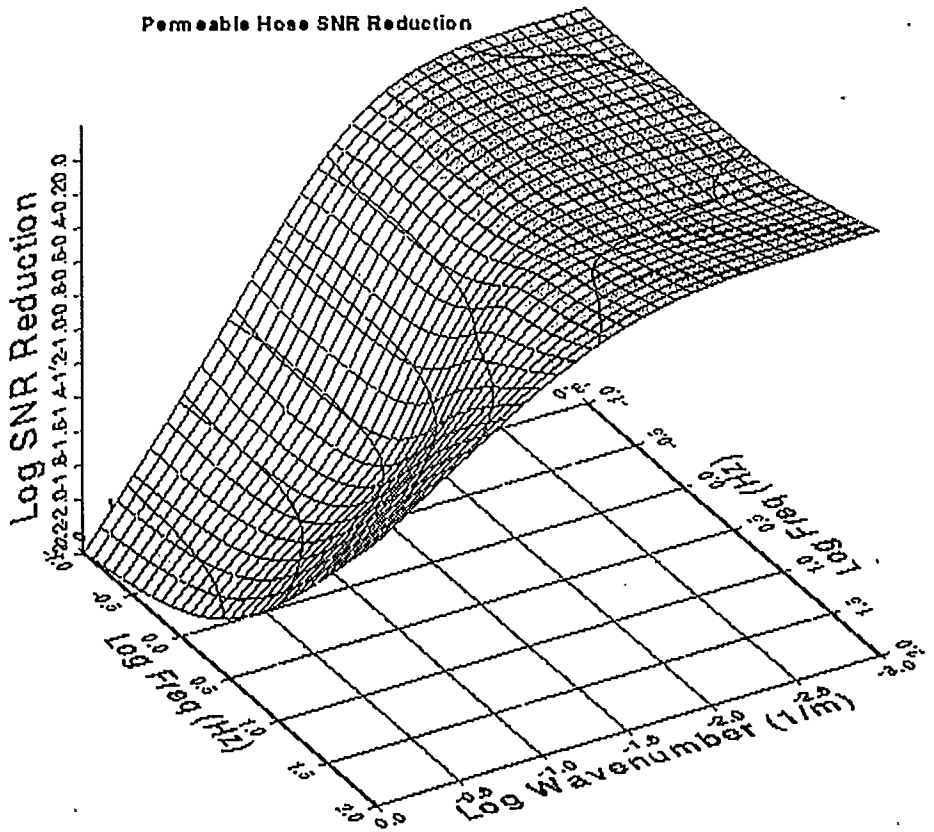

$$f_0 = 1/\tau_0 = RTe/(\pi a) > 1./(0.2\,\mathrm{sec})$$

$$\lambda_0 = 2\pi/\kappa_0 = [4\pi A\nu/(R\tau_0)]^{1/2} \approx 200m$$

Measurement of the hose time constant

The time constant changed by a factor of 2 with exposure to the elements over a 6 month period

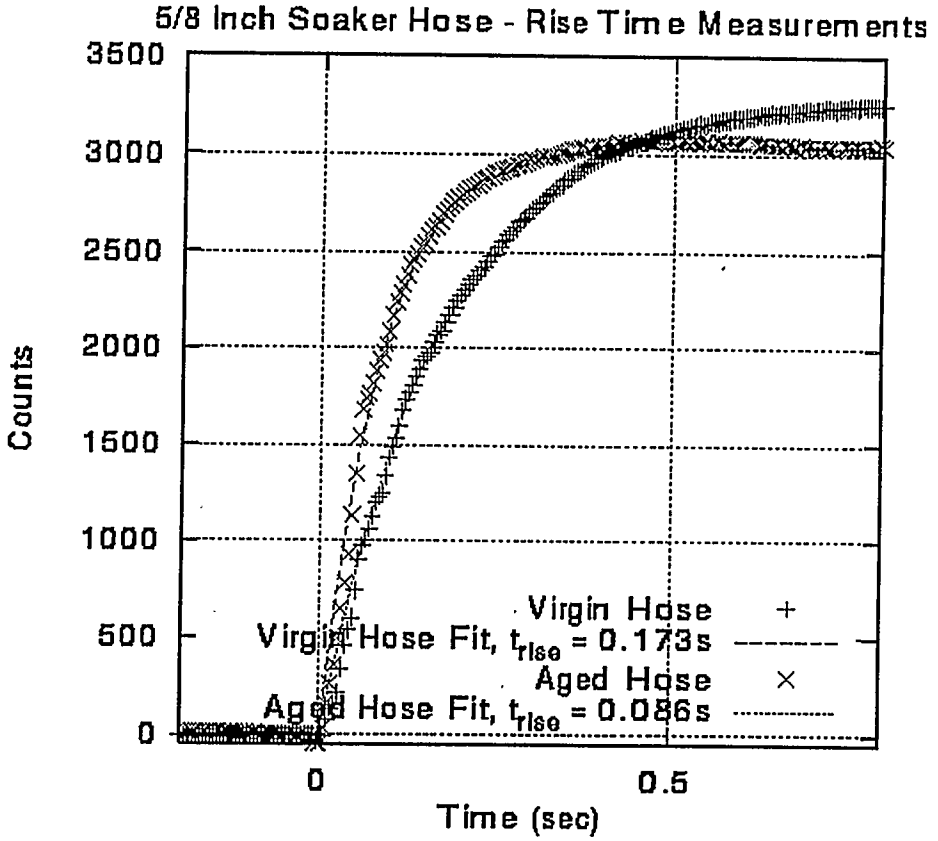

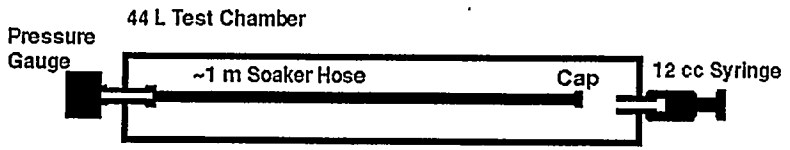

$$dV/V = dP/P = 0.0005$$

A Simple Diagnostic Procedure

The characteristic length measures how far the signal will travel down the hose before leaking back out into the atmosphere.

The older hose leaks into the atmosphere quicker.

The signal amplitude at the end of 10 m of hose is smaller for the older hose

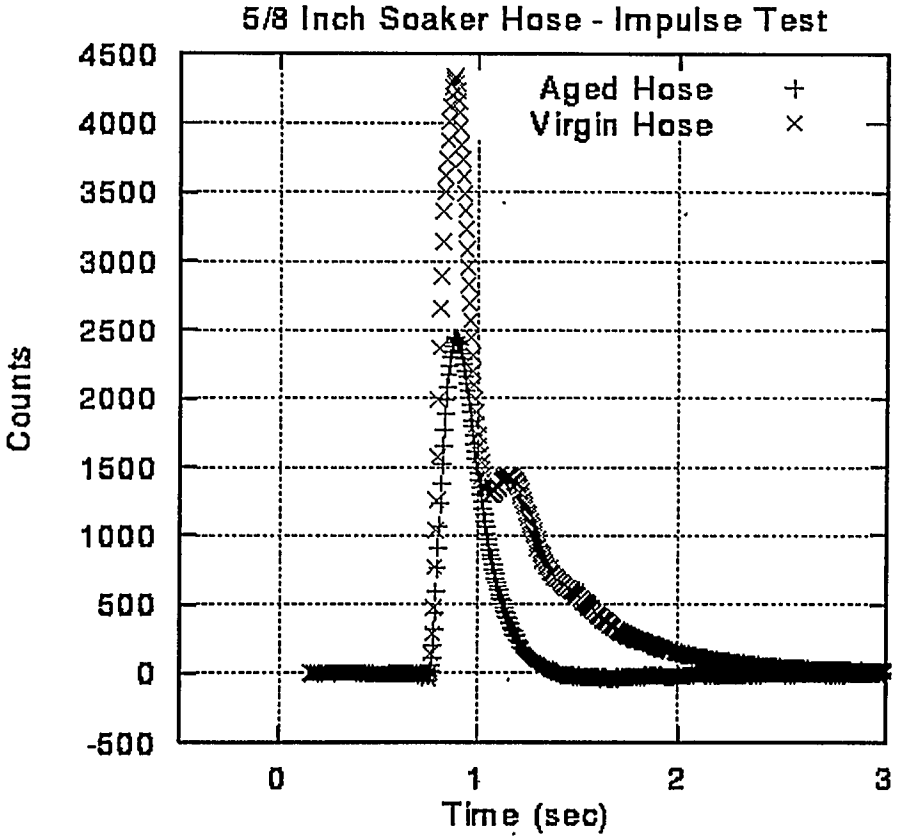

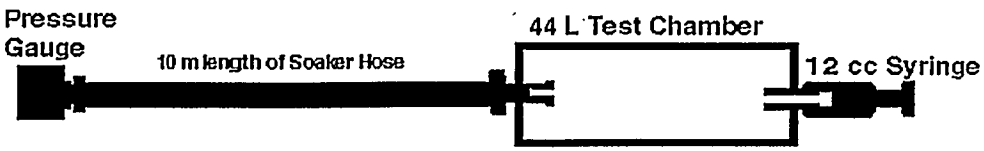

Helmholtz Oscillator

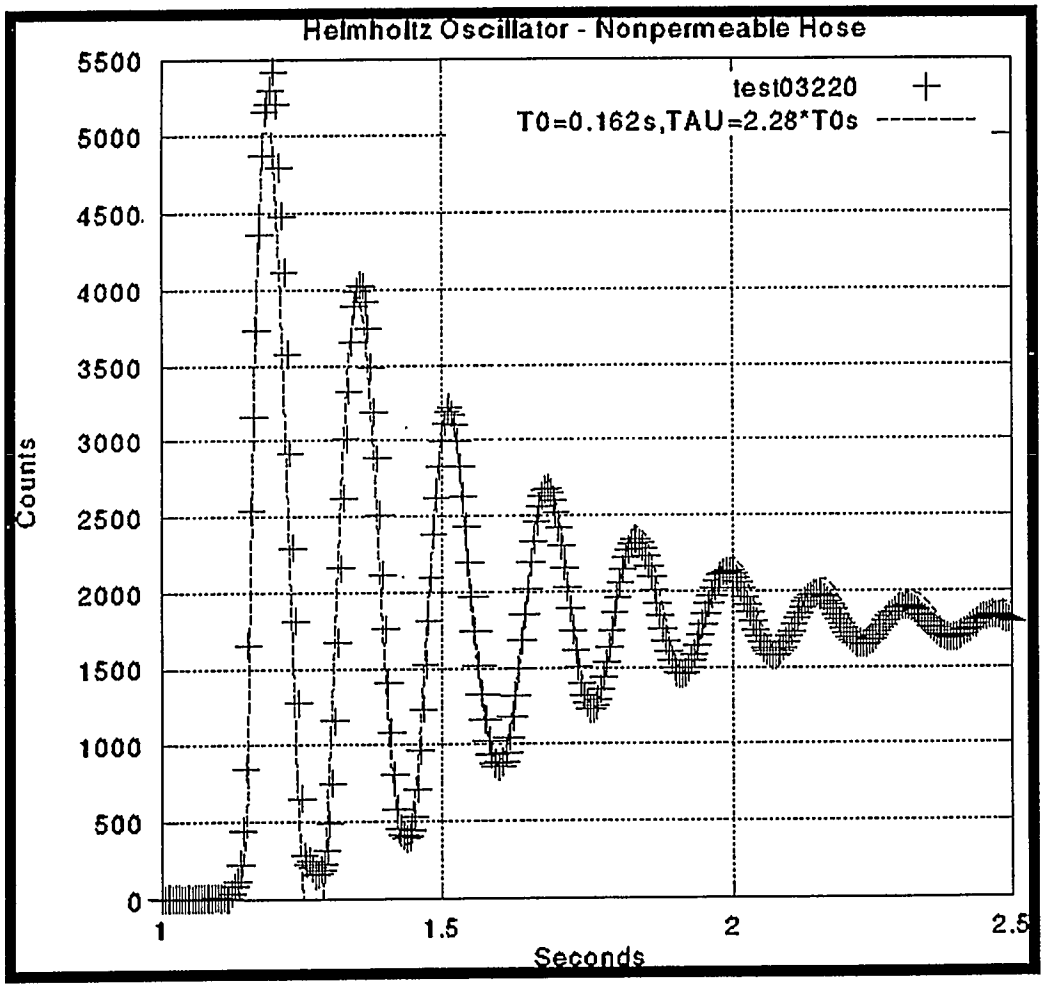

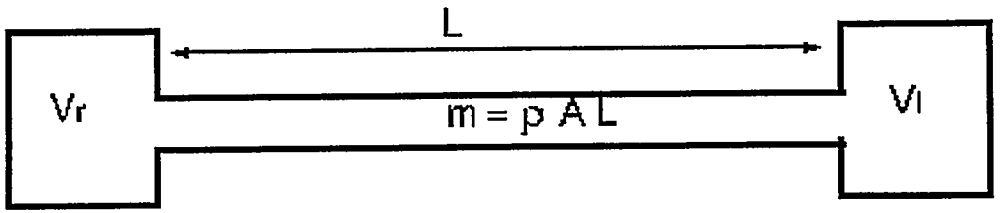

- A 0.32 m section of 5/8" non-permeable hose set up as a Helmholtz oscillator was used to determine the viscous drag constants
- Damping consistent with Pouisselle flow and nominal viscosity of air.

Finite Difference Modeling

- **Program: "Maxhose" - Standard F90 runs on UNIX and PC**
- **implicit Crank-Nicholson time stepping 2'nd order code**
- **simulates atmospheric loading, calibration/test volumes, and finite volume manifolds/transducers attached to a hose**
- **may be generalized to multiple hoses connected with finite volume manifolds**
- **may be driven with an arbitrary atmospheric pressure as a function of position and time to simulate wind noise and propagating signals**
- **future plans include Monte Carlo simulations of noise reduction properties of multiple hose configurations**

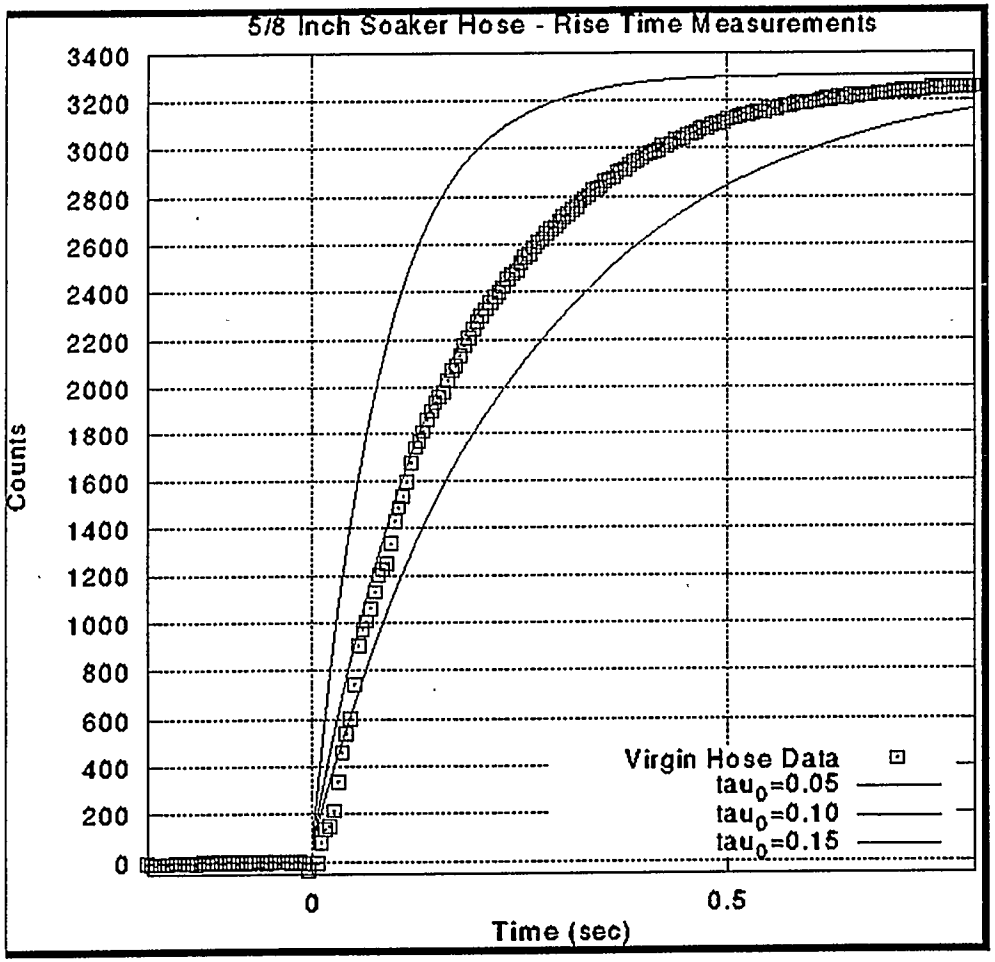

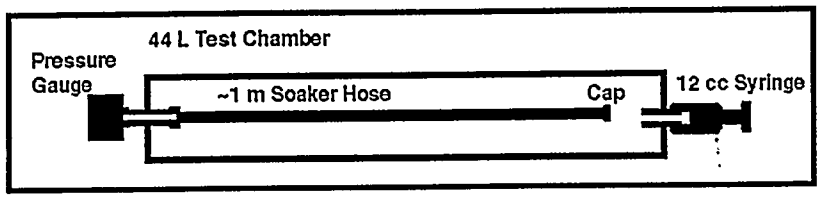

FD Modeling of Time Constant Measurement and Calibration

- dV/V = dP/P = 0.0005
- Test volume finite
- Finite pressure sensor volume, 3.8L
- Apparent hose time constant = 0.17 sec
- Real hose time constant = 0.10 sec

Modeling End-On Impulse Test

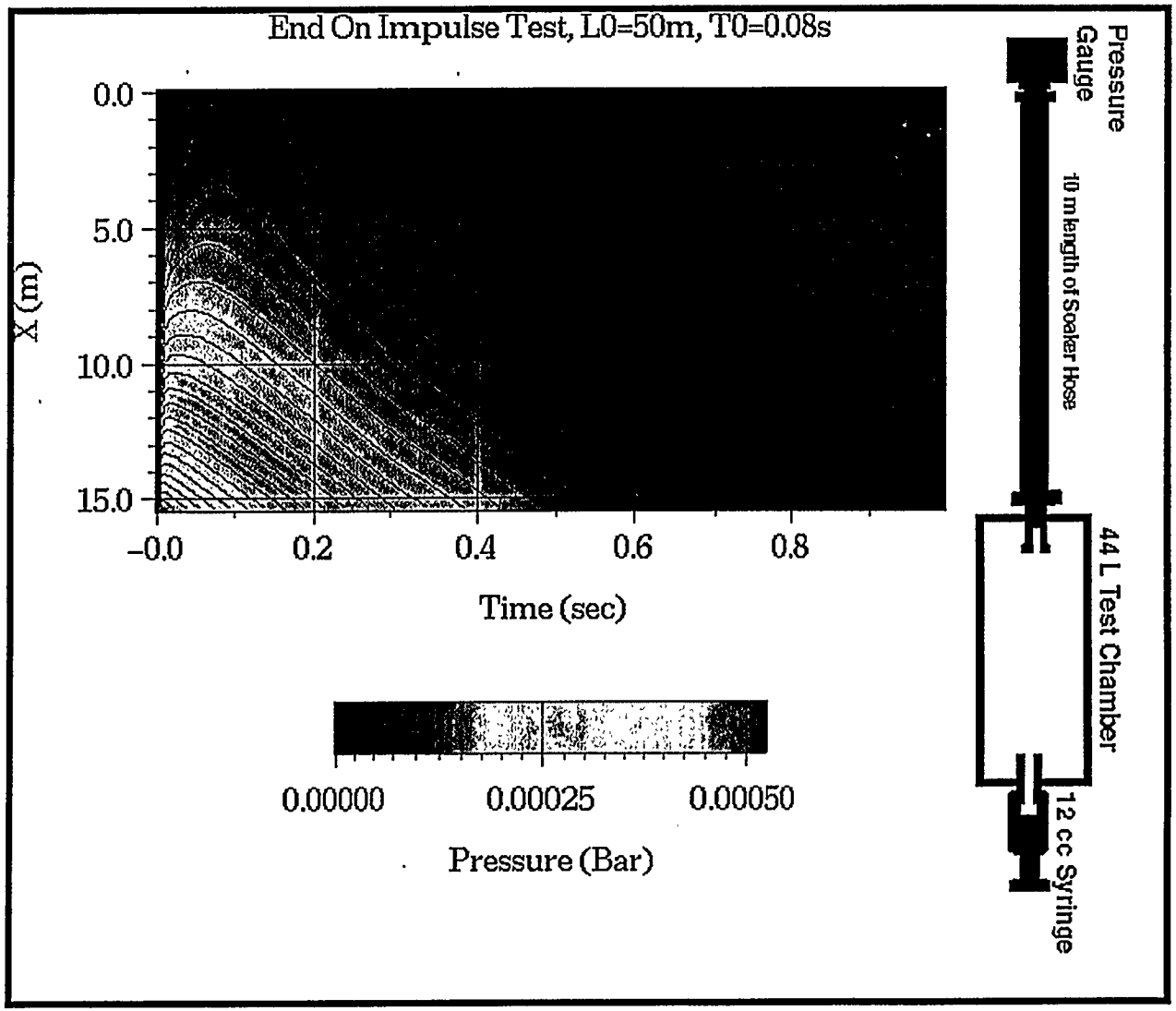

- The end-on impulse test demonstrates how a step function propagates down the hose
- The pulse is attenuated and delayed as the pulse leaks out into the atmosphere

Finite Difference Model of Pressure Inside Permeable Hose with Atmospheric Random White Noise Model

τ_0=0.1, λ_0=100m, RMS Noise = 0.0004 atm

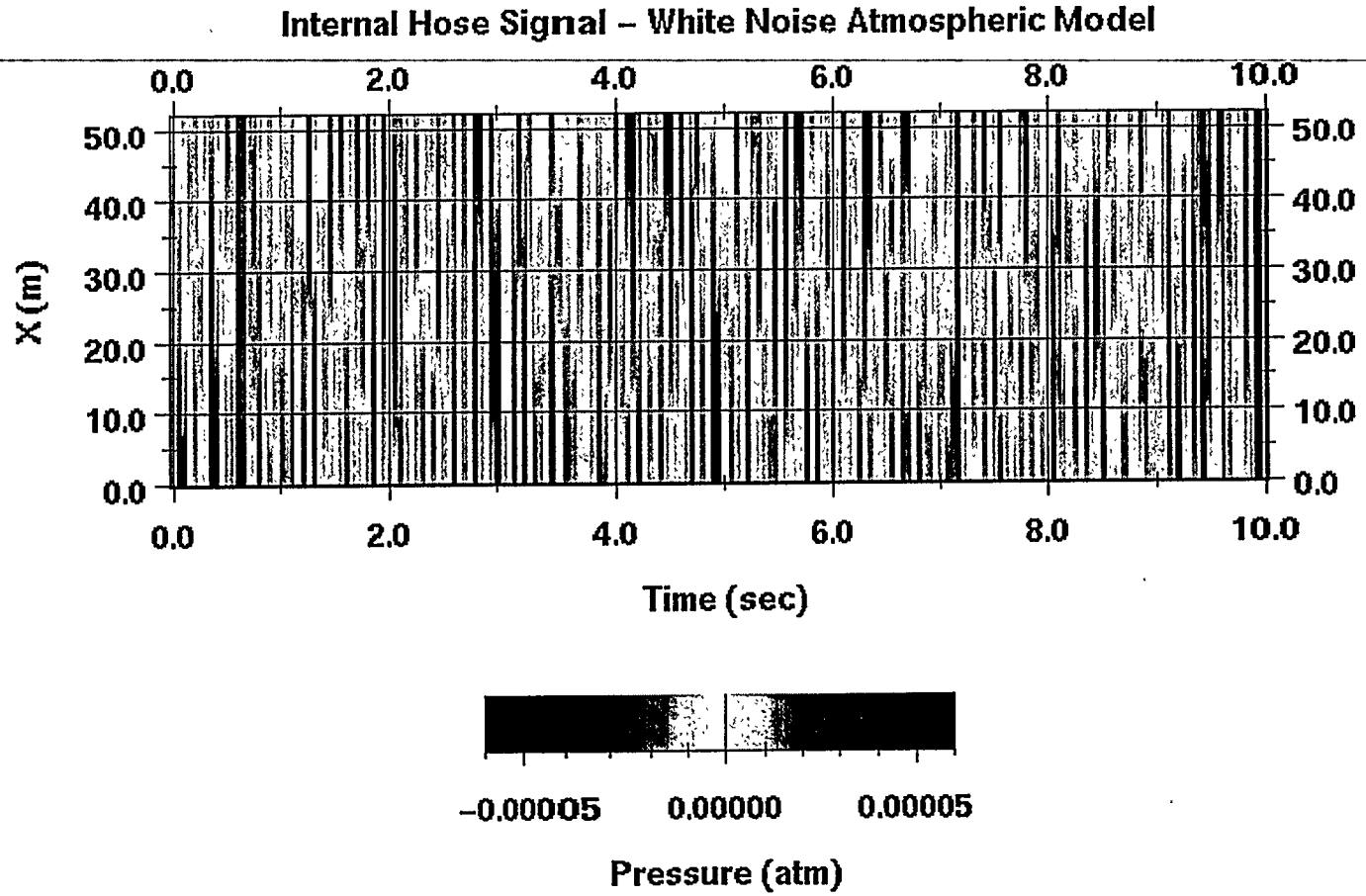

Atmospheric Turbulence Model proportional to ~1/K and ~1/F

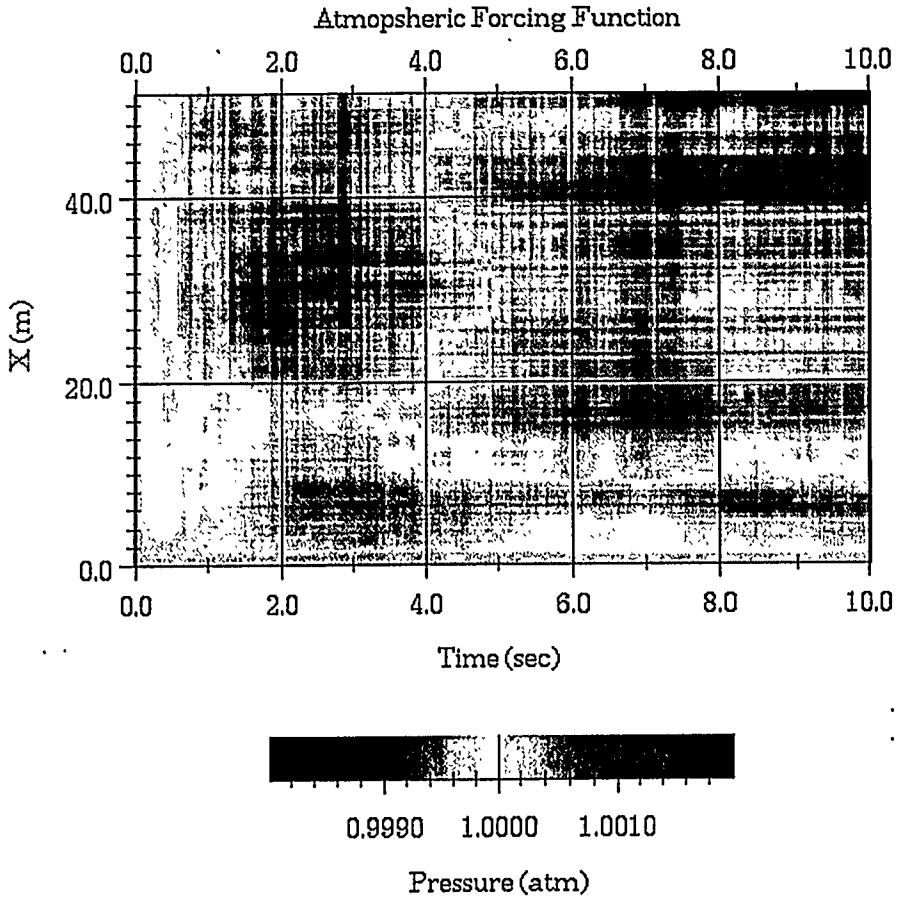

τ_0 =0.1s, λ_0 =100m

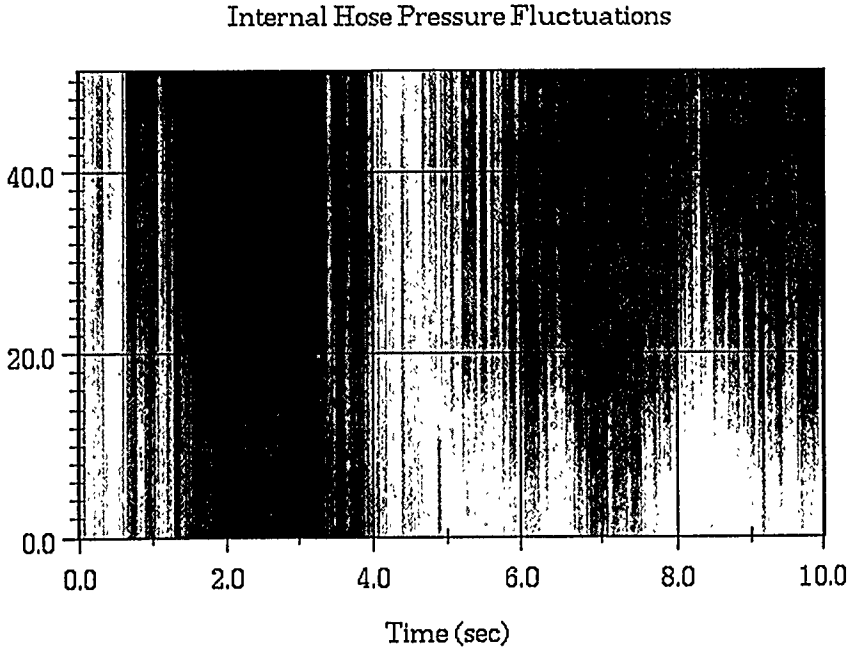

Output

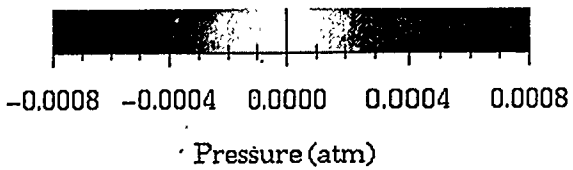

Finite Difference Modeling of Random Atmospheric Pressure Fluctuations

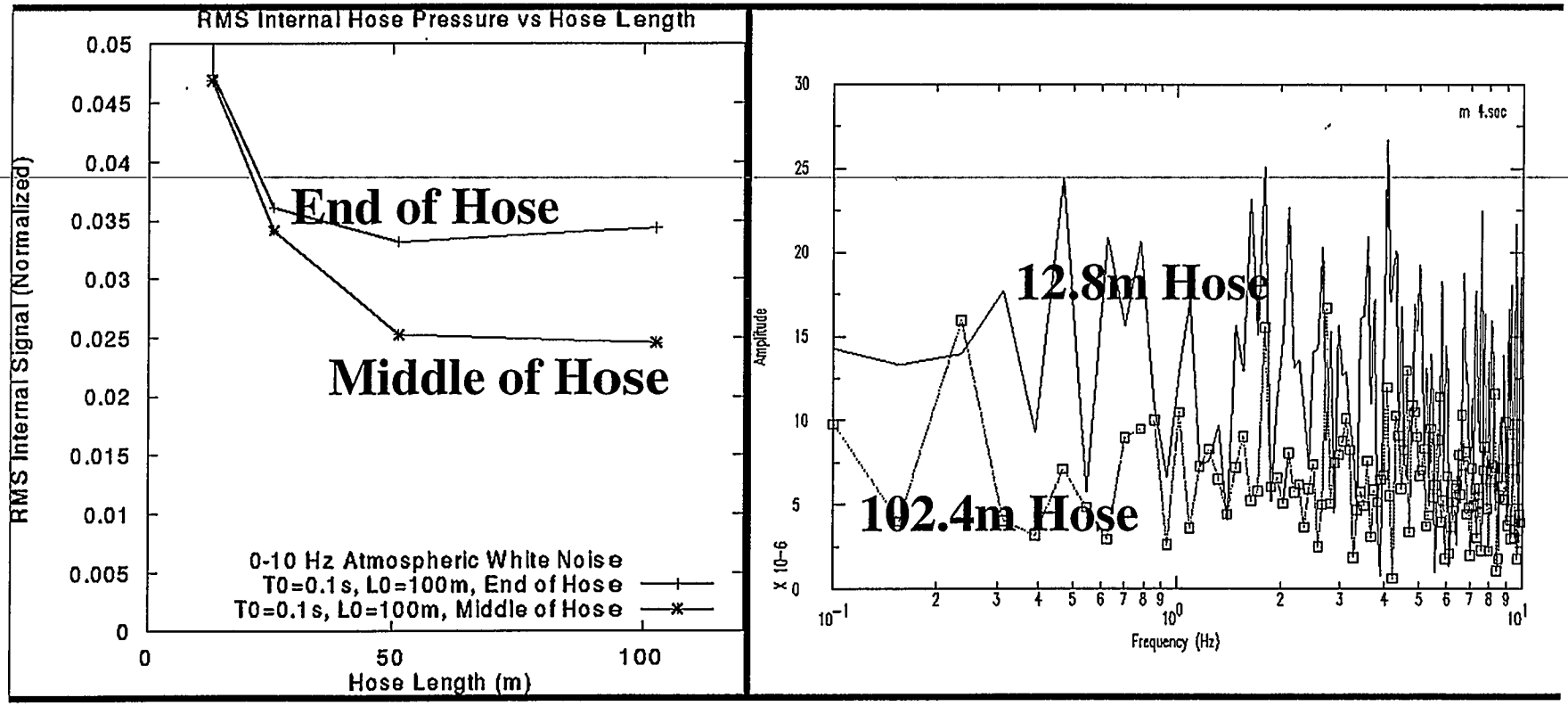

- Atmospheric pressure, Pa(x,t) = random white noise, τ_0 =0.1s, λ_0 =100m.
- Noise reduction at the end of a hose nears maximum for L = $\lambda_0/2$
- Maximum noise reduction in the middle of a hose nears maximum for L=$\lambda_0/2$

Maxwell TECHNOLOGIES
Federal Division

Summary

- We need to better understand the characteristics of hose arrays and their response to signals and noise before we can project the capabilities of the proposed IMS infrasound system of 50 to 60 stations worldwide
- The characteristic time and length of permeable hoses determine SNR improvements that can be expected from hose arrays
- Simple diagnostic methods may be devised to test hose systems
- The aging of hoses from the elements can decrease the potential SNR improvement by a factor of 2
- Numerical code, Maxhose, has been developed to model hoses
- Numerical modeling can be used with wind noise models to understand performance of hose configurations

NOISE REDUCERS FOR INFRASOUND DETECTION

Heinrich W. Haak and G. J. de Wilde

Royal Netherlands
Meteorological Institute
Seismology Division
DeBilt, The Netherlands

The Comprehensive Test Ban Treaty (CTBT) has brought renewed interest in infrasound detection. A worldwide network of sixty infrasound measurement stations are planned in the International Monitoring System.

Infrasound detection is also of importance for research of sonic booms and other natural and man-made low-frequency sound sources. Infrasound is usually detected with microbarographs or low frequency microphones. The main problem of infrasound detection is the reduction of background noise due to turbulent wind. Simple filtering in the frequency domain is not effective because the strong overlap of the noise frequency band and the frequency band of the signals under consideration. To be able to distinguish between noise and infrasound signals, usually array techniques are used. To improve the signal to noise ratio of the sensor itself, they are usually connected to the atmosphere by a noise reducing structure, which acts as a spatial filter. Recently we conducted experiments with star configurations of porous rubber hoses as noise reducers. The porous wall constitutes a distributed inlet for sound waves. It was found that porous hoses are effective in noise reduction. The porous hose can theoretically be treated as a leaky transmission-line. The propagation constant and the characteristic impedance are the main parameters and can be used to distinguish different types of commercial porous hoses. Standing-wave experiments in the frequency range 0.5-10 Hz with a porous tube of 12 mm inside diameter and 2 mm wall thickness have been performed to determine the impedance and the propagation constant. Good agreement with transmission-line theory was found. The slowness response of a star configuration of porous hoses depends highly on the diameter of the hoses and the impedance matching at end points and at branching points. Distortionless line design is possible when the flow resistance of the porous wall can be chosen as a free parameter. The attenuation of sound waves in commercial available porous hoses limits the physical dimensions of the noise reducers. Although porous hoses are effective in noise reduction, the question remains if they are robust enough for the intended purposes. Research of noise reducing structures of possibly more robust Daniels tubes is proposed in order to achieve a robust, linear, omnidirectional, effective noise reducing element. The air inlet points are most sensitive in almost every design. A right integration with the surface is essential. The problem of proper noise reducer design, therefore, is combining user demands with technological feasible and scientifically sound ideas.

Noise Reducers for Infrasound Detection

Hein W. Haak and Gerlof J. de Wilde

Royal Netherlands Meteorological Institute

Division of Seismology

KNMI

Contents

- Introduction
- Design variables of noise reducers
- Theory of acoustic transmission lines
- Calibration of porous hoses
- Future work
- Conclusions

Introduction

- Noise reducers essential for infrasound detection
- Large number of design variables
- Short time available for testing
- Not in current specifications of the IMS
- Few groups are working on the problem

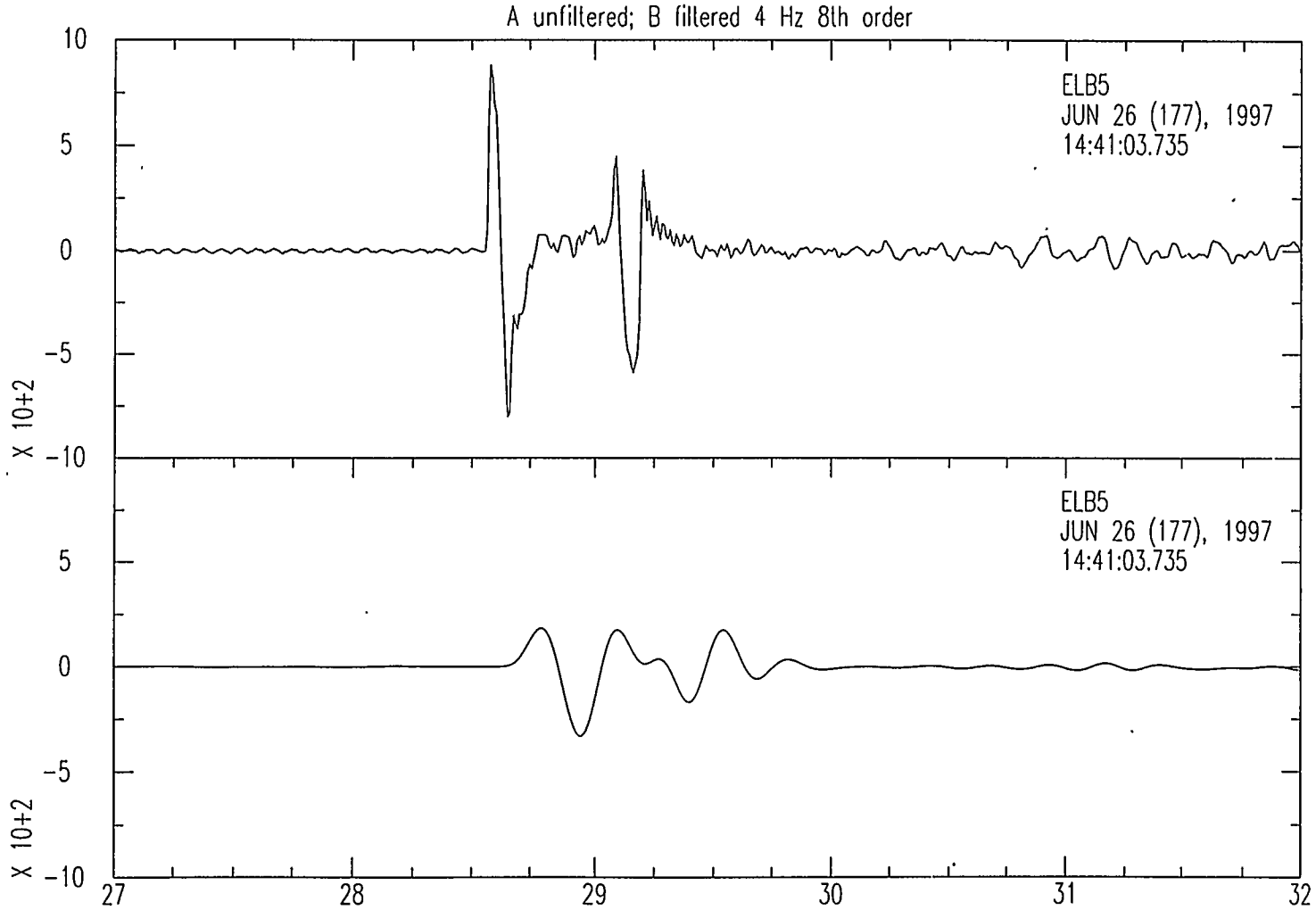
A unfiltered; B filtered 4 Hz 8th order
ELB5
JUN 26 (177), 1997
14:41:03.735
ELB5
JUN 26 (177), 1997
14:41:03.735
X 10+2
X 10+2
10
5
0
-5
-10
5
0
-5
-10
27
28
29
30
31
32

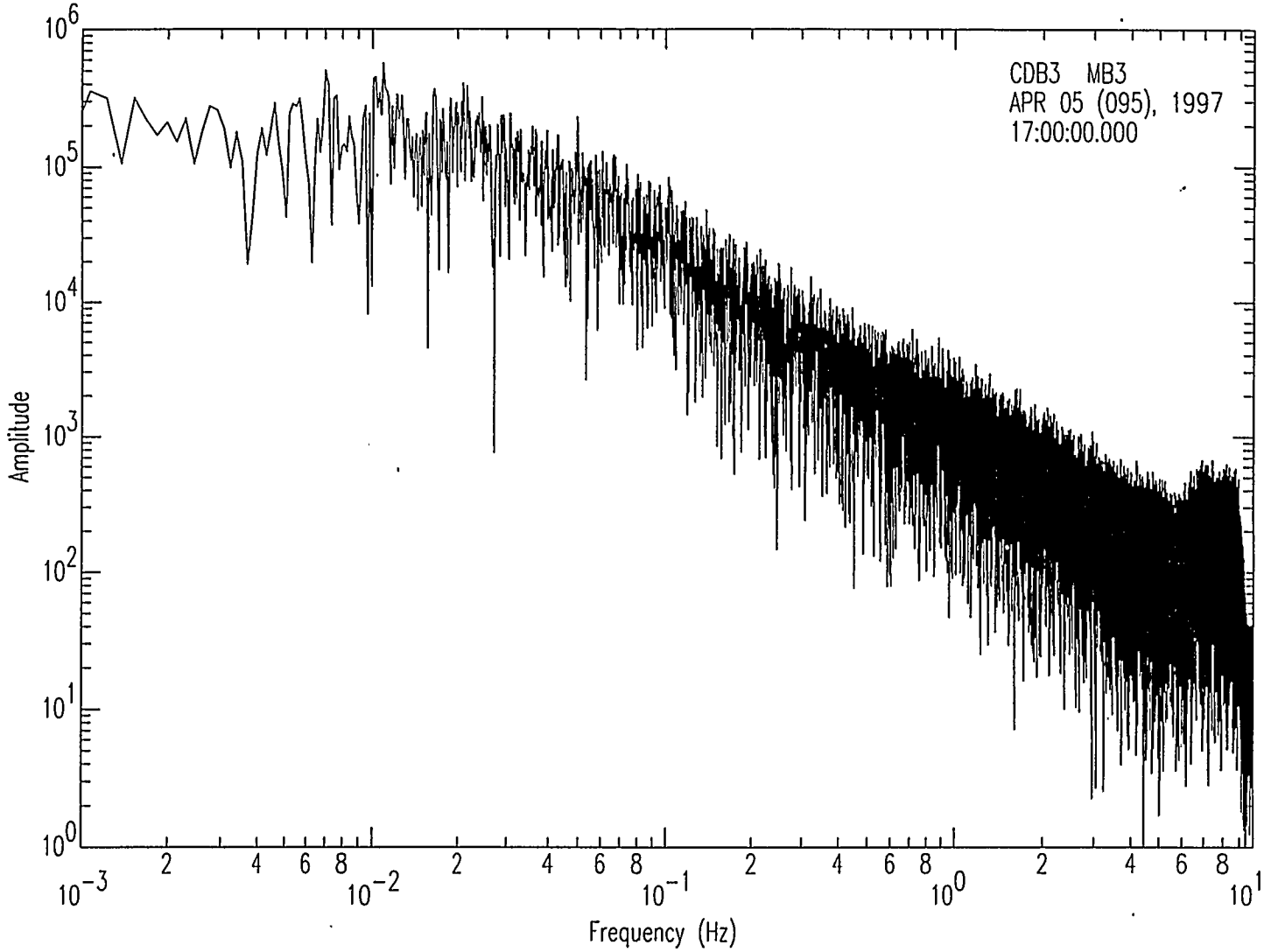
CDB3 MB3
APR 05 (095), 1997
17:00:00.000
Amplitude
Frequency (Hz)
10^6
10^5
10^4
10^3
10^2
10^1
10^0
10^{-3}
10^{-2}
10^{-1}
10^0
10^1
2 4 6 8

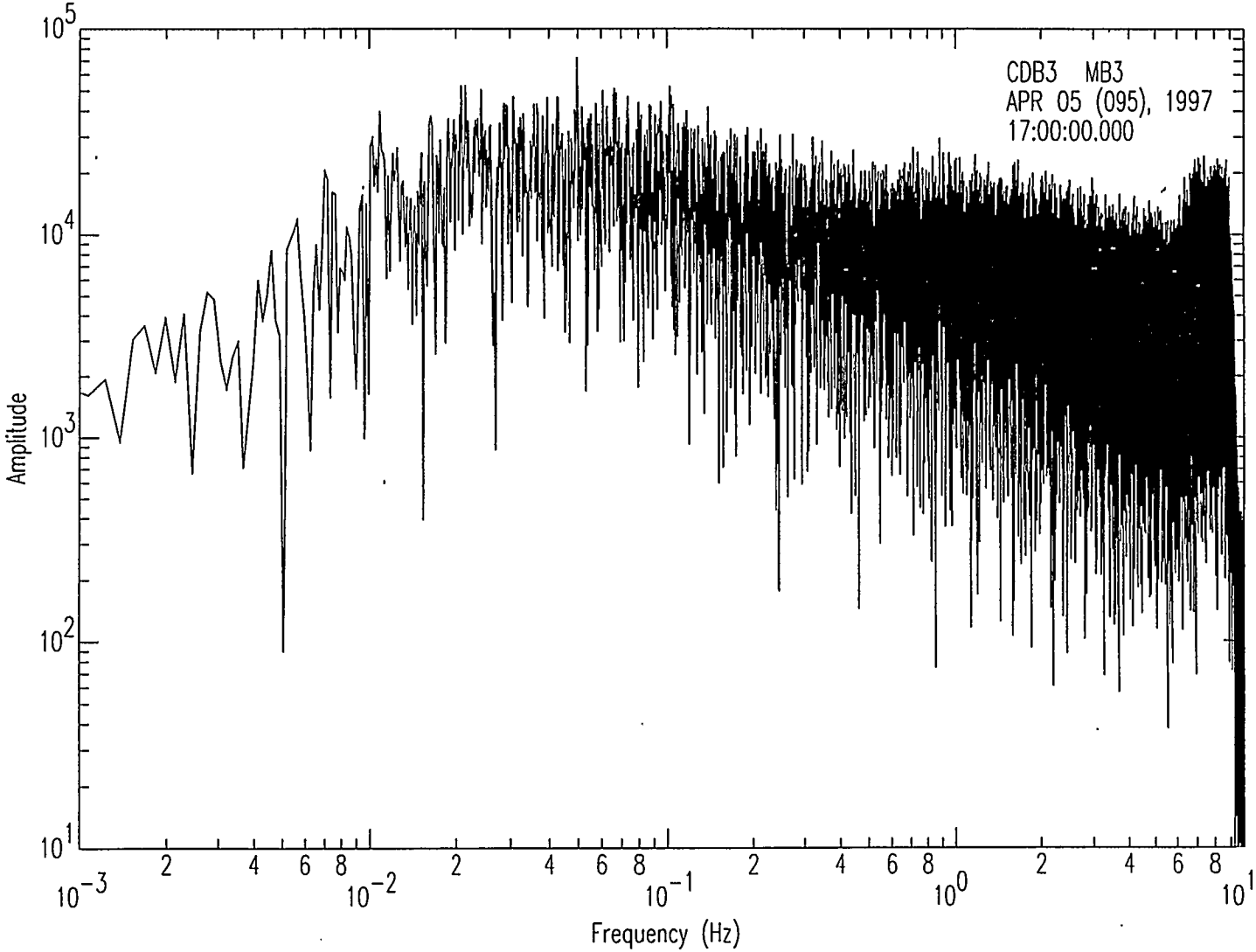
CDB3 MB3
APR 05 (095), 1997
17:00:00.000
Amplitude
Frequency (Hz)
10^5
10^4
10^3
10^2
10^1
10^{-3}
10^{-2}
10^{-1}
10^0
10^1
2
4
6
8

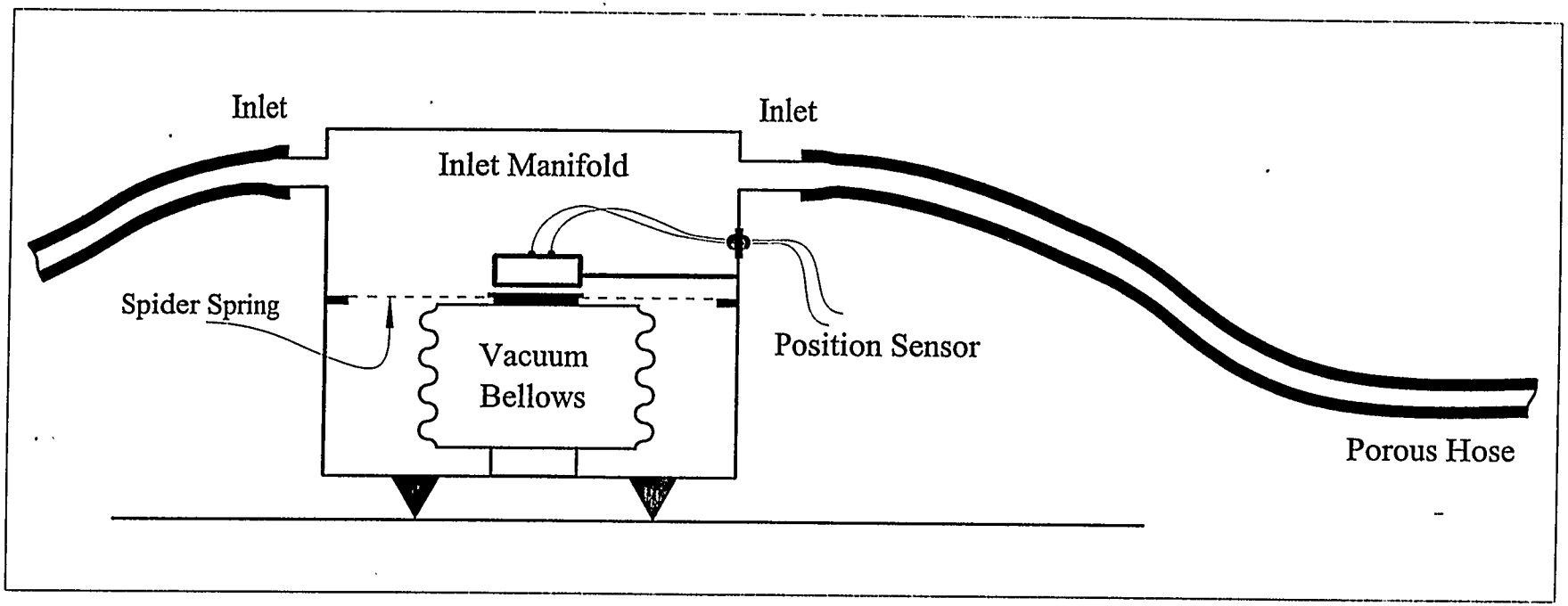
Inlet
Inlet
Inlet Manifold
Spider Spring
Vacuum
Bellows
Position Sensor
Porous Hose

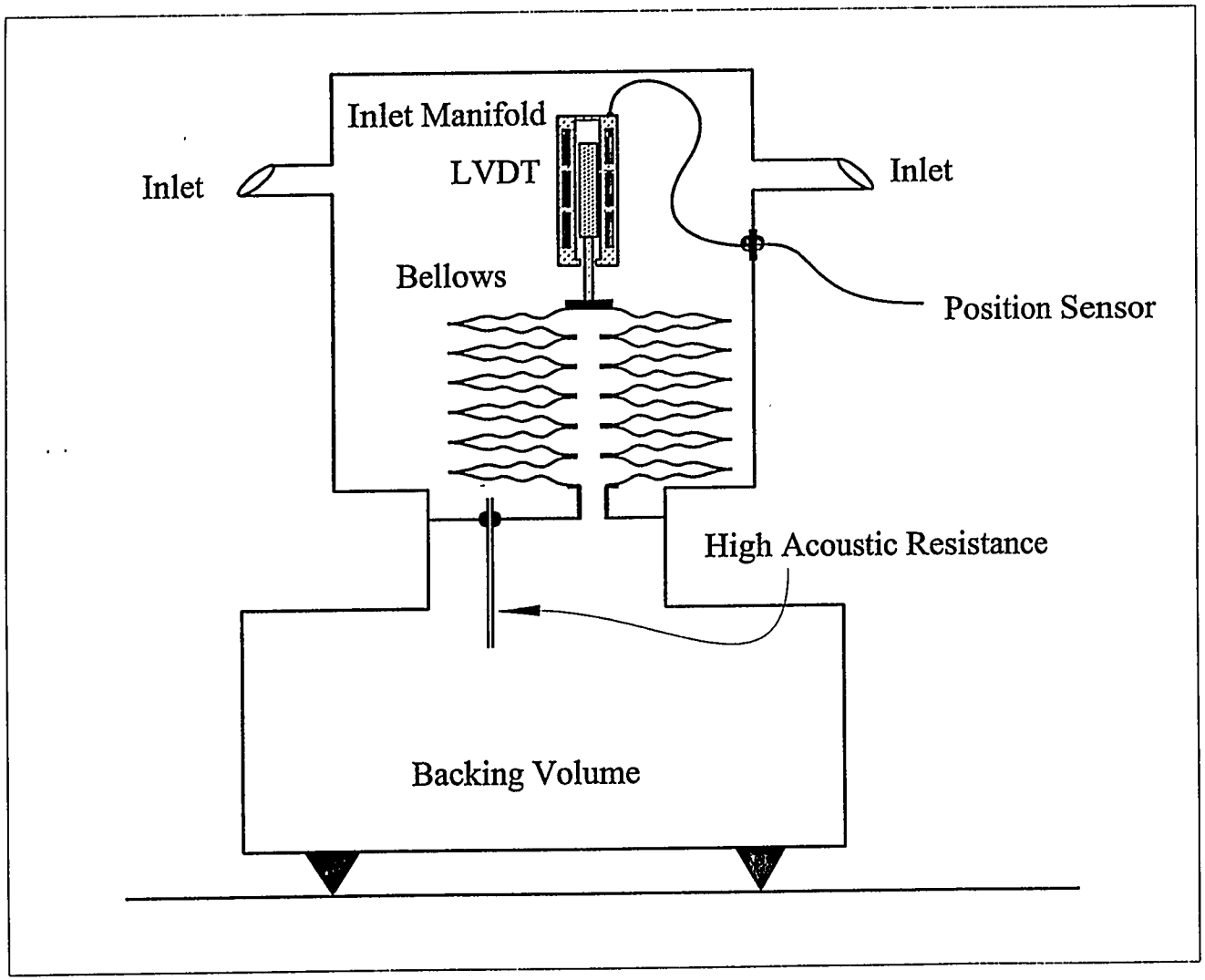
Inlet Manifold
LVDT
Inlet
Inlet
Bellows
Position Sensor
High Acoustic Resistance
Backing Volume

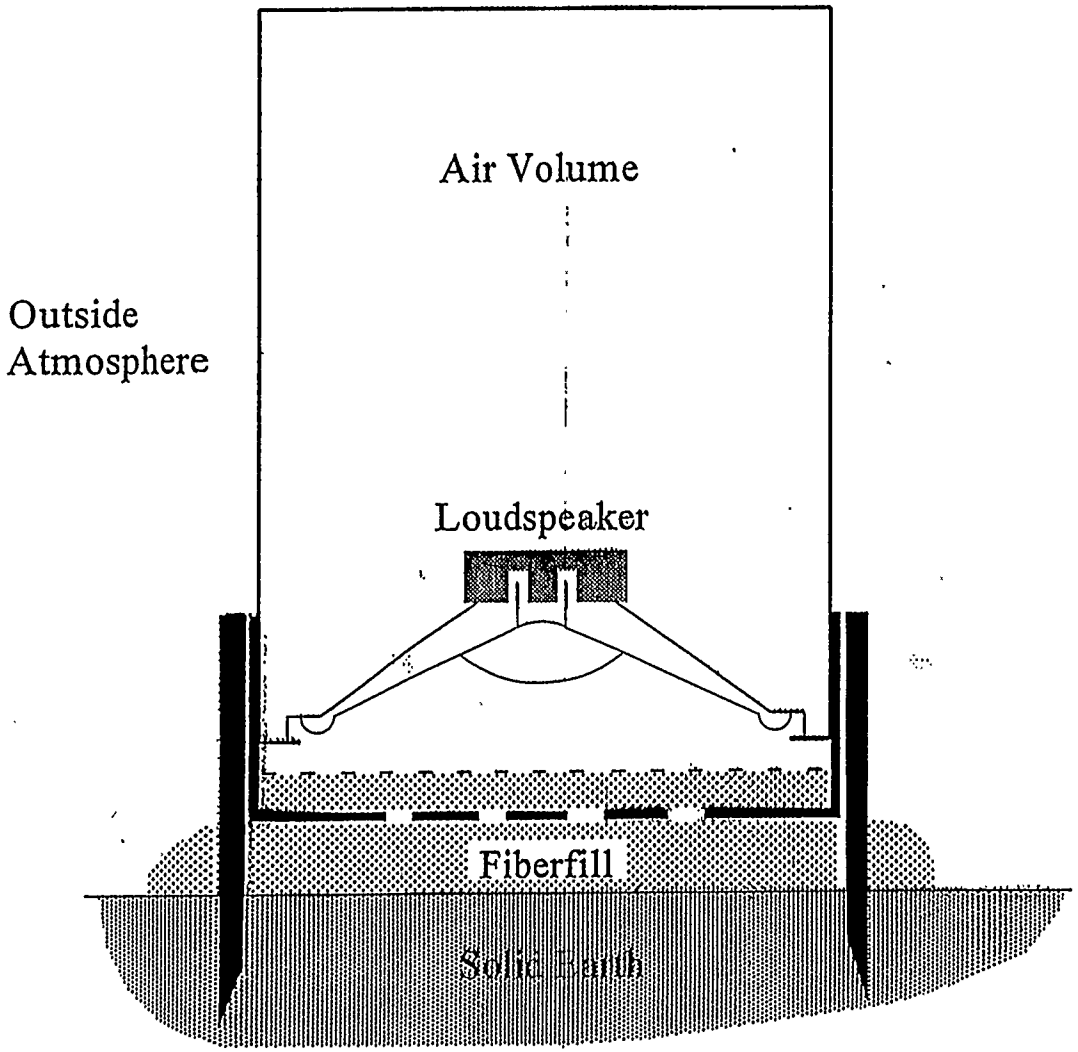
Air Volume
Outside
Atmosphere
Loudspeaker
Fiberfill
Solid Earth

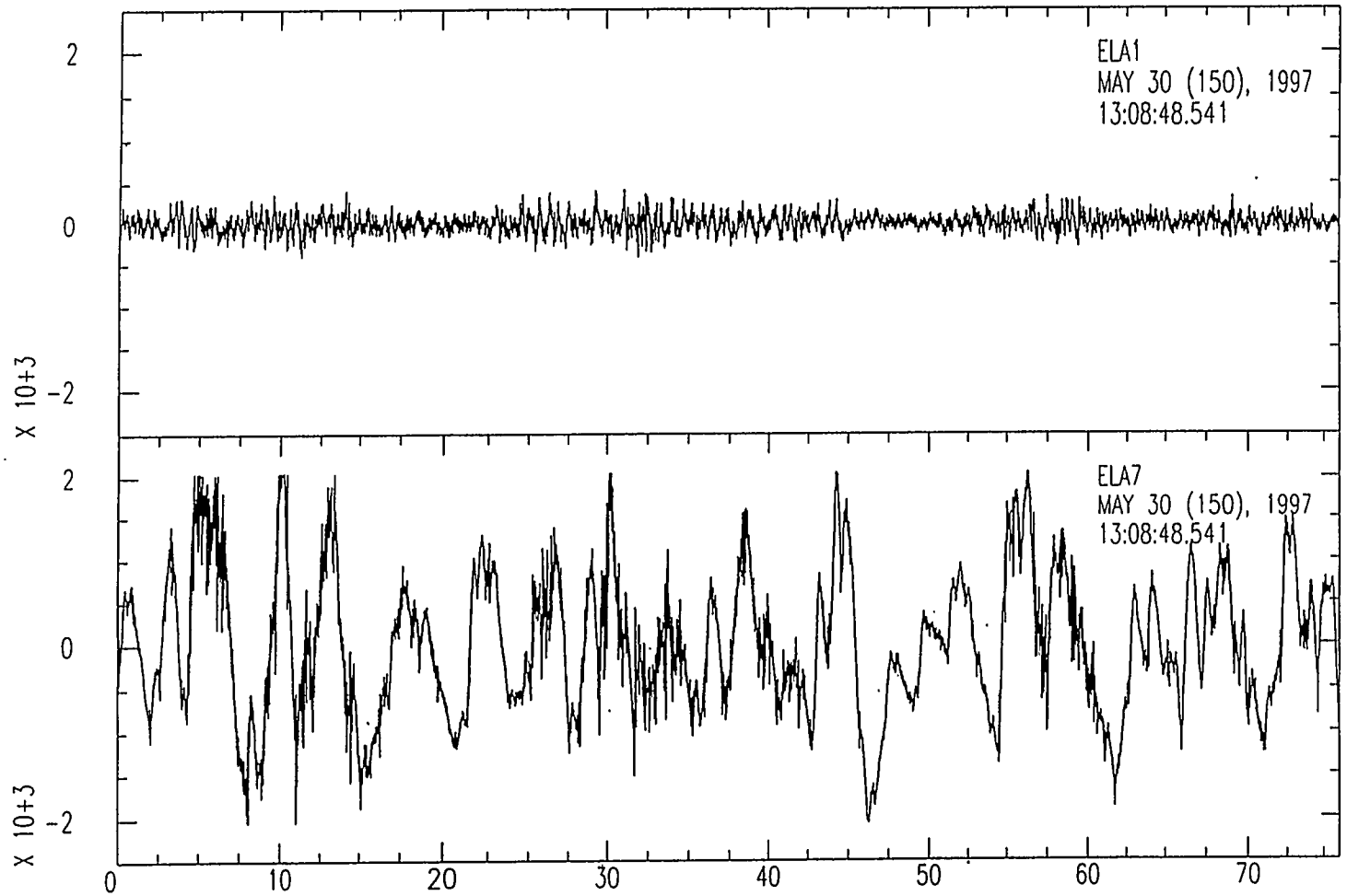

With Noise Reducer

Without Noise Reducer

Wind: 3 m/s

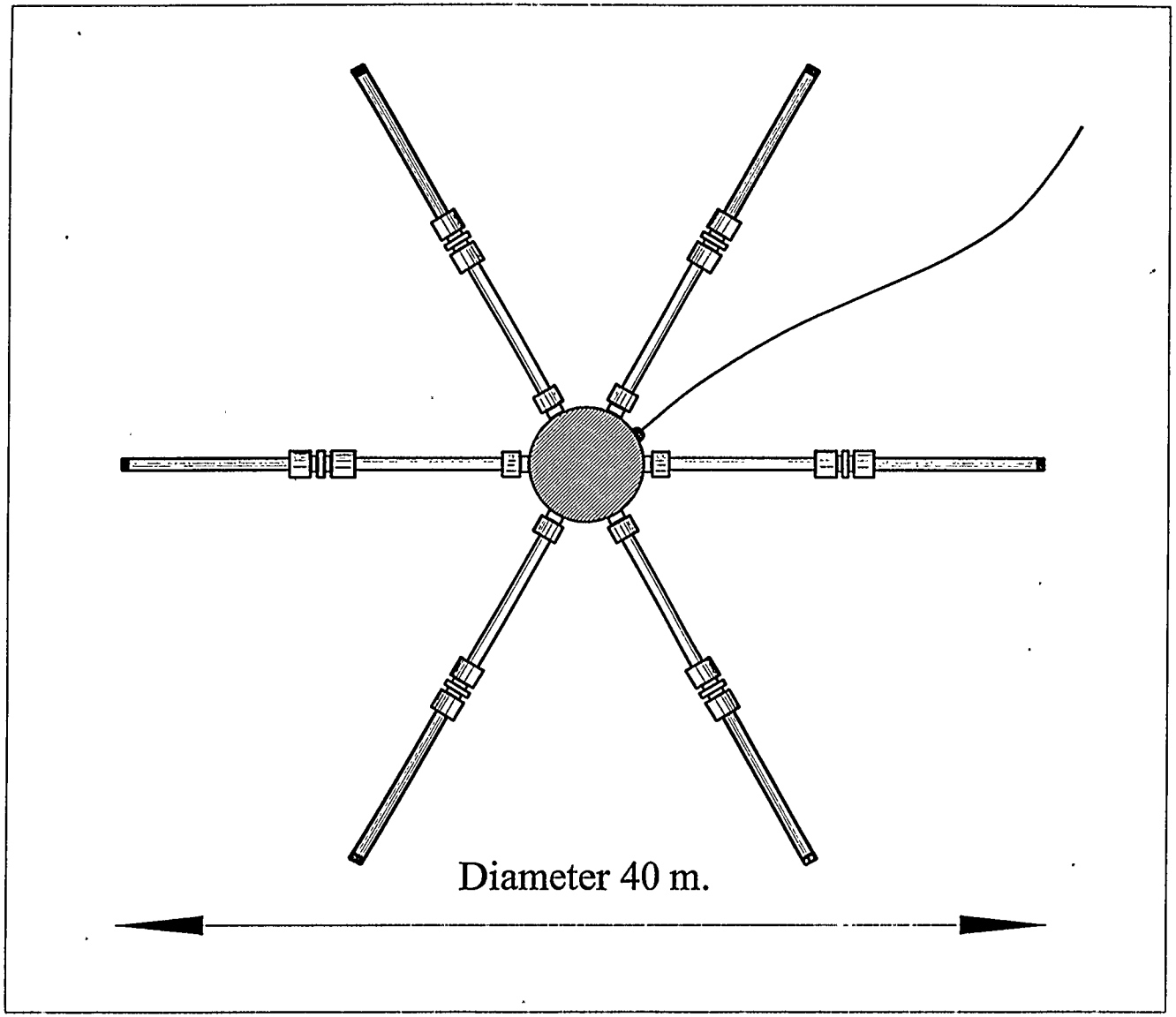
Diameter 40 m.

Design variables of noise reducers

- Dimension of noise reducer
- Vertical position of noise reducer
- Materials: stainless steel, plastics, rubber
- Inlet hole construction
- Surface structure
- Multi-sensor or analog integrator type

Theory of acoustic transmission lines

- Theory equivalent to lossy electrical wave guides
- Thermodynamic properties of air important
- Non-linear effects due to Bernoulli's Law
- Distortionless lines or
- Lines with impedance, velocity jump
- Matching with barograph and termination
- Branching, closed and low loss lines

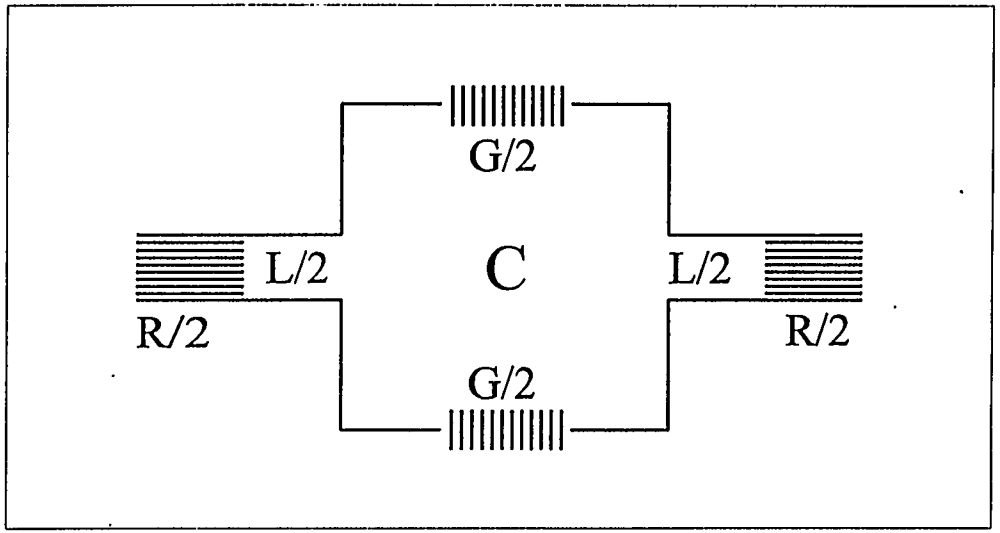
G/2
L/2
C
L/2
R/2
R/2
G/2

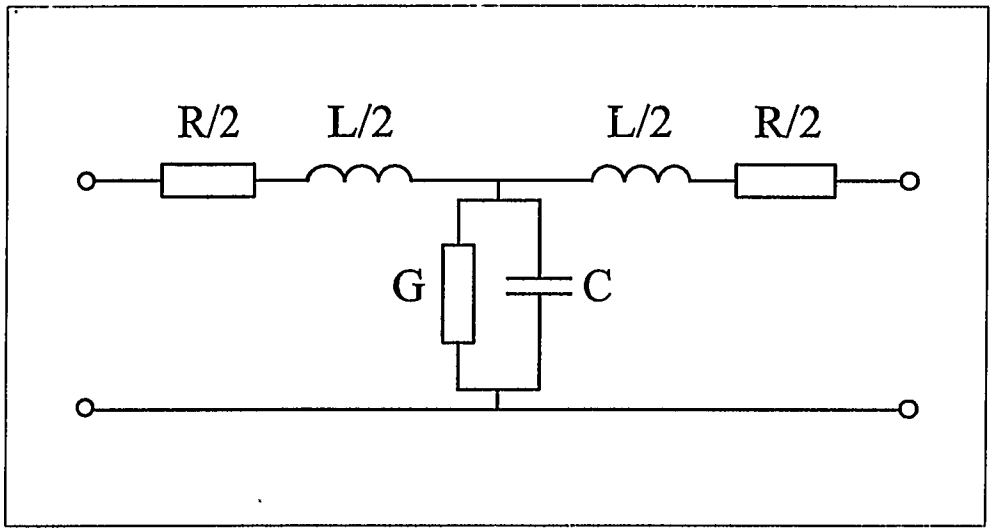
R/2
L/2
L/2
R/2
G
C

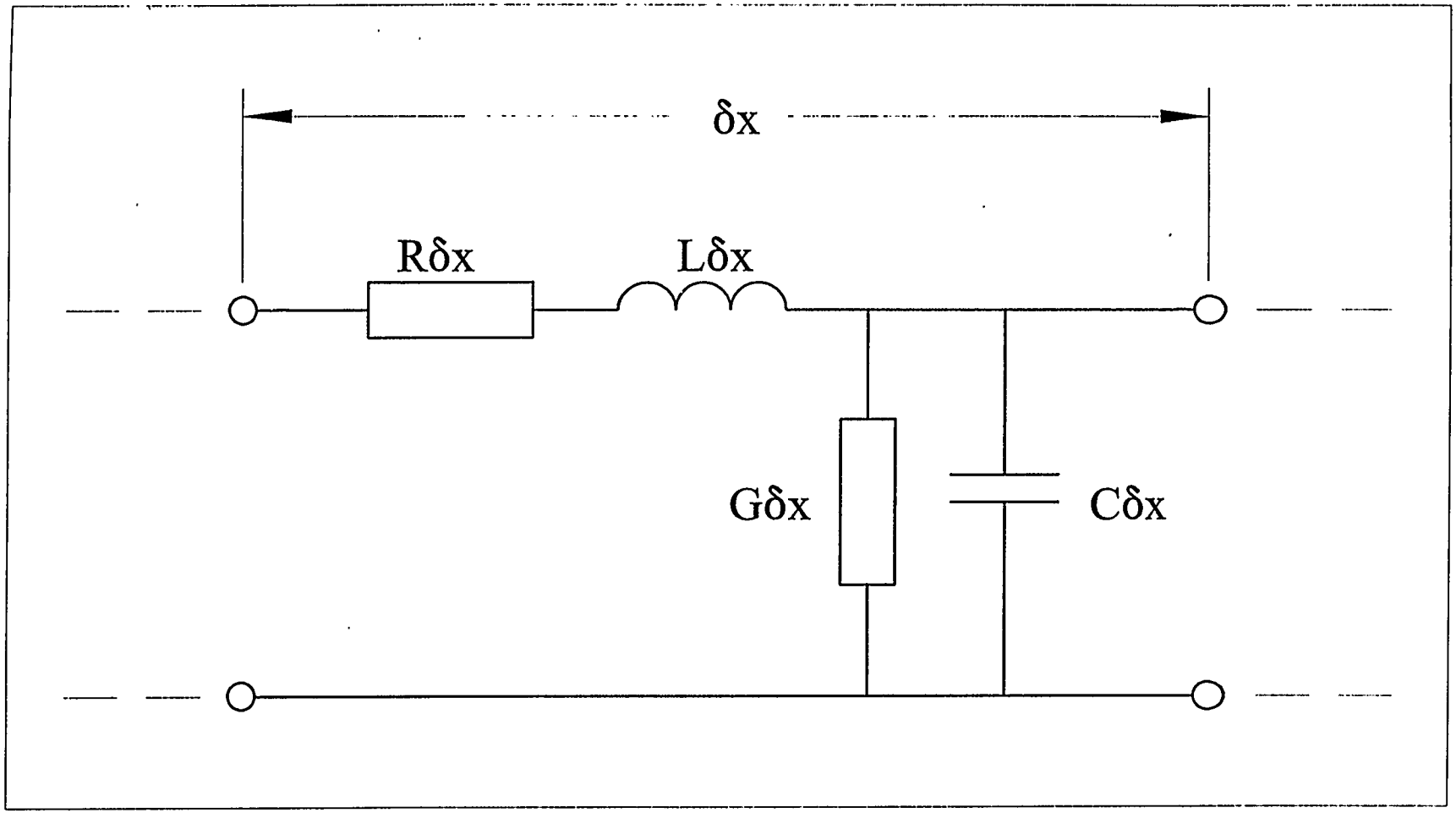
δx
Rδx
Lδx
Gδx
Cδx

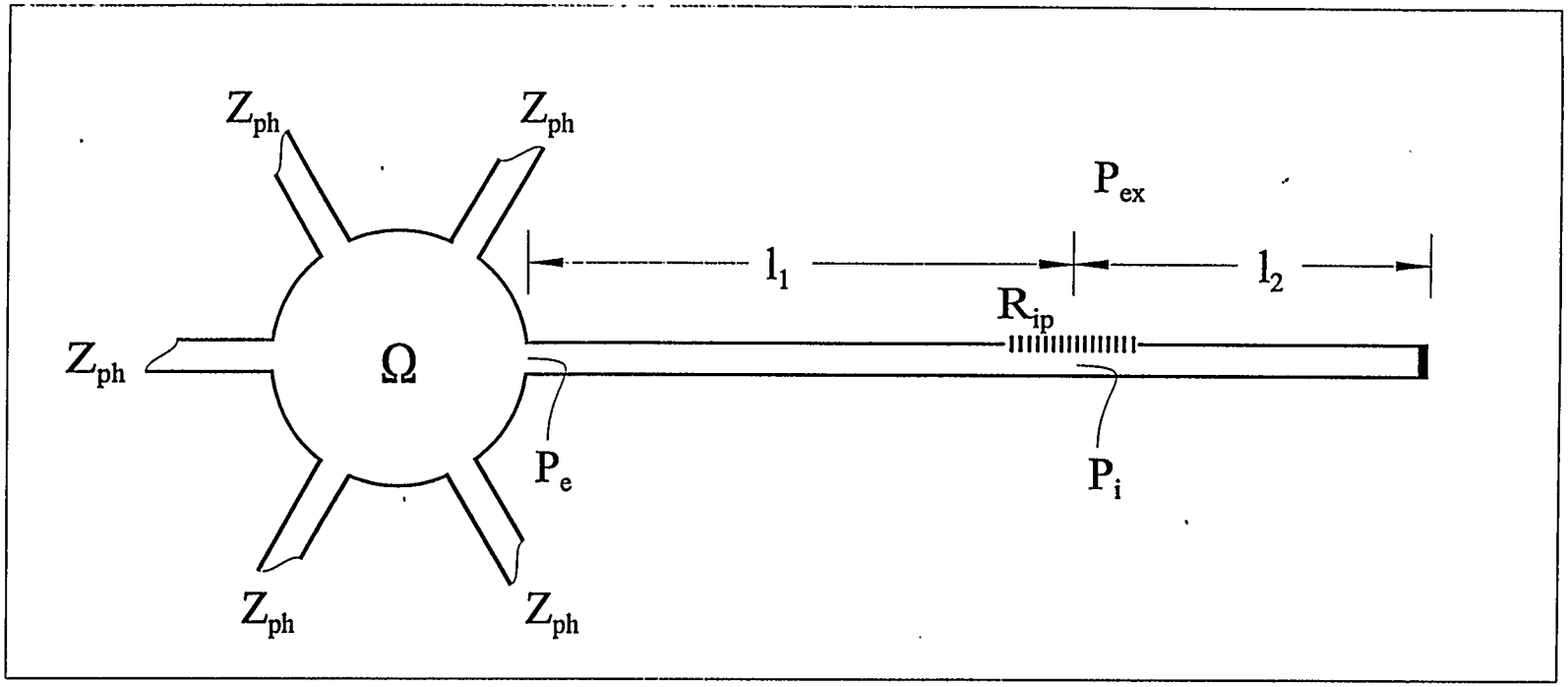
Z_{ph}
Z_{ph}
Z_{ph}
Z_{ph}
Z_{ph}
Z_{ph}
Ω
P_{ex}
l_1
l_2
R_{ip}
P_e
P_i

Linear acoustical transmission-line theory

The solution of the wave-equation for the pressure in a tube is given by

$$P(x,t) = (Ae^{-\Gamma x} + Be^{\Gamma x})e^{i\omega t}$$

where the propagation constant of the acoustical line is defined as

$$\Gamma = \sqrt{ZY} = \sqrt{(R+i\omega L)(G+i\omega C)}$$

The characteristic impedance is given by

$$Z_0 = \sqrt{\frac{Z}{Y}} = \sqrt{\frac{R+i\omega L}{G+i\omega C}}$$

The phase velocity in the line can be written as

$$v_{phase} = \omega / Im(\Gamma)$$

and the attenuation length is given by

$$L_{at} = 1/Re(\Gamma)$$

where *Im* and *Re* represent the imaginary and real parts.
For tubes with a *heat-conducting and rigid wall* the exact expressions for the series impedance Z and the shunt admittance Y are

$$Z = i(\omega\rho/\pi a^2)(1 - F_v e^{i\phi_v})^{-1}$$

$$Y = i(\omega\pi a^2/\rho c^2)(1 + (\gamma - 1)F_t e^{i\phi_t})$$

where ω is the angular frequency, ρ is the density of free air, a is the tube radius, c is the free-space speed of sound and γ is the ratio of specific heats at constant pressure and volume C_p/C_v.

Linear acoustical transmission-line theory of porous tubes

The admittance Y of the porous tube is effected by the porous wall in the following way

$$Y_{pt} = Z_{pw}^{-1} S^{-1} + Y$$

where Z_{pw} is the input impedance of the porous wall per unit area, S is the area of the inner wall surface per meter and Y the admittance for non-porous tube according to Benade's theory. The input impedance of the wall per unit area backed by the free air is given by

$$Z_{pw} = \frac{Z_{pm}\sinh(\gamma_{pm}d) + Z_{air}\cosh(\gamma_{pm}d)}{Z_{pm}\cosh(\gamma_{pm}d) + Z_{air}\sinh(\gamma_{pm}d)} Z_{pm}$$

where Z_{pm} is the characteristic impedance of the porous material per unit area, Z_{air} is the characteristic impedance of the air per unit area, γ_{pm} is the propagation constant of the porous material and d is the wall thickness. Expressions for the impedance and propagation constant of porous sound absorbing materials are:

$$Z_{pm} = \sqrt{(k\rho/h + \sigma/i\omega)\rho c^2/h}$$

with k the structure constant, h the porosity and σ the air resistance for steady air flow per unit area,

$$\gamma_{pm} = i\omega\sqrt{(k\rho/h + \sigma/i\omega)h/\rho c^2}$$

and the impedance of free air is given by

$$Z_{air} = \rho c$$

The parameter $F_v e^{i\phi_v}$ is defined as

$$F_v e^{i\phi_v} = \frac{2J_1[r_v\sqrt{(-i)}]}{r_v\sqrt{(-i)}J_o[r_v\sqrt{(-i)}]}$$

where the functions J are complex Bessel-functions and r_v is the ratio of tube radius and viscous boundary layer thickness and is defined as

$$r_v = a\sqrt{(\omega\rho/\eta)}$$

Here η is the viscosity of air. The parameter $F_t e^{i\phi_t}$ is defined in an analogous way with r_t, the ratio of tube radius and thermal boundary layer thickness, defined as

$$r_t = a\sqrt{\omega\rho C_p/\kappa}$$

where κ is the thermal conductivity.

We define R and ωL as the real and imaginary parts of the series impedance, associated with dissipation via viscous losses at the wall and storage of kinetic energy, and G and ωC as the real and imaginary parts of the shunt admittance, associated with thermal energy losses at the wall and potential energy of compression.

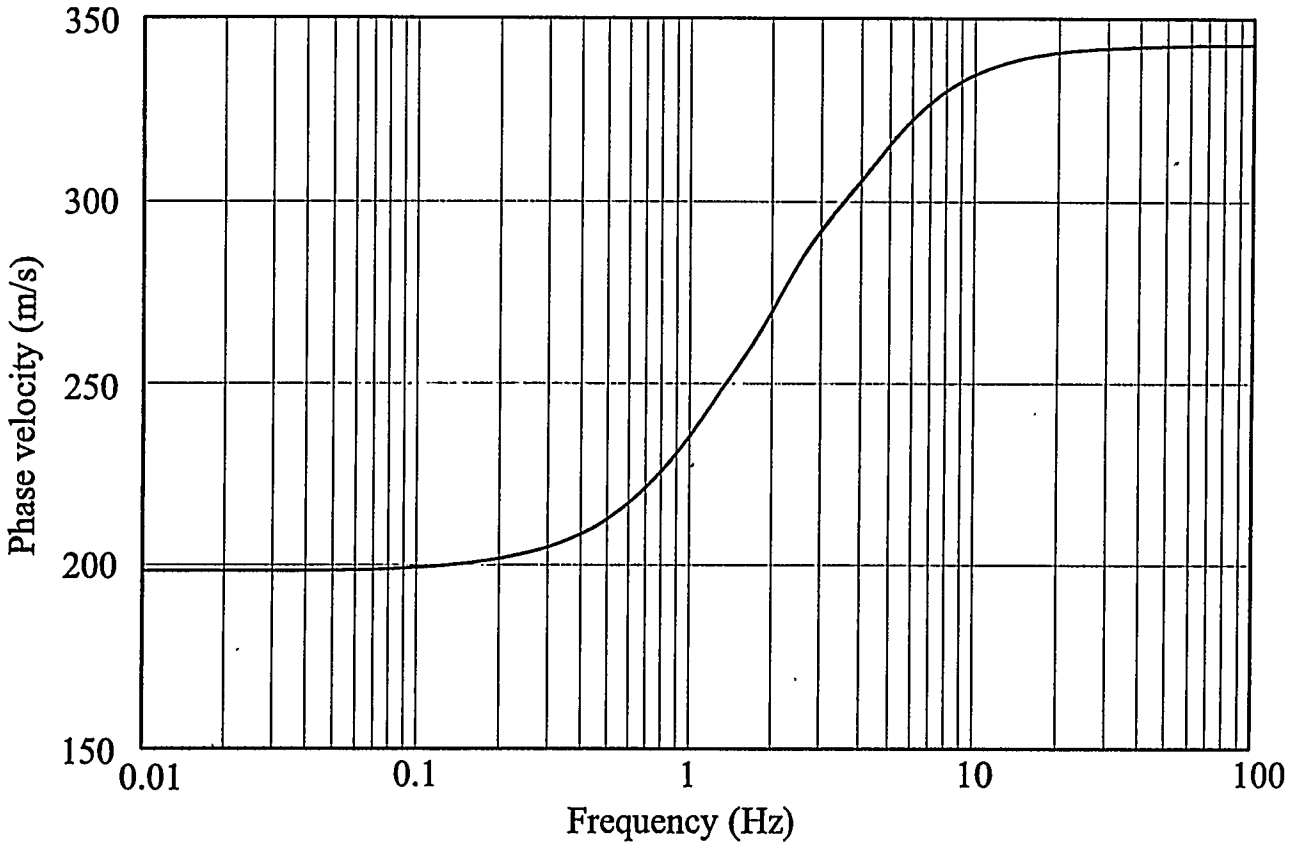
350
300
250
200
150
Phase velocity (m/s)
0.01
0.1
1
10
100
Frequency (Hz)

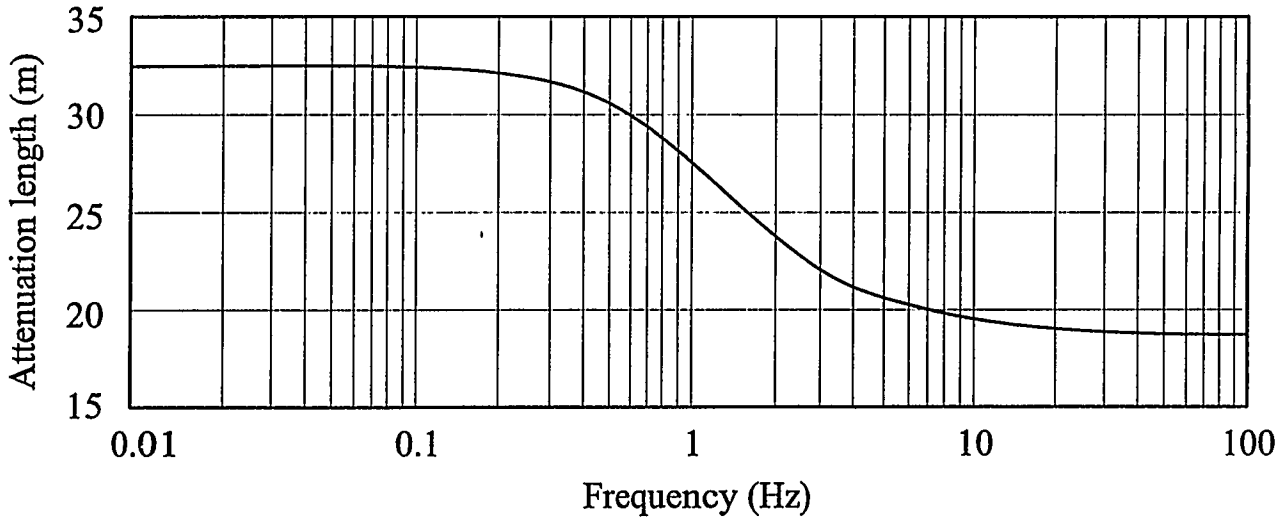
35
30
25
20
15
Attenuation length (m)
0.01
0.1
1
10
100
Frequency (Hz)

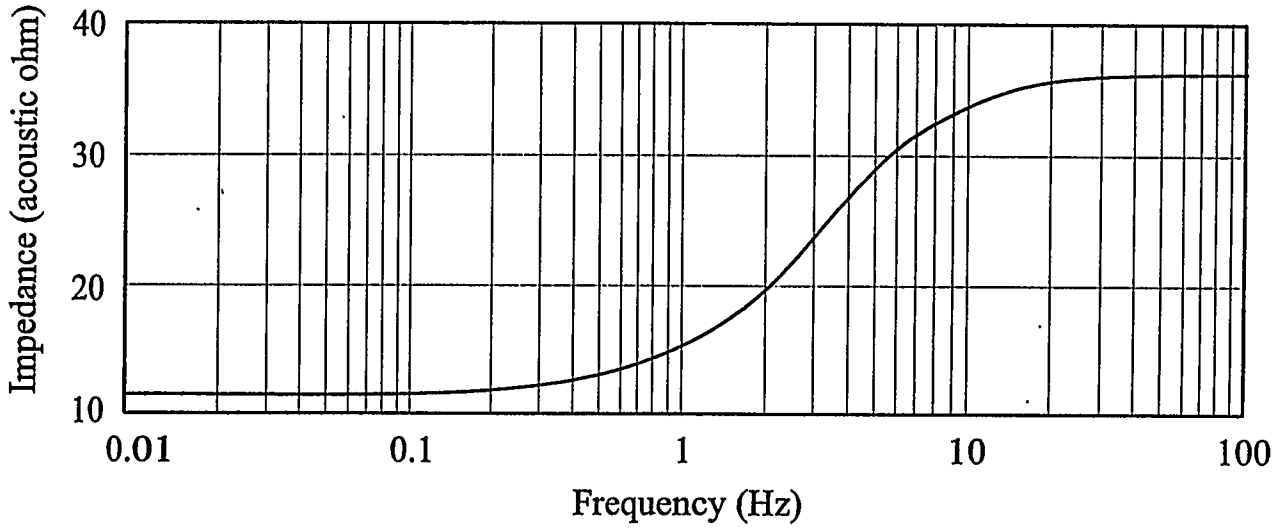
Impedance (acoustic ohm)
40
30
20
10
0.01
0.1
1
10
100
Frequency (Hz)

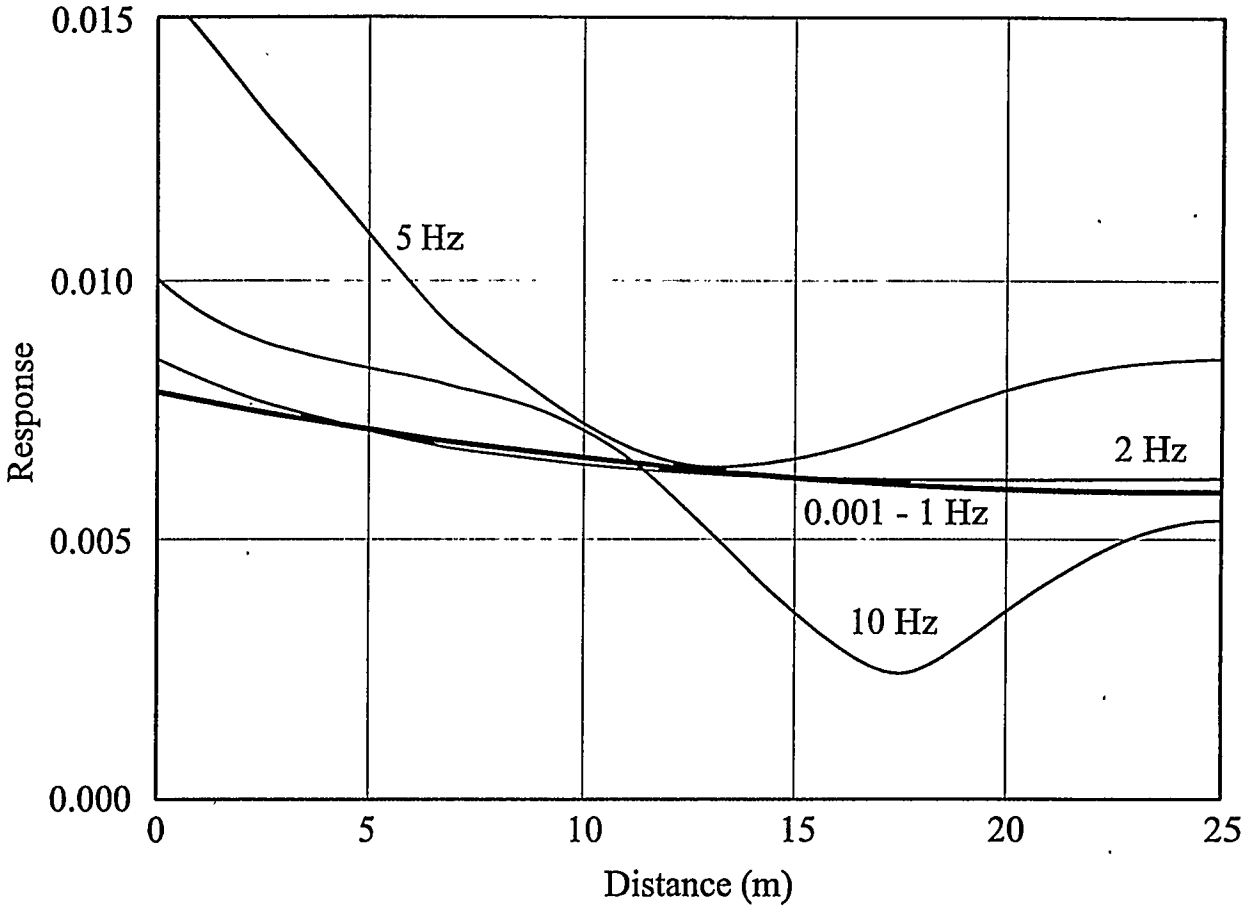
0.015
0.010
0.005
0.000
Response
0
5
10
15
20
25
Distance (m)
5 Hz
2 Hz
0.001 - 1 Hz
10 Hz

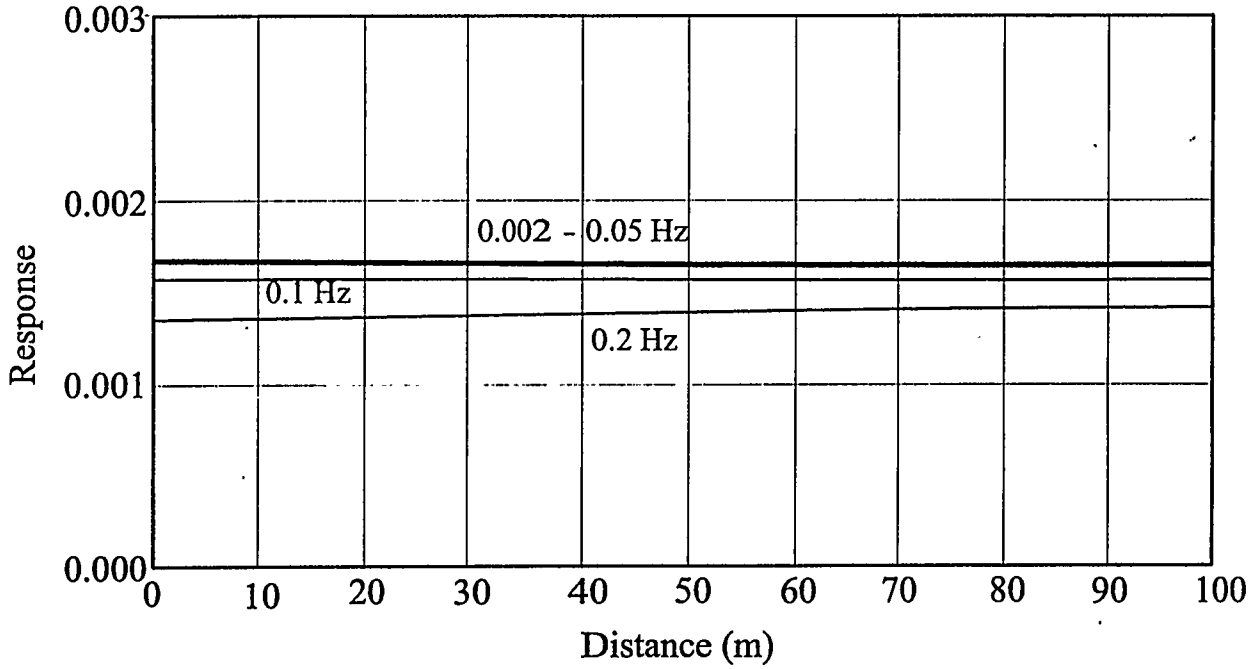
0.003
0.002
0.001
0.000
Response
0.002 - 0.05 Hz
0.1 Hz
0.2 Hz
0
10
20
30
40
50
60
70
80
90
100
Distance (m)

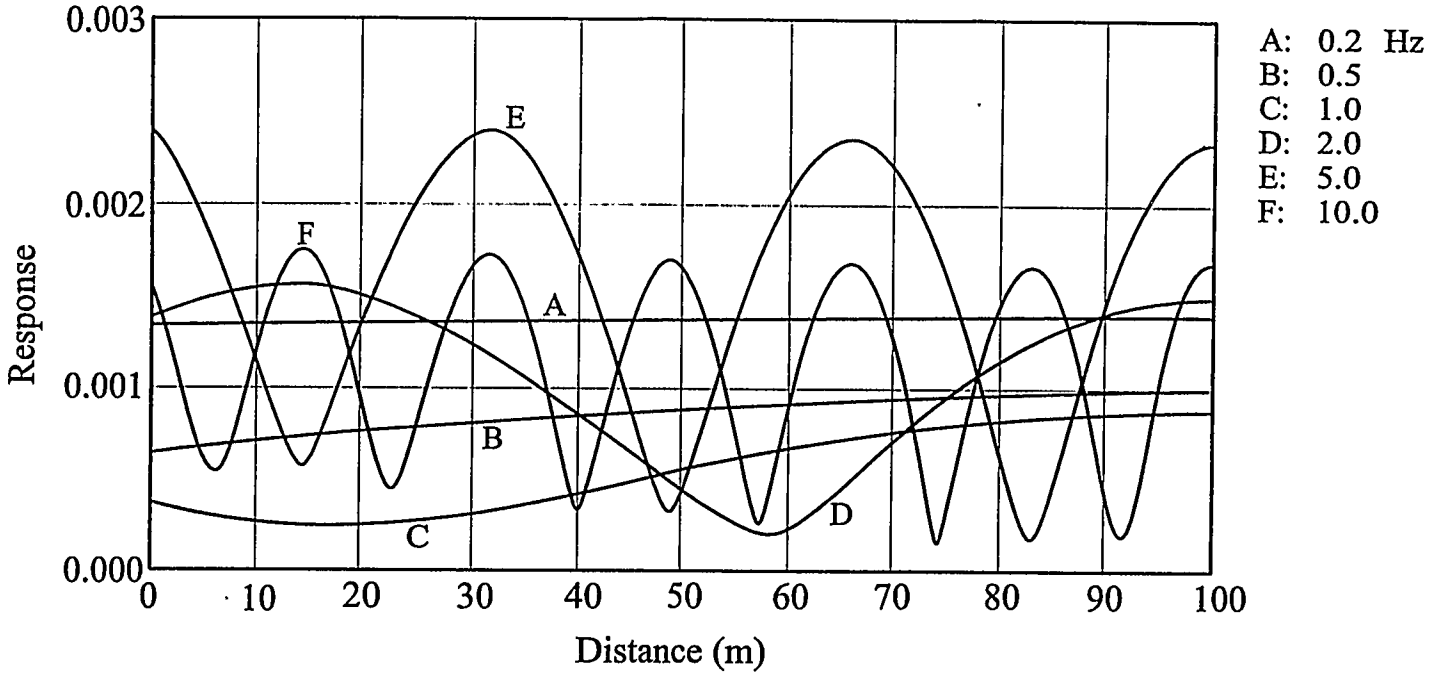
0.003
0.002
0.001
0.000
Response
0
10
20
30
40
50
60
70
80
90
100
Distance (m)
A
B
C
D
E
F
A: 0.2 Hz
B: 0.5
C: 1.0
D: 2.0
E: 5.0
F: 10.0

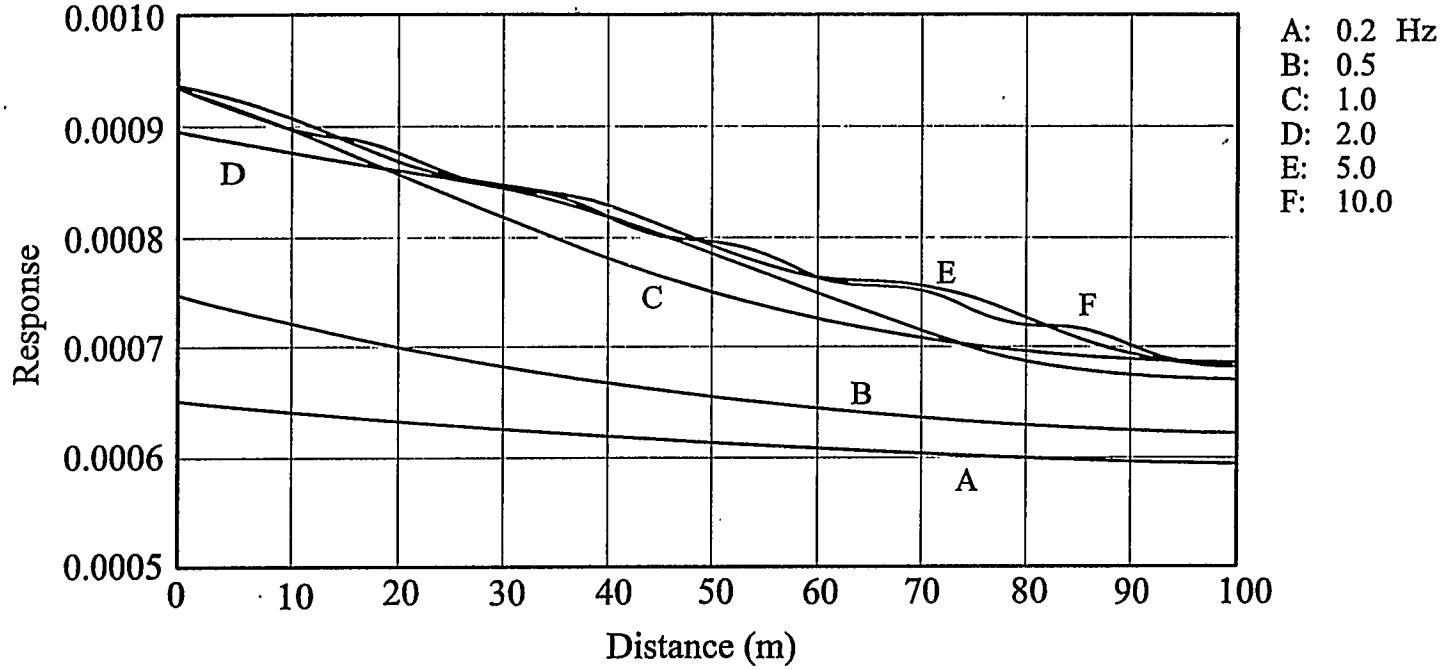
0.0010
0.0009
0.0008
0.0007
0.0006
0.0005
Response
0
10
20
30
40
50
60
70
80
90
100
Distance (m)
A
B
C
D
E
F
A: 0.2 Hz
B: 0.5
C: 1.0
D: 2.0
E: 5.0
F: 10.0

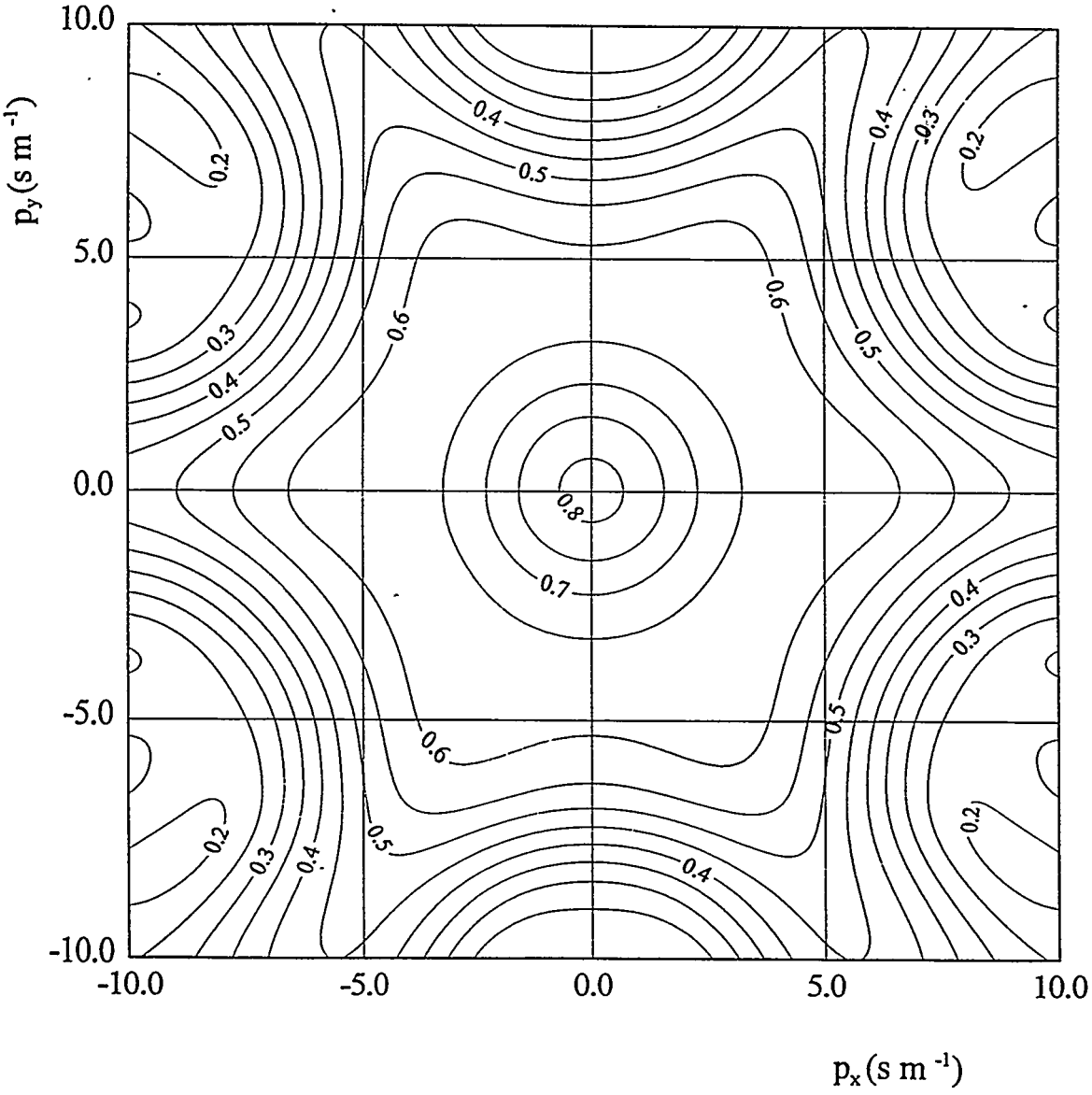
10.0
5.0
0.0
-5.0
-10.0
-10.0
-5.0
0.0
5.0
10.0
p_y (s m^{-1})
p_x (s m^{-1})
0.2
0.3
0.4
0.5
0.6
0.7
0.8
0.9

Calibration of porous hoses

- Calibrating procedure
- Results
- Testing with real signals
- Sensitivity to environmental circumstances

Royal Netherlands Meteorological Institute, Division of Seismology

KNMI

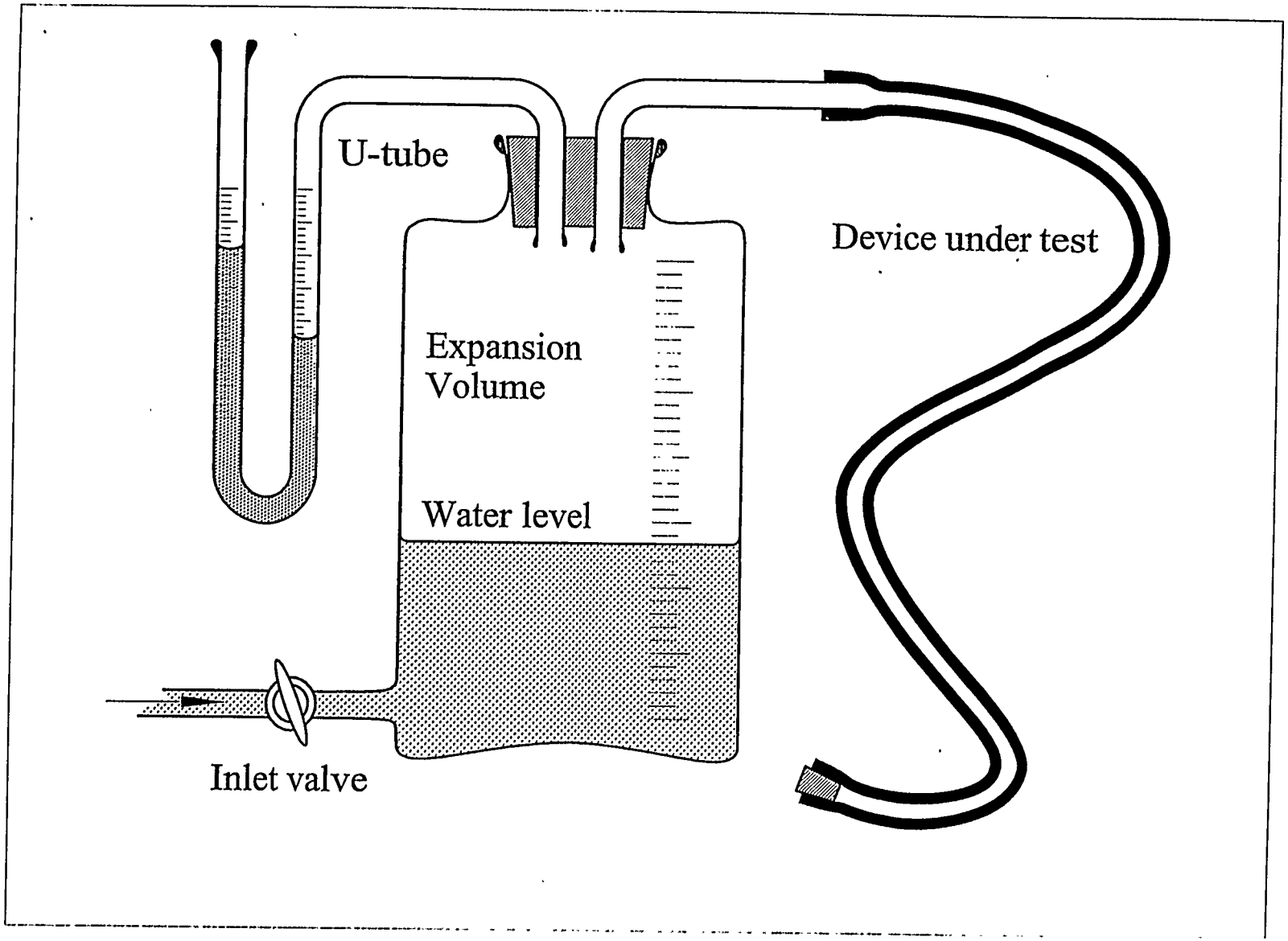
U-tube
Device under test
Expansion
Volume
Water level
Inlet valve

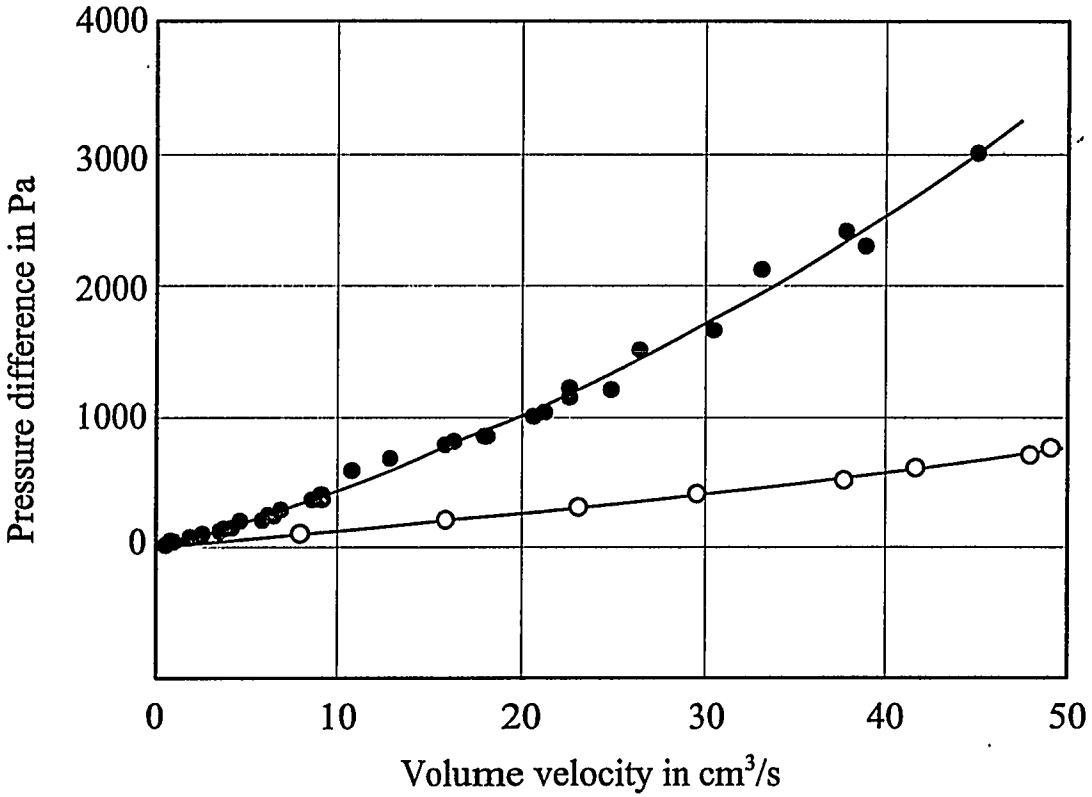
4000
3000
2000
1000
0
Pressure difference in Pa
0
10
20
30
40
50
Volume velocity in cm³/s

Transmission line model:
amplitude along the porous hose at 10 Hz

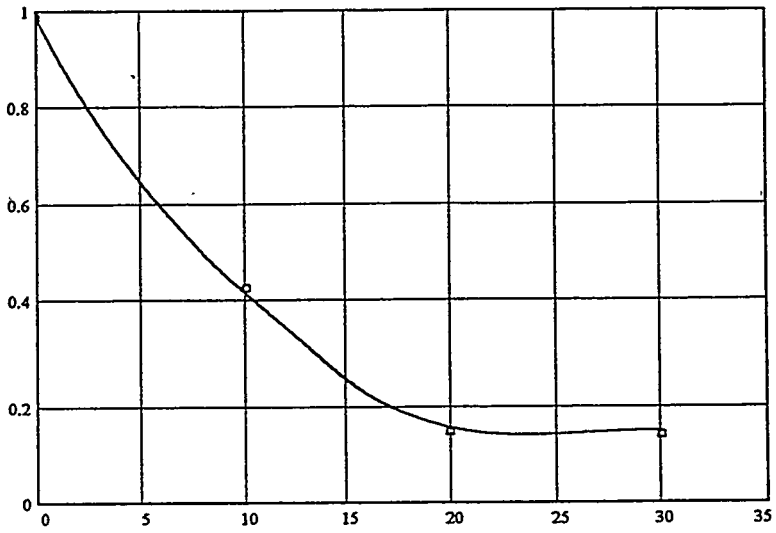

Transmission line model:
phase along the porous hose at 10 Hz

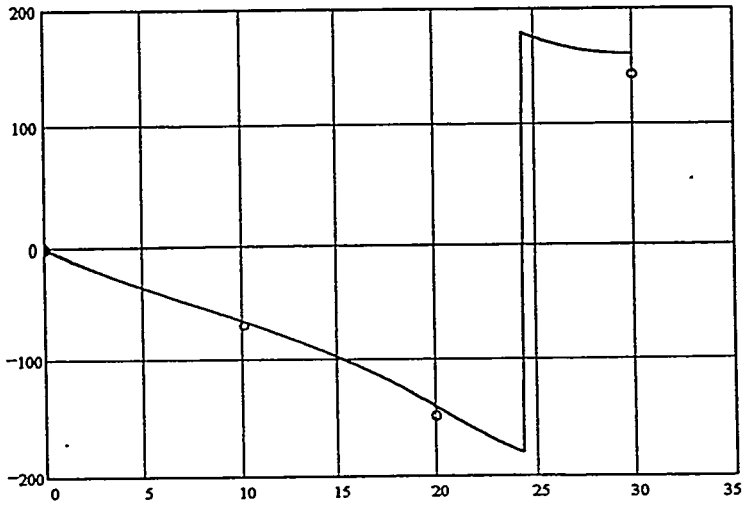

Propagation constant Γ (m^{-1})
as function of frequency

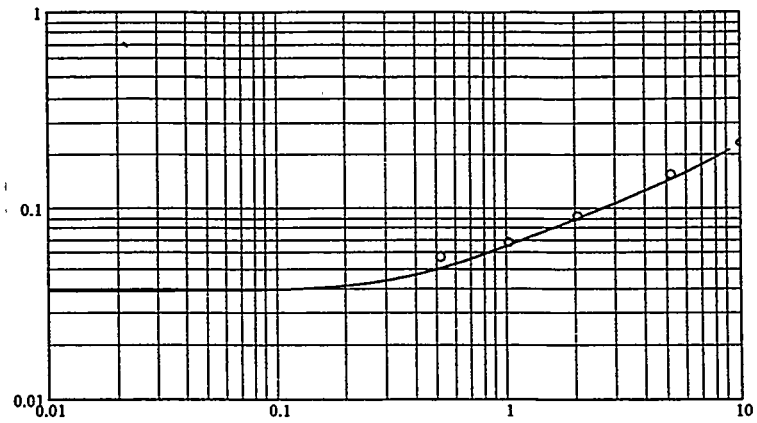

Characteristic impedance Z_0 ($kg\ m^{-4}\ sec^{-1}$)
as function of frequency

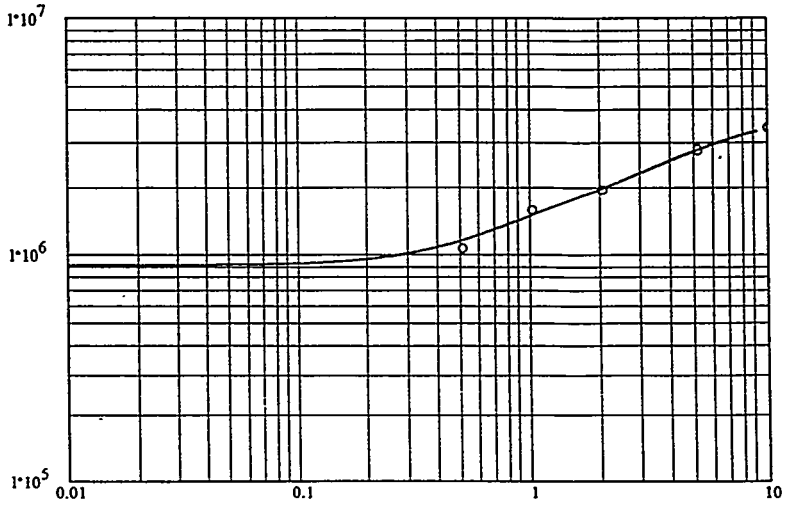

Phase velocity v_{phase} (m sec^{-1})
as function of frequency

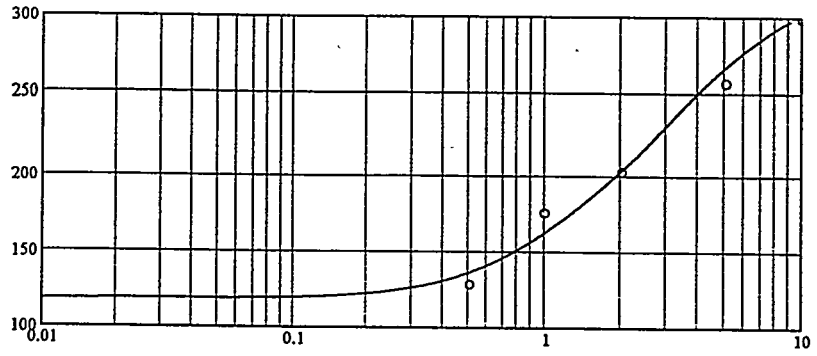

Attenuation length L_{at}(m)
as function of frequency

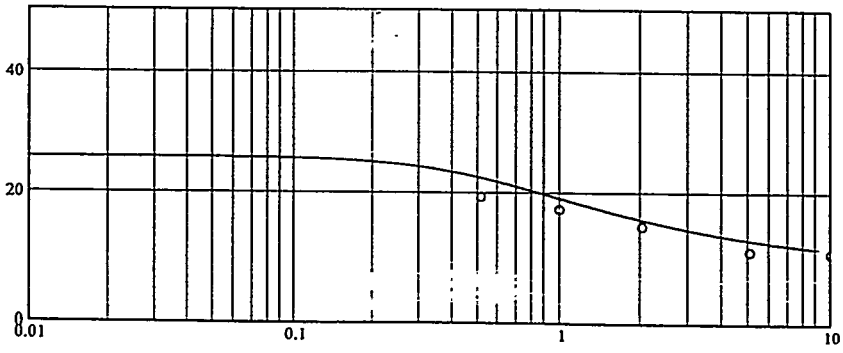

Future work

- Further work on noise reducer design
- Multi-sensor array
- Spatial structure of turbulent noise
- Influence of surface structure

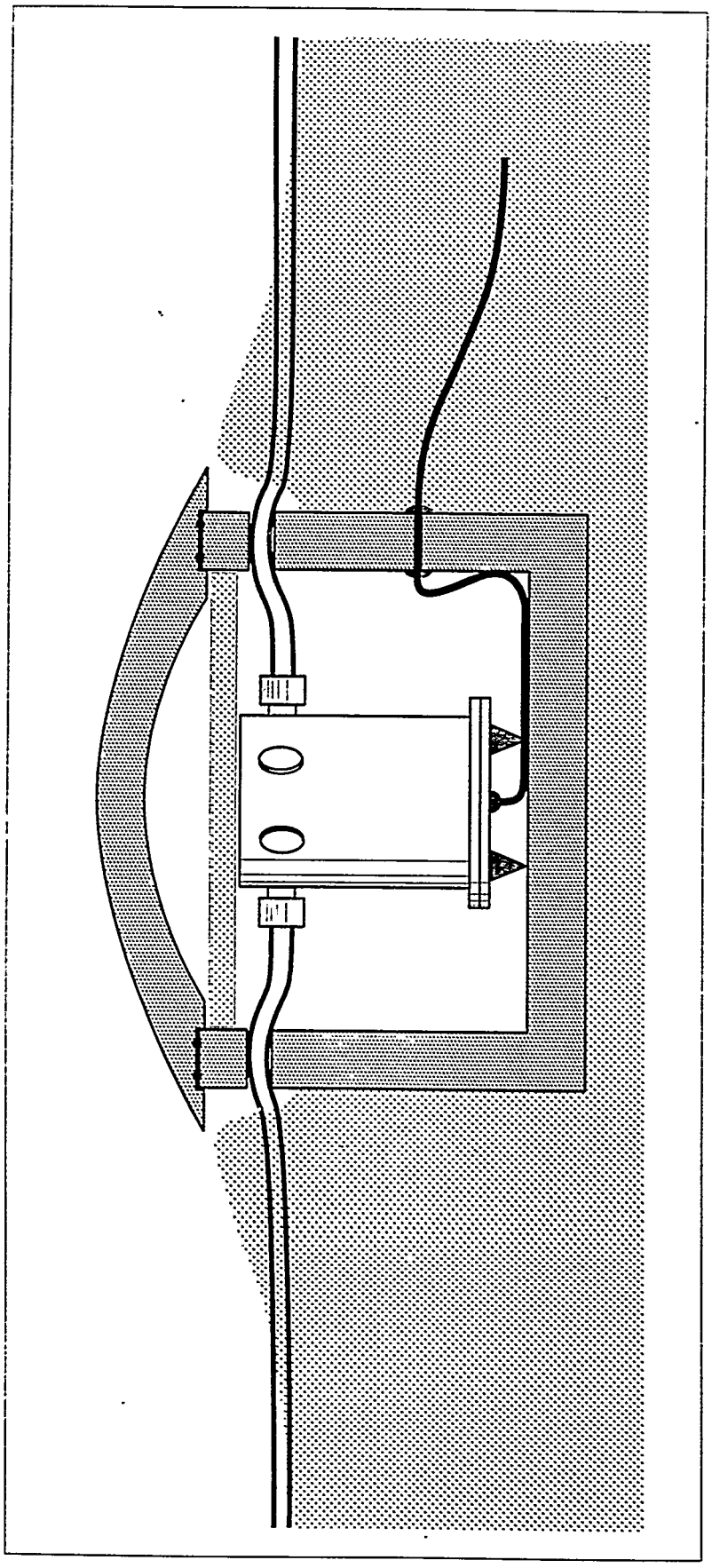

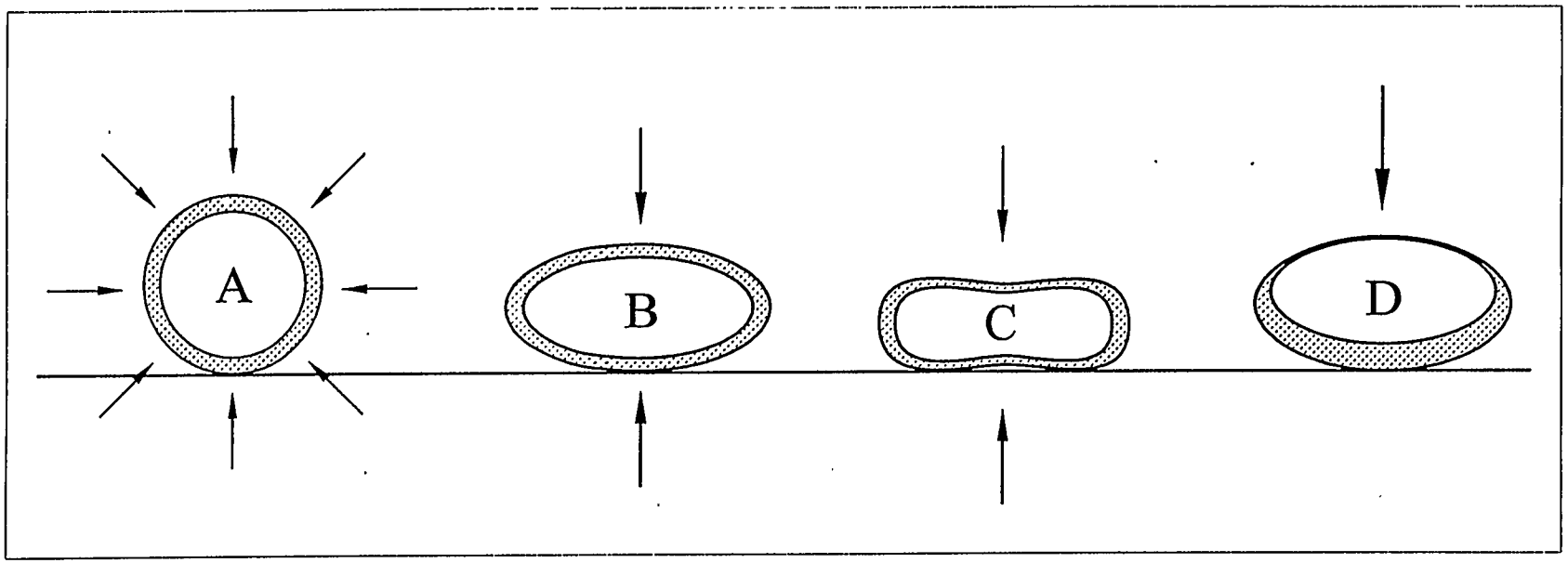
A
B
C
D

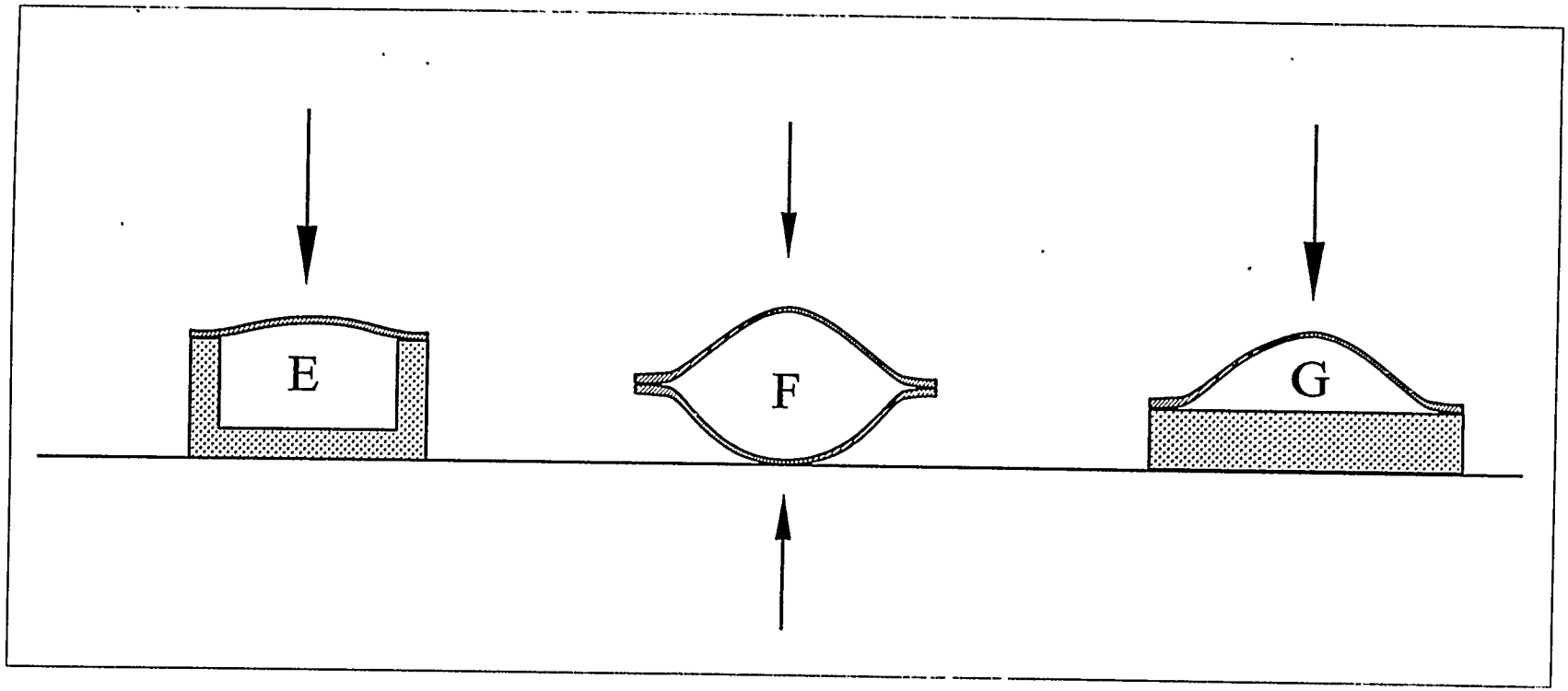
E
F
G

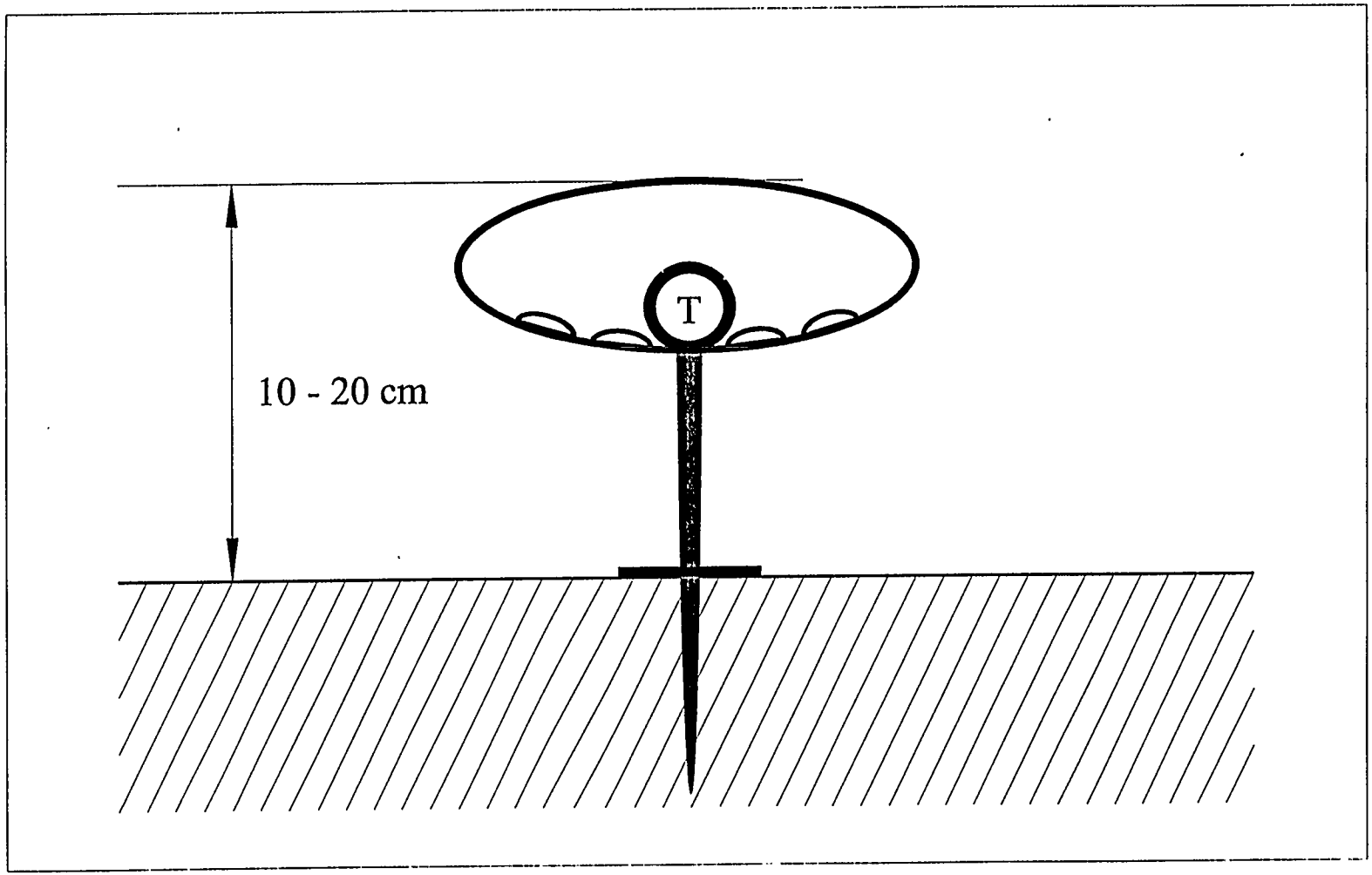
10 - 20 cm
T

Conclusions

- More work is needed on noise reducers
- In fast and close cooperation
- Contacts with PTS essential
- Evaluation of existing stations
- Decisions needed on noise reducer type
- Choice uniformity and site adaptation

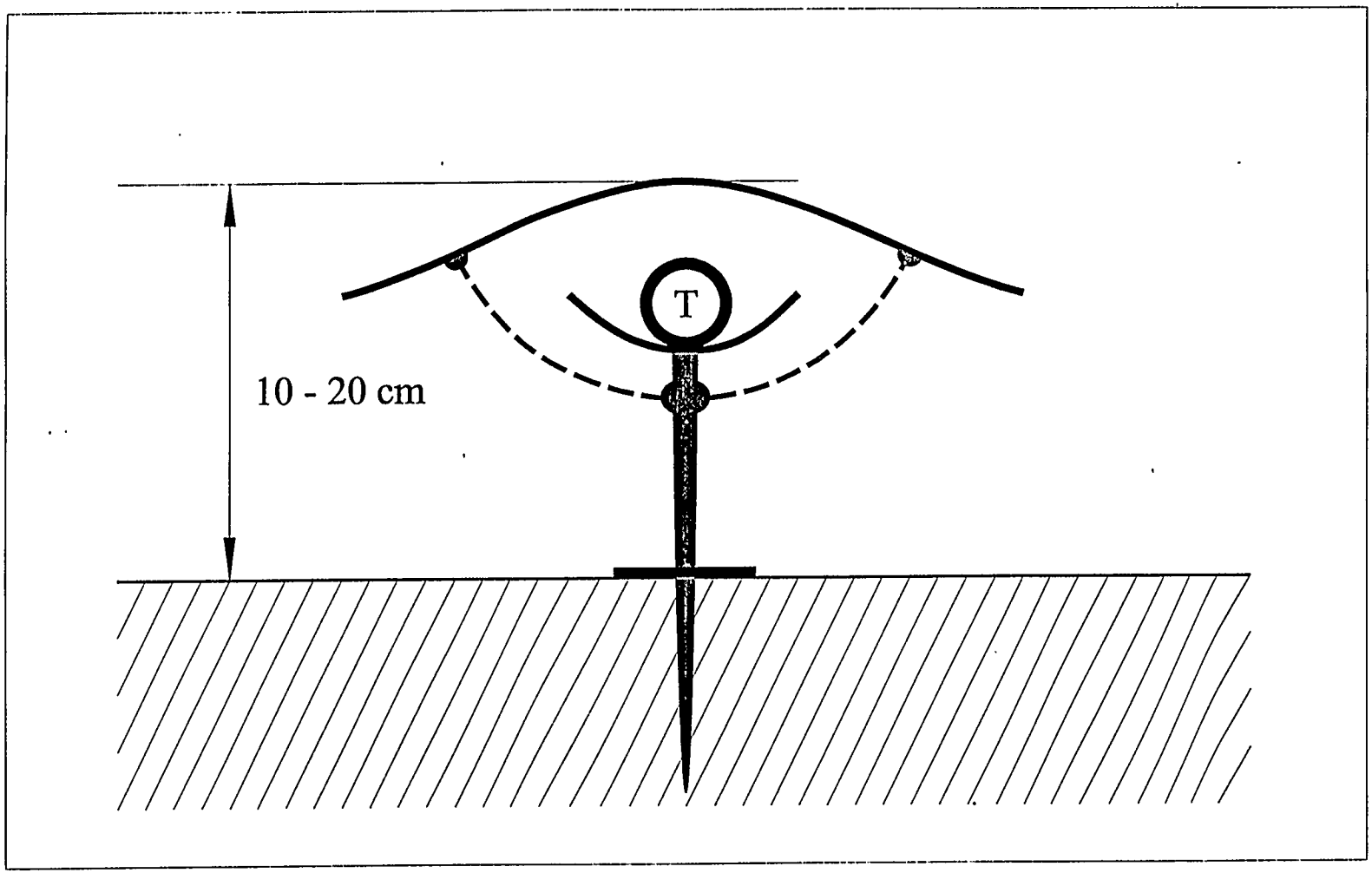
T
10 - 20 cm

Relationship between the Normalized Cross-Correlation Function and the F-Statistic of R. R. Blandford

C. N. Katz, Ph.D.
Division 206

01 August 1997

Science Applications International Corporation
Geophysical Systems Operation
10260 Campus Point Drive
San Diego, CA 92121

Digitally Sampled Time-Series Waveform Signal Data

$$x_i(n)$$

where n is the integer-valued time sample index, and where i is the integer-valued index (i.e., label) for the i^{th} of the I sensors; $i \in [1, I]$

Total Power in the Beam

$$B(k_0: N, n_0) = \sum_{n=n_0}^{n_0+(N-1)} \left| I \cdot b(n:k_0) \right|^2$$

Traditional Delay and Sum
(Plane Wave)
Beamform

$$b(n:\mathbf{k}_0)=\left(\frac{1}{I}\right)\cdot\sum_{i=1}^{I}x_i(n+\ell_i)$$

where the delays, ℓ_i, are given by the inner-product of the propagation vector, $\mathbf{k}_0$, and the vector positions of the I sensors, $\mathbf{r}_i$, as in:

$$\ell_i = -\mathbf{r}_i\cdot\mathbf{k}_0/\omega$$

Total Power in the Time-Series

$$P(\mathbf{k}_0: N, n_0) = \sum_{n=n_0}^{n_0+(N-1)} \left\{ \sum_{i=1}^{I} \left| x_i(n+\ell_i) \right|^2 \right\}$$

$$= \sum_{i=1}^{I} \left\{ \sum_{n=n_0}^{n_0+(N-1)} \left| x_i(n+\ell_i) \right|^2 \right\}$$

$$= \sum_{i=1}^{I} \left\{ p_i(\mathbf{k}_0: N, n_0) \right\}$$

The F-Statistic (definition)

$$F\text{-}S(\mathbf{k}_0{:}N, n_0) = \left(\frac{I-1}{I}\right) \cdot \left(\frac{\sum_{n=n_0}^{n_0+(N-1)} \left| \left\{ \sum_{i=1}^{I} x_i(n+\ell_i) \right\} \right|^2}{\sum_{n=n_0}^{n_0+(N-1)} \left\{ \sum_{i=1}^{I} \left| x_i(n+\ell_i) - b(n{:}\mathbf{k}_0) \right|^2 \right\}} \right)$$

Re-Expression of the Residuals (I)

$$\sum_{n=n_0}^{n_0+(N-1)} \left\{ \sum_{i=1}^{I} \left| x_i(n+\ell_i) - b(n:\mathbf{k}_0) \right|^2 \right\}$$

$$= \sum_{n=n_0}^{n_0+(N-1)} \left\{ \sum_{i=1}^{I} \left| x_i(n+\ell_i) \right|^2 + \sum_{i=1}^{I} \left| b(n:\mathbf{k}_0) \right|^2 \right\}$$

$$- \sum_{n=n_0}^{n_0+(N-1)} \left\{ \sum_{i=1}^{I} b(n:\mathbf{k}_0) x_i^*(n+\ell_i) + \sum_{i=1}^{I} x_i(n+\ell_i) b^*(n:\mathbf{k}_0) \right\}$$

Re-Expression of the Residuals (II)

$$= \sum_{n=n_0}^{n_0+(N-1)} \left\{ \sum_{i=1}^{I} \left| x_i(n+\ell_i) \right|^2 + I \cdot \left| b(n:\mathbf{k}_0) \right|^2 \right\}$$

$$- \sum_{n=n_0}^{n_0+(N-1)} \left\{ b(n:\mathbf{k}_0) \cdot I \cdot b^*(n:\mathbf{k}_0) + b^*(n:\mathbf{k}_0) \cdot I \cdot b(n:\mathbf{k}_0) \right\}$$

$$= \sum_{n=n_0}^{n_0+(N-1)} \left\{ \sum_{i=1}^{I} \left| x_i(n+\ell_i) \right|^2 \right\} - \left(\frac{1}{I} \right) \cdot \sum_{n=n_0}^{n_0+(N-1)} \left\{ \left| I \cdot b(n:\mathbf{k}_0) \right|^2 \right\}$$

Re-Expression of the Residuals (III)

$$\sum_{n=n_0}^{n_0+(N-1)} \left\{ \sum_{i=1}^{I} \left| x_i(n+\ell_i) - b(n:k_0) \right|^2 \right\}$$

$$= \left\{ \sum_{n=n_0}^{n_0+(N-1)} \left\{ \sum_{i=1}^{I} \left| x_i(n+\ell_i) \right|^2 \right\} \right\} - \left\{ \left(\frac{1}{I} \right) \cdot \sum_{n=n_0}^{n_0+(N-1)} \left| I \cdot b(n:k_0) \right|^2 \right\}$$

$$= P(k_0:N,n_0) - \left(\frac{1}{I} \right) \cdot B(k_0:N,n_0)$$

Re-Expression of the F-Statistic

$$F\text{-}S(k_0{:}N, n_0) = \left(\frac{I-1}{I}\right) \cdot \frac{B(k_0{:}\,N, n_0)}{\left\{P(k_0{:}\,N, n_0) - \left[\left(\frac{1}{I}\right) \cdot B(k_0{:}\,N, n_0)\right]\right\}}$$

Re-Expression of Total Power in the Beam

$$B(k_0{:}N, n_0) = \sum_{n=n_0}^{n_0+(N-1)} \left| \left\{ \sum_{i=1}^{I} x_i(n+\ell_i) \right\} \right|^2$$

$$= \sum_{n=n_0}^{n_0+(N-1)} 2 \cdot \mathrm{Re} \left\{ \sum_{i=1}^{I-1} \left\{ \sum_{j=i}^{I} \left\{ x_j(n+\ell_j) \cdot x_i^*(n+\ell_i) \right\} \right\} \right\}$$

$$+ \sum_{n=n_0}^{n_0+(N-1)} \left\{ \sum_{i=1}^{I} \left| x_i(n+\ell_i) \right|^2 \right\}$$

Expansion of Cross-Term

$$\sum_{n=n_0}^{n_0+(N-1)} 2\cdot \mathrm{Re}\left\{\sum_{i=1}^{I-1}\left\{\sum_{j=i}^{I}\left\{x_j(n+\ell_j)\cdot x_i^*(n+\ell_i)\right\}\right\}\right\}$$

$$=2\cdot\sum_{i=1}^{I-1}\left\{\sum_{j=i}^{I}\mathrm{Re}\left\{\sum_{n=n_0}^{n_0+(N-1)}\left\{x_j(n+\ell_j)\cdot x_i^*(n+\ell_i)\right\}\right\}\right\}$$

$$=2\cdot\sum_{i=1}^{I-1}\left\{\sum_{j=i}^{I}\tilde{c}_{ij}(\ell_j-\ell_i)\right\}$$

Un-Normalized Cross-Correlations

in terms of

Normalized Cross-Correlations

$$\sum_{n=n_0}^{n_0+(N-1)} 2\cdot \mathrm{Re}\left\{\sum_{i=1}^{I-1}\left\{\sum_{j=i}^{I}\left\{x_j(n+\ell_j)\cdot x_i^*(n+\ell_i)\right\}\right\}\right\}$$

$$=2\cdot\sum_{i=1}^{I-1}\left\{\sum_{j=i}^{I}\tilde{c}_{ij}(\ell_j-\ell_i)\right\}$$

$$=2\cdot\sum_{i=1}^{I-1}\left\{\sum_{j=i}^{I}\sqrt{p_i(k_0{:}N,n_0)\cdot p_j(k_0{:}N,n_0)}\,c_{ij}(\ell_j-\ell_i)\right\}$$

Final Form of Total Power in the Beam

$$B(\mathbf{k}_0{:}N,n_0)=$$

$$2\cdot\sum_{i=1}^{I-1}\left\{\sum_{j=i}^{I}\sqrt{p_i(\mathbf{k}_0{:}N,n_0)\cdot p_j(\mathbf{k}_0{:}N,n_0)}\;c_{ij}(\ell_j-\ell_i)\right\}$$

$$+\sum_{i=1}^{I}\left\{p_i(\mathbf{k}_0{:}N,n_0)\right\}$$

$$=2\cdot\sum_{i=1}^{I-1}\left\{\sum_{j=i}^{I}\sqrt{p_i(\mathbf{k}_0{:}N,n_0)\cdot p_j(\mathbf{k}_0{:}N,n_0)}\;c_{ij}(\ell_j-\ell_i)\right\}$$

$$+P(\mathbf{k}_0{:}N,n_0)$$

Expression of F-Statistic

in terms of

Normalized Cross-Correlation Functions

Total Power

Power in each sensor-channel

$$F\text{-}S(k_0{:}N,n_0)=\left(\frac{I\text{-}1}{I}\right)\cdot\frac{B(k_0{:}N,n_0)}{\left\{P(k_0{:}N,n_0)-\left[\left(\frac{1}{I}\right)\cdot B(k_0{:}N,n_0)\right]\right\}}$$

$$=(I-1)\cdot\frac{\left\{P(k_0{:}N,n_0)+\left[2\cdot\sum_{i=1}^{I-1}\left\{\sum_{j=i}^{I}\sqrt{p_i(k_0{:}N,n_0)\cdot p_j(k_0{:}N,n_0)}\;c_{ij}(\ell_j-\ell_i)\right\}\right]\right\}}{\left\{(I-1)\cdot P(k_0{:}N,n_0)+\left[2\cdot\sum_{i=1}^{I-1}\left\{\sum_{j=i}^{I}\sqrt{p_i(k_0{:}N,n_0)\cdot p_j(k_0{:}N,n_0)}\;c_{ij}(\ell_j-\ell_i)\right\}\right]\right\}}$$

Practical Consideration (I)

Ugly Question: "What happens if the sensor-channels are are characterized by different 'scales' or 'sensitivities' ?"

The CBF won't function properly & the F-Statistic's denominator will behave badly ... it won't be 'residuals.'

What can be done about this?"

Force each sensor-channel's time-domain waveform signal data to be zero-mean unit variance processes by explicitly:

☞ 'detrending' to zero-mean

☞ 'scaling' to unit variance

For Identical Power in each Sensor-Channel

$$F\text{-}S(k_0{:}N,n_0)=(I-1)\cdot\frac{\left\{I+\left[2\cdot\sum_{i=1}^{I-1}\left\{\sum_{j=i}^{I}c_{ij}(\ell_j-\ell_i)\right\}\right]\right\}}{\left\{I\cdot(I-1)-\left[2\cdot\sum_{i=1}^{I-1}\left\{\sum_{j=i}^{I}c_{ij}(\ell_j-\ell_i)\right\}\right]\right\}}$$

$$=\frac{\left\{1+(I-1)\cdot\left[\left[\frac{1}{\left[\frac{I\cdot(I-1)}{2}\right]}\right]\cdot\sum_{i=1}^{I-1}\left\{\sum_{j=i}^{I}c_{ij}(\ell_j-\ell_i)\right\}\right]\right\}}{\left\{1-\left[\left[\frac{1}{\left[\frac{I\cdot(I-1)}{2}\right]}\right]\cdot\sum_{i=1}^{I-1}\left\{\sum_{j=i}^{I}c_{ij}(\ell_j-\ell_i)\right\}\right]\right\}}=\frac{\left\{1+(I-1)\cdot\bar{c}(k_0{:}N,n_0)\right\}}{\left\{1-\bar{c}(k_0{:}N,n_0)\right\}}$$

Practical Consideration (II)

$64 Question: "Is wide-sense stationarity present in the scenario?"

Efficient Algorithms for Generating Normalized Cross-Correlation Functions

- Process Signal Data in Received-Time Registration Regardless of plane wave direction of arrival or magnitude phase velocity
- Depending upon the Integration Time (i.e., N) and the sensor geometry (i.e., MAX $(|\ell_j - \ell_i|)\ \forall\ i,j \in [1, I]$) a table of normalized cross-correlation functions may need to be generated and "sampled" in both time and lag

Relationship between F-Statistic
and Arithmetic Mean of
Normalized Cross-Correlation Functions

$$F\text{-}S(\mathbf{k}_0{:}N,n_0)=\left(\frac{I-1}{I}\right)\cdot\frac{B(\mathbf{k}_0{:}N,n_0)}{\left\{P(\mathbf{k}_0{:}N,n_0)-\left[\left(\frac{1}{I}\right)\cdot B(\mathbf{k}_0{:}N,n_0)\right]\right\}}$$

$$=\frac{\left\{1+\left(I-1\right)\cdot\bar{c}(\mathbf{k}_0{:}N,n_0)\right\}}{\left\{1-\bar{c}(\mathbf{k}_0{:}N,n_0)\right\}}=1+I\cdot\left(\frac{\bar{c}(\mathbf{k}_0{:}N,n_0)}{1-\bar{c}(\mathbf{k}_0{:}N,n_0)}\right)$$

$$=1+I\cdot(snr)_e$$

Sharpness with which the F-Statistic Changes in the presence of Coherent Energy

Calculate the Logarithmic Derivative:

$$\frac{1}{F}.\frac{\partial F}{\partial q} = \frac{\partial\left[\ell n(F)\right]}{\partial q}$$

where F is a continuous function of q

Where $F = \frac{1 + (I-1)\cdot\bar{c}}{1 - \bar{c}}$ and $F = 1 + I\cdot(snr)_e$

$$\frac{\partial[\ell n(F)]}{\partial q} = \left(\frac{F-1}{F}\right)\cdot\left[1+\left(\frac{F-1}{I}\right)\right]\cdot\frac{\partial[\ell n(\bar{c})]}{\partial q}$$

$$\frac{\partial[\ell n(F)]}{\partial q} = \left(\frac{1 + (snr)_e}{1 + [I\cdot(snr)_e]}\right)\cdot[I\cdot(snr)_e]\cdot\frac{\partial[\ell n(\bar{c})]}{\partial q}$$

$$\frac{\partial[\ell n(\bar{c})]}{\partial q} = \left(\frac{1 + [I\cdot(snr)_e]}{1 + (snr)_e}\right)\cdot\left[\frac{1}{I\cdot(snr)_e}\right]\cdot\frac{\partial[\ell n(F)]}{\partial q}$$

In the Limit of High $(snr)_e$

$$\frac{\partial\left[\ell n(\bar{c})\right]}{\partial q} \cong \frac{1}{(snr)_e} \cdot \frac{\partial\left[\ell n(F)\right]}{\partial q}$$

and conversely:

$$\frac{\partial\left[\ell n(F)\right]}{\partial q} \cong (snr)_e \cdot \frac{\partial\left[\ell n(\bar{c})\right]}{\partial q}$$

ABOUT ESTIMATION OF THE EXPLOSION SOURCES ENERGY BY REMOTE ACOUSTIC TECHNIQUES

Sergey N. Kulichkov

Institute of Atmospheric Physics
Russian Academy of Sciences
3 Pyzevsky, Moscow 109017, RUSSIA

The problem of estimation of explosion energy by using the remote acoustic method is discussed. The characteristics considered are the explosion energy E and the quantity I ("impulse") the product of the area of the wave profile S (in pressure-time coordinates) and the distance to the source. The quantity I remains unchanged along the path of infrasonic wave propagation and takes approximately the same values for tropospheric, stratospheric, and thermospheric arrivals. The records of infrasonic signals from air, surface, and underground explosions are considered as an example. The source energy varied between 300 kg and 2 kt; the distance between the sources and receivers was from 160 to 310 km. The records of more than 20 explosions were considered. Satisfactory agreement is observed between the values of I ("impulse") determined both in the vicinity of the sources and at great distances from them for different types of acoustic arrivals. The relation between the values of the explosion energy E and I-impulse is suggested.E(kt)= k*3.19*10(-11) I(kg/sec)(3/2). The coefficient k is determined from empirical data.

On the Estimation of Source Energy with the Aid of Remote Acoustic Techniques.

Sergey N. Kulichkov
Institute of Atmospheric Physics,
Russian Academy of Sciences.
3 Pyzevsky, Moscow 109017, RUSSIA
Tel: 7 (095) 233-4876, Fax: 7 (095) 233-1652;
E-mail:<postmaster@iaph.msk.su>

ABSTRACT. The problem of estimation of explosion energy by using the remote acoustic method is discussed. The I-"impulse" value, equal to the product of the wave profile area S (in the pressure-time coordinates) by the distance R between a source and a receiver, is used as a parameter characterizing a source. The quantity I remains unchanged along the path of infrasonic wave propagation and takes approximately the same values for tropospheric, stratospheric, and thermospheric arrivals. The records of infrasonic signals from air, surface, and underground explosions are considered as an example. The source energy varied between 300 kg and 2 kt; the distance between the sources and receivers was from 160 to 310 km. The records of more than 20 explosions were considered. Satisfactory agreement is observed between the values of E (explosions energy) determined both in the vicnity of the sources and at great distances from them for different types of acoustic arrivals. The relation between the values of the explosion energy E and I-"impulse" is suggested.

GENERAL GOAL.

To obtain a universal characteristic of infrasonic arrivals at long distances from explosions suitable to estimate explosion energy.

BACKGROUND.

SOURCE ENERGY RELATIONS

a. Semi-Empirical Approach of Mutschlecner and Whitaker (1988)

$$E_S(kt)=0.62\{(\Delta p_{p\text{-}p}(\mu bars)/4.69*10^4)\}^{1.471}10^{-0.259V_{\infty}(m/s)}R^2(km)$$

b. Semi-Empirical Approach of Reed (1972)

$$p(kPa)=11.8E(kt)^{0.4}R(km)^{-1.2},\quad E_o=(p/11.8)^{2.5}R^3$$

c. Semi-Empirical Approach of Sadovsky (see Gubkin,1978)

$$\Delta p(kg/sm^2)=0.83[E^{1/3}(kg)/R(m)]+2.7E^{2/3}/R^2+7.0E/R^3$$
$$E^{1/3}<R<10E^{1/3}$$

d. Approach of Landay (see Gubkin,1978)

$$\Delta p=1.35\{E^{1/3}(kg)/R[\ln(R(m)/2.7E^{1/3})]^{1/2}\} \quad [kg/sm^2]$$
$$10E^{1/3}<R$$

NONLINEAR EFFECTS.

The expression for the amplitude p and duration τ of the acoustic pulses at large distances from the sources, when nonlinear effects were pronounced, takes the forms (Bush,Kulichkov etc.1989)

$$p_a \sim f^{1/2}(2S_o r_o)^{1/2}(\rho_o c^3{}_o \varepsilon)^{1/2} r^{-1}\left[\int_{z_o}^{z_f} \{(æ_o\rho_o c^5{}_o/æ\rho c^5)^{1/2}/r_o \sin\alpha\} dz\right]^{-1/2}$$

$$\tau \sim (2S_o r_o)^{1/2}(\rho_o c^3 \varepsilon)^{-1/2}\left[\int_{z_o}^{z_f} \{(æ_o\rho_o c^5{}_o/æ\rho c^5)^{1/2}/r_o \sin\alpha\} dz\right]^{1/2}$$

$$p_a \tau r \approx (2S_o r_o)$$

where ρ is the density of air, ρ_o, c_o and S_o are the initial values or ρ, c and S at $z=z_o$, α is the grazing angle of the sound ray, æ is the cross-sectional area of the ray tube, $f=r^2 æ_o/æ^2{}_o$ is the focusing factor, $\varepsilon = 1.2$

DATA ANALYZED

The records of 23 explosions were considered (Kulichkov,1992).
There were:

(1) air explosions (Z=6-8 km,R=160-180km, E=300 kg- 1 t);
(2) surface explosions (R=290-310 km; E = 20 t-500 t)
(3) commercial subsurface explosions (R=186-240km; E=30- 2000 t)
(4) underground nuclear explosions.
(5) runs of surface explosions with an energy of 20--70 t regularly realized 1--2 times a month in 1989--1991 (when the SS-20 medium-range missiles were destructed).

SOURCE ENERGY RELATION

$$E_1=2.85*10^{-10}(I\ [kg/sec]/2)^{3/2}\ [kt]$$ Gubkin (1978)

$$I = SR$$

$$S= \int p(t)dt$$ (square of the "wave profile")

RESULTS OF CALCULATIONS

The acoustic records in the vicinity of explosions and at the distances R from explosions were analyzed (see examples in Fig.1)

The correlation between the values of E_o obtained at the distances R and R_o from the same explosion by using Reed's formula is presented in Fig. 2.

Great differences can been seen between the values of $E_o(R)$ and $E_o(R_o)$.

In contrast to this case, the same correlation between $E_1(R)$ and $E_1(R_o)$ obtained by using the formula:

$$E_1=2.85*10^{-10}(I\ [kg/sec]/2)^{3/2}\ [kt])$$

is satisfactory (see Fig. 3).

It follows from Fig.3 that the final correlation between the explosion energy and the parameters I for long distances from explosions can be written in the following form:

$$E_1= k*3.19*10^{-10}(I\ [kg/sec]/2)^{3/2}\ [kt]$$

coefficient k may be defined from empirical data.

CONCLUSIONS

To estimate explosion energy by using remote acoustic method ,the obtained relation E(I) may be used, as well as already known semi-empirical relations E(p,R).

REFERENCES

G.A.Bush, YE.A.Ivanov, S.N.Kulichkov,And M.V.Pedanov. Estimation of the Characteristics of a Pulsed Ground Source by Remote Acoustic Techniques. IZVESTIYA Academy of Sciences, USSR,Atmospheric and Ocean Physics,1989, V.25, No.11, p.p.861-866. (in English).

Gubkin,K.Ye. On similarity of explosions. Izv.Akad.Nauk SSSR,Fiz.Zemli,No.10 ,49-60,1978

S.N.Kulichkov.Long-Range Propagation of Sound in the Atmosphere,A Review. IZVESTIYA Academy of Sciences,USSR, Atmospheric and Ocean Physics, 1992, V.28, No.4, p.p.253-269 (in English).

Reed,J.W. Air blast overpressure decay at long ranges. J.Geoph.Res.,77,No.9,1623,1972.

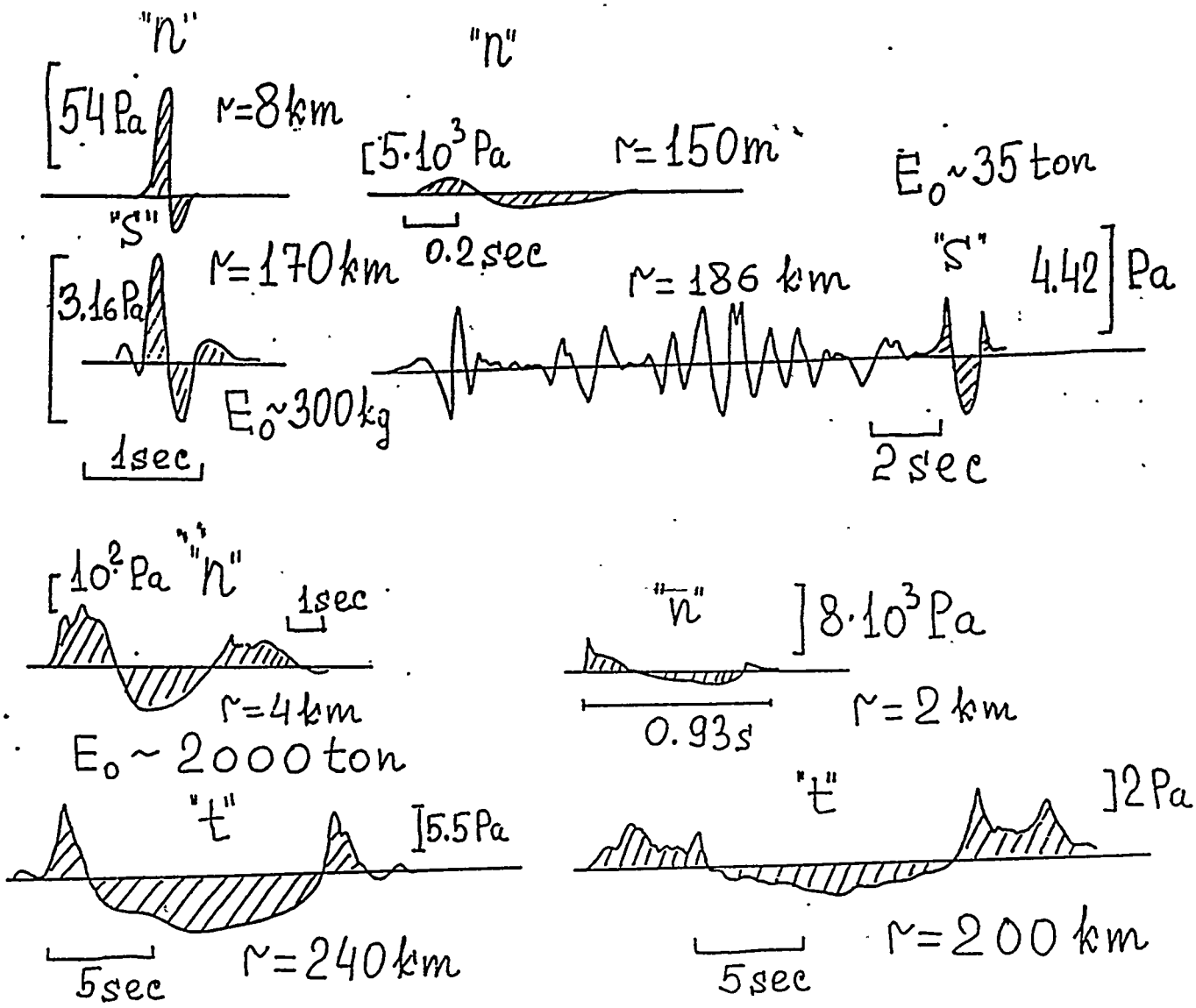

Figure 1.Samples of the acoustic records in the vicinity of explosions and at the distances R from explosions.

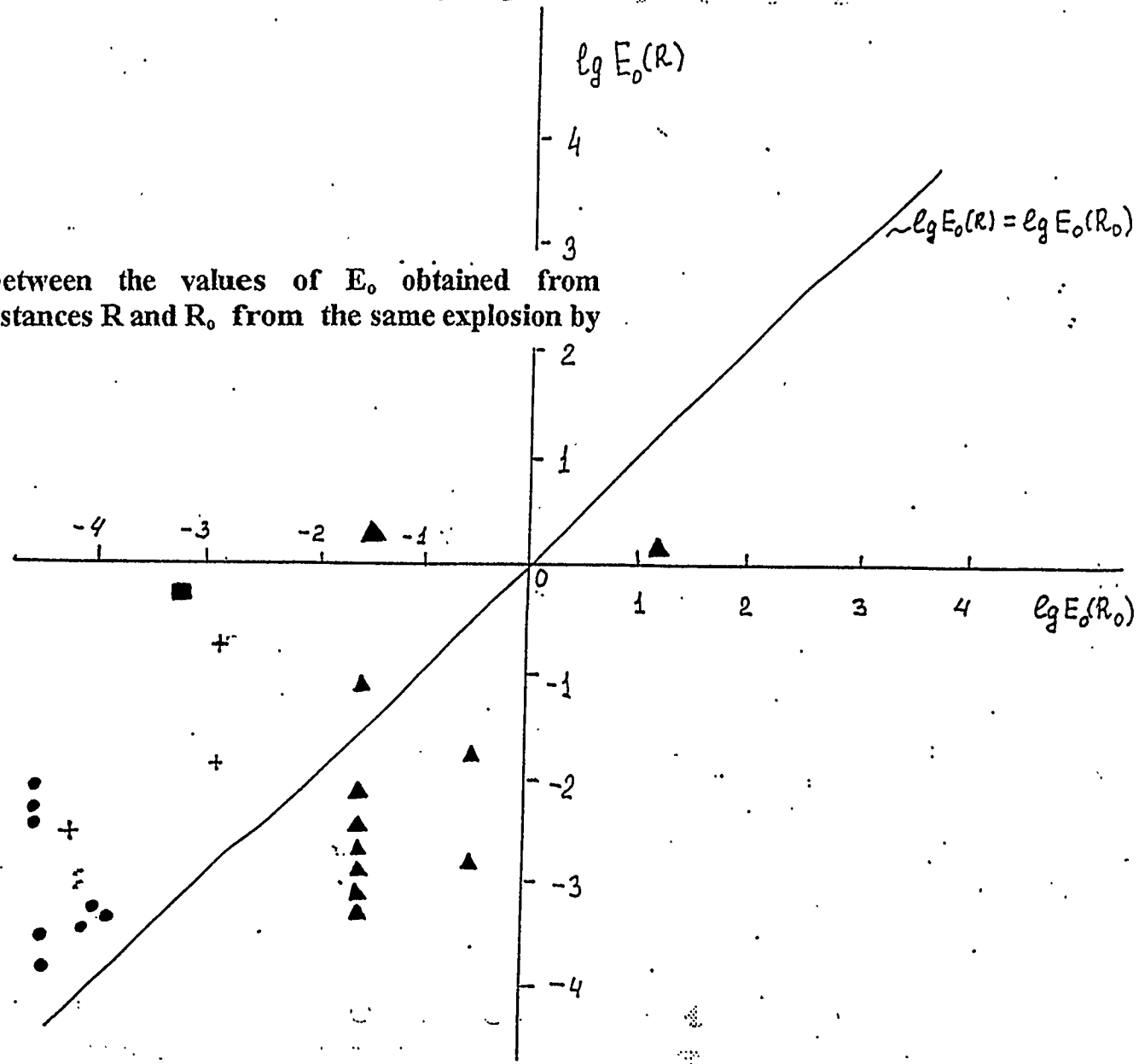

Figure 2. Correlation between the values of E_o obtained from experimental data at the distances R and R_o from the same explosion by using Reed`s formula:

$E_o = (p/11.8)^{2.5} R^3$

igure 3. Correlation between the values of E_1 obtained from xperimental data at the distances R and R_o from the same explosion by sing the formula:

$$E_1=2.85*10^{-10}(I\ [kg/sec]/2)^{3/2}\ [kt])$$

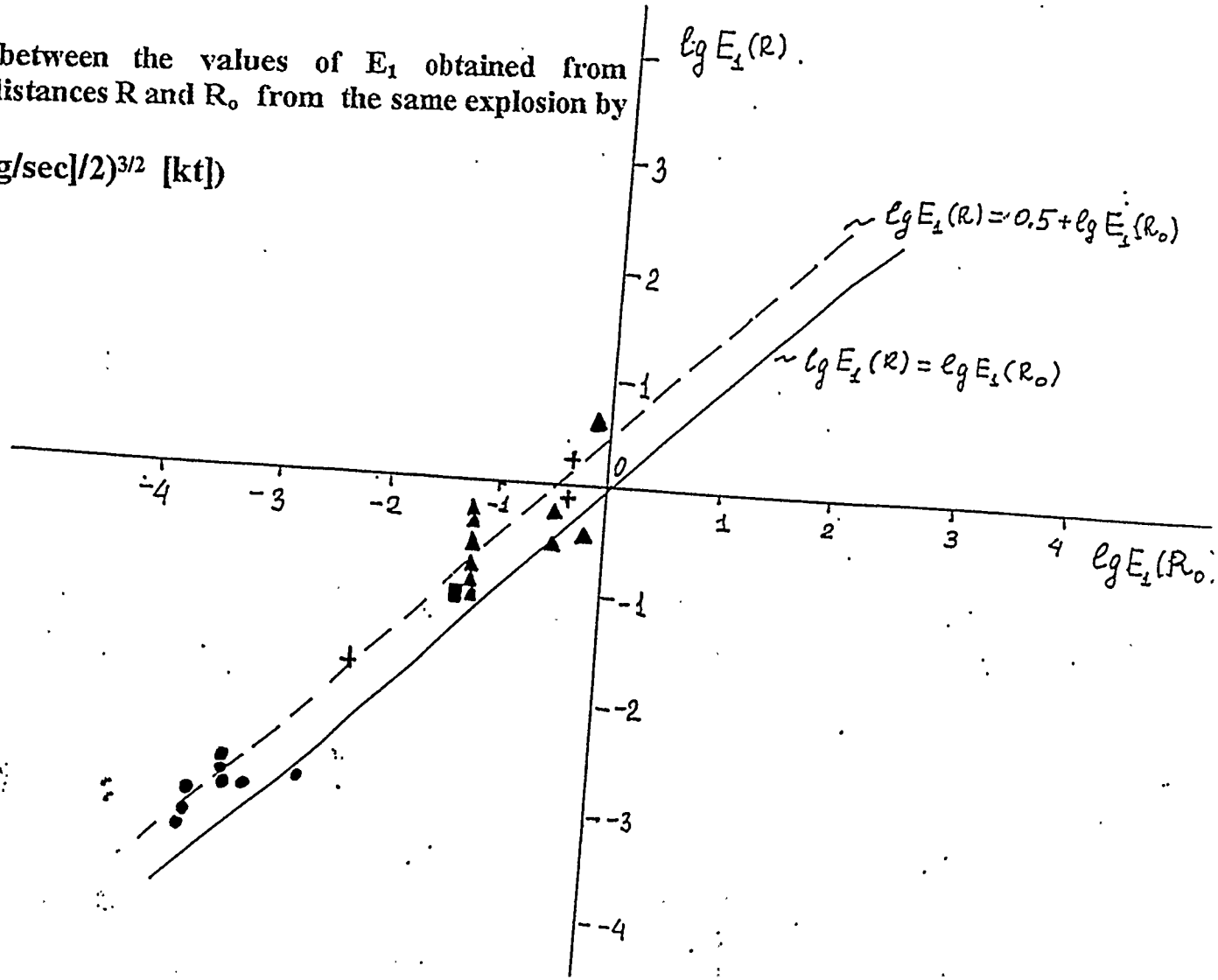

LONG-RANGE SOUND PROPAGATION FROM UNDERGROUND, SURFACE AND NEAR-SURFACE BURSTS WITH SMALL YIELDS

Sergey N. Kulichkov

Institute of Atmospheric Physics
Russian Academy of Sciences
3 Pyzevsky, Moscow 109017, RUSSIA

The results of the records of infrasonic waves from air, surface, and underground explosions at long distances from sources are presented. These data encompass source yields of 30 kg to 2000 tons and observation ranges of 120 to 980 km. The experiments were performed in runs of 3--5 in different regions, in different seasons, and with different intervals between the sources (from 15 min to a few days), but at the same relative position of the sources and observational points for one-type explosions. Infrasonic signals corresponding to the Lamb waves and also to stratospheric, mesospheric, and thermospheric arrivals were recorded. The results of the experiments, where the runs of explosions with an energy of 20--70 tons were regularly realized 1--2 times a month in 1989--1991 (when destructing the SS-20 medium-range missile)are presented too. Infrasonic signals in these experiments were recorded in the regions of geometric shadow at a distance of 300--310 km due to a partial reflection of infrasonic waves from inhomogeneous structures of acoustic refractive index at stratospheric and mesospheric altitudes. It is shown that the variations in the parameters of the inhomogeneous structure (cross wind, etc) of acoustic paths (including the time intervals up to 15 min) substantially affect the arrival azimuth and the standard parameters used in infrasonic monitoring to identify explosions and to estimate their energy.

Long-Range Sound Propagation from Air ,Surface, and Underground Small-Energy Explosions.

Sergey N. Kulichkov
Institute of Atmospheric Physics,
Russian Academy of Sciences.
3 Pyzevsky, Moscow 109017, RUSSIA
Tel: 7 (095) 233-4876, Fax: 7 (095) 233-1652;
E-mail:<postmaster@iaph.msk.su>

ABSTRACT. The results of the records of infrasonic waves from ionospheric,air, surface, and underground explosions at long distances from sources are presented. These data encompass source yields of 5 kg to 4000 tons and observation ranges of 120 to 980 km. The experiments were performed in runs of 3--10 explosions in different regions, in different seasons, and with different intervals between the explosions (from 1 min to a few days), but at the same relative position of the sources and receivers for one-type explosions. Infrasonic signals corresponding to the Lamb waves and also to stratospheric, mesospheric, and thermospheric arrivals were recorded. The results of the experiments, where the runs of explosions with an energy of 20--70 tons were regularly realized (1--2 times a month) in 1989--1991 (when the SS-20 medium-range missiles were destructed), are presented too . Infrasonic signals in these experiments were recorded in the regions of geometric shadow at a distance of 300--310 km due to a partial reflection of infrasonic waves from inhomogeneous structures of the acoustic refractive index in the stratosphere and mesosphere. It is shown that the variations in the parameters of the inhomogeneous structure of acoustic waveguides (including the time intervals up to 15 min) substantially affect the arrival azimuth and the standard parameters used in the infrasonic monitoring to identify explosions and to estimate their energy.

GENERAL GOALS.

The main objectives of the studies are the following:

(1)- to develop the methods of acoustic sounding of turbulent structures in the middle atmosphere and to study their time variations;

(2)- to study the influence of the atmospheric fine inhomogeneous structure on the standard parameters used in the infrasonic monitoring of small - energy explosions: the main period of infrasonic signals, their amplitude, duration, and dispersion;

(3)- to study the effect of time variations in atmospheric stratification (interseasonal, daily, and hourly variations, including the effect of internal gravity waves) on the parameters of recorded infrasonic signals;

(4)- to study the nonlinear and dissipative effects.

(5)- to study the effects of cross wind on the determined source azimuth.

EXPERIMENTS.

More than 100 experiments with explosions of different type and energy have been carried out (Kulichkov,1992).

Source energy varied between 5 kg and 4000 t;

The distance between sources and receivers varied between 120 and 980 km.

The experiments were carried out in different regions of Russia, in different seasons, and at different spatial orientations of acoustic paths. The experiments were carried out in runs of 3—10 explosions realized with different time intervals at one and the same relative position of sources and receivers.

The time intervals between explosions varied from 1 min to a few days.

TYPES OF EXPLOSIONS.

The following types of explosions were used as sources:

(1) ionospheric explosions (Z=120-150 km,E=5-15 kg);

(2) air explosions (Z=6-8 km,R=160-180km,
E=300 kg- 3 t);

(3) surface explosions (R=160-980 km; E = 30kg-500 t)

(4) commercial subsurface explosions
(R=186-450km;E=30- 4000t)

(5) underground nuclear explosions.

(6) runs of surface explosions with an energy of 20--70 t regularly realized 1--2 times a month in 1989--1991 (when the SS-20 medium- range missiles were destructed). (60 explosions).

Samples of the acoustic records in the vicinity of explosions of different type are presented in Fig.1-2.

EXPERIMENTAL RESULTS.

MINIMUM VALUES FOR EXPLOSION ENERGY SUFFICIENT TO RECORD STRATOSPHERIC AND THERMOSPHERIC ACOUSTIC ARRIVALS.

It is shown that the explosion energy of the order of 30—50 kg is enough for stable recording and further processing of stratospheric and thermospheric acoustic arrivals. (Fig.3.)(Kulichkov,1996).

MOLECULAR DISSIPATION.

In our experiments, no essential effects of molecular dissipation on the amplitudes of recorded infrasonic signals from explosions with an energy ranging from 5 kg was observed (Bush,Kulichkov etc.1997).
The dissipative absorption of high-frequency (about 7 Hz) acoustic signals recorded from the explosions with an energy of 5—15 kg at the ionospheric altitudes was found to be lacking. (Fig.4-5)

NONLINEAR EFFECTS.

Nonlinear effects noticeably manifest themselves when explosion energy exceeds 1 t. (Bush,Kulichkov etc. 1989)

At great distances from the sources, the amplitude and characteristic period of infrasonic signals are determined from the initial values of the magnitude I ("impulse"),the product of the wave profile area S (in the pressure-time coordinates), and the distance R to the explosion. (Fig.4)

BACKSCATTERING.

The results of the experiments show that the inhomogeneous structures of the acoustic refractive index with the values of the vertical gradients ($\partial c/\partial z$) of the effective sound velocity of the order of 50 m/sec/km exist in the middle atmosphere. It has been known earlier that the similar structures exist only in the atmospheric boundary layer. (Kulichkov,1996)

The inhomogeneous structures with great values of $\partial c/\partial z$ fill the upper atmosphere full. It is likely that an isolated layer with high $\partial c/\partial z$ is present in the mesosphere.

In all the experiments with explosions of 20—70 t , acoustic signals scattered from the inhomogeneous structures of the acoustic refractive index in the middle atmosphere were recorded in the zone of acoustic shadow (Fig.7). The corresponding profiles of the effective sound velocity are presented in Fig.8.(Kulichkov ,1996)

THE INFLUENCE OF VARIATIONS IN ATMOSPHERIC STRATIFICATION WITH DIFFERENT TIME SCALES ON THE CHARACTERISTICS OF RECORDED INFRASONIC SIGNALS FROM SMALL- ENERGY EXPLOSIONS.

Interannual and interseasonal variations

The maximum values of signal velocities for stratospheric, mesospheric, and thermospheric acoustic arrivals in the north and west directions from the sources are observed in July.(Kulichkov ,1996).(Fig.9)

The amplitudes of acoustic signals scattered from turbulent structures in the middle atmosphere take maximum values in July (Fig.9).

The general form of acoustic arrivals (both reflected and scattered) corresponds principally to interseasonal variations in atmospheric stratification. (Fig.7,10)

Daily and hourly variations

The sequence of stratospheric arrivals recorded at different time during a day is observed to vary (Fig.10). The general shape of reflected and scattered stratospheric arrivals remains unchanged during an hour (Fig.11).
The values of the amplitudes of registered signals can vary within an hour interval. It is probably due to the influence of gravity waves (Fig.9,11). (Kulichkov,1996)

MAIN PERIOD. GENERAL DURATION OF INFRASONIC SIGNALS FROM SMALL ENERGY EXPLOSIONS.

The main period of the "head" of stratospheric acoustic arrivals recorded in the audibility region corresponds to explosion energy. In this case, the characteristic period of arrival "tail" is determined by diffraction effects due to turbulent inhomogeneities in the middle atmosphere.

The main period of thermospheric arrivals also corresponds to explosion energy. At slightly oblique propagation (turning height is 115 km and path length is more than 500 km), the main period of thermospheric arrivals substantially varies due to the combination of the diffractive effects. (Fig.12)

The general duration of recorded acoustic arrivals from small energy explosions is mainly determined from the diffractive effects due to the presence of turbulent structures in the middle atmosphere (Fig 13).

The presence of a quasi-continuous component within the range between 0.5 and 2 Hz is noted for all the types of acoustic arrivals (stratospheric, mesospheric, and thermospheric).(see Figures)

EFFECTS OF CROSS WIND.

For acoustic signals propagating along the direction of the predominant stratospheric wind, only slight variations are observed in the measured azimuth of signal arrival. It makes sense to determine the azimuth of signal arrival for a high-frequency component of the signal spectrum (Fig.14).

CONCLUSIONS.

The fine inhomogeneous structure of the atmosphere substantially affects the parameters of infrasonic signals at great distances from small-energy explosions. Therefore the infrasonic monitoring of such explosions is a matter of some difficulty because of the frequency, amplitude and duration of infrasonic signals change essentially.

On the other hand, the presence of the atmospheric fine inhomogeneous structure opens some additional prospects in developing the methods of infrasonic monitoring. There appears a possibility to record infrasonic signals in the region of a geometric shadow from sources. Due to diffraction, the duration of recorded signals increases, and a quasi-periodic component appears in a frequency band between 0.5 and 2 Hz. All this facilitates the detection of infrasonic signals from small-energy explosions and their further analysis.

In developing the methods of infrasonic monitoring of small- energy explosions, one should take into account the diffraction effects caused by the influence of fine turbulent structures in the middle atmosphere on infrasonic signals at long distances from explosions. When choosing a spatial scale for the net-work of acoustic microphones, one should take into account the characteristic values of the vertical scales of turbulent structures in the middle atmosphere.

REFERENCES

G.A.Bush, YE.A.Ivanov, S.N.Kulichkov,And M.V.Pedanov. Estimation of the Characteristics of a Pulsed Ground Source by Remote Acoustic Techniques. IZVESTIYA Academy of Sciences, USSR,Atmospheric and Ocean Physics,1989, V.25, No.11, p.p.861-866. (in English).

G.A.Bush, YE.A.Ivanov, S.N.Kulichkov, and M.V.Pedanov. Some results of Recording Acoustic Signals from High-Altitude Explosions. IZVESTIYA Academy of Sciences ,RUSSIA, Atmospheric and Ocean Physics,1997, V.33, No.1, p.p.59-63.(in English).

S.N.Kulichkov.Long-Range Propagation of Sound in the Atmosphere,A Review. IZVESTIYA Academy of Sciences,USSR, Atmospheric and Ocean Physics, 1992, V.28, No.4, p.p.253-269 (in English).

S.N.Kulichkov. On Possibilities of Acoustic Method to Sound Turbulence in the Middle Atmosphere. Proceed.8th Int.Symp. on Acoustic Remote Sensing and Associated Techniques of the Atmosphere and Oceans. ISARS`96, 27-31 May,1996, Moscow,RUSSIA. G.65-G.74.

S.N.Kulichkov, A.I.Grachev, I.A.Sazonov. Long-Range Sound Propagation in the Atmosphere From Surface Small Energy Explosions. Ibid. p.p.4.1-4.6.

Figure 1. Samples of the acoustic records in the vicinity of the explosions of different types.
1- subsurface explosion (E~35 t); 2-surface explosion (E~50 kg);
3-air explosion (E~1 t);4 - surface explosion (E~260 t);
5- commercial subsurface explosion (E~2000 t);
6- commercial subsurface explosion (E~4000 t).

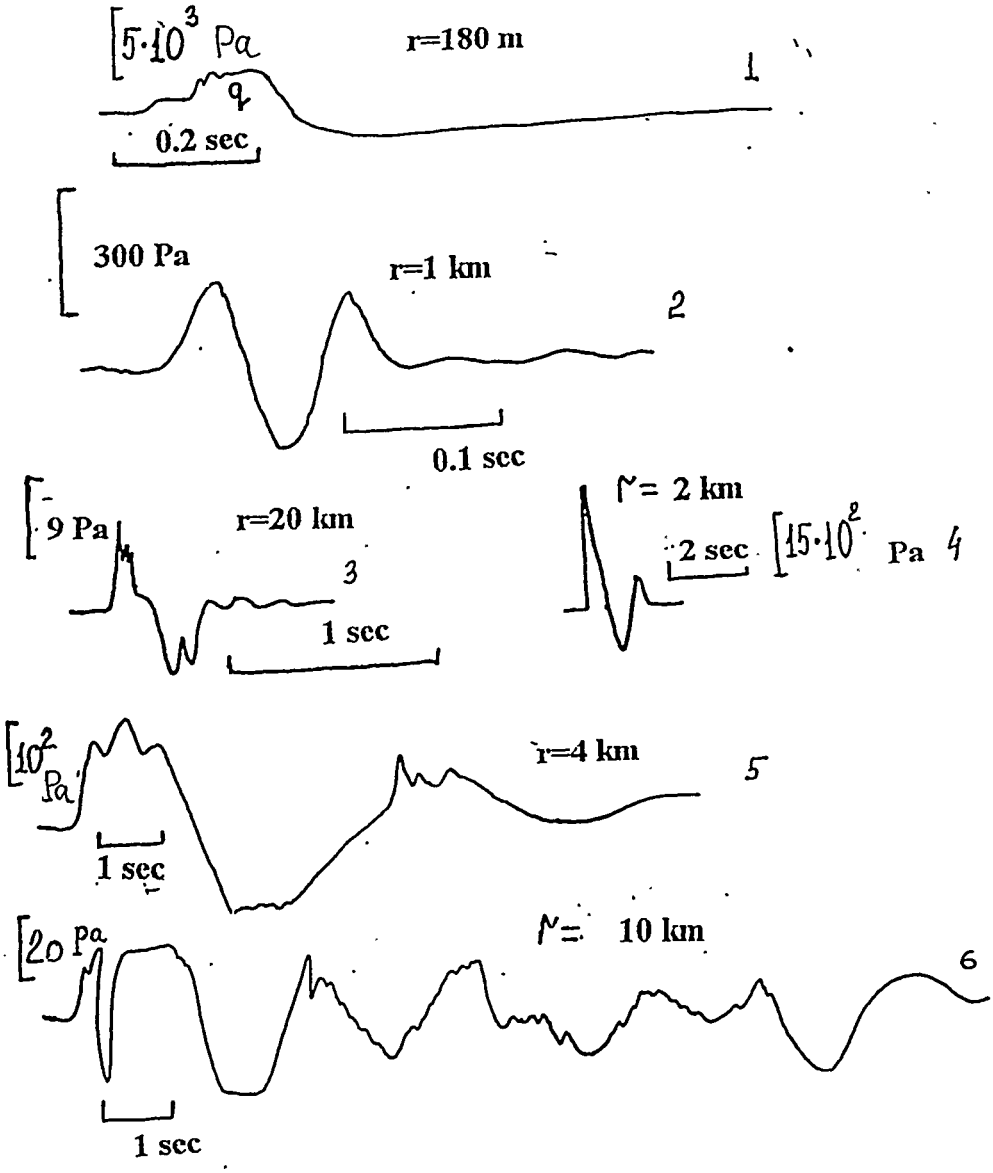

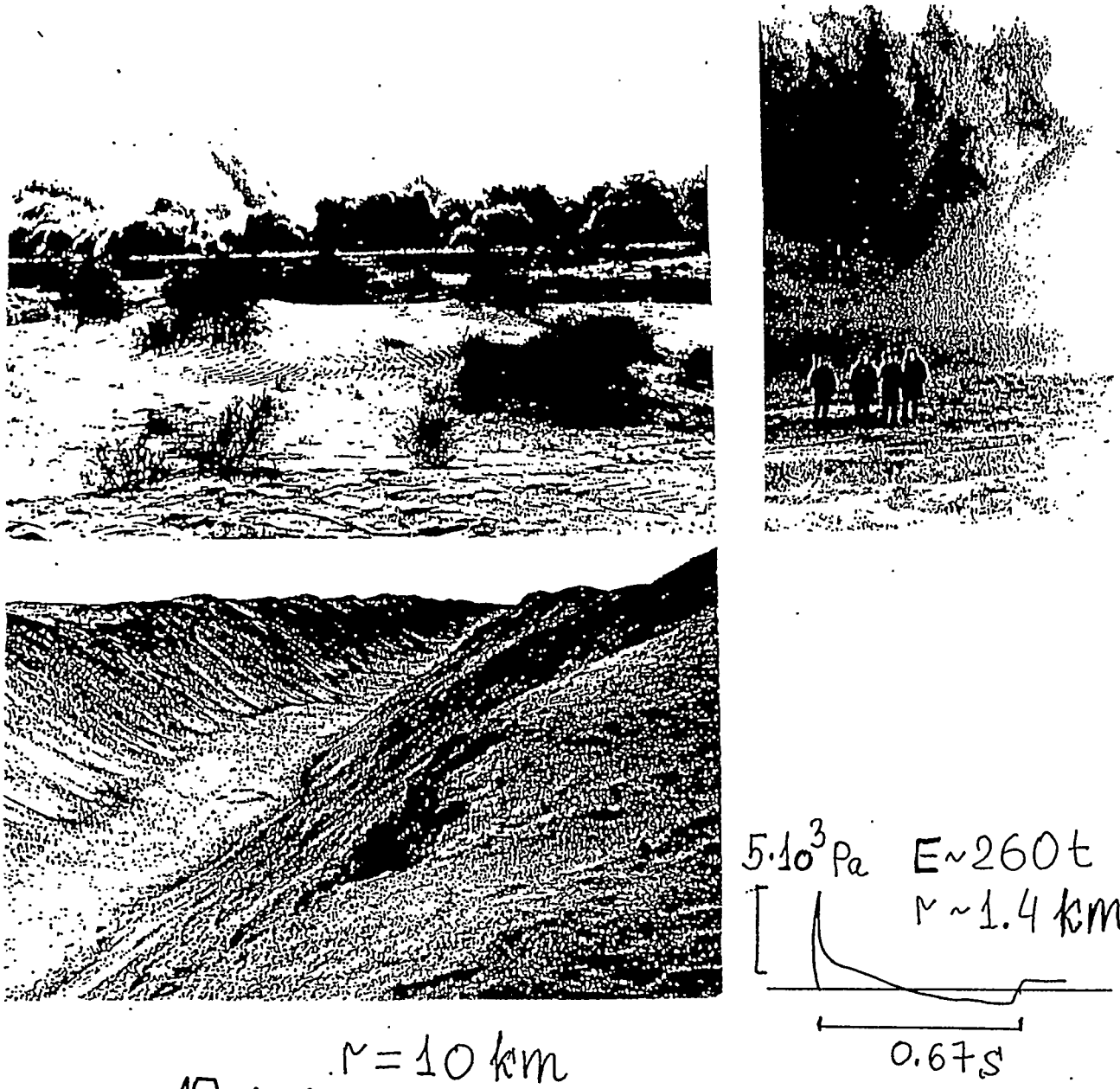

Figure 2. Photographs of a commercial subsurface explosion (L~ 4 km, depth h~15 m, E~4000 t) and a surface experimental explosion (E~260 t).

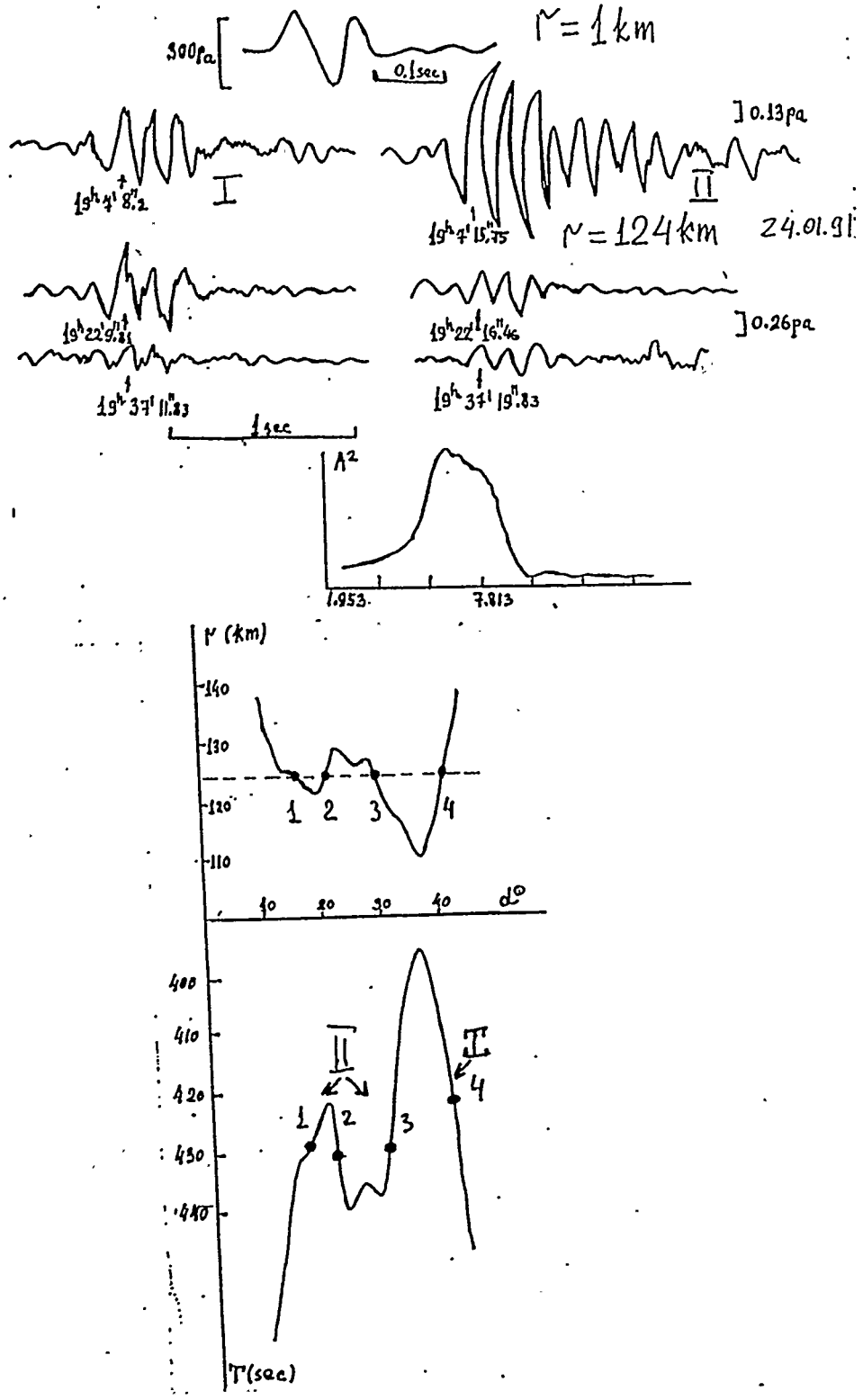

Figure 3. Acoustic records in the vicinity of a surface explosion (E~50 kg.) and at a distance of 124 km. Power spectrum. Results of trajectory calculations.

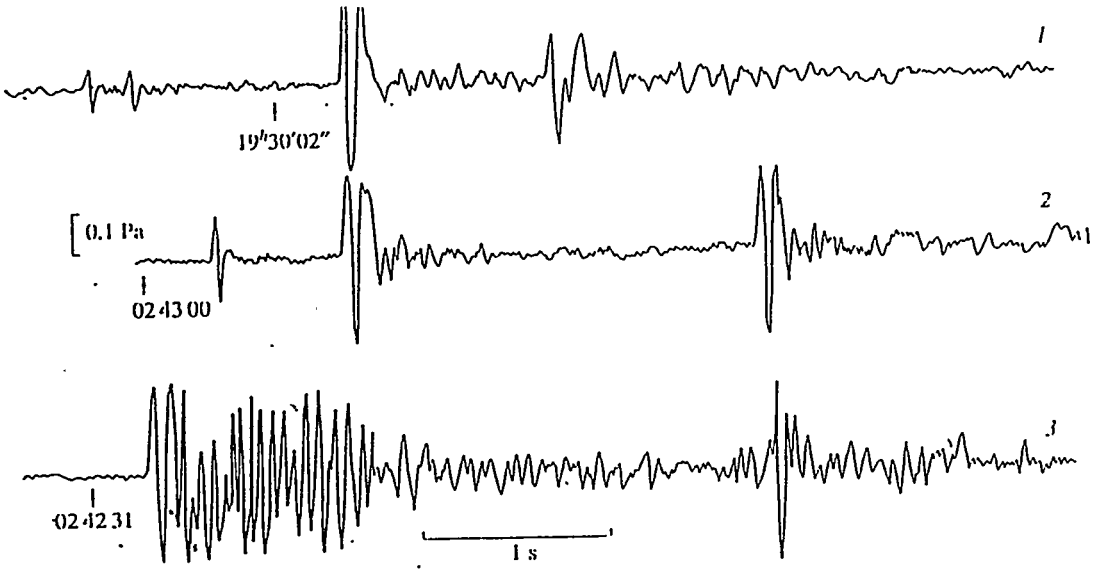

Figure 4. Surface acoustic records of the first arrivals of signals from the high-altitude explosions (*1*) on November 5, 1991 and (2) on November 6, 1991. (3) An acoustic signal from a meteor on November 6, 1991 (first arrival).

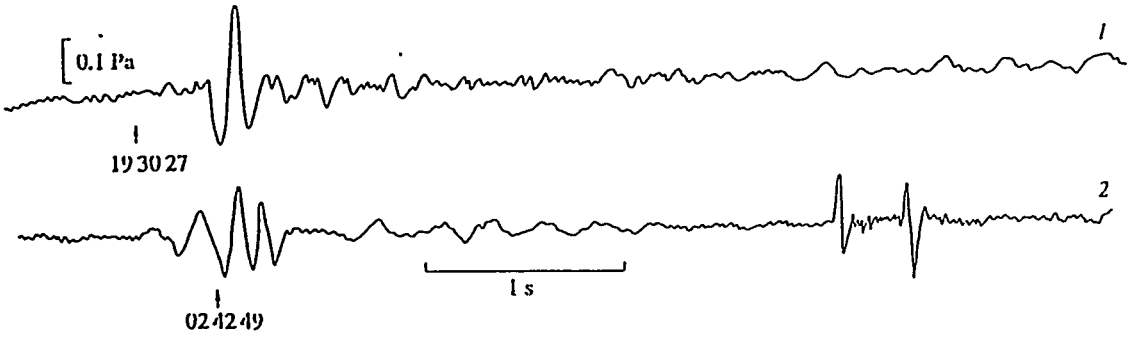

Surface acoustic records of the second arrivals of signals (*1*) from the high-altitude explosion on November 5, 1991 and (2) from a meteor on November 6, 1991.

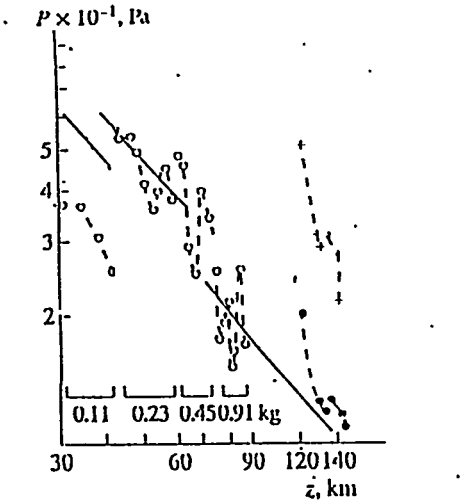

Figure 5. Amplitudes of acoustic signals, recorded at the earth's surface, from high-altitude explosions of different energy on the basis of the data of (○) [4] (up to the heights of 90 km) and (+) the present work (explosion heights 120–150 km). (●) The amplitude of acoustic pressure for explosions at heights above 120 km normalized by a multiplier $(E_0/E)^{-1/3}$, where E is the energy of explosion in kg TNT, $E_0 = 0.91$ kg TNT. The solid line specifies the semiempirical dependence $p(E, R) \sim 171.6(E_{kg})^{0.4}\ (R_{km})^{-1.2}$ proposed in [4] without taking into account molecular dissipation of

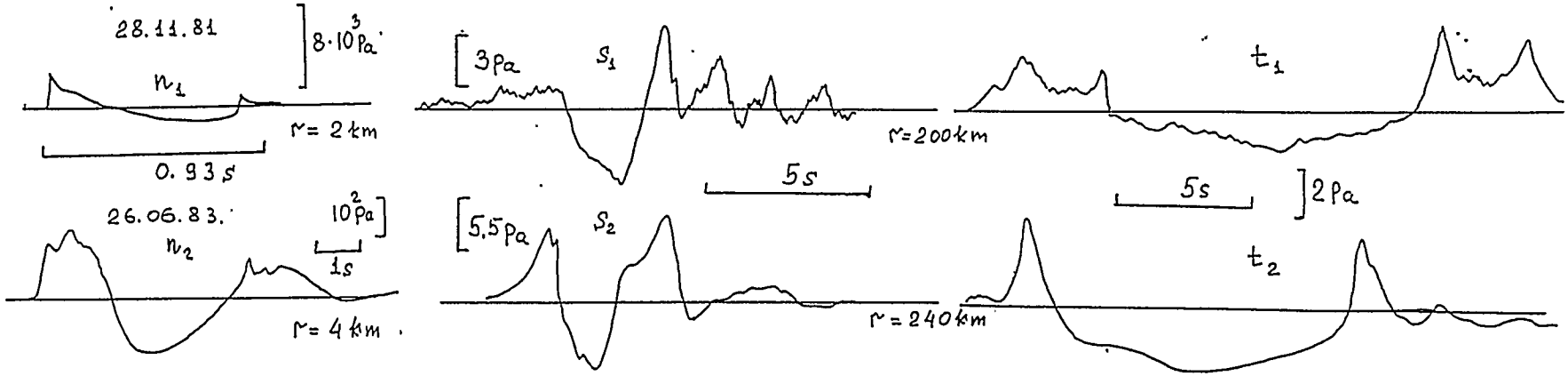

Figure 6. Results of the influence of nonlinear effects on infrasonic arrivals from a surface explosion (E~260t - 1) and a commercial subsurface exploson (E~2000 t - 2). n- records in the vicinity of explosions; s- stratospheric arrivals; t - thermospheric arrivals.

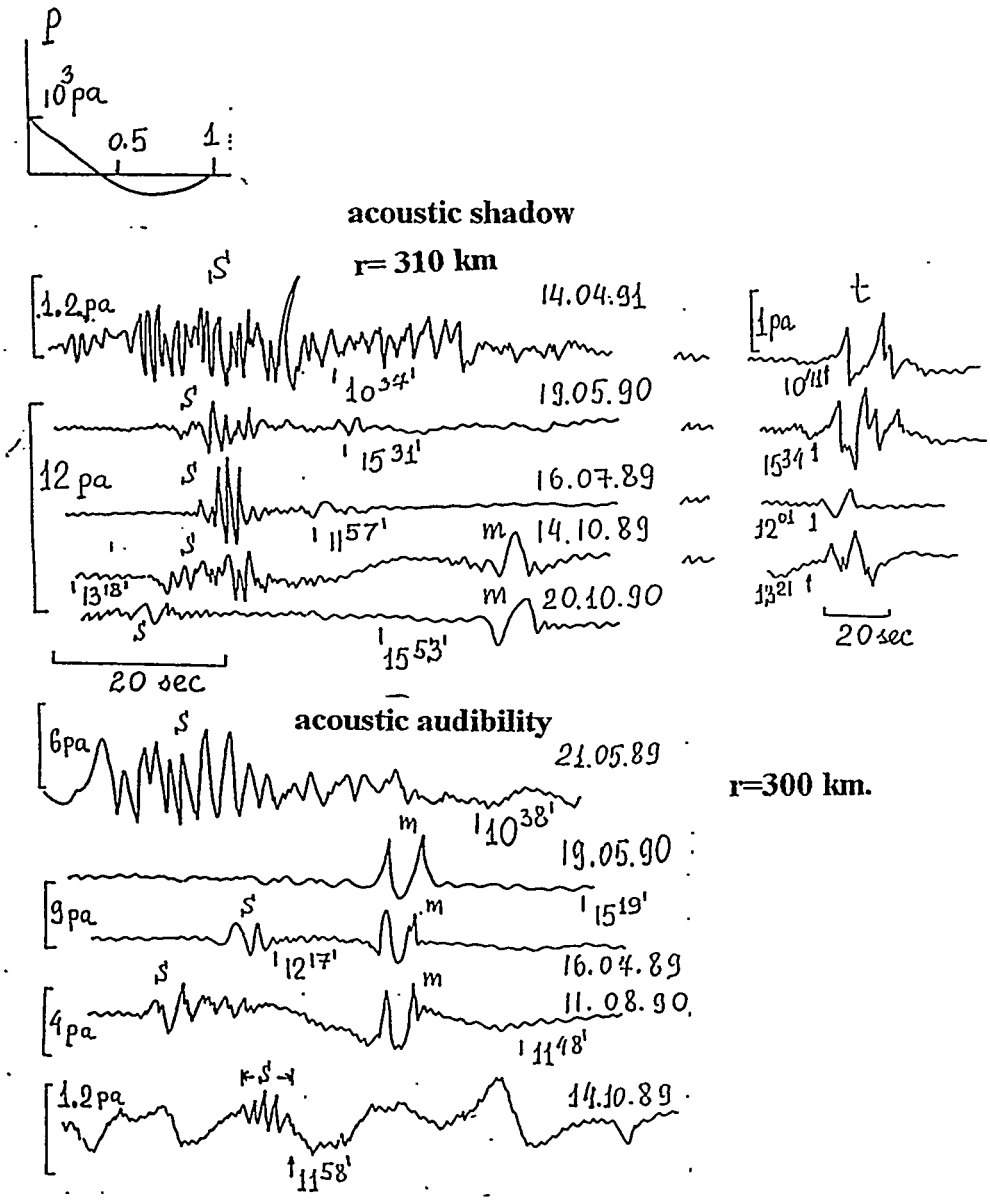

Figure 7. Samples of the acoustic records in the zones of acoustic shadow and acoustic audibility.
Stratospheric arrivals - s; Mesospheric arrivals - m ; Thermospheric arrivals - t .

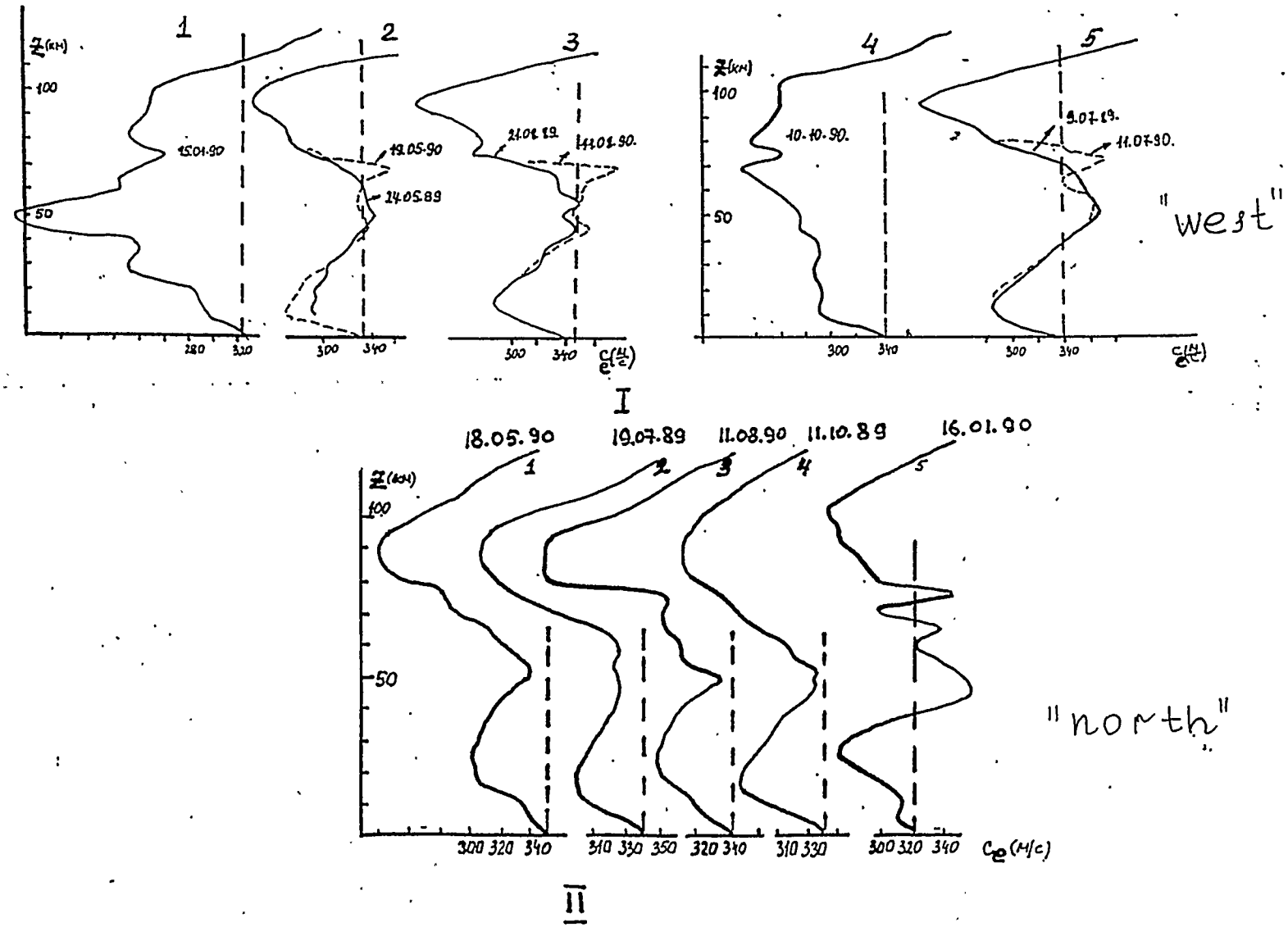

Figure 8. Samples of the profiles of effective sound velocities to the West and to the North from surface explosions.

Figure 9. Velocities of stratospheric (s); mesospheric (m) and thermospheric arrivals (t)

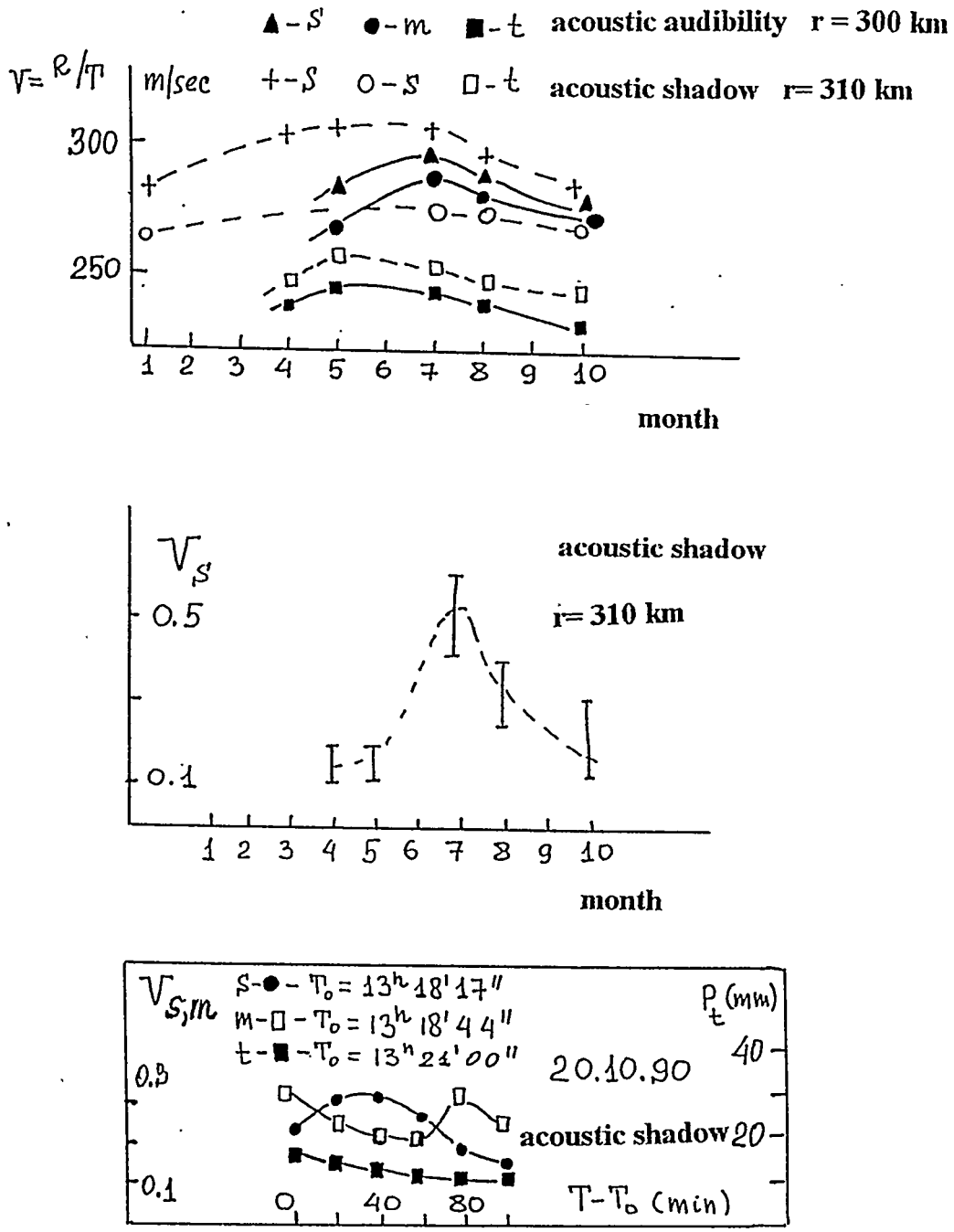

Interseasonal and daily variations of the coefficients of partial reflection of acoustic signals from turbulent irregularities of the acoustic refractive index in the middle atmosphere.

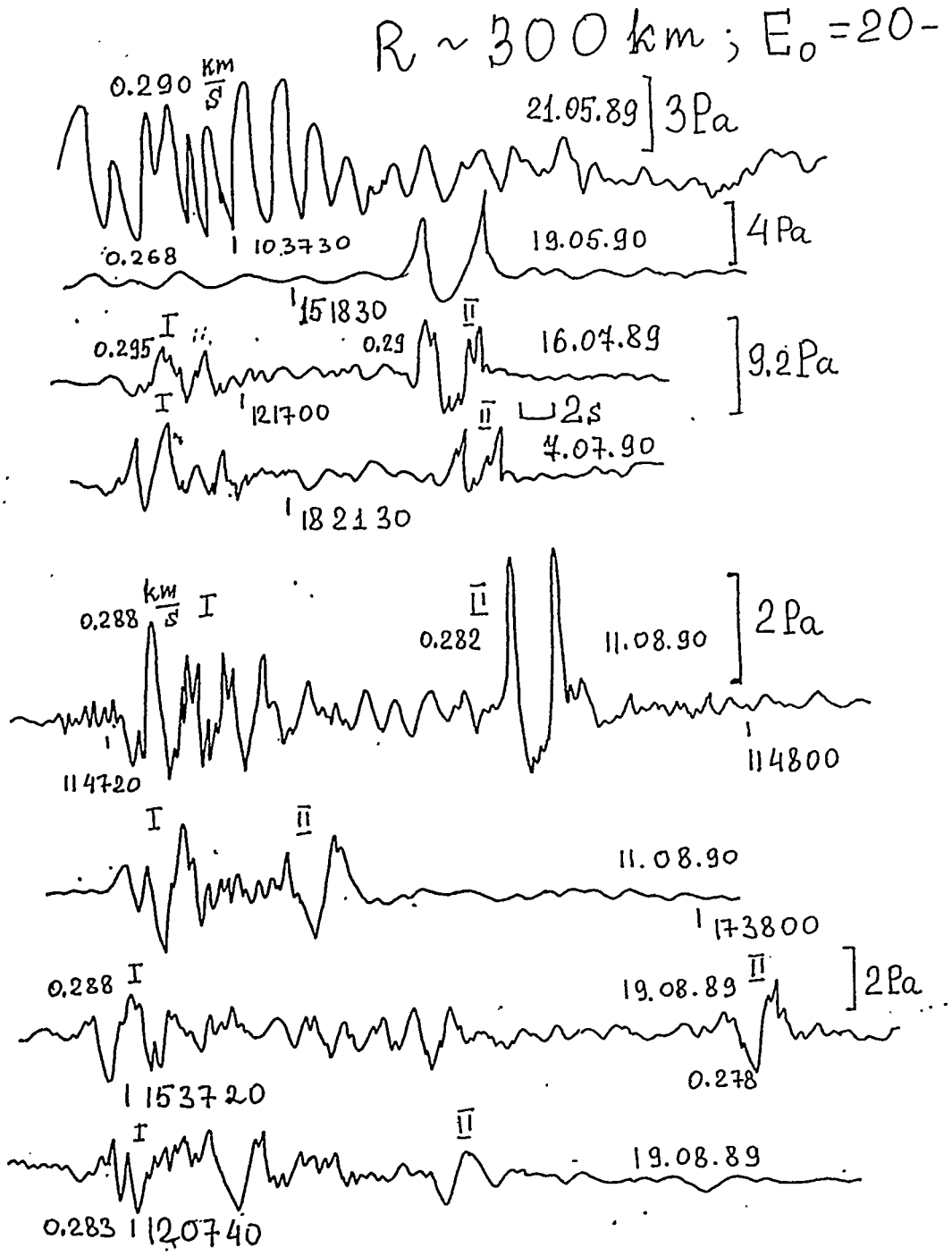

Figure 10. Interannual and interseasonal daily variations of stratospheric arrivals observed in the zone of audibility to the West from surface explosions with an energy of 20-70 t.

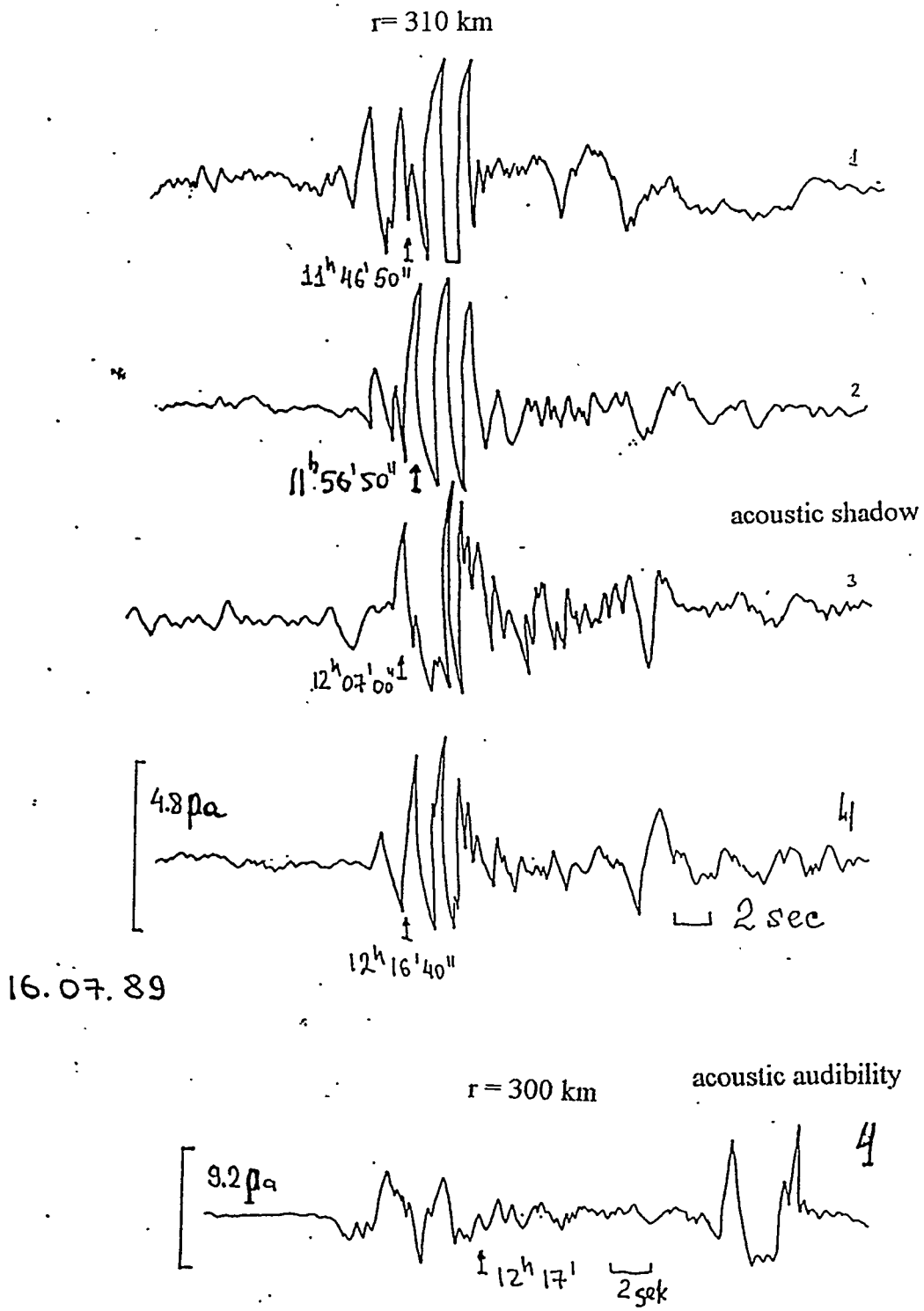

Figure 11. Samples of the acoustic records obtained in the zones of silence and audibility for the run of explosions with an energy of 20-70 t.

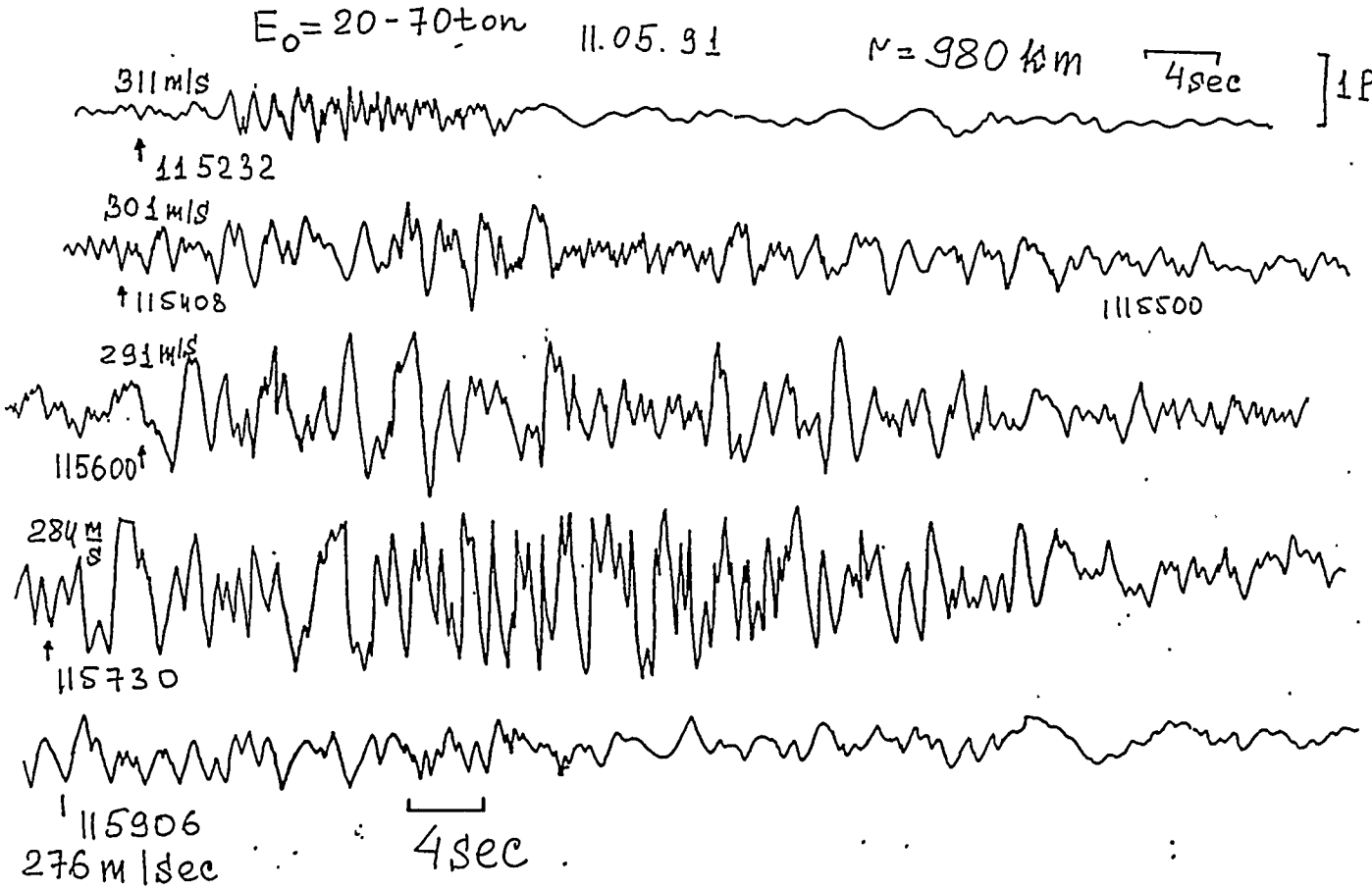

Figure 12 . Samples of the acoustic arrivals at a distance of 980 km from surface explosion with an energy between of 20-70 t.

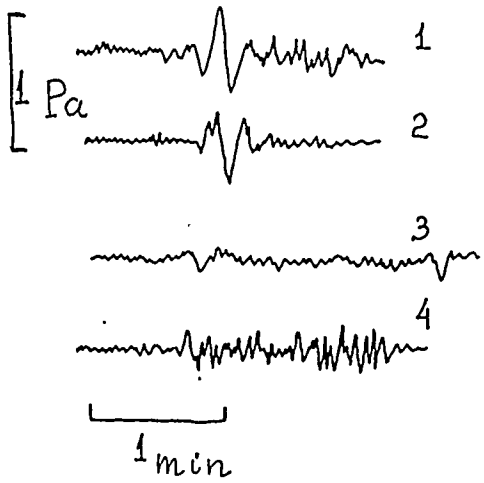

Types of thermospheric arrivals from volcano Sakura-Jima (M.Tahira. J.Met.Soc.Jap. 1988,66,1,17-26)

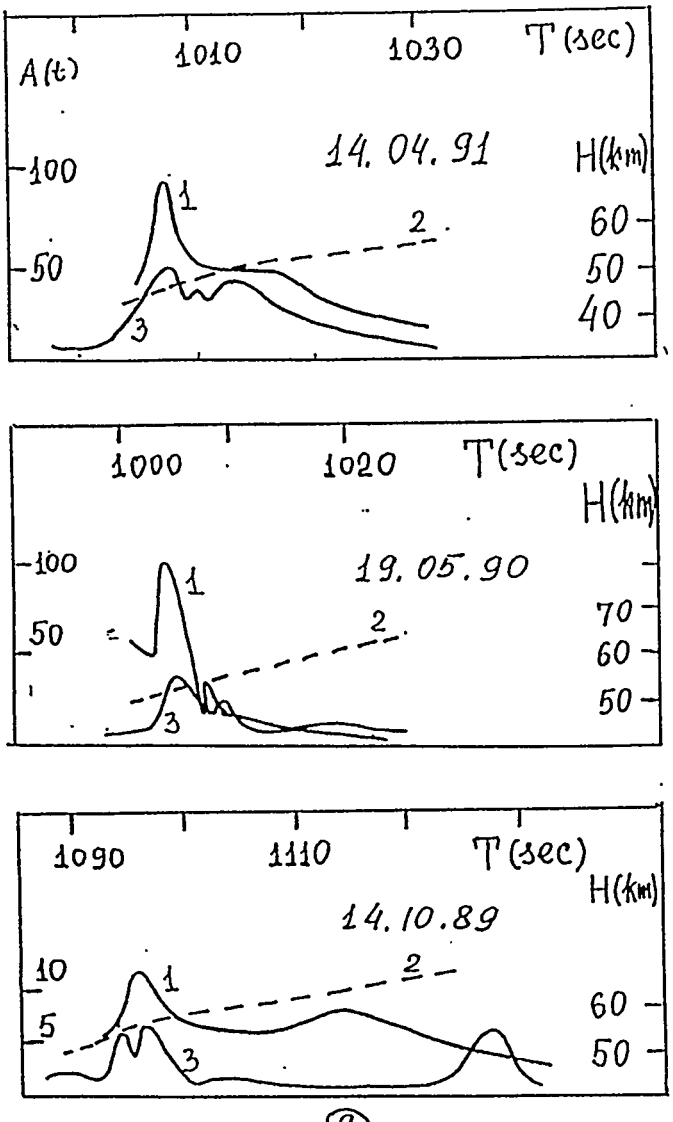

$A(t)=f^{1/2}(\cos\theta)^{-2.31}$

Figure 13.Values of A(t) (curve 1) for sound rays reaching the heights H of partial reflection (curve 2). Double amplitudes 2p(t) of recorded infrasound signals from explosion with an energy between 20-70 t.
Example of a profile of $\partial c/\partial z$ from experimental data.

Figure 14. Azimuths of the similar explosions (as function of spectral period) determined for different seasons from acoustic records in the zone of audibility at a distance of 300 km.

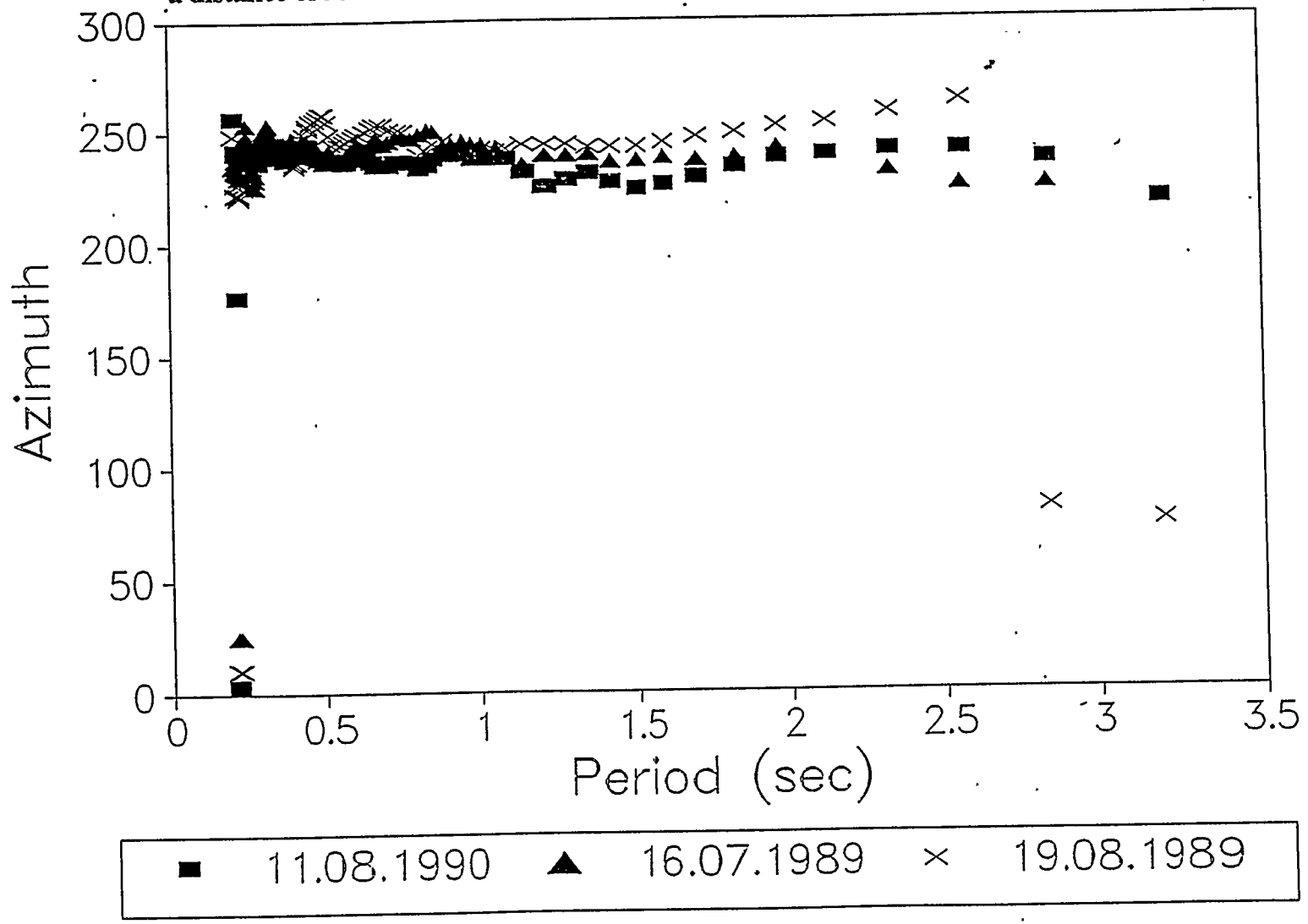

INFRASOUND MONITORING SYSTEM OF NUCLEAR EXPLOSION IN THE ATMOSPHERE

Jin Lai XIE

Institute of Acoustics
Chinese Academy of Sciences
Beijing 100080, China

Zhao Hua XIE

Computer Network Information Center
Chinese Academy of Sciences
Beijing 100080, China

Infrasound Program has been operating since 1965, making routine measurements of low frequency atmospheric pressure waves in Institute of Acoustics, Chinese Academy of Sciences. Infrasound monitoring is a well-established method for detecting and locating nuclear explosions in the atmosphere, hailstorm, earthquake and so on. A properly designed system provides anti-jamming probe, data acquisition, dynamic spectrum and cross analysis, real-time display, measurement velocity, location, indication of yield in real--time, capabilities of the unique event identification, classification events, and data transfer. The performance specifications of the equipment for detecting and recording infrasonic waves, and some typical results we obtained infrasonic waves from nuclear explosions would be shown. We hope that it will make as good as possible for monitoring nuclear test in comprehensive nuclear test ban treaty.

INFRASOUND MONITORING SYSTEM OF NUCLEAR EXPLOSION IN THE ATMOSPHERE *

XIE Jin Lai

(Institute of Acoustics, Chinese Academy of Sciences, Bejing 100080)

XIE Zhaohua

(Computer Network Information Center, Chinese Academy of Sciences, Beijing 100080)

ABSTRACT Infrasound monitoring is a well-established method for detecting and locating nuclear explosions in the atmosphere, hailstorm, earthquake and so on. A properly designed system provides anti-jamming probe, data acquisition, dynamic spectrum, cross-correlation analysis, measurement velocity, location, indication of yield in real–time, capabilities of the unique event identification, classification events, and data transfer. We, Institute of Acoustics, Chinese Academy of Sciences, provide performance specifications for the necessary equipment. It will make as well as possible for monitoring nuclear test in comprehensive nuclear test ban treaty.

1 INTRODUCTION

In the fifties to early seventies, there were frequent nuclear tests in the atmosphere, by means of our equipment we can determine when and where these tests being carried out and the equivalence of the nuclear bombs. Some typical recorded waveforms show the distinct differences at different distances (hundreds of kilometers) are discontinuous and separate obviously into three groups with increasing amplitudes.

This kind of discontinuity is featured for explosive waves. The dominant components are "high frequencies" with periods ranging from 2 to 10 sec. The recorded waveforms at moderate distance (about two thousand km) are shared equally by "high frequencies" with average period about 1 min and "low frequencies" with period about 6 min. The waveforms at far distance (about 10 thousand km, concerning the French nuclear test held in South Pacific in 1968) show that high frequencies all die out but only low frequencies

* The project is supported by National Natural Science Foundation of China

with periods about 120 min remain.

2 Equipment for detecting and recording infrasonic waves:

(1) Block diagram of complete system as shown Fig. 1

Our self-devised equipment has the advantages in simplicity and economy, in the easiness of operation and maintenance, and also in the intuition of results. The complete system consists of anti-interference receivers, digital wave-shape recorder and devices for signal transmission, processing and reserving.

(2) Transducers

The condenser type has the advantages in small volume, high sensitivity (30 millivolts per Pascal in general) and wide frequency responses (with high responses in low frequency range and uniform response characteristics within a wider frequency range; the frequency response characteristics can be adjusted by the acoustic compliance of the diaphragm), and thus suits to receive infrasonic waves with periods 0.1–200 sec. (Measurement range as 0.1–1000 sec.)

(3) Array

These microphones are seldom used singly, but often used to construct an array, or in equivalence, to be attached with some auxiliary devices. There are two purposes for doing so: for anti–jamming and for direction–finding or source–locating.

Direction-finding or source-locating array: One cannot determine the direction of coming wave by using a single microphone, but can do so by three microphones. If one wants to locate the wave source, however, at least three microphones are needed. The basic construction for this goal is triangular array.

From the time difference between the arrival of waves at any two elements of such an array, the arrival angle of a wave can be determined, and two such angles can determine the location of source (the intersection of two corresponding lines). Generally, the wave velocity is unknown, so at least two sets of such combination are required in order to eliminate the wave velocity, and at the same time, the unknown velocity can thus be determined also.

The actual array adopted in our field measurements is in the form of multi-element array in orthogonal lines.

Such arrays are designed to study the accuracy of the triangular array and the random characteristics of infrasonic wave propagation. Using this large-scale array, one can calculate the deflection obtained from various triangular arrays of different scales in detecting the same source.

3 NEW CONSTRUCTION

This system is included as followings:

3.1 Hardware configuration:

(1) CSH-5 type condenser infrasound microphone, sensibility 0.01 Pa, period range 0.1 $\sim$ 200 s, dynamic range 80 dB;

(2) Anti-jamming array;

(3) Pentium 586/166 MHz PC, memory 16 MB, harddisk 2 GB, Floppy 1.44 MB, moduration/demoduration 2.88 Mbps;

(4) 53 cm display;

(5) A/D and D/A data converter card;

(6) Chart recorder.

3.2 Software configuration and data processing as shown fig. 2

(1) Data acquisition program; (2) Dynamic spectrum analysis; (3) Real-time display; (4) Dynamic spectra represent; (5) Data compress; (6) Front grand and back; (7) Waveform display; (8) Measurement velocity; (9) Locating; (10) Windows95; (11) Matlab.

4 NETWORK DESIGN

The density of the network determines its detection and location capability. A single array station can provide information on the direction of the explosion as seen from the detector site, but only a rough estimate of range. Detection by two array stations will give a rough position, and detection by three or more array stations provides high accuracy location. Three infrasound stations have been established in China, such as Beijing, Kung Ming

and Hang Zhou city.

5 INFRASOUND NOISE FIELD AND ANTI–JAMMING ARRAY

Infrasound noise field investigation has been made and anti–jamming arrays have been used in Beijing Infrasound Station.

Since the infrasonic signals are quite weak in some cases but the background noise is relatively strong, such that the former are frequently submerged. The noises come mainly from the pressure fluctuations due to wind or local turbulences. The common feature of these disturbances lies in the fact that their correlation scales are much smaller compared with the acoustic wavelengths. Therefore the signal-to-noise ratio can be raised by technique of space filtering on the basis of time filtering. Two forms of anti–jamming receiving equipment are developed basing on this idea: long tube with uniform cross-section as a "line-series microphone" and "circular" of microphones.

We have designed four specifications of long tube with different lengths (110, 200 and 400 meters respectively). different inner radii (25 and 38mm) and different spacings between adjacent inlet ports (2, 3 and 4 meters). The selection of impedance* of the inlet ports (nylon or syringe needles) is important, its optimal value can be selected in accordance with the period of the signal to be received. A good selection will guarantee the signal to pass smoothly but cut out the high frequency noise rapidly. The selection of the spacing between adjacent inlet ports is also a key point. In doing this, the correlation under different wind velocities must be taken into consideration. The total length of array is limited by the high frequency components of the signal. In general, the length ought to be shorter than the half wavelength of the high frequency component. Thus the long tube array is mainly available for wind noise of shorter periods. A series of experiments have been carried out with these arrays. We received infrasonic waves in atmosphere by two transducers simultaneously. They are situated close to each other, one is connected to a pipe array and the other one is not. Some typical results are shown here.

* $R=8\eta/\pi r^4$ (η= air viscosity; l=effective length; r=inner radius of inlet port)

As can be see, the effect of array is obvious. The periods of the infrasonic signal recorded are ranging between 3–30 sec. and the amplitudes between 0.2–5 Pa. As for the wind with velocity 6–7 m/s, the fluctuation has been reduced from 3 Pa to 0.3 Pa after passing through the array.

We have designed also a circular infrasonic array with eighteen microphones, which are spread uniformly along three concentric rings, and an extra microphone used for comparing with the array is situated at the center.

A great number of experiments had been carried out at various noise levels caused by various wind speeds under different weather conditions to verify the anti-jamming effect of the array. The experimental results show that the reduction of wind noise is quite obvious. An example for moderate wind speed is shown.

REFERENCES

[1] Documents of Conference on Disarmament: CD/NTB/WP. 156 (1994, 8, 16); 176 (1994, 8, 24); 181 (1994, 9, 6); 184 (1994, 11, 30); 212 (1995, 2, 13); 224 (1995, 3, 16); 283 (1995, 12, 15).

[2] Bedard A.J. Jr. and Greene, G.E., Case study using arrays of infrasonic microphones to detect and locate meteors and meteorites, *J. Acoust. Soc. Am.*, 1981, **69**(5): 1277–1279.

[3] XIE Jin Lai, ACTA ACUSTICA, 1991, **16**(3): 230–234; *Chinese Journal of Acoustics*, 1991, **10**: 311–316.

[4] XIE Jin Lai, ACTA ACUSTICA, 1986, **11**(5): 276–286; *Chinese Journal of Acoustics*, 1986, **5**: 271–279.

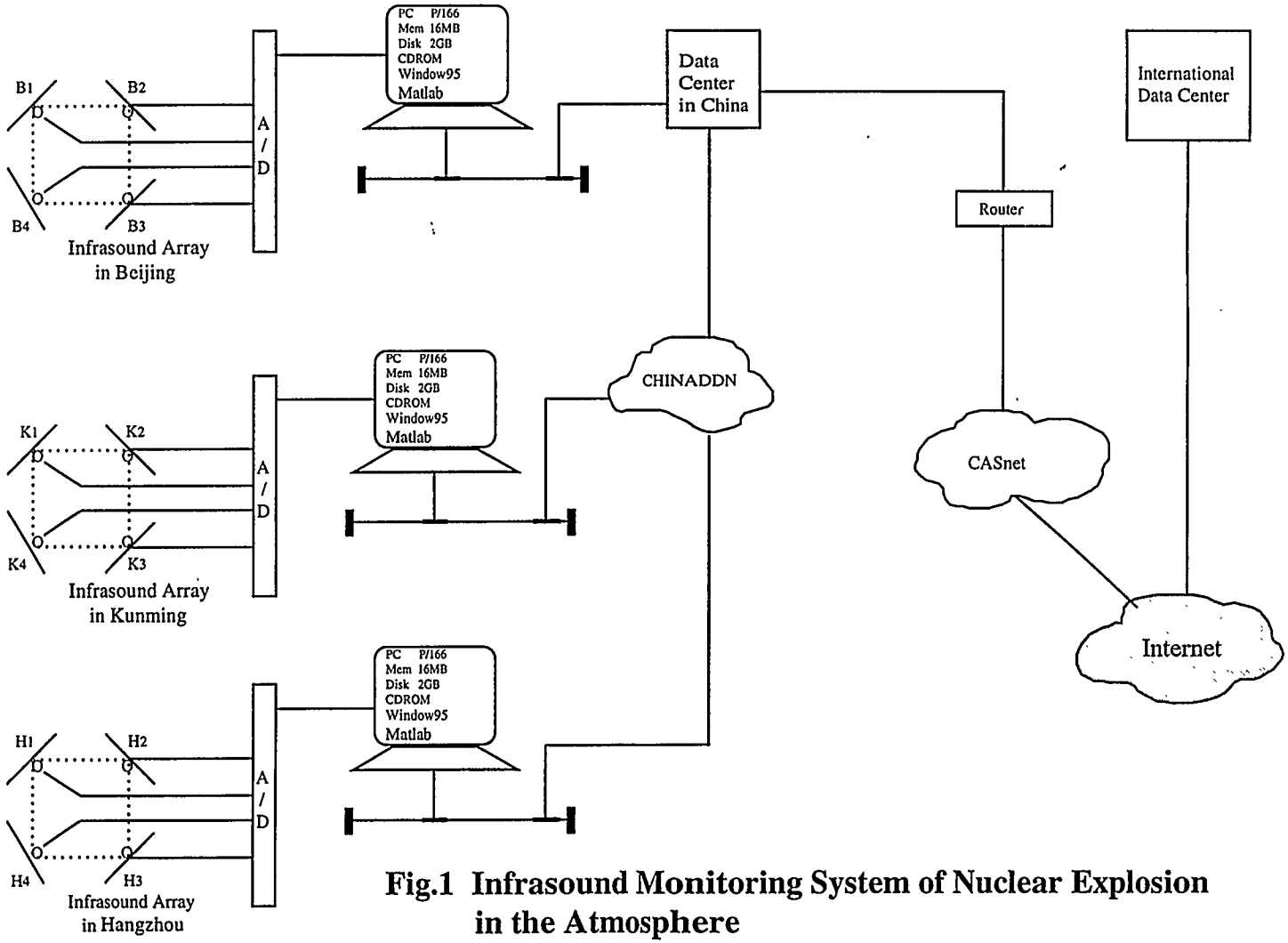

Fig.1 Infrasound Monitoring System of Nuclear Explosion in the Atmosphere

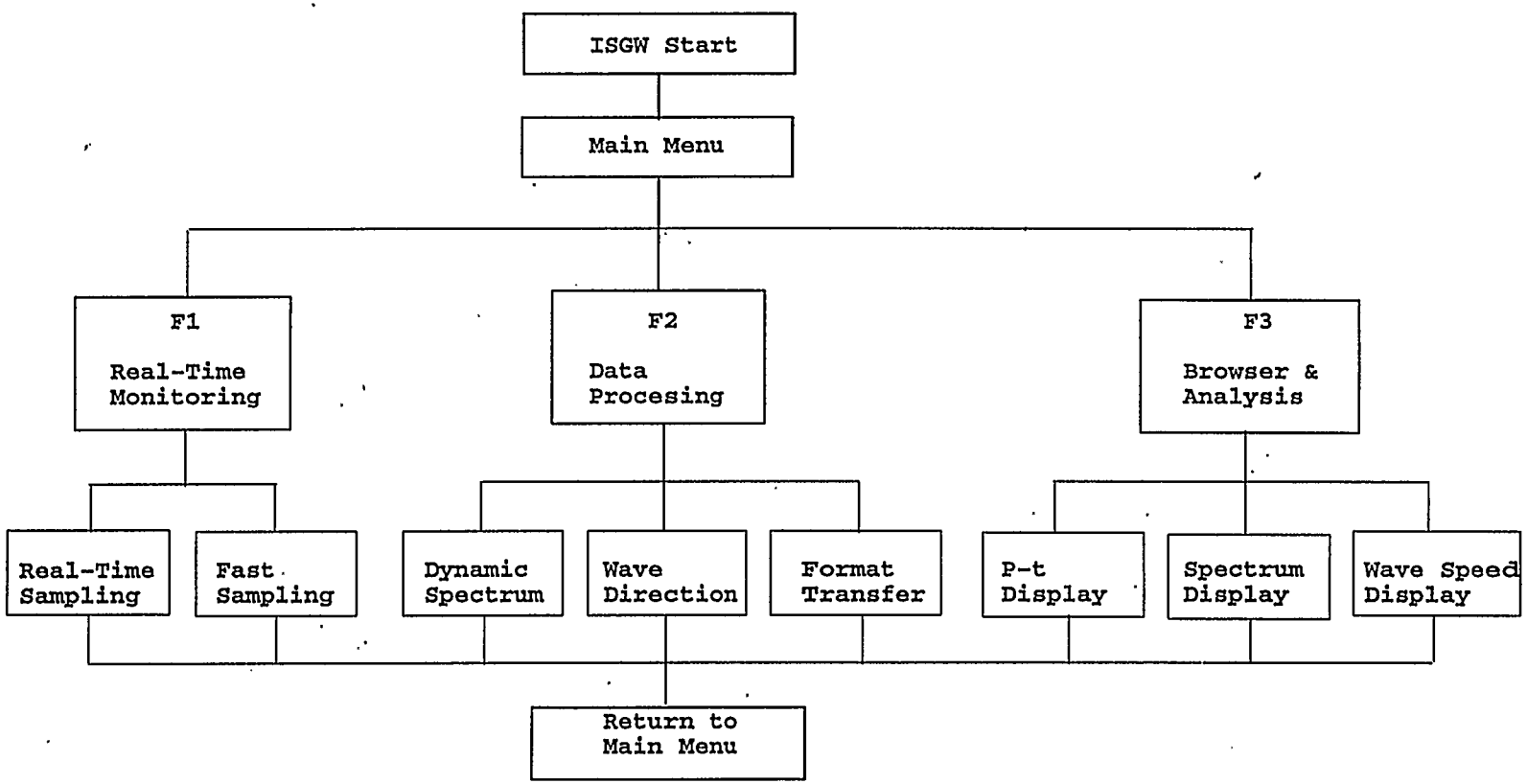

Fig.2 Infrasound Program Diagram of Nuclear Explosion in the Atmosphere

DEVELOPMENT OF A PROTOTYPE INFRASOUND SYSTEM

Rod Whitaker

Los Alamos National Laboratory

Dale Breding

Sandia National laboratories
Sponsored by DOE

Under Department of Energy sponsorship, Sandia and Los Alamos National Laboratories cooperated to develop a prototype infrasonic array that could be used as part of the International Monitoring System. The USG or foreign countries could procure these commercially available systems based on this prototype to fulfill their Comprehensive Test Ban Treaty (CTBT) obligations. The prototype is a four-element array in a triangular layout as recommended in CD/NTB/WP.224 with an element at each corner and one in the center. The initial array spacing will be 1 km.

The prototype infrasound system has the following objectives:

- Provide a prototype that reliably acquires and transmits near real-time infrasonic data to facilitate the rapid location and identification of atmospheric events.
- Provide documentation that could be used by the US and foreign countries to procure infrasound systems commercially to fulfill their CTBT responsibilities.

Infrasonic monitoring is an effective, low cost technology for detecting atmospheric explosions. The low frequency components of explosion signals propagate to long ranges (few thousand kilometers) where they can be detected with an array of sensors.

LANL's expertise in Infrasound systems and phenomenology when combined with Sandia's expertise in providing verification quality systems for treaty monitoring make an excellent team to provide the prototype infrasound sensor system.

By September 1997, we will have procured, integrated, evaluated and documented the Prototype Infrasound System. Final documentation will include a system requirements document, an evaluation report and a hardware design document. The hardware design document will describe the various hardware components used in the Infrasound Prototype and their interrelationships. Final versions of all documents are available from the bibliography on the CTBT R&D web site, URL: http://www.ctbt.rnd.doe.gov/.

Infrasound Workshop

Development of a Prototype Infrasound System

Rod Whitaker
Dale Breding

Department of Energy
Los Alamos

Infrasound Workshop
August 25-28, 1997

Collaborators

Rod Whitaker
Doug ReVelle
Tom Armstrong
LANL

Dale Breding
Pat Fleming
Tim Draelos
Dick Kromer
SNL

Tom Sandoval
Bechtel NV

Tim McDonald
J&M Systems

Outline

- Objectives
- System Overview
- Prototype Status
- Prototype Evaluation
  - Sensor
  - Digitizer
  - Authenticator
  - System
- Summary and Recommendations

Infrasound Prototype Development Objectives

- Provide a prototype that reliably acquires and transmits near real-time infrasonic data to facilitate the rapid location and identification of atmospheric events
- Provide documentation that could be used by the US and foreign countries to procure infrasound systems commercially to fulfill their CTBT responsibilities

Introduction
Prototype Block Diagram

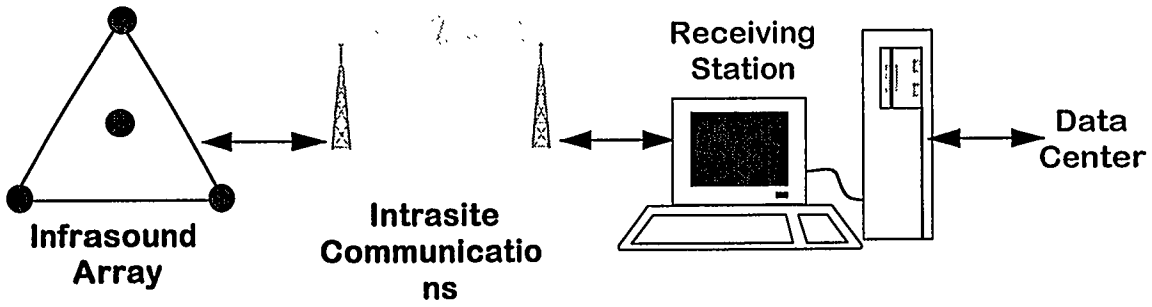

Introduction
Sensor Pictures

- Sensor has been re-packaged to accommodate the infrasound prototype data surety features

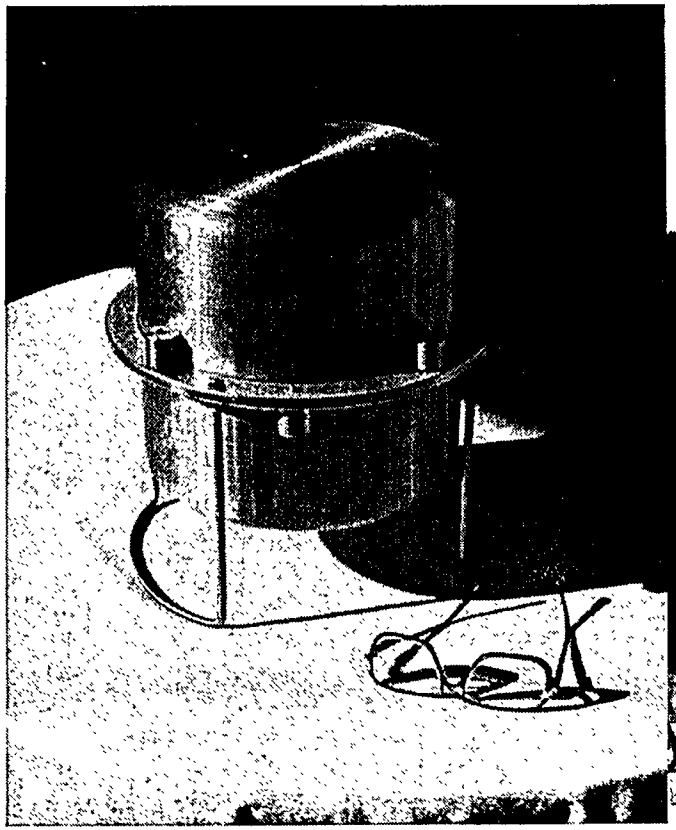

10" diameter

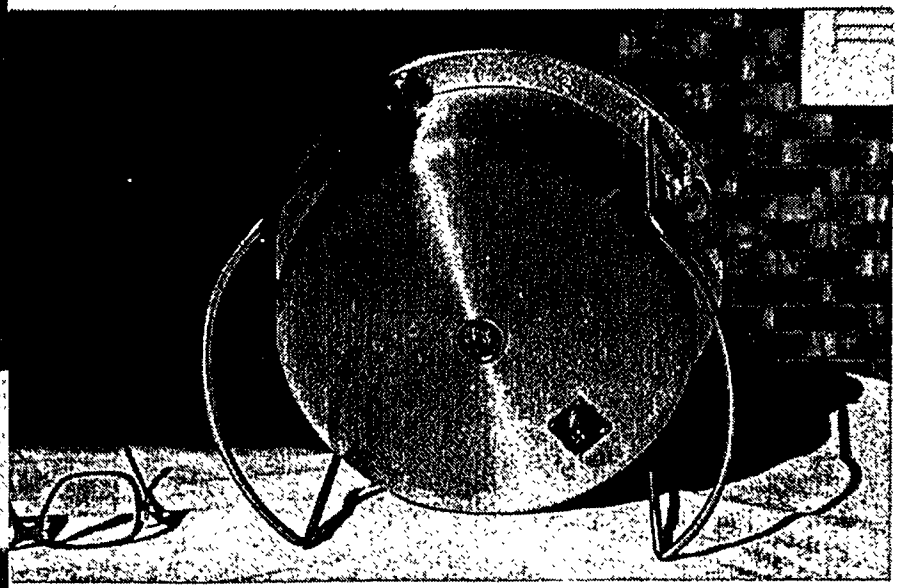

Introduction
Detailed Prototype Block Diagram

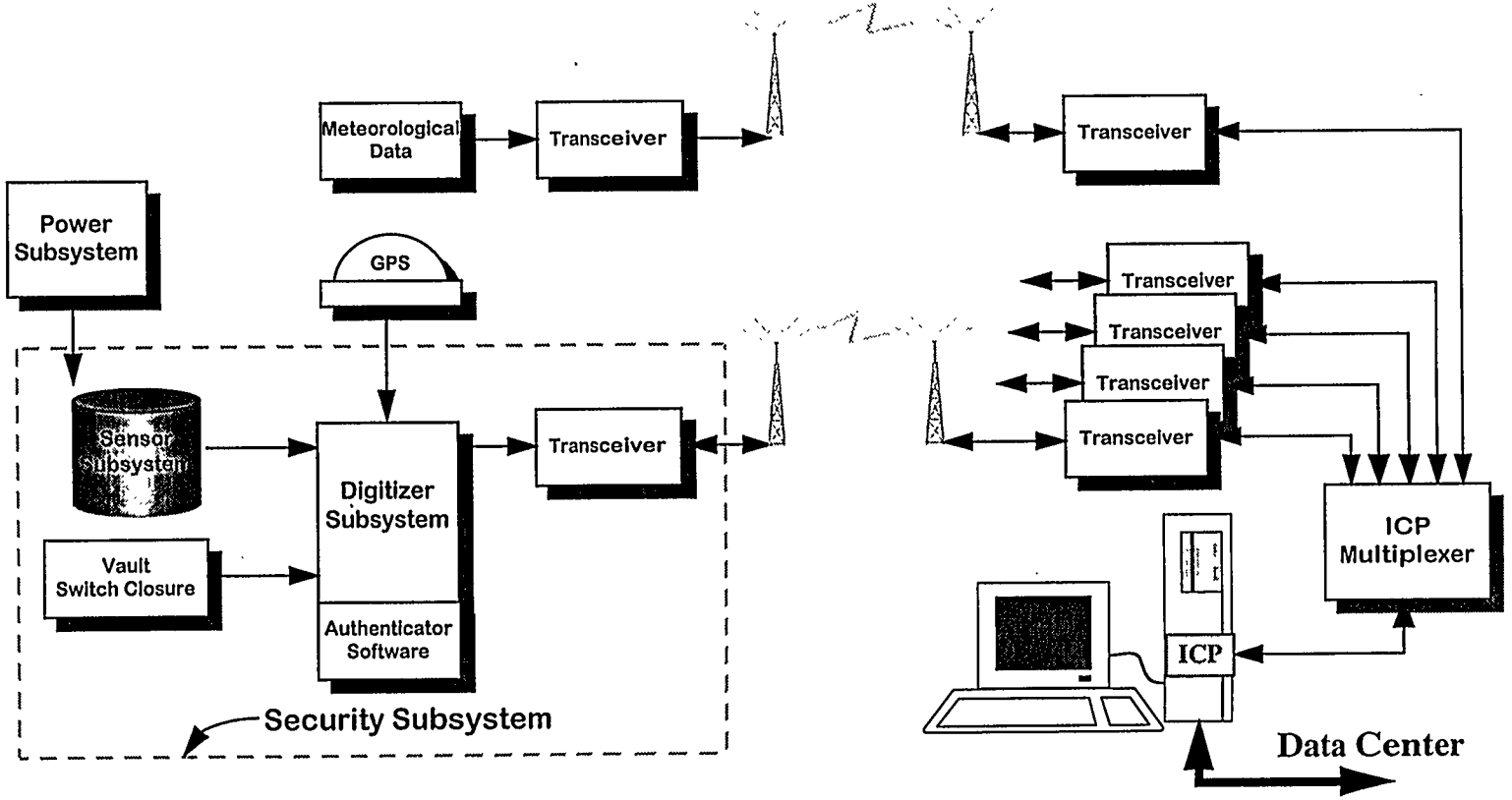

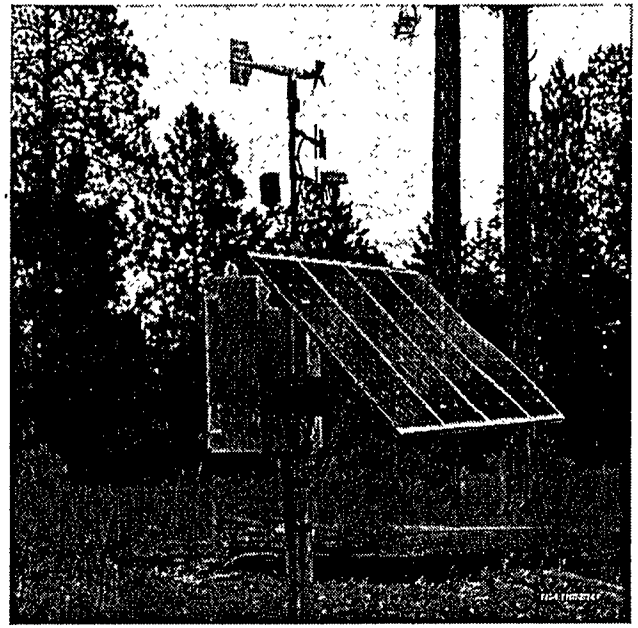

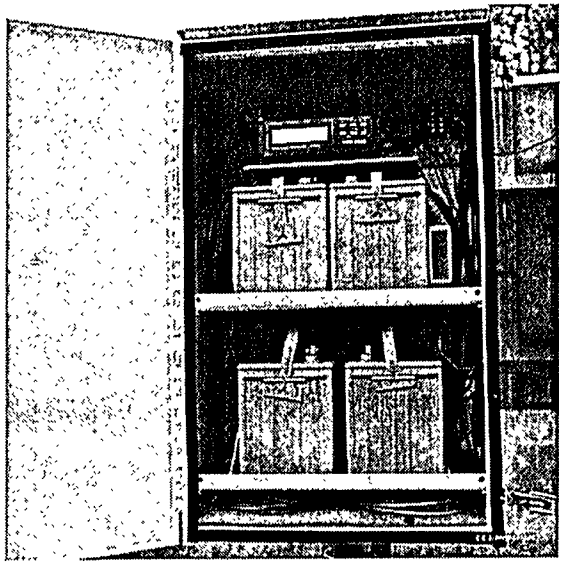

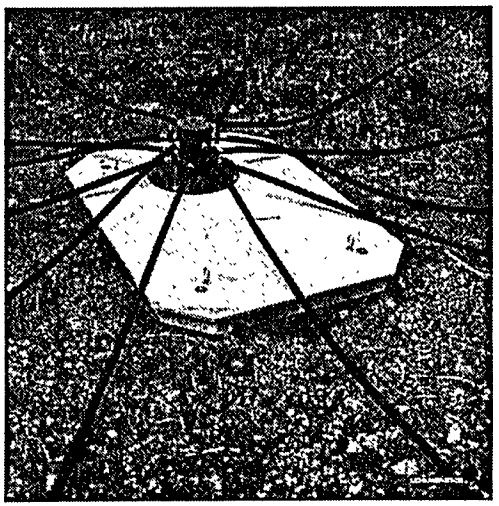

Above: Solar panels, battery box and weather station (for center only)

Upper right: Interior of battery box

Lower right: Manifold, hoses and box top

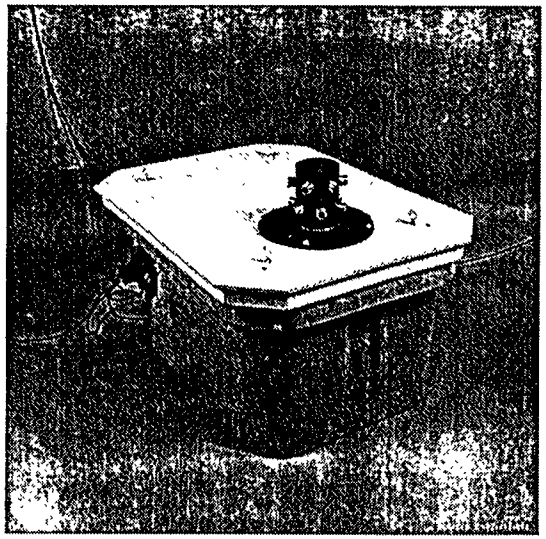

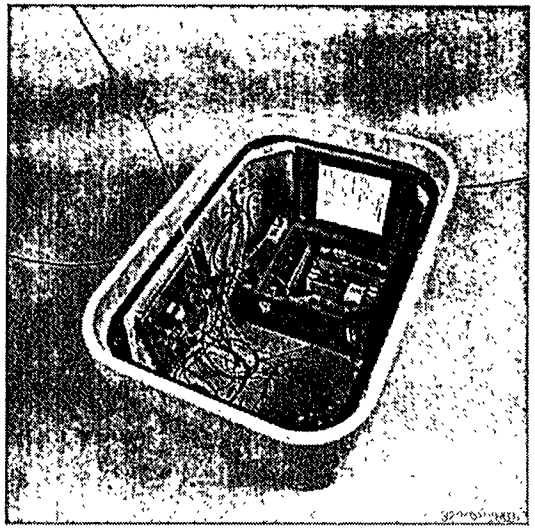

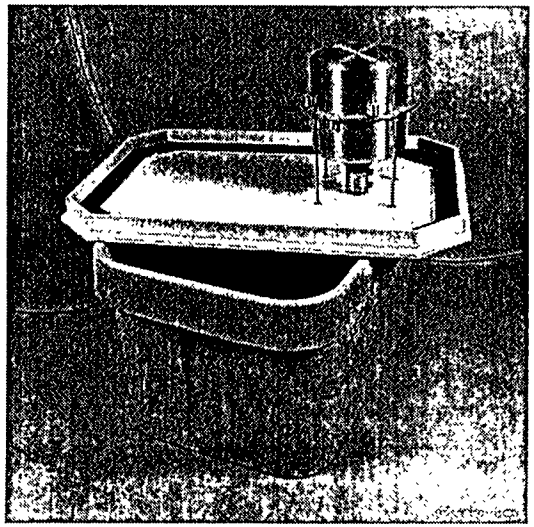

Upper left: system enclosure box
Upper right: interior components
Left: sesnor

System security is provided by housing equipment in enclousre.

Infrasound Workshop

Infrasound Prototype Data Acquisition System

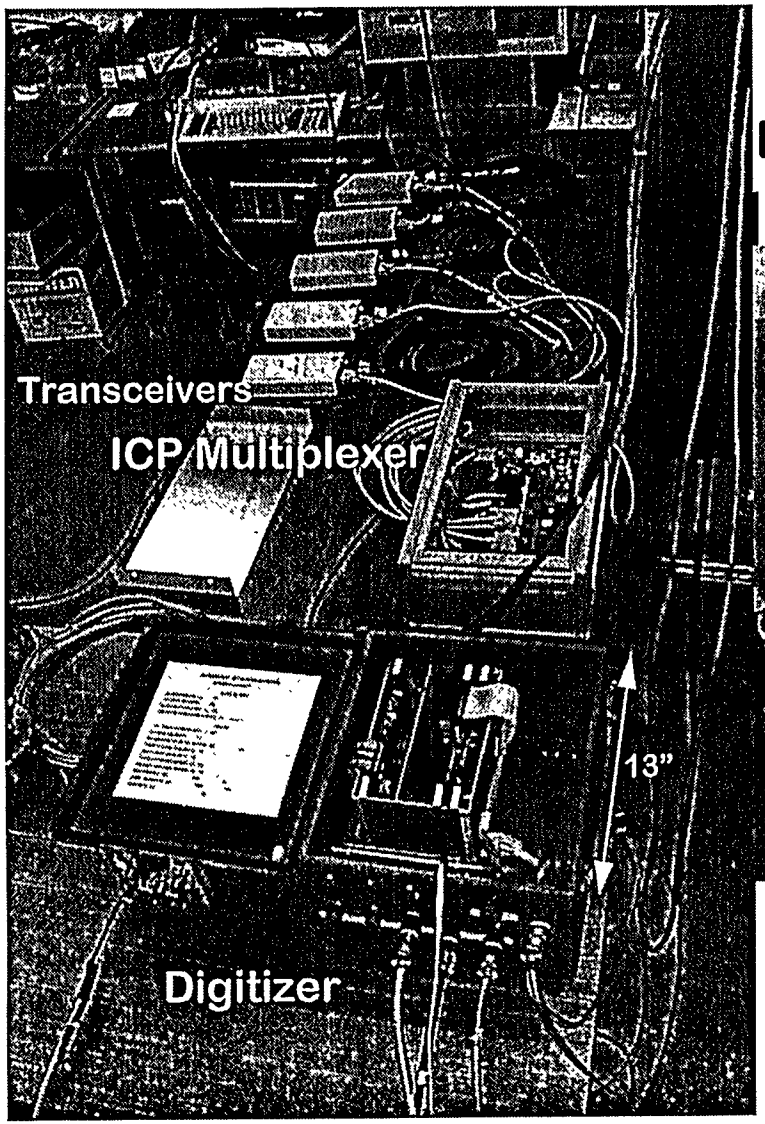

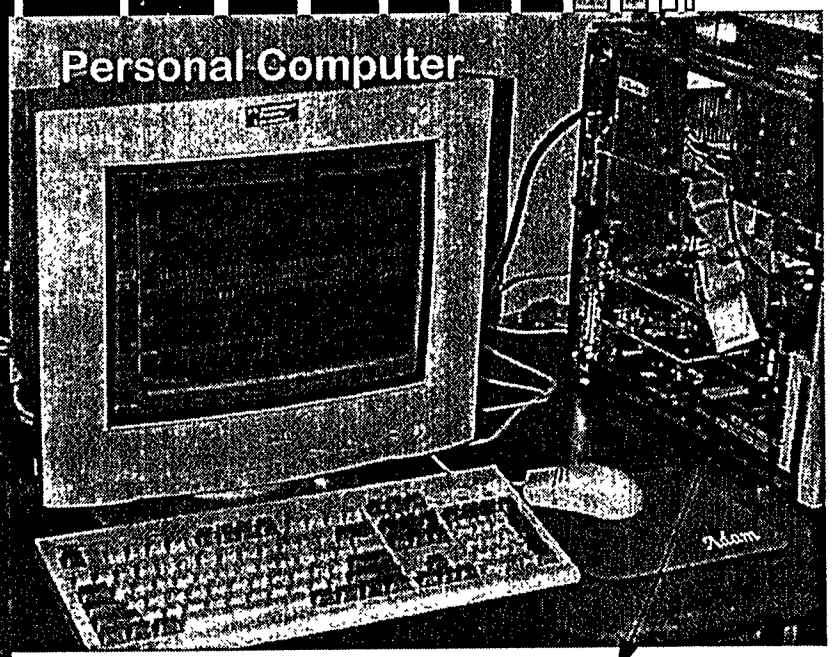

Intelligent Communications Processor (ICP) board

Prototype Status

- System integration/installation
  - Begun ~5/5/97
- Demonstration Test And Evaluation (DT&E)
  - August 5-7, 1997
  - Sensor, Digitizer and Authentication systems test
  - Test against System Requirements in SRD
- Operational Testing to begin in September, 1997
- Demonstration at Informal International Infrasound Workshop, 25-28 August 1997

DT&E Results
Sensor

- Calibration at LANL
  - Piston phone calibration chamber
    - Sets calibration constant to 0.04 volts per μbar (low gain)
    - Calibrates over the frequency range from 0.16 to 4.0 Hz
  - Theoretical transfer function
- Testing at the SNL FACT site
  - Coherence - tool for broadband sensor comparisons
  - Dynamic Range - sensor self noise down better than 80 dB from clip @ 1.0 Hz
  - Step calibration to derive transfer function

Meets CD and PREP COMM/WGB requirements

Infrasound Sensor Theoretical Response Curves

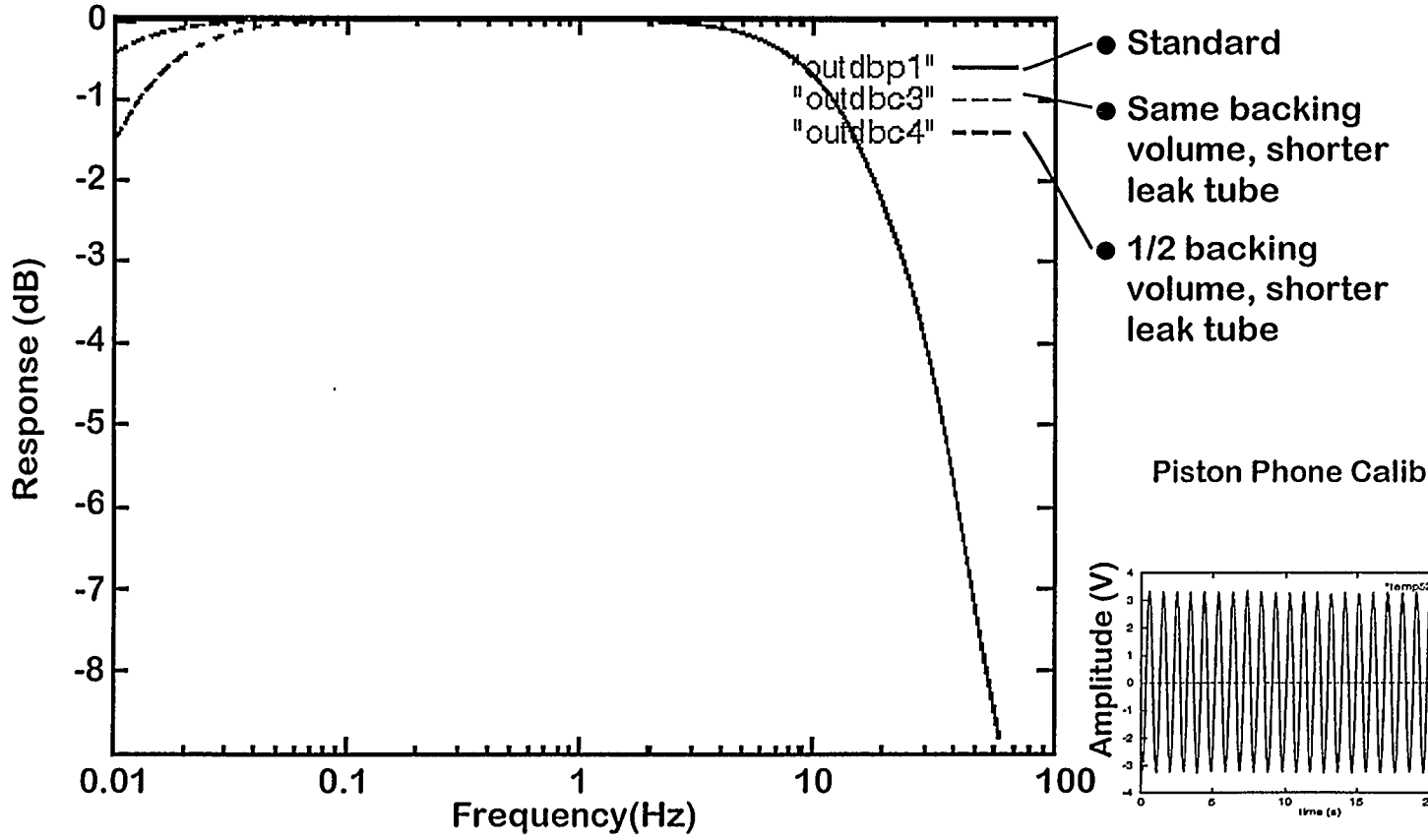

- Standard
- Same backing volume, shorter leak tube
- 1/2 backing volume, shorter leak tube

Piston Phone Calibration

DT&E Result
Digitizer

- Dynamic range measured at better than 120 dB
- Resolution measured at better than 20 bits
- Bandpass measured from DC to 3.75 Hz at 10 sps
- Accuracy measured to better than 1%
- GPS timing accuracy measured to better than 1 ms

Digitizer exceeds CD PREP COMM /WGB Requirements

DT&E Results
Authenticator

- The prototype writes 5 blocks of authenticated Alpha Protocol data to disk
- At Sandia we:
  - transferred to SNL the 5 blocks of data,
  - transferred to SNL a signature verification test program,
  - inspected the test program, and
  - ran the test program to verify data authentication

Sandia verified data authentication

Other System Components

- Solar power system well designed with variety of power options
- Alpha format data to the US NDC
- Tamper protection with closure indication at host station
- Sucessfully tested spread spectrum with integral CRC

Documentation will allow US and Foreign Countries to procure systems

● System Requirements Document	Completed 8/12/96
● Program Plan	Completed 8/12/96
● System Test Plan	~9/97 from web site
● Test Procedures	~9/97 from web site
● Test Report	~9/97 from web site
● Hardware Design Document	~9/97 from web site.

SUMMARY

- DT&E verified meeting system requirements in SRD
- Full documentation will be available
- Transition now to operational phase
- One sensor with higher noise level
- Resolving RF modem settings for optimum operation

TEST AND EVALUATION OF THE CHAPARRAL PHYSICS MODEL 4.11 INFRASOUND SENSOR FOR CTBT INFRASOUND ARRAY APPLICATION

Richard. P. Kromer and T. S. McDonald

Sandia National Laboratories
Cooperative Monitoring Technologies
Department 5736
Albuquerque, NM, 87185-0655

The Sandia National Laboratories has tested and evaluated the Chaparral Physics Model 4.11 prototype infrasound sensor to CTBT requirements. The sensor was characterized by using a piston-phone chamber to set and measure sensor sensitivity. Multiple sensor side-by-side coherence analysis testing provided a measure of sensor relative gain and phase; sensor self-noise was computed using this technique. The performance of the sensor calibration circuitry was evaluated. Sensor performance was compared to CTBT requirements. The Chaparral sensor met or exceeded all CTBT requirements. (Sandia is a multiprogram laboratory operated by Sandia Corporation, a Lockheed Martin Company, for the United States Department of Energy under contract DE-ACO4- 94AL85000).

Prototype Infrasound System

Test and Evaluation of the Chaparral Model 4.11 Infrasound Sensor for CTBT Infrasound Array Application

Presented by Dick Kromer

at the

DOE Informal Infrasound Workshop

August 26-28, 1997

Collaborators

Rod Whitaker
LANL

Dale Breding
Dick Kromer
Tim McDonald/API
SNL

Tom Sandoval
Bechtel NV

TEST AND EVALUATION OF THE CHAPARRAL PHYSICS MODEL 4.11 INFRASOUND SENSOR FOR CTBT INFRASOUND ARRAY APPLICATION

The Sandia National Laboratories has tested and evaluated the Chaparral Physics Model 4.11 prototype infrasound sensor to CD and WGB requirements. The sensor was characterized by using a piston-phone chamber to set and measure sensor sensitivity. Multiple sensor side-by-side coherence analysis testing provided a measure of sensor relative gain and phase; sensor self-noise was computed using this technique. The performance of the sensor calibration circuitry was evaluated. The Chaparral sensor meets or exceeds all CD and WGB requirements.

Prototype Infrasound System

Sensor Pictures

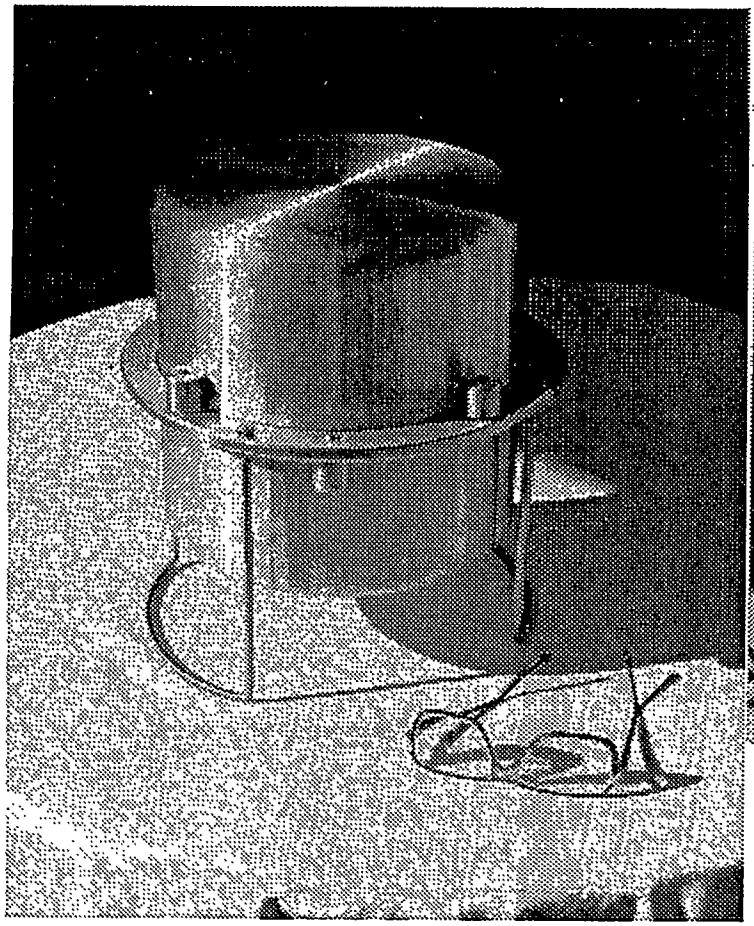

10" diameter

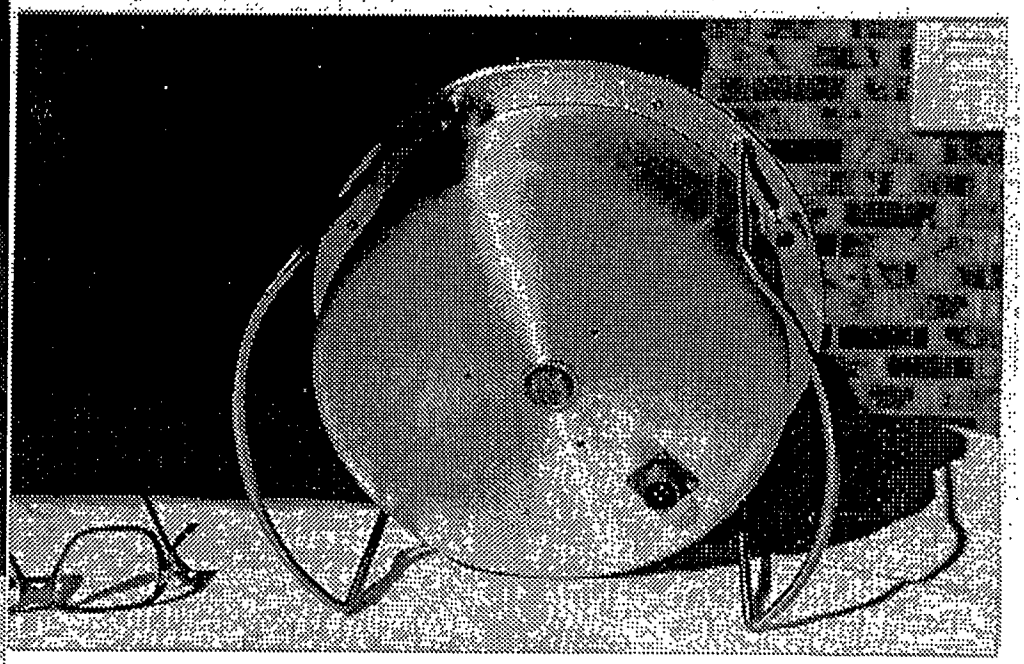

Sensor Requirements

CD/NTB/WP.224/.283

- Response - Flat over .02-5 Hz
- Resolution - .01 Pa @ 1Hz
- Dynamic Range - 80dB

PrepCom WGB/TL/8 (Rev.4)

- Response - Flat over .02-4 Hz
- Resolution - .001 Pa
- Dynamic Range - 108 dB
- Sensor noise - 18 dB below minimum acoustic noise (5 mPa @ 1.0 Hz)

Prototype Infrasound System

CD/NTB/WP.224/.283 PrepCom WGB/TL/8 (Rev.4)

Response - Flat .02-5 Hz Response - Flat .02-4 Hz

Infrasound Sensor Theoretical Response Curves

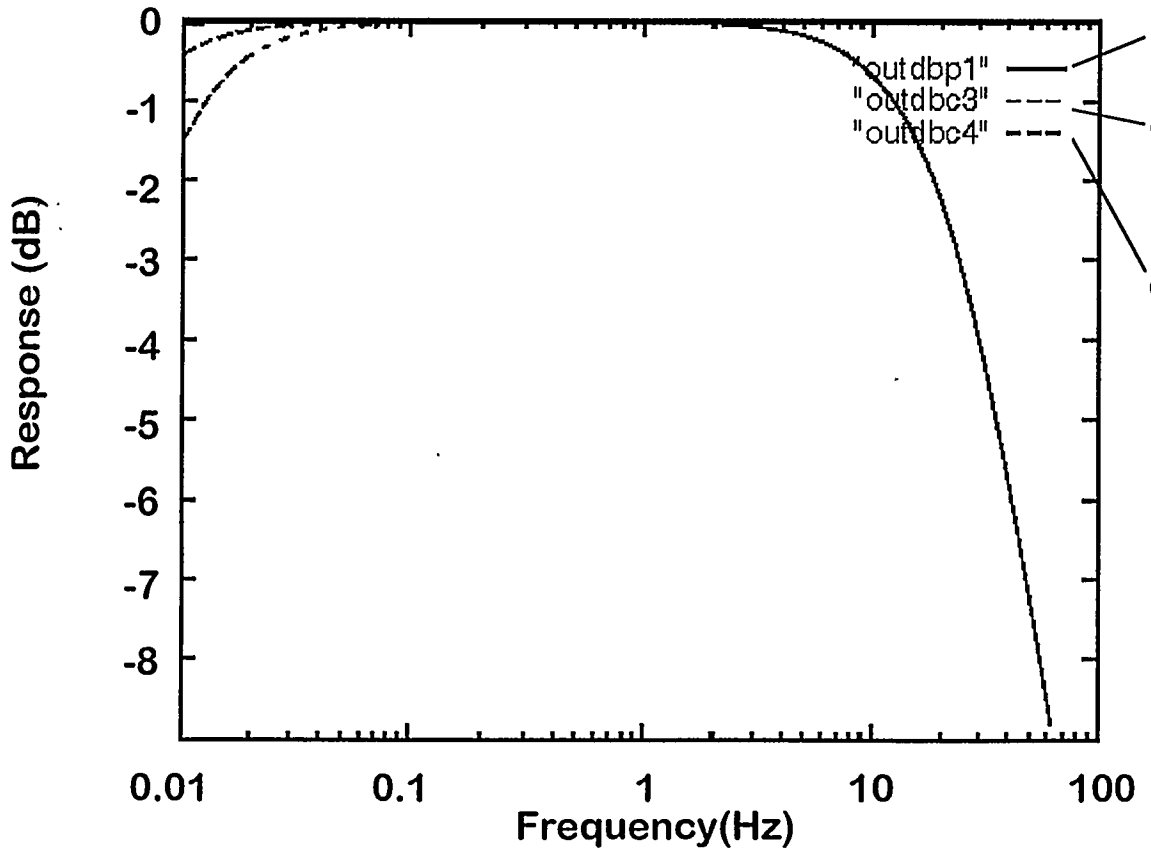

- Standard
- Same backing volume, shorter leak tube
- 1/2 backing volume, shorter leak tube

Piston Phone Calibration

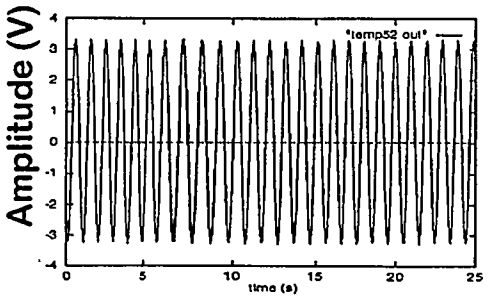

Prototype Infrasound System

CD/NTB/WP.224/.283 PrepCom WGB/TL/8 (Rev.4)

Resolution - .01 Pa @ 1 Hz Resolution - .001 Pa

- Resolution calculation is based on the ability to resolve .01 or .001 Pa peak-to-peak

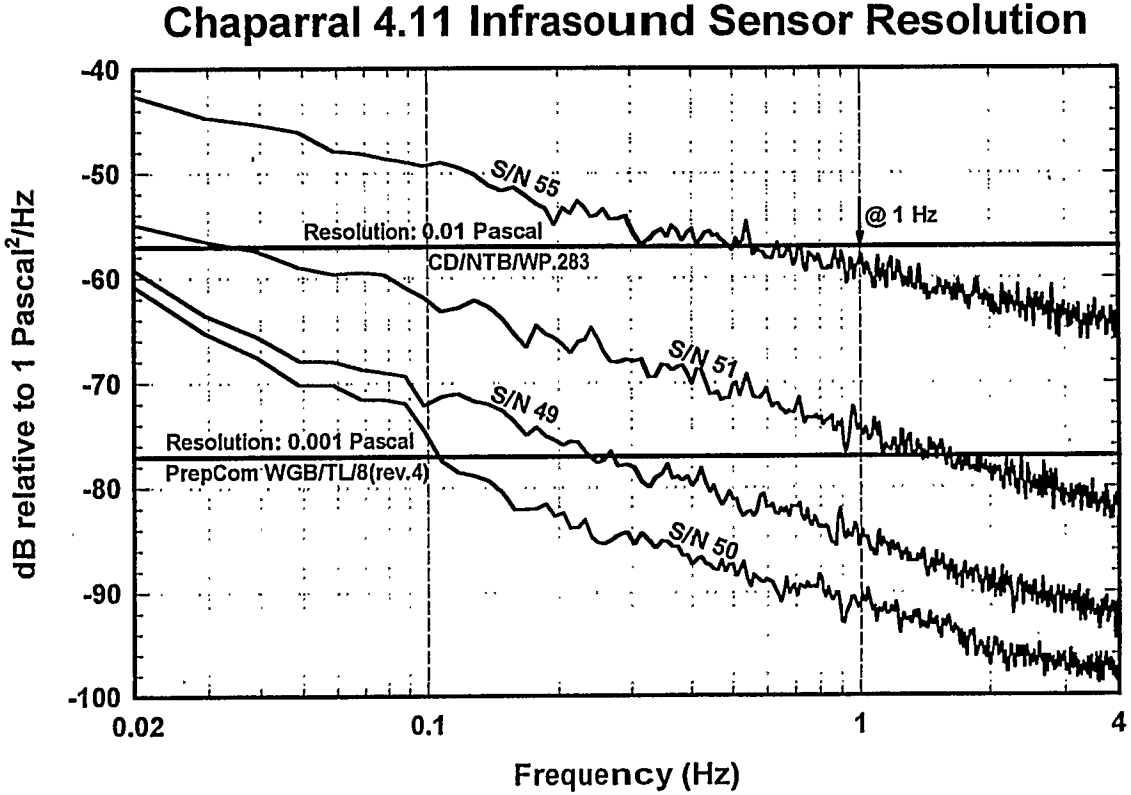

CD/NTB/WP.224/.283

Dynamic Range - 80 dB

- The Maximum Potential Dynamic Range (MPDR) of a sensor is determined by the ratio of the RMS value of the maximum sensor output to the RMS value of the sensor self-noise.

Maximum Potential Dynamic Range (MPDR)
Chaparral 4.11 Infrasound Sensor

Sensor Number	RMS Sensor Full-scale/ RMS Sensor Self-noise	Dynamic Range
49	7.07V/ 76.8μV	99.2 dB
50	7.07V/ 51.6μV	102.7 dB
51	7.07V/ 209μV	90.6 dB
55	7.07V/ 1001μV	76.9 dB

PrepCom WGB/TL/8 (Rev.4)
Dynamic Range - 108 dB

Chaparral 4.11 Prototype Infrasound System Performance

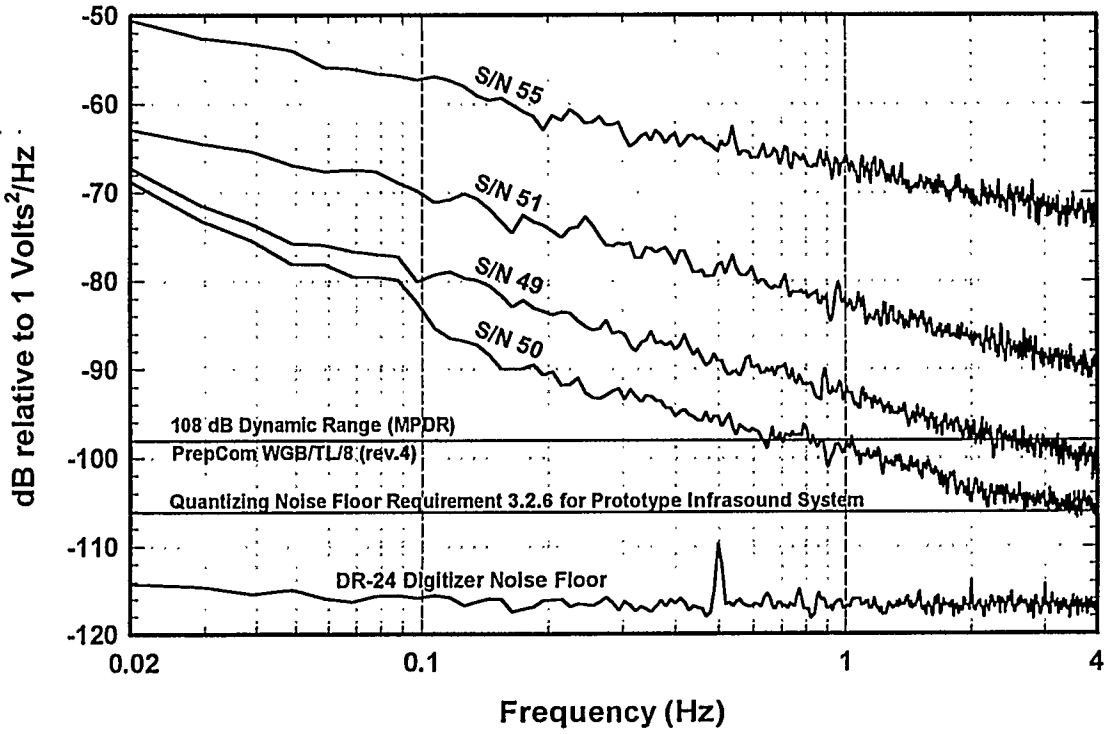

- WGB specification of 108 dB Dynamic Range is interpreted to be System Dynamic Range.
- Dynamic Range requirement for Prototype Infrasound System is 116 dB.
- Actual Prototype Infrasound System Dynamic Range is 126 dB.

PrepCom WGB/TL/8 (Rev.4)

Sensor Noise - 18 dB below minimum acoustic noise (5 mPa @ 1.0 Hz)

Sensor Side-by-Side Coherence Analysis: Sensor Noise

Chaparral 4.11 Infrasound Sensor Noise

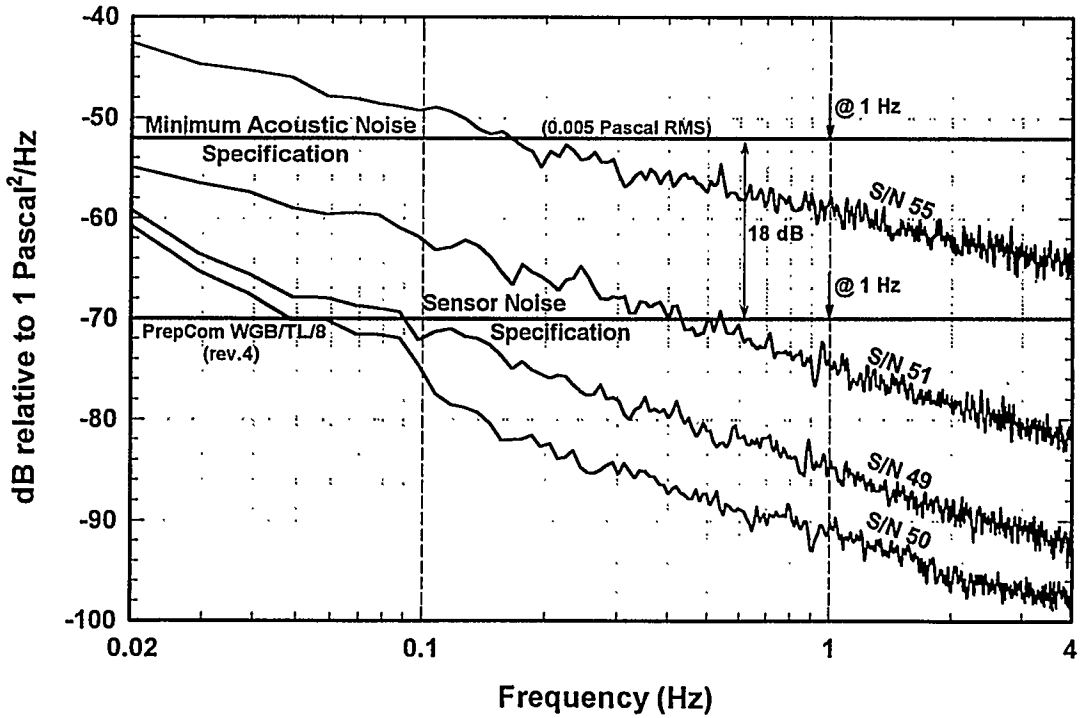

Sensor Sensitivity Test
Calibrate sensor to 400 mV/Pa

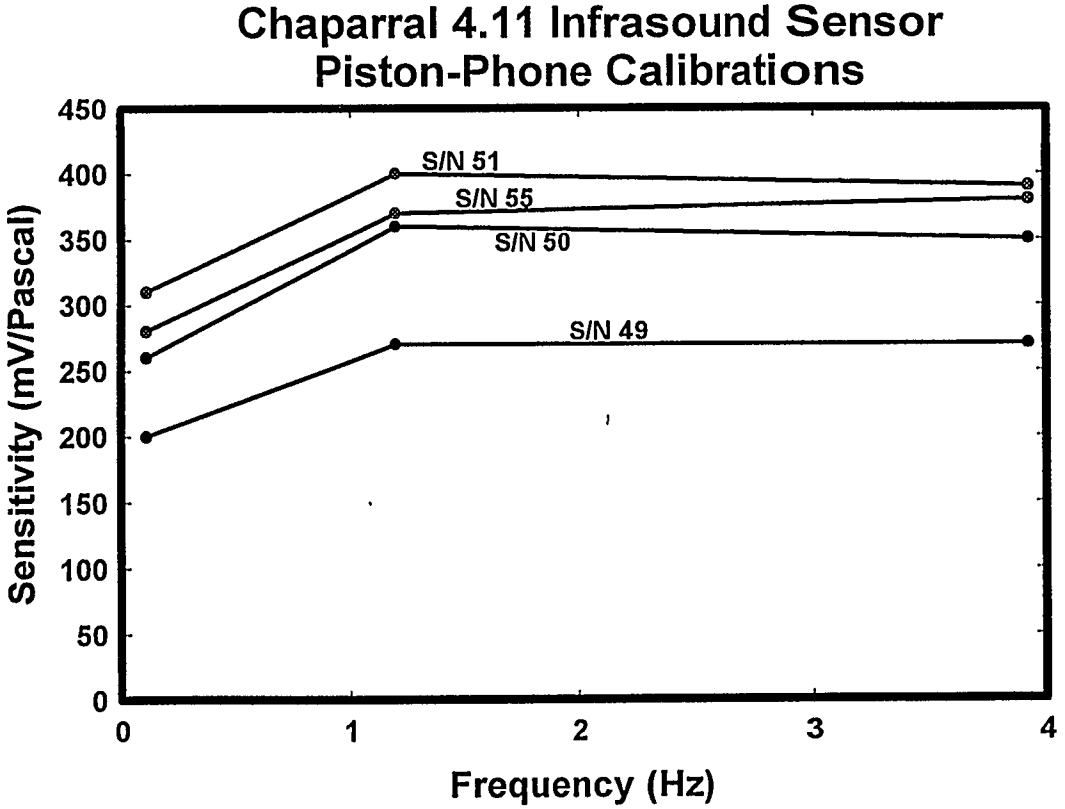

Piston-phone Calibrations

- Set sensor to 400mV/Pa
- Low frequency setting on piston-phone inaccurate due to air leakage around pistion-phone
- Reference pressure gauge needed to measure piston-phone output accurately to be able to calibrate sensors to 5%

Prototype Infrasound System

TEST AND EVALUATION OF THE CHAPARRAL PHYSICS MODEL 4.11 INFRASOUND SENSOR FOR CTBT INFRASOUND ARRAY APPLICATION

Report on the Infrasound Sensor Evaluation will be available on the DOE Web page

- www.ctbt.rnd.doe.gov

NUMERICAL MODELING OF LONG RANGE INFRASONIC PROPAGATION

James H. Hunter, Jr.

University of Florida

Rodney W. Whitaker

Los Alamos National Laboratory

We present calculations of long range infrasonic propagation using a modified version of the Pierce normal mode code, which includes atmospheric winds. Our modifications include a WKB procedure for the determination of the modes which is more suitable for our frequency range than the method in Pierce's original program. The yields of current interest are somewhat lower than considered in Pierce's original work. After summarizing our approach we will discuss results for a series of ideal ducts with and without winds. This will be followed by application to one of the large surface ammonium nitrate fuel oil tests at White Sands Missile Range. Comparison to observations of this event made at two Los Alamos infrasound arrays will be included.

Infrasound Workshop

NUMERICAL MODELING OF LONG RANGE INFRASOUND PROPAGATION

James H. Hunter, Jr.
University of Florida
and
Rodney W. Whitaker
Los Alamos National Laboratory

Infrasound Workshop August 25-28, 1997

ABBREVIATIONS

- HE : high explosive
- ANFO : ammonium nitrate and fuel oil
- DNA: Defense Nuclear Agency
- DSWA : Defense Special Weapons Agency (formerly DNA)
- kt : kiloton

BACKGROUND

- Research as part of monitoring large HE events
- Series of DNA tests provided uniform source for propagation studies
- Extended work of Pierce and co-workers
  - Allan D. Pierce, Joe Posey and Wayne Kinney
- Incorporated WKB approach for mode location due to higher frequencies of interest

CASES CONSIDERED

- Ideal Ducts
- isothermal
  - rigid lids (half-space above)
  - with and without winds in duct
  - winds in half-space no wind in duct
- Particular large DNA ANFO test: Minor Uncle
  - 2440 tons on surface
  - three stations - Los Alamos; St. George, UT, Nevada Test Site
  - White Sands Missile Range rocketsonde for winds

Pierce potentials

$$\phi_1 = \frac{i}{\Omega} p^{1/2} v_z$$

$$\phi_2 = \frac{i}{\Omega} p^{1/2} \vec{\nabla} \bullet \vec{v}$$

Differential Equations

$$\frac{d\phi_1}{dz} = a_{11}\phi_1 + a_{12}\phi_2$$

$$\frac{d\phi_2}{dz} = a_{21}\phi_1 + a_{22}\phi_2$$

where

$$a_{11} = -a_{22} = gk^2/\Omega^2 - \gamma g/(2c^2)$$

$$a_{12} = 1 - k^2c^2/\Omega^2$$

$$a_{21} = gk^2/(\Omega^2 c^2) - \Omega^2/c^2$$

Combined equation

$$\frac{d^2\phi_1}{dz^2} - (a_{11}^2 + a_{12}a_{21})\phi_1 - \left[\frac{d\ln a_{12}}{dz}\frac{d\phi_1}{dz} - a_{11}\left(\frac{d\ln a_{12}}{dz} - \frac{d\ln a_{11}}{dz}\right)\phi_1\right] = 0$$

Simplified equation

$$\frac{d^2\phi_1}{dz^2}(z^1 + q^2(z)\phi_1(z) = 0$$

where

$$q^2(z) \equiv -k^2\left[\begin{matrix}1-\Omega^2(z)/k^2c^2(z)-\omega_g{}^2(z)/\Omega^2(z)+\\ \omega_a{}^2(z)/k^2c^2(z)\end{matrix}\right]$$

WKB Integrals

$$\int_o^{zL} q(z)dz = \frac{\omega}{v_p} I = (m+\frac{\theta_o}{\pi})\pi$$

$$I = \int_o^{zL} \frac{\sqrt{\left[v_p - v(z)\right]^2 - c(z)^2}}{c(z)} dz$$

Lid conditions

$$tan^{-1}(qz_L) = \frac{\omega\sqrt{(v_p - v)^2 - c^2}}{v_p c} z_L = (m+\frac{\theta_0}{\pi})\pi$$

$$\theta_o = \tan^{-1}\left[\frac{c_L\sqrt{c_L^2 - (v_p - v_L)^2}}{c\sqrt{(v_p - v)^2 - c^2}} \frac{(v_p - v)^2}{(v_p - v_L)^2}\right]$$

$$\Omega = \omega - \vec{k} \bullet \vec{v}$$

g is the acceleration of gravity

γ is the ratio of specific heats

IDEAL DUCT CALCULATIONS

time to go 2 r is $$t = \frac{2R}{C} = \frac{2r}{C\cos\theta} = \frac{\{(2r)^2 + (2z)^2\}^{1/2}}{C}$$

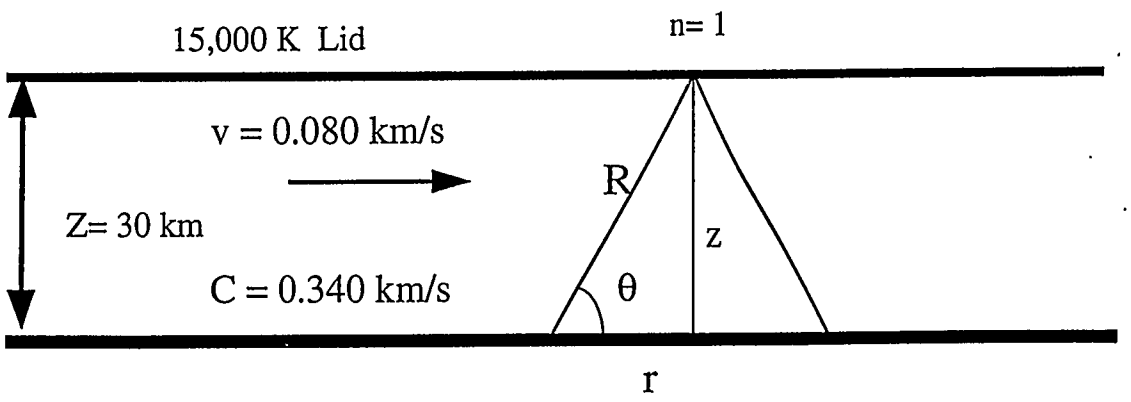

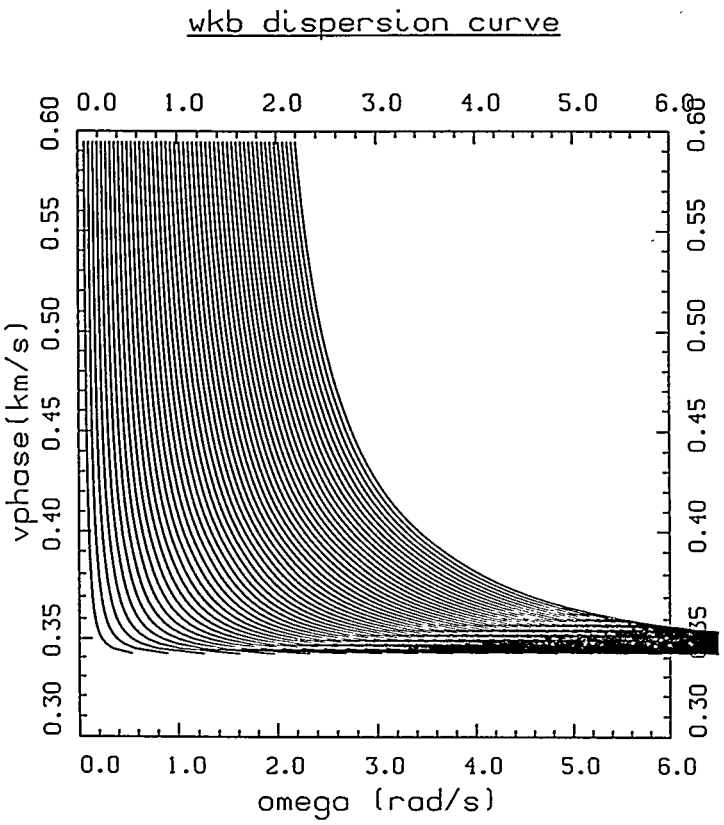

Isothermal
no wind
30 km height

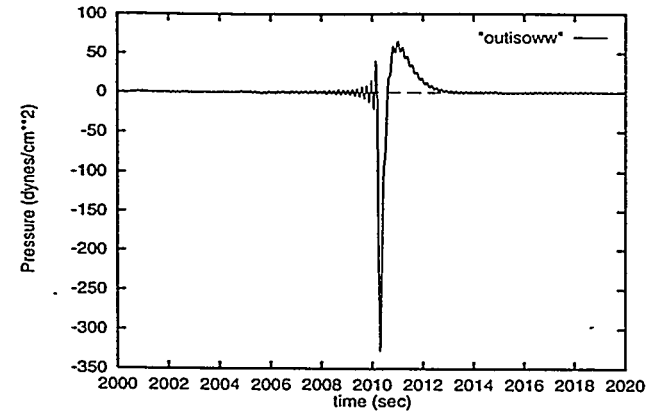

With wind
820.8 km
389 dynes/cm**2 pp

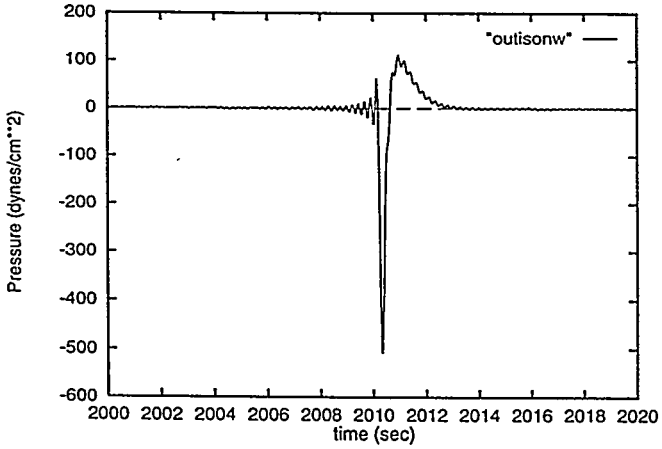

No Wind
660 km
620 dynes/cm**2 pp

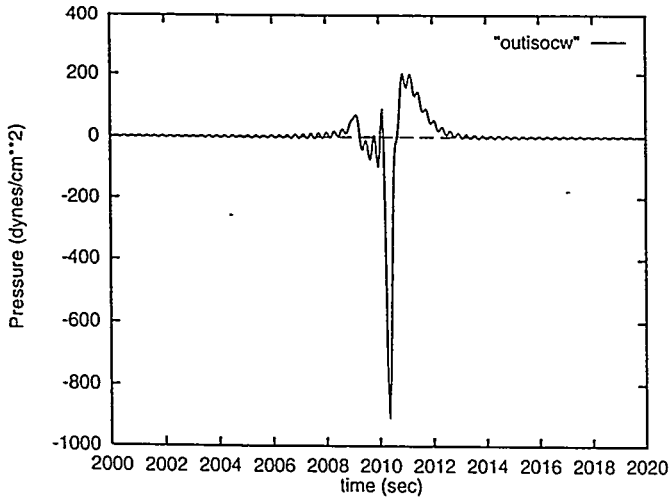

Counter wind
499.2 km
1095 dynes/cm**2 pp

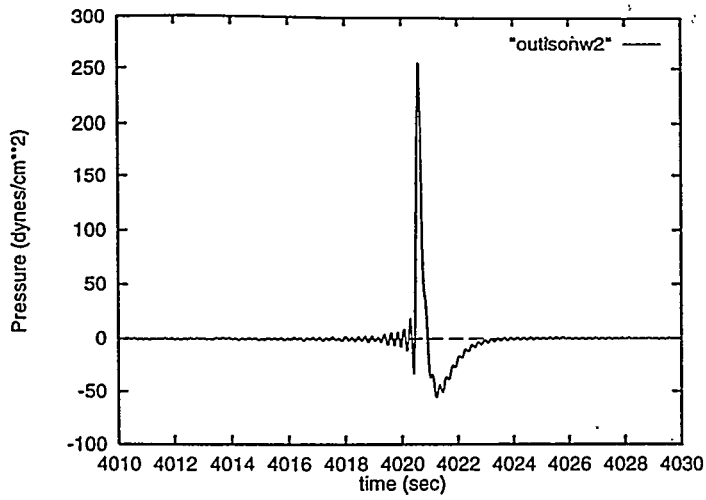

No wind
1320 km
310 dynes/cm**2 pp

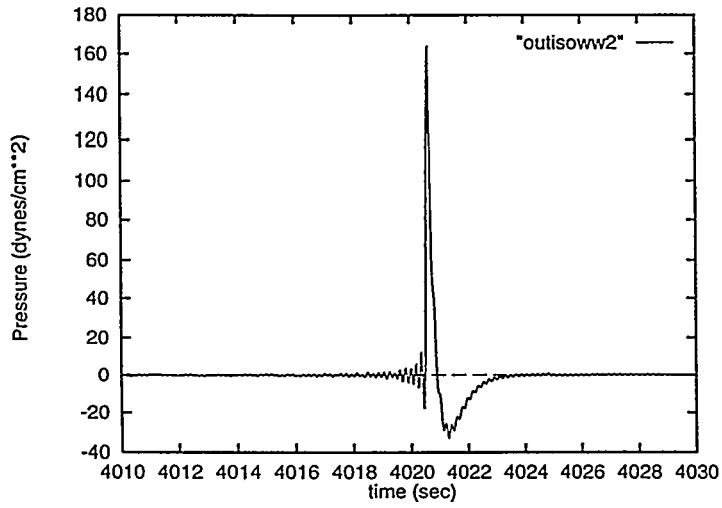

With wind
1641.6 km
196 dynes/cm**2 pp

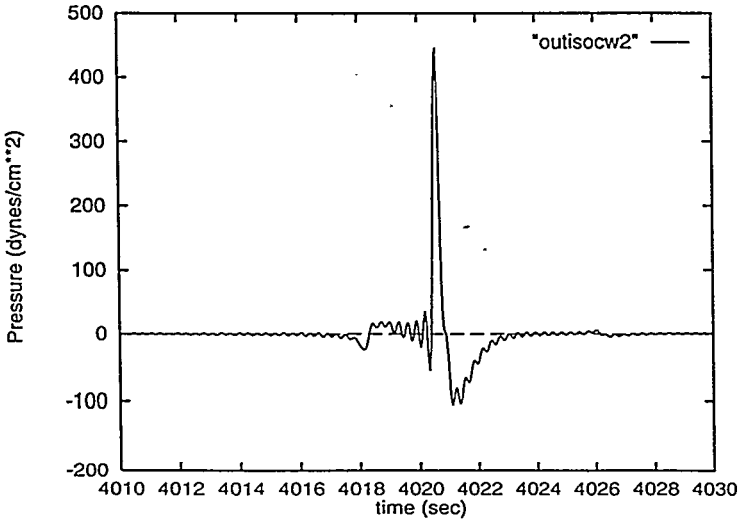

Counter wind
998.4 km
544 dynes/cm**2 pp

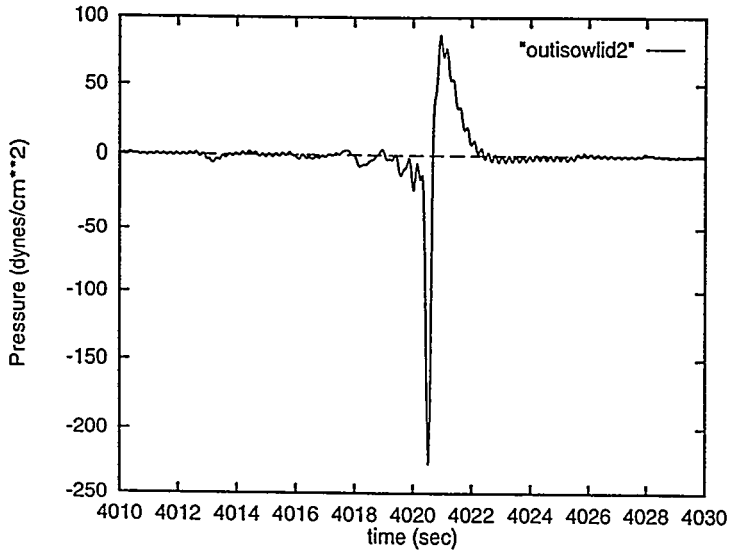
"outisowlid2"
Pressure (dynes/cm**2)
100
50
0
-50
-100
-150
-200
-250
4010 4012 4014 4016 4018 4020 4022 4024 4026 4028 4030
time (sec)

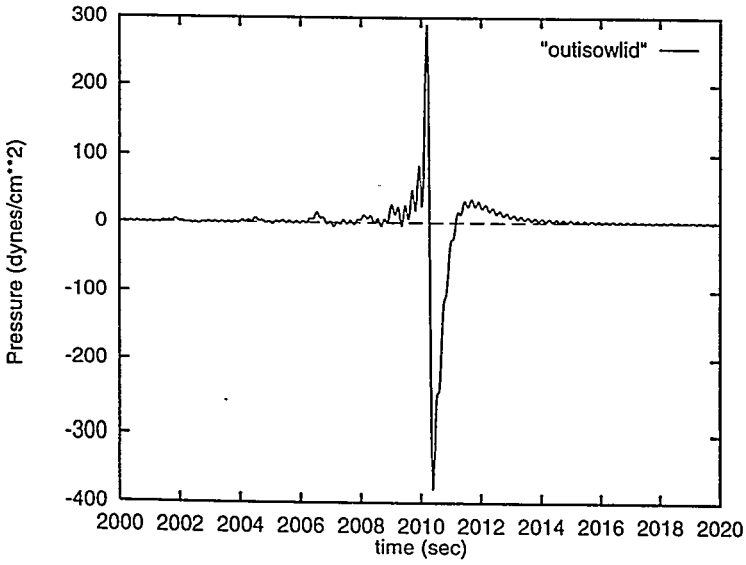
"outisowlid"
Pressure (dynes/cm**2)
300
200
100
0
-100
-200
-300
-400
2000 2002 2004 2006 2008 2010 2012 2014 2016 2018 2020
time (sec)

MINOR UNCLE

- June 10, 1993
- DNA airblast effects test
- 2440 tons ANFO
- Surface hemisphere
- Probably last large scale test for some time

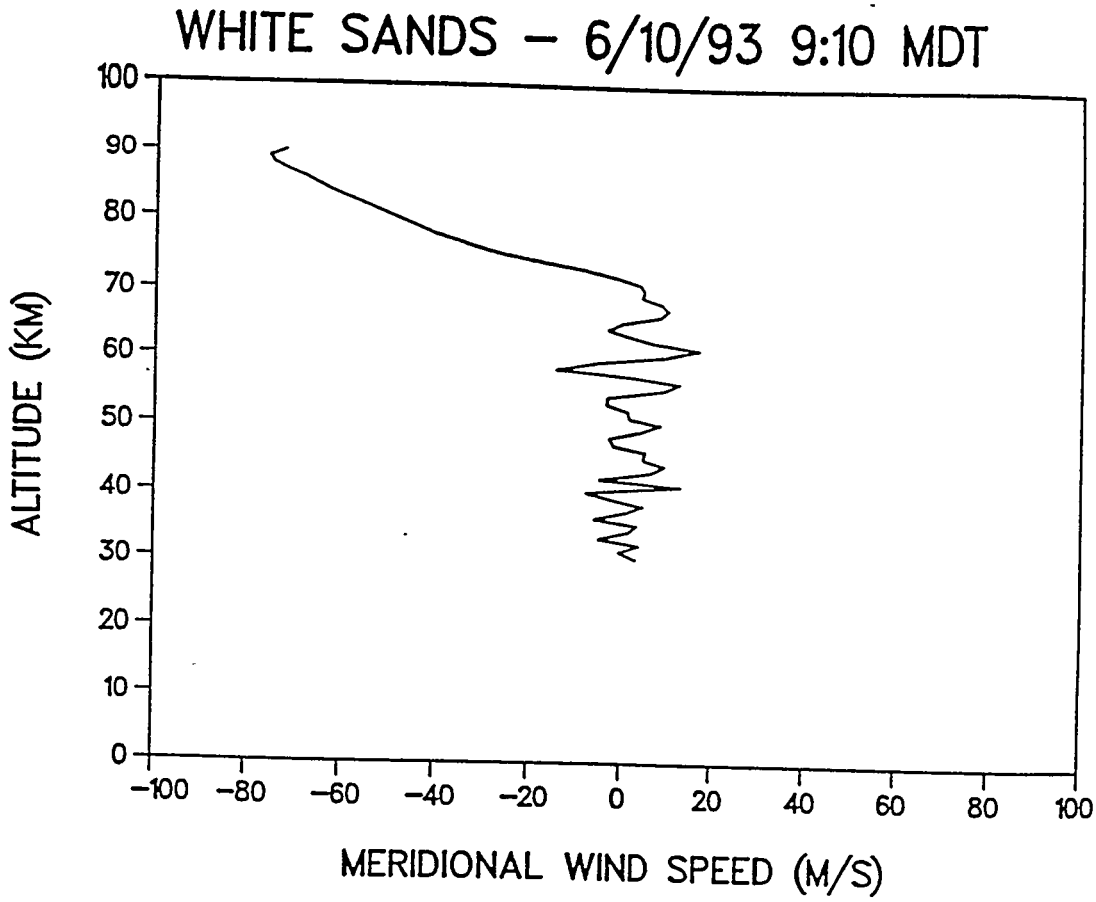
WHITE SANDS – 6/10/93 9:10 MDT
ALTITUDE (KM)
100
90
80
70
60
50
40
30
20
10
0
−100
−80
−60
−40
−20
0
20
40
60
80
100
MERIDIONAL WIND SPEED (M/S)

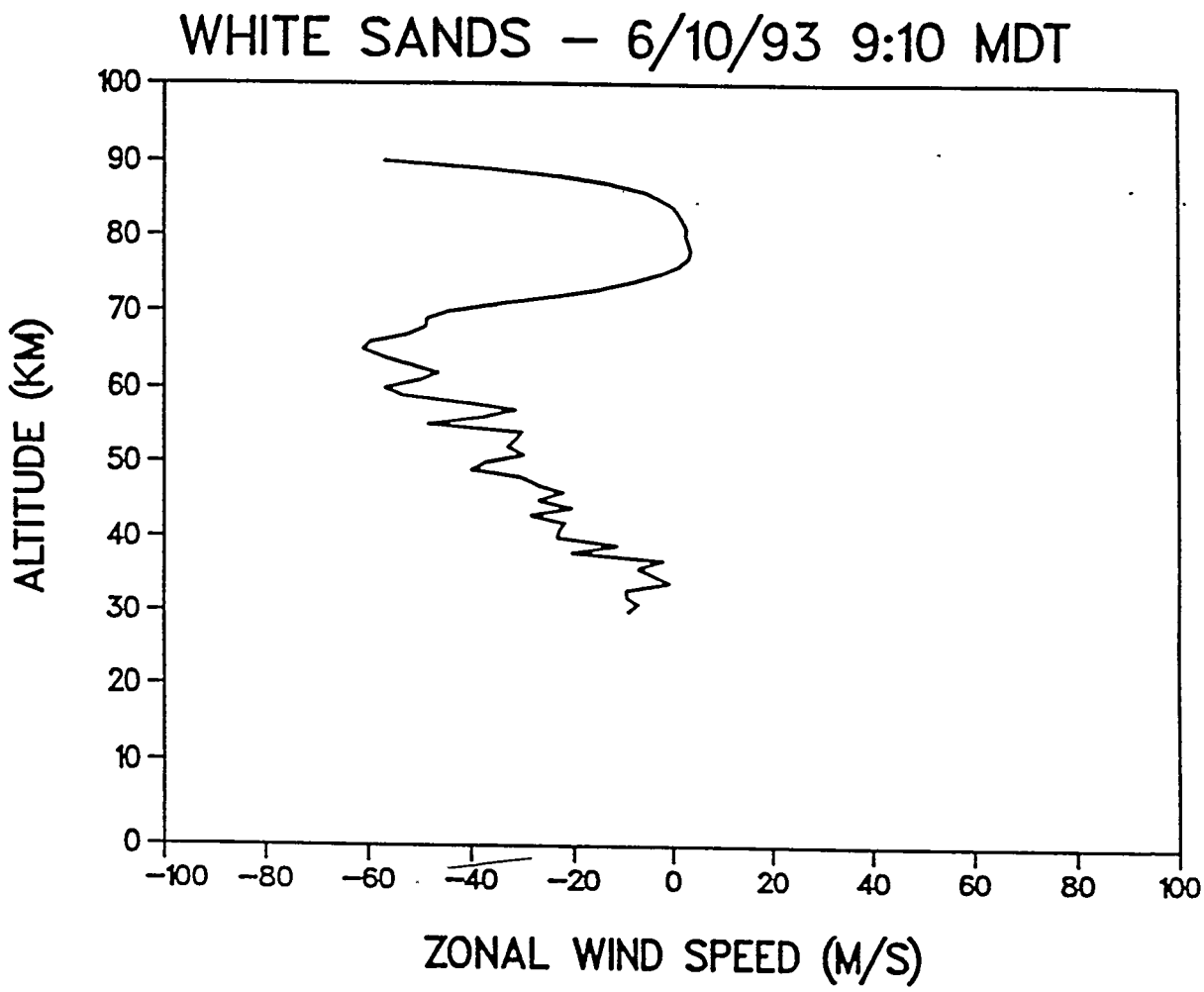
WHITE SANDS – 6/10/93 9:10 MDT
ALTITUDE (KM)
100
90
80
70
60
50
40
30
20
10
0
−100
−80
−60
−40
−20
0
20
40
60
80
100
ZONAL WIND SPEED (M/S)

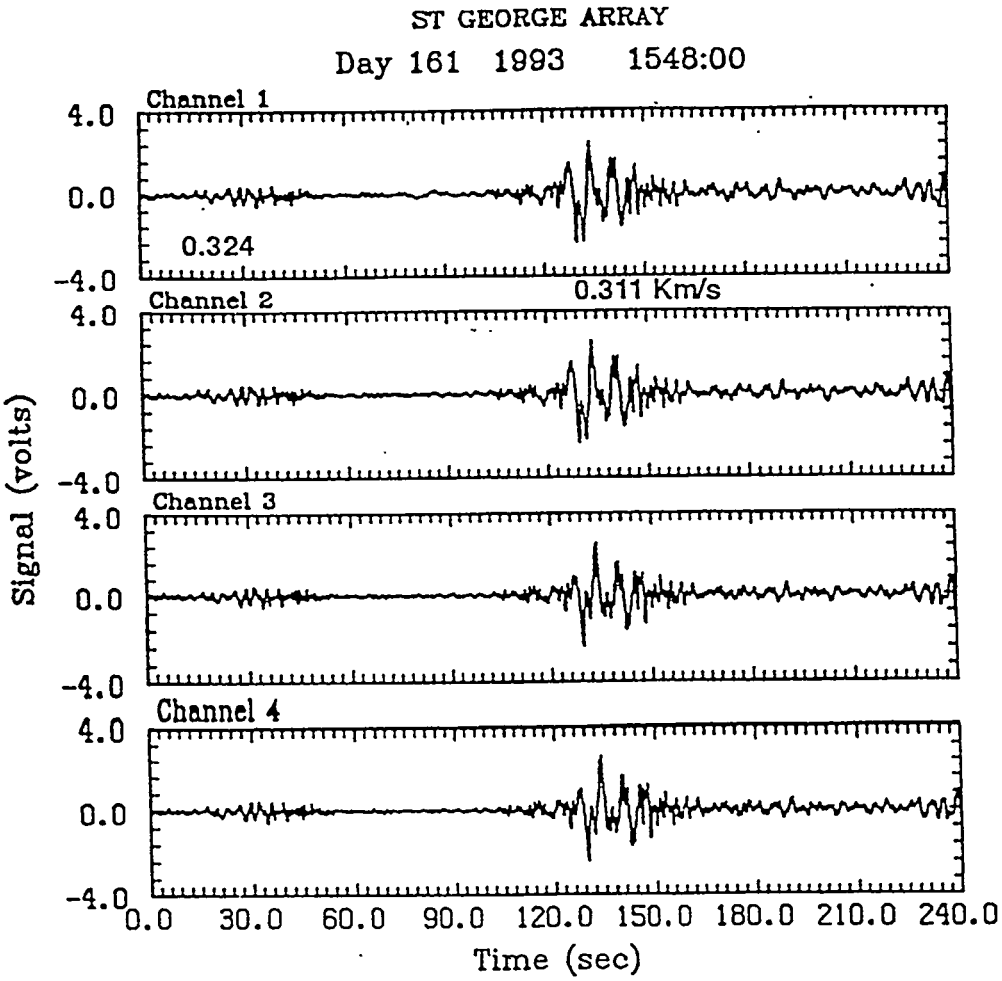
ST GEORGE ARRAY
Day 161 1993 1548:00
Channel 1
Channel 2
Channel 3
Channel 4
4.0
0.0
-4.0
0.324
0.311 Km/s
Signal (volts)
0.0 30.0 60.0 90.0 120.0 150.0 180.0 210.0 240.0
Time (sec)

Figure 6

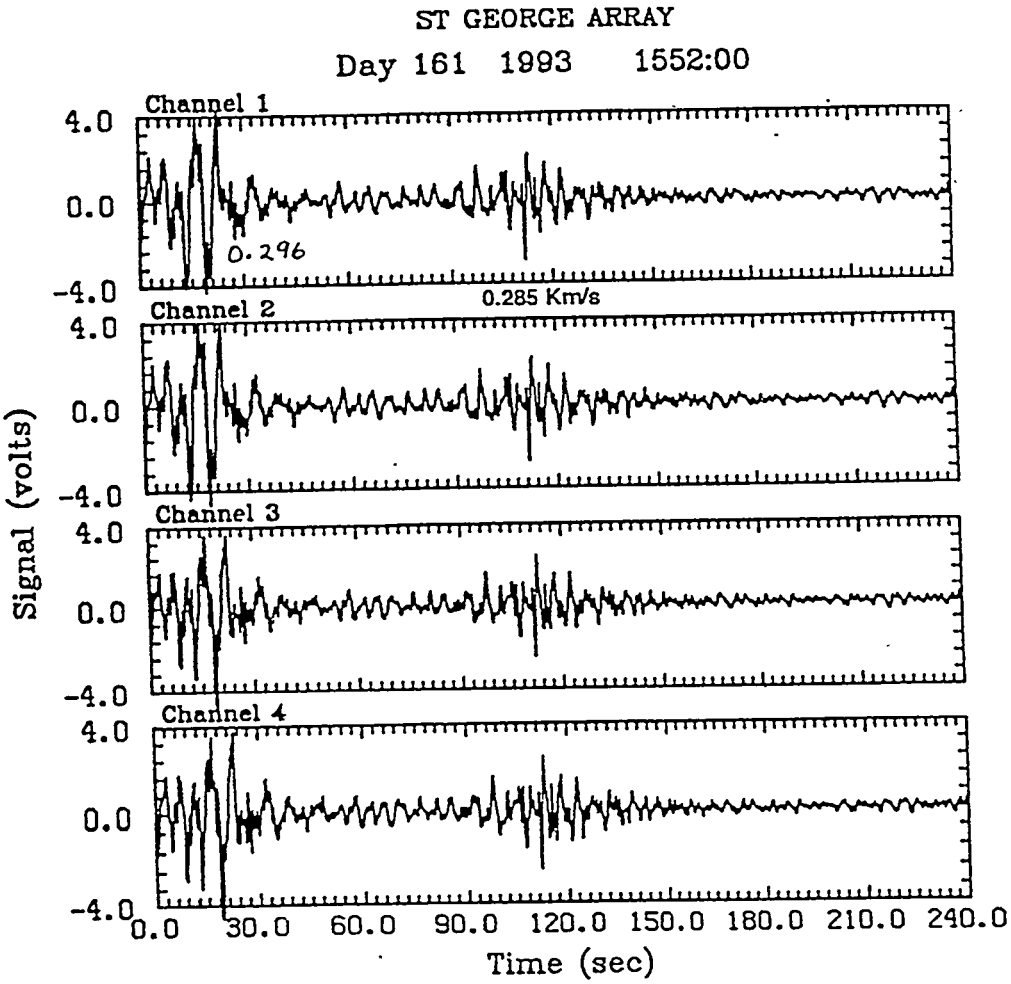
ST GEORGE ARRAY
Day 161 1993 1552:00
Channel 1
Channel 2
Channel 3
Channel 4
4.0
0.0
-4.0
0.296
0.285 Km/s
Signal (volts)
0.0
30.0
60.0
90.0
120.0
150.0
180.0
210.0
240.0
Time (sec)

Figure 7

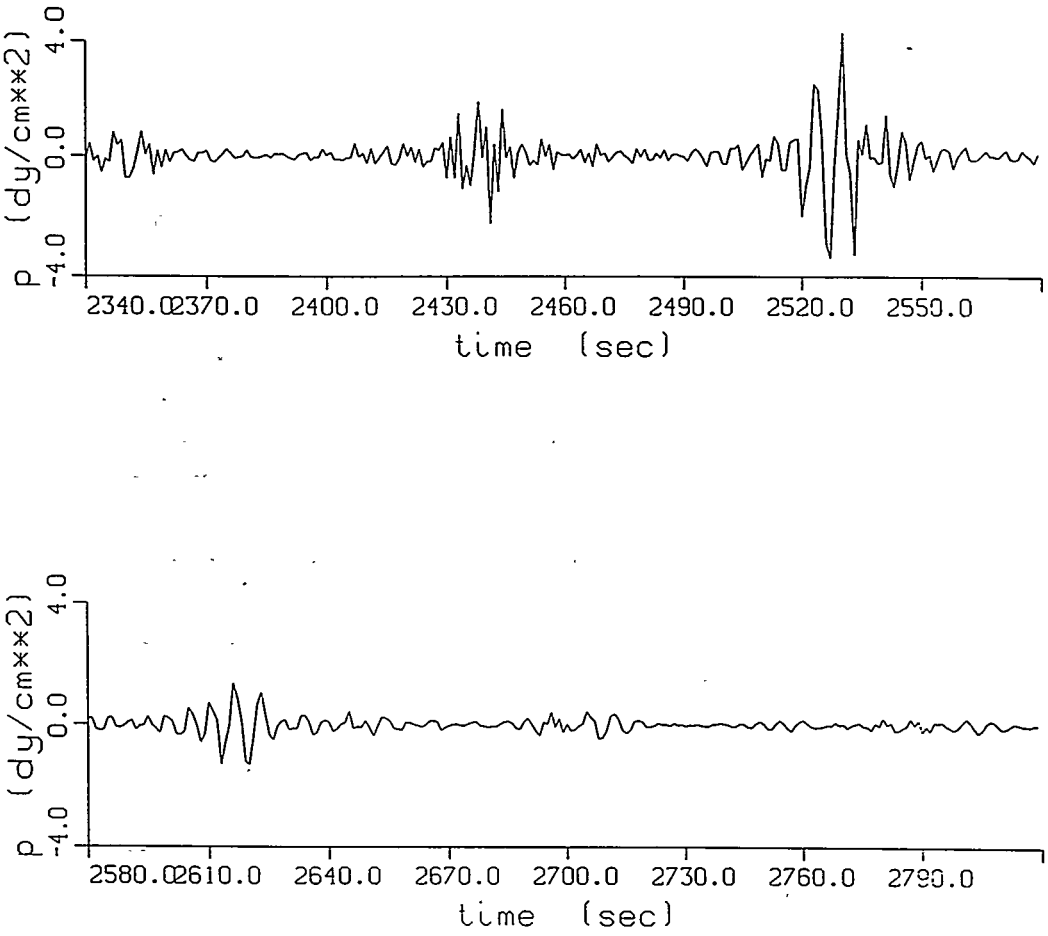

Normal mode calculation of Minor Uncle at St. George
750 km range

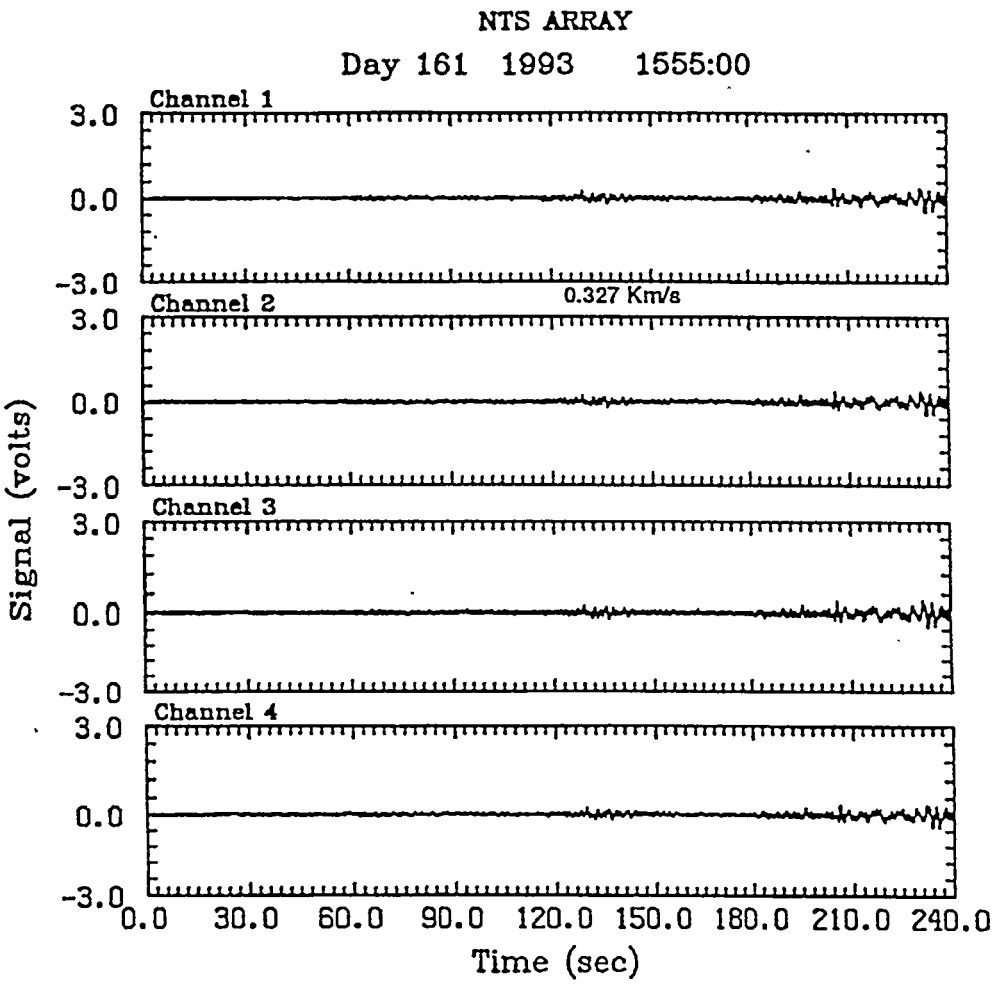
NTS ARRAY
Day 161 1993 1555:00
Channel 1
Channel 2
0.327 Km/s
Channel 3
Channel 4
3.0
0.0
-3.0
Signal (volts)
0.0 30.0 60.0 90.0 120.0 150.0 180.0 210.0 240.0
Time (sec)

Figure 8

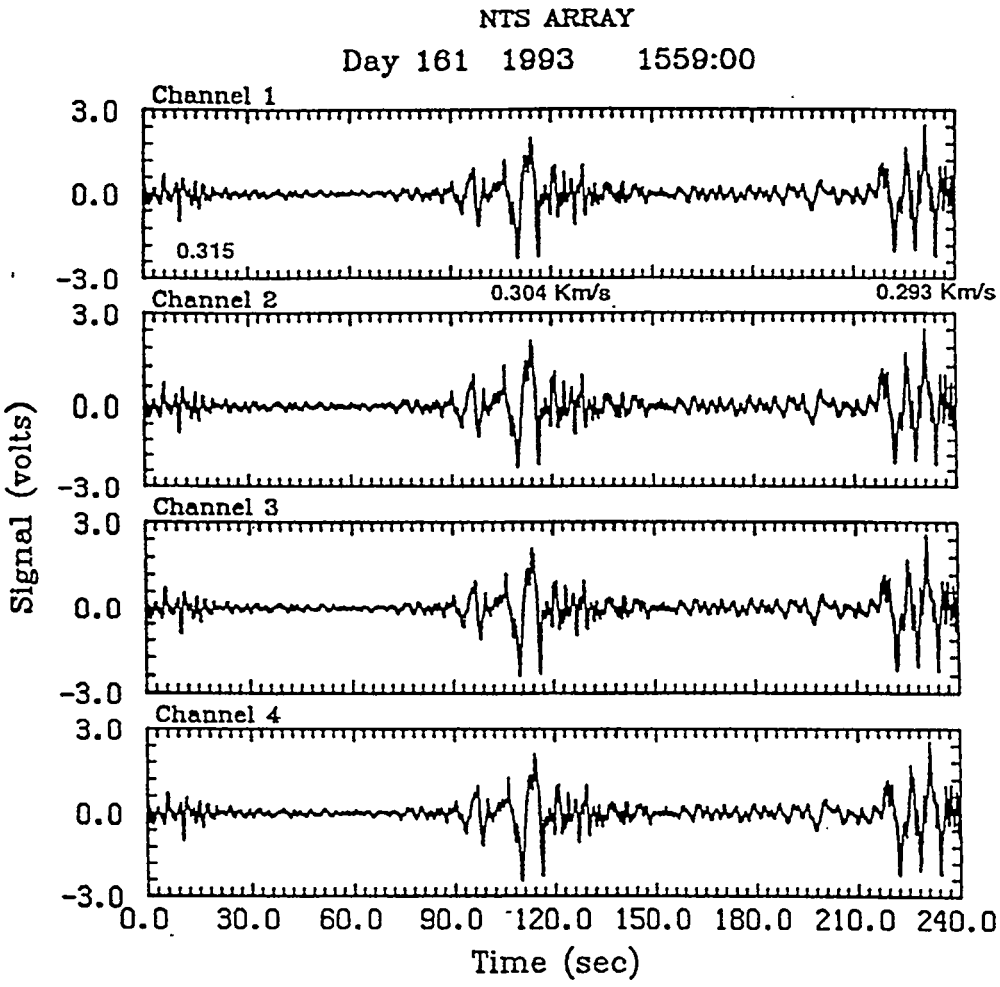
NTS ARRAY
Day 161 1993 1559:00
Channel 1
3.0
0.0
-3.0
0.315
0.304 Km/s
0.293 Km/s
Channel 2
3.0
0.0
-3.0
Channel 3
3.0
0.0
-3.0
Channel 4
3.0
0.0
-3.0
Signal (volts)
0.0 30.0 60.0 90.0 120.0 150.0 180.0 210.0 240.0
Time (sec)

Figure 9

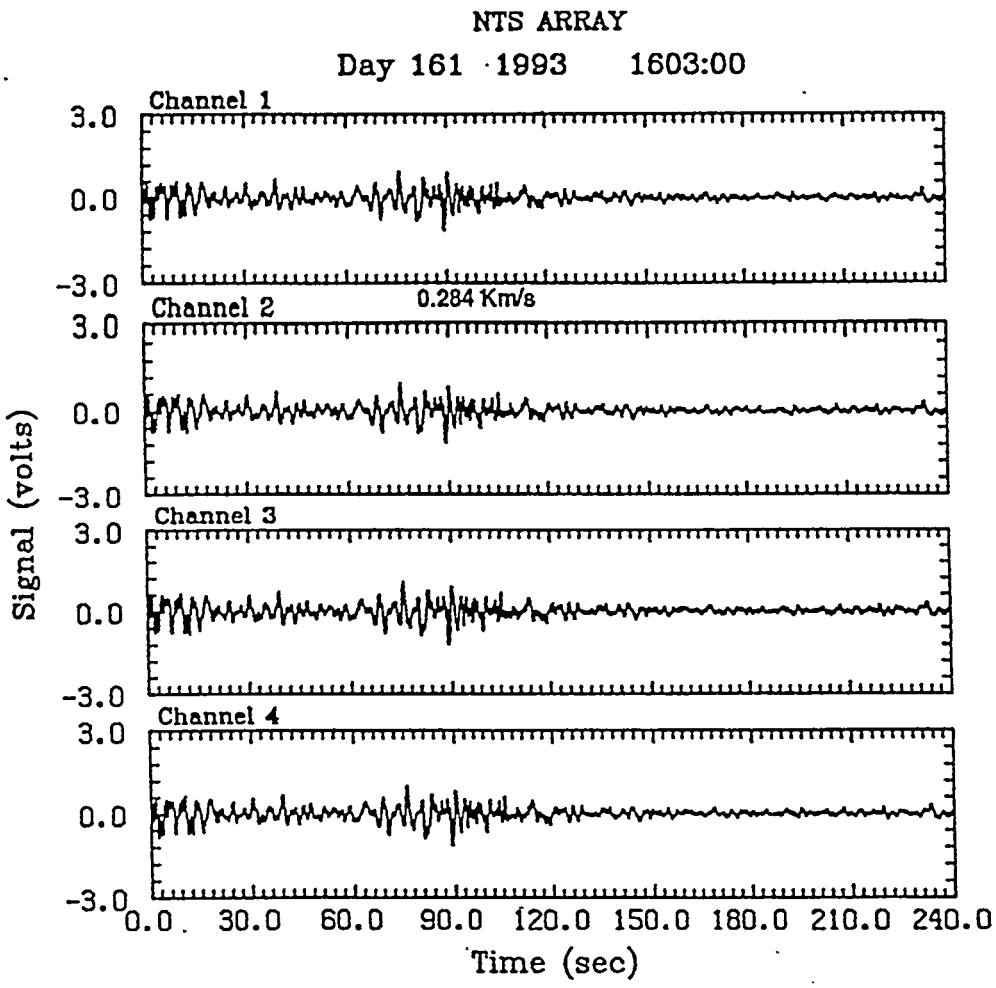
NTS ARRAY
Day 161 1993 1603:00
Channel 1
3.0
0.0
-3.0
0.284 Km/s
Channel 2
3.0
0.0
-3.0
Channel 3
3.0
0.0
-3.0
Channel 4
3.0
0.0
-3.0
Signal (volts)
0.0 30.0 60.0 90.0 120.0 150.0 180.0 210.0 240.0
Time (sec)

Figure 10

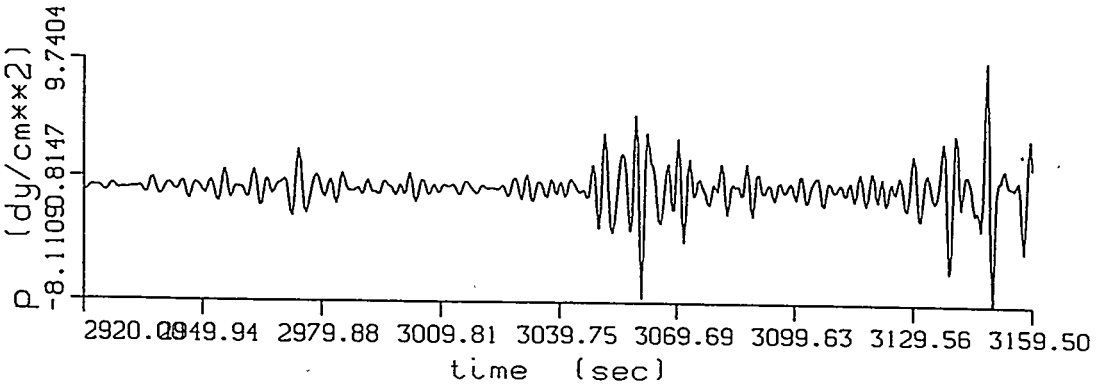

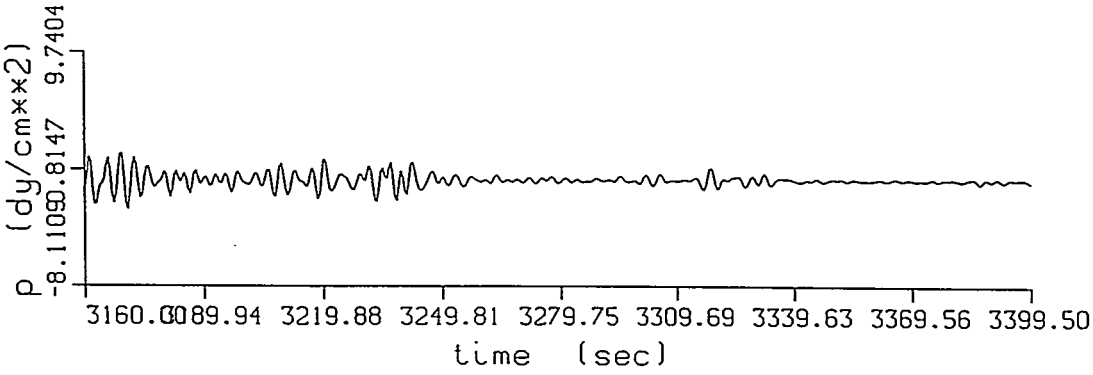

Normal mode calculation of Minor Uncle for Nevada Test Site 920 km range

SUMMARY

- Pierce code is good computational tool for long range propagation calculations
- WKB mode location sucessfully implemented for higher frequencies for lower yield sources
- Proper inclusion of wind fields

PROPAGATION CONDITIONS AND LOCALIZATION OF INFRASONIC SOURCES

Ludwik Liszka

Swedish Institute of Space Physics
Umea Division
Sorfors 634
S-90588 Umea, Sweden

Studies of long-distance infrasound propagation indicate lateral deviation of rays, probably due to horizontal gradients of wind and temperature. At distances around 2000 km differences between observed and calculated angle-of-arrival of the order of 10 degrees are observed. The phenomenon is clearly seen on recordings of infrasonic signals from Concorde. There is another problem in localization of infrasonic sources using multistation observations. Even if two stations are located as close as 300 km it is not certain that the same source will be observed at both stations due to both differences in local meteorological conditions and due to different propagation conditions. There is thus a need to develop techniques to estimate the distance to the source from recordings made at a single station. There is also a need to verify the distance information obtained from multistation measurements of the angle-of-arrival. Two different methods using: - the shape of infrasonic spectrum, - the anisotropy of the crosscorrelation field on the groundare presented.

TRAVEL TIMES FOR INFRASONIC WAVES IN THE ATMOSPHERE

Milton Garcés

Alaska Volcano Observatory
Geophysical Institute, University of Alaska
Fairbanks 99775-7320, USA

Sergey N. Kulichkov

Institute of Atmospheric Physics
Russian Academy of Sciences
3 Pyzevsky, Moscow 109017 Russia

A fast ray-theoretical method for computing travel times and transverse offsets of infrasonic waves propagating in a stratified, windy atmosphere has been developed and utilized to identify distinct phases in infrasonic recordings of pressure signals generated by chemical explosions detonated in Russia. The theory accounts for distinct infrasonic phases caused by the arrival of the Lamb wave (L), and by tropospheric (T), stratospheric (S), and thermospheric (I) ducting. Multiple branches for the last three phases may appear because of discontinuities in the effective sound speed gradient in each region. Using atmospheric temperature and wind velocity profiles up to heights of 200 km, theoretical travel time plots will be used to interpret the arrival times of infrasonic waves recorded by a linear acoustic network with an aperture of 300 -310 km. Future implementations of this method may be used for rapid and more precise locations of infrasonic sources.

Travel Times for Infrasonic Waves in the Atmosphere

Milton A Garcés
Alaska Volcano Observatory, Geophysical Institute
University of Alaska, Fairbanks

Sergey Kulichkov
Institute of Atmospheric Physics
Russian Academy of Sciences

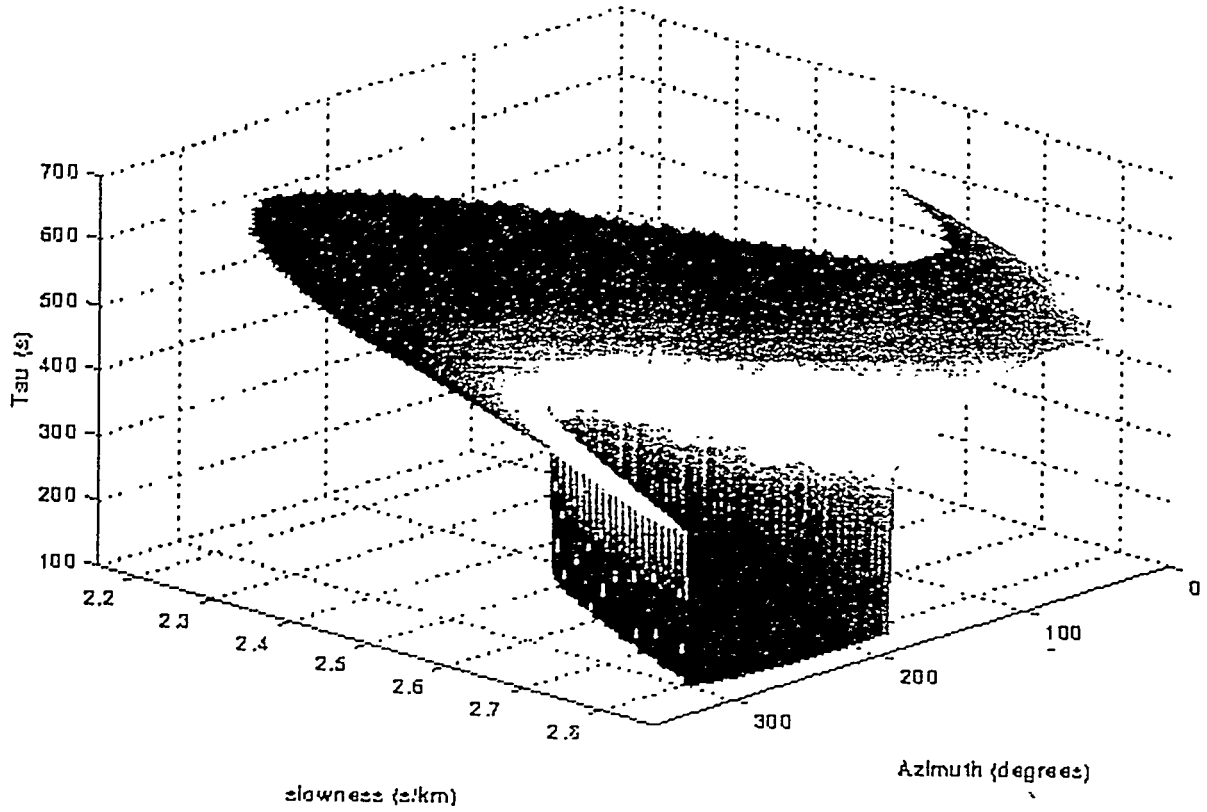

DOE/LANL Infrasound Workshop
Santa Fe, New Mexico
August 25-29, 1997

Travel times for infrasonic waves in the atmosphere

Milton A. Garcés (Alaska Volcano Observatory, Geophysical Institute, University of Alaska, Fairbanks: milton@giseis.alaska.edu) and Sergey Kulichkov (Institute of Atmospheric Physics, Russian Academy of Sciences: mail_adm@omega.ifaran.ru)

Overview

A theoretical model that permits travel time estimates in a stratified atmosphere with negligible vertical and shear winds was developed in the work of *Garcés et al.* (1997). This presentation focuses on the application of this theory to the comparison of predicted and observed arrival times of stratospheric (S) and thermospheric (I) phases at a distance of 300-310 km generated by 20-70 ton explosions detonated in Russia on August of 1990. An acoustic network of three B&K 4147 pressure microphones with a bandpass of 0.1-10 Hz recorded I phases at an azimuth of 5 degrees from North and 245 degrees from North (measured from the epicenter), and S phases at an azimuth of 245 degrees from North. The theoretical model predicted the presence of these phases, but the predicted arrival time for the I waves at 5° was approximately 100 s too late, and the S waves at 245° arrived approximately 60 s too early. The I waves at 245° were within 10 s of the observed values. Yet, the model correctly predicted the presence of distinct S branches arriving within 20 s of each other, which were observed in the acoustic data.

For operational applications, it is possible to use as input data the temperature and wind velocity vectors to compute theoretical travel time curves as a function of azimuth. The predicted time and distance of the first arrival, and the slope of the travel-time curve for specific branches at different angles may be stored and used to identify distinct branches in infrasonic data. A more sophisticated approach would involve the interpolation of the tau function over ray parameter-azimuth space. In contrast to the travel time, range, and transverse offset, the tau function is a monotonic function of the ray parameter for each branch, and thus permits convenient interpolation. The travel time and range for a specific ray parameter can be promptly computed once the interpolated tau function is known, and may provide more accurate determinations of travel time curves for infrasonic waves in the atmosphere.

References

Garcés, M. A., R. A. Hansen, K. Lindquist (1997). *Travel times for infrasonic waves propagating in a stratified atmosphere.* Geophys. J. International (Submitted).

Kulichkov, S. N. (1992). *Long-range propagation of sound in the atmosphere, a review.* Izvestiya, Atmoshperic and Oceanic Physics, 28, 253-265.

Travel Time Determinations in a Stratified Atmosphere

Basic Equations

Ray parameter, p, for given sound speed, c, and horizontal wind velocity along the ray path, u.

$$p = \frac{\sin\theta}{c}\left(1+\frac{u\sin\theta}{c}\right)^{-1}$$

Let s = 1/c. Travel time, T, range along the ray direction, X, and transverse offset, Y, of a propagating wave over a specific ray path:

$$T = \int_C s^2\left(s^2 - \frac{p^2}{(1-pu)^2}\right)^{-\frac{1}{2}} dz \ ,$$

$$X = \int_C \left(\frac{p}{(1-pu)} + s^2 u\right)\left(s^2 - \frac{p^2}{(1-pu)^2}\right)^{-\frac{1}{2}} dz \ ,$$

$$Y = \int_C \left(s^2 v\right)\left(s^2 - \frac{p^2}{(1-pu)^2}\right)^{-\frac{1}{2}} dz \ .$$

The above equations reduce to their standard forms when the wind velocity vanishes.
The Legendre transformation defines the intercept time, τ:

$$\tau = T - pX$$

or

$$\tau = \oint (1-pu)\left[s^2 - \frac{p^2}{(1-pu)^2}\right]^{\frac{1}{2}} dz \ .$$

Tau is a monotonic function of the ray parameter, p, and it does not exhibit square root singularities of X, Y and T.

Construct an interpolation function for τ up to its turning point, and transform tau into a continuous function of ray parameter.

The range for a specific ray parameter (or launch angle), p_k, can be obtained from

$$\left.\frac{d\tau}{dp}\right|_{p_k} = -X_k$$

and the travel time for a specific arrival at a given range from

$$T_k = \tau(p_x) + p_k X_k \ .$$

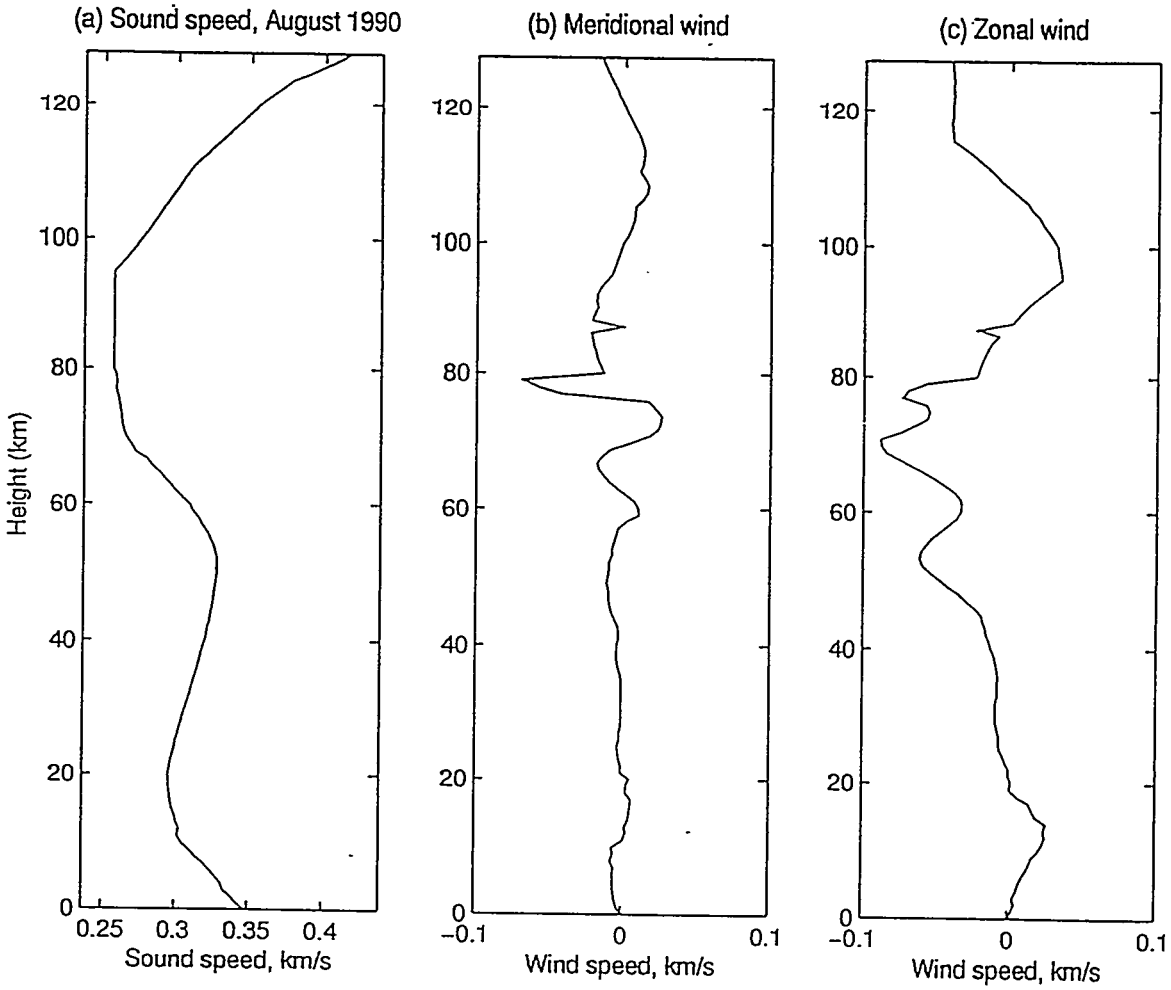
(a) Sound speed, August 1990
(b) Meridional wind
(c) Zonal wind
Height (km)
0
20
40
60
80
100
120
0.25
0.3
0.35
0.4
Sound speed, km/s
−0.1
0
0.1
Wind speed, km/s
−0.1
0
0.1
Wind speed, km/s

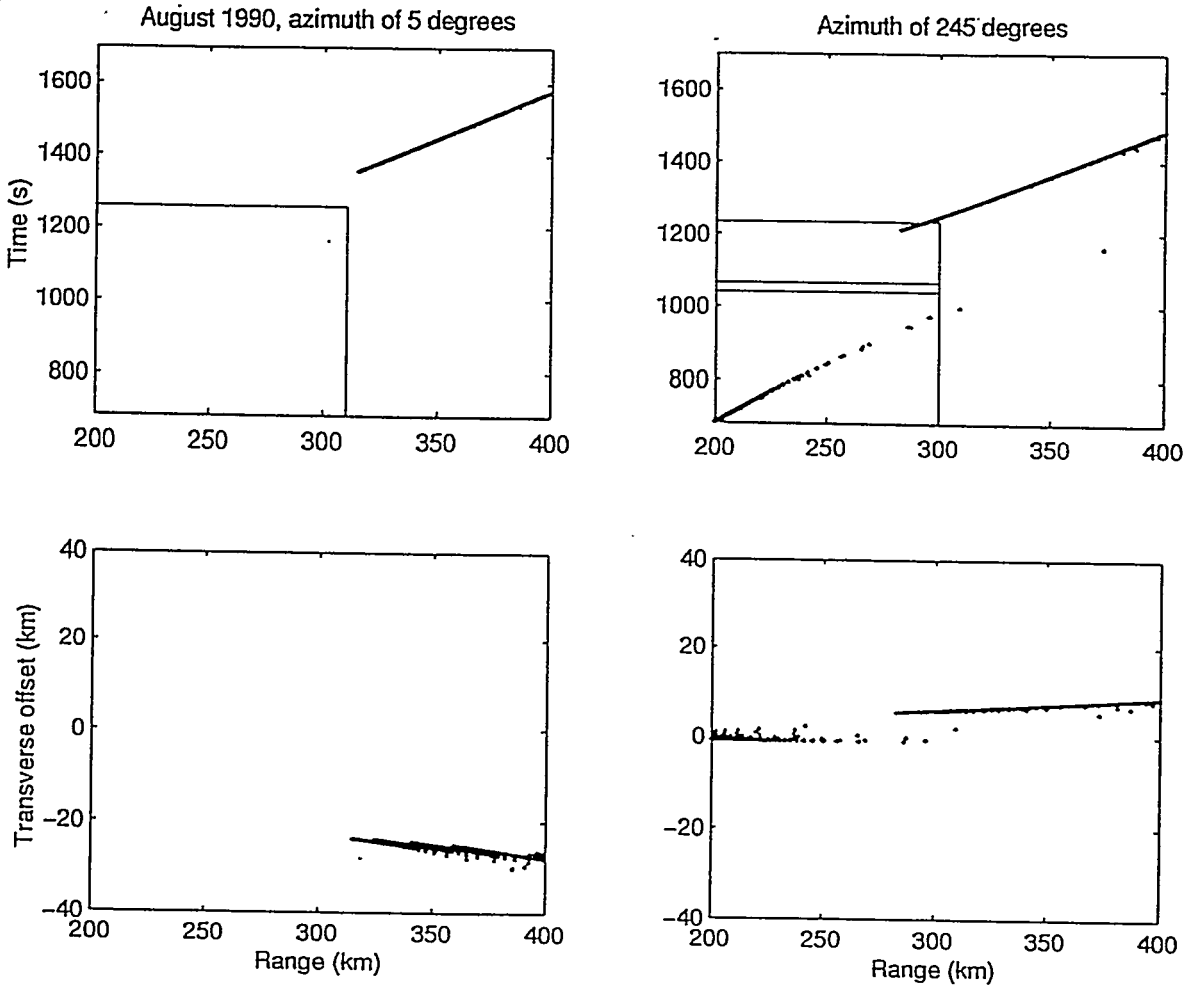
August 1990, azimuth of 5 degrees
Azimuth of 245 degrees
Time (s)
1600
1400
1200
1000
800
200
250
300
350
400
Transverse offset (km)
40
20
0
−20
−40
Range (km)

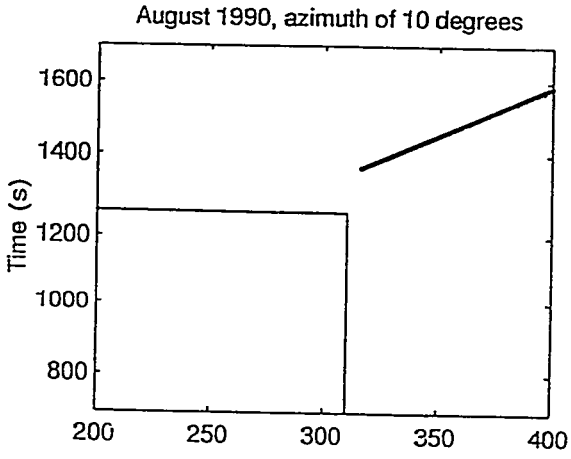
August 1990, azimuth of 10 degrees
Time (s)
1600
1400
1200
1000
800
200
250
300
350
400

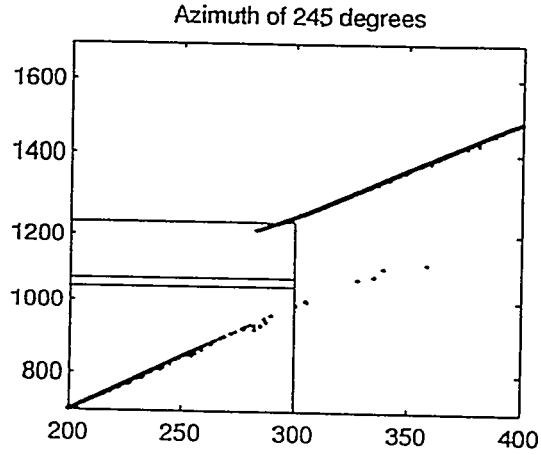
Azimuth of 245 degrees
1600
1400
1200
1000
800
200
250
300
350
400

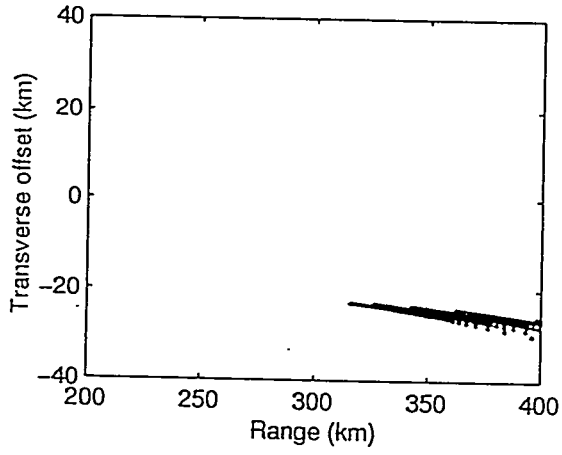
Transverse offset (km)
40
20
0
−20
−40
200
250
300
350
400
Range (km)

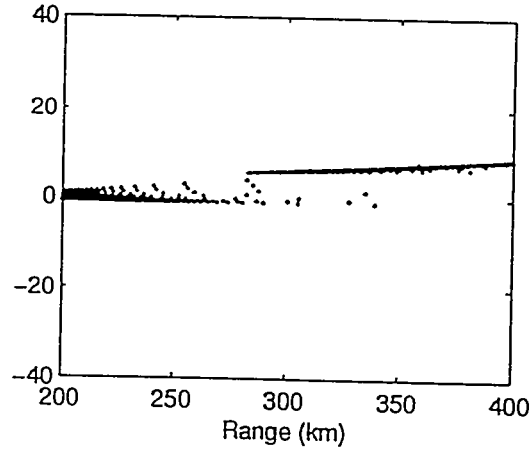
40
20
0
−20
−40
200
250
300
350
400
Range (km)

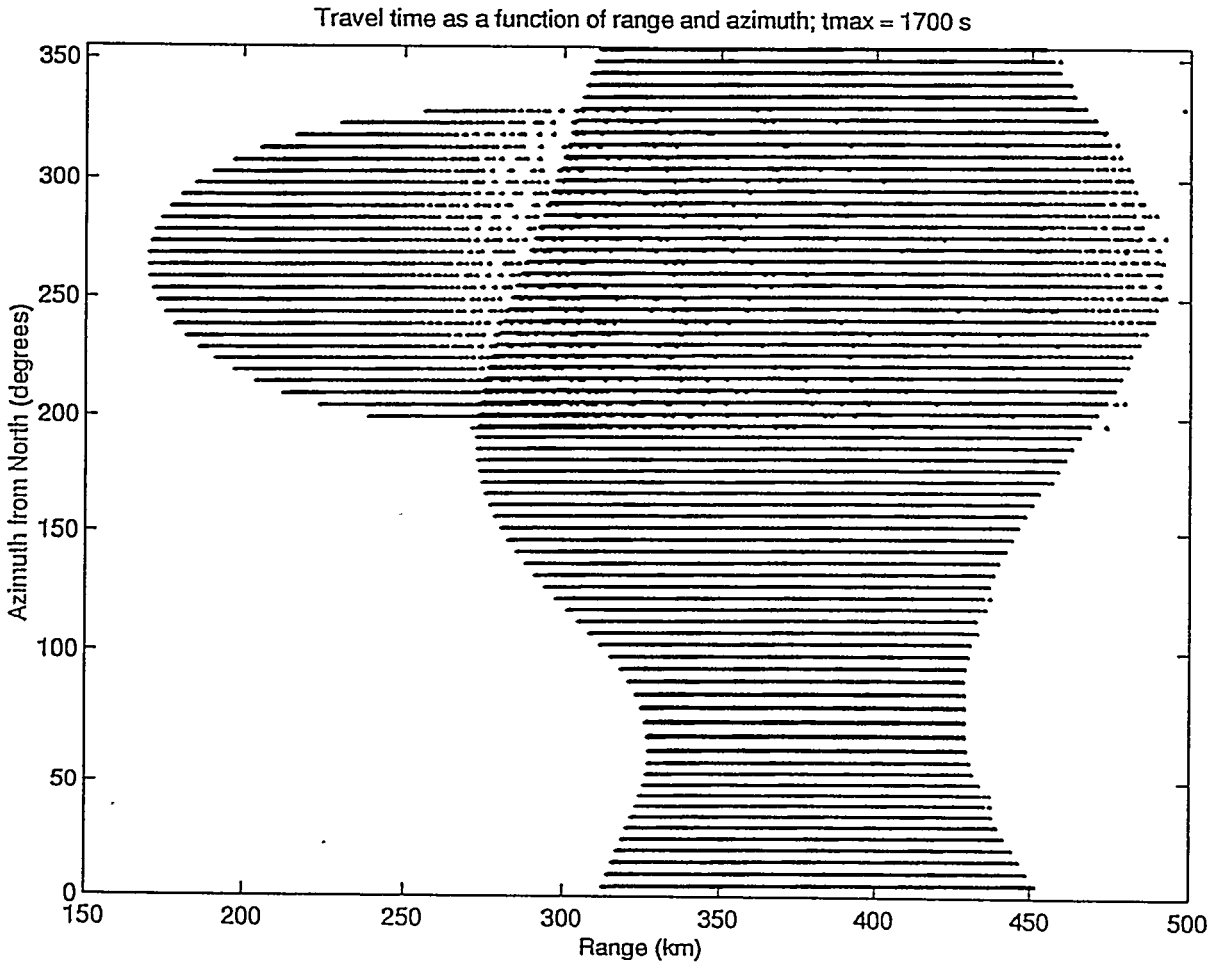
Travel time as a function of range and azimuth; tmax = 1700 s
Azimuth from North (degrees)
350
300
250
200
150
100
50
0
150
200
250
300
350
400
450
500
Range (km)

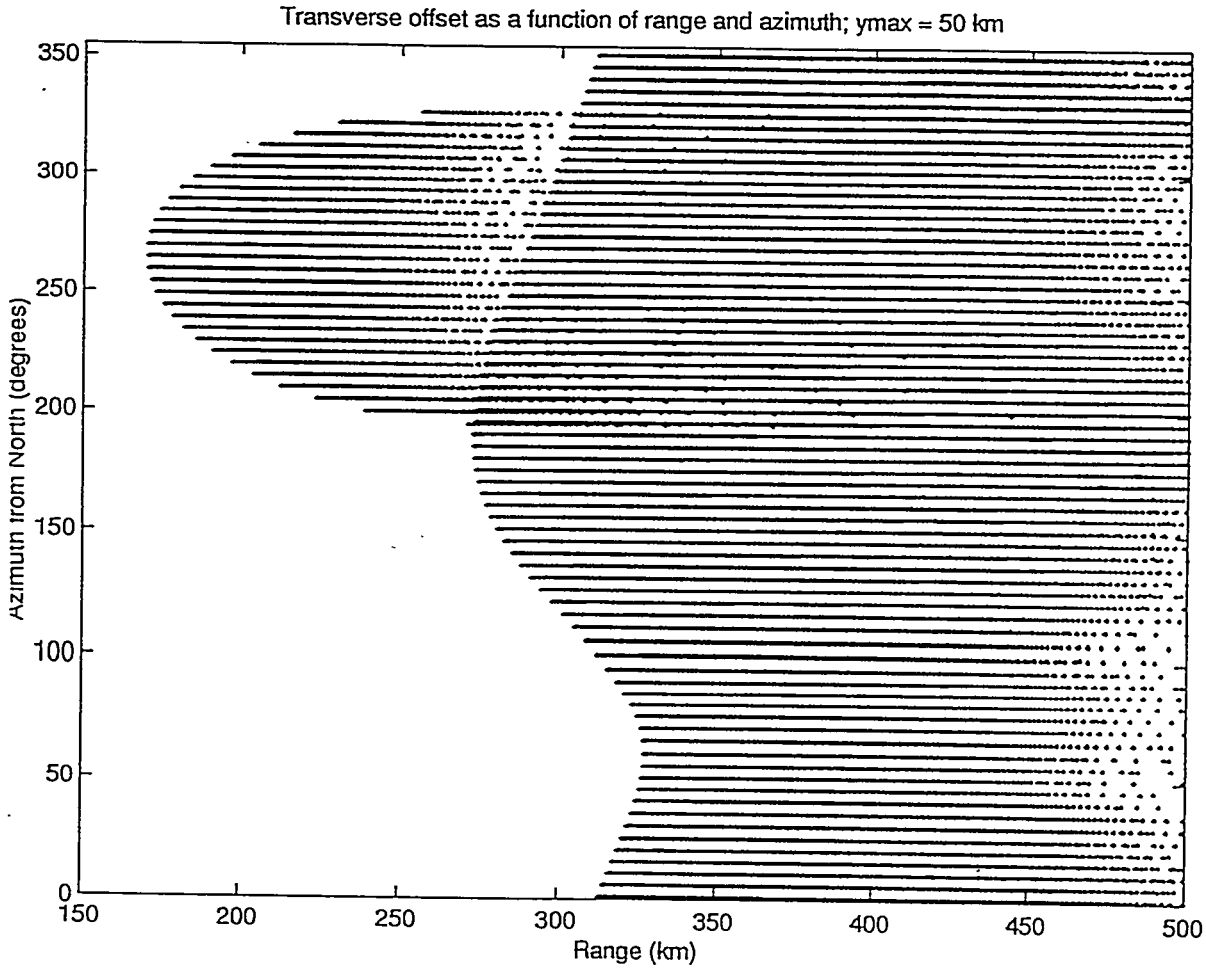
Transverse offset as a function of range and azimuth; ymax = 50 km
Azimuth from North (degrees)
350
300
250
200
150
100
50
0
150
200
250
300
350
400
450
500
Range (km)

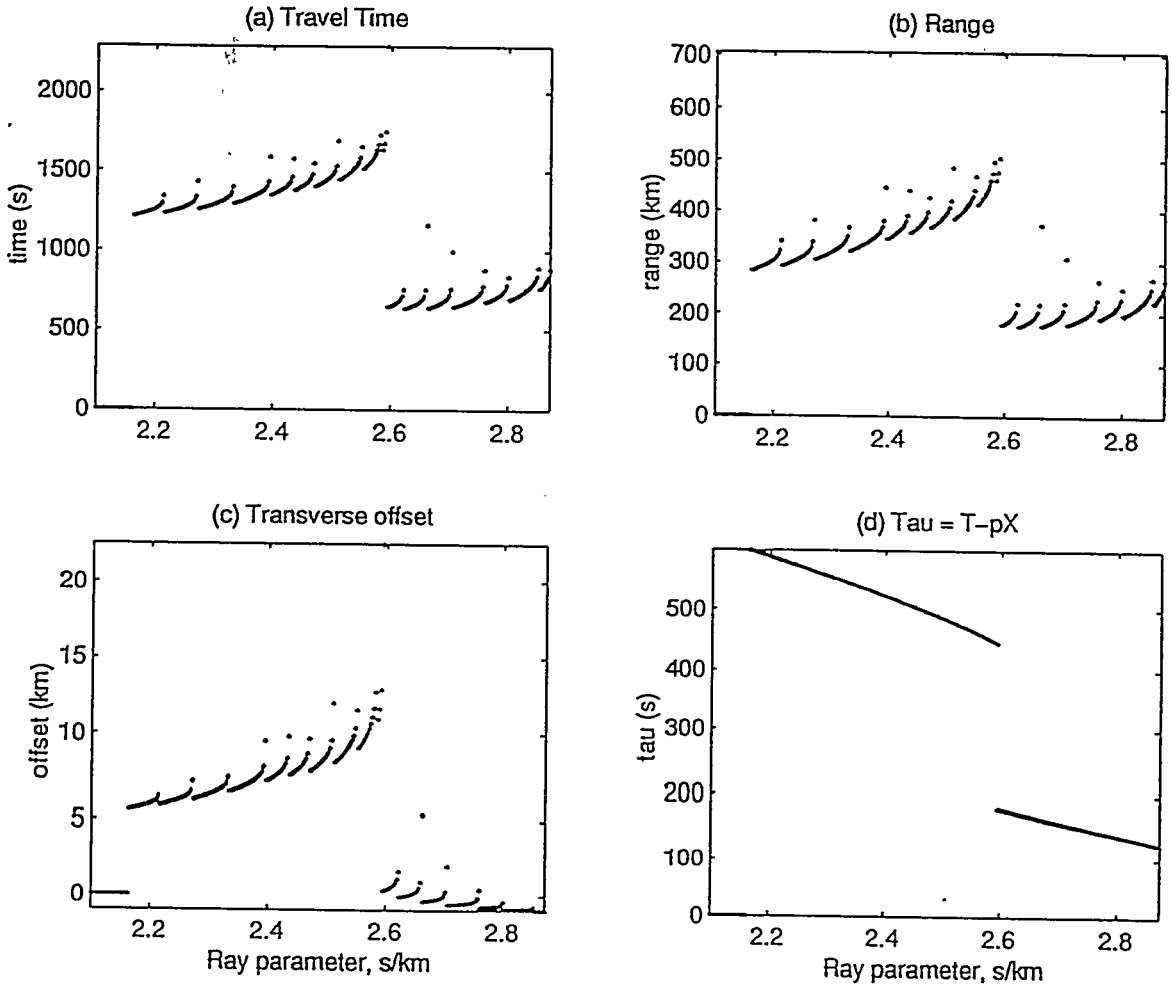
(a) Travel Time
time (s)
2000
1500
1000
500
0
2.2
2.4
2.6
2.8
(b) Range
range (km)
700
600
500
400
300
200
100
0
2.2
2.4
2.6
2.8
(c) Transverse offset
offset (km)
20
15
10
5
0
2.2
2.4
2.6
2.8
Ray parameter, s/km
(d) Tau = T–pX
tau (s)
500
400
300
200
100
0
2.2
2.4
2.6
2.8
Ray parameter, s/km

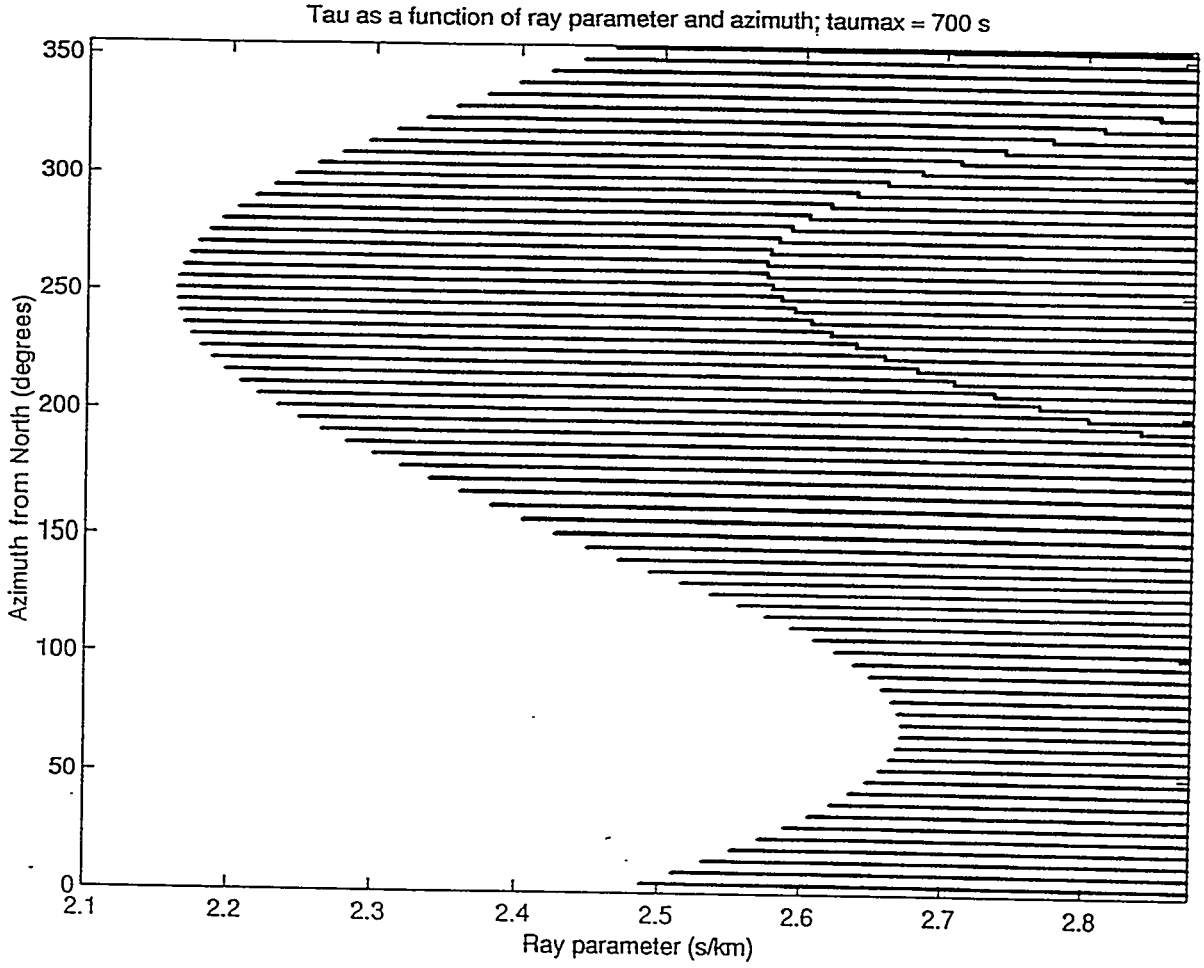
Tau as a function of ray parameter and azimuth; taumax = 700 s
Azimuth from North (degrees)
350
300
250
200
150
100
50
0
2.1
2.2
2.3
2.4
2.5
2.6
2.7
2.8
Ray parameter (s/km)

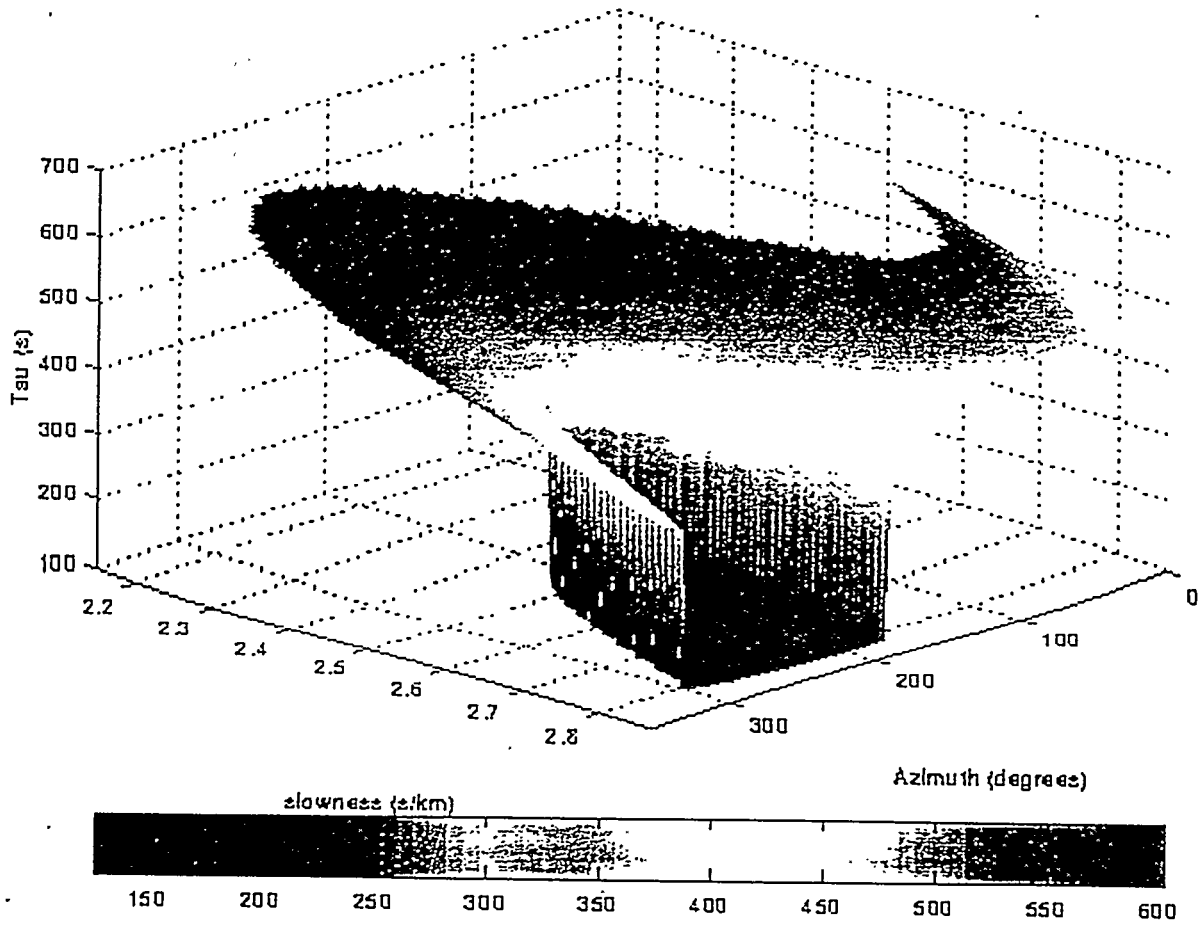
700
600
500
400
300
200
100
Tau (s)
2.2
2.3
2.4
2.5
2.6
2.7
2.8
0
100
200
300
Azimuth (degrees)
slowness (s/km)
150
200
250
300
350
400
450
500
550
600

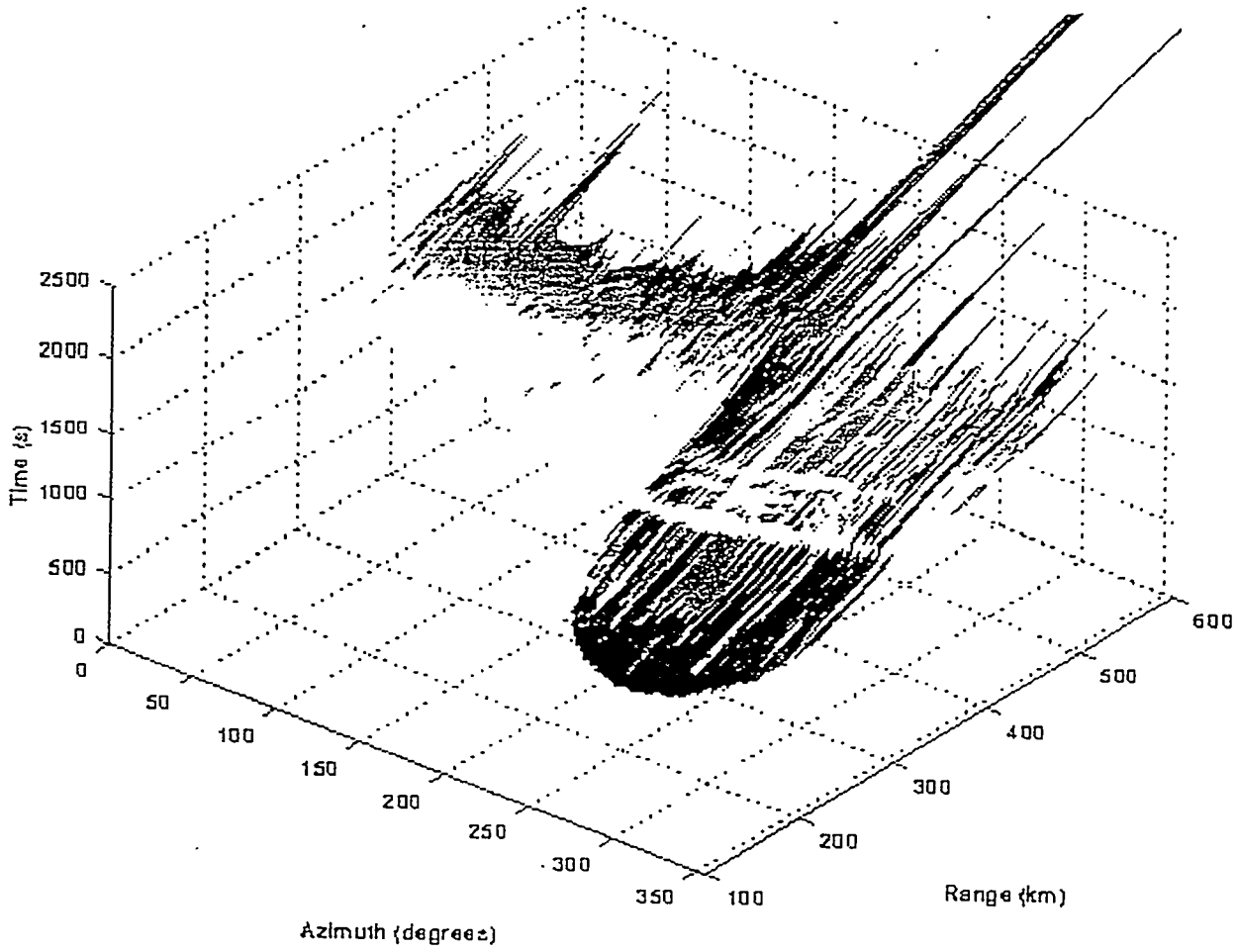
2500
2000
1500
1000
500
0
Time (s)
0
50
100
150
200
250
300
350
Azimuth (degrees)
100
200
300
400
500
600
Range (km)

Concluding Remarks

- A ray-theoretical model was utilized to compare observed and predicted arrival times for infrasonic waves ducted in the stratosphere and the thermosphere.

- Predicted S and I phases can be identified in the infrasonic data.

- Deviations in the arrival times of predicted and observed phases may be due to atmospheric changes, shearing or vertical winds, or diffraction.

- Travel time curves as a function of azimuth can be used for the identification of distinct branches observed in infrasonic data.

- Interpolation of the τ function over ray parameter and azimuth may permit the construction of more accurate travel time curves and efficient algorithms for source location.

INFRASOUND FROM MINING EXPLOSIONS, SPACE SHUTTLES AND METEORS

Eugene Herrin

Southern Methodist University

Seismic and infrasonic signals have been recorded at TXAR from explosions in Mexico, Texas, New Mexico and Arizona when the stratospheric winds were favorable. The effect of these winds has been found to be very significant to distances as great as 700km. Acoustic N waves and seismic "shuttle quakes" have been observed from the NASA space shuttle on landing orbits at distances up to 150km from TXAR. The unusual and distinctive characteristics of the shuttle quakes result from elastic bow-wave propagation resulting from the intersection of the acoustic conical wave with the earth's surface. Infrasonic signals and, in a few cases, seismic signals have been observed from meteors. These observations also show the importance of the stratospheric winds for infrasound detection.

INFRASOUND FROM MINING EXPLOSIONS, SPACE SHUTTLES, AND METEORS

Contributions by:

Jessie Bonner
Sarah Deering
Paul Golden
Eugene Herrin
Tao Liu
Gordon Sorrells
Jack Swanson
Ileana Tibuleac

Southern Methodist University
Department of Geological Sciences
Dallas, Texas 75275
(214)-768-2760

http://www.geology.smu.edu

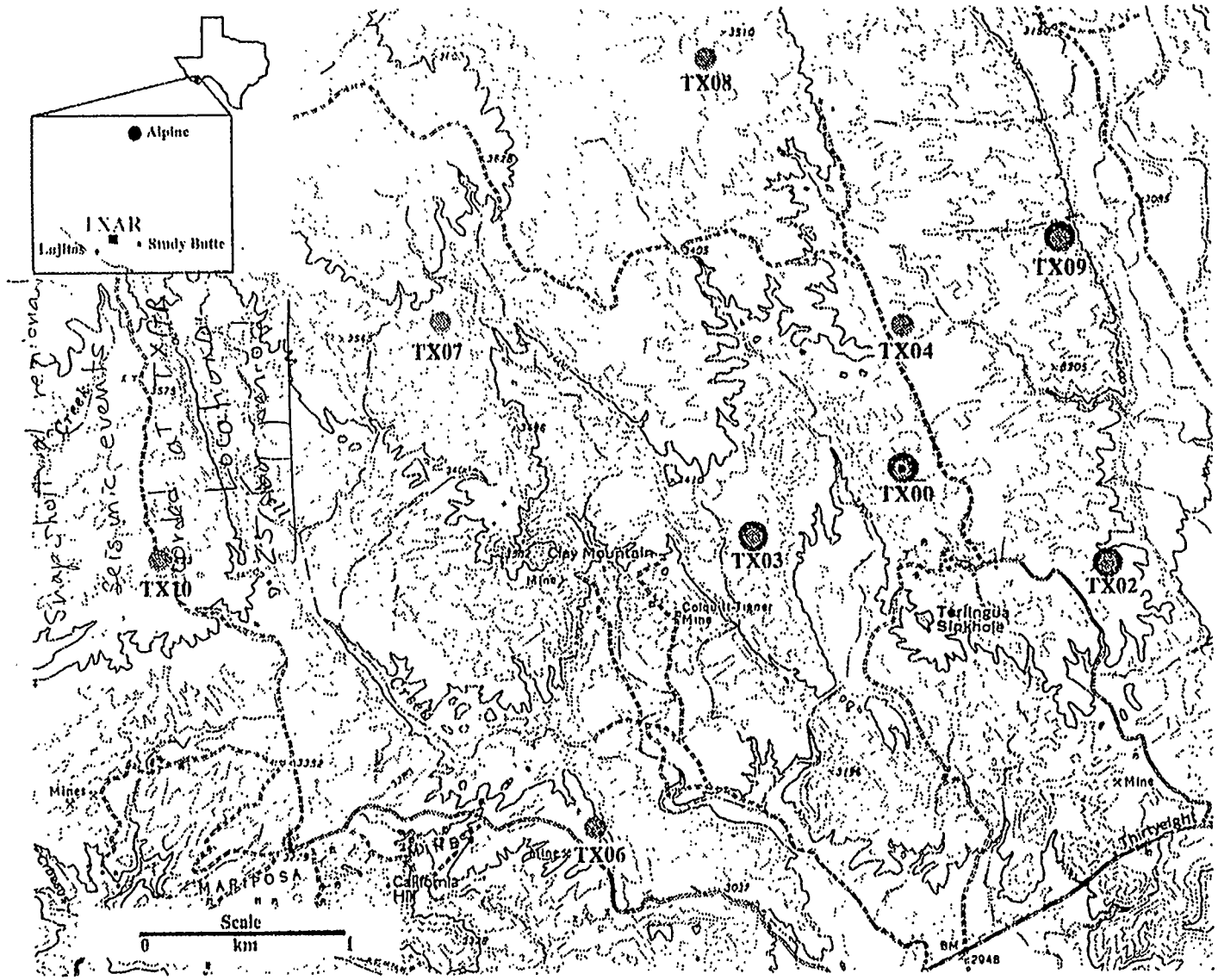

Map of the TXAR array showing the locations of all the elements (acoustic sensors shown in red):

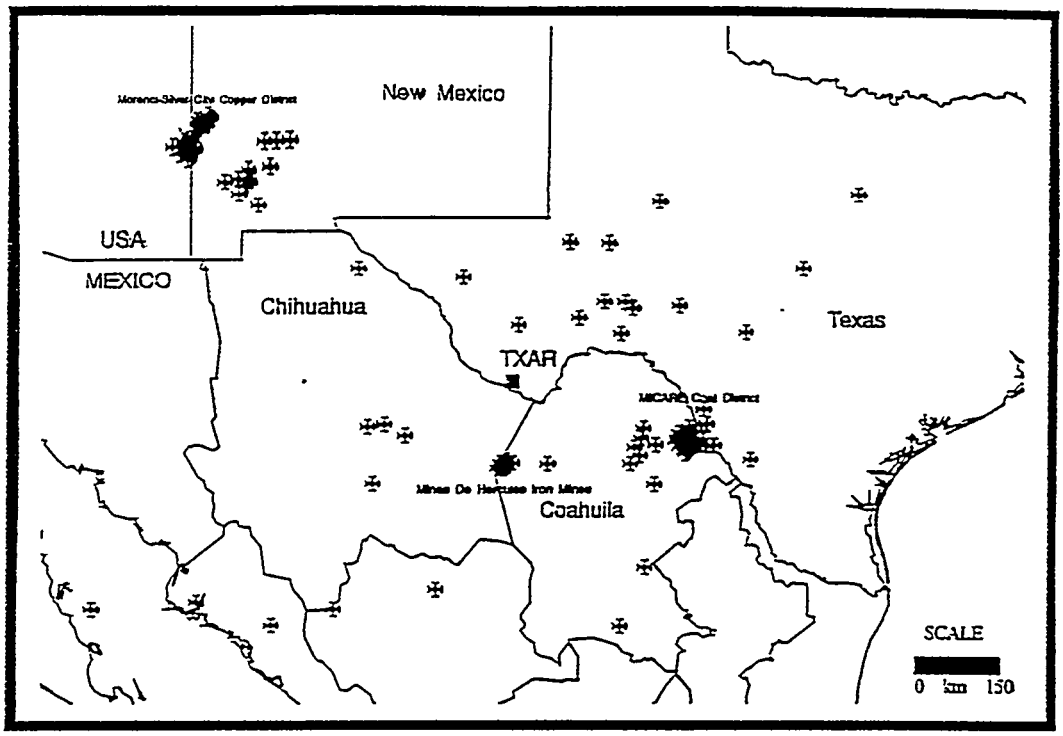

Locations of events recorded at TXAR between July 15, 1996 and August 10, 1996.

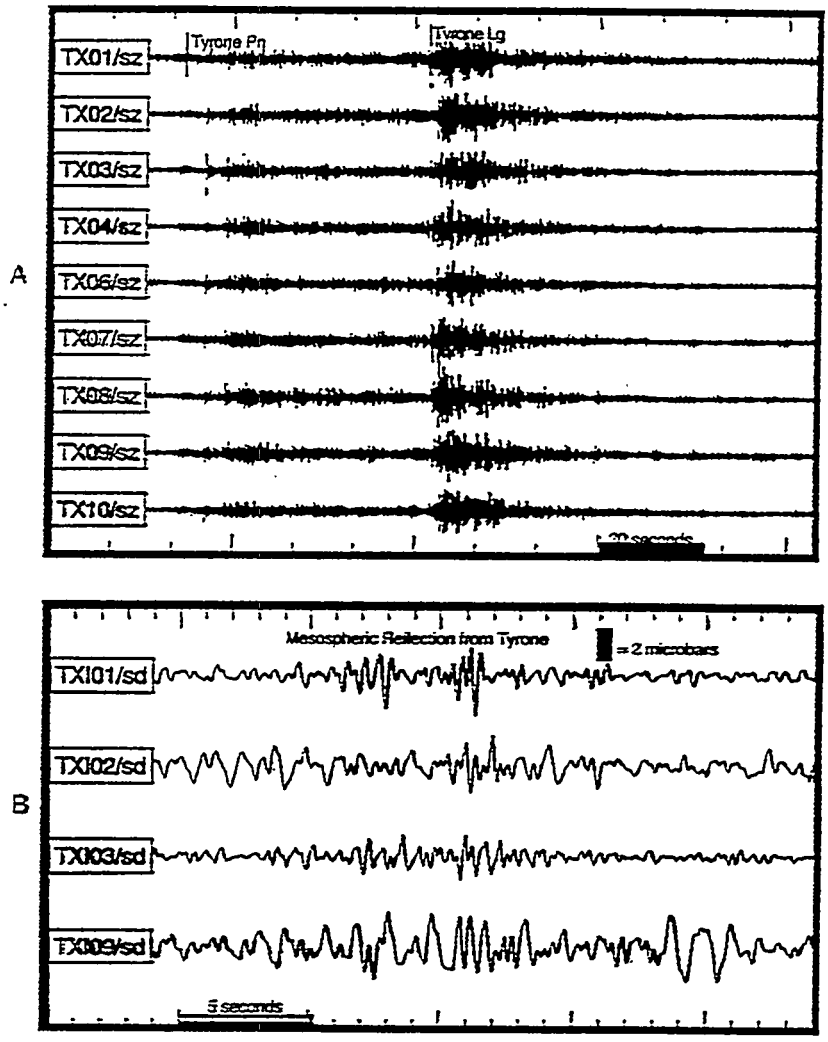

Seismograms (A) and microbarograms (B) from an explosion at the Tyrone Copper mine in western New Mexico.

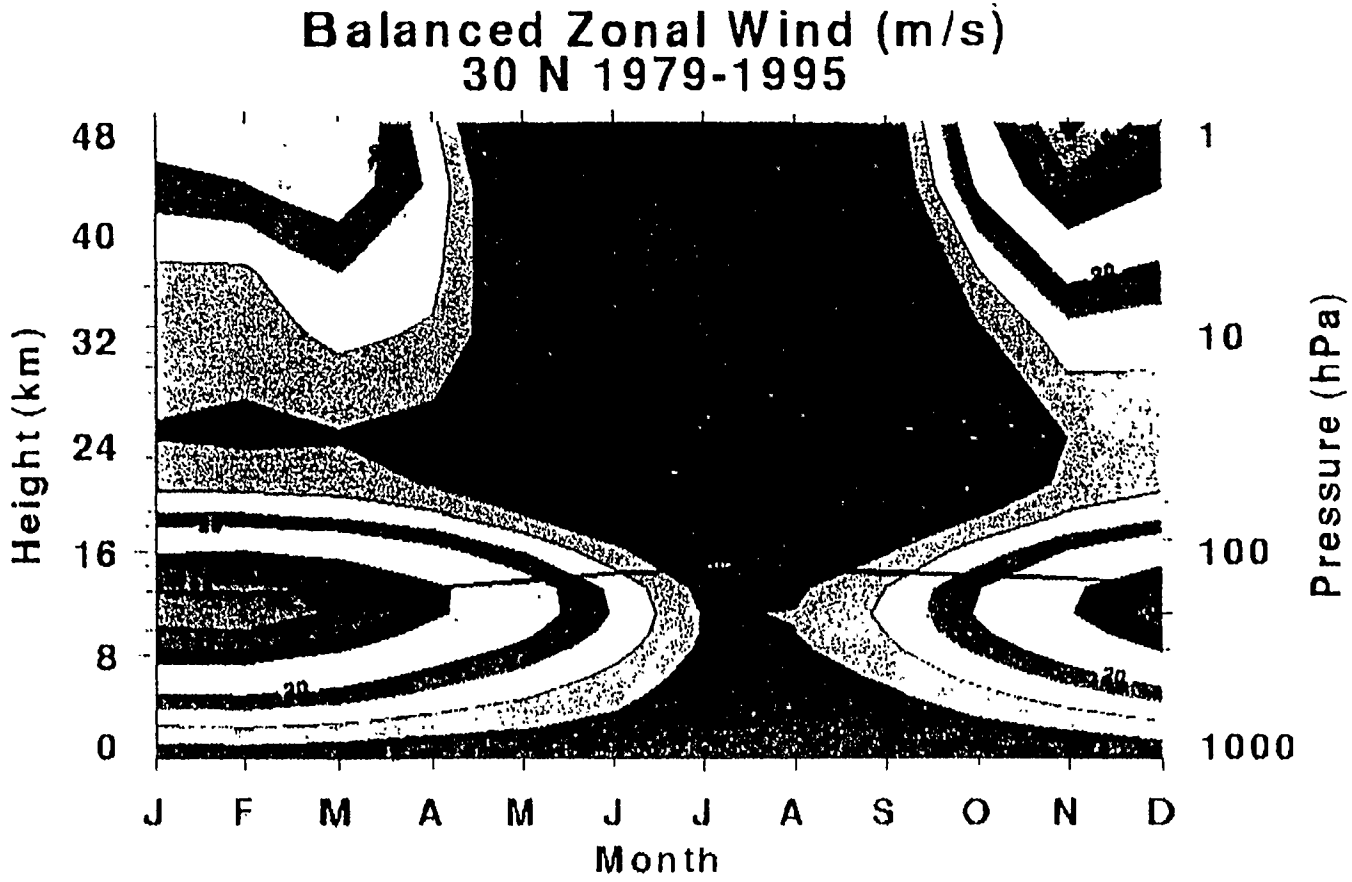

P. Newman (NASA), E. Nash (ARC), R. Nagatani (NCEP CPC)

Balanced zonal winds at 30° N, latitude. Wind from the west (positive) is indicated by warm colors, from the east (negative) by cool colors.

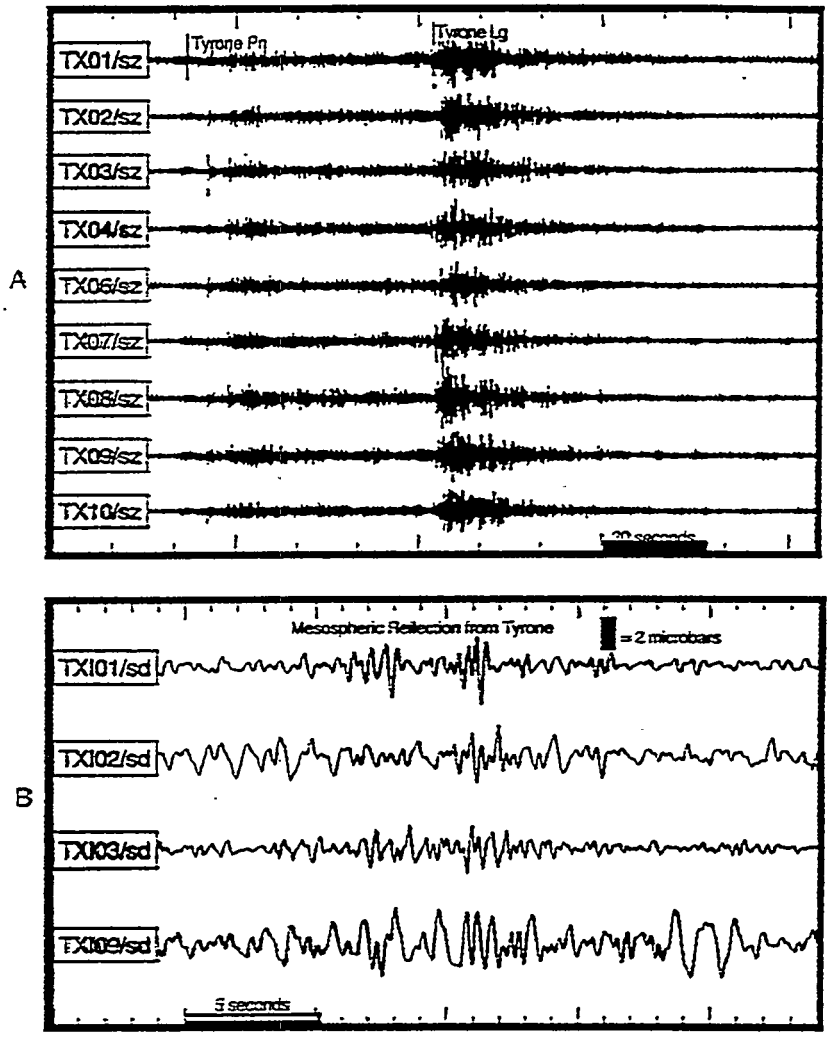

Seismograms (A) and microbarograms (B) from an explosion at the Tyrone Copper mine in western New Mexico.

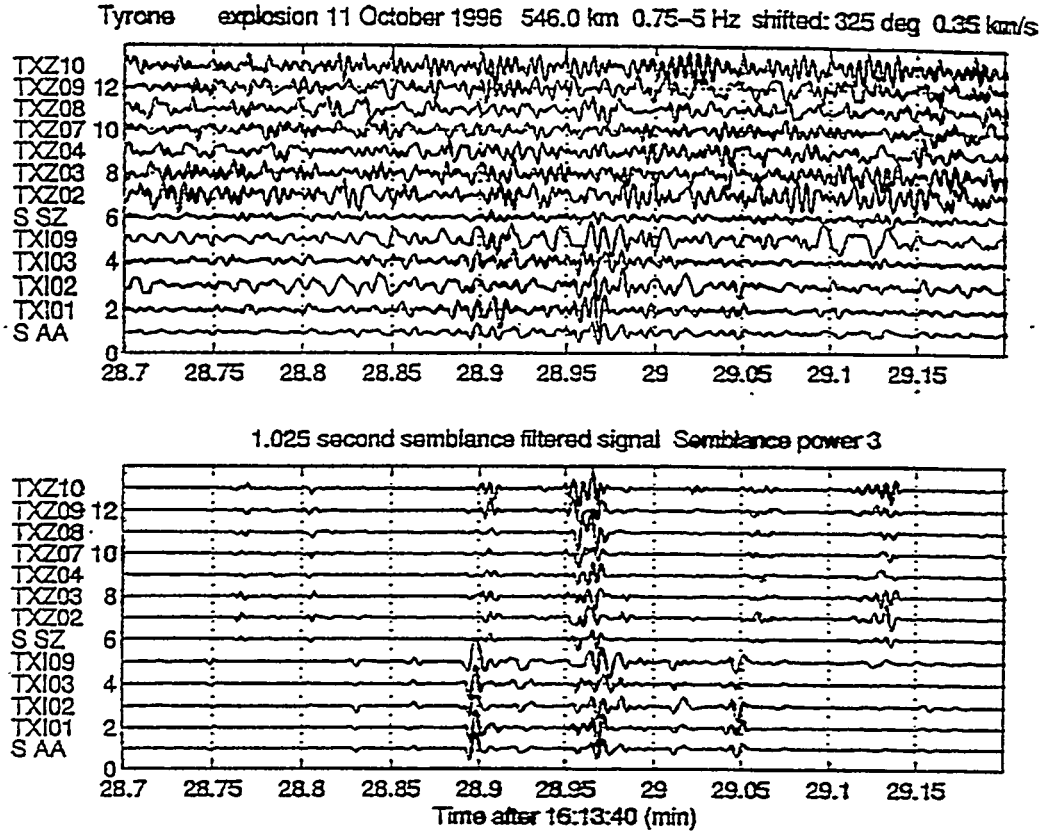

Results of semblance processing on seismo-acoustic data at TXAR.

CONCLUSIONS

- The results of the TXAR seismo-acoustic experiment illustrate that infrasound signals generated by commercial explosions are detectable in the 0.5-5.0 hertz bandwidth and can be observed at a distances up at least 680 kilometers from the source. Furthermore, it may be inferred from these results that the sources of the majority of commercial explosive seismic events will be identifiable by the detection of associated infrasound signals when:

  - the magnitudes of the seismic events are greater than about $m_b = 2.5$

  - their source to receiver distances exceed about 175-200 kilometers;

- the events occur during a time period and at locations such that the reception point is located stratospherically "downwind" from the sources.

Low Pressure Storm Front– February 13, 1997

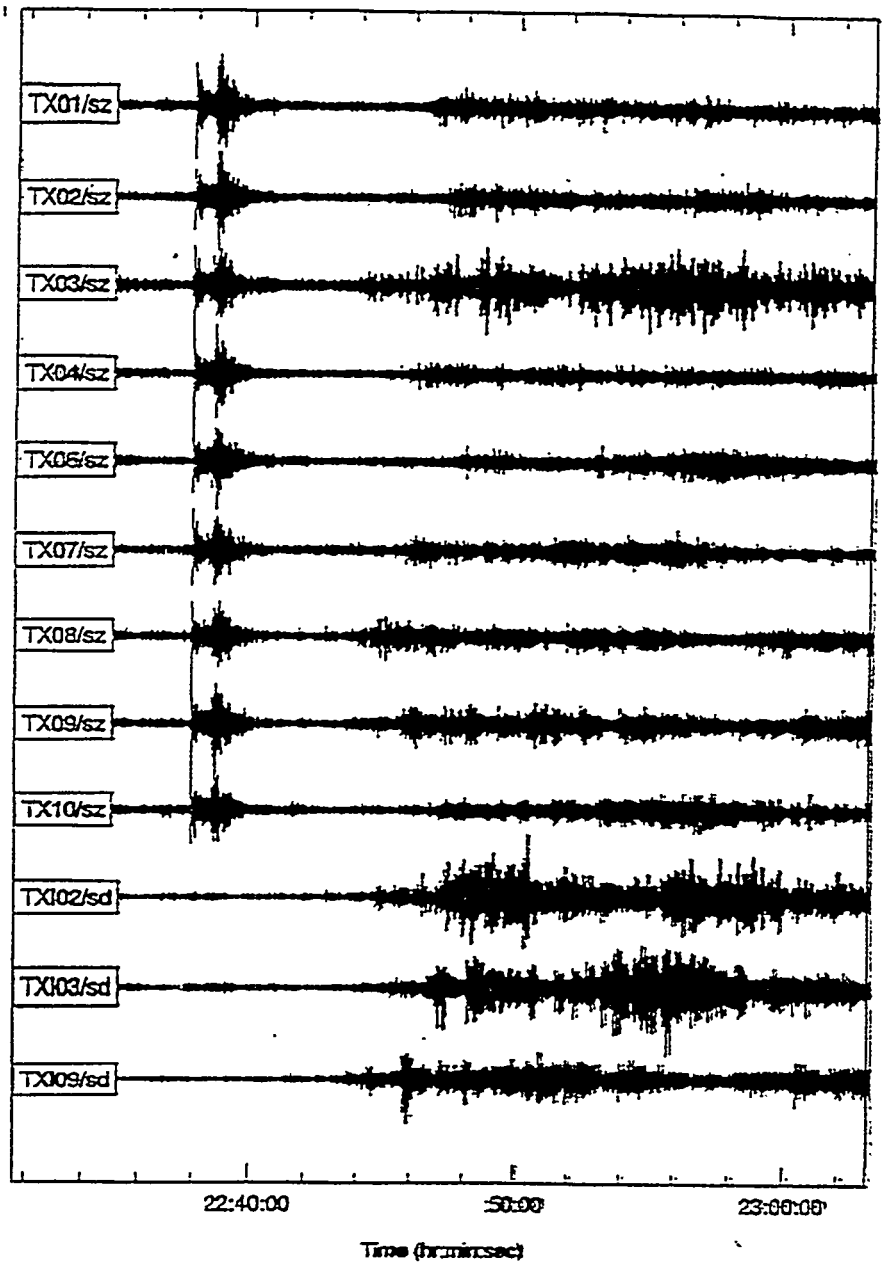

Arrival of a weather front at TXAR on Feb. 13, 1997. Noise levels are significantly increased on the seismic and acoustic channels as a result of the storm's passage.

Local Explosion-- February 11, 1997

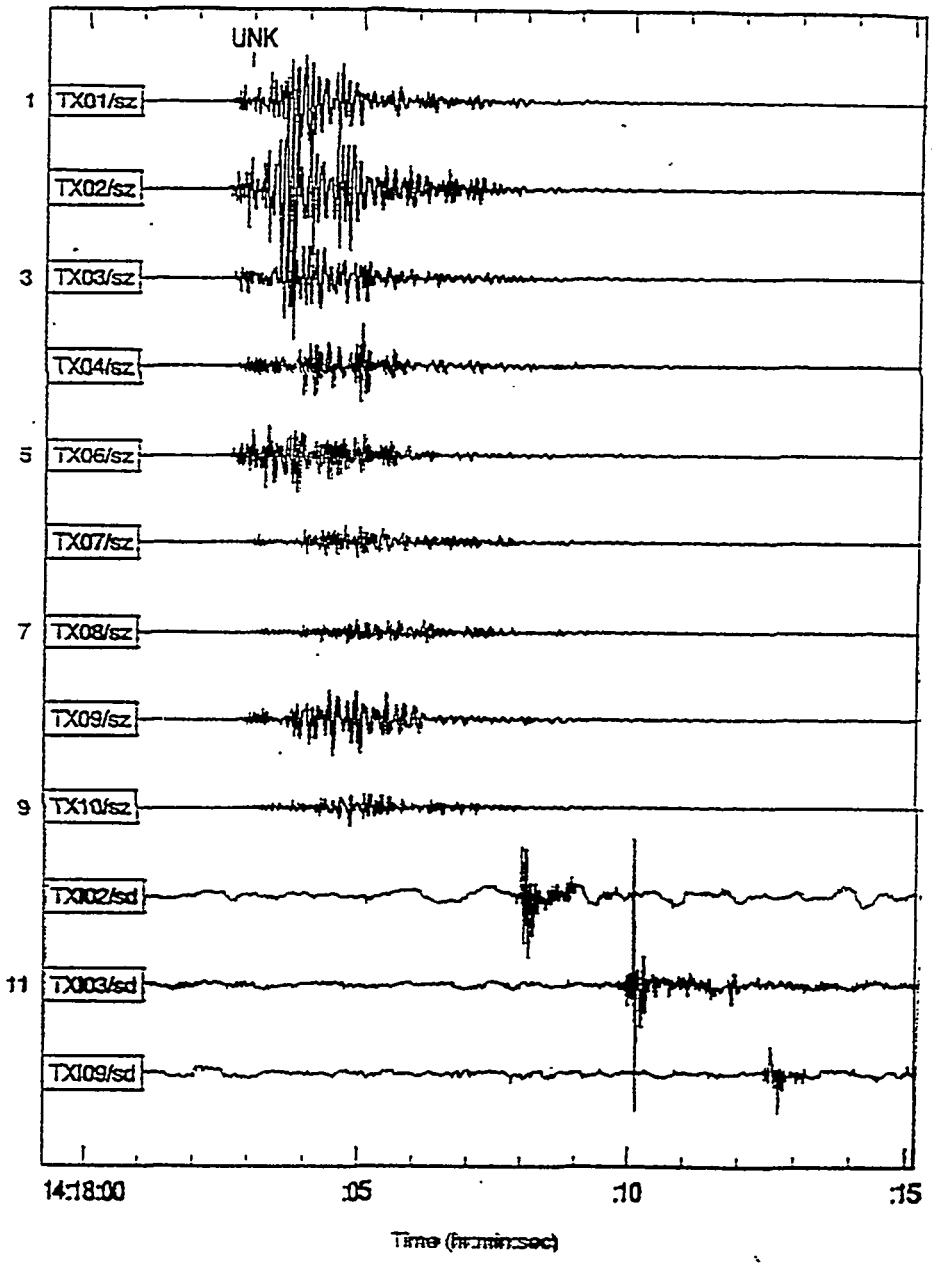

Local seismic event thought to be from an explosive source due to associated infrasound signals.

STS-70 Discovery July 22, 1995 Landing Time: 12:02:00 UTC Passed ~ 50 km to the South of TXAR

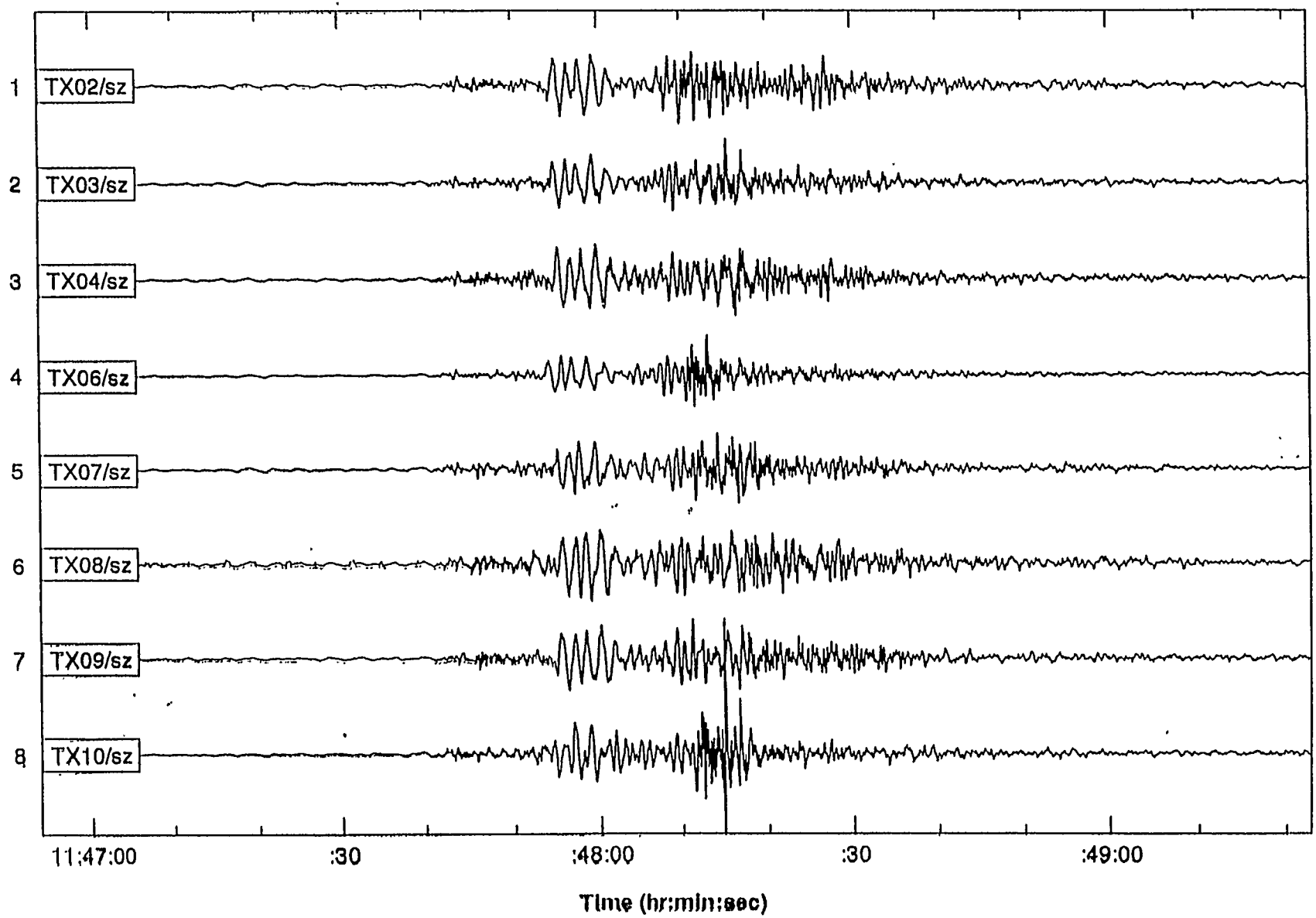

STS-82 Discovery February 21, 1997 Landing Time: 08:32:26 UTC Passed ~ 55 km to the South of TXAR

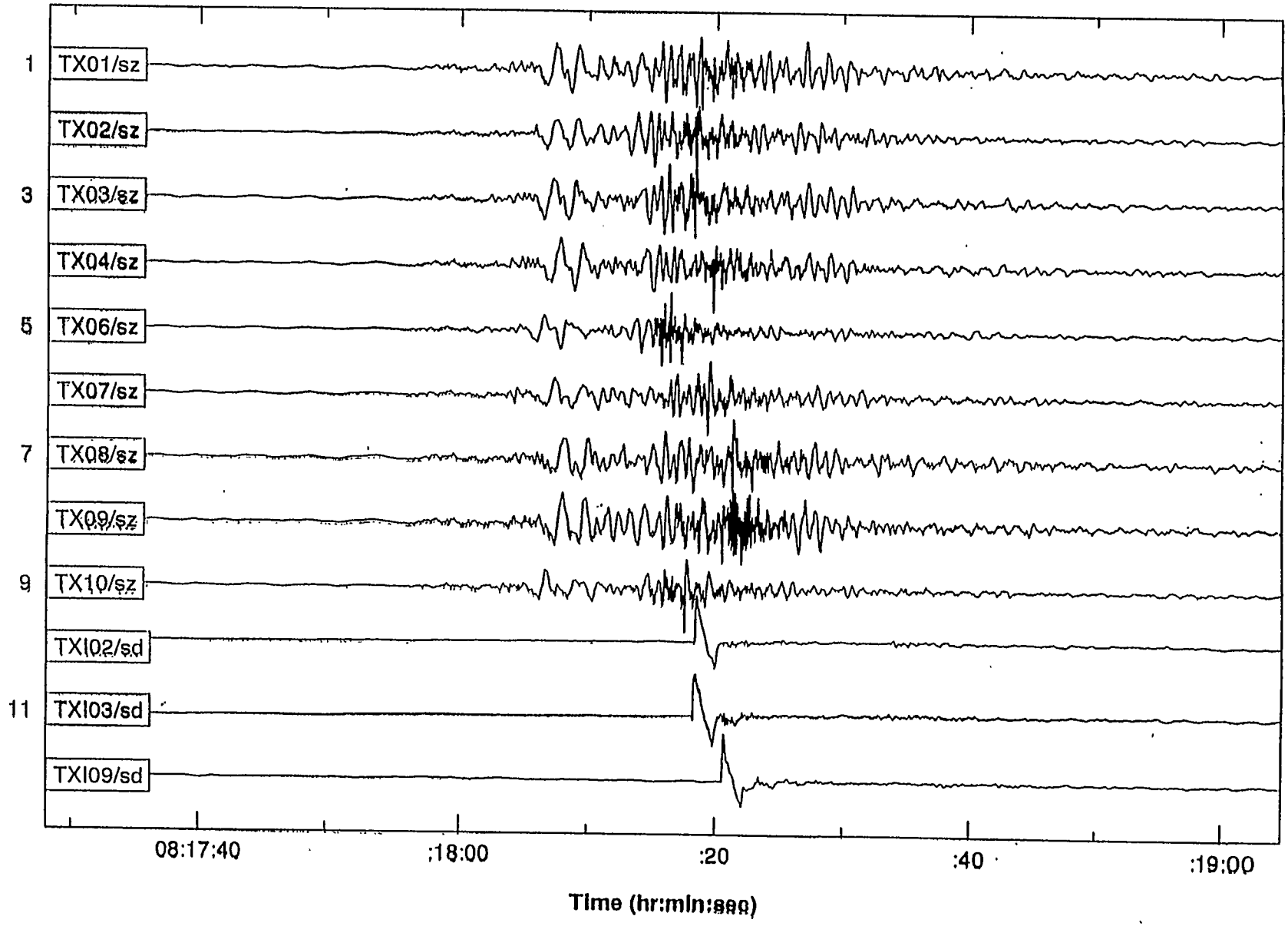

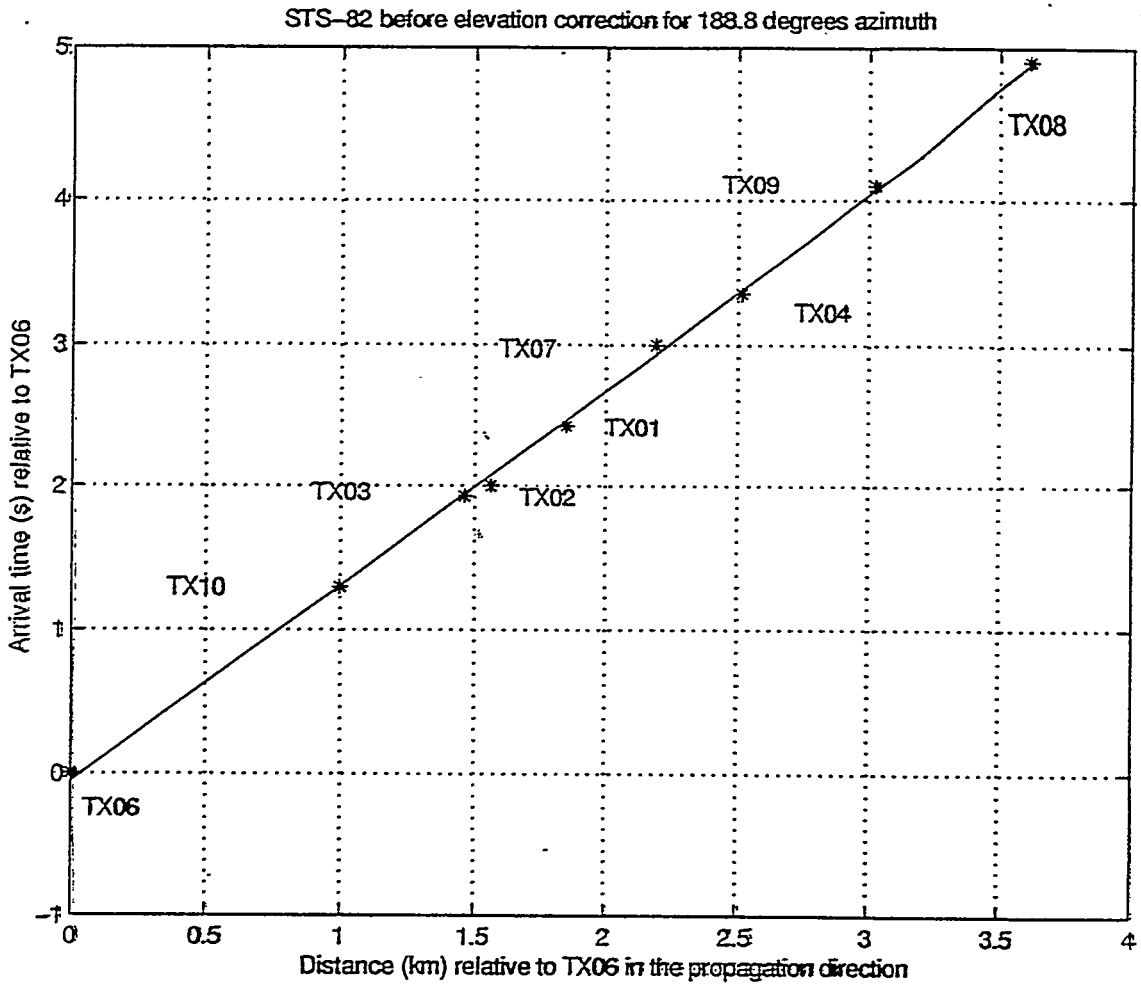
STS–82 before elevation correction for 188.8 degrees azimuth
Arrival time (s) relative to TX06
Distance (km) relative to TX06 in the propagation direction
TX08
TX09
TX04
TX07
TX01
TX02
TX03
TX10
TX06
5
4
3
2
1
0
−1
0
0.5
1
1.5
2
2.5
3
3.5
4

SHUTTLE LANDING GROUNDTRACKS

STS-78

STS-69 STS-75

STS-70 STS-82

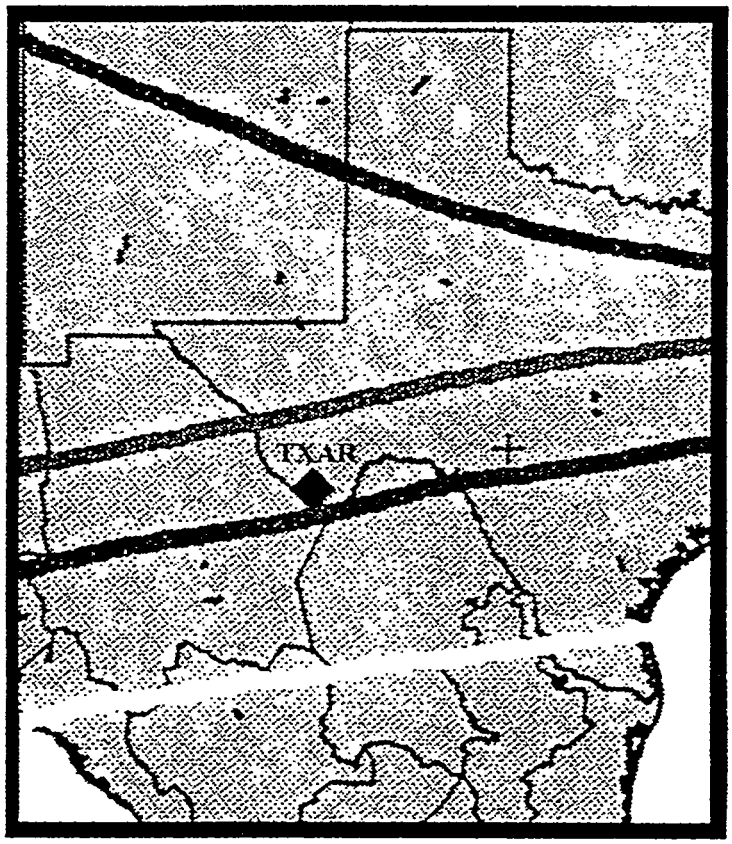

Groundtracks for shuttle missions are available through NASA's web pages.

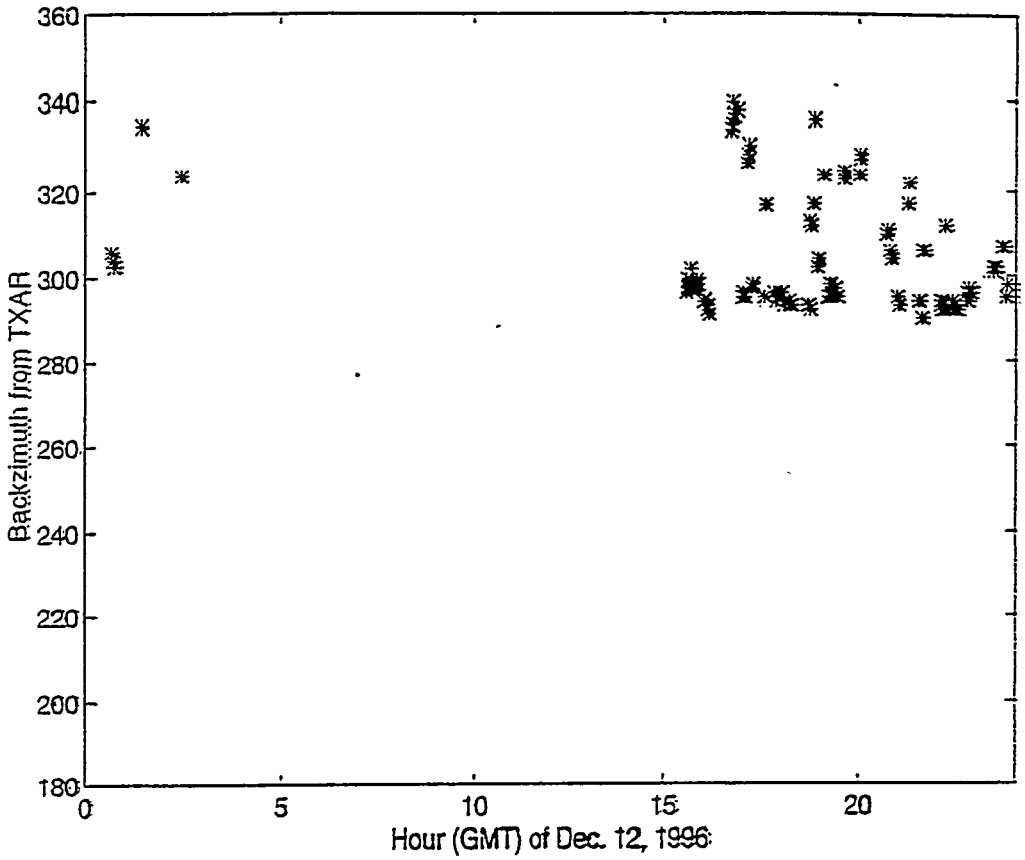

Arrival times for infrasound signals recorded on Dec. 12, 1996 plotted against backazimuth. These events are suspected to be from the Geminid meteor shower.

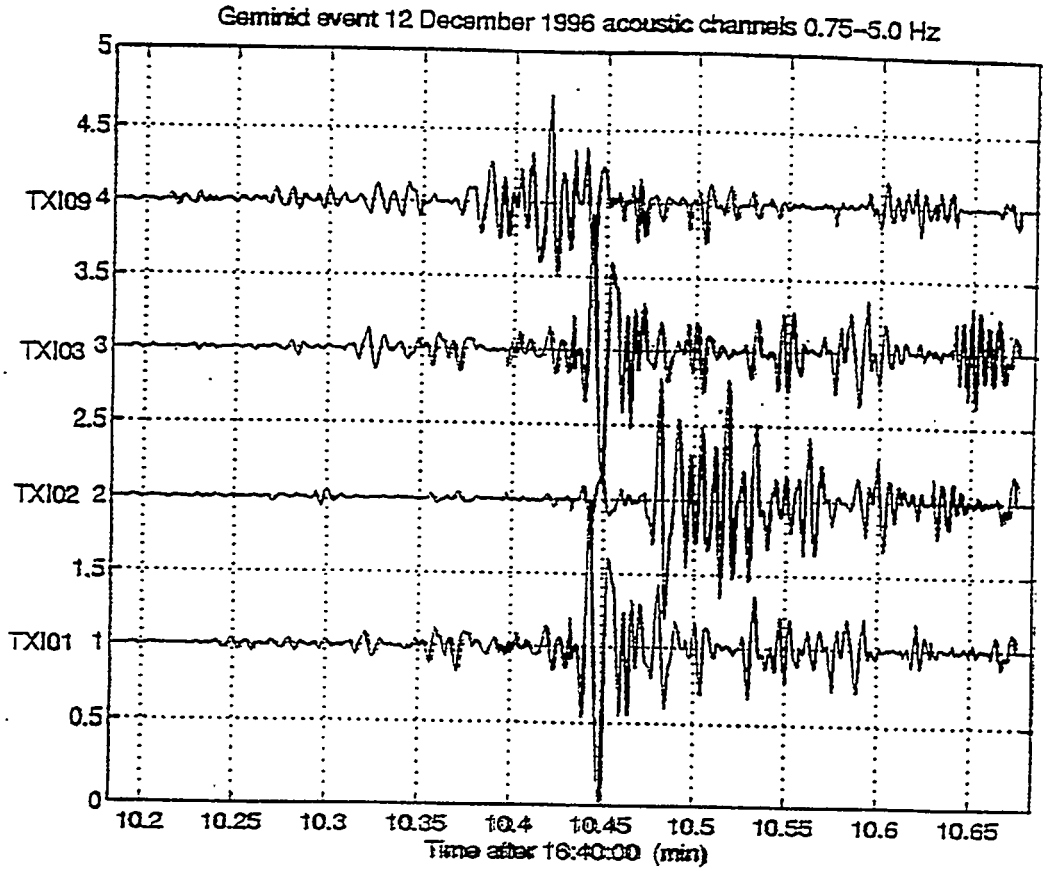

Infrasound signal thought to be the result of the Geminid meteor shower of December, 1996.

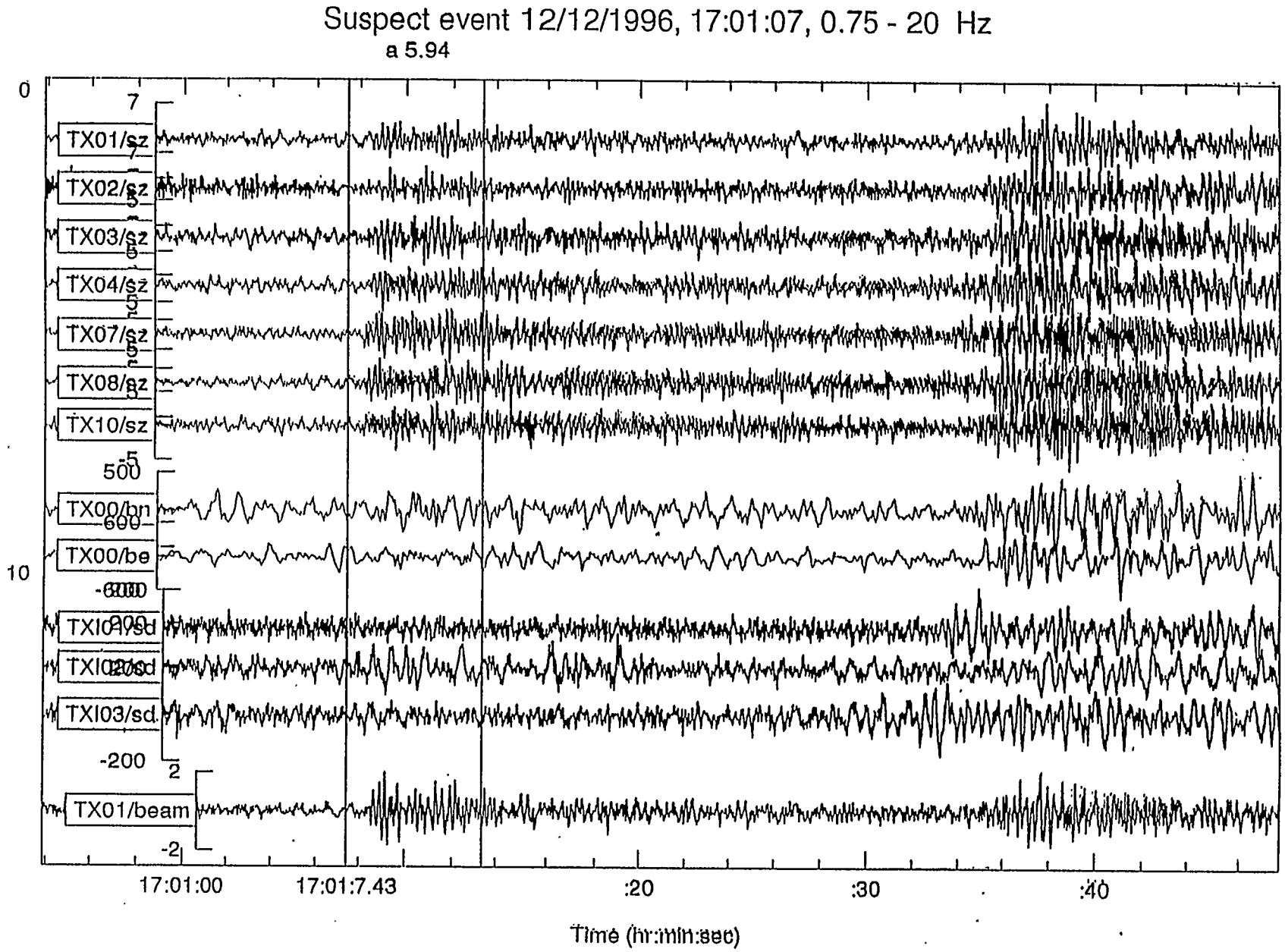
Suspect event 12/12/1996, 17:01:07, 0.75 - 20 Hz
a 5.94
0
10
TX01/sz
TX02/sz
TX03/sz
TX04/sz
TX07/sz
TX08/sz
TX10/sz
TX00/bn
TX00/be
TX01/sd
TX02/sd
TX03/sd
TX01/beam
7
-7
5
-5
500
-600
-200
2
-2
17:01:00
17:01:7.43
:20
:30
:40
Time (hr:min:sec)

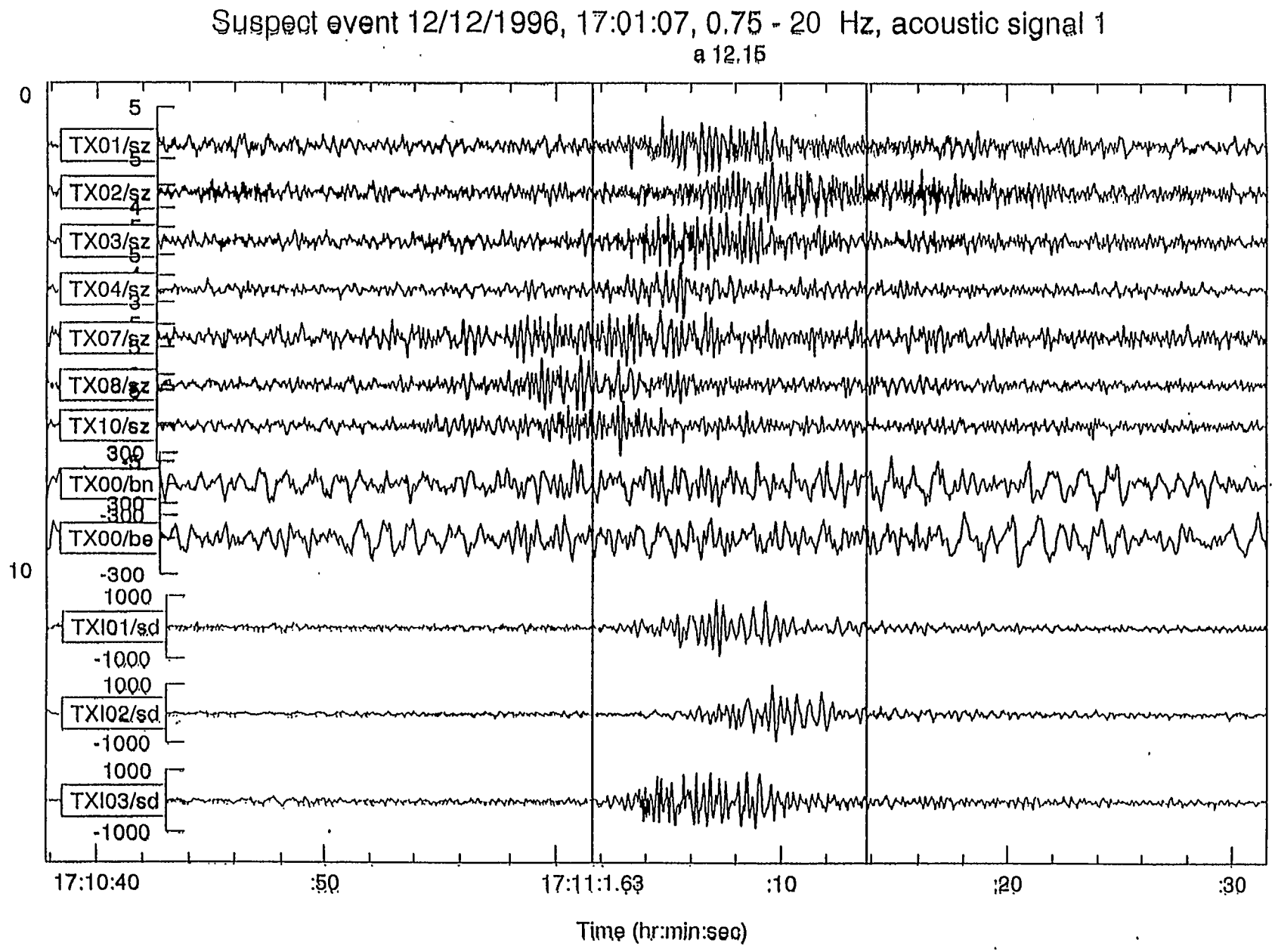
Suspect event 12/12/1996, 17:01:07, 0.75 - 20 Hz, acoustic signal 1
a 12.15
0
10
TX01/sz
TX02/sz
TX03/sz
TX04/sz
TX07/sz
TX08/sz
TX10/sz
TX00/bn
TX00/be
TXI01/sd
TXI02/sd
TXI03/sd
5
4
3
2
300
-300
1000
-1000
17:10:40
:50
17:11:1.63
:10
:20
:30
Time (hr:min:sec)

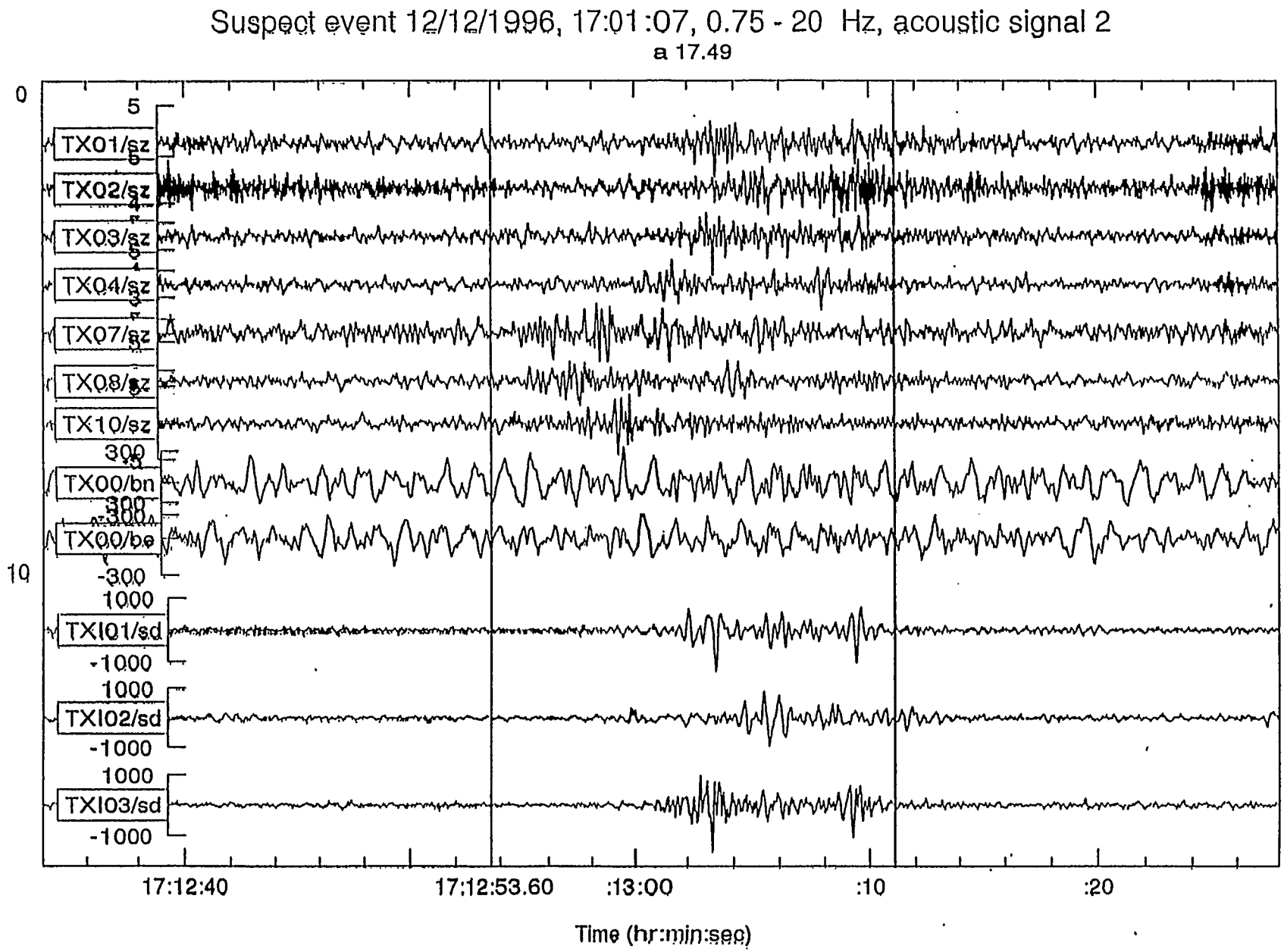
Suspect event 12/12/1996, 17:01:07, 0.75 - 20 Hz, acoustic signal 2
a 17.49
0
10
5
TX01/sz
TX02/sz
TX03/sz
TX04/sz
TX07/sz
TX08/sz
TX10/sz
300
TX00/bn
-300
TX00/be
-300
1000
TXI01/sd
-1000
1000
TXI02/sd
-1000
1000
TXI03/sd
-1000
17:12:40
17:12:53.60
:13:00
:10
:20
Time (hr:min:sec)

SEISMIC EVENT THE RESULT OF METEOR EXPLOSION ?

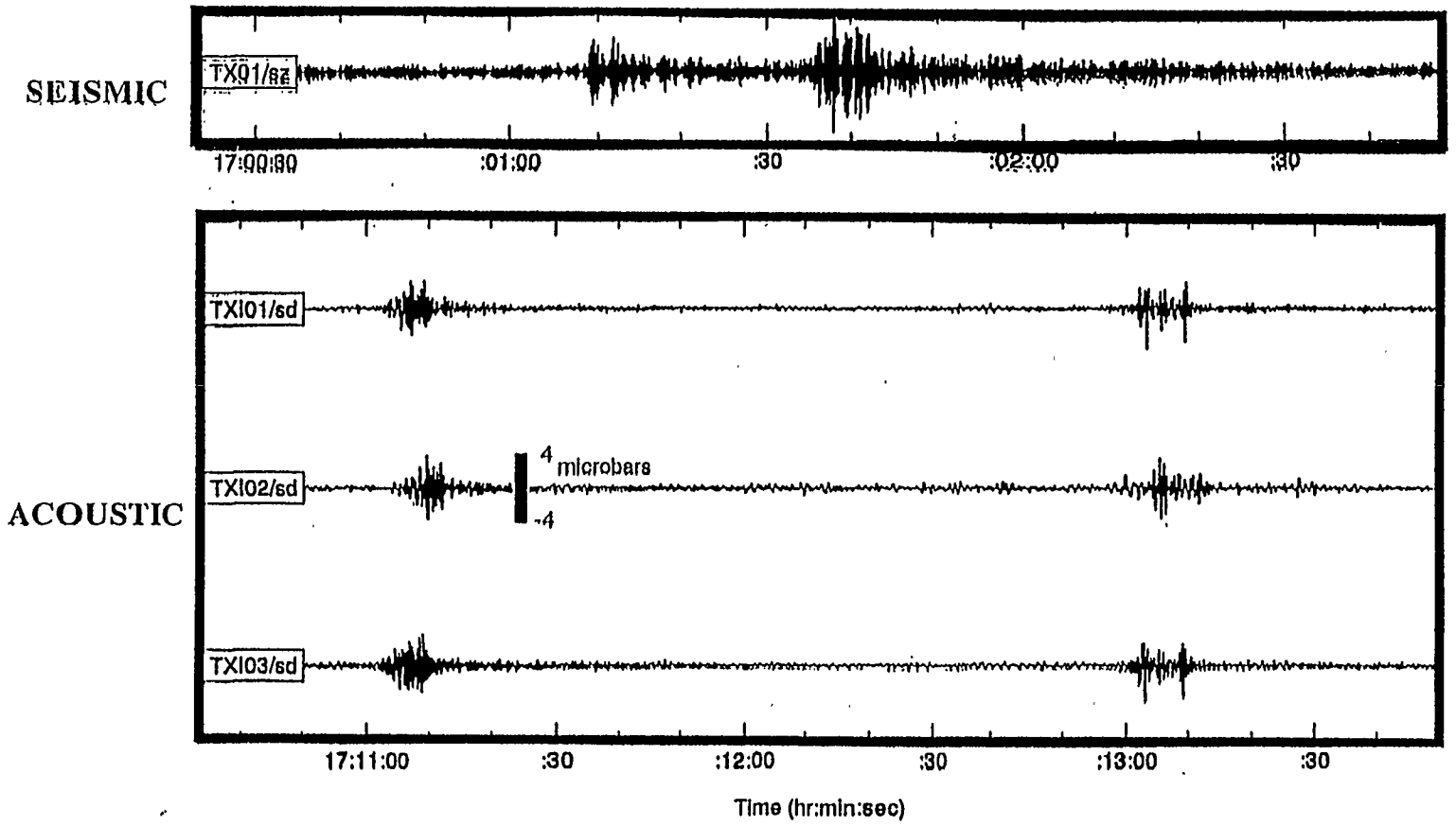

SEISMIC
Long: 104.7 W 30.9 N
SE of Van Horn, TX
Backazimuth: 330
mb:0.7 mLg: 1.0
Distance:201 km

ACOUSTIC
EVENT 1: Backazimuth 329 Vel: 0.35
EVENT 2: Backazimuth 331 Vel:0.36

SUMMARY

- A number of features may be used to group regional seismic events into clusters.

- Associated infrasonic signals can be used to identify some of the clusters as commerical explosions.

- Seismic events that do not fall into the usual categories - commercial explosions and earthquakes - may be identified using both seismic and acoustic data. Examples are shuttle quakes and bolide quakes.

THE INFRASOUND BACKGROUND FOR HIGH LATITUDE CTBT STATIONS

Charles R. Wilson

Geophysical Institute,
University of Alaska, Fairbanks Alaska

Examples are presented of typical infrasonic signals observed from natural sources at Fairbanks, Alaska (64.9 deg. North) and Windless Bight, Antarctica (77.7 deg. South) to illustrate the infrasound background to be expected at future high latitude CTBT sites.

Mountain Associated (MAW), Volcanic eruption (VOL), and Auroral infrasonic waves (AIW), within the passband of 0.01 to 0.1 Hz, were observed with a microphone array of 4km to 6km spacing, while Microbaroms (MB) from marine storm standing-sea-waves, within the passband from 0.1 to 1.0 Hz, were observed on a small array with ~1.0km spacing. For each infrasonic signal individual microphone waveform traces as well as a phase-aligned overlay trace for maximum correlation together with the horizontal trace velocity, the azimuth of arrival, and the maximum values of the six inter-microphone cross-correlation coefficients (cmax) are given for both the raw unfiltered data and for the Pure State filtered data to illustrate the often great increase in signal-to-noise ration after Pure State filtering F. Diagrams are also shown of Azimuth of Arrival and Horizontal Trace Velocity as a function of time for typical infrasonic wave episodes of MAW, VOL, AIW and BM. The typical signals that are presented were selected from a Geophysical Institute six station-years of historical digital data that has recently been transferred to CD-ROMs using a Matlab format. This digital infrasonic data archive is now available for testing infrasonic signal detection and analysis algorithms.

Atmospheric Infrasonic Waves of Natural Origin

By Charles R. Wilson, Professor of Geophysics
Emeritus, Geophysical Institute
University of Alaska, Fairbanks, Alaska
E-mail: 76654.2724@CompuServe.com

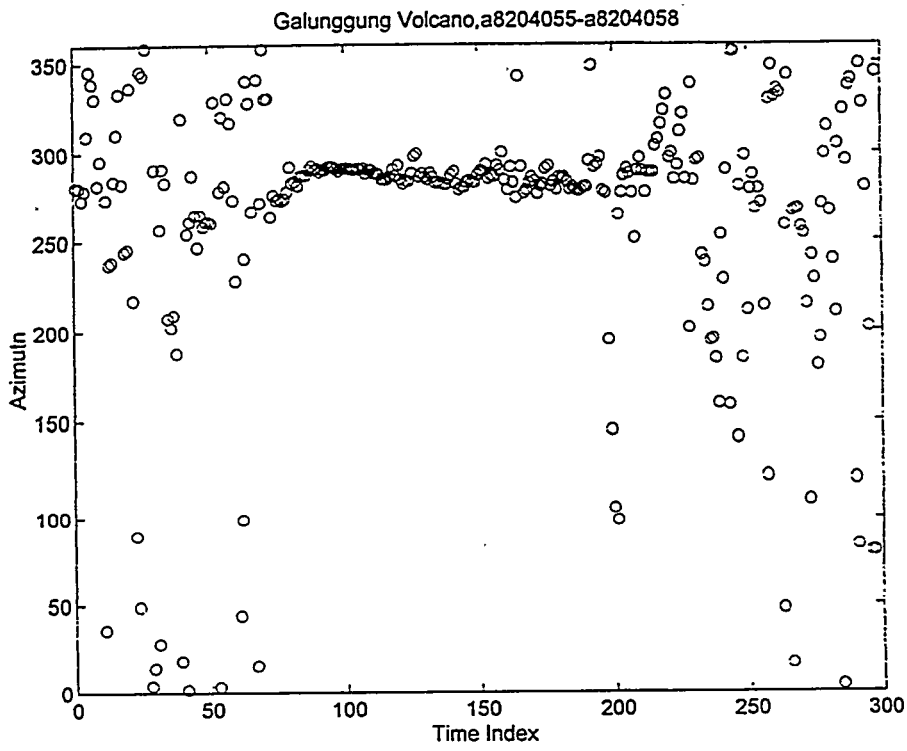

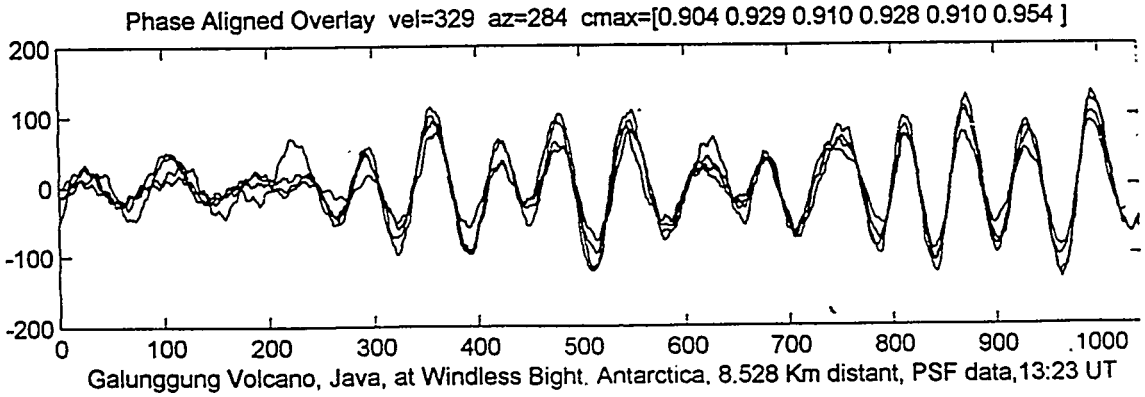

Auroral Infrasonic Waves (AIW)

In the passband from 10 to 100 second periods, auroral infrasonic waves (AIW) are frequently observed on the night side of the earth by infrasonic microphone arrays both in the high latitude auroral regions as well as at lower latitude stations, at distances up to 1,000 km from the source auroral arcs. AIW are occur at all seasons of the year with maximum activity around the Equinoxes. Their diurnal characteristics depend on the latitude of the observing station, with a maximum frequency of occurrence usually around local magnetic midnight in the auroral zone. AIW substorms are highly correlated with negative bays in geomagnetic activity and they can last for periods from only a few hours to all night long. AIW are infrasonic bow waves that are generated by the transverse supersonic motions of large scale auroral electrojet arcs that develop, high in the ionosphere, during periods of intense auroral activity. The infrasound produced by auroral arc supersonic motions is highly anisotropic propagating to the earth's surface as bow waves directly beneath the supersonic auroral arcs, with a delay times of about six minutes following zenith passage of the arc over the observing station, (see Fig. 2). The propagation vector of the AIW bow wave is parallel to the direction of motion of the supersonic auroral arc and to the total horizontal magnetic disturbance vector that is associated with the westward electrojet current flowing within the auroral arc itself, (see Fig.3). The azimuth of arrival for AIWs from the same source arc will frequently diverge by as much as 45 degrees, as observed successively at two infrasonic stations that are hundreds of kilometers apart, if the higher latitude station is in the front shock region of the bow wave while the lower latitude array is in the side-shock region, (see Fig. 2). Propagation to great distances takes place by reflection at the surface of the initial bow wave and subsequent ducting in the atmospheric sound channels to lower latitudes. Because the infrasound generated by aurora motions is not isotropic but highly directional, it is not possible to triangulate on the source region of AIW by the use of a network of infrasonic arrays as would be the case of volcanic infrasonic signals. The spectral characteristics of AIW observed at great distances from their sources differ from those observed at auroral zone stations in that the high frequency components of the AIW have are filtered out by multiple high level reflections along the ray path, (see Fig. 4 and 5). The diurnal variation in the azimuth of arrival of AIW, in the auroral zone, is totally dependent on the morphology of auroral motions along the auroral oval during the development of magnetic substorms, (see Fig. 6). At Fairbanks, Alaska AIW are observed to arrive first from the NE in the evening, from N around magnetic midnight and from the NW in the morning hours, (see Fig. 7).There is a great asymmetry in the production mechanism of AIW such that no AIW have ever been observed that result from poleward moving supersonic auroral arcs even though these auroral arcs may contain strong electrojet currents,(see Fig. 8). This asymmetry effect in AIW production is thought to be associated with Lorentz force,($\mathbf{J} \times \mathbf{B}$), coupling mechanism between the auroral electrojet current **J** and the neutral gas that produces the infrasonic bow wave in the auroral electrojet arcs in the lower ionosphere. The AIW horizontal trace velocity,(the speed with which the signal crosses the microphone array), varies from 300 m/sec to almost 1,000 m/sec, with an average value of about 500 m/sec. The high trace velocities occur only near the source arcs. AIW have inverse dispersion with the higher frequency components arriving first. The periods of AIW vary from 10 to 100 seconds with maximum spectral power around 70 second periods. The pressure amplitude of AIW varies from 0.5 to 20 microbars. In the near-field zone, under the source arcs, the AIW wave-packets are highly coherent across microphone arrays with sensor spacing of up to six km.

Two examples are shown ,after Figure8, of AIW signals observed at Fairbanks from an historical digital data set from 1984. The waveform data, for both the unfiltered raw data and the Pure-State filtered data (PSF), from each microphone as well as a phase-aligned overlay of all

channels are shown giving the trace velocity, azimuth of arrival, and the maximum cross-correlation coefficients (cmax) between microphone pairs. The spectral characteristics are given for the AIW for each of the four channels. The first AIW signals shown for 03/22/84 from 09:41 to 09:55 UT have a period around 50 seconds, while the two AIW signals at 09:11 and 09:18 on 04/08/84 have spectral energy at periods of 20 and 13.5 seconds.

Bibliography for Auroral Infrasonic Waves

Chimonas, G. , Infrasonic Waves From Auroral Arcs, 1977, J. of Gepphys. Res. vol. 82, No. 25 , p 3573

Chimonas, G. and W. R. Peltier, The Bow Wave Generated by an Auroral Arc in Supersonic Motion, Planet. and Space Sci., vol 18, p 599, 1970

Chrzanowski, P., et. al. ,Tvaveling Pressure waves Associated with Geomagnetic Activity, J. Geophys. Res. ,vol 66, 3727-33, 1961

Collier, J. L., Masters Thesis, Morphology of Microbaroms at Windless Bight, Antarctica and Fairbanks, Alaska, University of Alaska at Fairbanks, May 1983

Feder, J. A. and Banks, W.R., 1970, Auroral Infrasonic Wave Mechanism, Dept. of Applied Physics, U.C.S.D., La Jolla, California

Maeda, K. and J. M. Young, Propagation of Pressure Waves Produced by Auroras, J. of Geomagnetism and Geoelectricity, vol 18, 275-299, 1966

Nichparenko, S.; Masters Thesis, Aurorally Associated Infrasonic Waves, University of Alaska, College, Alaska.

Olson, J.V., Noise Suppression using data-adaptive polarization filters: Application to infrasonic arrays, J. Acoust Soc. Am., vol 72, 5, November 1982

Susumu Kato and Takato Kawakami, Theory of gravity wave emission from moving sources in the upper atmosphere, J. of Atmos. and Terr. Physics, vol 39, pp581-588, 1977

Swift, D. W., The generation of auroral infrasonic waves by electrojets, J. Geophys. Res., 78, 8205, 1973

Wilson, C. R. , Auroral infrasonic and ionospheric absorption substorms, J. Atmos.and Terr. Phys., vol. 74, 4511-4522, 1970

Wilson, C. R. , Auroral infrasonic substorms, The Radiating Atmosphere, McCormac (ed.), Reidel Publishing Co., Dordrecht-Holland, 1971

Wilson, C. R. , Auroral infrasonic wave generation mechanism, J. Geophys. Res., vol. 77, 1820-1843,1972

Wilson, C. R. , Auroral infrasonic waves and poleward expansions of auroral substorms at Inuvik, N.W.T., Canada, Geophysical Journal of R.A.S., vol. 26, 179-181, 1971

Wilson, C. R. , Auroral infrasonic waves, J. Geophys. Res., vol. 74 , 1812-1836, 1969a

Wilson, C. R. , Infrasonic pressure waves from the aurora, a shock wave model, Nature, vol. 214, No. 511, 131-133, 1967

Wilson, C. R. , Infrasonic wave generation by aurora, J. Atmos. Terr Physics, vol.37, 973-988,1975

Wilson, C. R. , Infrasonic waves from moving auroral electrojets, J. of Planet. and Space Physics , vol. 17, 1107, 1969b

Wilson, C. R. , R. D. Hunsucker and J. G. Romick, An auroral infrasonic substorm investigation using Chatanika radar and other geophysical sensors, Planet. Space Sci., vol. 24, 1155-1175, 1976

Wilson, C. R. , Seasonal variations in auroral infrasonic wave activity, J. Geophys. Res., vol. 78, 4801,1973

Wilson, C. R. , Trans-auroral zone auroral infrasonic wave observations, Planet. Space Sci., vol. 22,151-173,1974

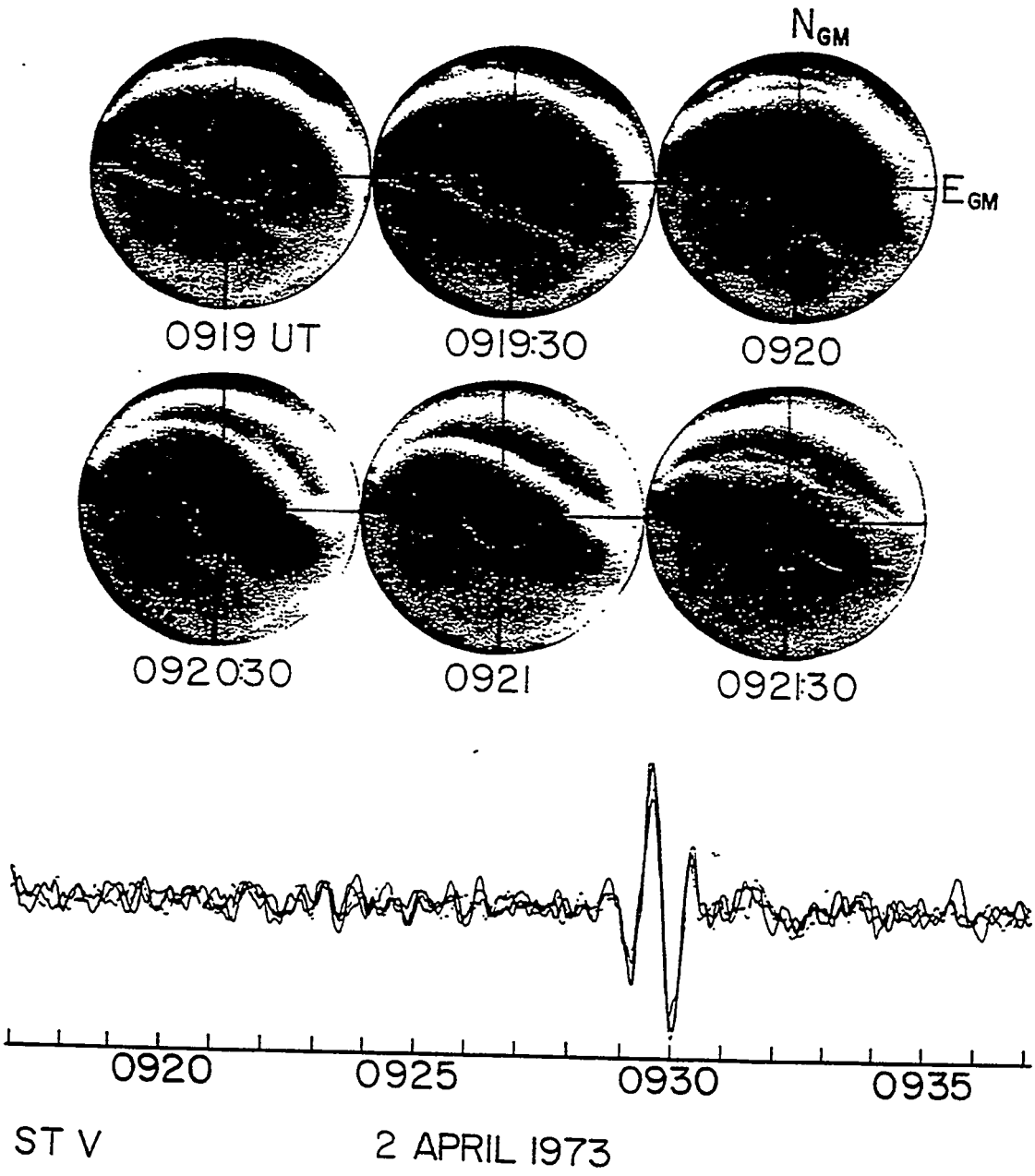

Figure 1. AIW observed at Steven's Village , Alaska that was generated by the supersonic motion of the auroral arc from 0920 to 0921UT from geomagnetic NE to SW. The true azimuth of arrival of the AIW was from 43 degrees and Vt=400m/sec.

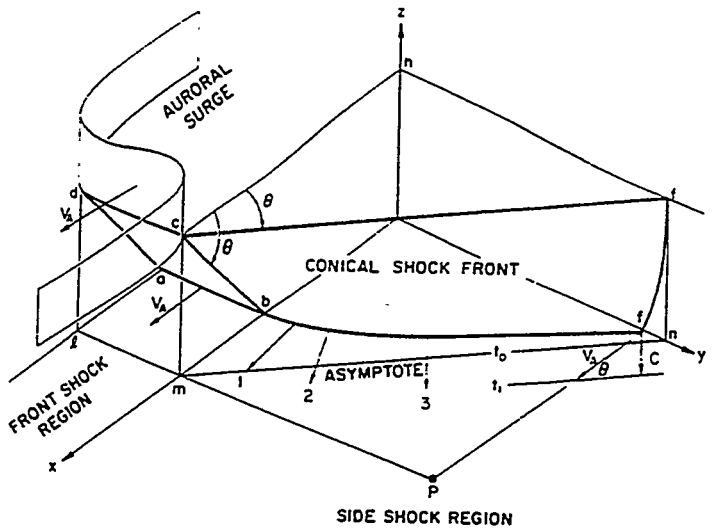

Figure 2. AIW bow wave surface geometry for an auroral arc surge traveling with supersonic motion in the positive x direction. The xy plane is the earth's surface. The mach angle of the bow wave is given by the arcsin(sound speed / auroral speed). In the front shock region the AIW trace velocity is equal to the auroral arc velocity. In the side shock region the azimuth of arrival for the AIW is divergent and the trace velocity asymptotically approaches the speed of sound at the surface.

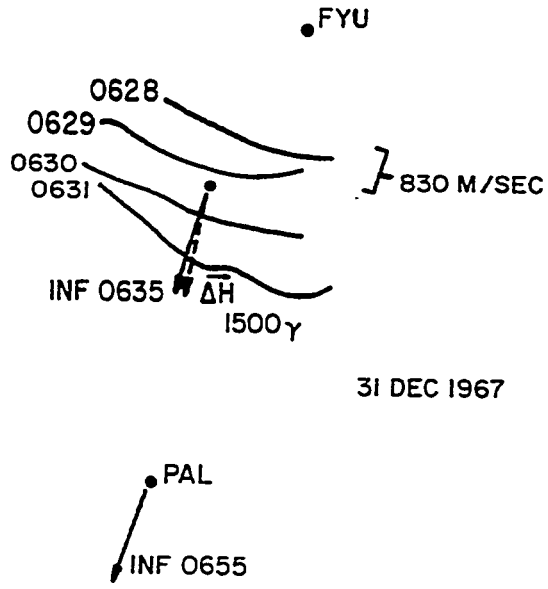

Figure 3a. Projection on to the earth's surface of a supersonic auroral arc at 1 min intervals showing motion parallel to that of AIWs that were generated by the arc as observed at College (0635UT) and later at Palmer (0655UT). The magnetic perturbation, (delta H), at College of 1500 gamma is shown parallel to the direction of the AIW.

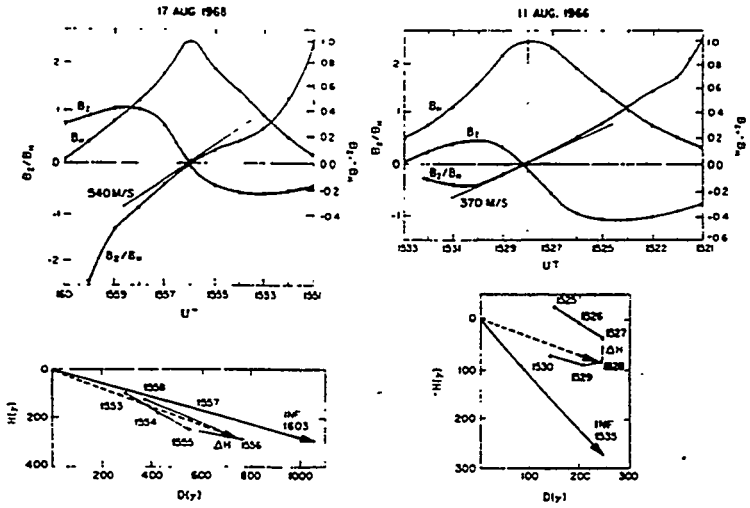

Figure 3b Horizontal (Bh) and vertical (Bz) components of the magnetic perturbation vs time from a moving auroral electrojet arcs that generated AIW observed at College after the zenith passage of the arc.The slope of the tangent of Bz / Bh at the zenith crossing time gives the speed of the auroral arc. Delta H , the horizontal magnetic disturbance vector and the AIW propagation vector (INF) are approximately parallel for the two events shown.

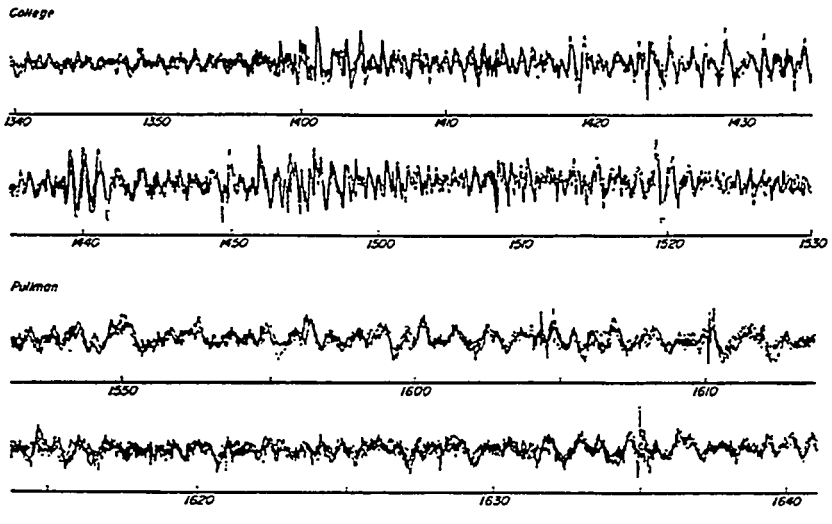

Figure 4. Portions of the AIW infrasonic substorm records from College,Alaska and Pullman, Washington showing the different character of the AIW from the same auroral substorm. The Pullman signals are of lower trace velocity and have longer periods.

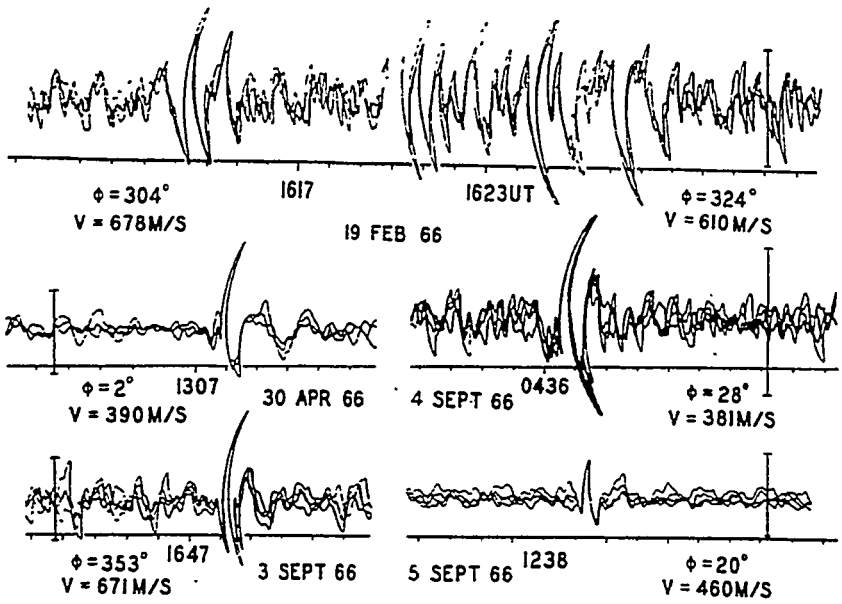

Figure 5. AIW signals observed in the auroral zone in Alaska at College and Palmer where the infrasonic array was in the front shock region resulting in higher frequency components in the wave-packets.

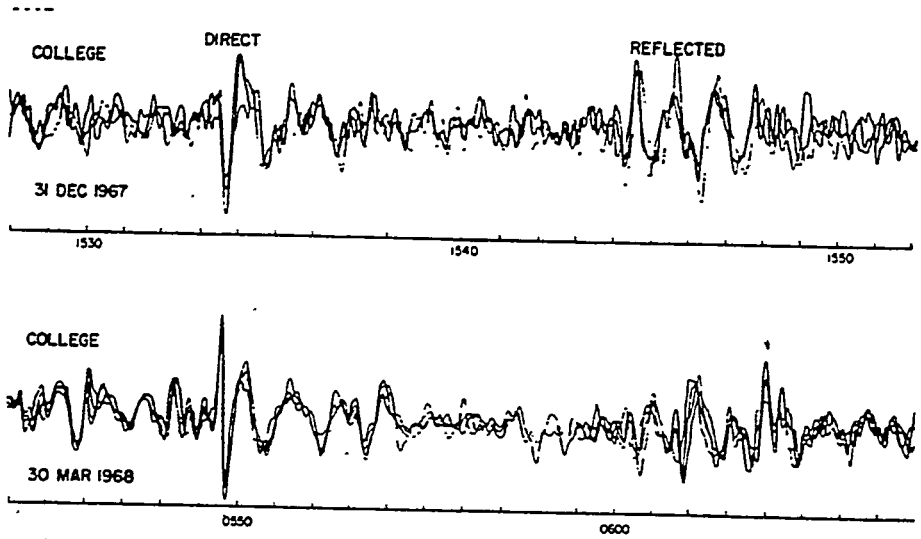

Fig. 18. Examples of direct and reflected AIW at College showing 12-minute delay time for the reflected mode of propagation.

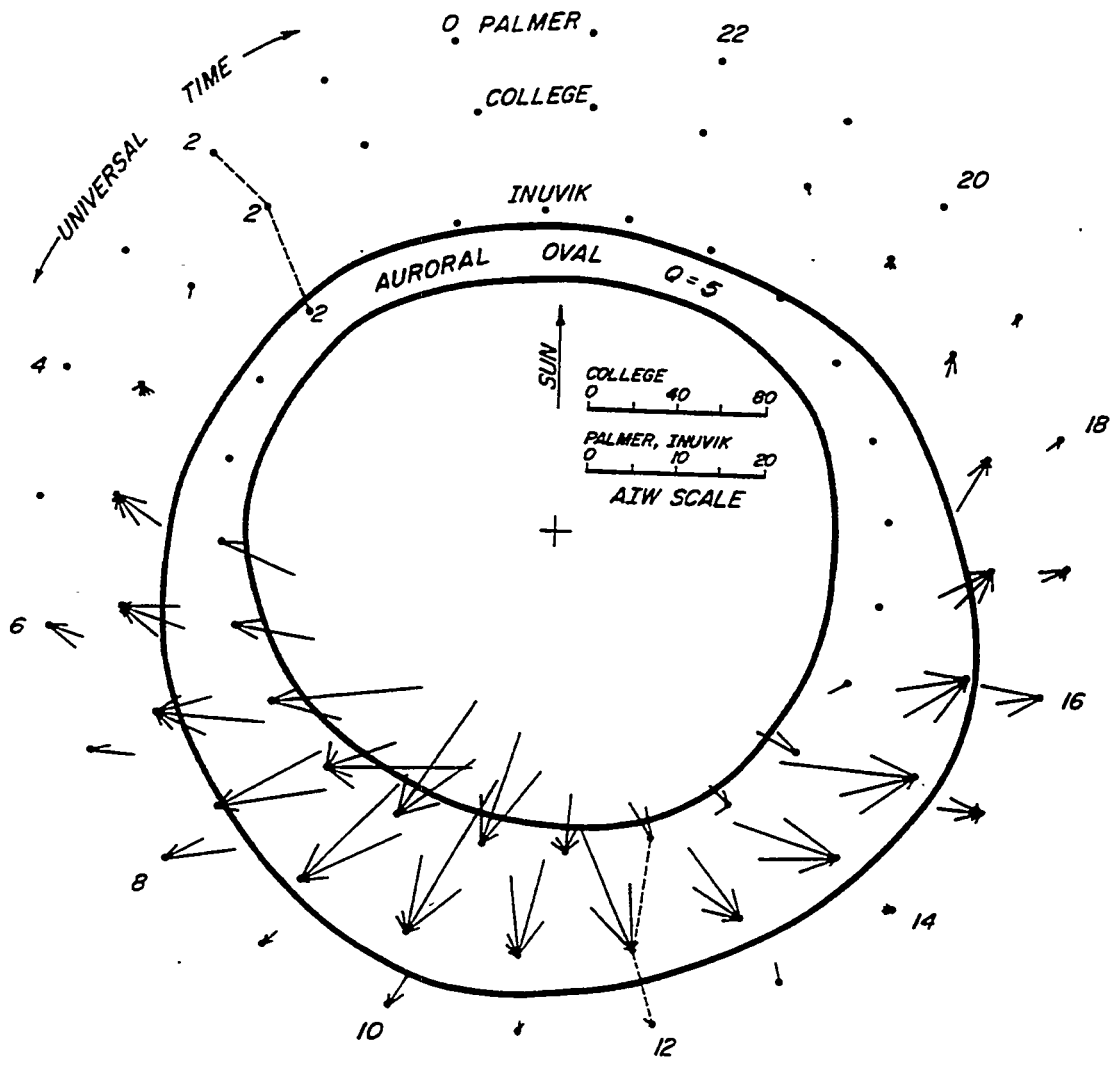

Figure 6. Number of AIW as a function of azimuth of arrival, plotted at the locations of Inuvik, College or Palmer, as these stations rotate with time throughout the night beneath the fixed auroral oval, for each hour of UT and each 20 degrees of azimuth.

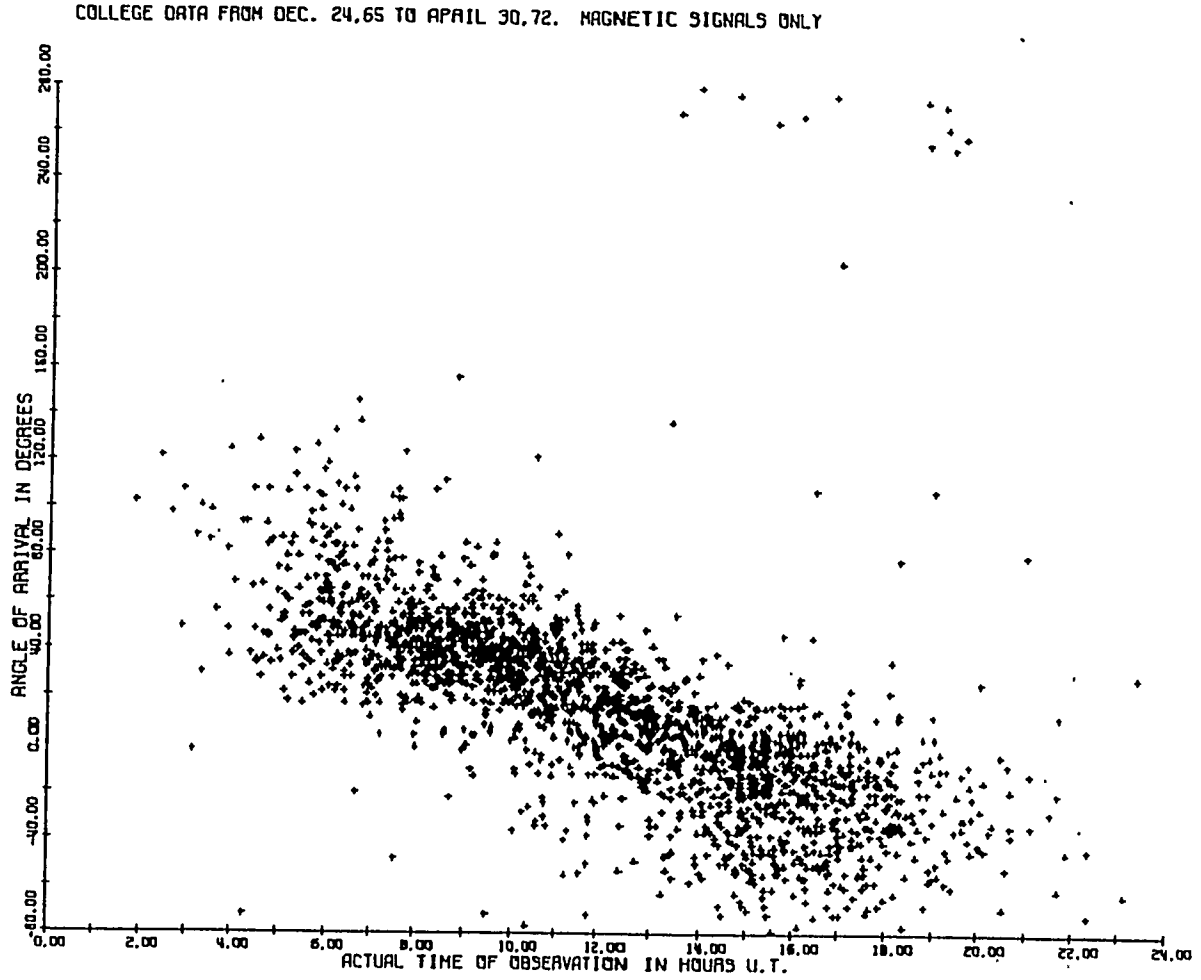

Figure 7. Azimuth of arrival vs. actual time of observation of 1564 AIW observed at College, Alaska from Dec. 24, 1965 to June 28, 1970. True North is at 0.00.

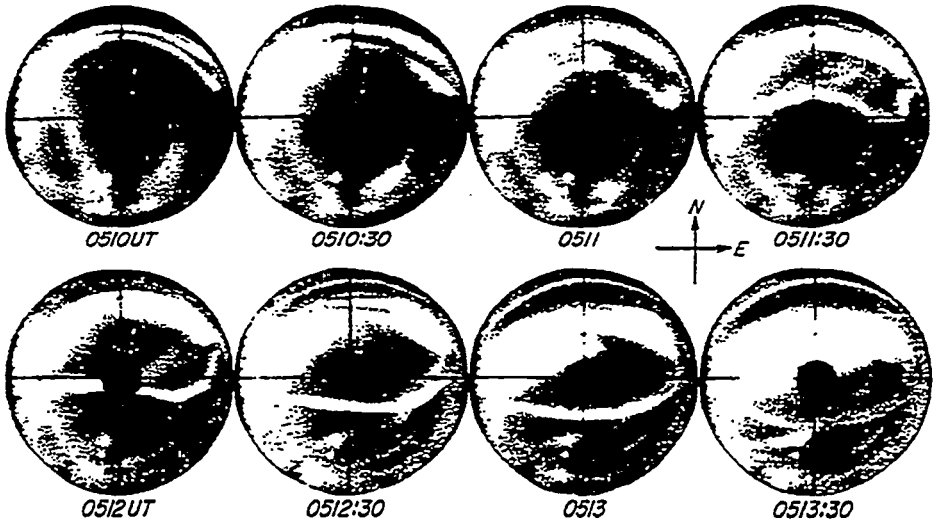

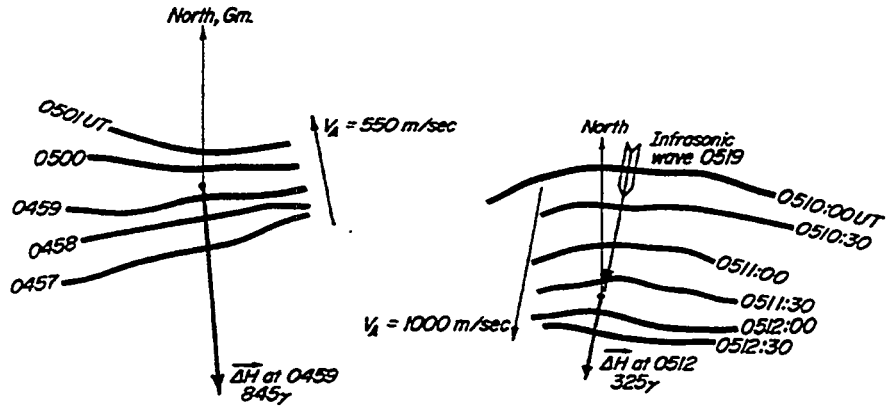

INUVIK, 6 DECEMBER 1969

Figure 8. All sky camera pictures of supersonic auroral arcs moving poleward from 0457 to 0501 at 550m/sec , and equatorward from 0510 to 0512:30 at 1,000m/sec. Although strong electrojet currents were flowing in both arc systems, as shown by the large values of the magnetic perturbation delta H , only the equatorward moving arc produced an AIW at Inuvik at 0519 demonstrating the basic North - South asymmetry in the AIW generating mechanism.

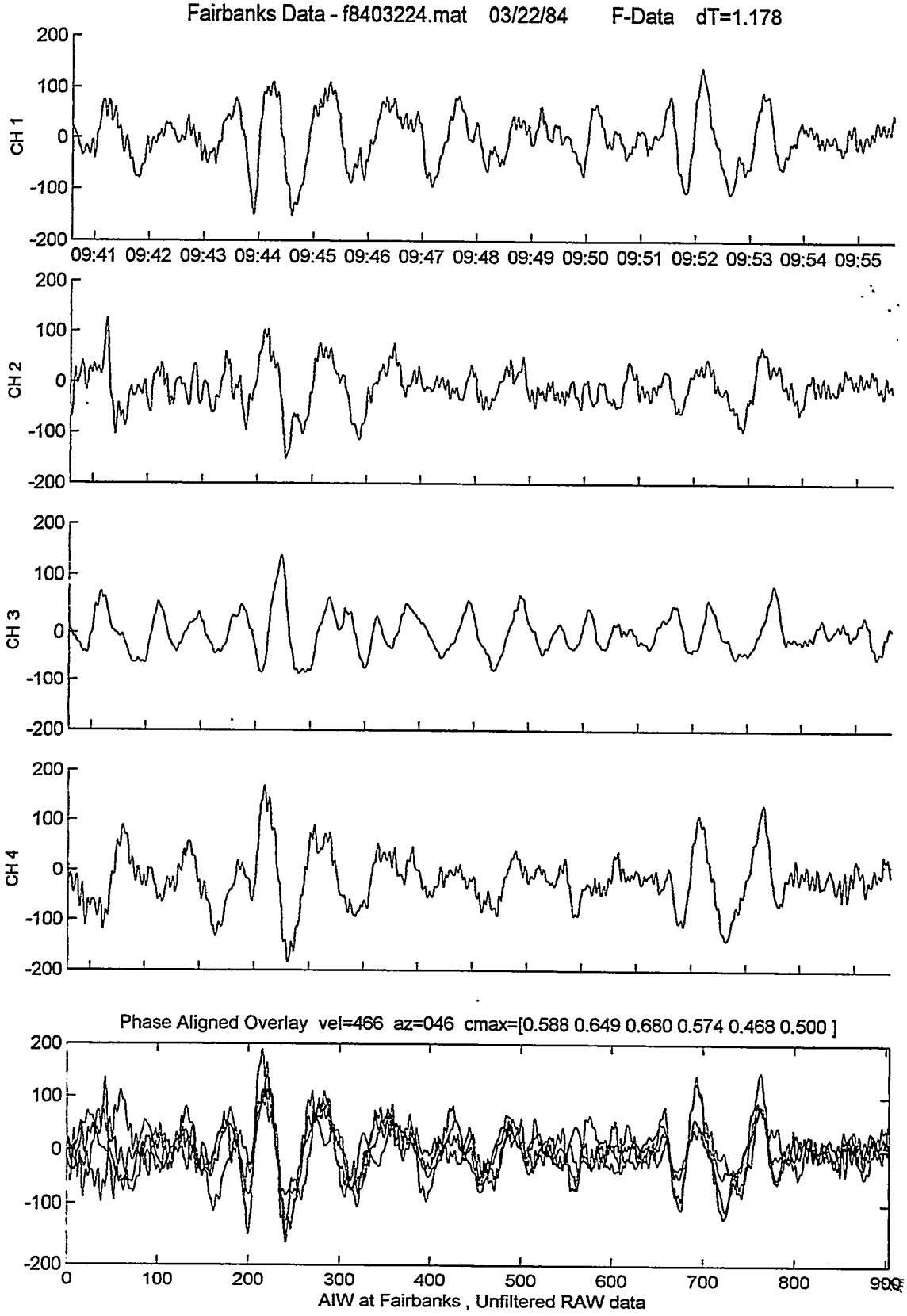
Fairbanks Data - f8403224.mat 03/22/84 F-Data dT=1.178
CH 1
CH 2
CH 3
CH 4
200
100
0
-100
-200
09:41 09:42 09:43 09:44 09:45 09:46 09:47 09:48 09:49 09:50 09:51 09:52 09:53 09:54 09:55
Phase Aligned Overlay vel=466 az=046 cmax=[0.588 0.649 0.680 0.574 0.468 0.500]
0 100 200 300 400 500 600 700 800 900
AIW at Fairbanks , Unfiltered RAW data

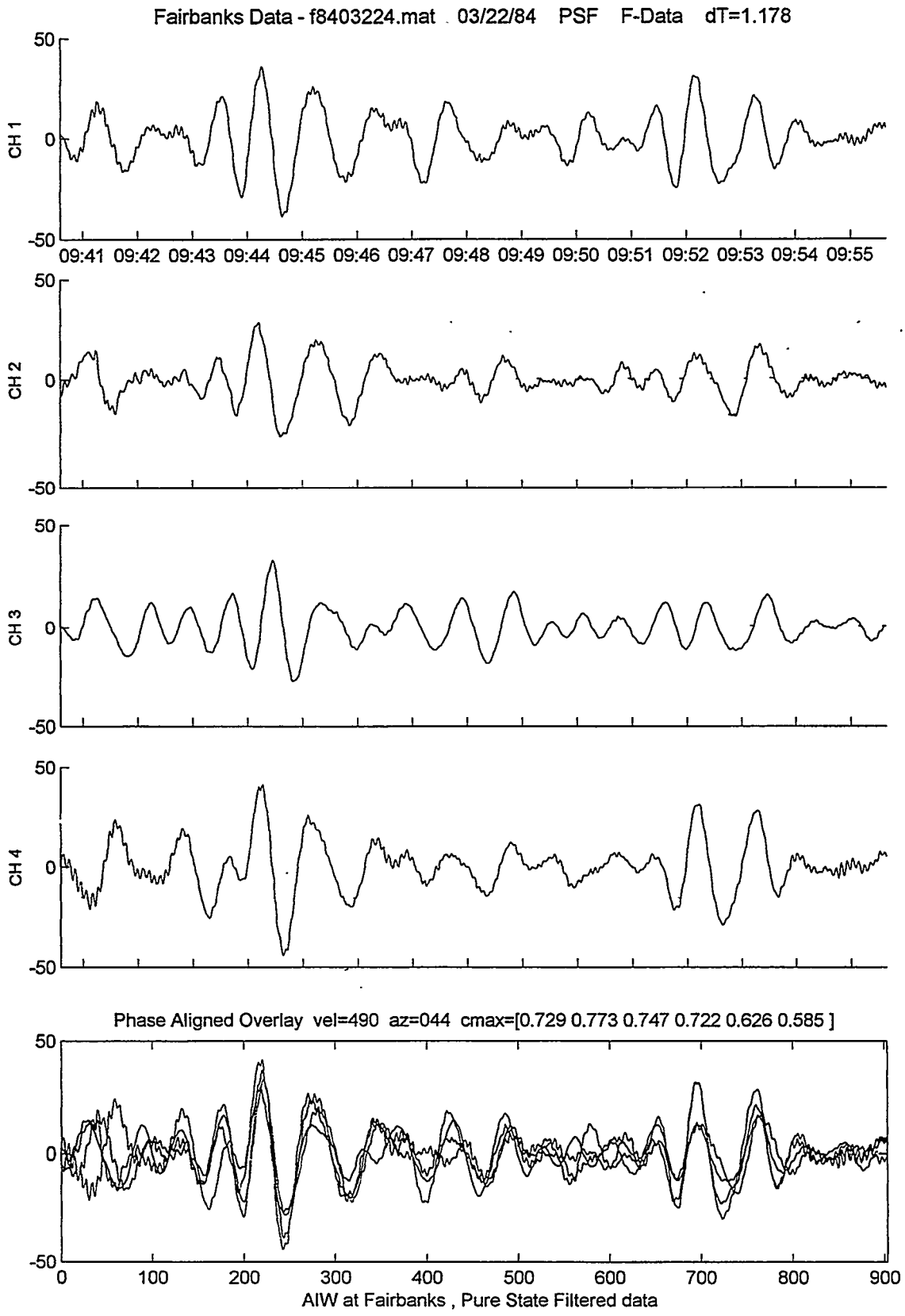
Fairbanks Data - f8403224.mat 03/22/84 PSF F-Data dT=1.178
CH 1
CH 2
CH 3
CH 4
50
0
-50
09:41 09:42 09:43 09:44 09:45 09:46 09:47 09:48 09:49 09:50 09:51 09:52 09:53 09:54 09:55
Phase Aligned Overlay vel=490 az=044 cmax=[0.729 0.773 0.747 0.722 0.626 0.585]
0 100 200 300 400 500 600 700 800 900
AIW at Fairbanks , Pure State Filtered data

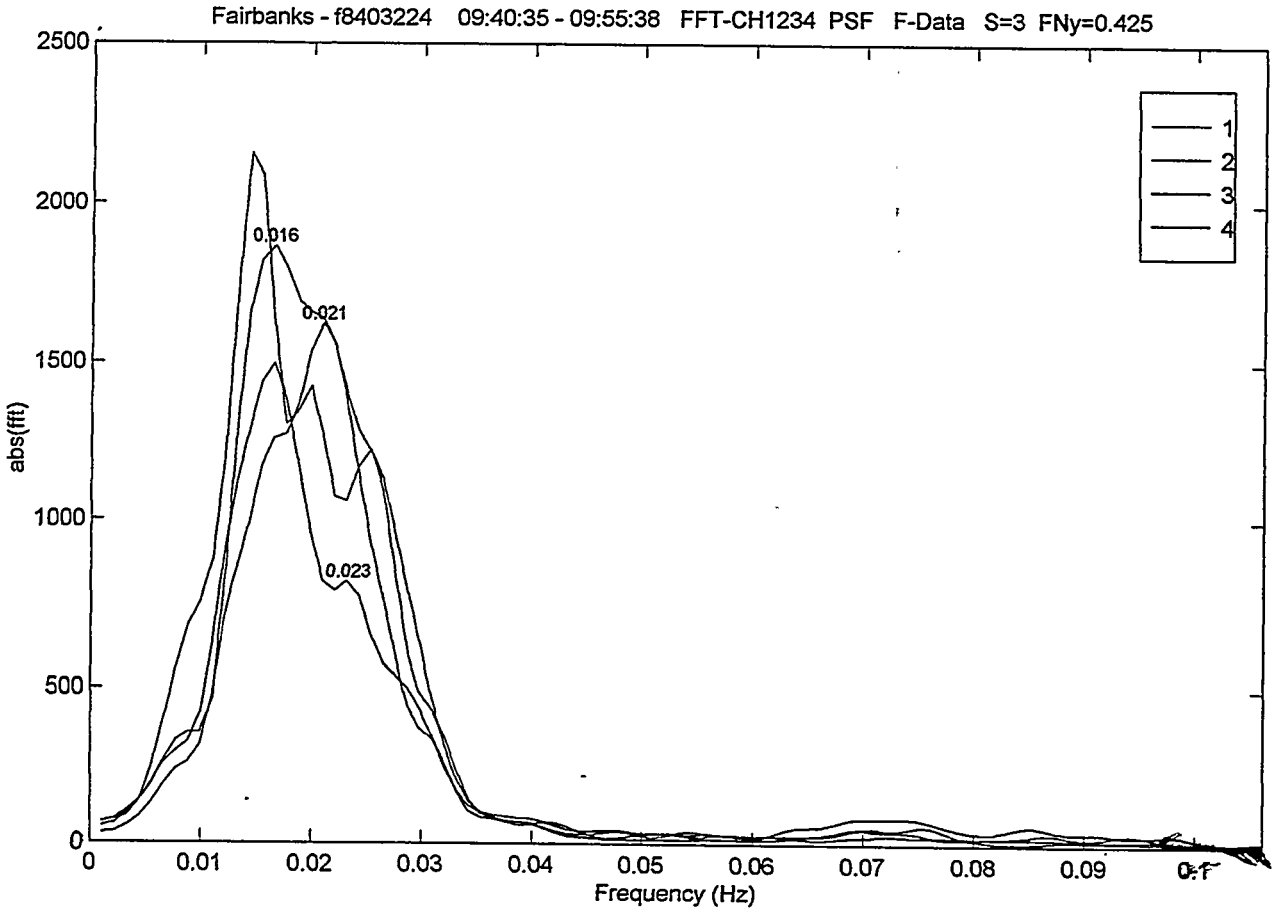
Fairbanks - f8403224 09:40:35 - 09:55:38 FFT-CH1234 PSF F-Data S=3 FNy=0.425
2500
2000
1500
1000
500
0
abs(fft)
0.016
0.021
0.023
1
2
3
4
0
0.01
0.02
0.03
0.04
0.05
0.06
0.07
0.08
0.09
Frequency (Hz)

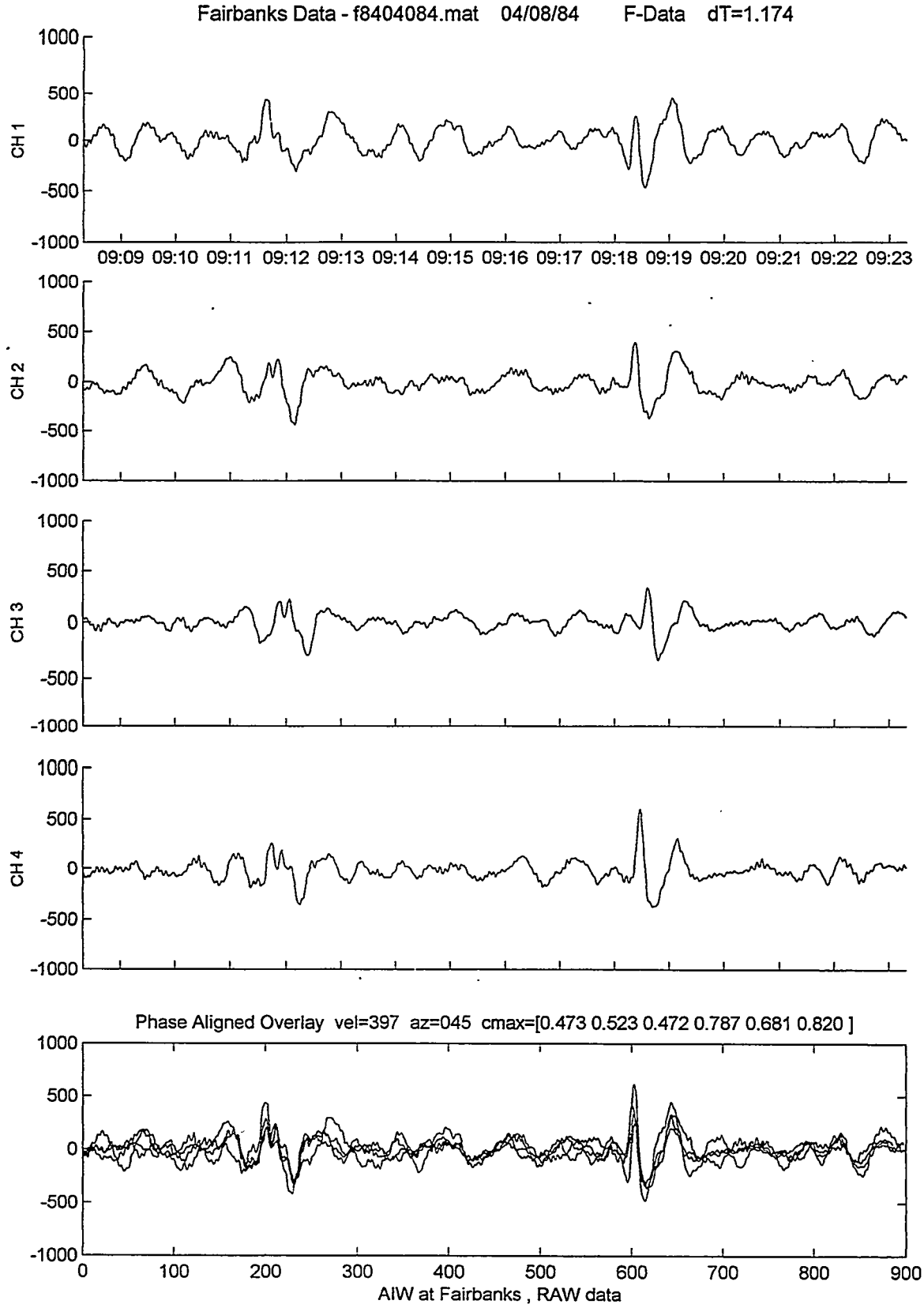
Fairbanks Data - f8404084.mat 04/08/84 F-Data dT=1.174
CH 1
CH 2
CH 3
CH 4
1000
500
0
-500
-1000
09:09 09:10 09:11 09:12 09:13 09:14 09:15 09:16 09:17 09:18 09:19 09:20 09:21 09:22 09:23
Phase Aligned Overlay vel=397 az=045 cmax=[0.473 0.523 0.472 0.787 0.681 0.820]
0 100 200 300 400 500 600 700 800 900
AIW at Fairbanks , RAW data

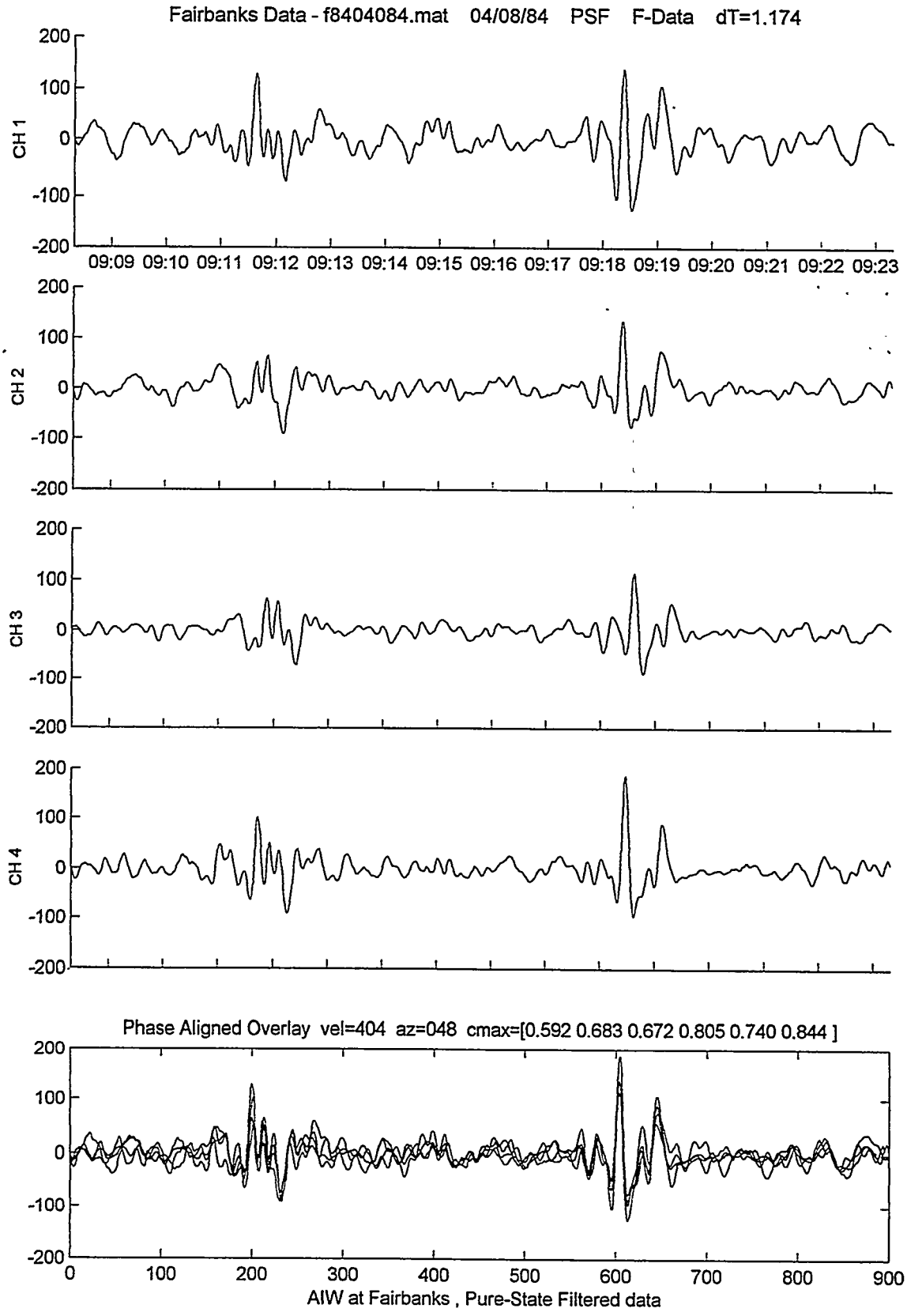
Fairbanks Data - f8404084.mat 04/08/84 PSF F-Data dT=1.174
CH 1
CH 2
CH 3
CH 4
200
100
0
-100
-200
09:09 09:10 09:11 09:12 09:13 09:14 09:15 09:16 09:17 09:18 09:19 09:20 09:21 09:22 09:23
Phase Aligned Overlay vel=404 az=048 cmax=[0.592 0.683 0.672 0.805 0.740 0.844]
0 100 200 300 400 500 600 700 800 900
AIW at Fairbanks , Pure-State Filtered data

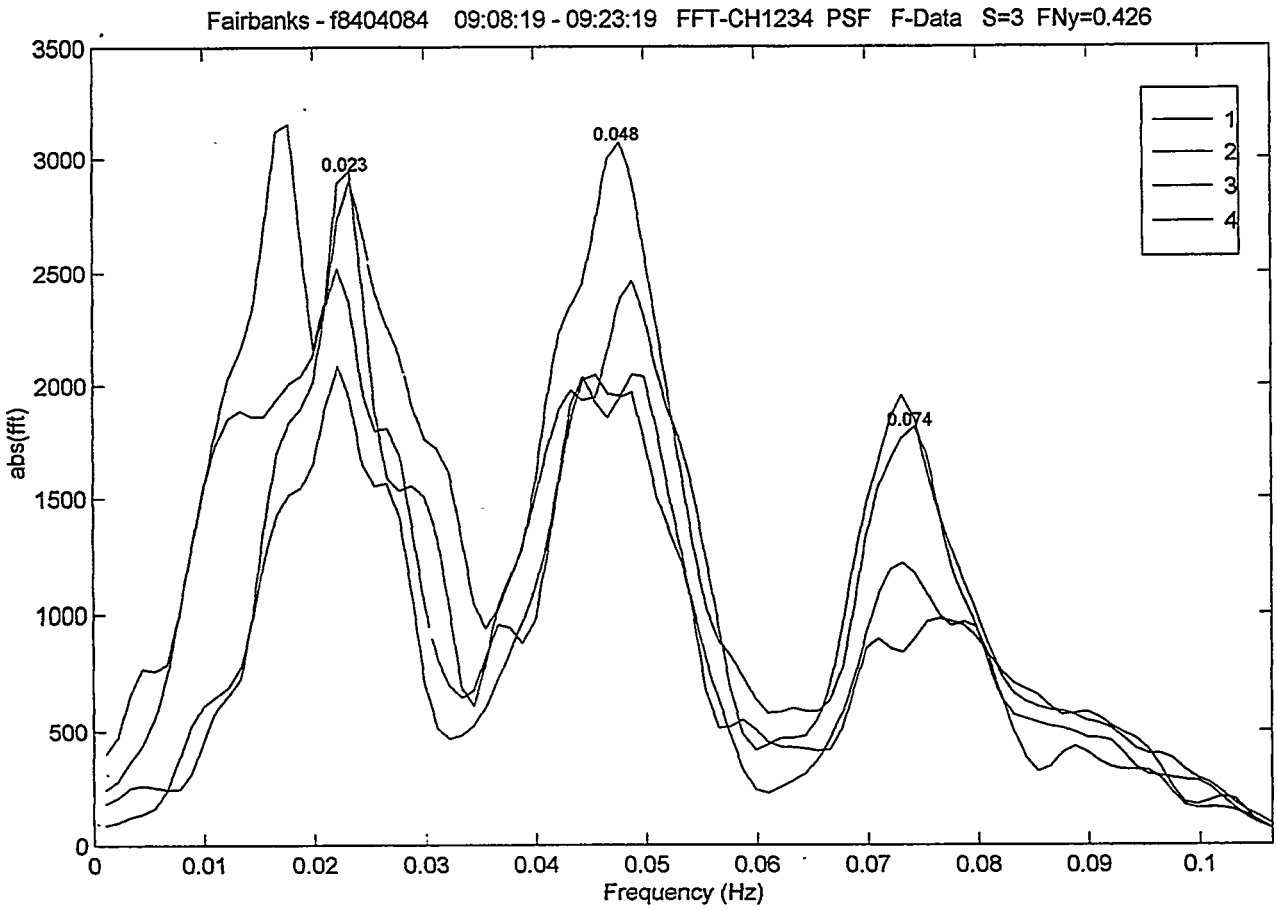
Fairbanks - f8404084 09:08:19 - 09:23:19 FFT-CH1234 PSF F-Data S=3 FNy=0.426
abs(fft)
Frequency (Hz)
0.023
0.048
0.074
1
2
3
4
0
500
1000
1500
2000
2500
3000
3500
0.01
0.02
0.03
0.04
0.05
0.06
0.07
0.08
0.09
0.1

Aerodynamic Infrasound (MAW)

Infrasonic waves , in the passband from 10 to 100 second periods, that last for many hours and propagate great distances , are radiated by the atmospheric turbulence that is generated when the tropospheric wind flow is interrupted by high mountain ranges. These mountain associated infrasonic waves (MAW) are observed at infrasonic stations all over the world. MAW that have been observed in Alaska and Antarctica are characterized by : (1) an average periods from 30 to 70 seconds, (2) long duration of quasi-sinusoidal wave form of a few microbars amplitude, (3) their fixed azimuth of arrival from definite directions depending on the particular station, (4) a total lack of diurnal variation of frequency of occurrence, (5) a strong tendency to be observed only during winter months, (6) their low average horizontal trace velocity of 325 m/sec. to 425 m/sec., (7) and the relatively poor quality of their phase coherence over the dimensions of the large microphone arrays at Fairbanks and Windless Bight. Examples are shown of the microphone traces time shifted to show coherent waves in Figure 1 of MAW observed at College (Fairbanks), Alaska for the three principle directions from which they arrive. These, as shown in Figure 2, are as follows: (1) 125^0 to 150^0 azimuth (the Saint Elias Range); (2) 200^0 to 230^0 (Alaska and Aleutian Ranges); and (3) 275^0 to 300^0 (Seward and Chukotsk peninsulas). The total lack of a diurnal variation in the frequency of occurrence at Fairbanks can be seen in Figure 3 for observations over a 42 month period of time. The seasonal variation of MAW at Fairbanks, as given in Figure 4, shows very few signals during the summer as compared with the winter months .The spectral characteristics of MAW change as the propagation distance increases. Thus the higher frequency of the wave train in Figure 1, for the December 4, 1967, is due to the fact that the source was Mt. McKinley, a 20,300 foot peak only a few hundred kilometers from Fairbanks. The waves from McKinley propagated via the lower sound channel while those observed on October 11,1968 from the Chukotsk Peninsula , coming from a much greater distance, arrived via the upper channel where the higher levels of reflection cause a filtering out of the higher frequency components and thus are of longer period.

Examples are shown in the following six figures, from the DataScan analysis system, of an MAW event from Mt. McKinley observed at Fairbanks with the digital system on March 3, 1984.The first two figures are of the waveform traces for RAW data and PSF data respectively with a phase-aligned overlay of all microphone channels at the bottom of each diagrams. The average value of the cross-correlation coefficients increased from 0.628 for RAW data to 0.765 for PSF data. The P value from PSF filtering has a maximum just above 0.60 as shown in the next figure. These low values for inter-microphone cross-correlation (cmax) and P parameter for multivariate coherence of all channels together are low which is typical for MAW waves. The spectral diagram, where abs(fft) is given as a function of frequency, for PSF data shows maximum energy at periods of 28.5 sec, 38.5 sec, and 55.5 sec. The last two figures for the Mt. McKinley MAW event of March 6, 1984 show the fixed azimuth of arrival at 215 degrees and the trace velocity variations for a 160 minute time window of data. The trace velocity of about 485 m/sec, that is shown in the last figure for the MAW event, must be corrected by a factor of 1/1.178 (to correct for the actual sampling interval being dT=1.178 instead of the assumed value of dT=1.00). Thus the correct velocity value determined by the least-squares analysis is 412 m/sec. The penultimate figure of azimuth versus time for this MAW event is another example of how well the least-squares detection algorithm locks on to the signal even though its coherence between microphones is only 0.6.

Bibliography for Aerodynamic Infrasound

Bedard, A. J. , Infrasound Originating Near Mountain Regions in Colorado, Journal of Applied Meteorology, vol 17, No 7, July 1978 page 1014

Goerke, V.H. and M.W. Woodward, Infrasonic Obersavation of a Severe Weather System, Monthly Weather Review vol 94, 395-398, 1966

Larson , Craine, Thomas and Wilson, Correlation of Winds and Geographic Features with Production of Certain Infrasonic Signals in the Atmosphere, Geophysical Journal of R. A. S. , 26, 201-214, 1971.

Lighthill, M.J., On Sound Generated Aerodynamically , Proc. Roy. Soc. of London, A, 211, 546-587, 1952.

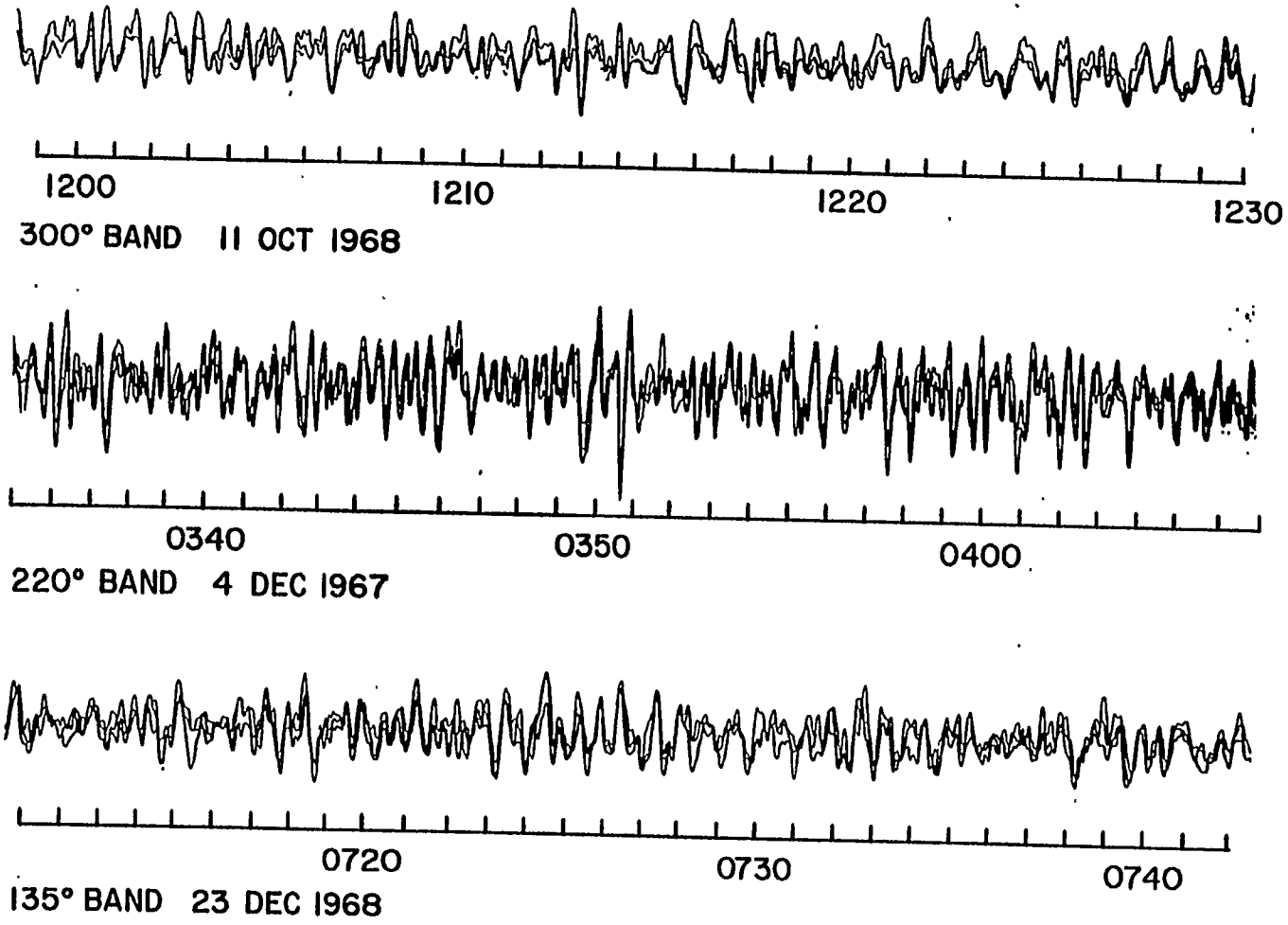

Fig. 1 Microbarograph traces of aerodynamic infrasonic waves at College, Alaska.

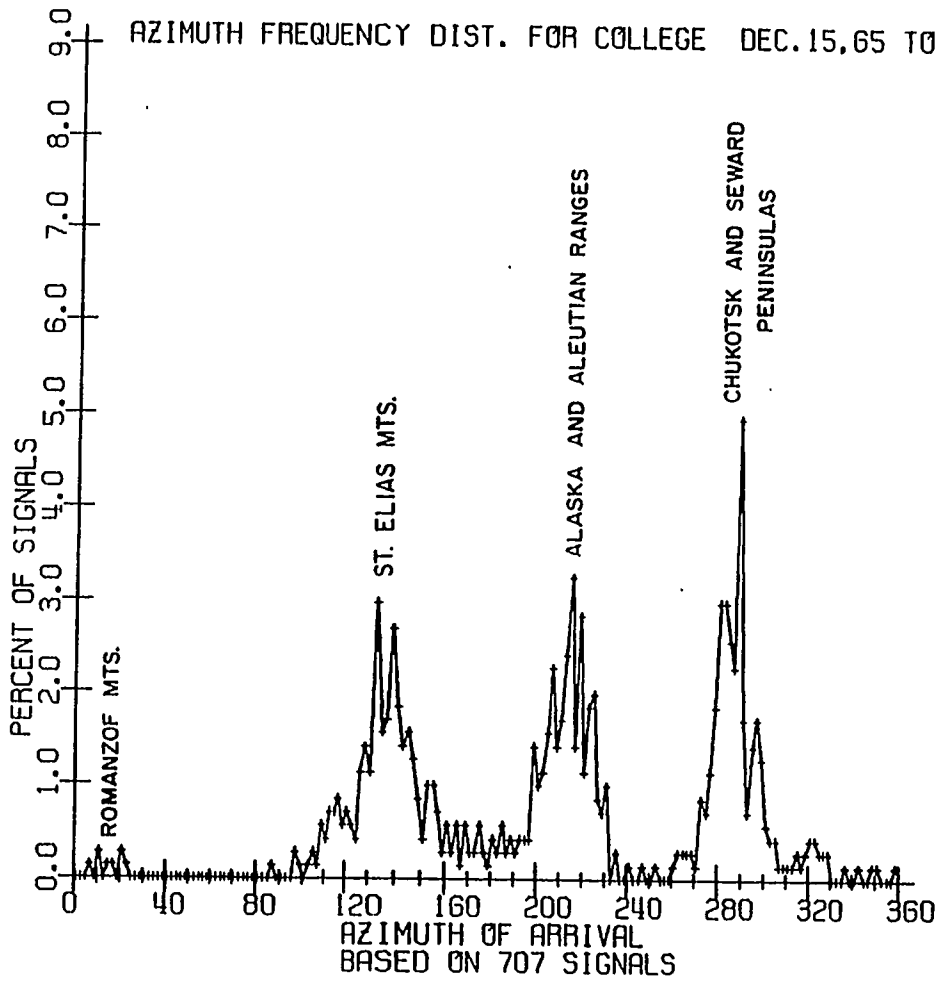

Figure 2. Azimuth of arrival bands for Mountain Associated Infrasound observed at College, Alaska over a 42 month period.

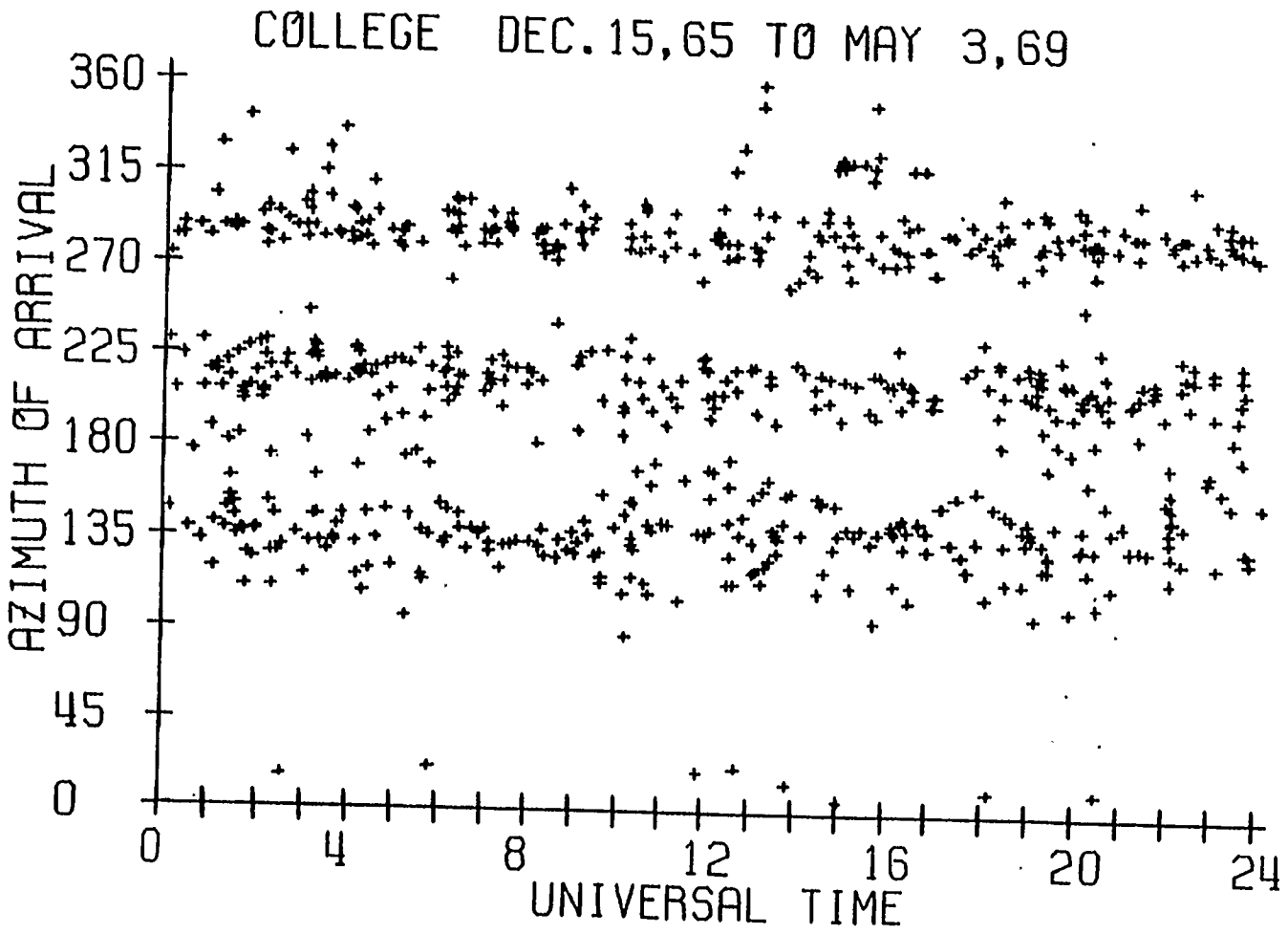

Figure 3. Azimuth of arrival bands for MAW showing total lack of diurnal variation in in frequency of occurrence.

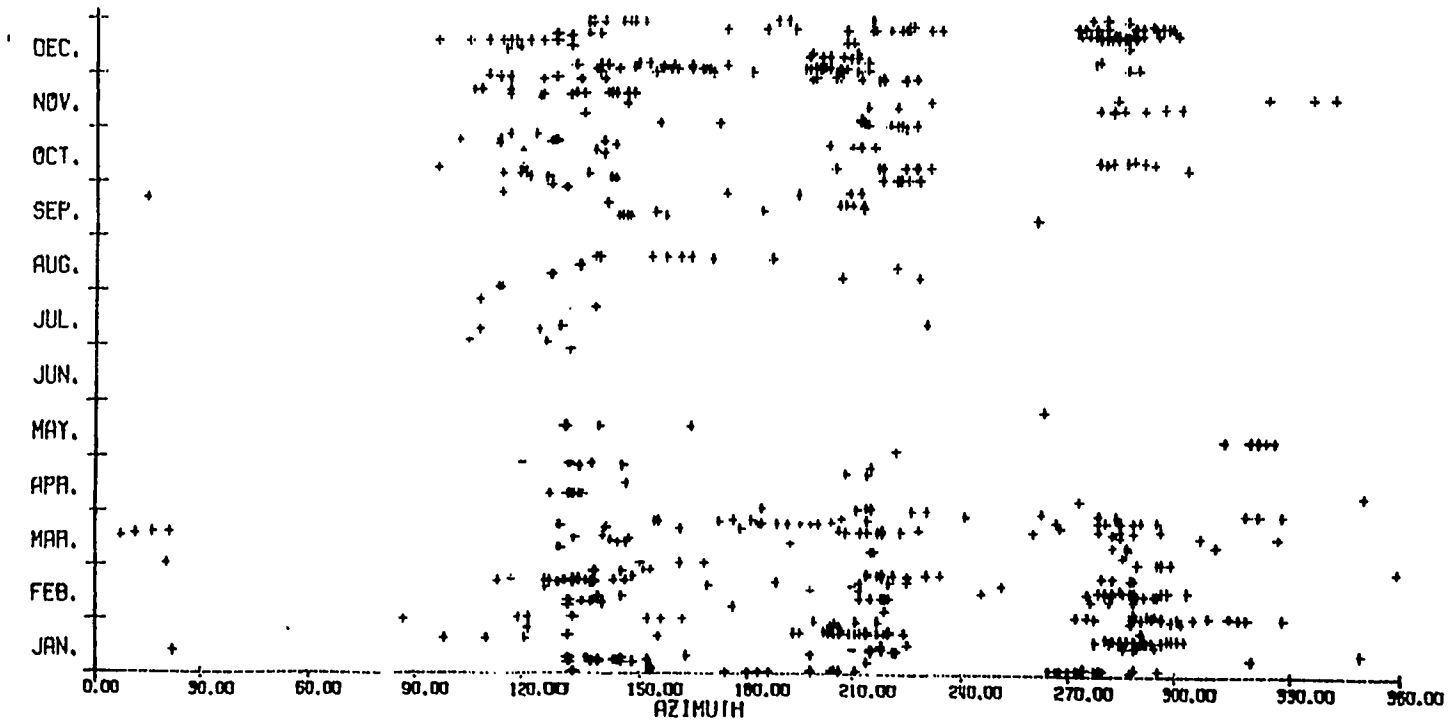

Figure 4. Seasonal variation in the azimuth of arrival for MAW at Fairbanks. Notice the lack of signals during the summer months.

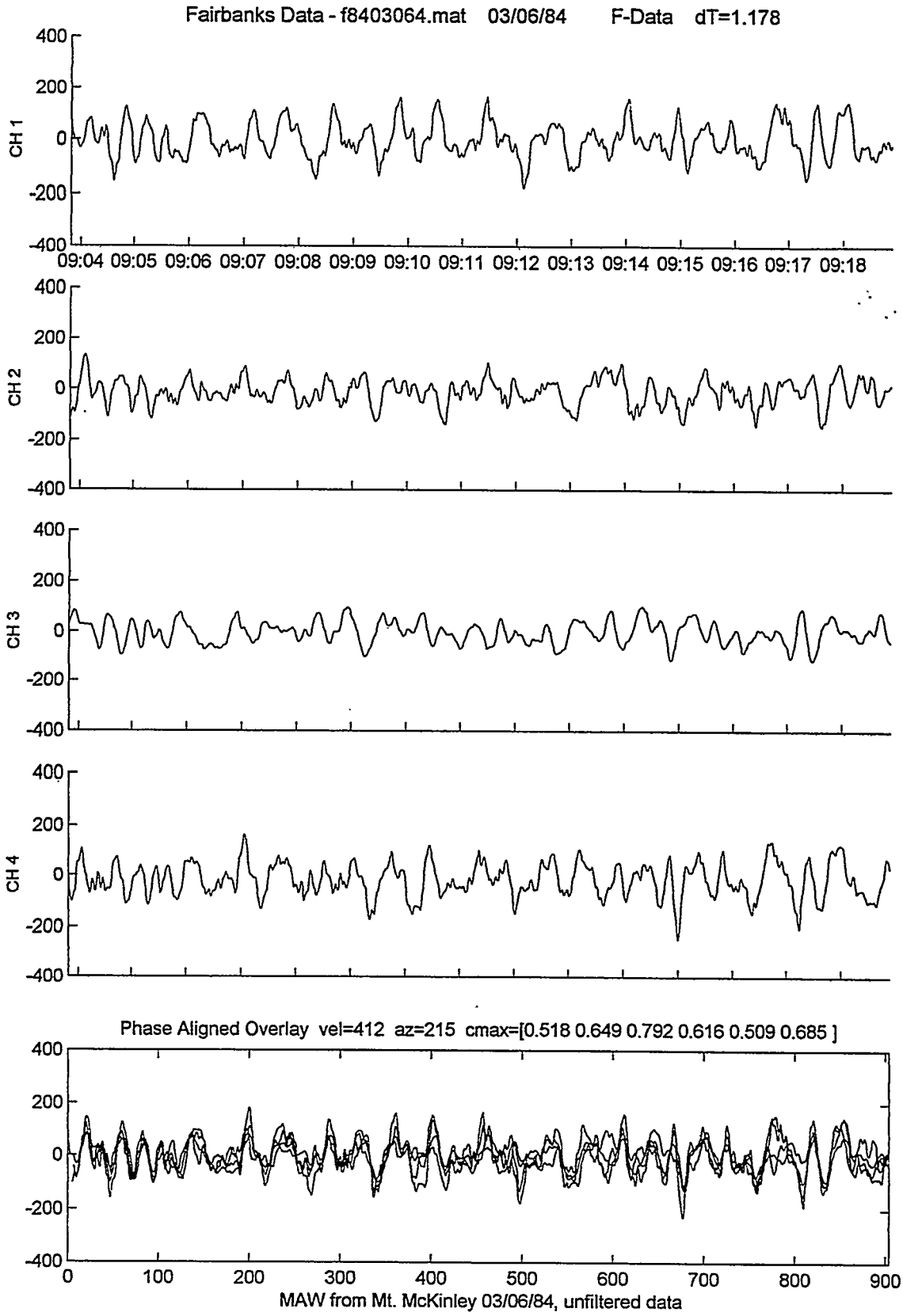
Fairbanks Data - f8403064.mat 03/06/84 F-Data dT=1.178
CH 1
CH 2
CH 3
CH 4
400
200
0
-200
-400
09:04 09:05 09:06 09:07 09:08 09:09 09:10 09:11 09:12 09:13 09:14 09:15 09:16 09:17 09:18
Phase Aligned Overlay vel=412 az=215 cmax=[0.518 0.649 0.792 0.616 0.509 0.685]
0 100 200 300 400 500 600 700 800 900
MAW from Mt. McKinley 03/06/84, unfiltered data

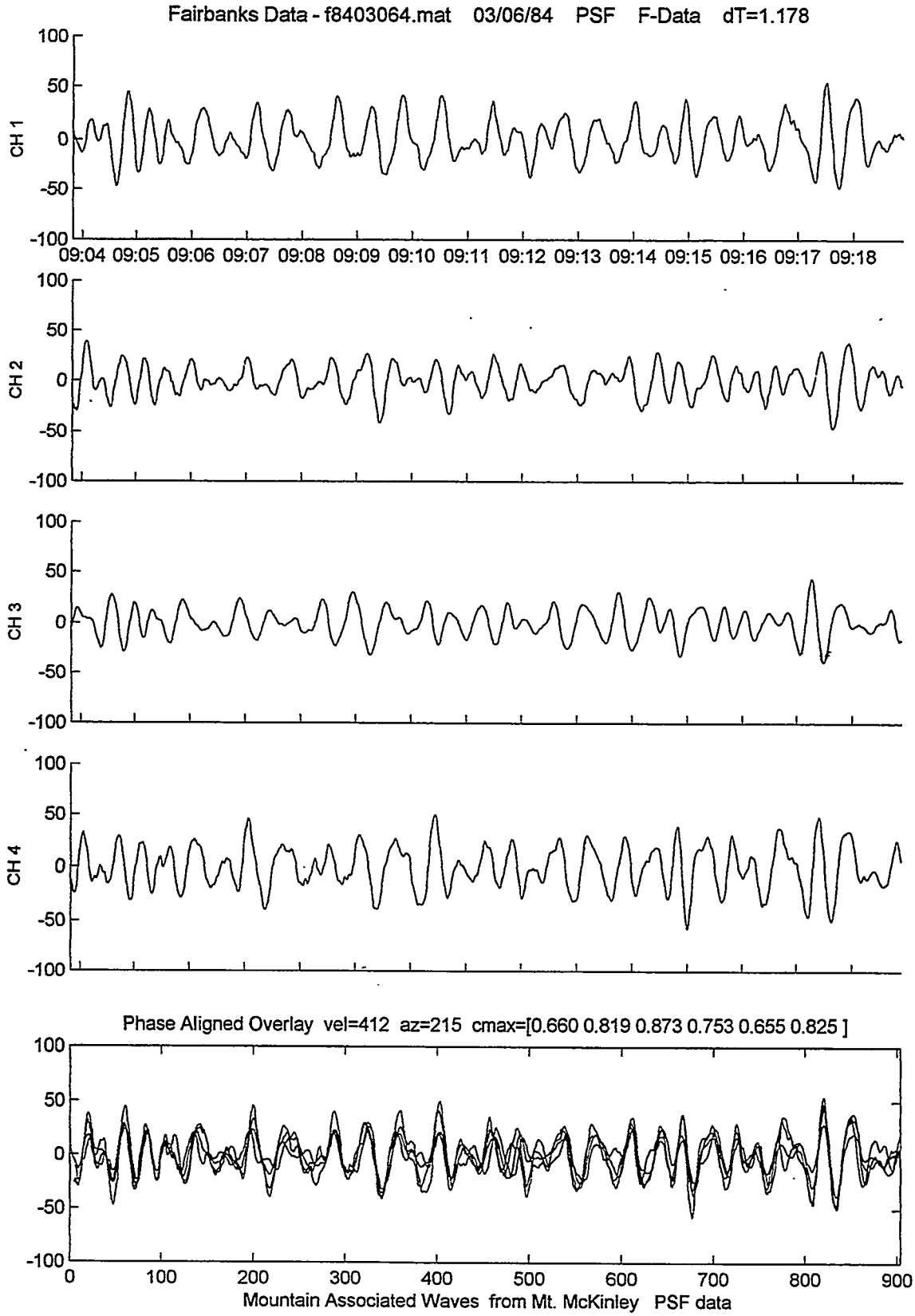
Fairbanks Data - f8403064.mat 03/06/84 PSF F-Data dT=1.178
CH 1
CH 2
CH 3
CH 4
100
50
0
-50
-100
09:04 09:05 09:06 09:07 09:08 09:09 09:10 09:11 09:12 09:13 09:14 09:15 09:16 09:17 09:18
Phase Aligned Overlay vel=412 az=215 cmax=[0.660 0.819 0.873 0.753 0.655 0.825]
0 100 200 300 400 500 600 700 800 900
Mountain Associated Waves from Mt. McKinley PSF data

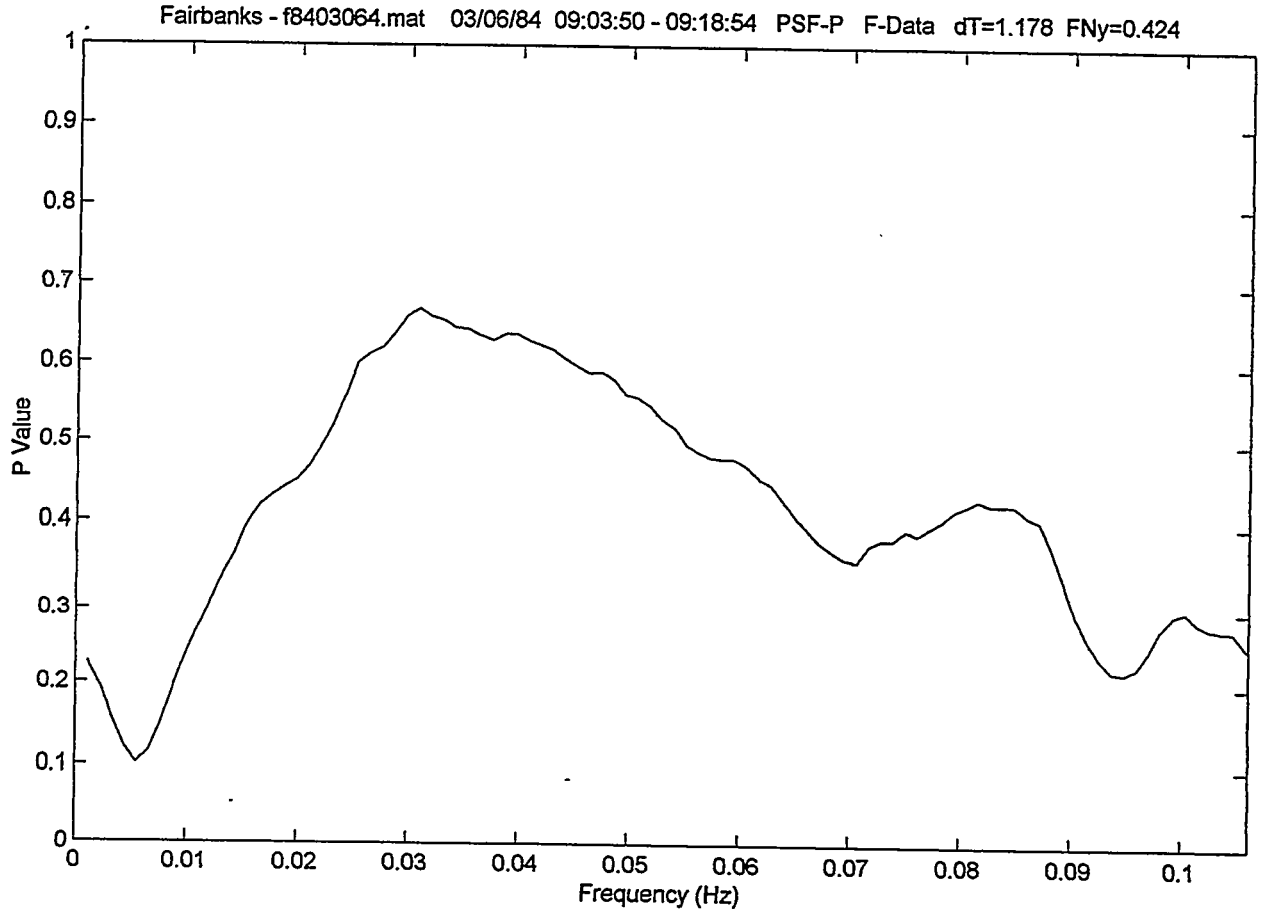
Fairbanks - f8403064.mat 03/06/84 09:03:50 - 09:18:54 PSF-P F-Data dT=1.178 FNy=0.424
P Value
Frequency (Hz)
0
0.1
0.2
0.3
0.4
0.5
0.6
0.7
0.8
0.9
1
0.01
0.02
0.03
0.04
0.05
0.06
0.07
0.08
0.09
0.1

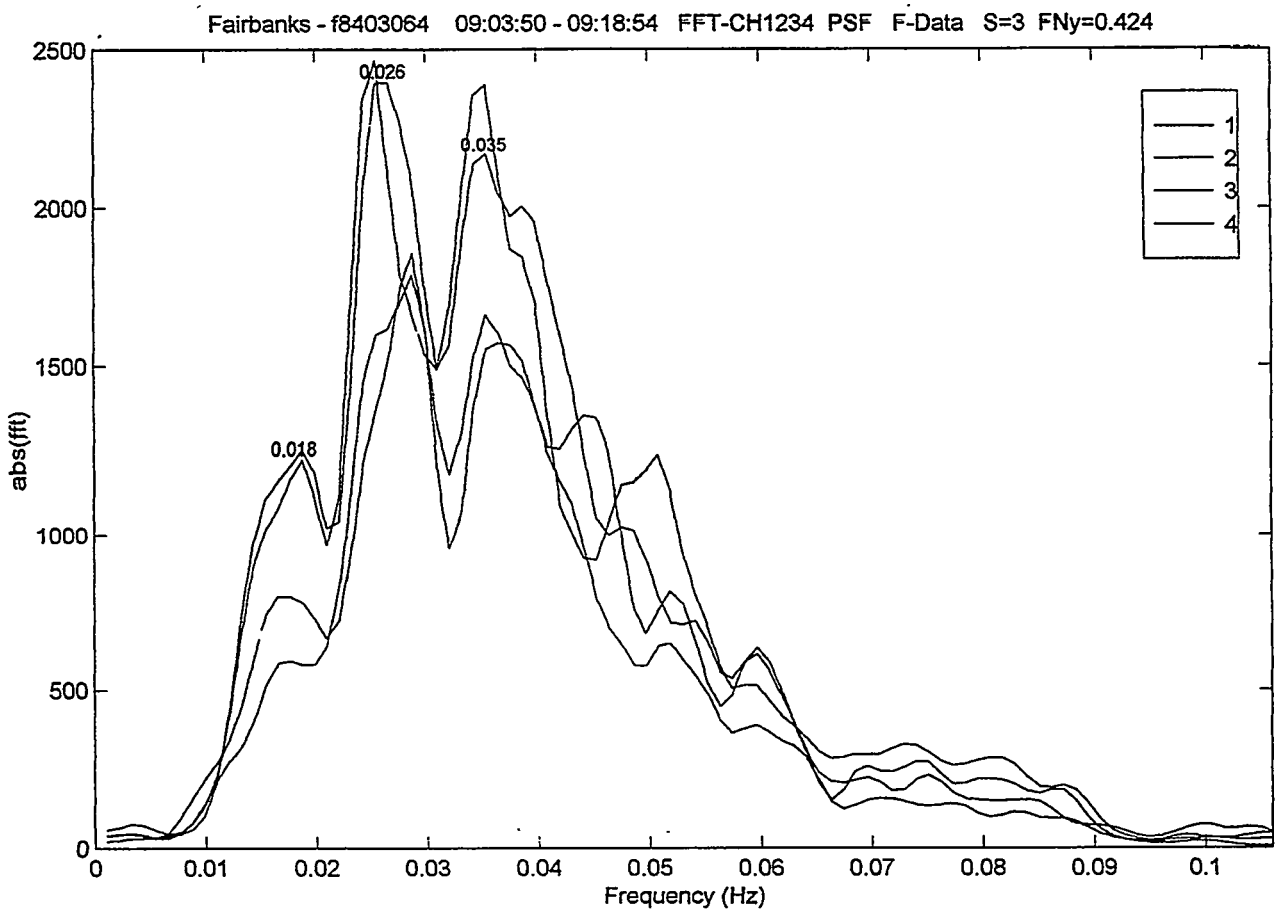
Fairbanks - f8403064 09:03:50 - 09:18:54 FFT-CH1234 PSF F-Data S=3 FNy=0.424
0.026
0.035
0.018
1
2
3
4
abs(fft)
Frequency (Hz)
2500
2000
1500
1000
500
0
0
0.01
0.02
0.03
0.04
0.05
0.06
0.07
0.08
0.09
0.1

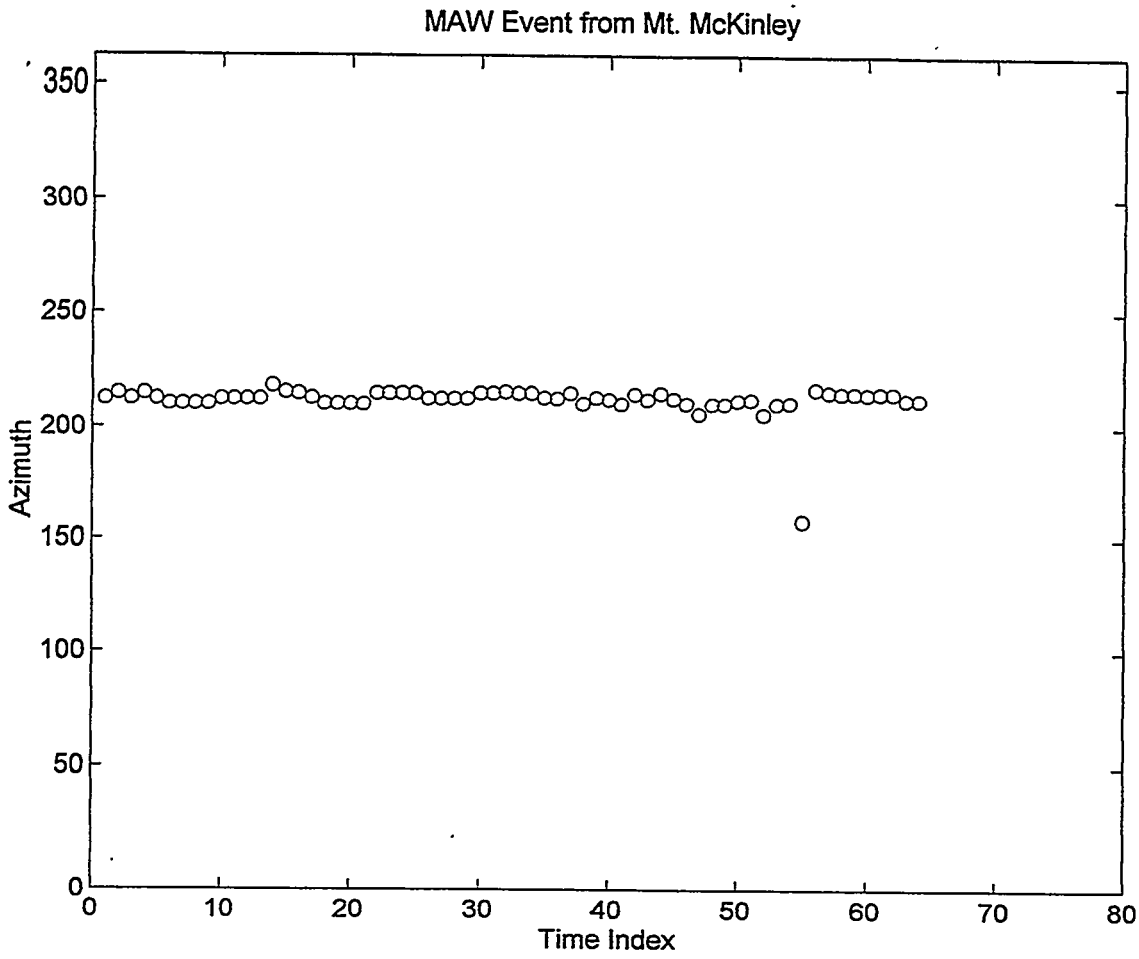
MAW Event from Mt. McKinley
Azimuth
Time Index
0
50
100
150
200
250
300
350
0
10
20
30
40
50
60
70
80

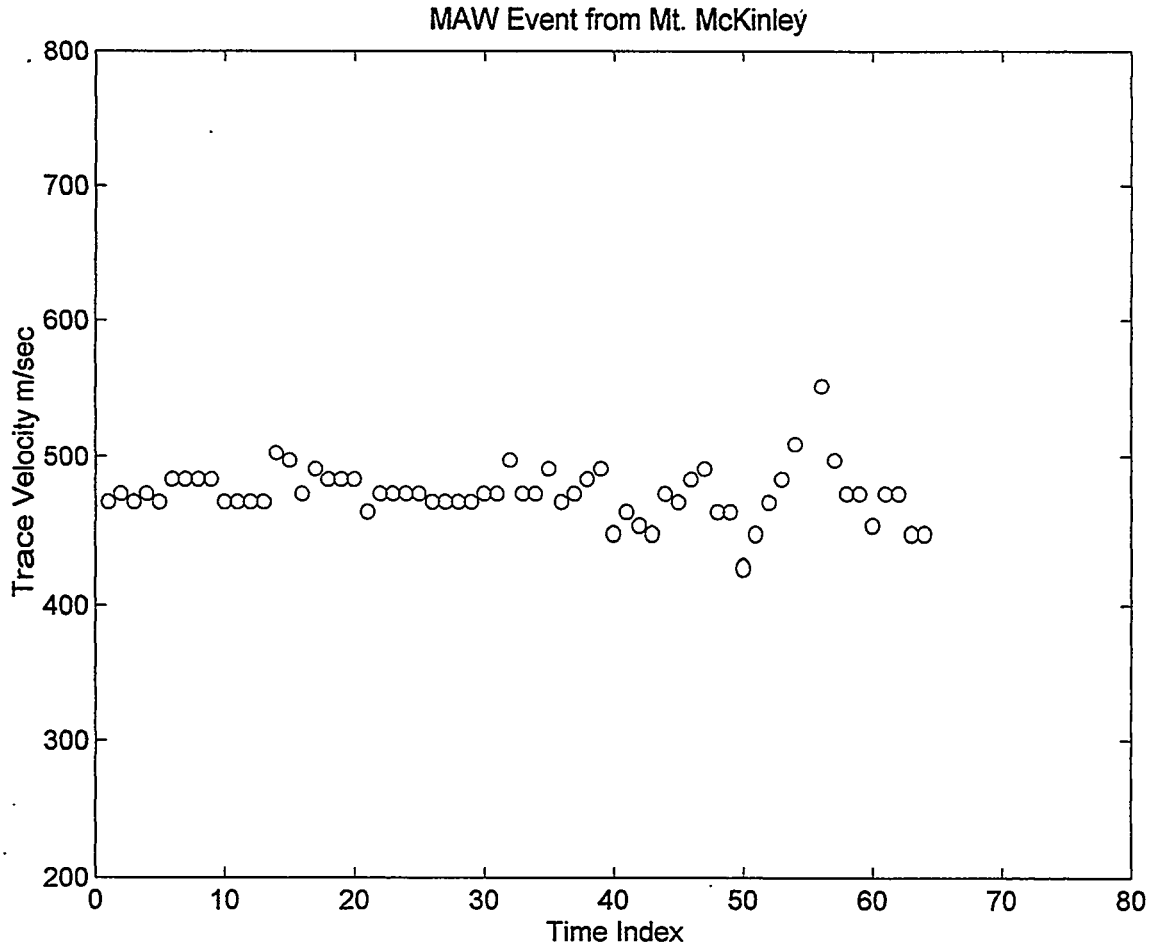
MAW Event from Mt. McKinley
Trace Velocity m/sec
800
700
600
500
400
300
200
0
10
20
30
40
50
60
70
80
Time Index

Volcanic Infrasound (VOL)

Depending on the scale size and violence of a volcanic eruption, traveling pressure waves may be generated by the eruption in the acoustic, infrasonic or even the internal-gravity wave modes, (see Fig. 1). Rapid collapse of a volcanic caldera of sufficient size can generate infrasonic waves in a manner similar to that resulting from under ground nuclear tests. The propagation of volcanic infrasonic waves from the eruption site to the infrasonic observatory depends on the atmospheric temperature and wind distribution along the path. The thermal structure of the atmosphere produces acoustic inversions in the sound speed profile in the mesosphere and the thermosphere. Over long distances infrasonic waves propagate in a reflection mode between the earth's surface and the acoustic inversions, giving zones of silence and zones of detectability on the ground as a series of rings concentric with the source. For distances greater than the first acoustical skip zone , the infrasonic wave may arrive via the upper and/or the lower sound channel, leading to a superposition of wave modes in the infrasonic wave train that may reduce waveform coherence across a microphone array, (see Figures 1 and 2). When the energy released by volcanic explosive eruptions is large enough, infrasonic waves can propagate around the earth by both direct and antipodal paths. Thus the May 1980 Saint Helens eruption produced infrasonic signals detected in Antarctica at Windless Bight on 19 May first at 0542UT from the direct path and again at 1615UT from the antipodal path. Over the twenty year period of operation by the Geophysical Institute of infrasonic observatories in Alaska, Canada, Sweden and Antarctica, infrasonic waves from volcanic eruptions have been detected from all over the world.. Examples are shown in Figures 2 and 3 of small impulsive type volcanic infrasonic signals that could easily be mistaken, at a single station, for an nuclear atmospheric test events because of their similarities of low trace velocity, amplitude and spectral characteristics. However, because volcanic infrasound is radiated isotropicaly, if the signal is detected at two stations, identification by triangulation of the volcanic source region should be possible.

Examples are shown, from a DataScan system, in the figures that follow of a volcanic infrasonic signal observed at Windless Bight, Antarctica from an eruption of Galunggung volcano in Java 8,538 km distant on April 5, 1982. The first figure gives the waveform traces from 13:23 to 13;44 UT of the unfiltered data. On the ordinate scale 100 is equal to 1.0 microbar of pressure disturbance. The second figure gives the same information for the Pure-State filtered data to remove incoherent noise. There is an increase in the average value of the cross-correlation coefficient (cmax) from 0.830 for the raw data to 0.948 for the PSF data. The third figure gives the spectrum of the PSF data with maximum values at periods of 83.3 seconds and 58.8 seconds. The small peak at 0.085 Hz is due to instrumental noise. The multivariate coherence parameter value P versus frequency in the next diagram has a strong maximum at 0.017 Hz as well. The last two figures for the Galunggung volcanic signal data show the effectiveness of the least-squares detection algorithm that was used to identify coherent signals in the DataScan analysis program that was operated online in real-time as the digital data was taken and archived. The penultimate figure displays the azimuth of arrival for a 10.6 hour period beginning at 10:42 UT before the volcanic signal was present and ending at 21:20 UT after the coherent volcanic signal had ended. There is a wide scatter in the azimuth data points until time index 75 when the Galunggung signal begins and after time index 200 when it ends. The same effect can be seen in the last figure for the trace velocity for the same data series. This volcanic signal wave train lasted for about five hours.

Bibliography for Volcanic Infrasound

Craine, L. and J. Thomas, Atmospheric sound signal from Galapagos volcanic eruption, A. U. G. Meeting, April 1, 1969

Donn, W. L. and N. K. Balachandran, Mt. Saint Helens eruption of 18 May, 1980; Air Waves and explosive yield, Science, 213, 539-541, 1981

Goerke, V. J., J. M. Young and R. J. Cook, Infrasonic observations of the May 14, 1963 volcanic explosion on the island of Bali, J. Geophys. Res., 70, 6017-6022, 1965

Harkrider, D. G. , Theoretical and Observed Acoustic Gravity Waves from Explosion Sources in the Atmosphere, J. Geophys. Res., vol. 69, No. 24, 1964

Simkin, T. and K. A. Howard, Caldera collapse in the Galapagos Islands, Science,169, 429-437, 1970

Symond, G., The eruption of Karkatoa and subsequent phenomena, Trubner, London, 1888 .

Wilson C.R, and R .B. Forbes, Infrasonic Waves from Alaskan Volcanic Eruptions, J. Geosphys Res., 74, 1812-1836, 1969d

Wilson C.R. and S. Nichparenko, Evidence of two sound channels in the polar atmosphere from infrasonic observations of the eruption of an Alaskan volcano, Nature, 211,163-165, 1966

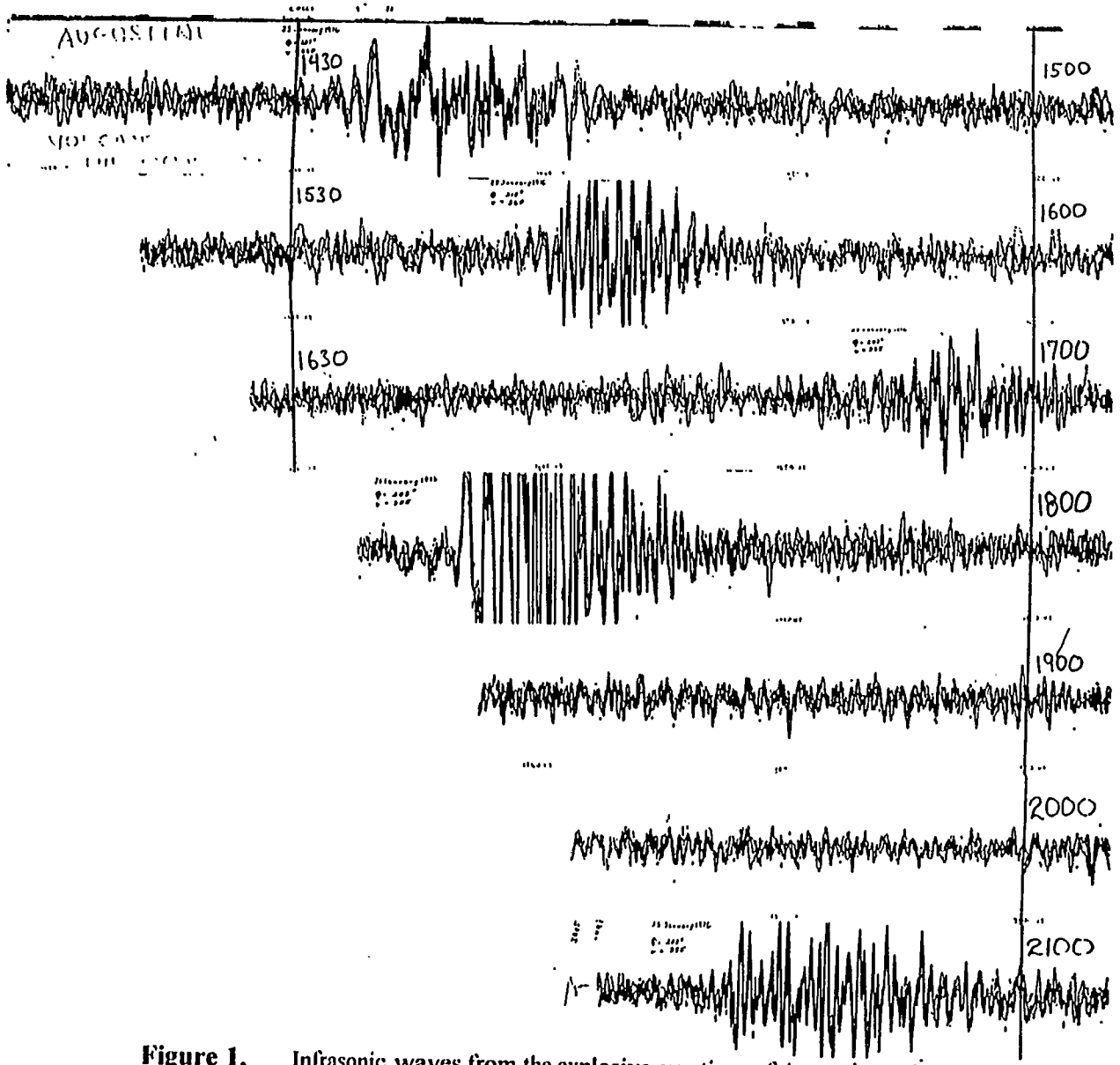

Figure 1. Infrasonic waves from the explosive eruptions of Augustine volcano 688 km SW of Fairbanks, Alaska 23 Jan. 1976. From 1800 to 2000 UT the vague coherence of mountain associated aerodynamic infrasound can be seen on the traces.

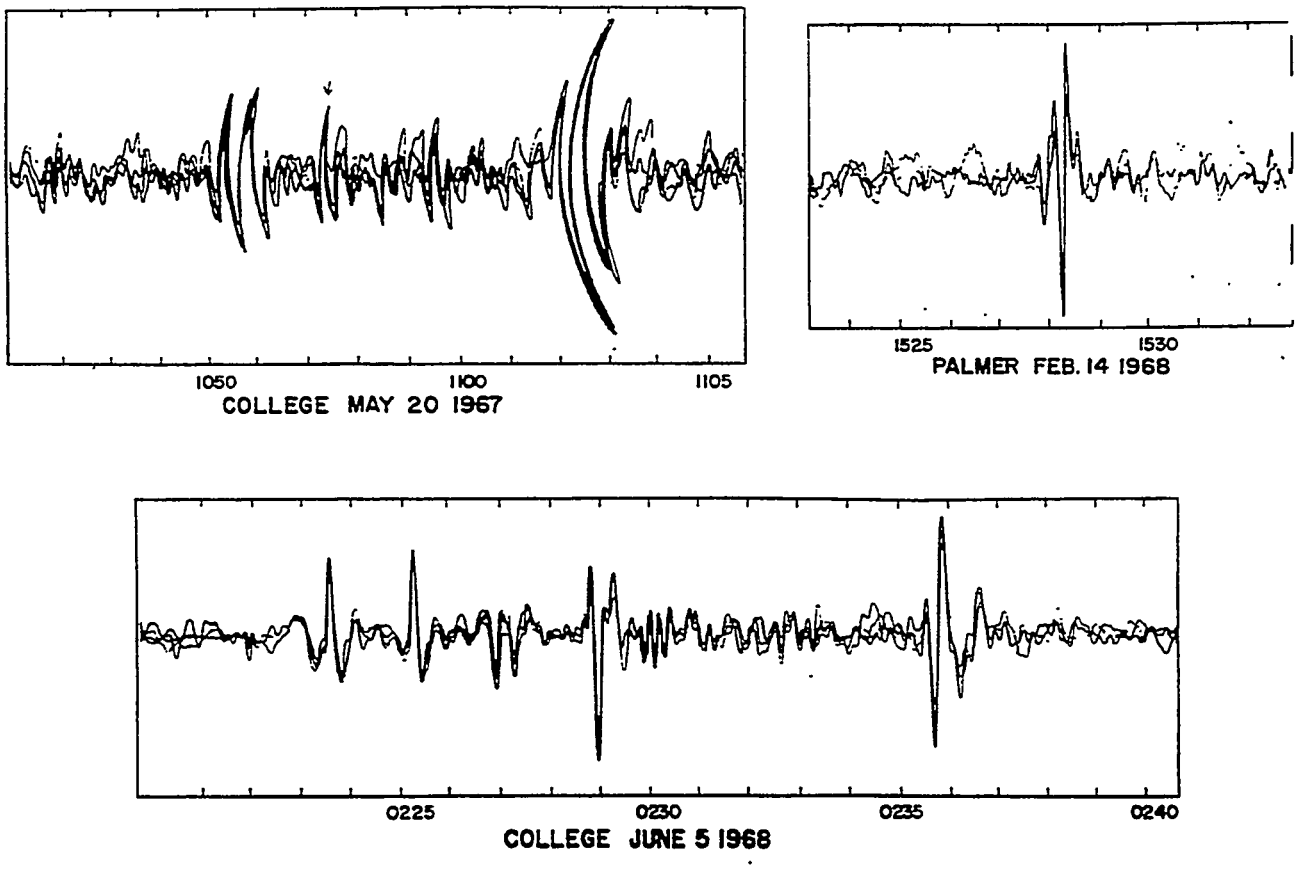

Figure 2. Microbarograph records for impulsive type volcanic eruptions of Trident and Redoubt volcanoes in Cook Inlet, Alaska that are 843 km and 510 km respectively from College.

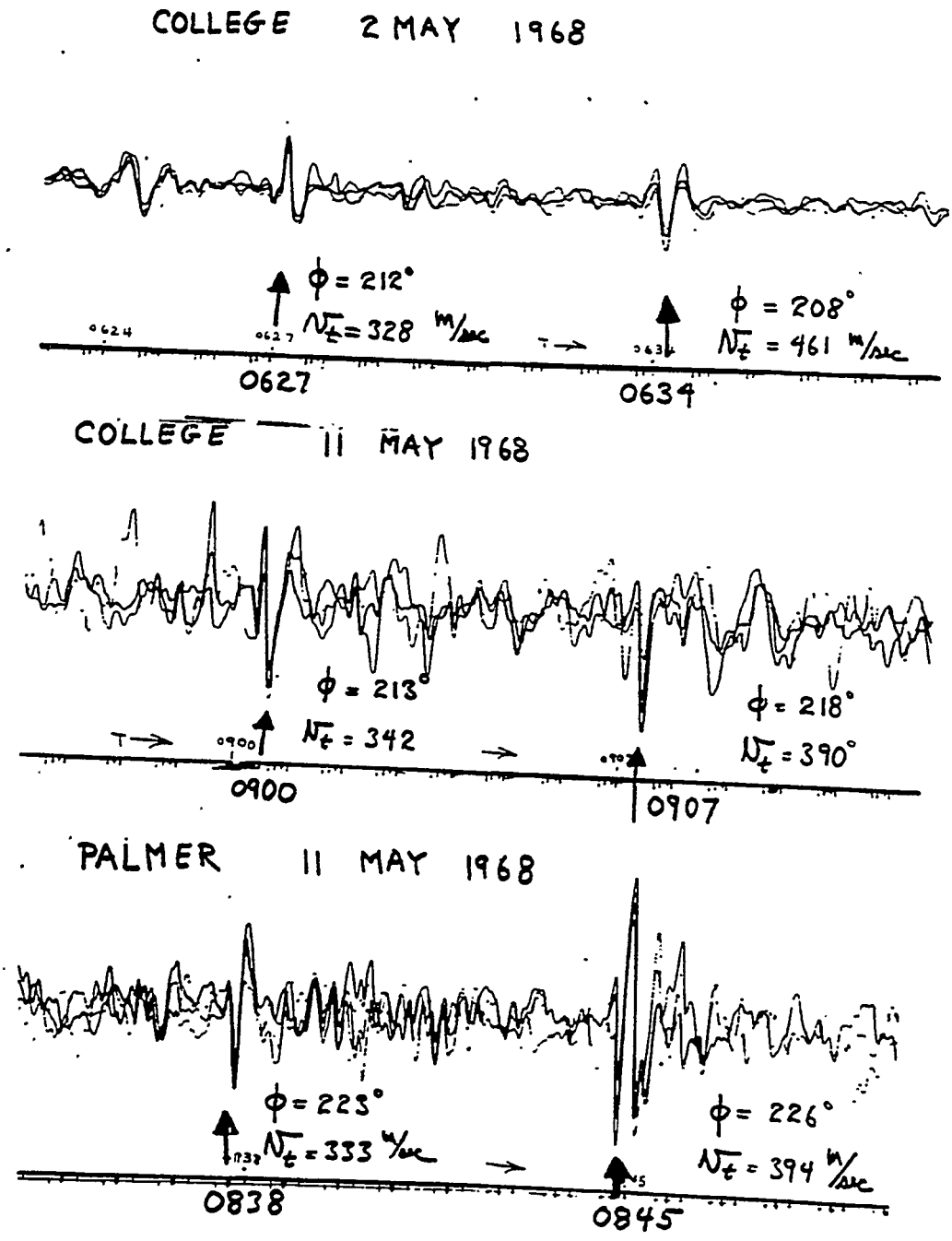

Figure 3. Volcanic infrasonic signals from unidentified eruptions of the Cook Inlet volcanoes. A much larger value of the trace velocity Vt can be seen in all three examples for the second signal propagating via the upper sound channel.

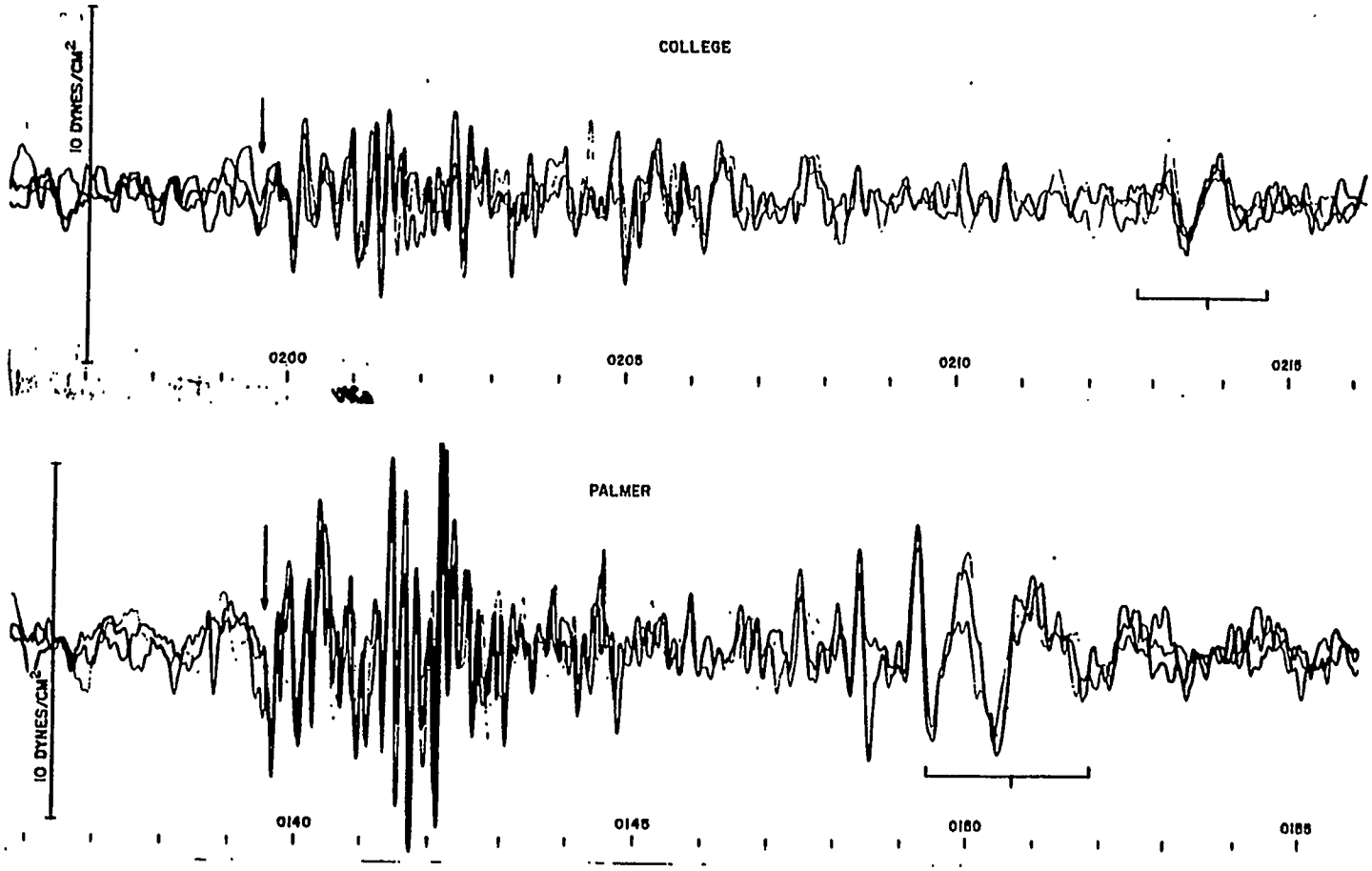

Figure 4. Infrasonic waves from the December 18, 1967 eruption of Trident volcano as observed first at Palmer and then at College. The average trace velocities for the first arrival was 326 m/sec , while for the second arrival Vt had a higher average of 443 m/sec for the two stations.

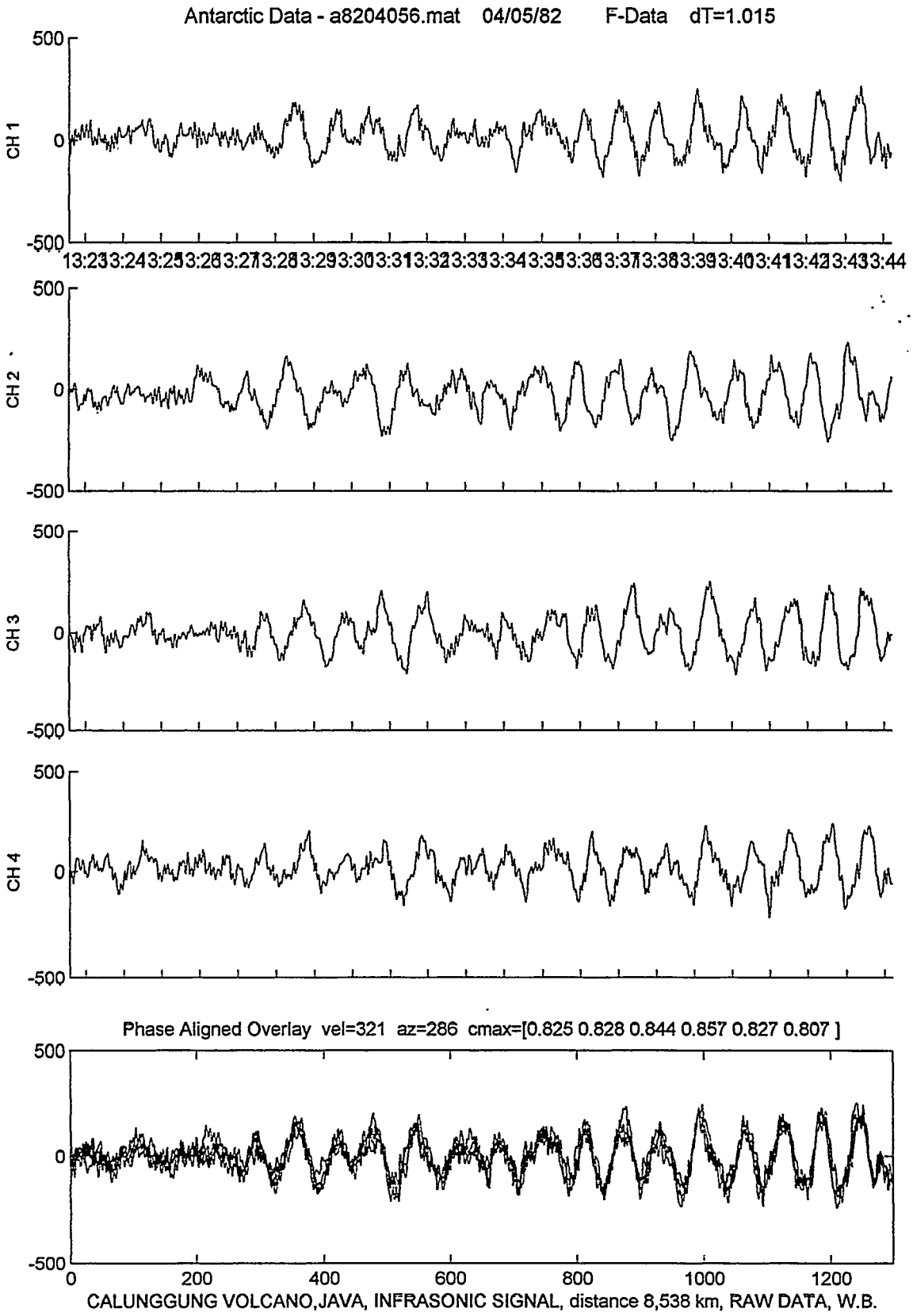
Antarctic Data - a8204056.mat 04/05/82 F-Data dT=1.015
CH 1
CH 2
CH 3
CH 4
500
0
-500
13:23 13:24 13:25 13:26 13:27 13:28 13:29 13:30 13:31 13:32 13:33 13:34 13:35 13:36 13:37 13:38 13:39 13:40 13:41 13:42 13:43 13:44
Phase Aligned Overlay vel=321 az=286 cmax=[0.825 0.828 0.844 0.857 0.827 0.807]
0
200
400
600
800
1000
1200
CALUNGGUNG VOLCANO,JAVA, INFRASONIC SIGNAL, distance 8,538 km, RAW DATA, W.B.

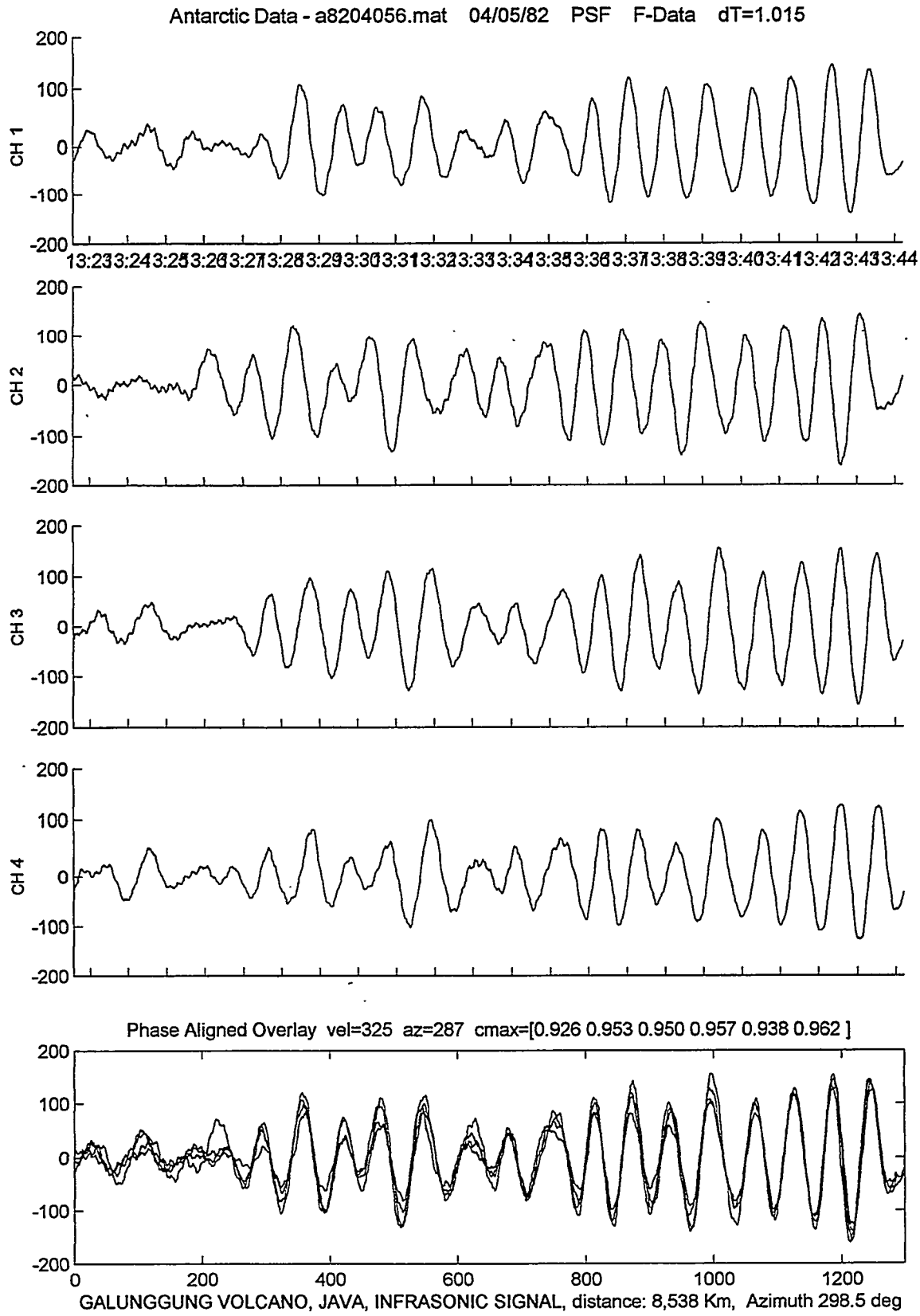
Antarctic Data - a8204056.mat 04/05/82 PSF F-Data dT=1.015
CH 1
CH 2
CH 3
CH 4
200
100
0
-100
-200
13:23 13:24 13:25 13:26 13:27 13:28 13:29 13:30 13:31 13:32 13:33 13:34 13:35 13:36 13:37 13:38 13:39 13:40 13:41 13:42 13:43 13:44
Phase Aligned Overlay vel=325 az=287 cmax=[0.926 0.953 0.950 0.957 0.938 0.962]
0
200
400
600
800
1000
1200
GALUNGGUNG VOLCANO, JAVA, INFRASONIC SIGNAL, distance: 8,538 Km, Azimuth 298.5 deg

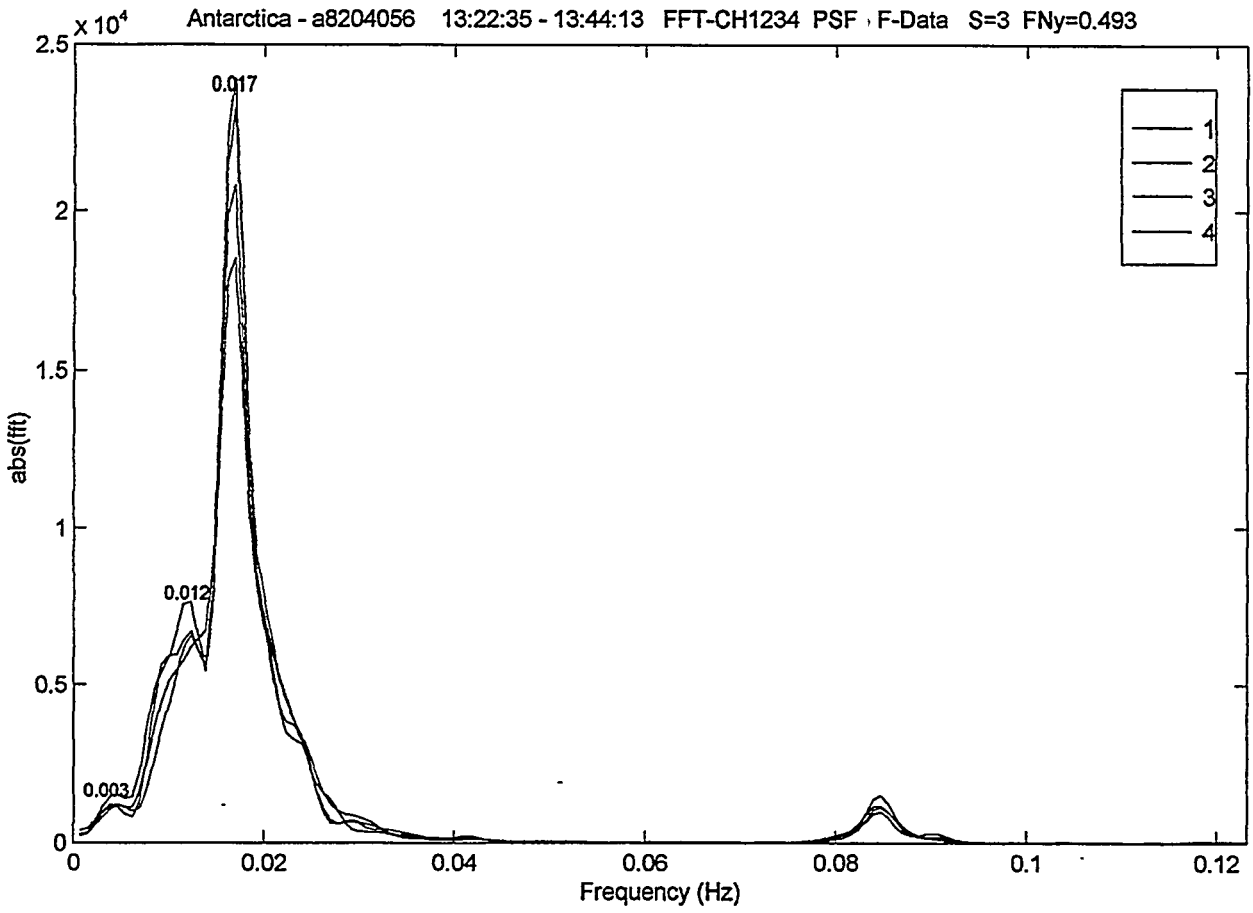
x 10^4
Antarctica - a8204056 13:22:35 - 13:44:13 FFT-CH1234 PSF , F-Data S=3 FNy=0.493
2.5
2
1.5
1
0.5
0
abs(fft)
0.017
0.012
0.003
1
2
3
4
0
0.02
0.04
0.06
0.08
0.1
0.12
Frequency (Hz)

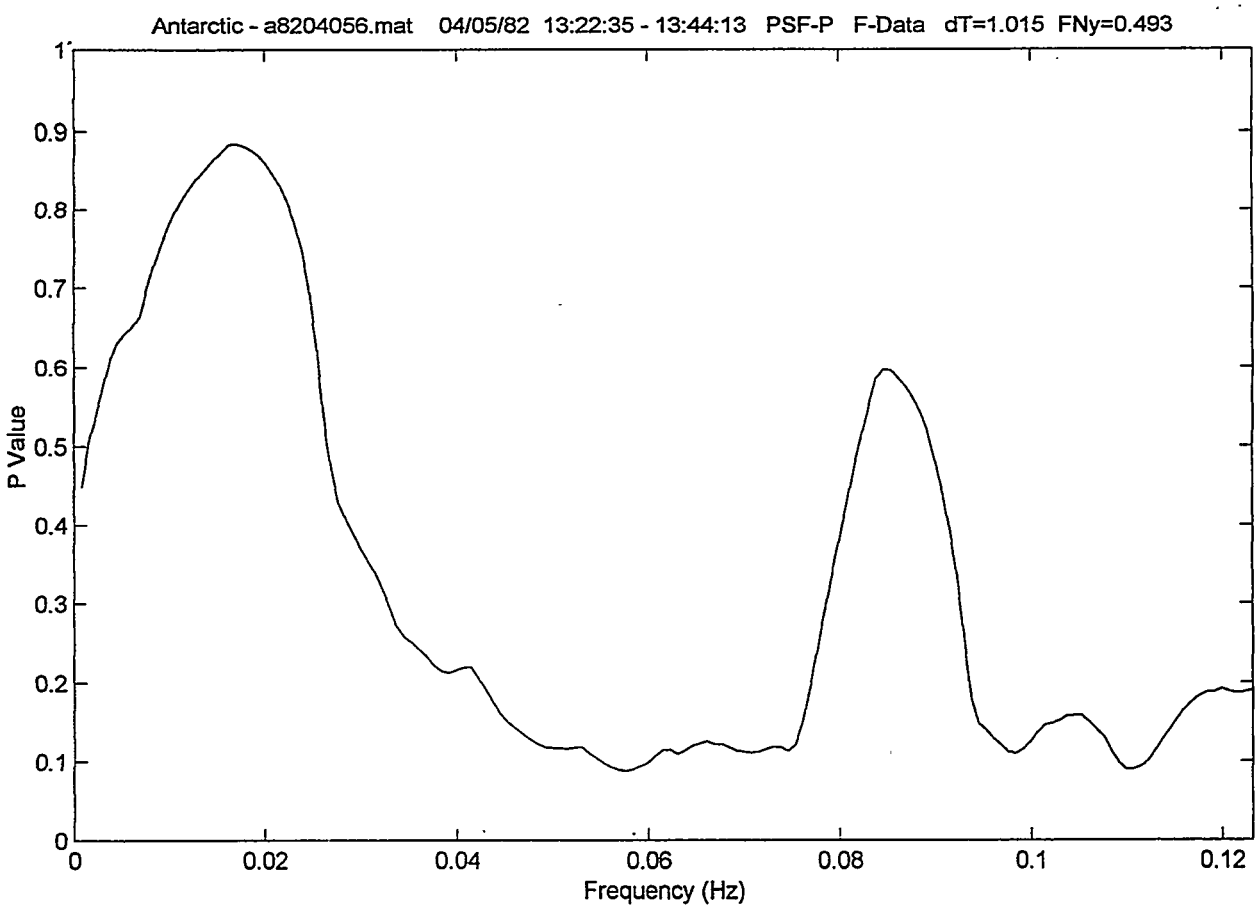
Antarctic - a8204056.mat 04/05/82 13:22:35 - 13:44:13 PSF-P F-Data dT=1.015 FNy=0.493
P Value
Frequency (Hz)
0
0.1
0.2
0.3
0.4
0.5
0.6
0.7
0.8
0.9
1
0.02
0.04
0.06
0.08
0.12

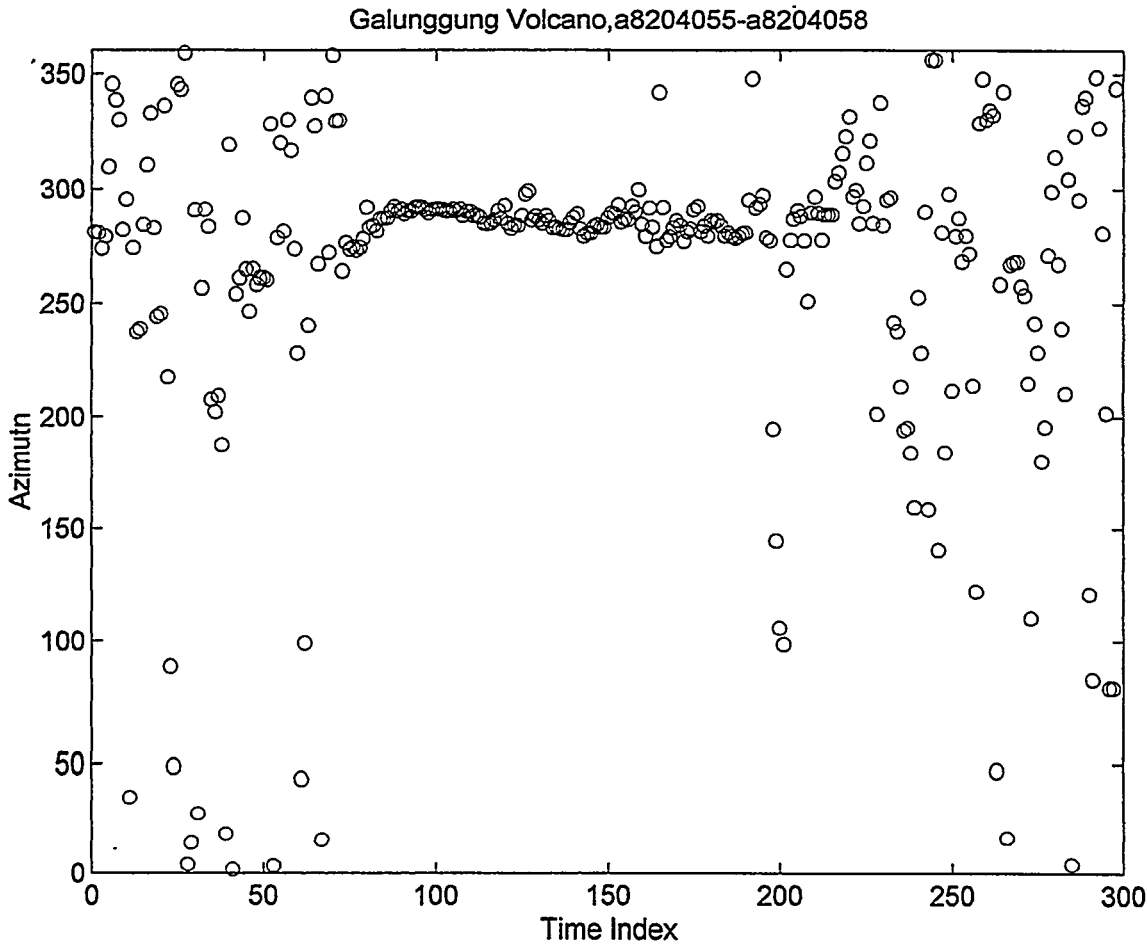
Galunggung Volcano,a8204055-a8204058
Azimutn
Time Index
0
50
100
150
200
250
300
350

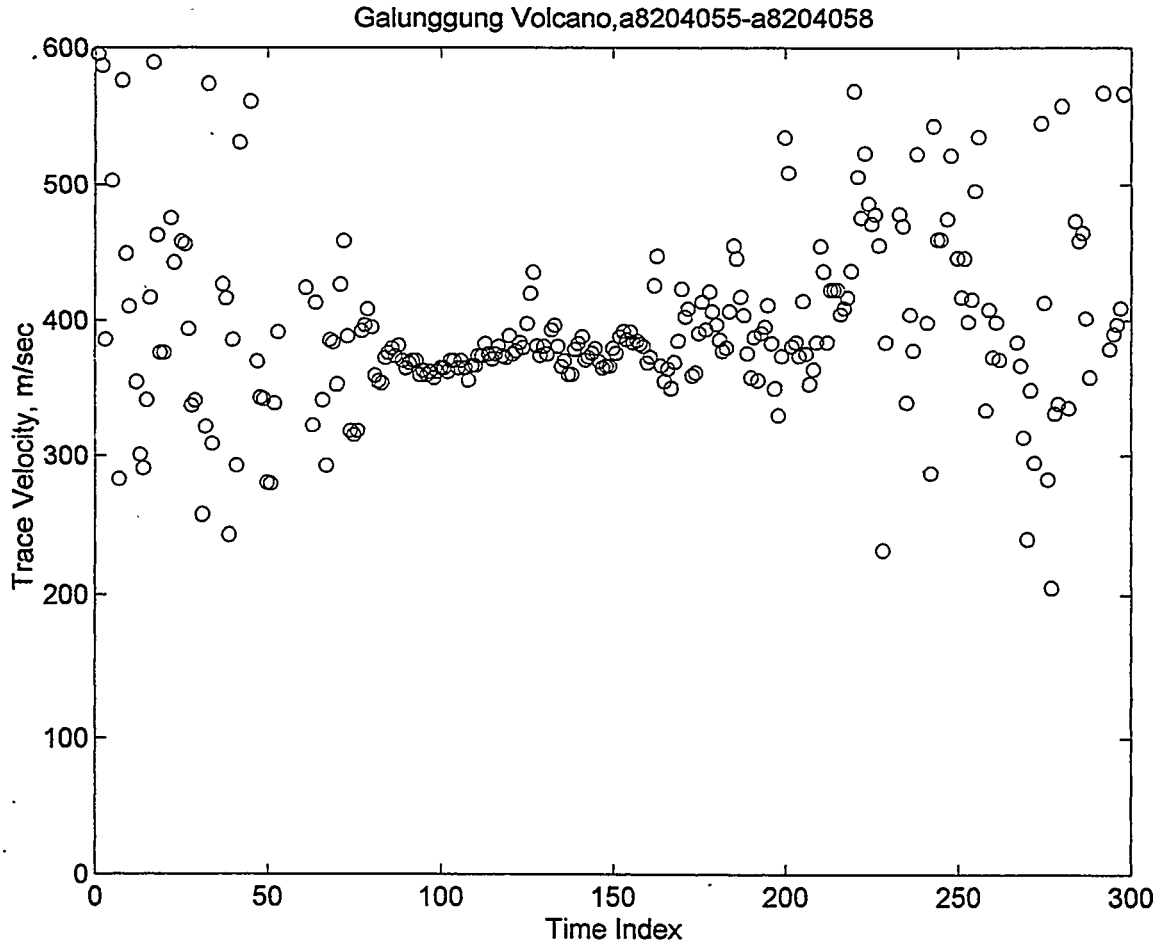
Galunggung Volcano,a8204055-a8204058
Trace Velocity, m/sec
Time Index
0
100
200
300
400
500
600
0
50
100
150
200
250
300

Microbaroms (MB)

Standing-wave patterns on the sea surface in marine storms produce infrasonic waves, called microbaroms (MB), with three to eight second period and amplitudes of a few microbars, that will propagate great distances with little dispersion or attenuation. The seasonal variations in occurrence of marine storms as well as the effect of upper level winds in the atmospheric sound channels will jointly determine the seasonal and diurnal variations of occurrence for MB. The observed trace velocity for a MB wave packet, that is observed at distances greater than the first acoustical skip-zone, will be modified from its intrinsic value by the addition of the component (in the direction of propagation of the MB) of the upper level wind at the height of the reflection in the atmospheric sound channel. The direction bands from which MB will be received are different for each observing station depending on the station location with respect to the surrounding oceans and marine storm source regions. Examples are shown in the figures that follow of microbaroms observed at Fairbanks on 01/26/84 from a storm in the Gulf of Alaska from an azimuth of 195 to 200 degrees. The MB data were obtained with a triangular microphone array of side length of about one kilometer and with a frequency passband of 0.10 Hz to 1.0 Hz.. The wave-packet like nature of microbarom events as a string of successive "pearls" can be seen in the second waveform figure that shows a 7 minute time window for the MB event. The multivariate coherence parameter P from Pure-State filtering is shown, as a function of frequency, for the MB event. The P value can be seen to peak at a value of 0.82 at a frequency of about 0.2 Hz. The peak in the spectral energy diagram for this same MB event, is also at 0.2 Hz. The penultimate figure in the BM diagram series shows, for a seven hour time window, the consistent azimuth of arrival from 195 to 200 degrees, from the Gulf of Alaska, for the MB event on 01/26/84. The trace velocity and azimuth of arrival for successive individual microbarom wave-packets can vary over a wide range that depends on the scale size of the marine storm source and its distance to the infrasonic array. The last figure in the Fairbanks 01/26/84 MB event series shows the fluctuations in the trace velocity within a band from about 290 m/sec to 350 m/sec for the same time period.

The theory of the generation mechanism of MB that agrees well with their characteristics, as observed at Fairbanks and in Antarctica, was developed by Posmentier (1967). He proposed that the oscillation of the center of gravity of the air above the standing-wave patterns on the surface of the sea would cause the radiation of infrasound of a frequency double that of the standing-waves themselves. The observed frequency range for microbaroms, from 0.125 Hz to 0.333 Hz, assures that microbaroms can be considered as nondispersive waves that can propagate long distances with little attenuation. Acoustic waves will be attenuated in amplitude by energy dissipation given by exp(-az) , where z is the distance traveled and a is the dissipation coefficient (Landau and Lifchitz, 1959). The dissipation coefficient for acoustic waves of frequency 0.25 Hz, (similar to that of microbaroms), increases with height from 5.1×10^{-7} at a 40 km altitude by almost four orders of magnitude to 3.0×10^{-3} at an altitude of 100 km. Thus microbaroms will suffer increasing energy dissipation with height. For very long propagation paths, where multiple reflections in the upper atmosphere occur, energy dissipation becomes important.

Infrasonic observations in both Fairbanks, Alaska and in Windless Bight, Antarctica have shown that MB waves are not coherent over the area of arrays with microphone spacing greater than a few kilometers. They could only be detected at either location where the inter-microphone distance was close to 800 meters at the Fairbanks and about 1,200 meters at the Windless Bight. In Antarctica the use of the pure-state filter in the digital system with the small microphone array at Windless Bight enabled the detection of microbaroms that were not detectable in the unfiltered data. The number of microbaroms as a function of azimuth for the year 1981 at Windless Bight are shown in Figure 5. There is a systematic variation ,due the upper level winds, in the average trace

velocity of microbaroms as a function of azimuth of arrival that is shown in Figure 6 for 1981 data at Windless Bight.

Bibliography for Microbaroms

Collier, J. L., Masters Thesis, Morphology of Microbaroms at Windless Bight, Antarctica and Fairbanks, Alaska, University of Alaska at Fairbanks, May 1983

Donn, W. L., and E. S. Posmentier, Infrasonic waves from the marine storm of 7 April 7, 1966, J. Geophys. Res.,72, 1 ,1967

Donn, W.L. and E.S. Rind, Microbaroms and the temperature and wind of the upper atmosphere, J. Aimos. Sci., 29,156,1972

Posmentier, E. S., A Theory of Microbaroms, Geophys. .J. R. Ast. Soc., 13,487, 1967

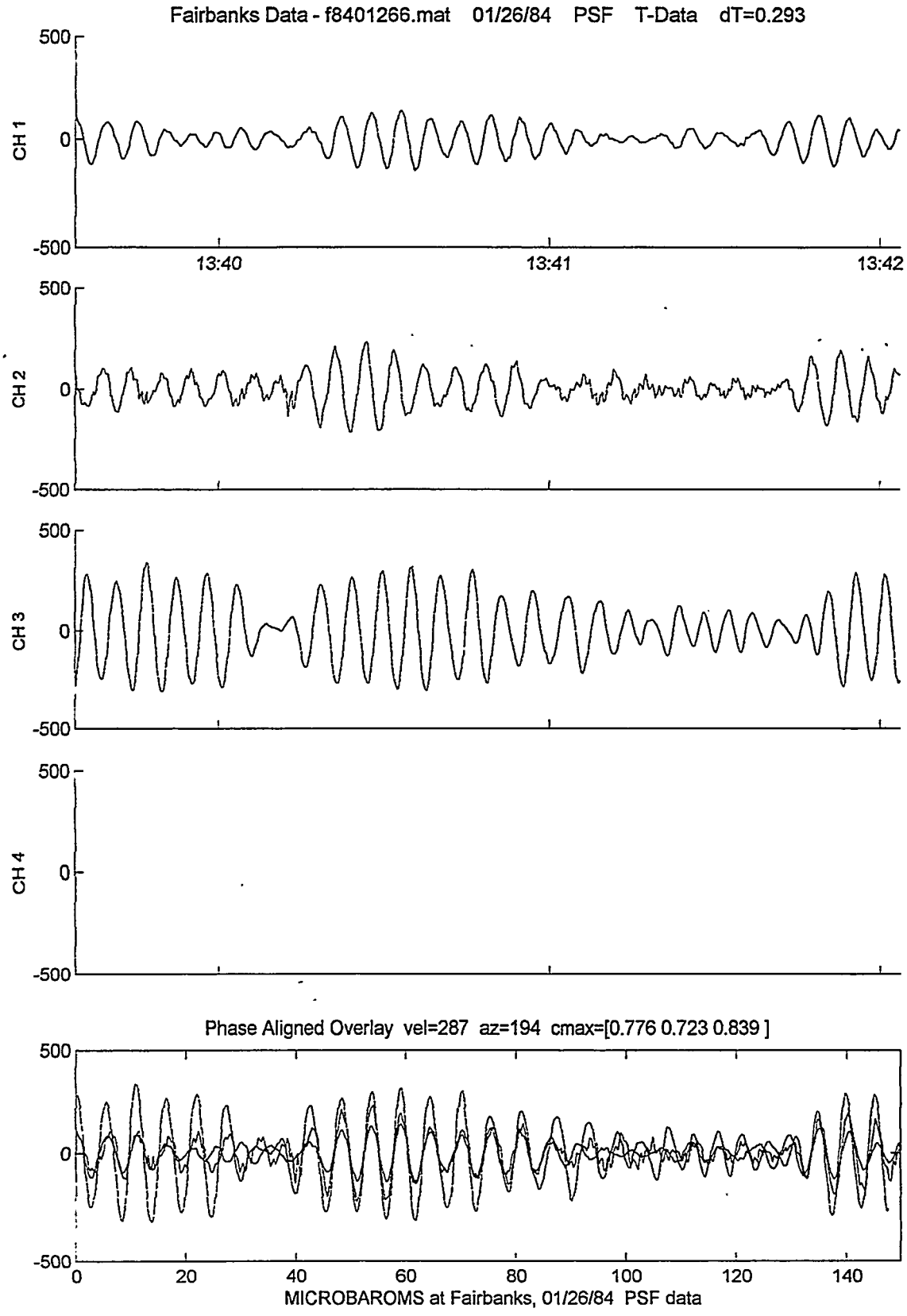
Fairbanks Data - f8401266.mat 01/26/84 PSF T-Data dT=0.293
CH 1
CH 2
CH 3
CH 4
500
0
-500
13:40
13:41
13:42
Phase Aligned Overlay vel=287 az=194 cmax=[0.776 0.723 0.839]
0
20
40
60
80
100
120
140
MICROBAROMS at Fairbanks, 01/26/84 PSF data

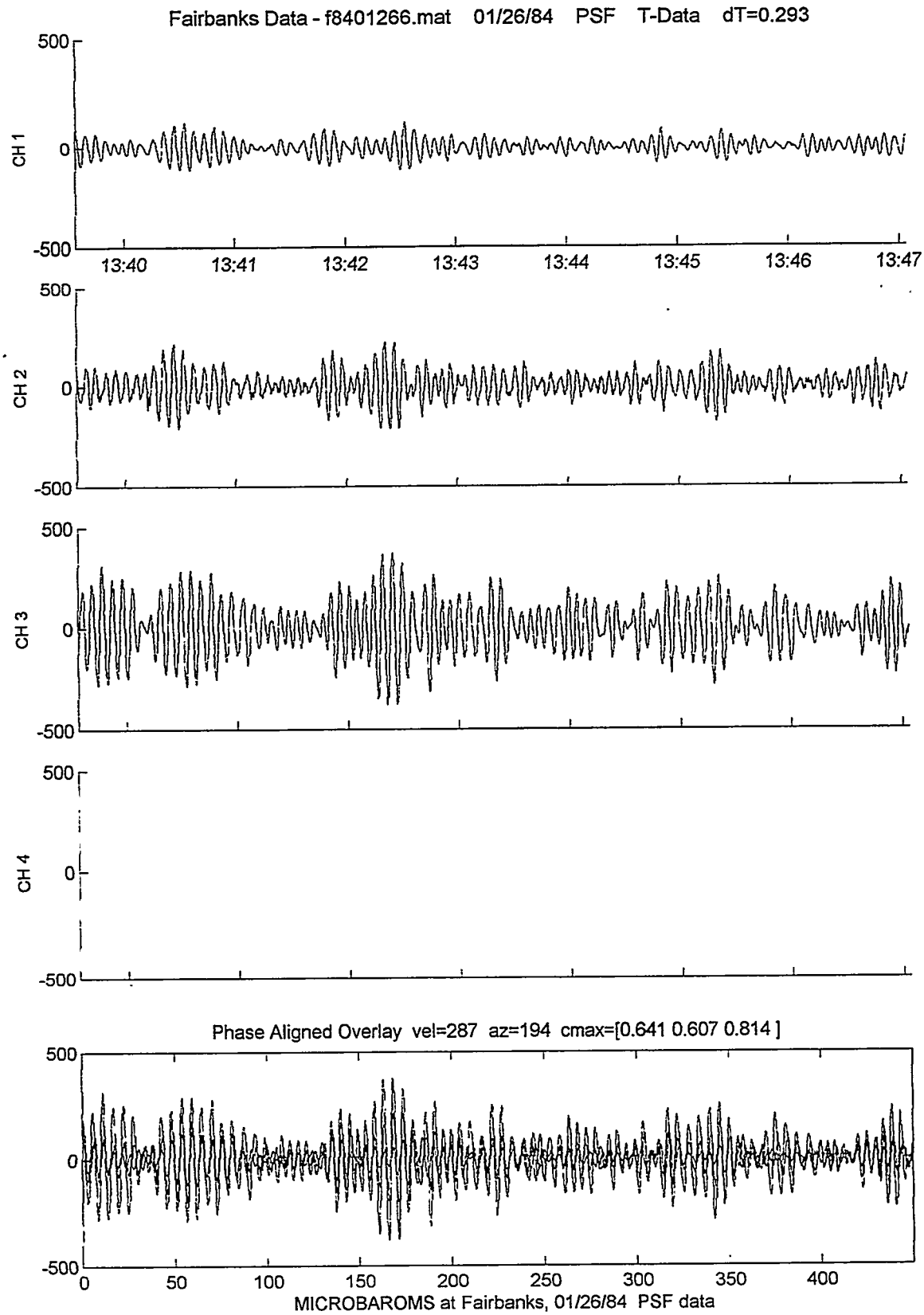
Fairbanks Data - f8401266.mat 01/26/84 PSF T-Data dT=0.293
CH 1
CH 2
CH 3
CH 4
500
0
-500
13:40
13:41
13:42
13:43
13:44
13:45
13:46
13:47
Phase Aligned Overlay vel=287 az=194 cmax=[0.641 0.607 0.814]
0
50
100
150
200
250
300
350
400
MICROBAROMS at Fairbanks, 01/26/84 PSF data

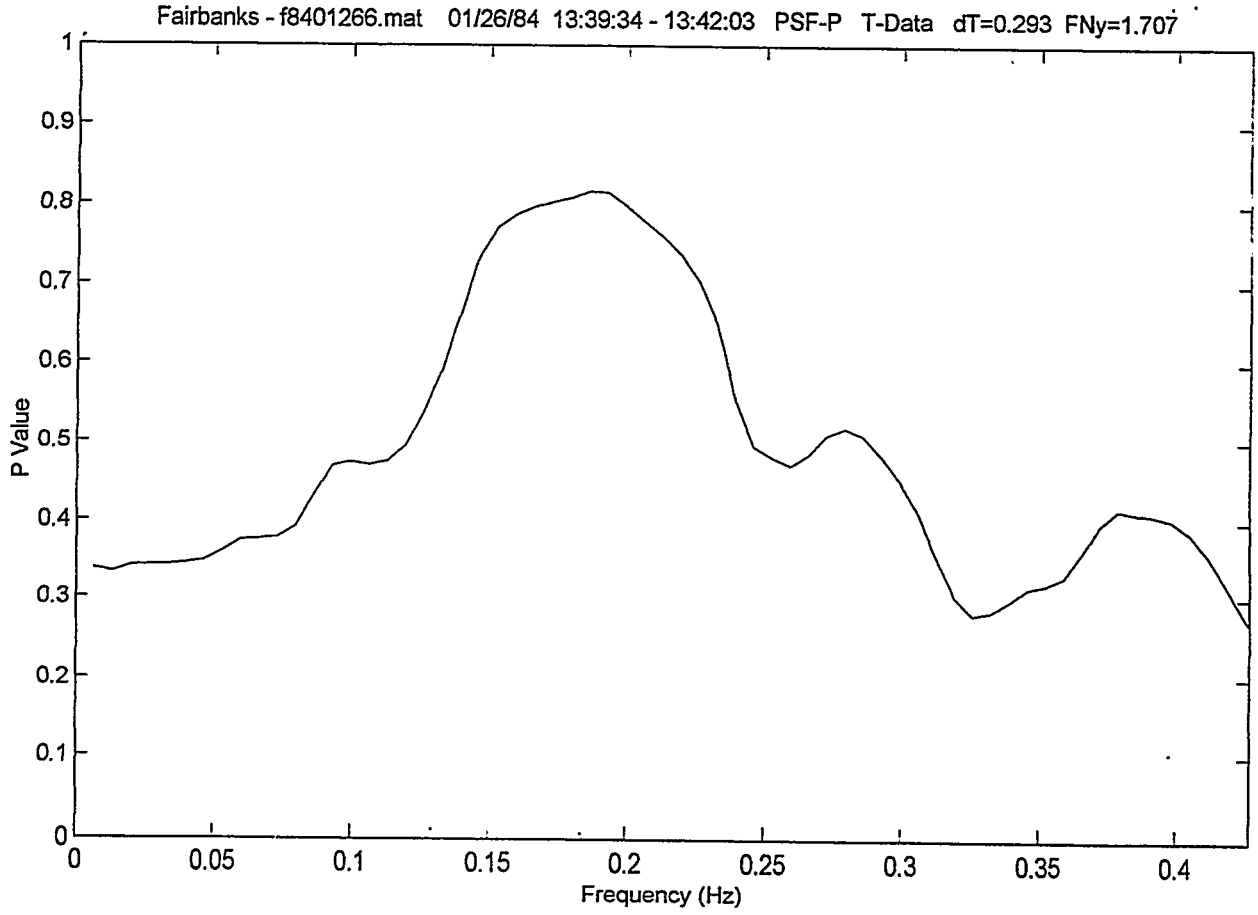
Fairbanks - f8401266.mat 01/26/84 13:39:34 - 13:42:03 PSF-P T-Data dT=0.293 FNy=1.707
P Value
Frequency (Hz)
0
0.1
0.2
0.3
0.4
0.5
0.6
0.7
0.8
0.9
1
0.05
0.15
0.25
0.35

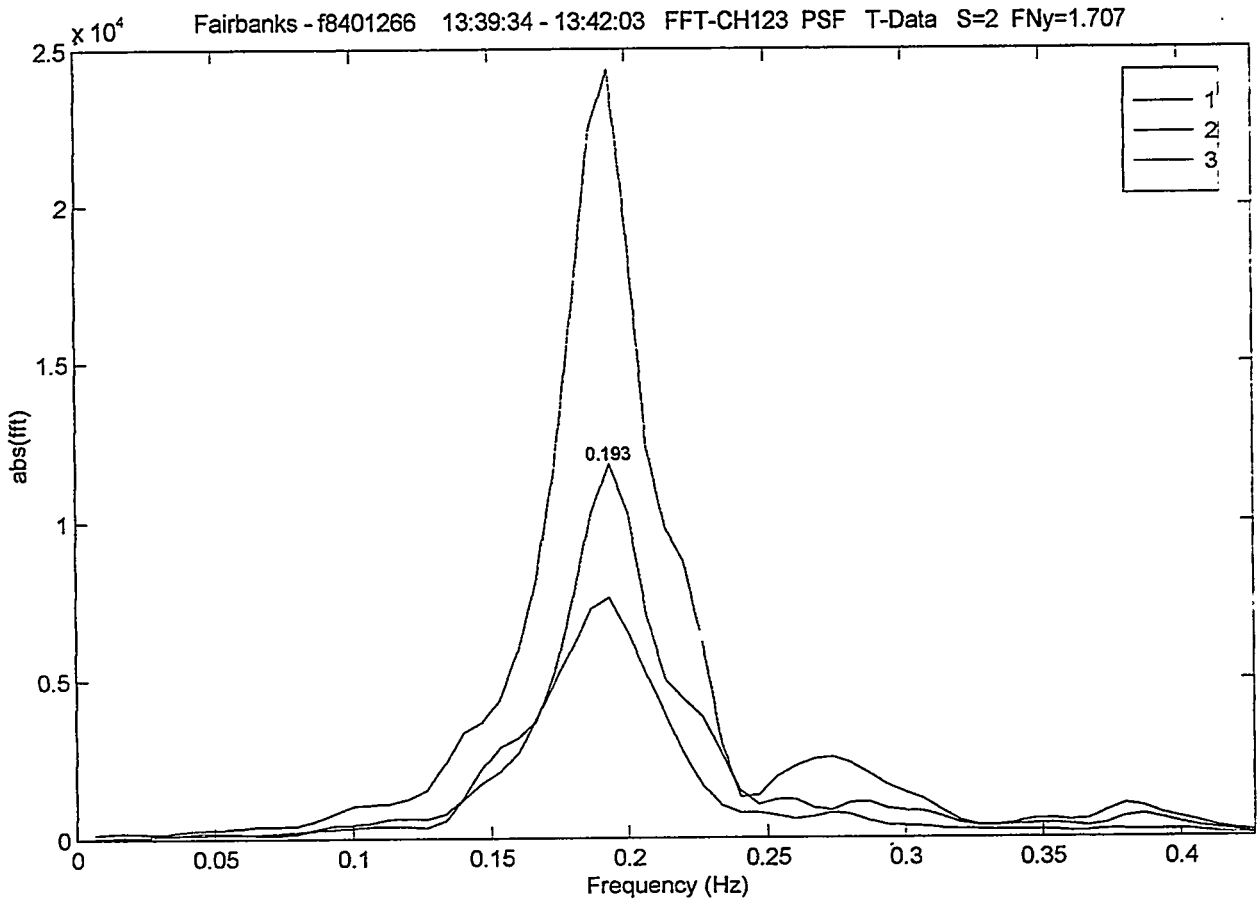
x 10^4
Fairbanks - f8401266 13:39:34 - 13:42:03 FFT-CH123 PSF T-Data S=2 FNy=1.707
2.5
2
1.5
1
0.5
0
abs(fft)
0.193
1
2
3
0
0.05
0.1
0.15
0.2
0.25
0.3
0.35
0.4
Frequency (Hz)

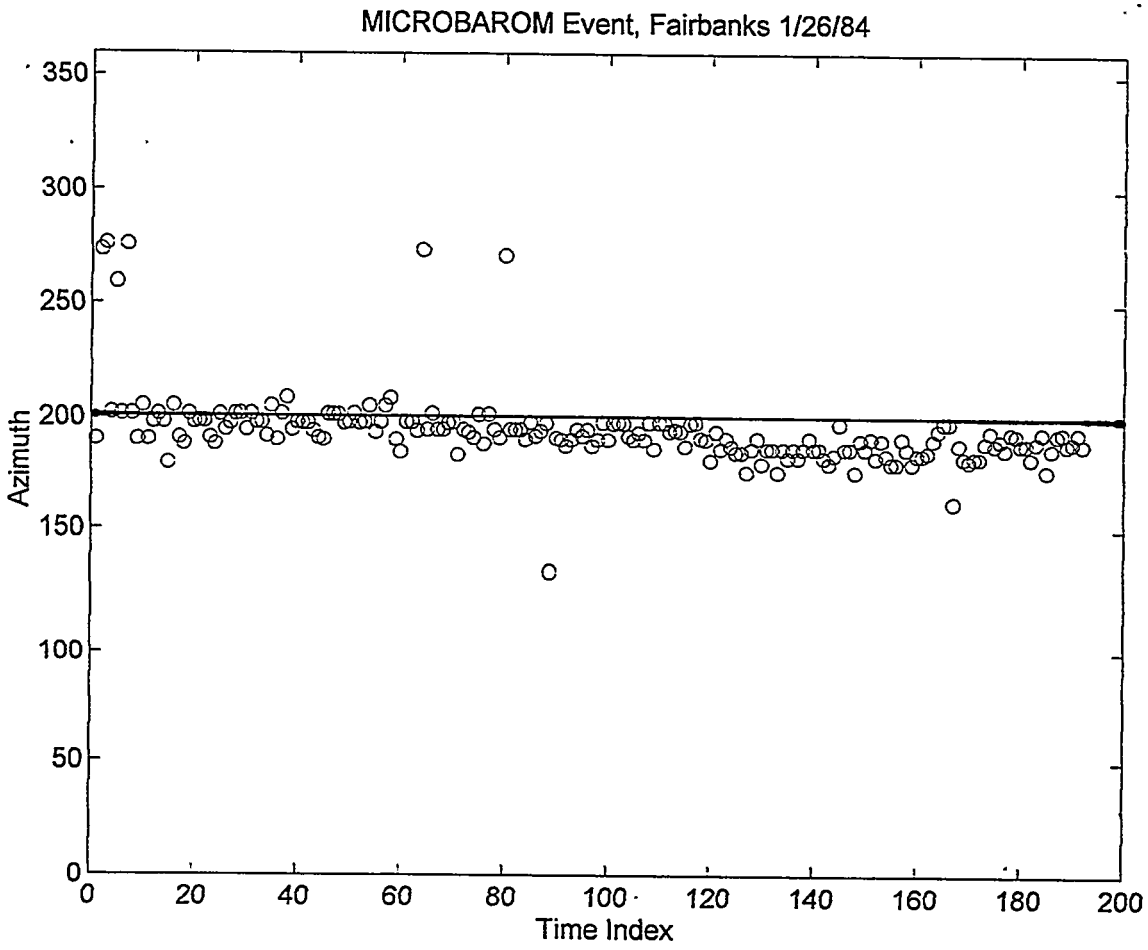
MICROBAROM Event, Fairbanks 1/26/84
Azimuth
Time Index
0
50
100
150
200
250
300
350
0
20
40
60
80
100
120
140
160
180
200

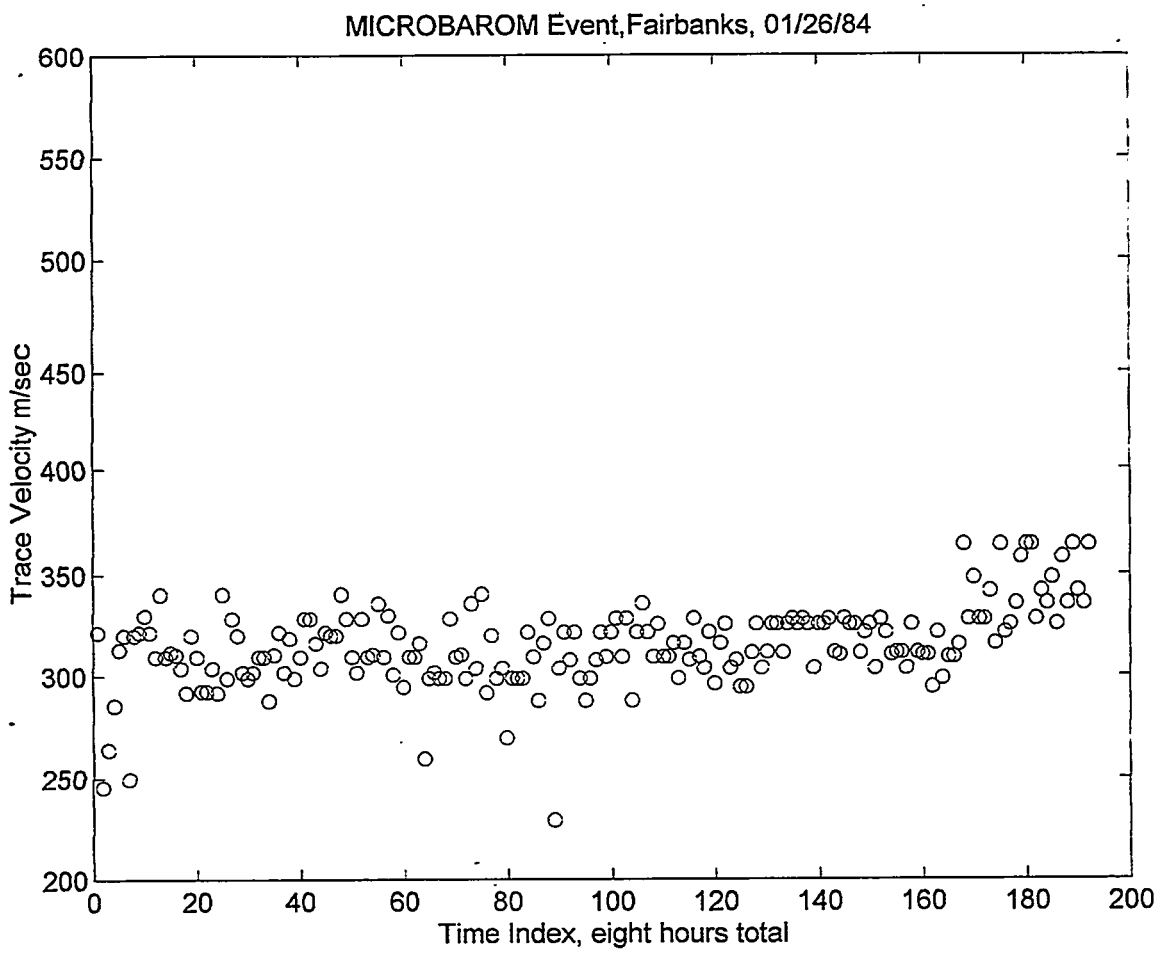
MICROBAROM Event,Fairbanks, 01/26/84
Trace Velocity m/sec
600
550
500
450
400
350
300
250
200
0
20
40
60
80
100
120
140
160
180
200
Time Index, eight hours total

Infrasound from Earthquakes

Infrasonic waves in the passband from 10 Hz to 0.01 Hz are generated by sudden ground displacements that occur in earthquakes and in under ground tests of nuclear weapons. There are two types of infrasonic signals the are associated with earthquakes. First ,as the seismic Rayleigh wave from an earthquake sweeps across an array of infrasonic microphones at seismic wave speeds, the vertical component of the ground motion of the Rayleigh wave causes the radiation of infrasound into the atmosphere at the microphone sites. The period of the Rayleigh wave generated infrasound is identical to that of the Rayleigh wave itself. Second, impulsive ground motion in the epicenter region of an earthquake will generate infrasonic waves that travel far from the source as was the case for the great Alaska earthquake of 1964. The infrasonic waves generated in the epicenter region by ground motion of an earthquake are of longer period (10 to 100 seconds) depending on the horizontal scale size of the ground displacement. An example is shown in Figure 1 from the Fairbanks infrasonic array of earthquake infrasound observed on 28 February 1979 from a magnitude 7.3 earthquake 640 km away with epicenter near Cape Yakataga, Alaska. The Rayleigh wave infrasound was observed at 2130 UT as the surface seismic wave crossed the microphone array. The air wave generated in the epicenter region arrived about 30 minutes later at 2202 UT with a trace velocity of 320 m/sec propagating via the stratospheric sound channel. Because of the particular azimuth of arrival of the wave, this second signal is thought to be associated with the motion of the Mount Logan massif as the earthquake seismic waves shook the mountain. The period of the Rayleigh wave signal was about 20 seconds while that of the second signal from Mount Logan is longer with components up to 100 seconds. The original analogue records from the Yakataga earthquake were hand digitized every 1.8 seconds and low pass filtered to remove high frequency contamination from the digitization process and then pure state filtered to produce the records shown in Figure 2. The most obvious feature of the pure state filtered data is the clarity of the onset of the arrival of the infrasonic waves at the array as shown in Figure 2. The pure state filtering of the data resulted in an overall enhancement of the signal to noise power at 0.01 Hz of approximately two orders of magnitude. The efficacy of this treatment by pure state filtering of the infrasonic microphone data results from the fact that the principal noise source, boundary layer turbulence, is uncorrelated over the scale size of the array. The spectra of the air wave signal at 2200 UT from one of the Fairbanks array microphones are shown in Figure 3 for the raw data, and in Figure 4 for the data after pure state filtering. There is considerable enhancement of the contrast between the central peaks and the noise in these spectra (raw data versus pure state filtered data). This filtering at 0.01 Hz gives an overall signal to noise enhancement of 20 db.

Rayleigh wave infrasonic signals have been detected numerous times in Antarctica at the Windless Bight array that is located on the floating Ross Ice Shelf. The area of the floating ice shelf is tens of thousands of square miles with a thickness of 800 feet. Surface seismic waves couple to the Ross Ice Shelf from the contiguous mountain ranges to the west and south and from the grounded glaciers of East Antarctica. The microphone traces from two of the sensors at Windless Bight are given in Figure 5 for a Rayleigh Wave infrasonic signal observed on December 30, 1976. From the one minute time marks at the bottom of the traces one can see that the arrival of the waves at the two microphones was virtually simultaneous. The amplitude of the signal was about three to five microbars.

Bibliography for Earthquake Infrasound

Bedard,A.J., Seismic Response of Infrasonic Microphones, J. of Research National Bureau of Standards, vol. 75C, 1971

Donn, W.L. and E.S. Posmentier , Ground -Coupled Air Waves from the Great Alaskan Earthquake, J.G.R. vol 69, No. 24, 5357, 1964

Mikumo, T. , Atmospheric Pressure Waves and Tectonic Deformation Associated with the Alaskan Earthquake of March 28,1964, J. Geophys. Res. vol. 73 , 1968

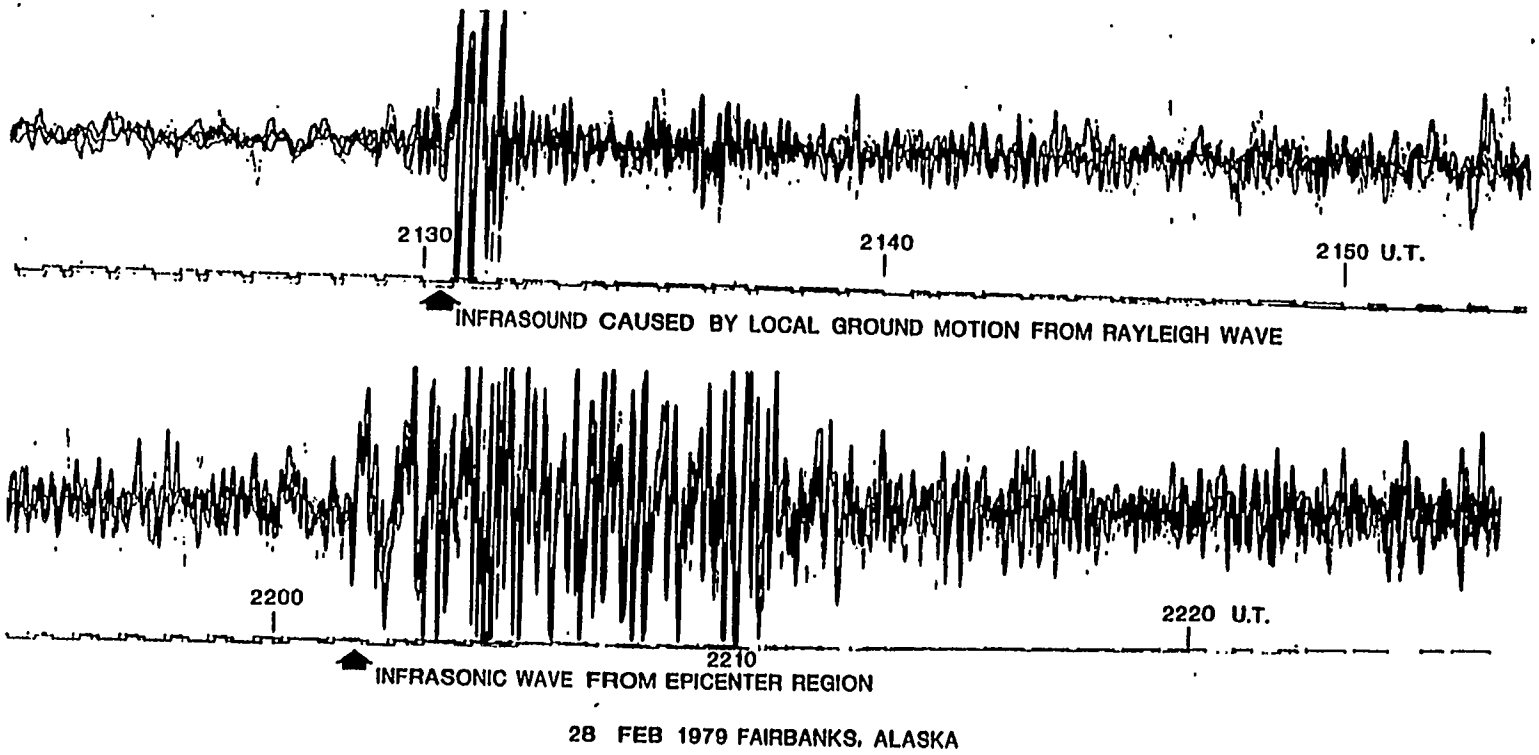

Figure 1, Infrasound from earthquake at Cape, Yakataga, Alaska .

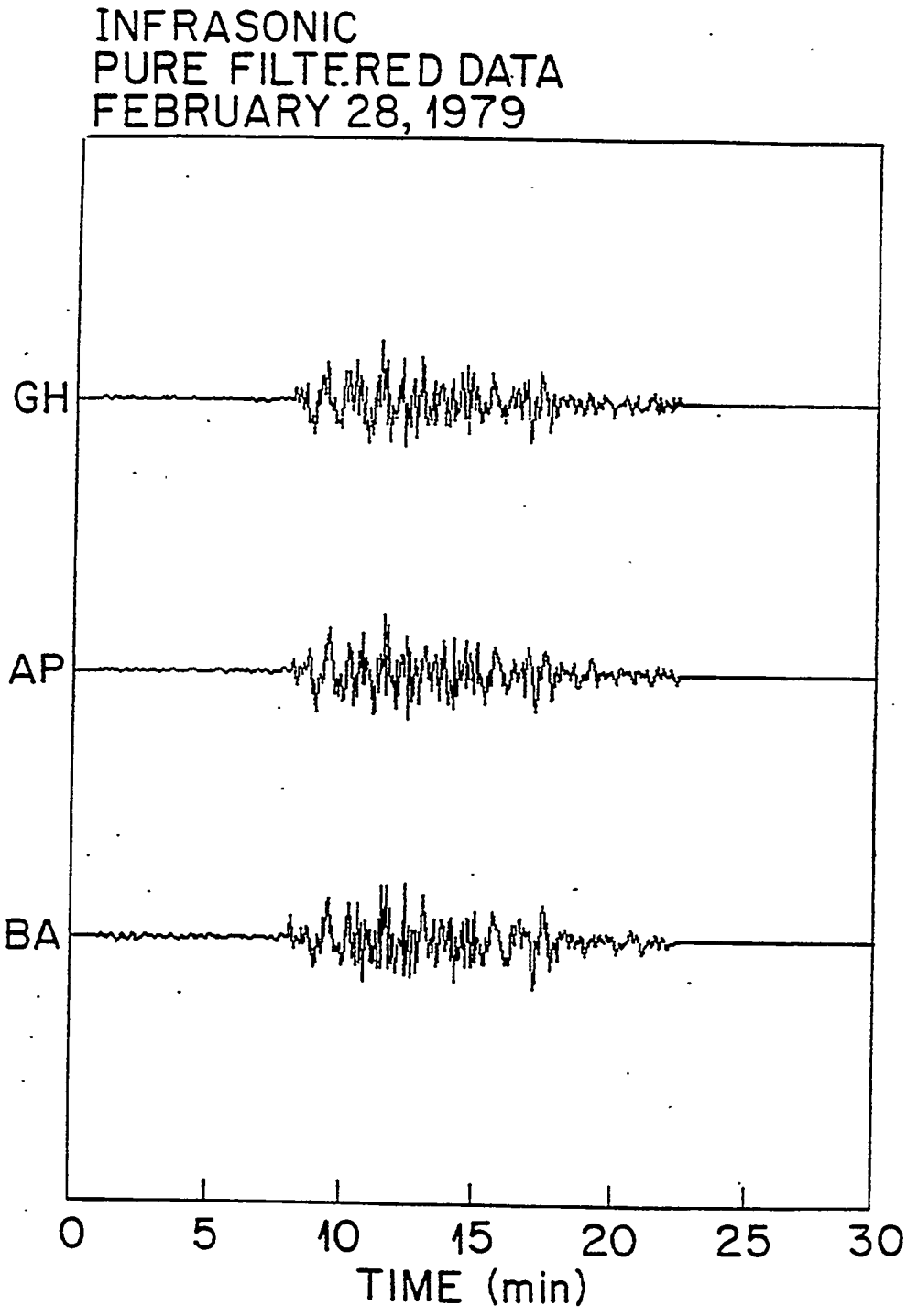

Figure 2 , Fairbanks infrasonic array data for Yakataga earthquake, pure state filtered.

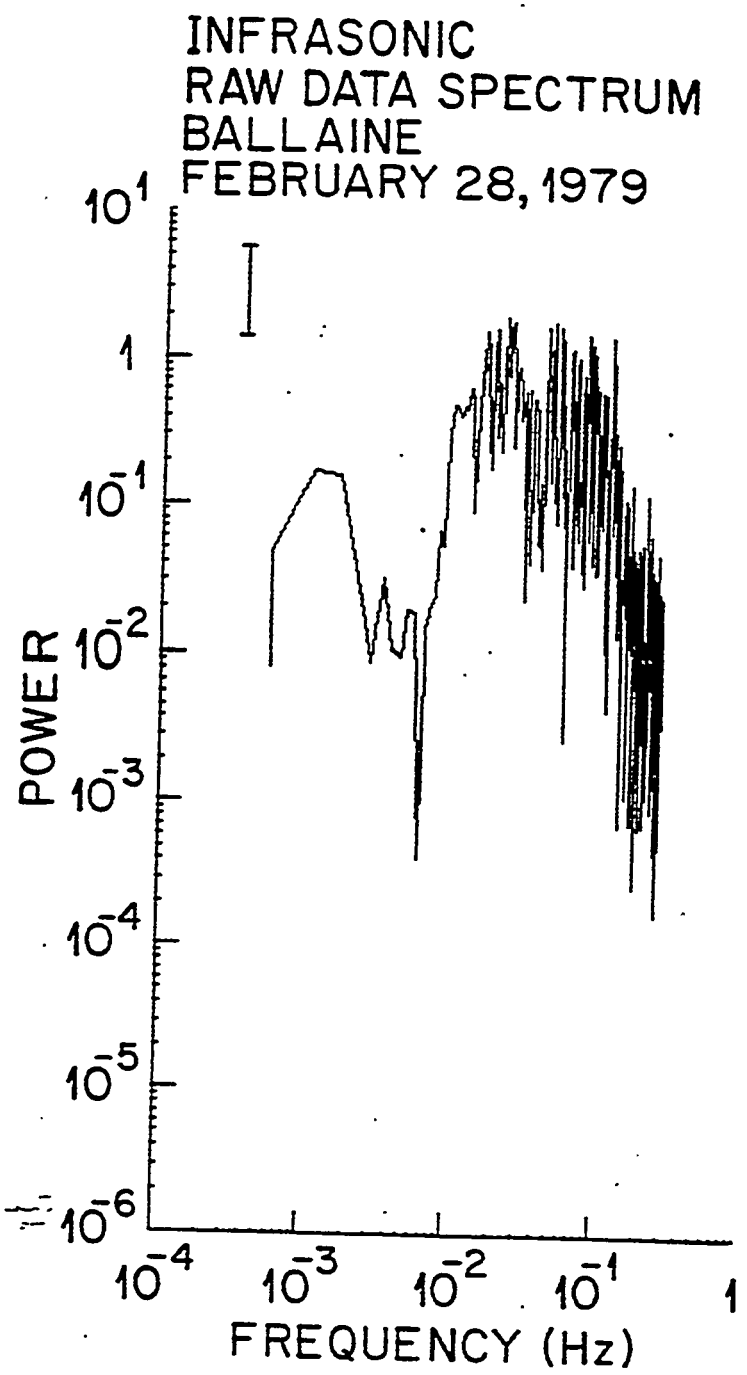

Figure 3, Raw data spectrum , Yakataga earthquake infrasound.

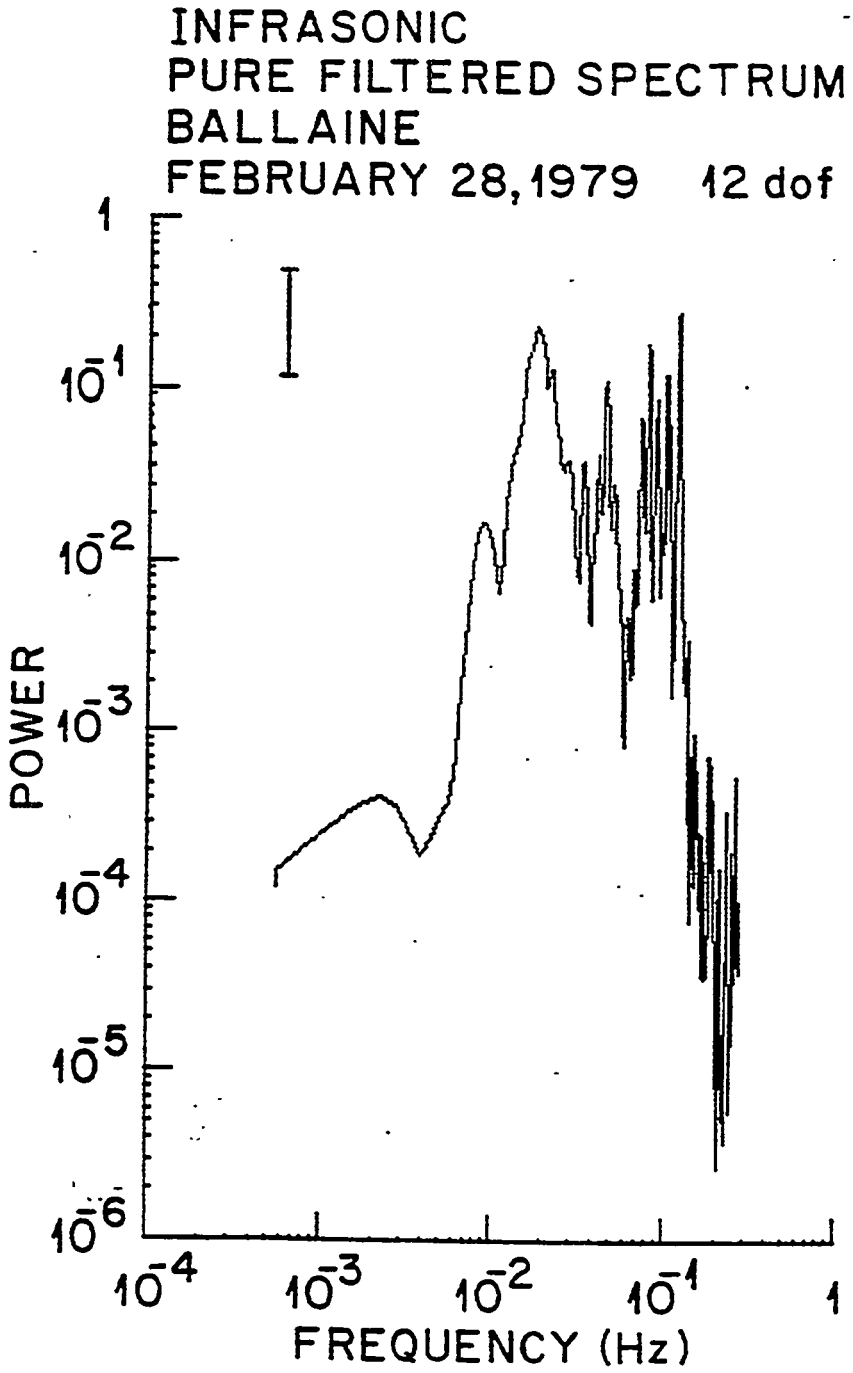

Figure 4, Pure filtered data spectrum, Yakataga infrasound.

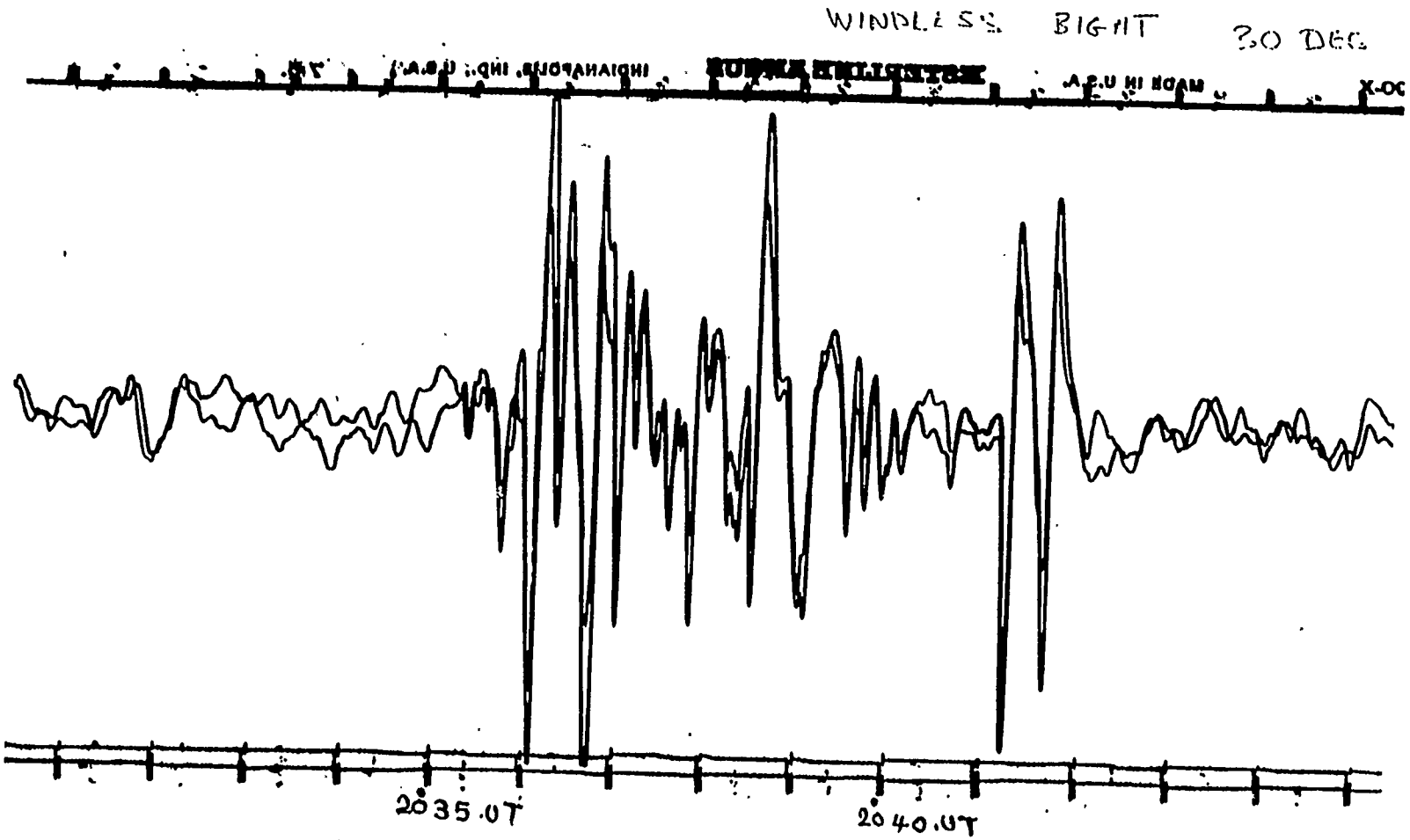

Figure 5, Raylcigh wave generated local infrasound on Ross Ice Shelf at Windless Bight, Antarctica, 2035 UT , 30 December 1976.

BOLIDES AS EXPLOSIVE INFRASONIC SOURCES: CTBT IMPLICATIONS

Douglas O. ReVelle

Los Alamos National Laboratory
Los Alamos, New Mexico 87545

Among the natural explosive sources of infrasound in the atmosphere, bolides (meteor-fireballs) rank as a major candidate along with volcanic eruptions for generating false alarm signals in the CTBT IMS system. This means much more work is needed to fully evaluate these bodies as infrasonic sources. This includes collaborative work with the US DoD satellite community and may include cooperation with the hydroacoustic and seismic communities as well. In this talk we will categorize bolides as infrasonic sources including the development of the line and modified line source blast waves from the fundamental bolide entry parameters. We will also consider refractive propagation effects on these signals at relatively close range from the standpoint of ray theory. Finally, we will discuss the interpretation of these signals at the ground at long ranges from the source. The development of the blast waves depends critically on the depth of penetration of bolides into the atmosphere. This, in turn, depends upon the composition, entry angle, size, velocity and rate of ablation of the bolide, etc. From other studies we know of at least five different, unique compositions whose tensile and compressive strength ranges from very strong(nickel-iron materials) to extremely weak, fragile cometary materials. This factor also greatly influences the number and size of major break-up events that can occur, i.e., gross-fragmentation effects. At the largest observable sizes there is also a tendency for weaker and consequently higher velocity bodies. The source energies corresponding to bolides that have previously produced detectable infrasound at the ground ranges from about 1e-5 kt to >10 Mt (TNT equivalent). This correspond to bodies large enough to reach a level of near-continuum flow (small Knudsen number) while still traveling at high Mach number. The very narrow Mach cone of the bolide generates a characteristic velocity pattern which is circular for vertical entry and which becomes a highly elongated ellipse as the entry angle becomes more horizontal. Consequently, the line source acoustic radiation pattern is highly directional and the range of altitudes from which infrasound can reach the ground depends critically on both the atmospheric temperature and wind structure aloft and on the altitude region penetrated. The consequences of this line source geometry are that for very steep entries the acoustical signals are likely to propagate horizontally and thus be much more influenced by refractive effects. For shallow entries the rays are traveling nearly vertically (in the entry plane) and thus subject to far less refractive influences. We will also summarize and evaluate the current techniques available for estimation of the bolide source energy for either point or line source geometry. These include various approaches that incorporate either wave amplitude information only or include both the wave amplitude and wave period information for the acoustic signals. We will also consider methods based on the presence of the Lamb wave and also methods that combine these approaches. Finally, we will consider the corresponding bolide influx rate implications as a function of their source energy. At a bolide source energy exceeding 0.1 kt, for example, we have estimated from the AFTAC bolide data (1960-1974) that there are about 30 bolides/year impacting the Earth's atmosphere. (This work is supported by the U.S. Department of Energy under contract No. W-7405-ENG.)

Infrasound Workshop for CTBT Monitoring

Bolides as Explosive Infrasonic Sources: CTBT Implications

Douglas O. ReVelle

Earth and Environmental Sciences Division
Los Alamos National Laboratory
Los Alamos, New Mexico 87545

Infrasound Workshop, D.O. ReVelle
Sante Fe, New Mexico, August 25-28, 1997

Summary of Presentation

- Introduction
- Line and modified line source models: Bolides as aerodynamic infrasonic sources
- Refractive propagation effects and source location
- Theoretical and semi-empirical methods: Source energy estimation
- Influx rate of large bolides: CTBT expectations
- Summary and conclusions

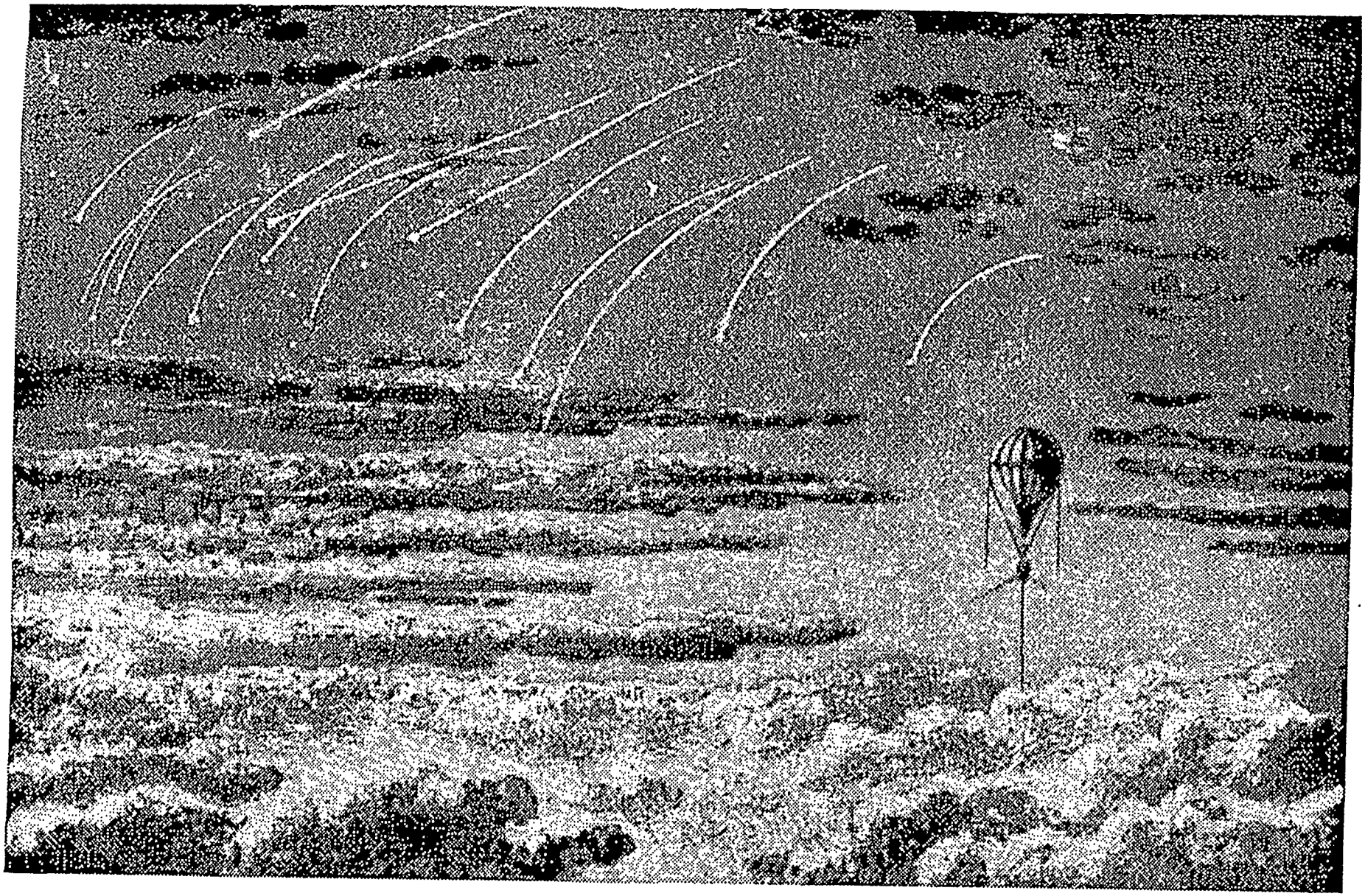

FIG. 1-1. A drawing by Albert Tissandier, entitled "Shooting Stars Seen from a Balloon, 1870," which originally appeared in the book "Travels in the Air," edited by James Glaisher, 1871. (*Reproduction courtesy of King Penguin Books, Ltd.*)

Bolide Compositions

- **A. Iron:** $\rho = 7.7 \cdot gm/cm^3$
- **Melting dominant: Mass < 2·10(5) kg;** $\sigma = 0.0743 \cdot sec^2/km^2$
- **Vaporization dominant:** $\sigma = 0.0124 \cdot sec^2/km^2$
- **B. Olivine-Bronzite (Ordinary) Chondrite:**
- $\rho = 3.7 \cdot gm/cm^3; \sigma = 0.020 \cdot sec^2/km^2$
- **C. Carbonaceous Chondrite:**
- $\rho = 1.85 \cdot gm/cm^3; \sigma = 0.040 \cdot sec^2/km^2$
- **D. Regular Cometary Material:**
- $\rho = 0.93 \cdot gm/cm^3; \sigma = 0.080 \cdot sec^2/km^2$
- **E. Weak Cometary Material: (Draconids)**
- $\rho = 0.34 \cdot gm/cm^3; \sigma = 0.22 \cdot sec^2/km^2$

Summary: Bolide Size and Source Energy

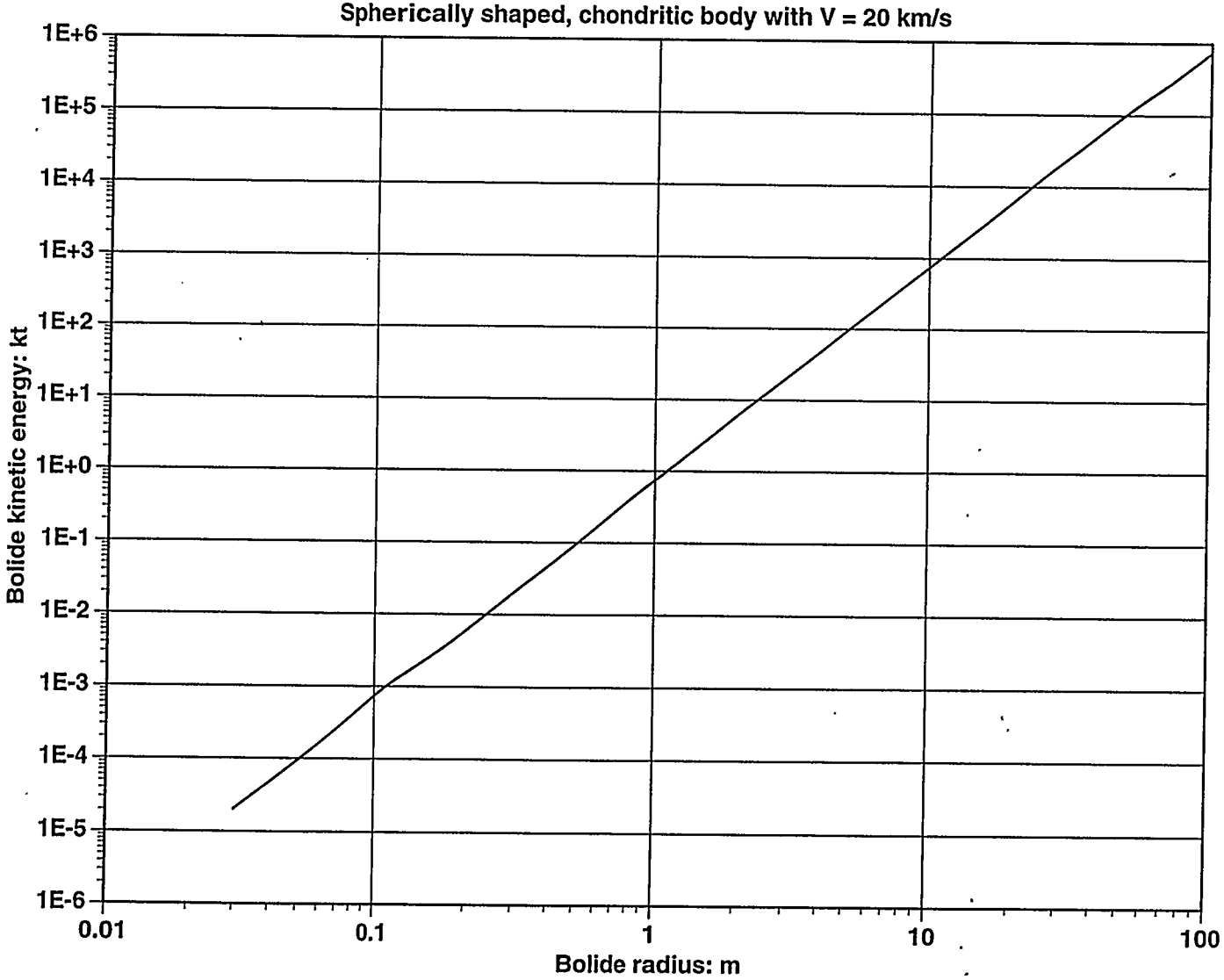

Summary:
Bolide Size and Source Energy

Radius: m	Bolide source energy (*)
0.03	0.02 t
0.04	0.047 t
0.05	0.093 t
0.1	0.741 t
0.5	92.6 t
1	0.741 kt
2	5.93 kt
3	20.0 kt
4	47.4 kt
5	92.6 kt
10	0.741 Mt
20	5.93 Mt
30	20.0 Mt
40	47.4 Mt
50	92.6 Mt
100	740.7 Mt

(*) Assumes a spherically shaped, chondritic bolide (ρ=3.7 g/cc) with V=20 km/s.

Modeling of Bolides as Infrasonic Sources

- Key similarity numbers: Hypersonic aerodynamics
  - Knudsen no., Kn << 1: Near-continuum flow
  - Mach no., Ma >> 1: V = 11.2 to 73.2 km/sec
  - Reynolds no., Re >> 1: Turbulent flow regime
- Key aerodynamic diagnostic parameters:
  - Surface pressure/modified ballistic entry ratio
  - Variations in dimensionless ablation efficiency
  - % of kinetic energy remaining at the end height
- Stagnation point analysis done assuming:
  - > 10 deg (Steep entry angle restriction)
  - Single-body model with constant shape factor

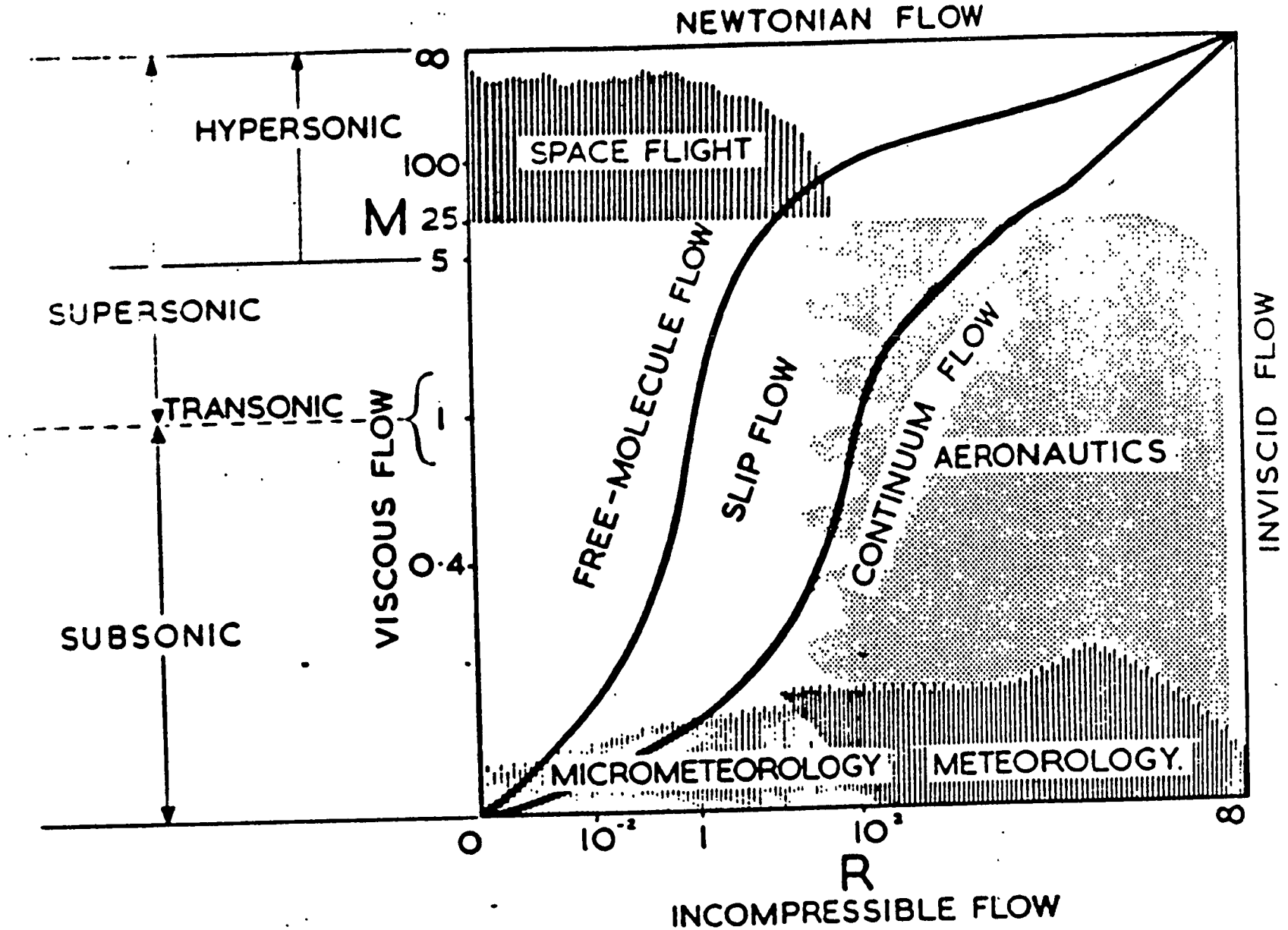
NEWTONIAN FLOW
HYPERSONIC
SUPERSONIC
TRANSONIC
SUBSONIC
M
∞
100
25
5
1
0·4
VISCOUS FLOW
SPACE FLIGHT
FREE-MOLECULE FLOW
SLIP FLOW
CONTINUUM FLOW
AERONAUTICS
MICROMETEOROLOGY
METEOROLOGY.
INVISCID FLOW
0
10⁻²
1
10²
∞
R
INCOMPRESSIBLE FLOW

Line Source and Modified Line Source Bolide Modeling

- Line source blast waves: Hypersonic flow analogy
  - Ma >>1 and dV/dt = 0; Very narrow Mach cone
- Line source energy deposition:
  Nonlinear blast wave relaxation radius: Ro
  - Ro $\propto$ Square root of Energy per length/pressure
    Ro $\cong$ Mach no. X diameter (Non-fragmenting)
  - Ro ranges from 10 m to > 10 km (Tunguska)
  - Source energy ranges from 10(-5) kt to > 10 MT
- Point source relaxation radius: Rs
  - Rs $\propto$ Cube root of Source energy/pressure
- Acoustic period $\propto$ Ro (or Rs) /acoustic phase speed

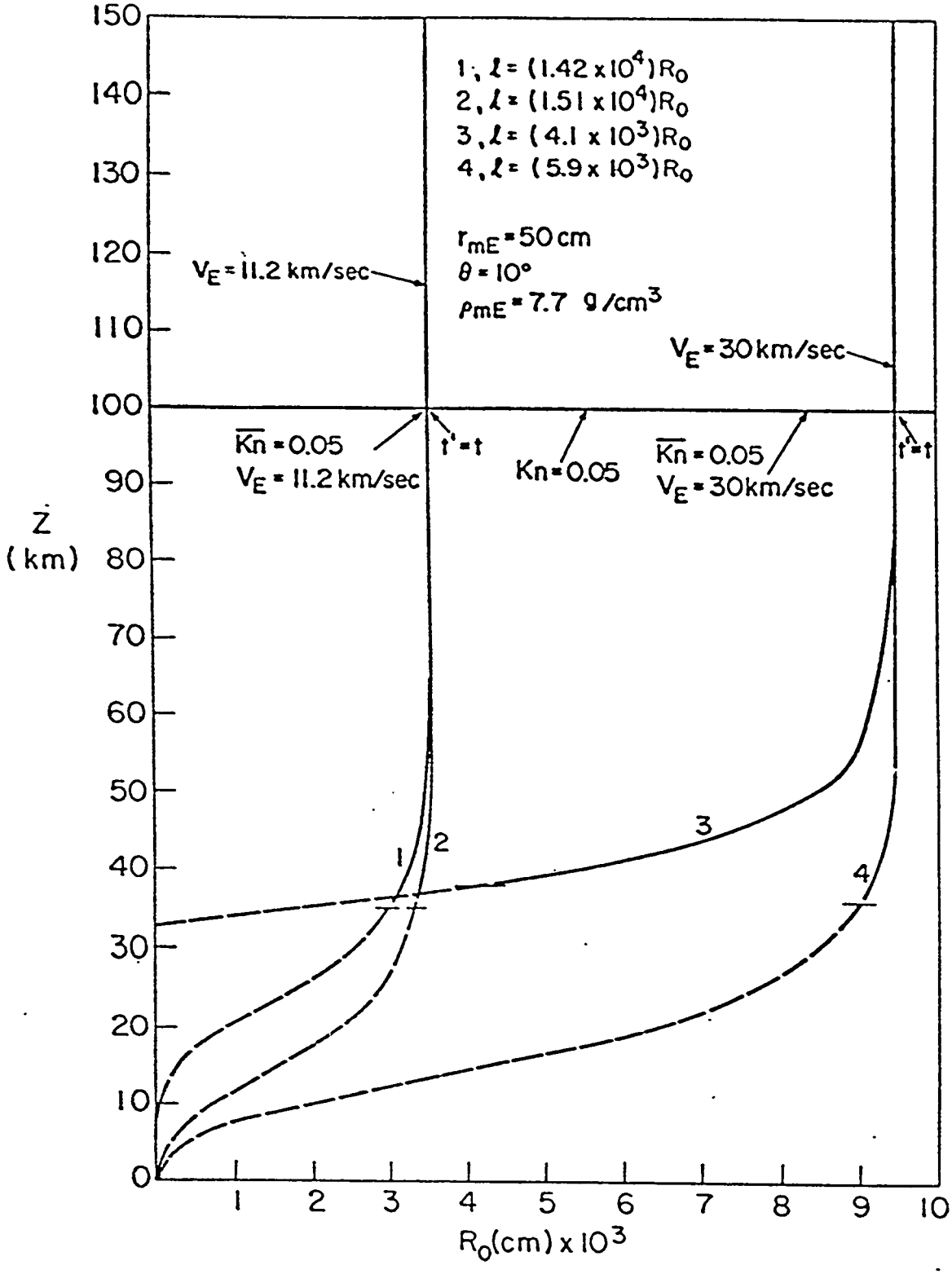

Figure 72. Cylindrical blast wave radius as a function of altitude (curves 2 and 4, $\sigma=0$; curves 1 and 3, $\sigma=5\cdot10^{-12}$ sec^2/cm^2; for all curves dashed portion represents altitude region for which cylindrical blast wave theory is not applicable to hypersonic flow), $\theta=10^{\circ}$, $d_m=100$ cm, $\rho_m=7.7$ g/cm^3.

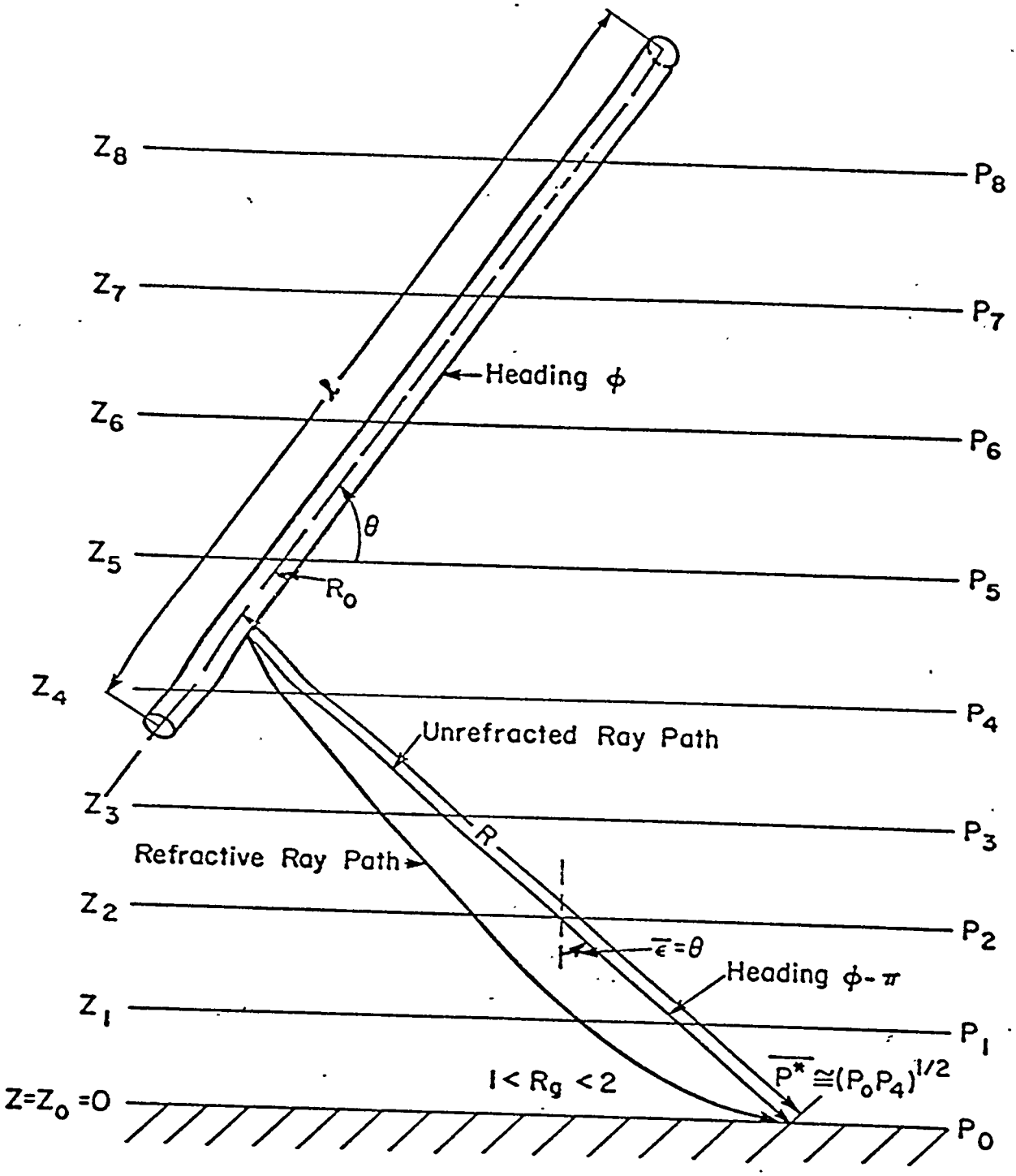

Figure 99. Source, observer geometry for a horizontally stratified atmosphere in the entry plane.

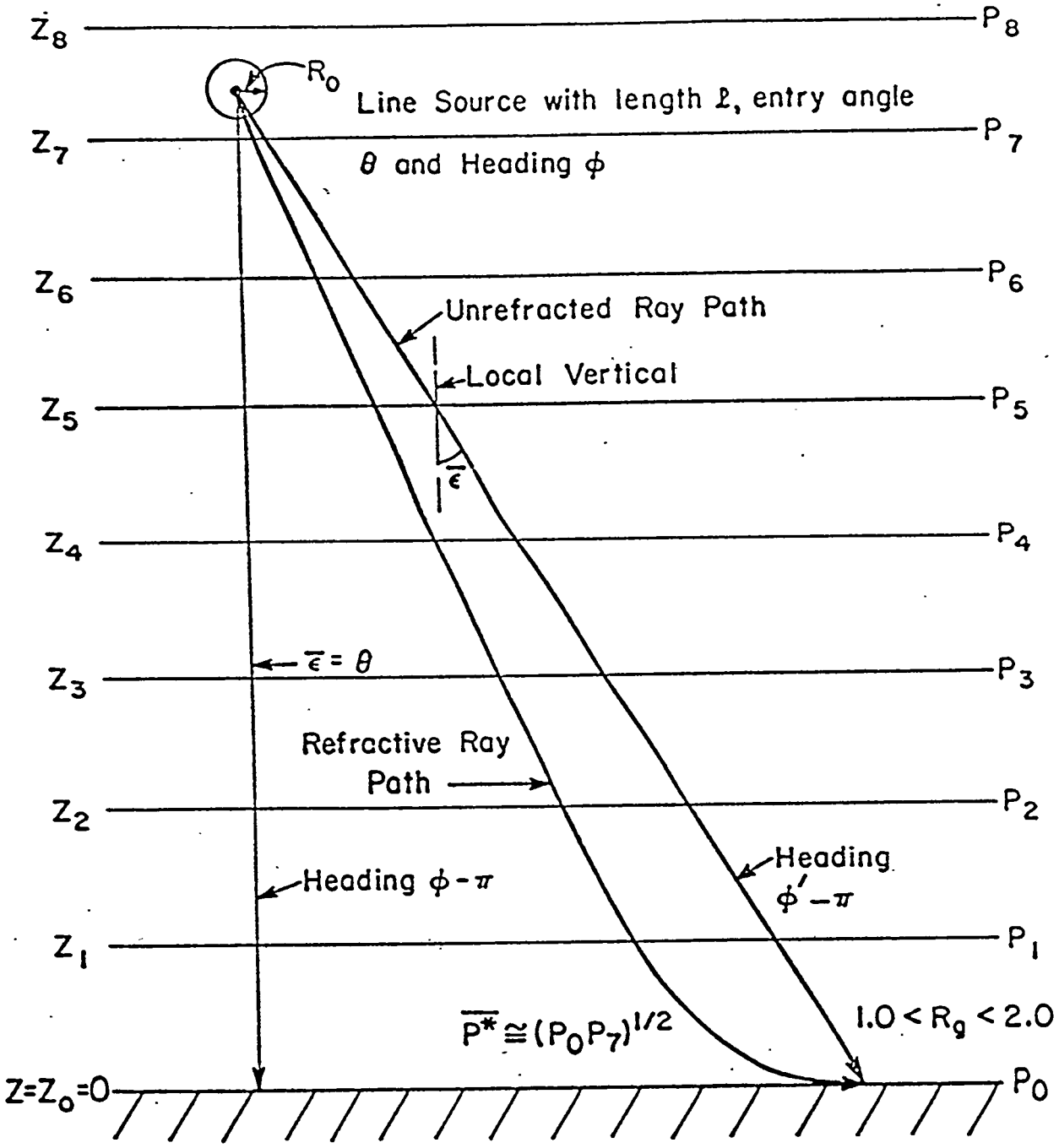

Figure 100. Source, observer geometry for a horizontally stratified atmosphere out of the entry plane.

Modeling of Bolide Infrasound Propagation

- **Source inclusion: Aerodynamics of large bolides**
  - **Near-field hydrodynamics/blast wave scaling- $R << \lambda$ with nonlinearity dominant to R = Ro**
  - **λ proportional to Ro**
- **Primary infrasonic propagation approaches:**
  - **Ray theory: Far-field; $R >> \lambda$**
    - **High frequency limit; Ray paths computed**
  - **Multi-modal analyses: $R \geq 2H^2 / \lambda$**
    - **Low frequency waves: Diffraction and constructive/destructive interference**
  - **Lamb wave approach: Fundamental mode**

Ray Theory Modeling in Perfectly Stratified Media: I.

Acoustical wave dynamics- Two fundamental propagation constants for plane waves in perfectly stratified media:

i) Characteristic velocity (Horizontal trace speed), K
ii) Wave normal heading (NOT ray heading)

I. Point Source Emission: Trace Velocity

$$K = c_s / \cos\theta' + V_H \cos\Delta = Cons\tan t \cdot ; \cdot \Delta = \phi'(z) - \psi'(z)$$

Infrasound Workshop, D.O. ReVelle
Sante Fe, New Mexico, August 25-28, 1997

Ray Theory Modeling in Perfectly Stratified Media : II

Inner audibility zone: Analytic result and Numerical integral

$$D = 2 \cdot (T_0 \, z_s / \Gamma)^{0.5}$$

$$D = \int_O^z [c_s(z) \cos\theta' + V_H(z) \cos\Delta] \{dz / (c_s(z) \sin\theta')\}$$

II. Line source emission: Trace Velocity
For V(z)>> Adiabatic sound speed

$$K = c_s / \cos\theta' \cdot \{\cos^2\theta' + (1 - 2\Delta\phi/\pi)^2 \sin^2\theta'\}^{0.5} + V_H \cos\Delta$$

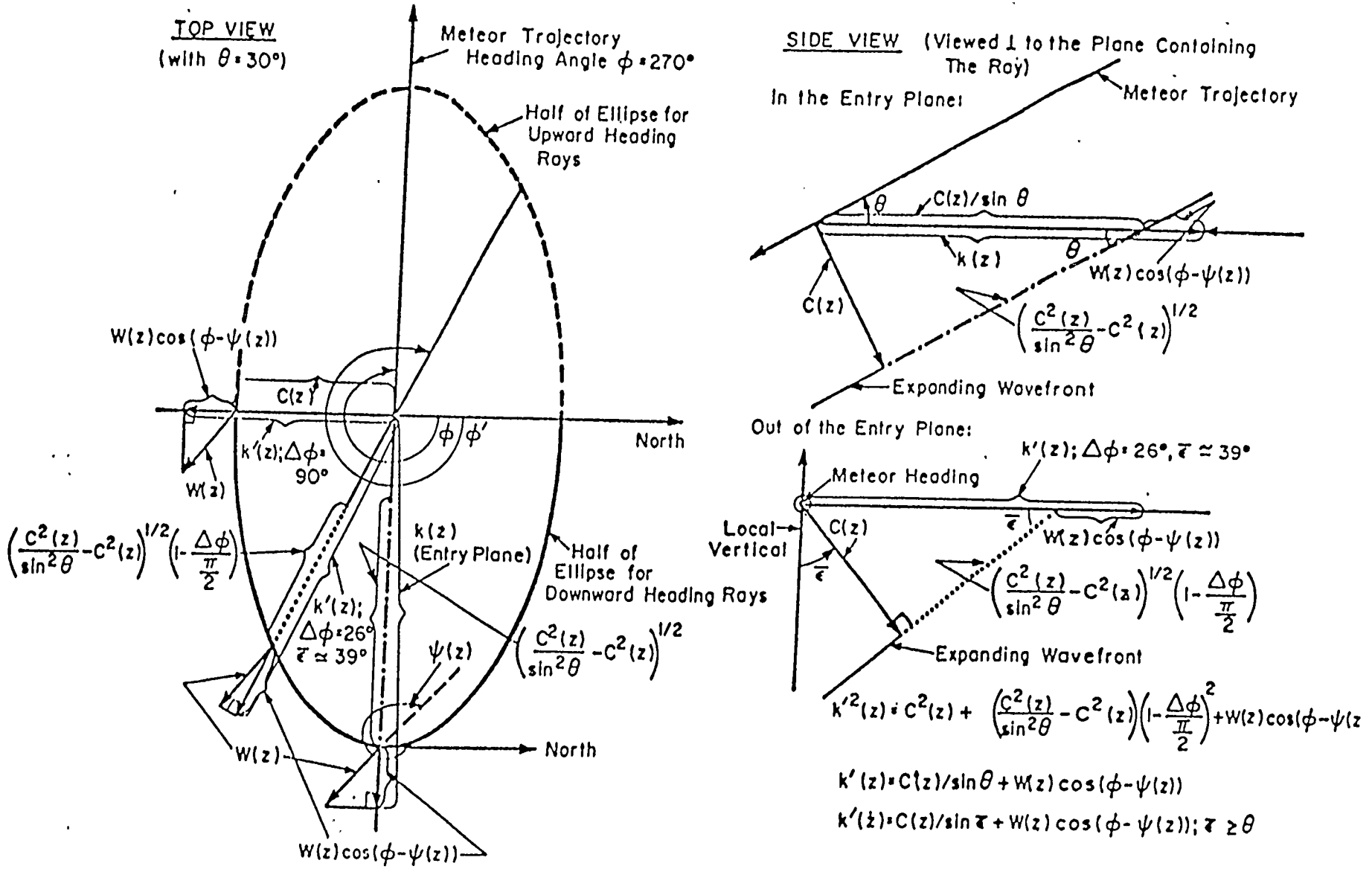

Figure 76. Characteristic velocity geometry out of the entry plane with steady wind, $\alpha=0^{\circ}$ (concluded).

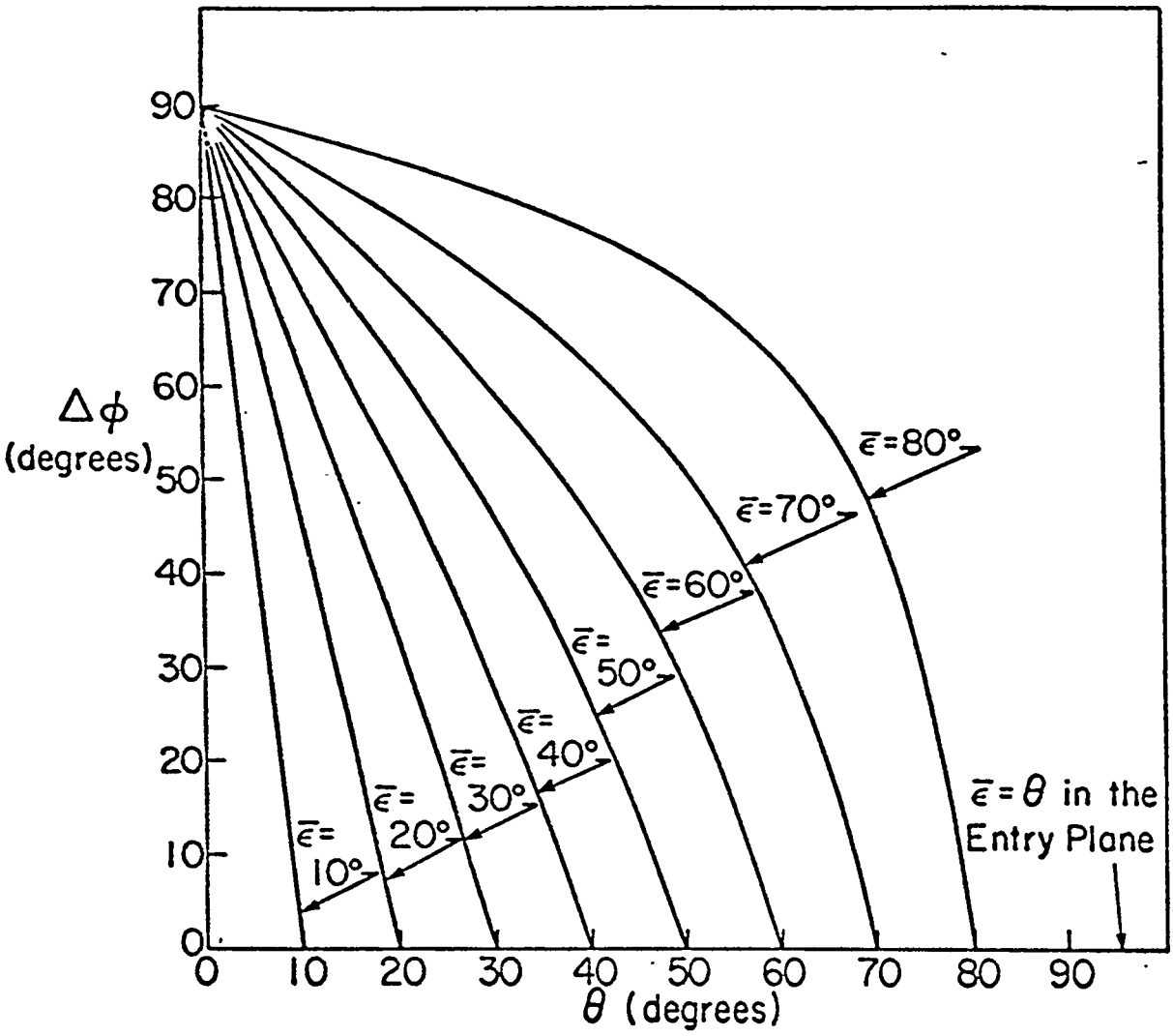

Figure 116. Zenith angle of the ray as a function of the azimuth interval outside of the entry plane and of the entry elevation angle of the meteor.

Line Source Refraction Effects

- Key variables for "local" ground observations:
  - Entry angle, θ (with respect to the horizon)
  - Observer's position away from the entry plane
  - Vertical temperature and wind structure
  - Horizontal gradients: Frontal activity, etc..
- Deduced behavior: $\theta' \equiv \pi/2 - \theta$
  = Elevation angle of the wave normal
  - Steep entry produces waves arriving horizontally and which are likely to be refracted upward away from the ground
  - Shallow entry produces waves arriving steeply which are less subject to refractive effects

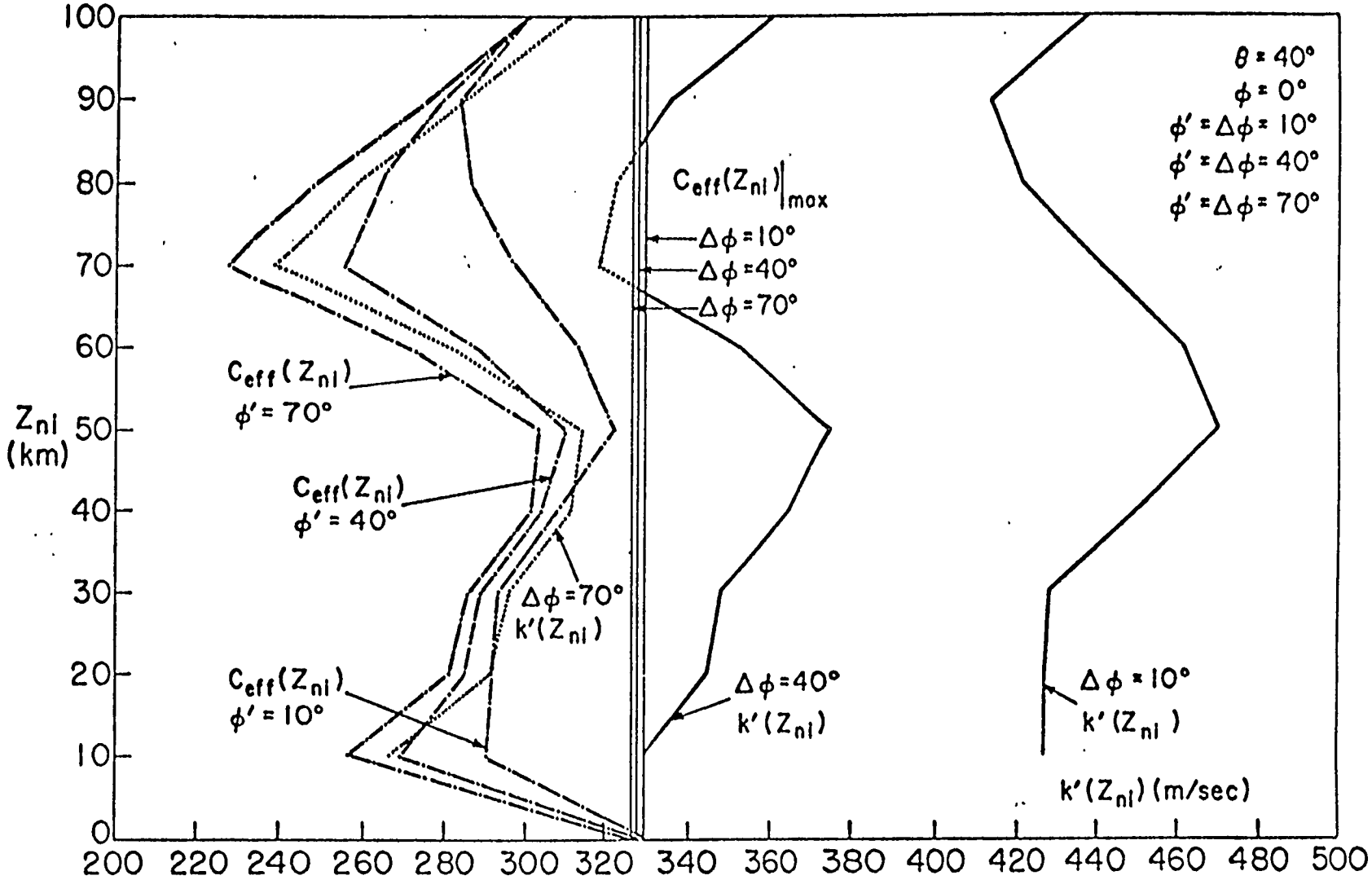

Figure 84. Effective sound velocity and characteristic velocity as a function of altitude out of the entry plane, $\phi=0^{o}$, $\Delta\phi=10^{o}$, 40^{o} and 70^{o}; propagation in January for ray heading West of South, $\theta=40^{o}$. Dotted portions of curves represent situations for which ray paths to the ground are not allowed.

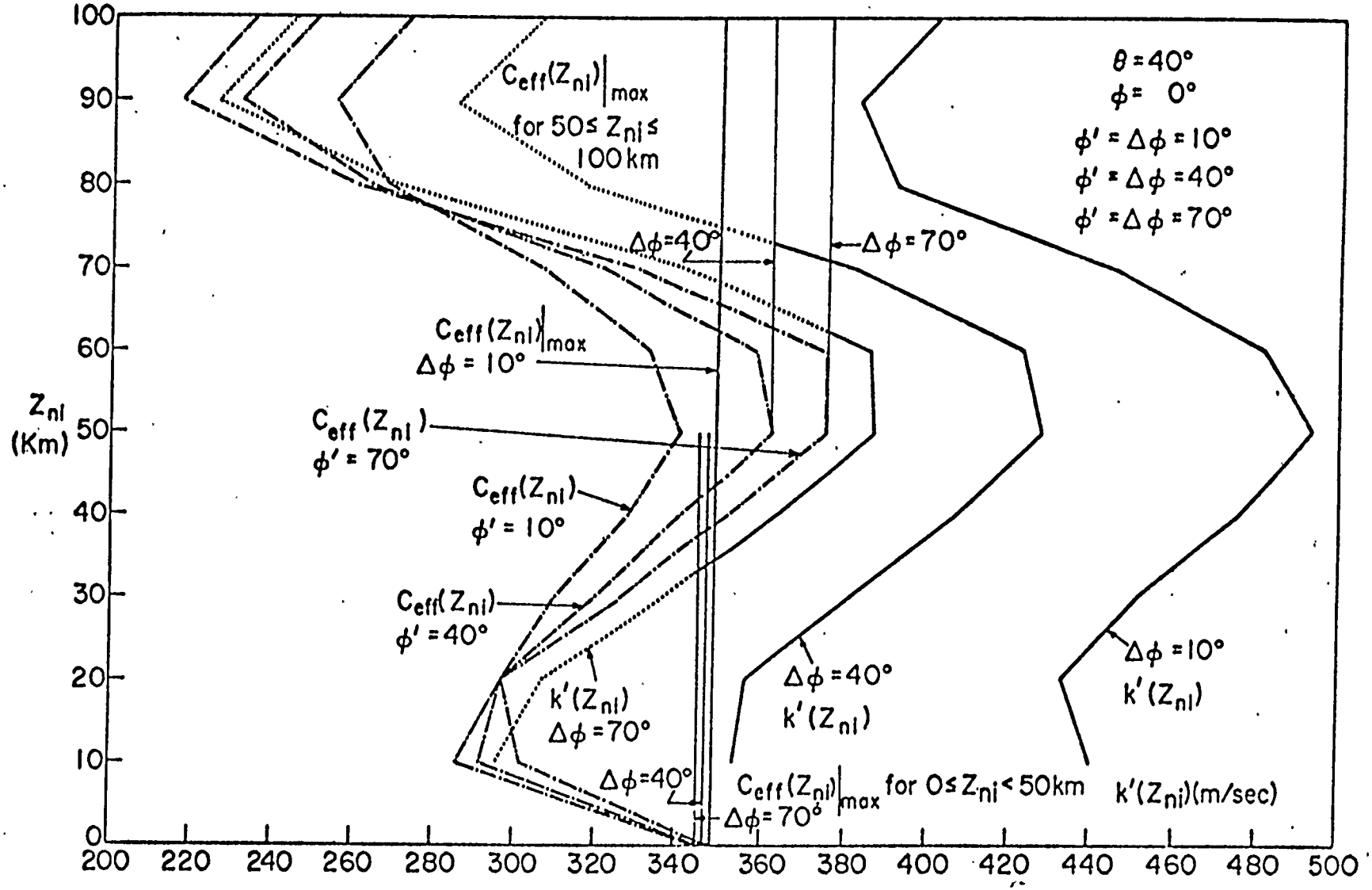

Figure 87. Effective sound velocity and characteristic velocity as a function of altitude out of the entry plane, $\phi = 0°$, $\Delta\phi = 10°$, $40°$ and $70°$; propagation in July for ray heading West of South, $\theta = 40°$. Dotted portions of curves represent situations for which ray paths to the ground are not allowed.

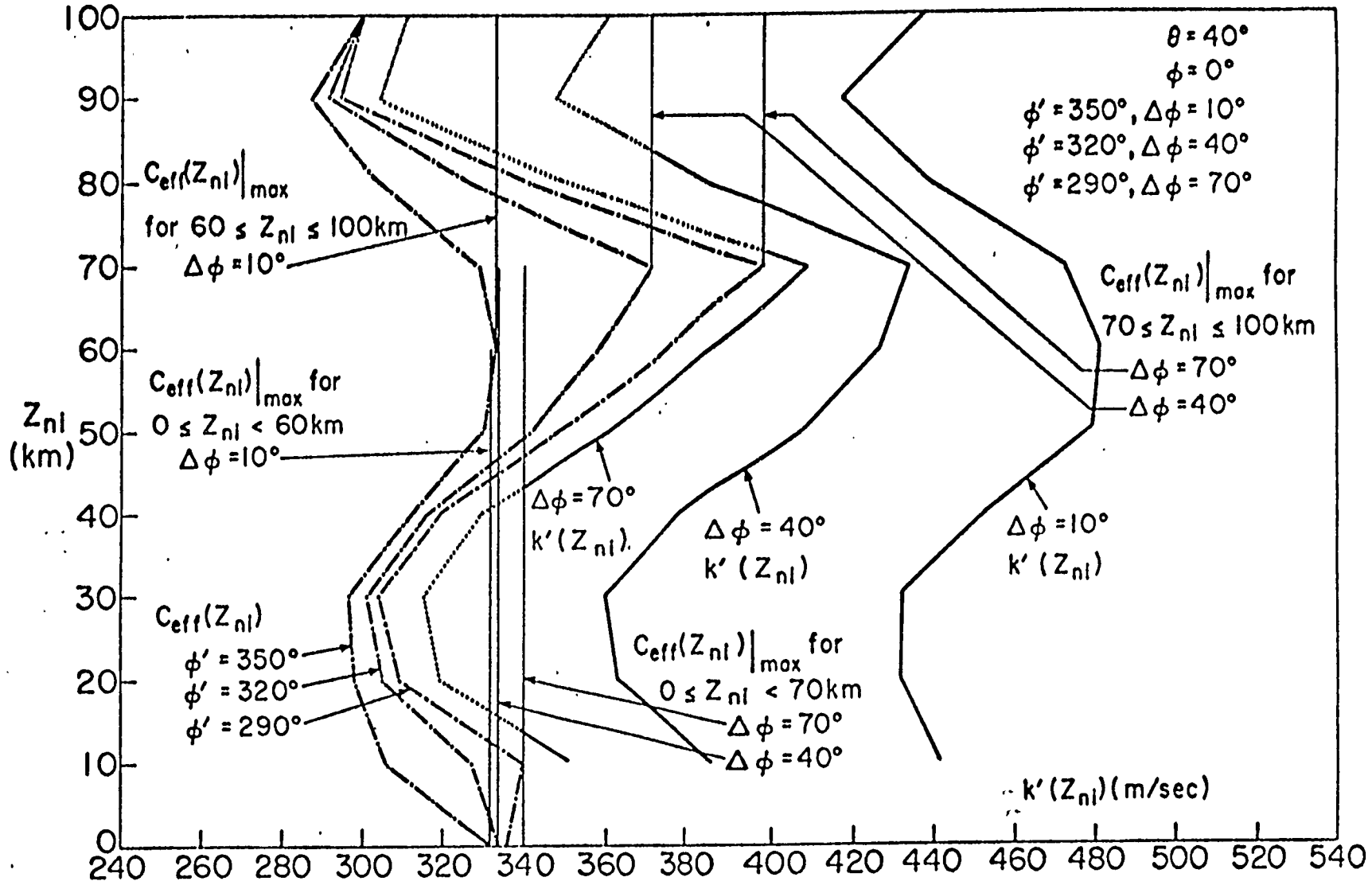

Figure 90. Effective sound velocity and characteristic velocity as a function of altitude out of the entry plane, $\phi=0^{o}$, $\Delta\phi= 10^{o}$, 40^{o} and 70^{o}; propagation in January for ray heading East of South, $\theta=40^{o}$. Dotted portions of curves represent situations for which ray paths to the ground are not allowed.

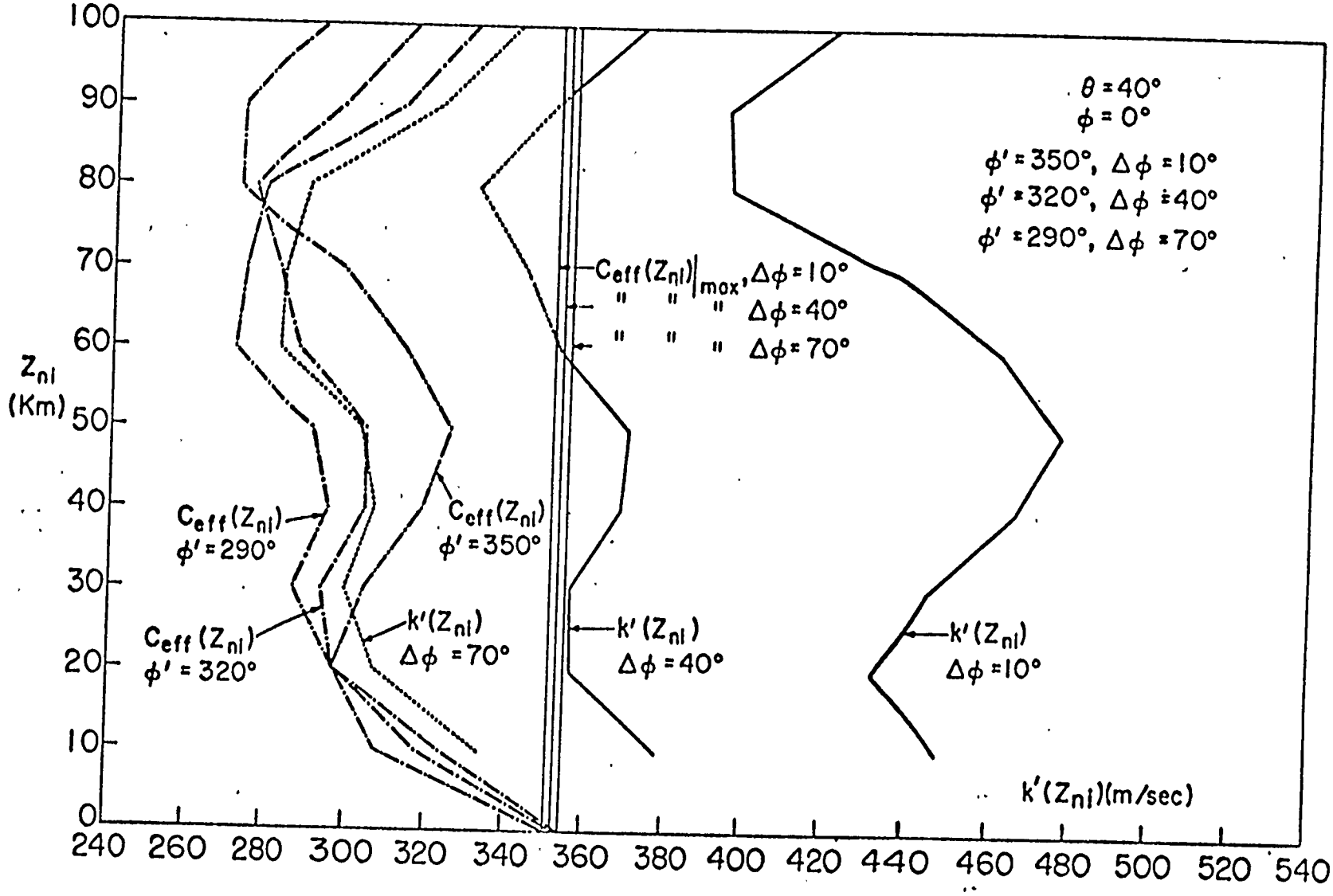

Figure 93. Effective sound velocity and characteristic velocity as a function of altitude out of the entry plane, $\phi=0^{o}$, $\Delta\phi= 10^{o}$, 40^{o} and 70^{o}; propagation in July for ray heading East of South, $\theta=40^{o}$. Dotted portions of curves represent situations for which ray paths to the ground are not allowed.

Bolide Source Energy: Available Approaches

- AFTAC Semi-empirical wave period approach: Olmstead and Leies (1979): Near-surface sources
- LANL Wind-corrected amplitude: Mutschlecner and Whitaker (1988); Near-surface sources
- Acoustic efficiency: Cox (1958); ReVelle (1980); ReVelle and Whitaker (1995);Near-surface sources
- Line source amplitude/period and wave period method: ReVelle (1976); Source altitudes included
- Lamb wave mode approach:Pierce-Posey (1971)
- Combined Lamb/wind-corrected approach: ReVelle and Whitaker (1996): Near-surface source
- Pierce(1976): Point source, multi-modal synthesis

Infrasonic Source Energy Relationships: I

I. Lamb Wave Approach: Pierce-Posey (1971)

$$Y = 13\Delta p \cdot \{r_E \sin(r/r_E)\}^{1/2} \cdot H_p \cdot (c_s P_L)^{3/2}$$

II. AFTAC- Semi-empirical Regression: Olmstead-Leies (1979)

Acoustic Period at Maximum Amplitude

$$P = 5.922Y^{0.299}; Y \leq 10^2 kt$$

$$P = 7.447Y^{0.242}; Y > 40kt$$

Alternatively:

$$\log Y = 3.34 \log P - 2.58; Y \leq 10^2 kt$$

$$\log Y = 4.14 \log P - 3.61; Y > 40kt$$

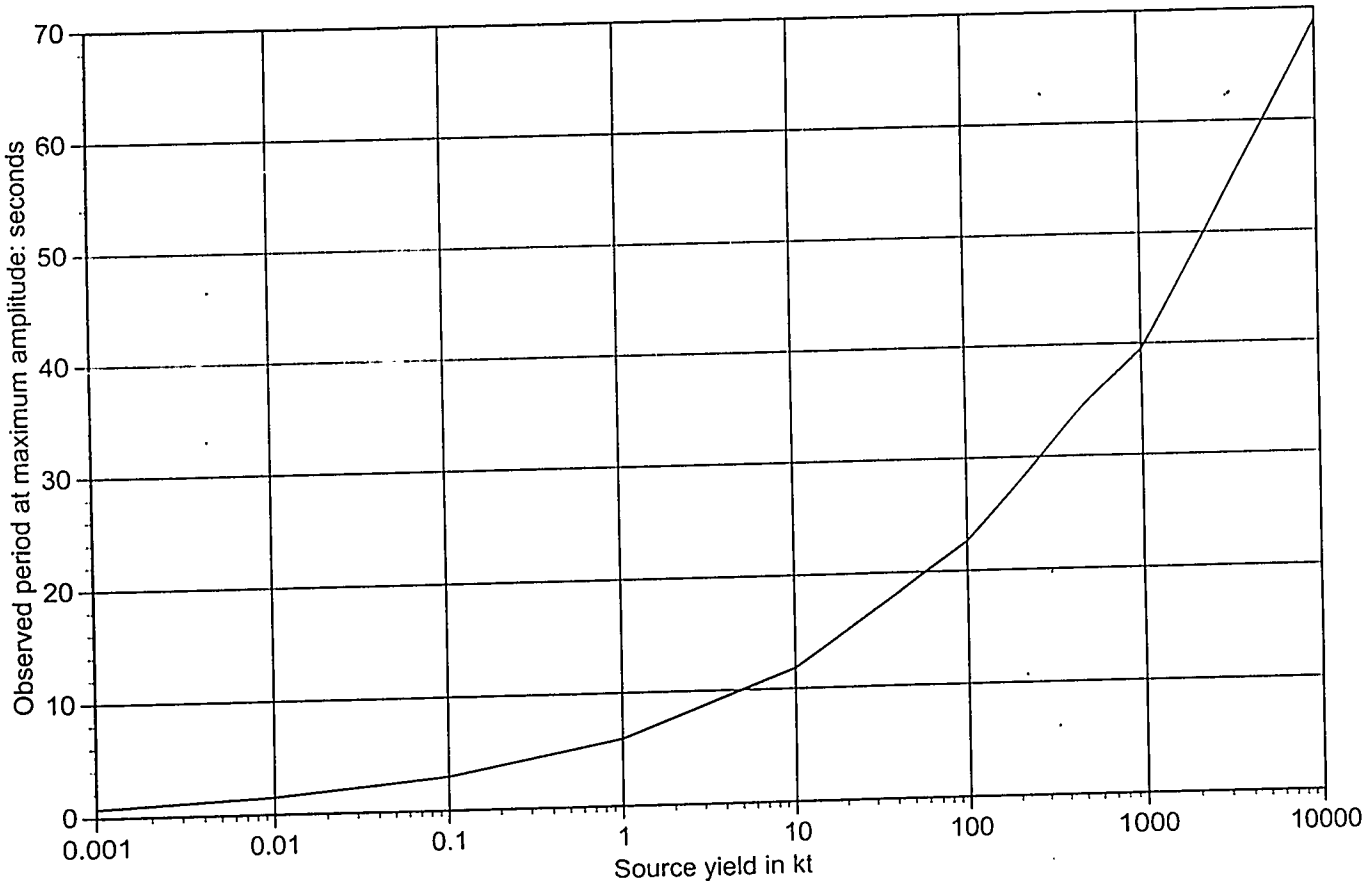
70
60
50
40
30
20
10
0
Observed period at maximum amplitude: seconds
0.001
0.01
0.1
1
10
100
1000
10000
Source yield in kt

Infrasonic Source Energy Relationships: II

III. LANL- Wind-corrected amplitude:
Mutschlecner and Whitaker (1988)

$$E_s(kt) = 0.62 \cdot \{(\Delta p_{p-p}(\mu bars)/4.69 \cdot 10^4)\}^{1.471} 10^{-.0259 \cdot V_{so}(m/sec)} \cdot R^2(km)$$

IV. Acoustic efficiency approach: Cox (1958); ReVelle(1980):

$$E_s(J) = [(2\pi \cdot R^2)/(\varepsilon_{ac} \cdot \Delta)] \cdot \int_0^{\tau_p} \{\Delta p^2{}_{o-p}/(\rho c_s)\} dt$$

V. Line source bolide: Amplitude/period method: ReVelle (1976)

$$E_s(J) = K \cdot R^3 \cdot \{\Delta p_{o-p}/p_{gm}\}^4 \cdot \{c_s^3/V_m\}$$

where:

$$K = 11.5 \cdot \pi \cdot \rho_m \quad \text{and} \quad p_{gm} = \{p_o \cdot [p_o \cdot exp(-\int_0^{z_r} dz/H_p(z))]\}^{0.5}$$

Bolide Sources: Summary of Observed Infrasonic Waves

- For > 22 detections: L and S type observed arrivals
  - Observed periods: 0.5 sec to > 5 min
  - Observed amplitudes (p-p): 0.2 - 160 microbars
  - Observed durations: 2 min to > 25 min
  - Observed trace velocities: 330 to 1200 m/sec
  - Predicted source energies: 0.00001 kt to > 10MT
  - Observed ranges: 150 to > 14,000 km
- Signal characteristics similar to other explosive sources: Lamb waves, multi-path arrivals, etc.
- Observed seismic signals: Air-coupled Rayleigh waves
- Direct Earth impact waves (Revelstoke, 4/01/1965)

Table III. Summary of Basic Meteoroid Airwave Events Taken by the U.S. Air Force During the Period From 1960-1974.

Date	Source Location	Origin Time	Total Range	Source Energy (*)
1: (**) 11/2/60	9N, 43E	0022 GMT	2488 mi.	10 kt
2: 9/26/62	30N, 35E	1545 GMT	688 mi.	20 kt
3: 9/27/62	32N, 60E	1529 GMT	518 mi.	30 kt
4: 8/3/63	51S, 24E	1645 GMT	7038 mi.	1100 kt
			8590 mi.	" "
5: 11/30/64	18N, 123W	0310 GMT	3243 mi.	10 kt
6: 1/3/65	21N, 68E	2151 GMT	2008 mi.	0.2 kt
7: 4/1/65	49N, 117W	0548 GMT	1552 mi.	0.24-2.4 kt (***)
			2173 mi.	" "
8: 6/12/66	51N, 164E	0905 GMT	4150 mi.	8 kt
			2750 mi.	" "
			1800 mi.	" "
			3000 mi.	" "
9: 1/8/71	30N, 40E	1826 GMT	8632 mi.	6 kt
10: 4/14/72	13S, 78E	1613 GMT	2300 mi.	14 kt
			2700 mi.	" "
			3400 mi.	" "
			4850 mi.	" "
			8000 mi.	" "
			8550 mi.	" "

(*) 1 kt TNT = 4.185*10(12) Joules; Assuming E_s= 2*Yield

(**) Originally estimated by the Air Force to be 1 kt

(***) The average E_s of about 1.3 kt is from E.M. Shoemaker (personal communication, 1972) using a multi-modal analysis from Pfeffer and Zarichny (1963). E_s= 26 kt was used for the NEO influx calculations, but since equation (3) predicted 44.6 kt, our influx is likely to be too low. Also, in Table VIA., E_s for Revelstoke was about 69 kt. Bayer and Jordan (1967) located its ground impact using infrasonic and seismic waves from multiple stations in the U.S. and Canada.

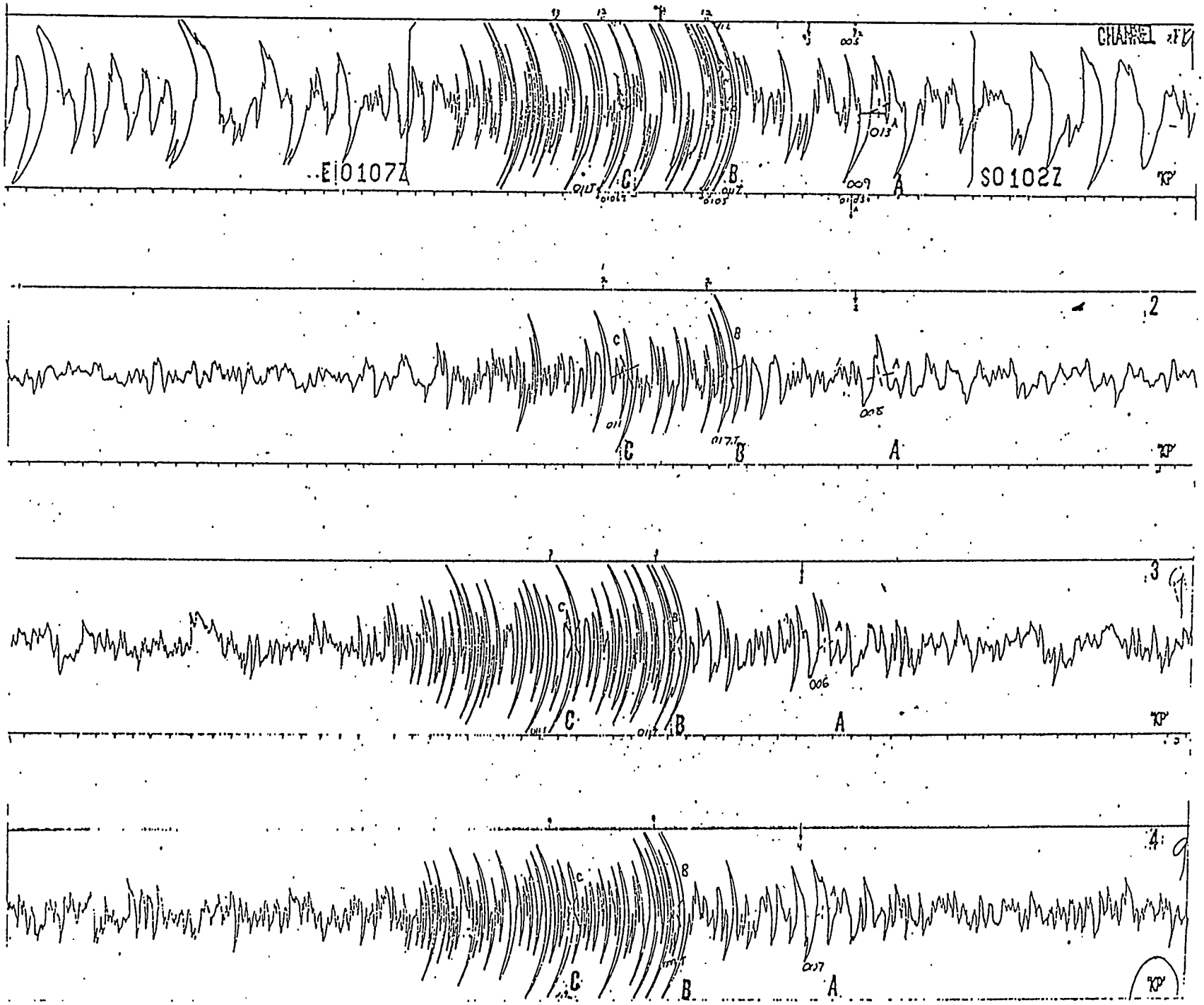
CHANNEL
E10107Z
S01022
C
B
A
2
3
4

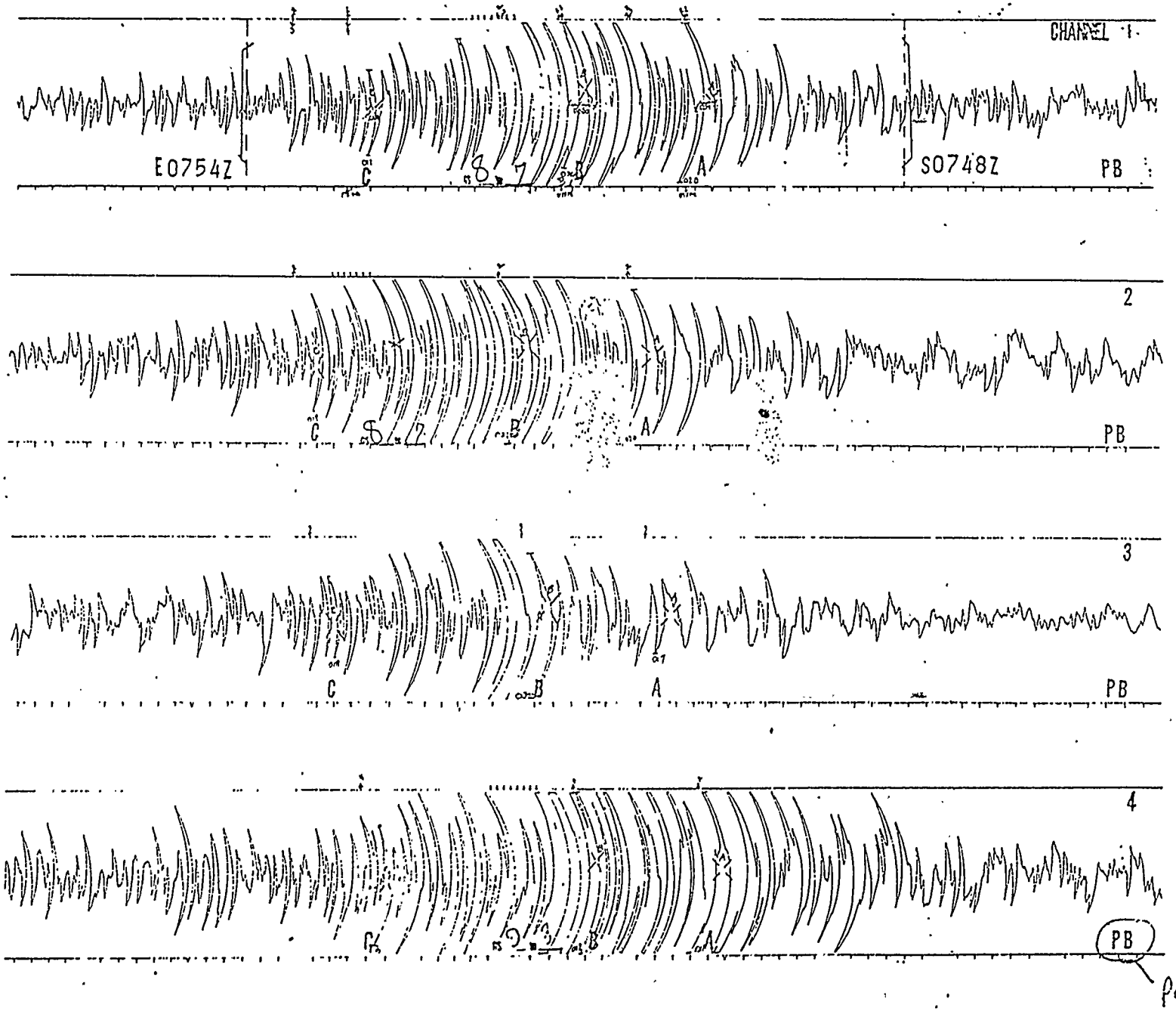
CHANNEL 1
E0754Z
C
B
A
S0748Z
PB
2
C
B
A
PB
3
C
B
A
PB
4
C
B
PB
POS

Station POSTER BOY

3 August 1963

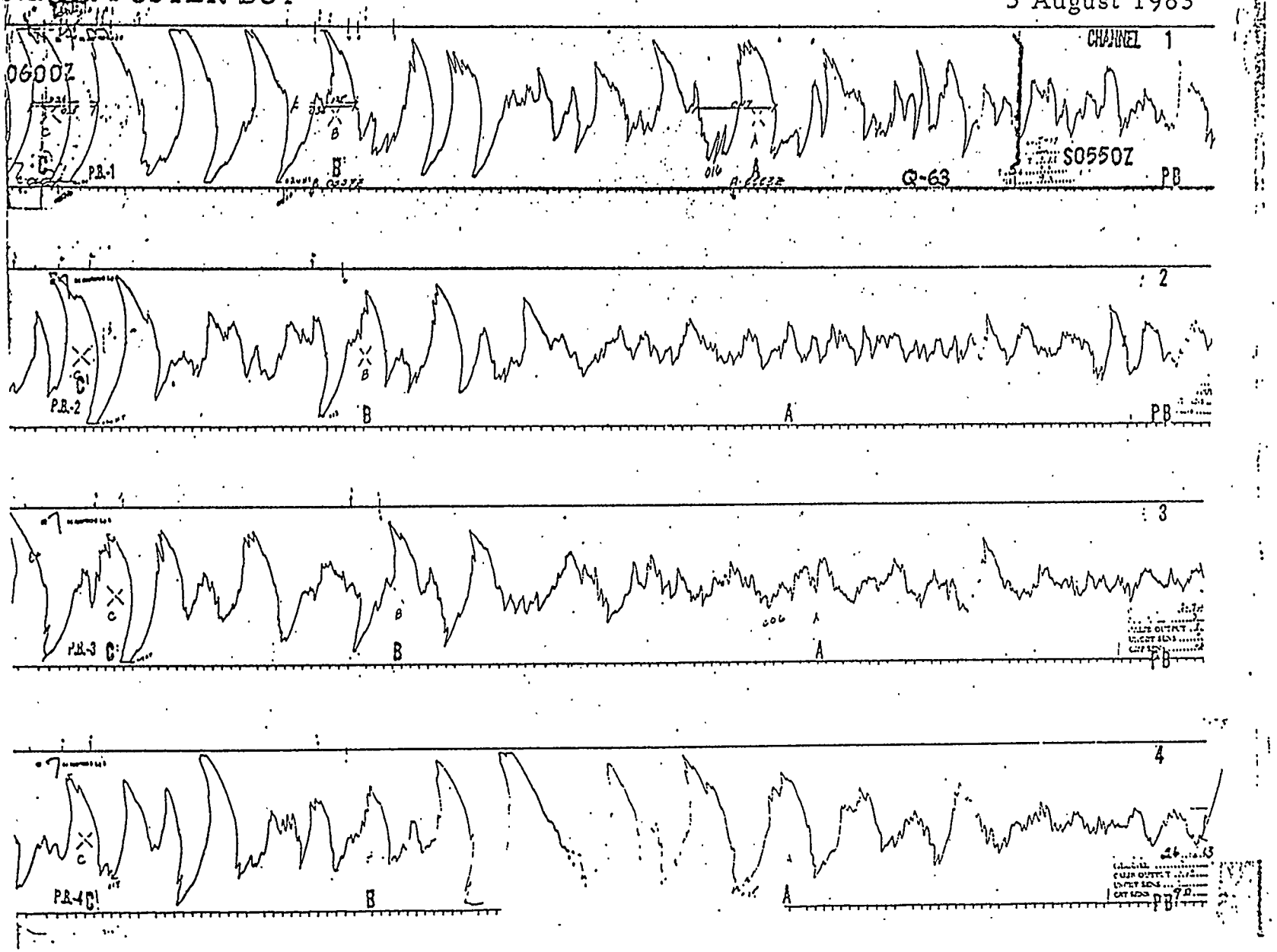

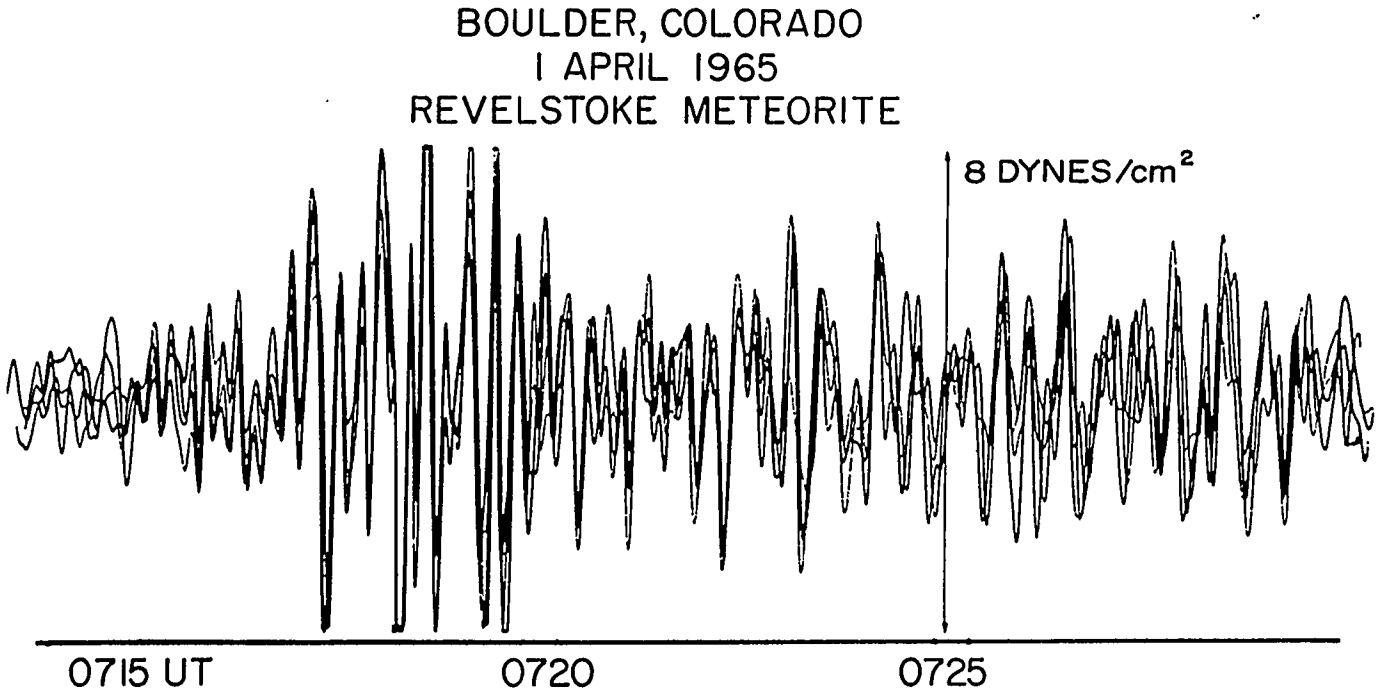
BOULDER, COLORADO
1 APRIL 1965
REVELSTOKE METEORITE
8 DYNES/cm²
0715 UT
0720
0725

Acoustic and Infrasonic Bolide Detections

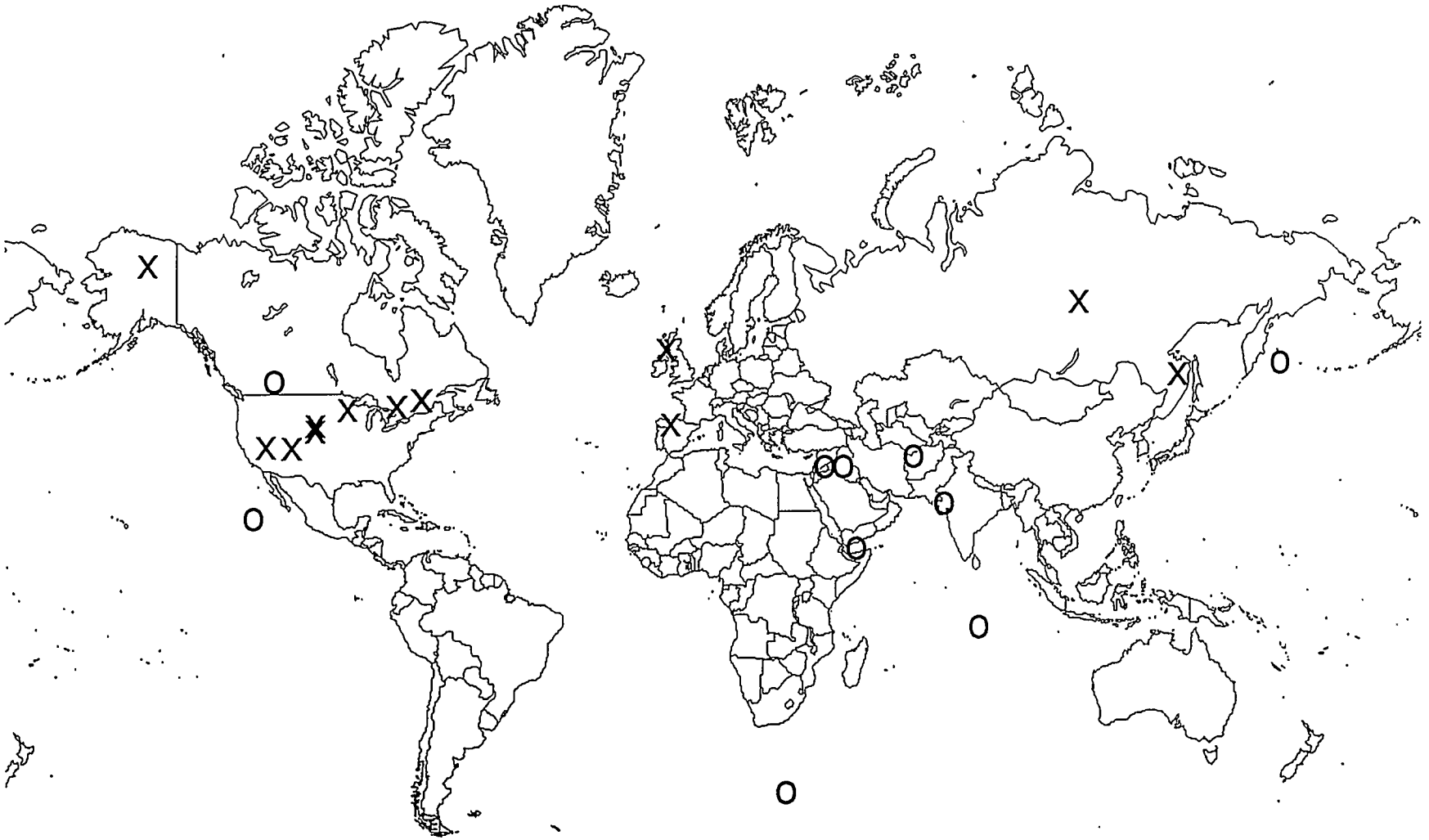

Cumulative Bolide Influx Rate: Infrasonic Determinations

- **Knowing:**
  - **Number of events at each source energy**
  - **Detection probability Vs yield, range and season**
  - **Time of AFTAC infrasound network operation**
- **Assuming:**
  - **Low-altitude explosive source < 15-20 km**
  - **S type ducting from point/line source emission**
  - **Great circle path: Source location for > 2 arrays**
- **Predict: Number of bolides per year over Earth:**

$$N(\geq E_s : kt) = 7.17 E_s^{-0.731}; r^2 = 0.9243$$

CTBT False Alarm Rate Implications

- Implications of cumulative bolide influx rate:
  - 10,000-30,000 bolides/year at an energy > 0.00001 kt: If the nominal detection range is 200 km, a single station could record 5-10/year.
  - Up to 12 bolides/year at an energy > 1 kt: Nominal detection range is about 2500 km.
  - One bolide/year at an energy > 15 kt: Detection likely at ranges of 14,000 km from the source.
  - One bolide in 120 years at an energy > 10 MT: Detection expected over most of the globe
- Rates are confirmed by US DoD satellite data, but are lower limits compared to other data (by 10 X).

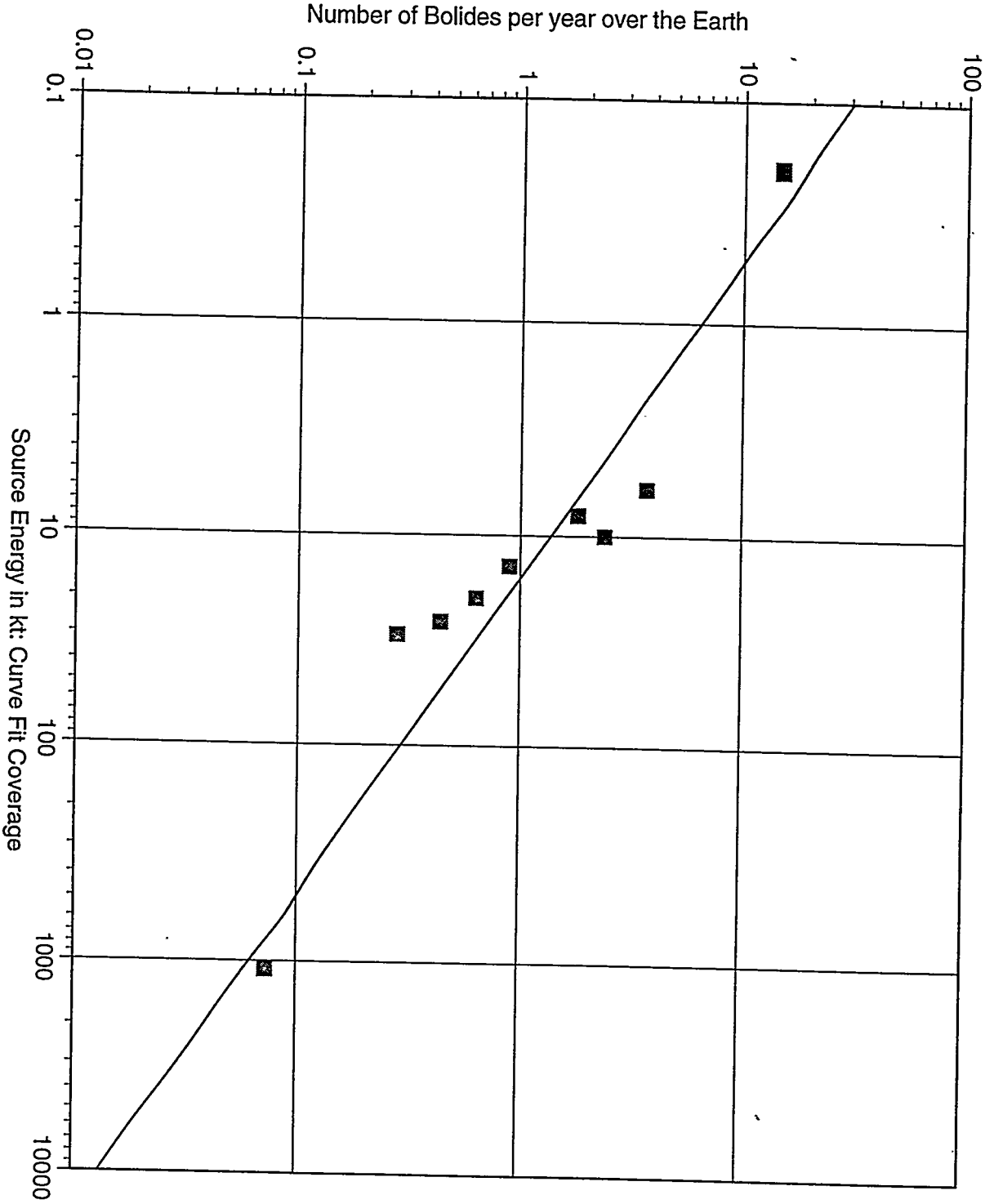
Number of Bolides per year over the Earth
0.01
0.1
1
10
100
Source Energy in kt: Curve Fit Coverage
0.1
1
10
100
1000
10000

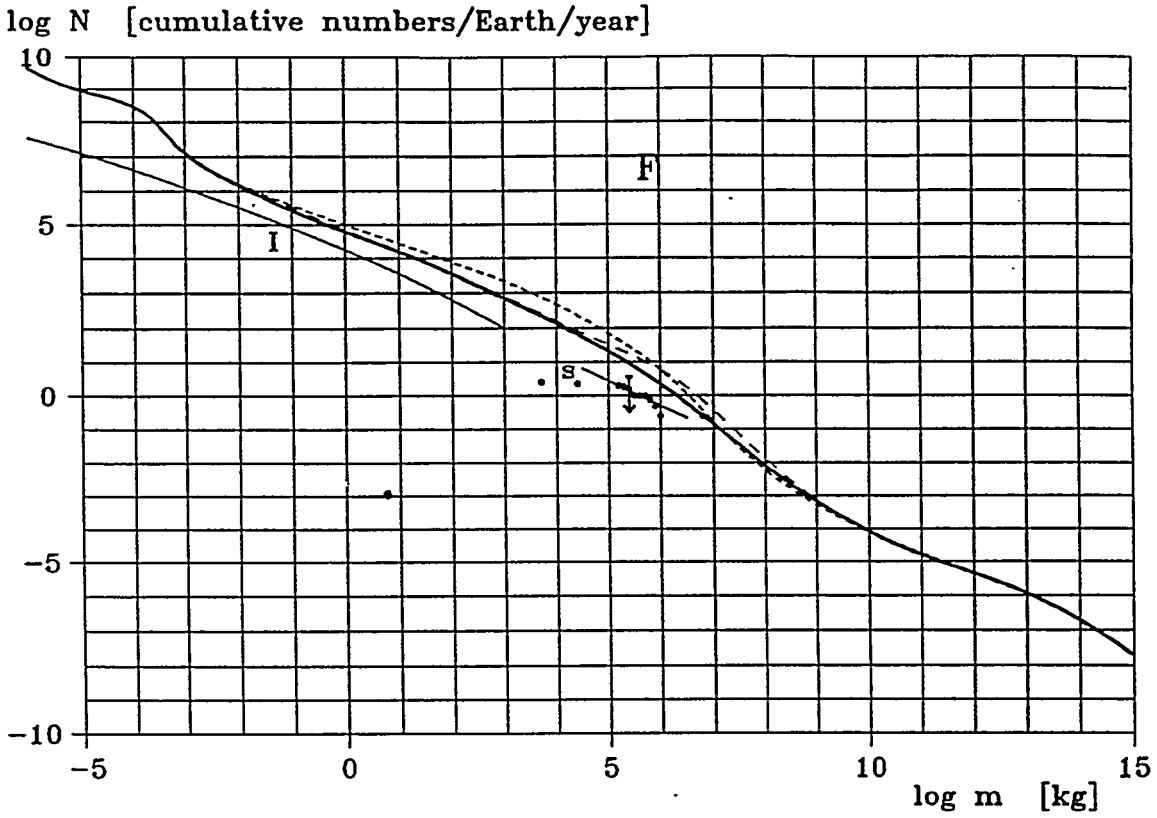

Figure 1. Common logarithm of cumulative numbers N (all bodies with masses larger than the given mass m) of interplanetary bodies coming to the entire Earth's surface per year are plotted against common logarithm of the mass m. The thick line : resulting fluxes of all bodies. The thin line from $\log m = -6$ to $\log m = 3$ denoted 'I': fluxes of the type I bolides (stony bodies, for larger masses meteorite dropping). The thin line from $\log m = 4.5$ to $\log m = 6.5$ denoted 's': fluxes from recording sounds of superbolides (the dots are the individual values of cumulative numbers defining the thin line: Ref. 5). The arrow at $\log m = 5.4$: satellite observed superbolides interpreted as belonging to type I (stony bodies); because separation of type I and II superbolides was not possible[7] , only the upper limit can be given (the base of the arrow) and the arrow symbol means: 'less than the given value'. - - - the cumulative flux curve of all bodies as published in Ref. 1 before calibration with the new Lost City mass. – – – the cumulative flux curve of all bodies as published in Ref. 2 (without calibration for the new Spacewatch statistics in Ref. 10). The enormously high flux announced by Frank[31] is denoted by 'F'.

Recent LANL Bolide Detections

- November 21, 1995: COLORADO Bolide
  - Video/audio camera in Colorado Springs
  - Some Ground observers reports
  - DoD satellite detection
  - Los Alamos array: LANL infrasound
- October 4, 1996: CALIFORNIA Bolide
  - > 200 Ground observers reports
  - NTS and Pinedale arrays: LANL infrasound
  - DoD satellite detection
  - 31 Caltech seismic detections (LA area): All signals converge near Little Lake, California.

Summary and Conclusions

- Bolides as explosive infrasonic sources:
  - ♦Fundamental parameter, Ro, blast radius
  - ♦Amplitude and wave period proportional to Ro
- Propagation effects limit infrasound arrivals:
  - ♦ Atmospheric temperature and wind effects
  - ♦Angle of entry and depth of penetration effects
- Source energy estimation using several techniques
  - ♦Ray, modal, Lamb wave, semi-empirical, etc.
- Earth influx rate (Deep-penetrating part of total):
  - ♦Up to one dozen/year at > 1 kt
  - ♦One bolide/year at > 15 kt

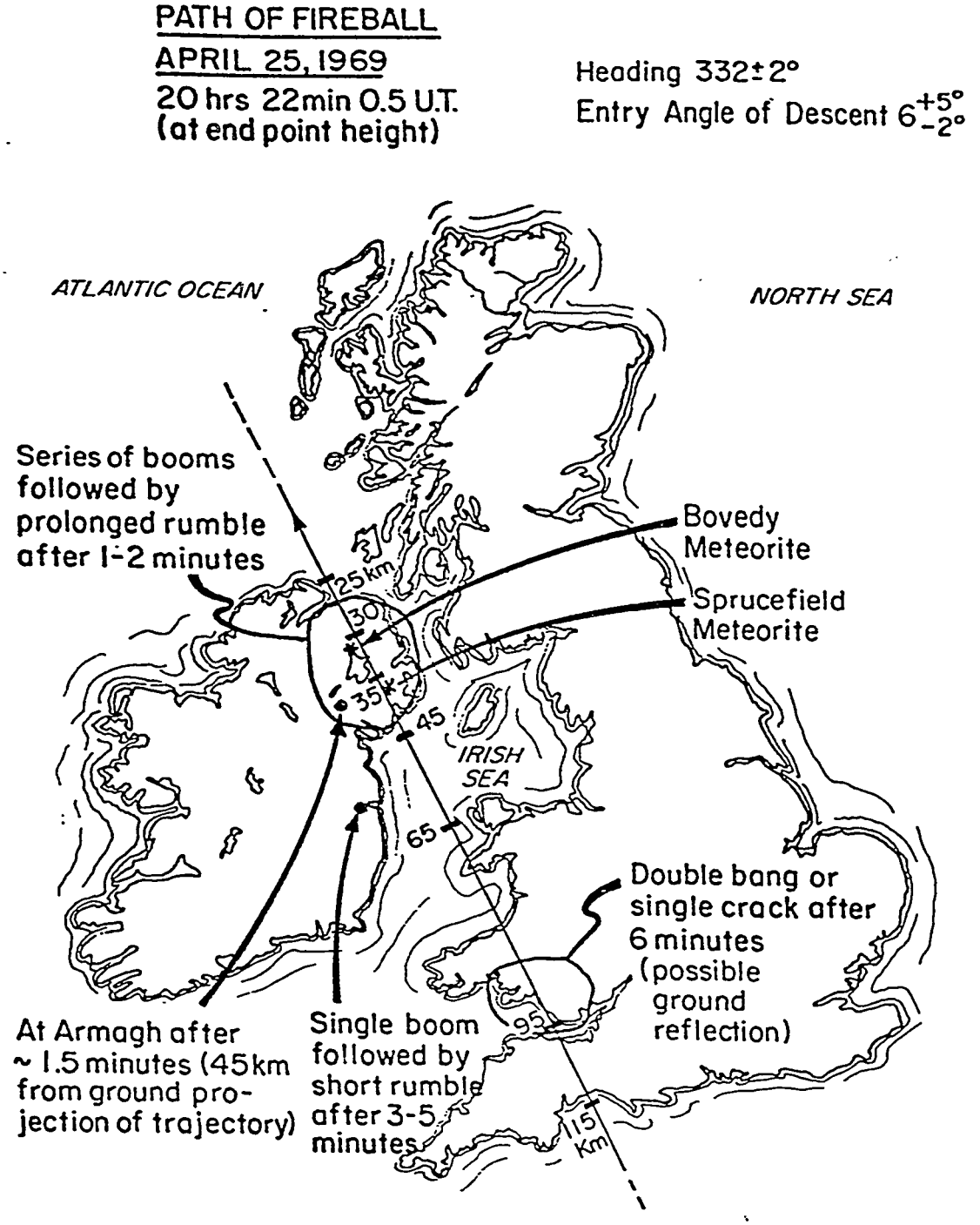

Figure 125. Ground projection of the entry of the British Fireball of April 25, 1969, after Hindley and Miles, 1970.

Abstract submitted but presentation not given because author could not attend.

ON THEORETICAL FUNDAMENTALS OF INFRASOUND PROPAGATION IN AN INHOMOGENEOUS MOVING ATMOSPHERE

Vladimir E. Ostashev

Department of Physics
New Mexico State University
Las Cruces, NM 88003-8001, U.S.A
(On leave from Institute of Atmospheric Physics
Russian Academy of Sciences
Moscow 109017, Russia)

The book [1] deals partly with theoretical fundamentals of infrasound propagation in an inhomogeneous moving atmosphere. The main goal of the presentation is to briefly review the results presented in [1]. First, we consider the historical review of extensive studies of infrasound propagation from large explosions on the ground, which were done in the first half of the century. Then, starting from a system of linearized equations for fluid dynamics, both classical and new equations for acoustic and internal-gravity waves in a stratified moving or turbulent atmosphere are systematically derived. The main results of geometrical acoustics in an inhomogeneous moving atmosphere are presented. In particular, the recently derived refraction law for an infrasound ray in a stratified moving atmosphere is considered. This law allows one to study deflection of the ray from a vertical plane containing source and receiver. The wave theory of infrasound propagation in a stratified moving atmosphere is considered. This theory gives various approaches for calculating a form of infrasound impulse propagating in an atmosphere. Finally, we consider the recently developed theory of wave propagation in an atmosphere with temperature and wind velocity fluctuations. (This material is based partly upon work supported by the U.S. Army Research Office under contract number DAAH04-95-1-0593.)